
Science
15 June 2012 | $10
AAAS

CONTENTS

Volume 336 Issue 6087

CONTENTS continued >>

page 1375

pages 1361, 1383, & 1396

COVER

View of a ceiling in Altamira Cave, Cantabria, Spain (original image rotated 180°). The multicolor (brown and red) bison depicted here date to ~18,000 years ago but were painted on top of earlier single-color artwork (red). New uranium-thorium dates on calcite crusts show that the large (~50-centimeter) double-claviform figure (center right) is at least 35,600 years old, indicating that, at the latest, cave painting here began shortly after humans first arrived. See page 1409.

Photo: Pedro Saura

pages 1394 & 1420

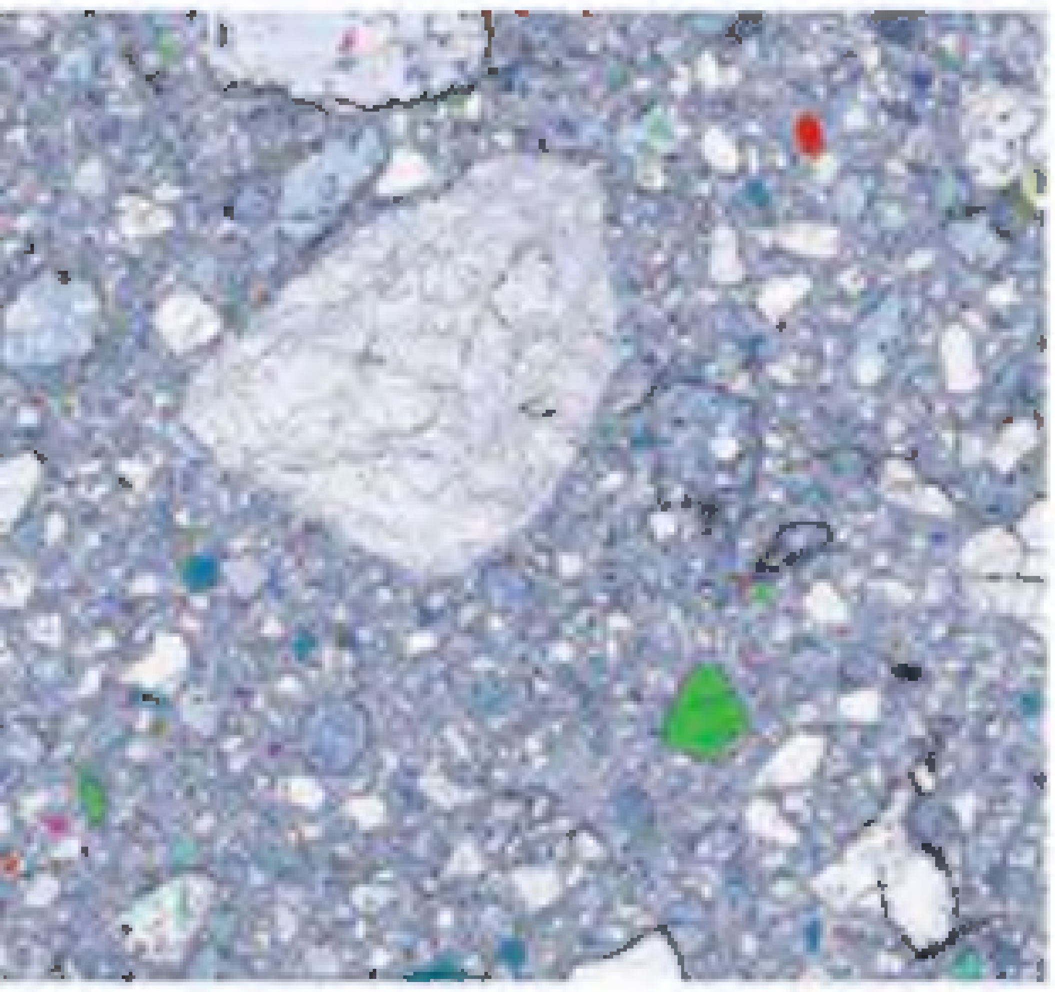

pages 1390 & 1426

pages 1368 & 1432

SCIENCEONLINE

SCIENCEXPRESS

www.sciencexpress.org

Universities, Key to Prosperity
C. O. Holliday
10.1126/science.1225457

Adenylate Cyclases of *Trypanosoma brucei* Inhibit the Innate Immune Response of the Host
D. Salmon et al.
Parasites release cyclic adenosine monophosphate when swallowed up by myeloid cells, thereby turning off a host defense pathway.
10.1126/science.1222753

Function, Targets, and Evolution of *Caenorhabditis elegans* piRNAs
M. P. Bagijn et al.
Piwi-bound piwi-interacting RNAs recruit endogenous small interfering RNAs to silence mobile genetic elements.
10.1126/science.1220952

Rapid Progression of Ocean Acidification in the California Current System
N. Gruber et al.
Rising concentrations of atmospheric carbon dioxide threaten to amplify the severity of ocean acidification in upwelling zones.
10.1126/science.1216773

Mitochondrial Import Efficiency of ATFS-1 Regulates Mitochondrial UPR Activation
A. M. Nargund et al.
When stressed, the mitochondrion reduces import of a transcription factor, which enters the nucleus instead.
10.1126/science.1223560

SCIENCENOW

www.sciencenow.org
Highlights From Our Daily News Coverage

Putting the Brakes on the Immune System
Researchers discover powerful but short-lived cells that rein in immune attacks.
http://scim.ag/Immune-Brakes

Aging Is Recorded in Our Genes
As we grow older, we lose DNA modifications that can protect against cancer and other diseases.
http://scim.ag/Age-Genes

Life Blooms Under Arctic Ice
Researchers discover green blooms of phytoplankton more than one meter below the surface.
http://scim.ag/Ice-Blooms

SCIENCESIGNALING

www.sciencesignaling.org
The Signal Transduction Knowledge Environment
12 June issue: http://scim.ag/ss061212

RESEARCH ARTICLE: The Transcription Factor TFEB Links mTORC1 Signaling to Transcriptional Control of Lysosome Homeostasis
A. Roczniak-Ferguson et al.

PODCAST
S. M. Ferguson and A. M. VanHook
Regulated nuclear translocation of a transcription factor maintains lysosomal homeostasis.

RESEARCH ARTICLE: The *lin-4* MicroRNA Targets the LIN-14 Transcription Factor to Inhibit Netrin-Mediated Axon Attraction
Y. Zou et al.
A microRNA instructs neurons when to stop axonal pathfinding.

PERSPECTIVE: S-Nitrosylation Signaling in *Escherichia coli*
I. Gusarov and E. Nudler
Two posttranslational modifications of a transcription factor enable bacteria to adapt to changes in NO and O_2.

SCIENCETRANSLATIONAL MEDICINE

www.sciencetranslationalmedicine.org
Integrating Medicine and Science
13 June issue: http://scim.ag/stm061312

EDITORIAL: Listen, Understand, Engage
A. Thomson and M. Watson
For more effective vaccine advocacy, scientists and policy-makers must translate and apply insights from the cognitive and social sciences to the way they communicate and engage with the public.

RESEARCH ARTICLE: Cell Carriage, Delivery, and Selective Replication of an Oncolytic Virus in Tumor in Patients
R. A. Adair et al.

FOCUS: The Virus That Came in from the Cold
J. C. Bell
Oncolytic reovirus is carried by cells to tumors and protected from neutralizing antibodies in the circulation.

RESEARCH ARTICLE: Myocardial Infarction Triggers Chronic Cardiac Autoimmunity in Type 1 Diabetes
R. V. S. R. K. Gottumukkala et al.

FOCUS: Autoimmune Diabetes Inflames the Heart
R. H. Eckel and G. S. Eisenbarth
Acute myocardial infarction triggers an autoimmune attack on the heart in a mouse model of type 1 diabetes and in human type 1 diabetic patients.

RESEARCH ARTICLE: Exome Sequencing Can Improve Diagnosis and Alter Patient Management
T. J. Dixon-Salazar et al.
Exome sequencing of 118 patients with neurodevelopmental disorders shows that this technique is useful for identifying new pathogenic mutations and for correcting diagnosis in ~10% of cases.

RESEARCH ARTICLE: Mucus-Penetrating Nanoparticles for Vaginal Drug Delivery Protect Against Herpes Simplex Virus
L. M. Ensign et al.
Mucus-penetrating particles improve drug delivery to the mucosal surface of the mouse vagina and deliver acyclovir for enhanced protection against vaginal herpes infection in mice.

RESEARCH ARTICLE: Successful Treatment of Ebola Virus–Infected Cynomolgus Macaques with Monoclonal Antibodies
X. Qiu et al.
Macaques survived infection with Ebola virus when treated starting at 24 hours after infection with a mix of three neutralizing monoclonal antibodies.

SCIENCECAREERS

www.sciencecareers.org/career_magazine
Free Career Resources for Scientists

Soldiers Becoming Scientists
M. Price
The Post-9/11 GI Bill and other programs are enabling some veterans to pursue careers in science.
http://scim.ag/SoldierScientists

Tooling Up: Interview Intangibles
D. Jensen
The most important aspects of your job interview are things you may not have thought about.
http://scim.ag/TU_Intangibles

SCIENCEPODCAST

www.sciencemag.org/multimedia/podcast
Free Weekly Show
On the 15 June *Science* Podcast: stressed-out grasshoppers, a new way to date cave paintings, counting the dead on a global scale, and more.

SCIENCEINSIDER

news.sciencemag.org/scienceinsider
Science Policy News and Analysis

SCIENCE (ISSN 0036-8075) is published weekly on Friday, except the last week in December, by the American Association for the Advancement of Science, 1200 New York Avenue, NW, Washington, DC 20005. Periodicals Mail postage (publication No. 484460) paid at Washington, DC, and additional mailing offices. Domestic individual membership and subscription (51 issues): $149 ($74 allocated to subscription). Domestic institutional subscription (51 issues): $990; Foreign postage extra: Mexico, Caribbean (surface mail) $55; other countries (air assist delivery) $85. First class, airmail, student, and emeritus rates on request. Canadian rates with GST available upon request, GST #1254 88122. Publications Mail Agreement Number 1069624. **Printed in the U.S.A.**

Change of address: Allow 4 weeks, giving old and new addresses and 8-digit account number. **Postmaster:** Send change of address to AAAS, P.O. Box 96178, Washington, DC 20090–6178. **Single-copy sales:** $10.00 current issue, $15.00 back issue prepaid includes surface postage; bulk rates on request. **Authorization to photocopy** material for internal or personal use under circumstances not falling within the fair use provisions of the Copyright Act is granted by AAAS to libraries and other users registered with the Copyright Clearance Center (CCC) Transactional Reporting Service, provided that $30.00 per article is paid directly to CCC, 222 Rosewood Drive, Danvers, MA 01923. The identification code for *Science* is 0036-8075. *Science* is indexed in the *Reader's Guide to Periodical Literature* and in several specialized indexes.

AAAS
ADVANCING SCIENCE, SERVING SOCIETY

EDITED BY STELLA HURTLEY

Environmental Determinism?

Earth's millions of species influence a wide range of environmental processes, including elemental cycling, the stability of ecosystems, and the goods and services they provide. **Naeem *et al.*** (p. 1401) review recent advances in the young and evolving field of biodiversity and ecosystem functioning, explore the extent to which the field is becoming a predictive science, and indicate how the field needs to develop in order to aid worldwide efforts to achieve environmental sustainability in the face of rising rates of extinction.

Dating Cave Paintings

A number of caves in Europe contain exquisite ancient art. Most of the art has been thought to be produced during the time of last glaciation by recently arrived modern humans, but dating of the art has been problematic because the art contains only minimal amounts of carbon for radiocarbon dating. **Pike *et al.*** (p. 1409; see the cover; see the Perspective by **Hellstrom**) have now obtained U-series dates on the calcite crusts that formed over the art from 11 caves in northwestern Spain. The ages from three caves are older than 35,000 years ago, and one dates to nearly 41,000 years ago. The earliest art used primarily red and was relatively formless; animal depictions appeared later. This dating is near the time of the arrival of modern humans and, because Neandertals were also present, complicates identifying the artists.

Spin Recovery

Spin-orbit interactions present in many semiconductors are used to manipulate the spin of an electron in spin-based electronics. However, this same interaction is also responsible for the loss of information contained in a spin when it changes its direction during the scattering off of impurities. **Sugimoto and Nagaosa** (p. 1413) describe a new quantity, twisted spin, which, unlike regular spin, survives the scatterings; moreover, because the spin-orbit interaction is turned off adiabatically, the lost spin information is retrieved.

Dynamic Responses >>

Expression of the tumor suppressor p53 is activated in response to cell stress. The dynamics of p53 activation can vary, depending on the stressor, resulting in either pulsatile or constant p53 levels; however, the functional consequence of these different dynamics is unclear. **Purvis *et al.*** (p. 1440) developed a method to control p53 dynamics in human cells. Pulsing p53 selectively activated genes involved in cell cycle arrest and DNA repair, allowing recovery from DNA damage. In contrast, sustained p53 promoted induction of terminal genes leading to cellular senescence. Thus, protein dynamics can affect cell fate decisions.

Dropping a Dimension?

In most magnetic materials, the exchange interaction causes the spins on the neighboring sites of a crystal lattice to align. In the absence of exchange interactions, dipolar interactions, which are highly orientation dependent, are also expected to be able to cause magnetism. **Kraemer *et al.***(p. 1416) present evidence for antiferromagnetism in a dipolar-coupled material, $LiErF_4$. Although a three-dimensional system, its critical behavior was more reminiscent of a two-dimensional material.

B-B Bond

Alkynes contain carbon-carbon triple bonds and represent a diverse class of organic compounds. In principle, valence rules suggest that the boron analog of an alkyne, with a B-B triple bond, ought to be accessible by appending a two-electron donor to each B atom. **Braunschweig *et al.*** (p. 1420; see the Perspective by **Frenking and Holzmann**) now present the synthesis, isolation, and crystallization of a solid, triple-bonded diboryne, with N-heterocyclic carbenes as the terminal substituents, which contains the expected linear bonding geometry.

Porous Blocks

Porous materials are widely used in separation processes and catalysis. **Seo and Hillmyer** (p. 1422) used block copolymers that naturally separate into domains to achieve a continuous network of pores. A chain transfer agent was used to direct the copolymerization of the two materials in situ to generate a structure with a percolating porous structure with pore sizes of a few nanometers and with tunable control over the polymer properties and extent of cross-linking.

The Rocks That Hit the Moon

The cratered surface of the Moon bears witness to the numerous impacts it has suffered. Chemical signatures of these impacts have been detected indirectly. Now, **Joy *et al.***(p. 1426, published online 17 May; see the Perspective by **Rubin**) report the detection and characterization of meteorite fragments preserved in ancient lunar regolith breccias from the Apollo 16 landing site. These meteoritic fragments represent direct samples of the population of small bodies traversing the inner solar system at around 3.4 billion years ago—the same time or just after the basin-forming epoch on the Moon.

Ancient Associations

Submarine seagrass meadows are critical to fisheries and coastline protection and provide feeding grounds for many endangered species, including dugongs and turtles, and serve as a nursery for coral reef fish. The persistence and maintenance of seagrass ecosystems have been mysterious, because accumulation of organic matter in the beds should rapidly lead to toxic sulphide levels in the sediment. Using a meta-analysis and a field study, **van der Heide *et al.*** (p. 1432) atttribute the 100-million-year success of seagrasses to a three-stage symbiosis. Seagrass beds worldwide contain high densities of small lucinid bivalves that have symbiotic

CREDITS (TOP TO BOTTOM): JEREMY PURVIS/HARVARD MEDICAL SCHOOL; SUGIMOTO ET AL.

sulphide-oxidizing bacteria in their gills. This association appears to relieve any sulphide stress for seagrasses, while the lucinids and their symbionts profit from the accumulation of degradable organic matter and oxygen release from seagrass roots.

Population Limits

Extensive pre-Columbian populations inhabited the central and eastern Amazon basin, as evidenced by the clearing and modification of forests. **McMichael *et al.*** (p. 1429) examined how far inland such activities may have extended by sampling soils across western Amazonia, including river bluffs, which were heavily occupied downstream. Little evidence of human disturbance across a wide region was found by looking for charcoal layers (which would suggest use of fire) and phytoliths, which trace local plants and would indicate the presence of crops. Furthermore, no ceramics or tools were found. Thus, pre-Columbian human populations seem to have been sparse in western Amazonia.

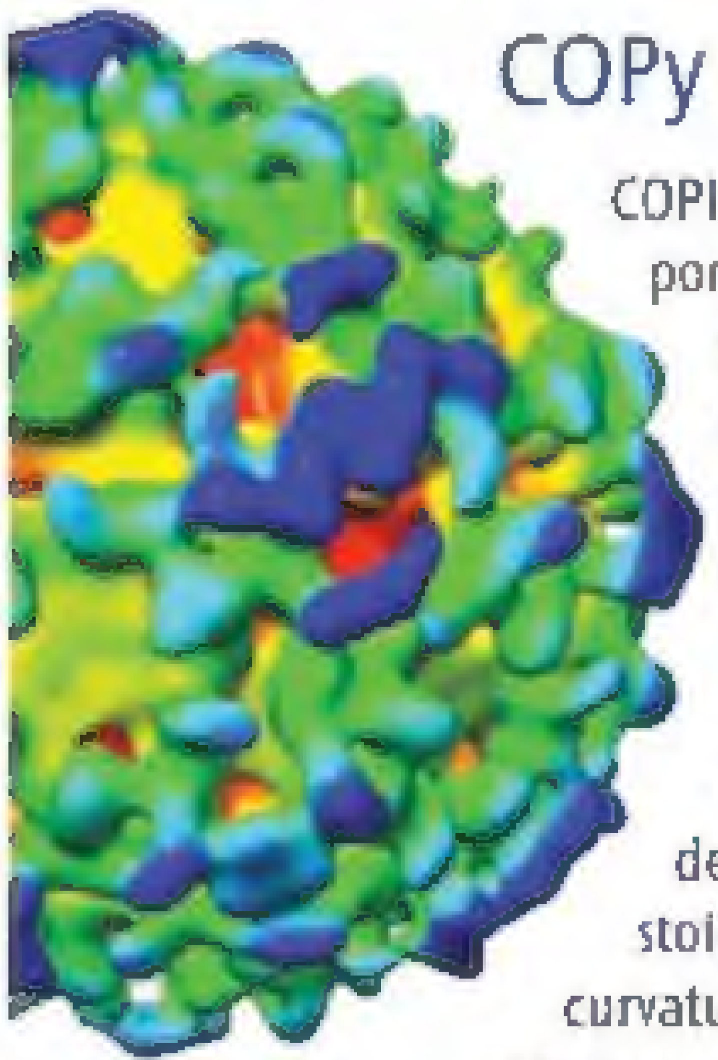

COPy Coat

COPI-coated vesicles are responsible for intracellular vesicular transport both within the Golgi and between the Golgi and endoplasmic reticulum. By applying subtomogram averaging from cryoelectron tomography data, **Faini *et al.*** (p. 1451, published online 24 May) were able to describe the complete three-dimensional structure for COPI-coated vesicles generated in a cell-free, membrane-budding reaction. The structures of multiple individual vesicles reveal assembly principles based on interactions that, unlike those for clathrin-coated vesicles, are not regular: The basic subunit can undergo significant conformational changes and assemble with different stoichiometries. This variability may allow the regulation of membrane curvature and vesicle size. Furthermore, forming a complete closed coat was not required to produce budded vesicles.

Fear Itself

A direct connection exists between aboveground communities and belowground soil microbiota: Soil microbes break down detrital inputs from above. Generally, it has been assumed that this relationship is largely driven by the soil community and the quality of the unconsumed plant-matter that makes up the majority of detritus in most ecosystems. However, **Hawlena *et al.*** (p. 1434) found that grasshoppers exposed to the threat of spider predation have an altered carbon to nitrogen ratio. When these grasshopper carcasses were subsequently integrated into the plant litter, they significantly slowed the decomposition rate, although there was no impact on the rate of decomposition of the grasshoppers themselves. Thus, the mere presence of predators, and the stress they impose, can have cascading trophic impacts and even influence the process of decomposition.

Reading the Leaves

Excess inputs of nutrients—a type of pollution known as eutrophication—threatens biodiversity and water quality in rivers and streams. **Woodward *et al.*** (p. 1438; see the Perspective by **Palmer and Febria**) studied how one key ecosystem process—leaf-litter decomposition—responds to eutrophication across a large nutrient pollution gradient in 100 European streams. Leaf breakdown was stimulated by low to moderate nutrient concentrations but was inhibited at high rates of nutrient loading.

Spatial Memory Perturbation

The hippocampus is important for learning and memory. However, it is not clear which patterns of neural activity in the hippocampus support specific mnemonic functions. **Jadhav *et al.*** (p. 1454, published online 3 May) developed a real-time analysis system to detect and selectively interrupt a certain type of hippocampal neuronal network event—sharp-wave ripples—during learning. In awake animals, loss of sharp-wave ripples and associated memory replay activity caused a learning deficit specific to spatial working memory but had no effect on reference memory. This learning deficit was present despite the preservation of place-field representations and replay activity during rest.

CREDIT: MARCO FAINI/EMBL

Carlos A. Nobre is a climate scientist and is the National Secretary for R&D Policies at the Ministry of Science, Technology, and Innovation of Brazil. He is a former chair of the International Geosphere-Biosphere Programme. E-mail: carlos.nobre@mct.gov.br.

UNsustainable?

NEXT WEEK, THOUSANDS OF PARTICIPANTS FROM GOVERNMENTS, THE PRIVATE SECTOR, NON-governmental organizations, and other stakeholders will gather in Brazil at a United Nations (UN) summit to secure political and economic commitments for sustainable development and to address new and emerging challenges. These objectives recall the 1992 UN Conference on Environment and Development, also held in Rio de Janeiro. Although political progress toward these goals has stagnated, in the intervening 20 years science and technology have moved on. The "Rio+20" meeting should be framed by these new developments.

Three notable global changes should affect the summit outcome. The most obvious is the degree of interconnectedness among nations, which would have been unimaginable in 1992. Today's global society is linked culturally, socially, and economically. Highly interconnected systems can confer remarkable stability, but they are prone to abrupt change, as shown by the global financial crisis and recent food security issues. We need to consider how to minimize such systemic risks.

Another shift has been the concept of the "Anthropocene," popularized in 2000 by the atmospheric chemist and Nobel Laureate Paul Crutzen and others who have recognized the substantial influence of human behavior on the Earth system. The word, defining a new geological epoch, symbolizes the idea that humanity has become a key driver of the Earth system, even perhaps pushing it beyond several planetary boundaries such as radiative forcing and biodiversity loss. It heralds a profound change in perspective that goes beyond geological nomenclature and into political, cultural, and economic spheres. The idea of the Anthropocene requires that nations reevaluate their relationship with the planet and each other to ensure the prosperity of current and future generations. Next week's summit must be seen against this backdrop.

The third change in the past 20 years has been geopolitical. Emerging economies such as Brazil, China, and India are growing into economic powerhouses that are critical to the future global sustainability agenda. Brazil has undergone vast transformations since hosting the Rio 1992 Summit. It has exceeded most UN Millennium Development Goals, including lifting 40 million people out of poverty. Amazon deforestation has declined by 77% in 7 years, and over 25% of the territory is protected as Conservation Units or Indian Reservations. If Brazil meets its voluntary targets on greenhouse gases, emissions will fall by 10 to 12% by 2020 as compared with 2005. 45% of Brazil's energy is renewable, such as hydropower and biofuels. But there has been slower progress in achieving universal sanitation and sustainable urban development and in reducing the environmental impact of large-scale agriculture.

On the table at Rio+20 are several building blocks that together could create momentum for a global transformation. Universal sustainable development goals should encompass social, economic, and environmental outcomes, underpinned by quantitative targets and indicators. A Sustainable Development Council with a direct mandate from the UN General Assembly could promote progress on goals. And regular analyses of emergent global sustainability must be coupled with a more coherent and strategic approach to evidence-based policy internationally. Future Earth, a 10-year international research program focusing on global sustainability solutions, is already planned. These efforts could be further strengthened by the oversight of a new office of Chief Scientific Advisor to the UN Secretary-General, which would help ensure that these actions together provide the start of a strong global innovation system.

In March 2012, the international research community convened the London Planet Under Pressure conference and released the State of the Planet Declaration (www.planetunderpressure2012.net), emphasizing that the risks to Earth's natural processes and our globally interconnected society are too great to ignore. Rio+20 should act as a catalyst for a sustainable development agenda that emphasizes holistic, equitable, and farsighted approaches to decision-making. Urgently needed is courageous leadership that commits to a long-term vision for our planet and its people.

– Carlos A. Nobre

10.1126/science.1225343

EDITED BY MARIA CRUZ AND KRISTEN MUELLER

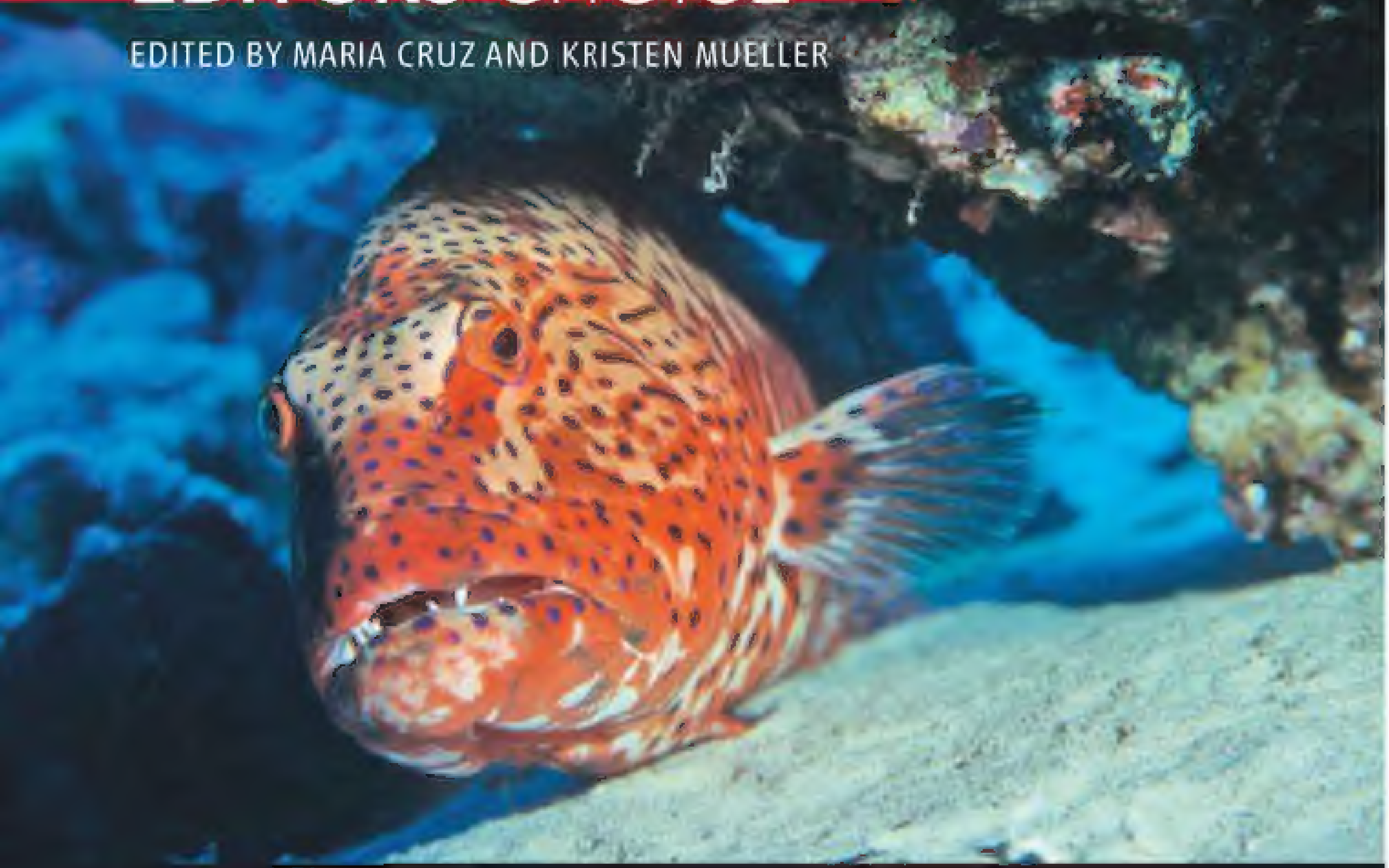

ECOLOGY

The Reef Next Door

Marine reserves have been repeatedly shown to conserve local populations of fish and other marine organisms, but whether they also help to replenish nearby fished areas has been more difficult to demonstrate. Harrison *et al.* tested whether connectivity between reserves and nonreserves in the Great Barrier Reef enhanced the recruitment of fish to fished reefs. First, they sampled hundreds of adults and performed genetic parentage analysis on two exploited reef species, the coral trout and stripey snapper, across three of the reserves. They then identified the parents of juveniles captured from 19 sites scattered across a 1000-km area encompassing reserves and harvest areas. The authors found that adults sampled within the reserves exported a majority of their offspring to intervening harvest areas (between 55 and 83%) and other reserves, but that a significant proportion remained within the reserve. They estimate that reserves (where fish are both larger and more abundant) contribute about half of the overall recruitment, despite being smaller in area. These results demonstrate that marine reserves benefit nearby harvested areas substantially and facilitate persistence of the overall network. — SNV

Curr. Biol. **22**, 10.1016/j.cub.2012.04.008 (2012).

ECONOMICS

Insuring Greater Health

What happens when health insurance is given to low-income individuals? Finkelstein *et al.* report on the 1-year outcomes after the state of Oregon enrolled roughly 10,000 uninsured adults, selected by lottery and with annual incomes of $10,000 or less, in Medicaid. They find, in comparison to those who were not selected, a 15 to 35% greater consumption of health care, as measured by the number of hospital admissions, prescription drugs taken, and outpatient visits, along with a 15 to 60% greater rate of compliance with preventive care, such as testing for blood cholesterol and mammograms. The increased use of medical services was consistent with the observation that the incidence of diabetes, hypertension, asthma, and depression in the people who were eligible for Medicaid but did not win the lottery was twice as high as in the general adult population. Objective measures of changes in physical health await in-person follow-up assessments, but one remarkable finding from the surveys is that the impact of health insurance on subjective well-being, at least in this context, is equivalent to what would be produced by a doubling of one's income. — GJC

Q. J. Econ. **127**, 10.1093/qje/qjs020 (2012).

MICROBIOLOGY

Corrosion Conundrum

Corrosion of iron leads to damage and failure of a variety of structures, including bridges and underground pipes. The electrochemical process occurs by the oxidation of metallic iron (Fe^0) to ferrous iron (Fe^{2+}), which creates iron oxide rust in the presence of oxygen. In anaerobic sediments, however, the purely chemical reaction is so slow that sulfate-reducing bacteria are mainly responsible for the corrosion of buried iron structures. In theory, the bacteria themselves could use the electrons generated during corrosion to drive their metabolism, but crusts precipitated on the iron surface would present a physical barrier to prevent the cells from coming in direct contact with the metallic iron. In laboratory and field experiments, Enning *et al.* found that the precipitating crusts on highly corroded iron surfaces were semiconducting, which provides an electrical path for electrons to travel between the iron surface and bacterial cells. To complete the electrochemical circuit, chimney-like structures in the crust allowed the passage of neutralizing ions. A sharp pH gradient inside the chimney promoted dissolution and pitting of the iron surface, and the released Fe^{2+} was incorporated into the chimney and crust. Inhibiting bacterial sulfate reduction in the subsurface may therefore reduce the economic costs associated with iron corrosion underground. — NW

Environ. Microbiol. 10.1111/j.1462-2920.2012.02778.x (2012).

ASTRONOMY

Active Galaxy

Like most other galaxies, the Milky Way hosts a massive black hole in its center. This hole is 4 million times more massive than the Sun, and although it currently lies dormant, it is expected that it experienced periods of activity as it grew by accreting gas and stars from its vicinity. Using data from the Fermi Large Area Telescope, Su and Finkbeiner report signs of that activity in the form of two gamma-ray jets, which emanate from the center of the Milky Way in nearly opposite directions. These jets are tilted at an angle of 15° from the north-south axis of the galaxy and extend to about the edge of two previously identified gamma-ray–emitting bubbles, which extend 27,000 light-years north and south of the galactic center. The southern jet has blown a tenuous gamma-ray–emitting cocoon as it propagated through the interstellar medium. The shape of this cocoon is similar to those of the radio-emitting cocoons produced by the jets of actively accreting black holes in distant galaxies. It is not clear whether the bubbles and the jets and cocoon system were produced concurrently. — MJC

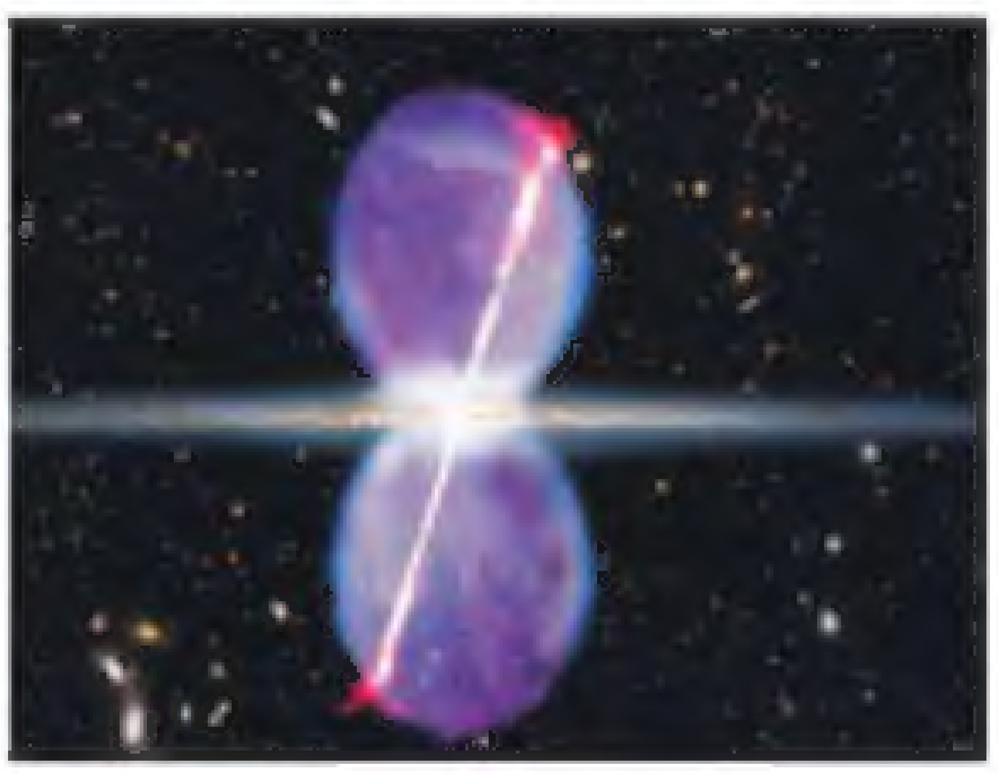

Astrophys. J. arXiv:1205.5852 (2012).

CREDITS (TOP TO BOTTOM): © ANNDREY NEKRASOV/ALAMY; DAVID A. AGUILAR (CFA)

www.sciencemag.org

Science

1200 New York Avenue, NW
Washington, DC 20005
Editorial: 202-326-6550, FAX 202-289-7562
News: 202-326-6581, FAX 202-371-9227
Bateman House, 82-88 Hills Road
Cambridge, UK CB2 1LQ
+44 (0) 1223 326500, FAX +44 (0) 1223 326501

Subscription Services For change of address, missing issues, new orders and renewals, and payment questions: 866-434-AAAS (2227) or 202-326-6417, FAX 202-842-1065. Mailing addresses: AAAS, P.O. Box 96178, Washington, DC 20090-6178 or AAAS Member Services, 1200 New York Avenue, NW, Washington, DC 20005

Institutional Site Licenses please call 202-326-6755 for any questions or information

Reprints: Author Inquiries 800-635-7181
Commercial Inquiries 803-359-4578

Permissions 202-326-7074, FAX 202-682-0816

Member Benefits AAAS Travels: Betchart Expeditions 800-252-4910; Apple Store www.store.apple.com/us/go/eppstore/aaas; NASA Federal, 1-888-NASA-FCU (1-888-627-2328) or www.nasafcu.com; Cold Spring Harbor Laboratory Press Publications www.cshl.press.com/affiliates/aaas.htm; GEICO Auto Insurance www.geico.com/landingpage/go51.htm?logo=17624; Hertz 800-654-2200 CDP#343457; Office Depot https://bsd.officedepot.com/portalLogin.do; Seabury & Smith Life Insurance 800-424-9883; Subaru VIP Program 202-326-6417; VIP Moving Services www.vipmayflower.com/domestic/index.html; Other Benefits: AAAS Member Services 202-326-6417 or www.aaasmember.org.

science_editors@aaas.org	(for general editorial queries)
science_letters@aaas.org	(for queries about letters)
science_reviews@aaas.org	(for returning manuscript reviews)
science_bookrevs@aaas.org	(for book review queries)

Published by the American Association for the Advancement of Science (AAAS), *Science* serves its readers as a forum for the presentation and discussion of important issues related to the advancement of science, including the presentation of minority or conflicting points of view, rather than by publishing only material on which a consensus has been reached. Accordingly, all articles published in *Science*—including editorials, news and comment, and book reviews—are signed and reflect the individual views of the authors and not official points of view adopted by AAAS or the institutions with which the authors are affiliated.

AAAS was founded in 1848 and incorporated in 1874. Its mission is to advance science, engineering, and innovation throughout the world for the benefit of all people. The goals of the association are to: enhance communication among scientists, engineers, and the public; promote and defend the integrity of science and its use; strengthen support for the science and technology enterprise; provide a voice for science on societal issues; promote the responsible use of science in public policy; strengthen and diversify the science and technology workforce; foster education in science and technology for everyone; increase public engagement with science and technology; and advance international cooperation in science.

Information for Authors
See pages 752 and 753 of the 10 February 2012 issue or access www.sciencemag.org/about/authors

Editor-in-Chief **Bruce Alberts**
Executive Editor **Monica M. Bradford**
News Editor **Colin Norman**

Managing Editor, Research Journals **Katrina L. Kelner**
Deputy Editors **R. Brooks Hanson, Barbara R. Jasny, Andrew M. Sugden, Valda J. Vinson**

Editorial senior editors/commentary Lisa D. Chong, Brad Wible; senior editors Gilbert J. Chin, Pamela J. Hines, Paula A. Kiberstis (Boston), Marc S. Lavine (Toronto), Beverly A. Purnell, L. Bryan Ray, Guy Riddihough, H. Jesse Smith, Phillip D. Szuromi (Tennessee), Valda Vinson, Jake S. Yeston, Laura M. Zahn (San Diego); associate editors Kristen L. Mueller, Jelena Stajic, Sacha Vignieri, Nicholas S. Wigginton; book review editor Sherman J. Suter; associate letters editor Jennifer Sills; editorial manager Cara Tate; senior copy editors Jeffrey E. Cook, Cynthia Howe, Harry Jach, Lauren Kmec, Barbara P. Ordway, Trista Wagoner; copy editor Chris Filiatreau; senior editorial coordinators Carolyn Kyle, Beverly Shields; editorial coordinators Joi S. Granger, Anita Wynn; publications assistants Ramatoulaye Diop, Le-Toya Mayne Flood, Aneera Dobbins, Jeffrey Hearn, Lisa Johnson, Dona Mathieu, Scott Miller, Jerry Richardson, Teresa R. Sakon, Brian White; editorial assistant Patricia M. Moore; executive editorial assistant Yolanda O Bannon (San Francisco); executive assistant Alison Crawford; administrative support Maryrose Madrid; editorial fellow Melissa R. McCartney

Editorial director, web and new media Stewart Wills; senior web editor Sarah Crespi; web editor Kerry Klein; web development manager Martyn Green; web developers Corinna Cohn, Andrew Whitesel

News deputy news editors Robert Coontz, David Grimm (Online), Eliot Marshall, Jeffrey Mervis, Leslie Roberts, John Travis; contributing editors Elizabeth Culotta, Polly Shulman; news writers Yudhijit Bhattacharjee, Adrian Cho, Jennifer Couzin-Frankel, Carolyn Gramling, Jocelyn Kaiser, Richard A. Kerr, David Malakoff, Greg Miller, Elizabeth Pennisi, Robert F. Service (Pacific NW), Erik Stokstad; web developer Daniel Berger; interns Jane J. Lee, Meghna Sachdev; contributing correspondents John Bohannon, Jon Cohen (San Diego, CA), Daniel Ferber, Ann Gibbons, Sam Kean, Eli Kintisch, Andrew Lawler, Mitch Leslie, Charles C. Mann, Virginia Morell, Gary Taubes; copy editors Melissa Raimondi, Linda B. Felaco; administrative support Scherraine Mack; bureaus San Diego, CA 760-942-3252, FAX 760-942-4979; Pacific Northwest 503-963-1940

Production director Wendy K. Shank; assistant managers Rebecca Doshi, Lori Murphy; senior specialists Steve Forrester, Chris Redwood, Anthony Rosen; Preflight director David M. Tompkins; manager Marcus Spiegler; specialists Jason Hillman, Tara Kelly

Art director Yael Fitzpatrick; associate art director Laura Creveling; senior illustrators Chris Bickel, Katharine Sutliff; illustrators Yana Hammond, Brocelyn Straub; senior art associates Holly Bishop, Preston Huey, Nayomi Kevitiyagala; art associates Kay Engman, Garvin Grullón; photo editor Leslie Blizard

Science International

Europe (science@science-int.co.uk) editorial: international managing editor Andrew M. Sugden; senior editor/commentary Julia Fahrenkamp-Uppenbrink; senior editors Caroline Ash, Stella M. Hurtley, Ian S. Osborne, Peter Stern; associate editor Maria Cruz; contributing editor Helen Pickersgill; editorial support Samantha Hogg, Alice Whaley; administrative support Janet Clements, Nicola Morris, John Wood; news: deputy news editor, u.k. Daniel Clery; contributing editor, europe Martin Enserink; contributing correspondents Michael Balter (Paris), Kai Kupferschmidt (Berlin), Gretchen Vogel (Berlin)

Asia Japan Office: Asca Corporation, Tomoko Furusawa, Rustic Bldg. 7F, 77 Tenjin-cho, Shinjuku-ku, Tokyo 162-0808 Japan; +81 3 6802 4616, FAX +81 3 6802 4615, inquiry@sciencemag.jp; asia news editor Richard Stone (Beijing: rstone@aaas.org); contributing correspondents Dennis Normile (Japan: +81 (0) 3 3391 0630, FAX +81 (0) 3 5936 3531; dnormile@gol.com); Hao Xin (China: cindyhao@gmail.com); Mara Hvistendahl (China, mhvisten@aaas.org); Pallava Bagla (South Asia, +91 (0) 11 2271 2896; pbagla@vsnl.com)

Executive Publisher **Alan I. Leshner**
Publisher **Beth Rosner**

Fulfillment Systems and Operations (membership@aaas.org); customer service supervisor Pat Butler; specialists LaToya Casteel, Michelle Ofordire, April Marshall; manager, data entry Mickie Napoleoni; data entry specialists Tarrika Hill, JJ Regan, Eva Mae Campbell

Business Operations and Administration director Deborah Rivera-Wienhold; business systems and financial analysis director Randy Yi; manager, fulfillment systems Frits Bunningh; systems analyst Nicole Mehmedovich; manager, business analysis Eric Knott; manager, business operations Jessica Tierney; business analysts Cory Lipman, Celeste Troxler, Christine Wehr; financial analyst Julia Nguyen; rights and permissions: administrator Emilie David; associate Elizabeth Sandler; marketing director Ian King; marketing managers Allison Pritchard, Alison Chandler, Julianne Wielga, Samantha Smith; marketing associates Aimee Aponte, Mary Ellen Crowley, Elizabeth Sattler, Rebecca Rillin; senior marketing executive Jennifer Reeves; director, site licensing Tom Ryan; director, corporate relations Eileen Bernadette Moran; senior publisher relations specialist Kiki Forsythe; publisher relations manager Catherine Holland; publisher relations, eastern region Phillip Smith; publisher relations, western region Ryan Rexroth; customer relations manager Iquo Edim; marketing manager Christina Schlecht; marketing associates Paulina Curto, Mitchell Edmund; electronic media: director Lizabeth Harman; assistant manager Lisa Stanford; production specialists Antoinette Hodal, Thomas Jaensch, Nichele Johnston, Kimberly Oster; project manager Trista Snyder; computer specialists Walter Jones, Kai Zhang; program director, aaas membercentral Peggy Mihelich

director, global collaboration, custom publications, advertising Bill Moran
commercial editor Sean Sanders: 202-326-6430
assistant commercial editor Tianna Hicklin 202-326-6463

Product (science_advertising@aaas.org); midwest Rick Bongiovanni: 330-405-7080, FAX 330-405-7081; east coast/e. canada Laurie Faraday: 508-747-9395, FAX 617-507-8189; west coast/w. canada Lynne Stickrod: 415-931-9782, FAX 415-520-6940; uk/europe/asia Roger Goncalves: TEL/FAX +41 43 243 1358; japan Makiko Hara: +81 (0) 3 6802 4616, FAX +81 (0) 3 6802 4615, ads@sciencemag.jp; china/taiwan Ruolei Wu: +86 1367 1015 294 rwu@aaas.org

worldwide associate director of *Science* careers Tracy Holmes: +44 (0) 1223 326525, FAX +44 (0) 1223 326532

Classified (advertise@sciencecareers.org); u.s.: midwest/west coast/south central/canada Tina Burks: 202-326-6577; east coast/industry Elizabeth Early: 202-326-6578; sales administrator Marci Gallun; europe/row sales Simone Jux, Lucy Nelson; sales assistant Kelly Grace; japan Yuri Kobayashi: +81 (0) 6627-9250; careerads@sciencemag.jp; china/taiwan Ruolei Wu: +86 1367 1015 294 rwu@aaas.org; advertising support manager Karen Foote: 202-326-6740; advertising production operations manager Deborah Tompkins; senior production specialist/graphic designer Amy Hardcastle; production specialist Yuse Lajiminmuhip; senior traffic associate Christine Hall; sales coordinator Shirley Young

AAAS Board of Directors retiring president, chair Nina V. Fedoroff; president William H. Press; president-elect Phillip A. Sharp; treasurer David E. Shaw; chief executive officer Alan I. Leshner; board Mary R. Berenbaum, Bonnie L. Bassler, Stephen L. Mayo, Raymond Orbach, Julia M. Phillips, Sue V. Rosser, David D. Sabatini, Inder M. Verma

AAAS
ADVANCING SCIENCE, SERVING SOCIETY

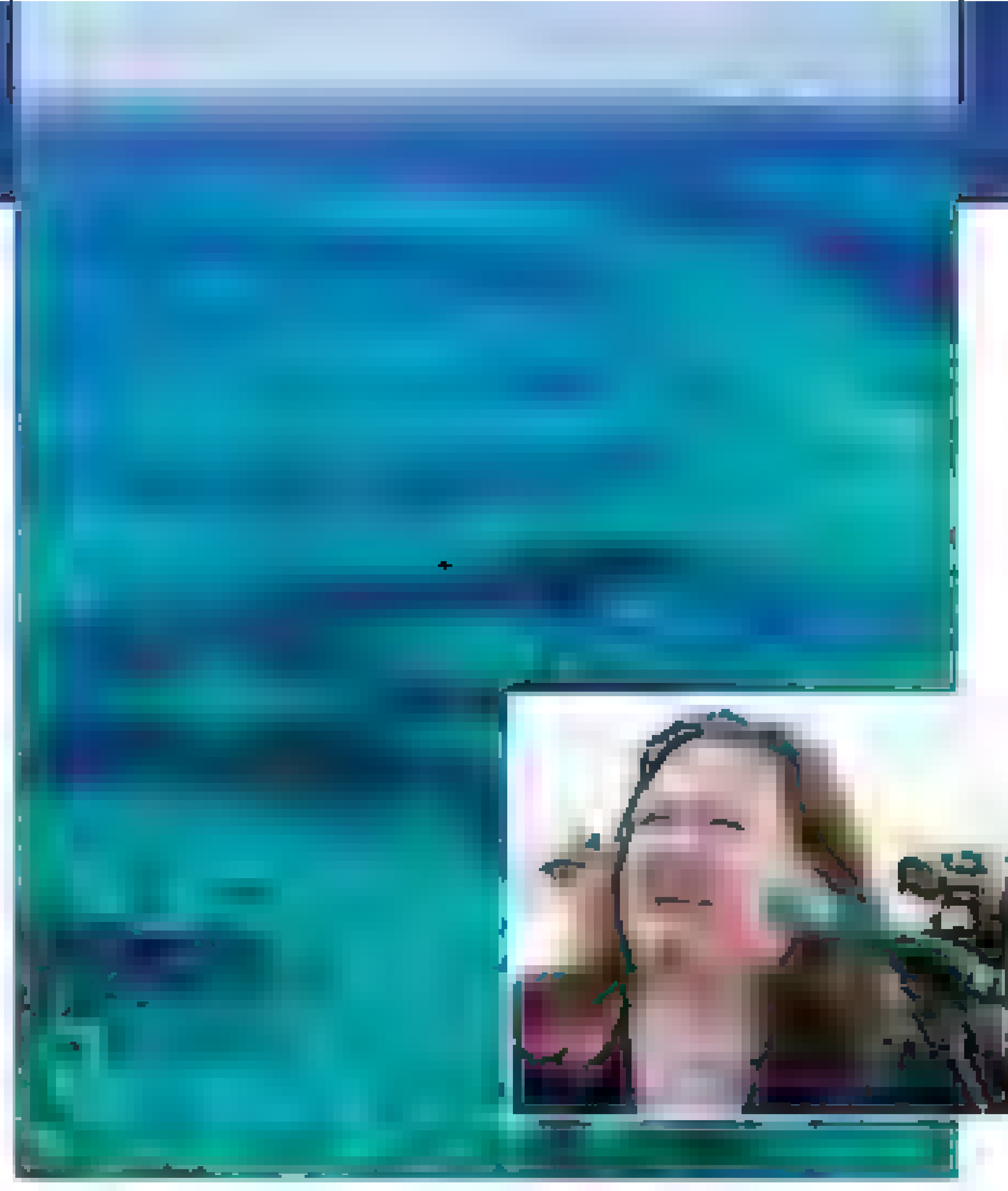

AROUND THE WORLD

Washington, D.C. 1

NASA Rover Will Contaminate Mars Samples

The Curiosity rover will definitely find evidence of an advanced civilization if it lands safely on Mars. That's because any rock samples the rover drills will be contaminated with bits of Teflon from the rover's machinery, NASA announced during a press teleconference on 11 June.

Curiosity's $2.5 billion mission includes searching for the carbon-containing molecular remains of any life that inhabited ancient Mars. The rover will use its Sample Analysis at Mars (SAM) instrumentation to analyze samples. To extract the rock samples, the rover will bang a drill bit into the rock — which will also rub off bits of Teflon from seals in the drill assembly. The Teflon — which is two-thirds carbon — can become mixed in with the sample, which will be vaporized for analysis.

The team is guardedly upbeat that it can overcome the problem: Paul Mahaffy of NASA's Goddard Space Flight Center in Greenbelt, Maryland, says team members can minimize the amount of Teflon getting into the analytical system by altering operation of the drill. Once in SAM, Mahaffy says, the compounds being analyzed are heated to a temperature at which Teflon decomposes, producing mostly small, easily identified compounds of carbon and fluorine. http://scim.ag/Teflonrover

Geneva, Switzerland 2

WHO Warns of Drug-Resistant Gonorrhea

Last week, the World Health Organization (WHO) warned that gonorrhea, which infects 106 million people in the world each year, could soon become untreatable. In its *Global action plan to control the spread and impact of antimicrobial resistance in* Neisseria gonorrhoea, released on 6 June, the public health arm of the United Nations sounds a dire note. "The loss of effective and readily available treatment options will lead to significant increases in morbidity and mortality," the authors write.

Gonorrhea, if left untreated, can lead to infertility in men and women and increases the risk of contracting and transmitting HIV. It can also cause blindness in children born to infected women. The gonorrhea pathogen is now resistant to many common antibiotics such as penicillin and tetracyclines; only one class of antibiotics, called cephalosporins, has remained effective. But in the last few years, Australia, Sweden, Japan, the United Kingdom, and other countries have reported cases of resistance to cephalosporins.

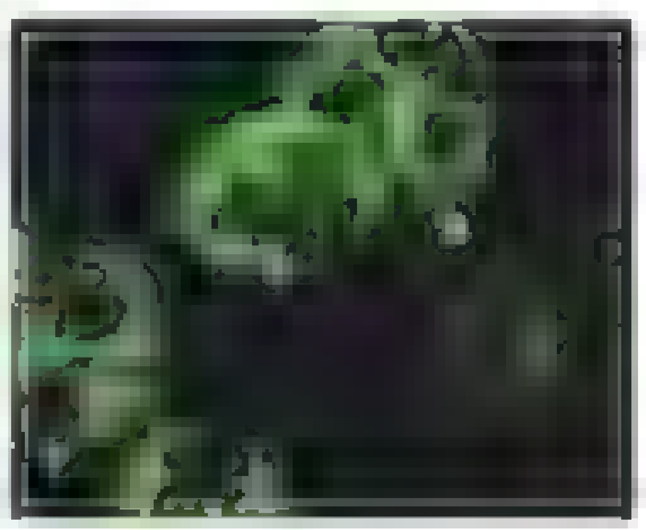

WHO is pushing for better surveillance of resistant strains, and the plan also calls for stricter prescription policies and more research into alternative treatment regimens for gonococcal infections.

Queensland, Australia 3

Fears of Damage to Great Barrier Reef Delay Mine

Citing concerns that a $6.4 billion coal mine planned in Queensland would cause significant damage to Australia's Great Barrier Reef, on 5 June Australia's federal minister for sustainability and environment, Tony Burke, halted the environmental clearances granted to the mine.

The week before, on 29 May, the Queensland government had approved the GVK-Hancock Coal mine, which is co-owned by the Indian infrastructure conglomerate GVK and billionaire miner Gina Rinehart (inset), the world's richest woman.

However, Burke said he could not sign off on the Queensland government's conditional approval, calling it "shambolic" and dangerously deficient. The mine and a planned rail link to the port, he said, could pose problems for the long-term conservation of the reef.

London 4

Bioethics Council: Mitochondrial Disease Therapy Is Ethical

In vitro fertilization techniques that could allow women with mitochondrial disease to bear healthy, genetically related children are ethical, provided the techniques prove

NOTED

>Physicists are past putting nails in the coffin of faster-than-light neutrinos; now they're planting the sod atop the idea's grave. As announced last week, all four of the particle detectors at Italy's Gran Sasso National Laboratory—as well as another team at Fermi National Accelerator Laboratory in Batavia, Illinois—have independently determined that neutrinos do not travel faster than light after all.

CREDITS (TOP TO BOTTOM): ISTOCKPHOTO.COM; TONY ASHBY/AFP/GETTYIMAGES; NASA; CDC/M. S. FERGUSON

Venus Silhouetted by the Sun

The start of Venus's 5 to 6 June transit in front of the sun is captured here by Japan's HINODE spacecraft. The image shows the "arc of Venus," the bright halo around the planet formed by sunlight refracted by the planet's atmosphere. Similar arcs around exoplanets transiting in front of their own, distant suns might also hold clues to those far-off planets' atmospheric compositions (*Science*, 11 May, p. 660).

"We're also going to learn a lot about our telescopes," says solar physicist Dean Pesnell, of NASA's Solar Dynamics Observatory in Greenbelt, Maryland. "[The transit] allows us to understand properties of telescopes that cause rings and ghost images, and can improve images of the sun based on that knowledge." And the transit was a great outreach opportunity, adds Pesnell, who helped host a public viewing of the event in Fairbanks, Alaska. "It was really exciting to watch the kids see something happen that they will probably never see again." The next transit will occur in 2117.

to be safe, according to a report released on 11 June by the Nuffield Council on Bioethics. Mitochondria, which are inherited only through the mother, are organelles that provide cells with energy. They carry their own genome, and mutations in mitochondrial genes can lead to a range of symptoms, including blindness, deafness, dementia, and muscle disorders.

Research groups have experimented with ways to transfer the genetic material from an egg with faulty mitochondria into a healthy egg. But the technique raises ethical questions: Any resulting child would carry genetic material from the mitochondrial donor. And any female child would pass the donated mitochondrial genome to her children. The Nuffield Council said that, provided the technique proves to be safe and effective, it would be ethical for families to use it. The techniques are not currently allowed in the United Kingdom, which prohibits any IVF treatment techniques in which sperm or eggs that have had any of their DNA altered are implanted in a woman's body. **http://scim.ag/mitoethics**

Sacramento, California **5**

California Rejects Tobacco Tax

Voters in California narrowly rejected a ballot measure on 5 June that would have increased the state tobacco tax by $1 a pack to raise an estimated $441 million a year for research on cancer and other tobacco-related illnesses.

Proposition 29, defeated by a vote of 50.8% to 49.2%, would have made California one of the world's largest funders of cancer research. Supporters, led by the American Cancer Society and the Lance Armstrong Foundation, argued that the measure would also save thousands of lives by discouraging smoking.

Tobacco companies and other opponents mounted a campaign against the measure and raised nearly $47 million to defeat it, including $27.5 million from tobacco company Philip Morris. Television and radio ads portrayed the measure as creating a burdensome bureaucracy that would do nothing to help the state's budget woes.

Paris **6**

French Research Unions Protest Funding Plan

On 6 June, members of the French scientific community announced the launch of legal action against the country's new government, hoping to prevent the development of national excellence clusters—which apparently offend the researchers' sense of égalité.

France's former president, Nicolas Sarkozy, launched the €7.7 billion Excellence Initiatives (IdEx) program in 2010 as part of a €21.9 billion boost to research and higher education. Sarkozy's government selected 8 clusters of universities and institutions to receive an IdEx award.

In a joint statement dated 14 May, the French National Trade Union of Scientific Researchers (SNCS-FSU) and the National Union of Higher Education Professors (SNESUP-FSU) said that because the IdEx program concentrates the resources of the national financial boost on a selected number of clusters, it threatens core principles—equality, democracy, and a collegial administration—dear to research and higher education in the nation.

The new minister for higher education and research, Geneviève Fioraso, has not yet responded to the legal actions, but told national newspaper *Le Monde* that the government would "reexamine the IdEx [projects] from every angle."
http://scim.ag/IdExprog

Washington, D.C. **7**

NASA Axes Mission to Study Black Holes, Neutron Stars

NASA has cancelled a mission to study the warping of space around black holes and map the structure of magnetic fields around neutron stars. The Gravity and Extreme Magnetism Small Explorer (GEMS), scheduled to be launched in 2014, was supposed to cost no more than $119 million. But after independent external reviews of the project found that the final costs were likely to exceed that cap by 20% to 30%, NASA pulled the plug on the project.

The agency has already spent $37 million on the design of instruments for the mission; it will cost another $13 million to close out the project. "One of the major contributors of the increased cost was that the technology development was more difficult and took longer than they [the mission planners] had originally estimated," Paul Hertz, head of NASA's astrophysics division, said, announcing the project's cancellation 7 June. GEMS was initiated under a cost-cap competition, Hertz says. "As such, the cost cap is a very important aspect of the project."

CREDITS (TOP TO BOTTOM): NAOJ/JAXA; NASA

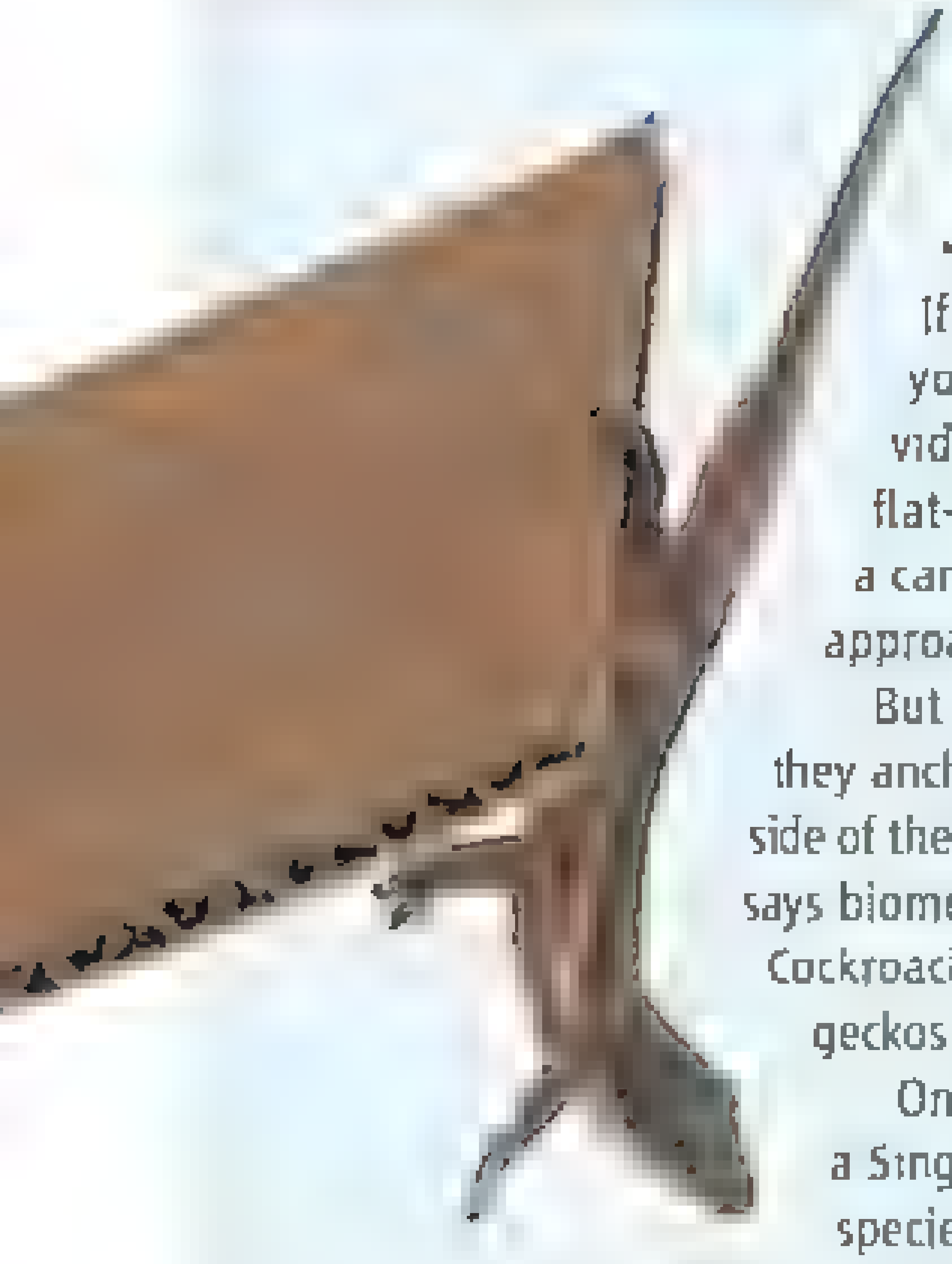

Random Sample

… And in the Center Ring: Animal Acrobats

If you've ever seen a cockroach or a gecko disappear before your eyes, science now knows where they go. High-speed video of American cockroaches (*Periplaneta americana*) and flat-tailed house geckos (*Hemidactylus platyurus*) running up a cardboard ramp reveals that both creatures barely s ow as they approach the edge.

But instead of launching into space like m niature ski-jumpers, they anchor their hind limbs and swing down, perching on the underside of the ledge. It's the first time scientists have observed th s behavior, says biomechanist Robert Full of the University of California, Berkeley Cockroaches use claws on their rear legs like grappling hooks, while geckos use claws and sticky hairs on their back feet.

One of Full's graduate students filmed flat-tailed house geckos in a Singapore forest performing the same maneuvers on ferns. Both species experience 3 to 4 *g* during these acrobatics, the researchers report online 6 June in *PLoS ONE*, similar to forces humans experience at the bottom of a bungee jump. They speculate that the 120-millisecond maneuver allows cockroaches and geckos to escape predators—such as a squealing human armed with a newspaper

BY THE NUMBERS

20% Percentage by which the Nobel Foundation will cut each Nobel Prize's cash award in 2012.

635,000 Number of martian craters at least 1 kilometer wide, according to a *Journal of Geophysical Research-Planets* study.

NEWSMAKERS

Paleoanthropologist Phillip Tobias Dies

The legendary grand old man of South African paleoanthropology, **Phillip Tobias**, died on 7 June in Johannesburg, South Africa, at age 86. Tobias spent most of his career as head of the anatomy department at the University of the Witwatersrand, Johannesburg, where he succeeded another one of the field's legends, Raymond Dart, discoverer of the first known australopithecine (*Science*, 28 October 2005, p. 608).

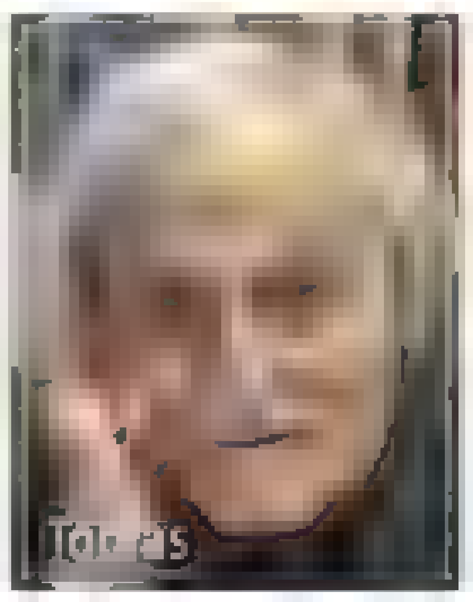

Tobias

Tobias is probably best known as the last surviving member of the three-man team that also included famed fossil hunter Louis Leakey, which reported the discovery of *Homo habilis* in 1964. Tobias was also noted for his outspoken opposition to the racist system of apartheid.

More recently, Tobias was enjoying the discovery of South Africa's latest contribution to paleoanthropology, a new species called *Australopithecus sediba*. "We were all thrilled by the discovery," Tobias told *Science* in an interview in his Johannesburg office last year. "We paleoanthropologists are young at heart, and never cease to have a sense of wonderment and excitement"

Forestry Center Gets New Head

Forestry and food security expert **Peter Holmgren** will be the next director general of the Center for International Forestry Research (CIFOR) in Bogor, Indonesia. A Swedish national, Holmgren has been at the United Nations' Food and Agriculture Organization (FAO) in Rome since 1998, where he has held a variety of positions related to forestry, climate change, and agricultural productivity. He is currently coordinating FAO's preparations for the United Nations Conference on Sustainable Development, Rio+20, being held in Rio de Janeiro, Brazil, starting 20 June.

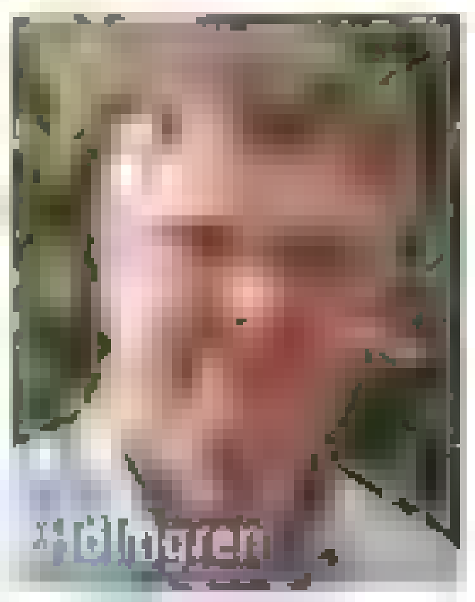

Holmgren

When he officially takes up his new position in September, Holmgren will succeed Frances Seymour, who has led CIFOR for 6 years. CIFOR is one of 15 members of the Consortium of International Agricultural Research Centers, which is working to reduce poverty and hunger and improve human health and nutrition through agricultural research. Holmgren says he wants to broaden the involvement of researchers and stakeholders to help promote evidence-based forestry policies and practices. "We need to bridge gaps between research and policy," he says.

FINDINGS

Bonobo Genome Sequenced

Completing the roster of genomes for great apes, researchers have sequenced the DNA of a bonobo. In *Nature* th s week, the team reports that humans share about one-quarter of our genes with bonobos or with common chimpanzees, but not with both types of ape.

When the team at the Max Planck Institute for Evolutionary Anthropology in Leipzig, Germany, analyzed the genome of a bonobo named Ulindi from the Leipzig Zoo, they found that bonobos and chimpanzees are still highly similar, sharing 99.6% of their DNA, even though their lineages split apart in Africa about 1 million years ago. The ancestors of both bonobos and chimpanzees diverged from human ancestors 5 million to 7 million years ago. About 1.6% of humans' DNA is shared with bonobos, but not with chimpanzees and about 1.7% of our DNA is shared with chimps, but not bonobos, the team found.

The function of the DNA we share exclusively with bonobos is not known, but may be connected to our immune systems and may reveal how the ancestors of humans, bonobos, and chimps evolved different responses to infectious diseases.
http://scim.ag/bonobogenome

Science LIVE

Join us on Thursday, 21 June, at 3 p.m. EDT for a live chat on **the science of organ transplants. http://scim.ag/science-live**

CREDITS (TOP TO BOTTOM): JEAN-MICHEL M[illegible]GEAU; ARDIAN JUSUF AND PAULINE JENN[illegible], COURTESY OF POLYPEDAL LAB UC BERKELEY; HANS HILLEWAERT/WIKIPEDIA CREATIVE COMMONS; RAASGAT/WIKIPEDIA; GIULIO NAPOLITANO

Travel advisory. Census questions about commuting to work, which some legislators regard as intrusive, offer the best data on regional transportation needs.

Social Scientists Hope for Reprieve From the Senate

The question would challenge the most astute political scientist: How do you prevent Congress from inflicting two potentially crippling blows to the social sciences without knowing when, or even if, they will occur and what form they will take?

The conundrum is real after the U.S. House of Representatives voted last month to prohibit the National Science Foundation (NSF) from funding political science research and to curtail the government's ability to monitor economic and demographic trends by eliminating the American Community Survey (ACS). The amendments were offered, respectively, by Representative Jeff Flake (R–AZ) and Representative Daniel Webster (R–FL) as part of a \$51 billion spending bill for 2013 covering the Commerce and Justice departments and several science agencies, including NSF and NASA. A parallel appropriations bill is now awaiting debate by the full Senate.

The House votes were fueled by ideological opposition to the social sciences and a broader effort to reduce overall federal spending. Detractors of the survey, conducted by the U.S. Census Bureau, also tapped a vein of antigovernment sentiment. However, because the reasons are amorphous, it's hard for advocates to know where to aim their counterpunches.

The business community is leading a full-court press to defend the ACS, a recent replacement for the long form of the decennial census with questions on housing, education, employment, transportation, and other topics (*Science*, 9 April 2010, p. 158). These defenders have explained to anyone who will listen that the data are essential for companies deciding where to locate and how to operate, for government agencies allocating nearly half-a-trillion dollars a year in federal assistance, and for a host of other purposes, from civil rights enforcement to public health initiatives.

"There is no substitute for this data in the private sector," says Diane Swonk, a past president of the National Association for Business Economics and chief economist at Mesirow, a Chicago-based financial services company. "To deliberately take off the table information that companies need to make important investment decisions is just cutting economic development off at the knees."

In contrast, the academic political science community has adopted a more passive, one-on-one defense of the discipline. Its professional society, for example, has urged members to write to lawmakers with examples of how their research has benefited society. "We believe that it's meritorious research," explains Michael Brintnall, executive director of the 15,000-member American Political Science Association. "We also think that it plays a role in understanding a range of national issues, from counterterrorism and nation-building to energy and health care."

Congress has questioned the value of the social sciences, including political science, in the past. The assault on ACS, however, features a new element: claims that the federally mandated questions are intrusive, and that census officials are harassing residents in conducting the needed follow-up to ensure a high response rate. Even so, the social science and business communities were caught off guard by the timing and substance of last month's amendments.

Flake's proposal was the last of 42 recorded votes in a debate that ran for 3 days from 8 to 10 May. His earlier attempt to trim \$1.2 billion from NSF's \$7 billion budget was defeated handily, attracting only 121 votes in the 435-member House. But Flake persuaded 217 colleagues to kick political science out of the NSF tent. The ban, if it becomes law, would not only end NSF's \$11-million-a-year research program but could also preclude political scientists from participating in any NSF initiative. (Five Democrats voted for the amendment, and 27 Republicans opposed it.)

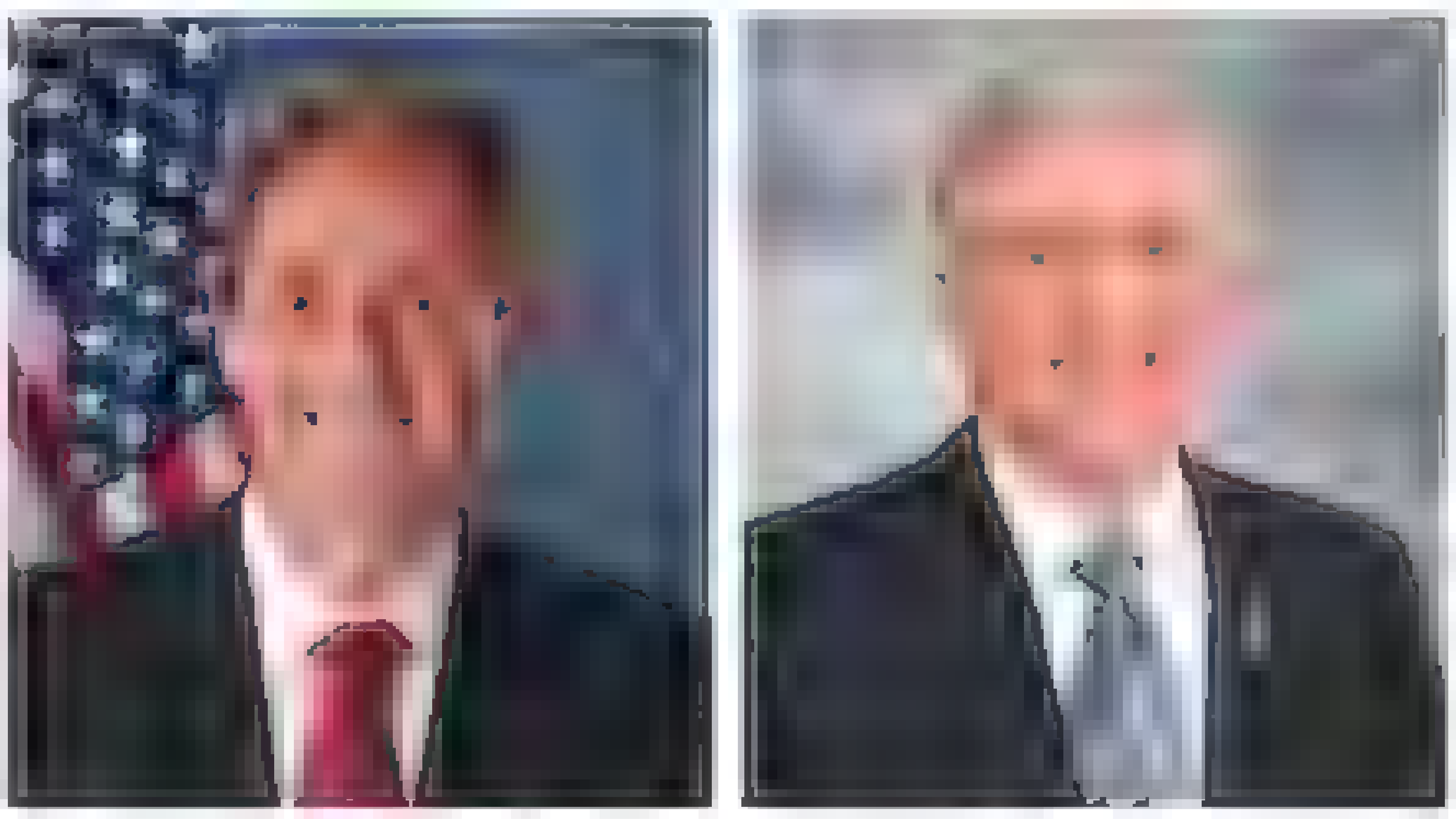

Stop signs. Jeff Flake (*left*) and Dan Webster led House opposition to political science research and the American Community Survey.

Flake says political science isn't sufficiently rigorous to warrant federal support when the government needs to spend less. Although he acknowledges that some of the research is valid, he believes there are other ways to pay for it.

Brintnall and others say they don't know if any senator is planning an amendment simi-

CREDITS: (TOP) ISTOCKPHOTO.COM; (LEFT) U.S. CONGRESS; (RIGHT) U.S. HOUSE OF REPRESENTATIVES

lar to Flake's. And they are heartened by the fact that the chair of the spending subcommittee who wrote the Senate version of the bill, Senator Barbara Mikulski (D-MD) offered a vigorous and successful defense of the field the last time it came under attack in 2009 from Senator Tom Coburn (R-OK). "The real challenge is to find someone on the other side of the aisle," Brintnall acknowledged, adding that it's even harder to recruit champions "when they don't know what they would be opposing."

The initial debate over ACS was about whether to make it voluntary. In March, a House panel held a hearing on a bill (H.R. 931) by Representative Ted Poe (R-TX) that would erase the criminal penalty for not responding to ACS, and Poe's amendment to the spending bill to achieve that goal was approved by a voice vote. But when Webster proposed axing ACS entirely, his motion carried by a vote of 232 to 190.

Senator Rand Paul (R-KY) introduced a bill (S. 3079) last month that would make every one of the 48 questions on ACS voluntary except for the name, address, and the number of people living in the dwelling. Although that measure has not advanced, ACS supporters fear that Paul could propose a similar amendment to the Commerce and Justice appropriations bill.

A Paul staffer wouldn't speculate on what he might do once the spending bill came up for debate. "It's not on the top of his list," the aide said. "But they should be worried," the aide added, referring to those who support the survey. "Nobody knew that it would pass the House, and I don't see why it would be off the table [in the Senate]." –JEFFREY MERVIS

MARINE ECOLOGY

Seagrasses Partner With Clams to Stay Healthy

Not much to look at and sometimes quite mucky, seagrass beds have been called the ugly ducklings of marine conservation. They lack the charisma of coral reefs, yet like reefs, these beds form a highly productive and diverse ecosystem, acting as the nursery for many kinds of fish as well as a home to sea turtles, manatees, birds, and a host of other sea creatures. Seagrasses help cycle nutrients, and experts estimate they provide $1.9 trillion in ecosystem services per year worldwide. At the heart of seagrasses' success—and the secret to efforts to restore the increasingly threatened ecosystem—may be a small clam.

Hidden workers. Tiny clams living in the roots of seagrass help keep the sediment a healthy environment.

On page 1432, marine ecologist Tjisse van der Heide of the University of Groningen in the Netherlands and colleagues describe a three-way partnership—between seagrasses, lucinid clams, and bacteria living in the clams—that likely keeps toxic sediments from building up and killing the seagrass. An appreciation of this partnership could lead to better success in seagrass restoration, Van der Heide suggests. "This study pointedly reminds us that we cannot study species in isolation. … Symbiosis is one of the fundamental mechanisms by which ecosystems become productive and robust," says Geerat Vermeij, an evolutionary biologist at the University of California, Davis.

Seagrasses are saltwater flowering plants that grow along coasts and make up 0.2% of the ocean's ecosystems. They produce an amount of biomass that beats that of the Amazonian rain forest and is on par with that of corn and sugar cane crops. Their roots and stems trap organic matter and sediment, causing buildups of rich mud that can be waist deep.

This muck is a potential threat to the grass: Decaying organic matter produces a lot of sulfide, creating what could be an unhealthy environment for plant roots. Researchers had assumed that the oxygen released from seagrass roots combined with enough of the surrounding sulfide to neutralize this toxic element. Not so. "We found that in most seagrass beds, it's much more complex," Van der Heide says. "They have a trick to speed up oxidation" that relies on a symbiotic relationship with bacteria that consume sulfides.

Van der Heide first began to suspect that the seagrass depended on bacteria while doing fieldwork in Mauritania. He and his colleagues found thousands of 1-centimeter lucinid clams living among the seagrass roots. Gills make up much of the clam's innards. That's where sulfide-oxidizing bacteria live. They sustain the clam by providing nutrients much in the way that zooxanthellae sustain coral.

Following up their clam observation, the researchers took 110 samples of seagrass beds with a 15-centimeter-wide tube that cut cores 20 centimeters deep into the sediment. They filtered out and weighed all the organisms in the sediment and dried and weighed the seagrass in each core. "The more bivalves we found in the core, the more seagrass we found in the core," suggesting a beneficial partnership, Van der Heide says.

Wondering if this cohabitation was unique to Mauritania, the researchers combed the literature for studies describing the communities inside other seagrass beds, finding 84 covering tropical, subtropical, and temperate sites on six continents. Lucinid clams were found associated with 11 of 12 seagrass genera, the one exception being a seagrass that grew on bare rock.

Next, Van der Heide explored the potential of this relationship in the lab. He grew seagrass alone, clams alone, and the two organisms

CREDITS: MARJOLIJN CHRISTIANEN; (INSET) LAURA L. GOVERS

together under different conditions, including one in which he and his colleagues injected sulfide into the sediment semiweekly. On its own, the seagrass was able to process some of the sulfide, but sulfide gradually increased in concentration and interfered with seagrass growth. The clams alone got rid of the introduced sulfide but didn't get any bigger. But both the clam and the seagrass thrived when together, getting rid of the sulfide and growing as well, Van der Heide's team reports. The roots seemed to provide the clams with more ready access to oxygen, which "was necessary for the bivalves to consume that sulfide in an efficient manner," Van der Heide explains.

"The elegant experimental design provides compelling evidence for the benefits of the interaction between seagrasses and the associated bivalve," says Carlos Duarte, a marine ecologist at the University of Western Australia in Perth.

The new understanding comes at a crucial time as seagrasses are in trouble. About 7% of seagrass beds disappear per year, a rate comparable to the loss of tropical rainforest. Yet the amount of carbon seagrasses sequester can be more permanent, in part because forest fires can eventually release the carbon from forests, while carbon stays buried in seagrass sediments for millennia, Duarte and his colleagues reported online 20 May in *Nature Geoscience*.

Coastal development, dredging, and declining water quality are mostly to blame for the current woes of seagrasses, though epidemics, severe weather, and destructive fishing practices have also contributed to their decline. Rising water temperature due to climate change is also taking a toll, Duarte says. Warming in the Mediterranean Sea could result in the functional extinction of a dominant seagrass there by mid-century, he and his colleagues reported online 20 May in *Nature Climate Change*.

Seagrass restoration is expensive, as large areas must be hand-planted, and less than a third of attempts succeed. In evaluating an area in decline, "it's probably smart not just to look at these plants but also to look at the bivalves present," says Van der Heide, who advocates transplanting the entire community.

Duarte is not completely convinced that adding lucinid bivalves in seagrass restoration programs will increase their success. But he values Van der Heide's study because it draws attention to the importance of considering biological interactions in planning seagrass recovery. "The discovery of this three-way symbiosis provides evidence for the key importance of biotic components."

–ELIZABETH PENNISI

Targeted. The Human Microbiome Project charted the bodily whereabouts of thousands of bacteria, including this gut microbe, *Enterococcus faecalis*.

CREDIT: U.S. CENTERS FOR DISEASE CONTROL AND PREVENTION

MICROBIOLOGY

Microbial Survey of Human Body Reveals Extensive Variation

Though perhaps less contemplated than the navel, the inside of the elbow seems nonetheless comfortingly familiar. Don't be fooled. Our bodies are home to trillions of microbes, and that patch of skin hosts an invisible ecosystem whose microbial members were virtually unknown until now. This week, a consortium involving 200 investigators from a variety of disciplines describes that elbow-dwelling microscopic community as well as more than a dozen others as part of the most thorough look ever at the microbial world on and within us.

By the time it is completed next year, this Human Microbiome Project (HMP) will have spent $170 million cataloging the microorganisms—and to a lesser extent, their genes—that live on 18 human body sites, sequencing 3000 relevant bacteria, and determining differences between the microbiomes of healthy and unhealthy people. "It's a great framework, reference, and tool to really understand the microbiome," says microbial ecologist Maria Gloria Dominguez-Bello of the University of Puerto Rico in San Juan.

The U.S. National Institutes of Health (NIH) started HMP in 2007 to jump-start a young field. When the effort was first conceived, researchers had hopes of generating a reference healthy microbiome, on par with the reference human genome, that the community could use to assess the role of microbes in health and disease. Two reports this week in *Nature* and 15 others in *PLoS ONE* and other journals, all from the HMP consortium, speak to the naïveté of that idea. "There's not a single reference human microbiome that we can compare everybody to," says George Weinstock, an HMP researcher at Washington University in St. Louis in Missouri. "You can have two healthy people whose microbiomes are fairly different."

The research released this week comes just as NIH is debating whether to launch an HMP follow-up and European nations are considering a successor to their own ambitious human gut microbiome effort, Metagenomics of the Human Intestinal Tract (MetaHIT) (*Science*, 8 June, p. 1246). For the HMP studies just published, researchers took samples from more than a dozen body sites covering the skin, nose, mouth, and gut in 242 healthy

people. (In men, 15 sites were sampled, in women, an extra three in the vagina.) They excluded participants with any signs of illness, even minor gum disease, as they wanted to get a sense of what a healthy microbiome looks like. Some people provided up to three samples over a 22-month period to assess whether their microbiomes were stable over time. In each sample, the researchers probed for copies of a DNA sequence, the 16*S* ribosomal subunit, that is used to identify organisms. And in 1300 of the 11,000 samples, they sequenced all DNA present to get a sense of what genes were at a particular body site.

HMP to date has generated 3.5 terabases of data, more than 1000 times the amount produced by the original Human Genome Project. "HMP is about the same size [as] all the previous microbiome studies put together," says Curtis Huttenhower, a computational biologist at Harvard School of Public Health in Boston. "No computational methods existed to analyze that scope of data."

"It's an impressive data set," adds Dusko Ehrlich, who coordinates Europe's MetaHIT, whose results were published last year.

Despite the lack of a clear-cut reference of a healthy microbiome, some patterns have emerged from the HMP data. They provide "dramatic and gratifying degrees of support for what were just some early and tantalizing leads" about our microbial partners, says David Relman, a microbiologist and infectious diseases clinician at Stanford University in Palo Alto, California, who is not part of HMP.

For one, no two microbiomes are alike. "There is a personalization of the microbiome that takes place in every individual," says HMP investigator Barbara Methé, a microbial ecologist at the J. Craig Venter Institute in Rockville, Maryland. There's also an incredible diversity of life across the body of each individual. The microbes on the forearm are starkly different from those on the teeth and equally different again from those in the gut or in the vagina.

Yet there are similarities across different people in, say, the forearm microflora, indicating that our microbial partners are not randomly distributed. Each body site had a few core or "signature" bacteria living there, with characteristic genes linked to that particular body site. "Different parts of the body see different configurations of organisms," Methé says.

Once they established the community makeup of each body site using the 16*S* data, the HMP researchers examined whether any of the microbes were known pathogens hiding out on or in the healthy subjects. They found no 16*S* genes from deadly germs such as those that cause cholera or botulism. But lurking in some places in some people were about 100 opportunistic pathogens, microbes that are known under certain circumstances to become dangerous. For example, they confirmed previously discovered hideouts of *Staphylococcus aureus*, infamous for having antibiotic-resistant strains: 30% of the subjects had this bacterium in their noses and 5% had it behind their ears. And they discovered hideaways of other less-well-known pathogens, Huttenhower says, such as *Gardnerella vaginalis*, *Haemophilus influenzae*, and *Treponema denticola*.

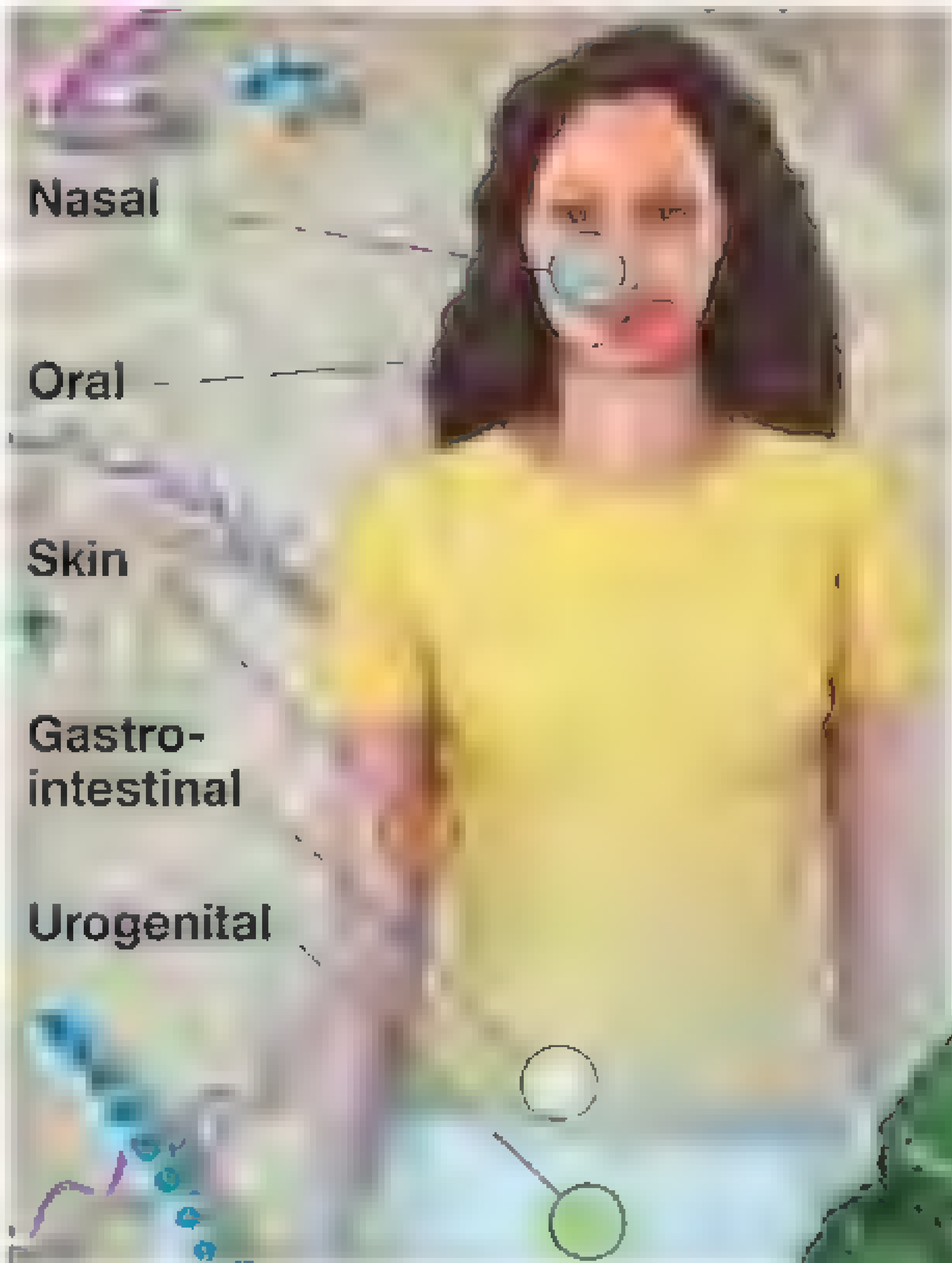

Spice of life. The different body sites studied by the Human Microbiome Project show extensive variety in their community compositions.

For a subset of the body samples, the researchers went beyond simply doing 16*S* identification of the microbes present. They fully sequenced most of the sample's DNA, trying to reveal the full array of genes available to microbes. Huttenhower and his colleagues assigned those genes to various cellular or metabolic pathways and thus were able to reconstruct how these microbes were functioning on the body.

That analysis revealed that even if the specific microbes present differ between body sites, core sets of microbial functions are shared by those sites. At each one, "the bugs are very different but the pathways are very similar," Huttenhower says. "If you go to different cities, you have different people with different last names and different backgrounds, but every city has people who are the bankers and the people who run the subway."

Some body sites had more bankers than subway workers, however. There were many microbial genes for simple carbohydrate processing in the mouth, where food flushes through quickly, for example. In contrast, the gut had more microbial pathways for processing complex carbohydrates.

It may eventually be possible to diagnose healthy microbiomes by the metabolic pathways they have functioning in them and to treat unhealthy microbiomes by restoring missing pathways or targeting pathways that are out of whack. "It could be a process that could be carried out by different bugs in different people," Huttenhower says, so it may be most efficient to go after pathways rather than the microbes themselves.

Some researchers contend that there's too much variety among human microbiomes to think in terms of a reference microbiome. But Methé argues that the HMP data establish the right range of organisms and pathways for each body site and thus do establish a reference of sorts. "If we can begin to understand what we think should be there and in what proportions, you can begin to tell the difference between a healthy state and a disease state," she says.

Because the functioning of our bodies is so intimately linked to the microbiome, the latter's DNA has been referred to as the "second human genome." But deciphering this second genome has proven a much tougher challenge than our first, Relman says. HMP "is the Human Genome Project to the 1000th power."

–ELIZABETH PENNISI

CREDITS: TOP TO BOTTOM: NIH MEDICAL ARTS AND PRINTING (INSET) UNITED STATES DEPARTMENT OF AGRICULTURE

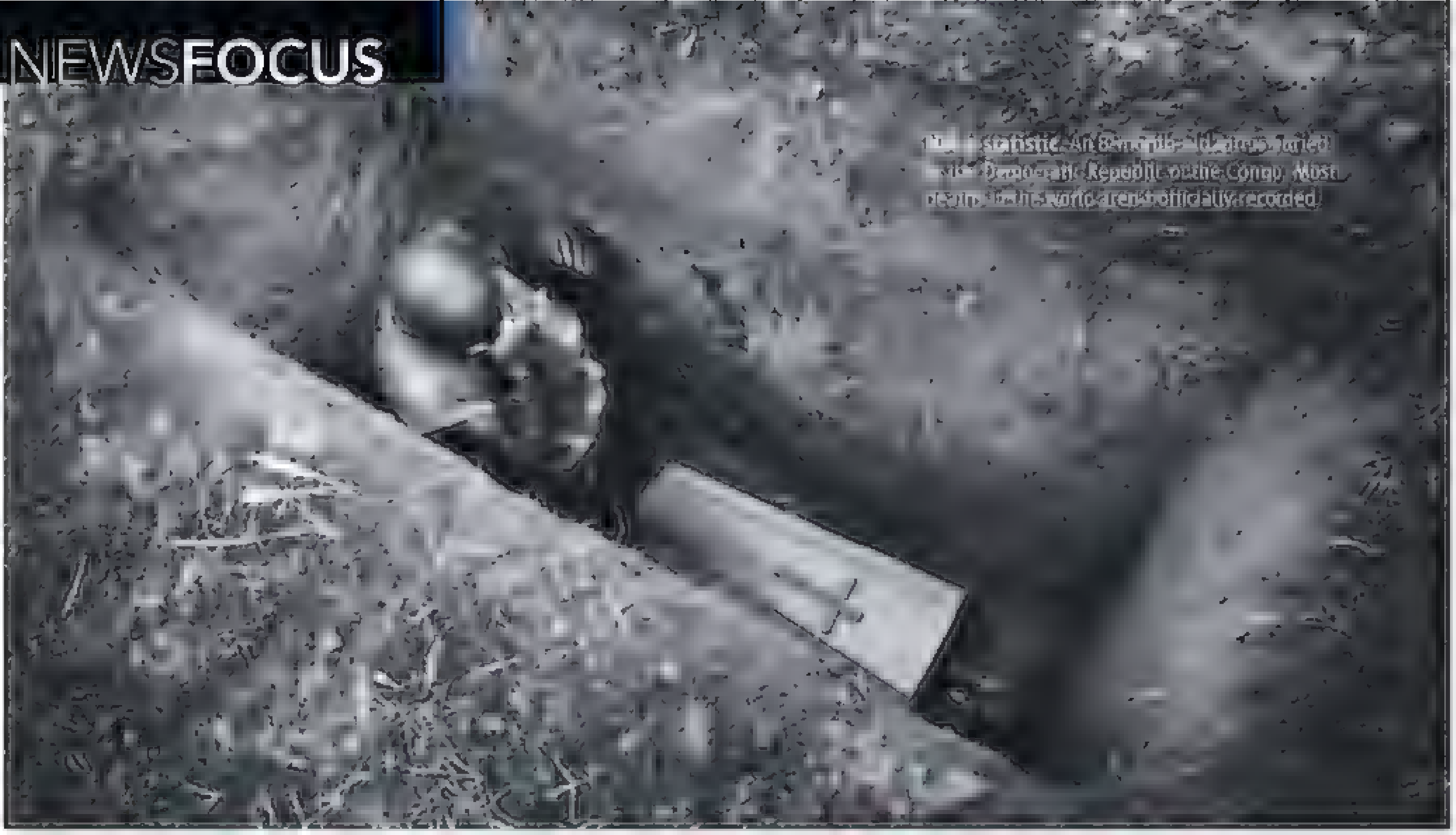

The statistic. An 8-month-old child is buried in the Democratic Republic of the Congo. Most deaths in the world aren't officially recorded.

How Do You Count the Dead?

Scientists agree they need better estimates for the death toll from the world's major killers. But they fiercely disagree on how to go about it

ONE OF THE BEST WAYS TO HELP THE living, says Prabhat Jha, is to count the dead. Understanding how many people die of which causes is invaluable for designing effective public health programs, says Jha, a global health expert at the University of Toronto in Canada. That's why he started an ambitious research project in India called the Million Death Study, which aims to record the causes of death for 1 million Indians between 1998 and 2014.

But counting the dead can be extremely difficult. The problem is that most of the world's deaths occur in places with few or no hospitals or doctors to record deaths and their causes. Last month, for example, an international research group published the latest statistics on global child mortality in *The Lancet*. They estimated that 7.6 million children under age 5 died in 2010, well over half from infectious diseases. But fewer than 3% of those deaths were medically certified—assigned a cause by a health worker and recorded in an official database. For the other 97%, the scientists are forced to make sophisticated guesses.

In doing so, they extrapolate from a patchwork of survey data, incomplete records, and research studies. Various groups use different statistical methods, however, sometimes resulting in very different numbers that are hotly debated. One study published in *The Lancet* in February, for example, found that 1.24 million people died from malaria in 2010; that's more than twice the estimate from the World Health Organization (WHO). Reactions from some in the malaria community were swift and harsh. "In terms of credibility I think public health science has been done a disservice by this paper," says Robert Snow, a veteran malaria epidemiologist at the University of Oxford in the United Kingdom and the Kenya Medical Research Institute in Nairobi.

Online
sciencemag.org
Podcast interview with author Gretchen Vogel (http://scim.ag/pod_6087)

The paper was only a preview of a much larger project counting deaths and disease prevalence by the Institute for Health Metrics and Evaluation (IHME) at the University of Washington, Seattle. The Global Burden of Disease, Injuries, and Risk Factors 2010 (GBD 2010) study is the most massive study of deaths and disease ever undertaken. It involves more than 1000 researchers and aims to assemble the cause of 1 billion deaths worldwide going back to 1980. It will be published in a series of papers later this year and is likely to trigger new debates.

Some say that's necessary and healthy. "It's always worth looking at different approaches," says Ties Boerma, director of measurement and health information systems at WHO. "We're all trying to make the best of incomplete and inaccurate data." Others worry that the sharply diverging estimates and the bickering will erode policymakers' trust in science. "Can you imagine if I'm a minister of health in a country and am faced with new numbers every 2 years?" asks Zulfiqar Bhutta, an expert on maternal and child health at Aga Kahn University in Karachi, Pakistan. "At some stage we've got to stop confusing people."

Patchy data

In the case of IHME's malaria study, the large gap between its estimate and WHO's was mainly due to one category: deaths of youth and adults in Africa. WHO estimated that in 2010, malaria killed 55,000 Africans over the age of 5; the IHME team concluded that the number was 435,000. Snow says that although WHO's numbers are too low, IHME's estimates, especially for adult deaths in Africa, are far too high. He notes that in several countries that keep very good records for malaria, such as Swaziland and Djibouti, IHME's formulas count more deaths than

CREDIT: MARCUS BLEASDALE/VII/CORBIS

documented malaria cases, a sign that they're fundamentally off.

The number of adult deaths surprised the IHME team as well, says epidemiologist and health economist Stephen Lim, the study's lead author. "There's lots of uncertainty," he concedes. "The data are patchy, particularly in the hardest-hit areas." However, after reexamining their data, the researchers remain convinced that their conclusions are on target. "Reasonable scientists will differ on a given point based on the evidence they have," says epidemiologist and global health expert Alan Lopez of the University of Queensland in Brisbane, Australia, another co-author. "We do not know who's right. We are simply following our evidence."

There is more at stake than academic reputations. Global health estimates help determine where billions of dollars in health funding goes. Campaigners use them to justify public health spending on certain causes, such as measles immunization campaigns or AIDS prevention. The numbers also help to measure whether a campaign has made any difference, and they are one of the ways policymakers determine whether they are spending their money wisely.

To understand how death-count studies can reach strikingly different results, consider one example. Suppose you're trying to find out how many people were sickened and killed by, say, pneumonia in Tanzania. The government's records of births and deaths are incomplete; only 17% of Tanzanian births are registered with officials, Boerma says. Hospitals have records, but they're not always accurate and up to date. Most important, most pneumonia patients never come to the hospital. They die at home without seeing a doctor who can make a diagnosis.

So health metrics experts gather the best data they can, first from government and hospital records, and then from surveys, clinical studies, or any other possible source. Birth history surveys, for example, ask women not only how many children they have but also how many times they have given birth, which helps identify children who were born and died without ever being noted in official records. In a technique called verbal autopsy, trained field workers ask relatives of a deceased person a standard series of questions and record a short narrative of events leading up to the death. Physicians—or sometimes computer programs—evaluate the information and assign a likely cause of death.

Researchers feed all the numbers into computer models that use sophisticated statistical techniques to fill in the gaps. Data on related circumstances such as rainfall, availability of clean water and health care, vaccine coverage, and mosquito densities—as well as data from nearby or comparable regions—all help the programs to churn out their estimates. The algorithms can fill in gaps in time as well as space. Data collected 5 years ago in one country can be combined with recent numbers from comparable sites to calculate current estimates.

Crunching the numbers

For their malaria estimates, Lim and his group generated thousands of models, which gave slightly different weights to various data sets. They then probed the models' accuracy by removing a subset of the data and testing each model's ability to predict the missing numbers. They used the same method to test so-called ensemble models, which combine individual models in different ways.

IHME's mathematical prowess is undisputed. "Their work has transformed the way we think about the metrics of disease," Snow says. Their approach "can be quite helpful. Gather all the data you can and see what they say," adds Ramanan Laxminarayan, director of the Center for Disease Dynamics, Economics & Policy in New Delhi and Washington, D.C. But powerful computers can't make up for data that are simply too sparse, Laxminarayan says. The result "has to fit with some sort of on-the-ground validation." For example, those who dispute IHME's malaria findings note that in the hardest-hit regions of Africa, most adults develop partial immunity to malaria, so a new infection is rarely deadly. If IHME's numbers are right, they would throw doubt on decades of malaria immunology and epidemiology, Snow says.

The controversy stems primarily from IHME's choice of data sets. The team made a systematic effort to find as many verbal autopsy studies as possible, turning up thousands of studies. They then used computer programs to adjust for misclassified or unclear causes of death. But many researchers question whether verbal autopsies are a reliable way to measure malaria deaths, especially in adults.

Even when a patient is alive, lab tests are often the only way to tell whether a sudden fever is caused by malaria, dengue, meningitis, or Japanese encephalitis. Some scientists contend that an accurate diagnosis based on a family's description of symptoms weeks or months after a death is impossible. "The tool is blunt," Snow says. For determining whether an adult fever death was due to malaria, "it is probably as good as flipping a coin."

Jha counters that even if diagnosing an individual fever death as malaria is unreliable, researchers can check the population-level

DIFFERENT STUDIES, VERY DIFFERENT NUMBERS

SOURCE CREDITS (LEFT TO RIGHT): IHME AND WHO WORLD MALARIA REPORT 2011; CENTER FOR GLOBAL HEALTH RESEARCH, UNIVERSITY OF TORONTO; SWAROOP ET AL., BULL. WORLD HEALTH ORGAN.; WORLD HEALTH ORGAN.; C. LIPPAUX, BULL. WORLD HEALTH ORGAN.; GUIDELINES FOR THE CLINICAL MANAGEMENT OF SNAKE BITES IN THE SOUTH-EAST ASIA REGION: WHO REG OFFICE FOR S.E. ASIA; KASTURIRATNE ET AL., PLOS MED; MOHAPATRA ET AL., PLOS NEGL TROP DIS.

results by looking at the proportion of fever deaths that were caused by various diseases, taking into account other factors such as parasite prevalence or viral transmission patterns. Lim's IHME colleagues have conducted several studies to find out how accurate verbal autopsies are. In those analyses, Lim says, verbal autopsy actually seems to underestimate malaria deaths.

WHO, in contrast, uses verbal autopsy data primarily for malaria deaths in children younger than 5 and in areas of low malaria transmission. (Most researchers agree that among common childhood diseases, malaria is distinct enough that verbal autopsy data are reliable.) WHO's main source of data are national registration and hospital records, which most experts say vastly undercount malaria deaths. For adult deaths in regions with heavy malaria burdens, WHO estimates the number of people living in areas with high, low, or no risk of malaria and uses mathematical models to extrapolate death rates based on the childhood numbers.

Filling the gaps. A field worker in Bangladesh trained to conduct verbal autopsies asks a relative of a deceased person about the circumstances that led to the death.

Epidemiological terrorism

WHO's methods receive plenty of criticism as well, and IHME's malaria numbers are not the first to diverge from WHO's estimates. Jha's Million Death Study, carried out with Indian colleagues, has also come up with significantly higher death totals, especially among adults. The researchers are monitoring 14 million people in 2.4 million Indian households that constitute a statistically representative sample of the population. Surveyors visit regularly to record births and deaths; if they hear of a recent death, a second field worker conducts a verbal autopsy. Two independent physicians evaluate the information and assign a cause of death. If they disagree, a third physician decides.

Local support for the project "was phenomenal," Jha says. "We throw these mortality numbers around. But for the families, [each death] is a tragedy"—and in many cases, the survey is the first time someone with authority is paying attention. "These invisible deaths become visible."

Jha likes to refer to his work as "epidemiological terrorism," because it tends to explode public health experts' assumptions. For malaria, the team put India's annual death toll at 200,000 in a 2010 publication—more than 13 times WHO's estimate—with most deaths occurring among people aged 15 and older. Those numbers were controversial, but many experts said they could be plausible; malaria rates are lower in India than in sub-Saharan Africa, so adults have less natural immunity and are at greater risk of dying.

Disputes about numbers aside, the study is revealing important patterns that can help policymakers, Jha says. In April 2011, the group reported that an estimated 50,000 people per year in India are dying of snakebites. (Other estimates had suggested it was 50,000 worldwide.) The country's snakebite deaths were concentrated in certain areas, the study found—an estimated 8700 occurred in the state of Uttar Pradesh alone. That suggests directing antivenom supplies to high-risk areas could save lives.

The study has also found dramatic regional differences in death rates from cervical cancer, the leading cause of cancer deaths among Indian women. Rates in Muslim-majority areas are significantly lower than in Hindu-majority regions, perhaps because male circumcision reduces the risk of sexual transmission of the human papillomavirus (HPV), which causes cervical cancer. It also suggests, Jha says, that focusing HPV vaccination campaigns in high-prevalence regions might have the most effect. "None of these questions were hypothesized when we started the Million Death Study," he says.

More feuds expected

The global health community is bracing for more explosions when the GBD 2010 results are published later this year. IHME plans to release complete and comparable estimates for the global death and disability caused by more than 200 conditions in 1990, 2005, and 2010. Observers from many fields "will see patterns and results that are surprising," Lopez promises. New feuds are sure to result.

Everyone agrees that the way to resolve those fights is to collect more complete information on the ground. "There is much more expenditure on places like IHME that are taking the data and churning them through black box models" than on strengthening reporting systems, Laxminarayan says.

But so far, several attempts to improve the developing world's health record-keeping have come up short. In 2005, the Bill and Melinda Gates Foundation and WHO established the Health Metrics Network (HMN) to strengthen national health information systems. That's the right goal, says Kenneth Hill, a demographer at Harvard School of Public Health in Boston; improving civil registration systems is "where the world needs to go." It's not there yet, however. "It's safe to say HMN has been a complete failure," Hill says. "We really don't know how to improve registration systems. There hasn't been enough systematic research."

In countries without strong central registration systems, families and community officials have few incentives to register births or deaths, he says. "In most developing countries, bureaucracy is awful. Digging a hole is a hell of a lot simpler" than registering a loved one's death with local authorities.

There are some positive signals, however. New technologies—cell phones and Internet access—are starting to have an impact, Snow says. "People are beginning to send real-time information to health authorities," he says, and the supply of commodities to manage malaria, such as drugs and diagnostic tests, are now tied to providing reliable stock and disease information.

Such information could help researchers come closer to a set of numbers they all can agree on. In the meantime, Jha hopes policymakers will see good news in a few things all studies agree on: for instance, that malaria deaths, especially among children, have fallen thanks to control programs. Similar success is possible if authorities take adult malaria seriously, as well, he says: "That message was a bit lost in the shouting about the numbers."

–GRETCHEN VOGEL

CREDIT: INSTITUTE FOR HEALTH METRICS AND EVALUATION

Toad stopper. Shine is on friendly terms with this cane toad, but he wants to protect Australia from its relatives

PROFILE: RICK SHINE

The Reluctant Toad Killer

Australia's cane toad problem has distracted Rick Shine from the animals he truly loves, but the biologist may have an effective way to slow their invasion

While growing up in Brisbane in the 1950s, Rick Shine chased big bluetongue lizards in the neighbors' yards. By high school in Canberra, he was bringing home deadly brown snakes. "I can only wonder at my parents' forbearance," he says.

When Shine began college at Australian National University, he didn't yet know what he wanted to do in life, but then zoologist Richard Barwick showed him an appealing future. "Dick was the first professional reptile biologist that I ever met," Shine says. "The light went on quite brightly when I recognized that there was such a thing as a career studying reptiles."

Shine, also smitten with the ideas of Darwin and the other giants of evolution, decided to pursue research and was soon applying evolutionary theory to the reptiles and amphibians that had fascinated him from a young age. In the 1980s, by then on the faculty at the University of Sydney, Shine set up a research station at Fogg Dam near the aptly named Australian town of Darwin, where he could study the ecology of the local pythons year after year.

And then, in 2004, the cane toads came to Fogg Dam.

Cane toads (*Bufo marinus*) have spread west from the Queensland coast since 1935, when Australian sugar growers, desperate to control beetles that were eating their crops, released several thousand young toads into their fields. The toads, native to Central and South America, had reportedly eaten enough similar beetles in Hawaii to improve sugar yields there, and they were considered less destructive than chemical pesticides. But Australia, with no native toads and plenty of suitable habitat, proved to be cane toad heaven. That soon created a new problem: The foreign amphibians produce a toxin that is deadly to many of the native predators that gobble them up. As the toads spread, a wave of death struck snakes, freshwater crocodiles, and other Australian animals. Today, cane toads are one of the continent's worst invasive species and number in the hundreds of millions.

Finding himself on the leading edge of the invasion, Shine knew the toads would likely eradicate many of the animals he had studied for decades, so he reluctantly turned his attention to the unwelcome guest. "It was an extraordinary opportunity for a scientist," he says, but it was also "so very bittersweet. … I thought we'd find out a lot about toads and do some great science, but we'd have very little actual management impact."

Less than a decade later, Shine's research has paid off, with dozens of findings covering basic toad biology and how the toads interact with Australia's native fauna, and even the discovery of a potentially new mechanism of evolution. Shine "is carrying on first-class 19th century natural history using 21st century techniques," says John Endler, a veteran evolutionary biologist at Deakin University in Victoria, Australia.

But the 62-year-old herpetologist's biggest breakthrough may be a recently devised strategy to turn the toad's own toxins against the invader. Shine has explored other ways to stop the animal's spread, but this time he believes he has struck gold. "I think that this will be the centerpiece of future efforts to control invasive cane toads," he predicts.

Team *Bufo*

Walk into Shine's Sydney lab and you'll see a place full of the critters he would have loved to collect as a kid—snakes, frogs, lizards, a chameleon, and, of course, a couple of cane toads, including one named Gwendolyn. Shine spends less time in the lab and the field than he once did. "I probably just get in the way," he says—but he has successfully resisted calls to pull him into university administration. Still, now that he is at the forefront of Australia's cane toad problem, Shine frequently finds himself in front of television cameras and community groups. He also spends a lot more

CREDIT: TERRI SHINE

time writing about cane toads for journals and magazines these days. "I enjoy the process of writing," he says. "I suspect I would've been writing trashy crime novels if I hadn't been a professional scientist."

That love of writing certainly helped Shine produce the more than 750 papers he's authored in his career. Shine also modestly credits many of his published findings to the "sheer luck" of being in the right place at the right time, as well as having a small army of students and collaborators—he currently supervises about 20 scientists, including some postdocs and research assistants who have each stuck around for more than a decade.

Shine chooses hard-working, motivated people and then guides them softly, says Ben Phillips, an evolutionary biologist at James Cook University in Townsville, Australia, and a former Shine student. Phillips describes his mentor as "quite unbosslike" and "very easygoing." Shine is constantly listening to the people in his lab, Phillips says, and then "he puts a lot of effort into trying to improve what you're doing."

"Team *Bufo*," as Shine's group is sometimes known, has garnered respect from the invasion biology community. "Shine's involvement in [cane toad research], with his laboratory and his linkages and his way of working, where he gets on with many people, has vastly improved our knowledge of the biology of the toad," says veteran invasion biologist Tony Peacock, CEO of Australia's Cooperative Research Centres Association.

Shine says he approaches topics with a willingness to be wrong. "I'm still appalled at my own inability to guess the right answer before we actually gather the data."

Take away the cane toad research, and Shine's resume is still full of first-class natural history discoveries. By studying the ecology and life histories of snakes in Australia and around the world, for example, he has provided fresh insight into the evolution of live birth (most reptiles lay eggs, but more than 2000 species give birth) and why male snakes are bigger than females in certain species, while the opposite is true in others (males tend to grow larger in species whose males have to fight other males during the mating season). Shine "really observes and thinks about what the animals are doing and lets the hypothesis be generated by their natural world, which is the characteristic of a real scientist," Endler says.

In 2008, Shine and former student Daniel Warner, now at Iowa State University in Ames, finally provided experimental evidence for a 1970s-era theory for why some species have temperature-dependent sex determination. In certain reptiles—including all crocodilians, for example—nest temperature skews offspring gender ratio. Evolutionary biologists Eric Charnov and James Bull posited that there must be an evolutionary benefit for letting environmental conditions determine gender instead of genetics, but no one had been able to confirm that, in part because the phenomenon occurs in mostly long-lived animals.

But Shine, who had been a postdoc in Charnov's lab, and Warner turned to the Jacky dragon, an Australian lizard with

Snake study. Much of Shine's career has focused on Australia's native animals, such as pythons.

a life cycle of only a few years in which both sexes are born if nest temperatures are between 27°C and 30°C, but only females are born if it's colder or hotter. Hormonally manipulating the eggs in one experiment so that males were born outside the intermediate temperature range, the pair maintained those Jacky dragons in enclosures and showed that they didn't reproduce as well as typical males, an evolutionary disadvantage expected under the Charnov-Bull theory. "The sons that had been produced at the temperatures that normally produce sons were far more successful than sons that had been produced at any other temperature," Shine says. "And the reverse went for the girls."

Killer robot toads

For almost a decade, cane toads have distracted Shine from the Jacky dragon, snakes, and other native animals he loves to study. Fifty years ago, no one would have thought that the cane toads would make it to his research station in Fogg Dam so quickly. The toads had initially traveled west steadily at about 10 kilometers per year. But then the amphibians at the front of the invasion began to change with every generation. The new offspring developed longer legs that enabled them to hop farther. And they didn't rest as much, hopping more frequently than previous generations of the toad, and thus moving longer distances on average. They also followed straighter paths and had greater endurance than the toads in the east—they could travel a kilometer or more each night. "You get these bizarre, robot cane toads that are designed to do nothing but hurtle as fast as possible, as straight as possible, across the landscape," Shine says.

The adaptations carried a price—about 10% of these toads now develop spinal arthritis—but the result was an invasion front that is now moving at a rate of 50 kilometers each year. "I've come to have a sneaking admiration for the toads," Shine says. "They're an extraordinary invasion machine."

The longer Shine and his colleagues studied the toads, the more they became convinced that the amphibians' evolution was more complex than natural selection alone. They concluded there was another mechanism at work, one that Shine last year dubbed "spatial sorting" in an article in the *Proceedings of the National Academy of Sciences*. If you look at the population of cane toads spreading from east to west, toads at the front of the invasion in the west are the ones that have dispersed most quickly. When these toads on the leading edge breed, some of their offspring are naturally even faster dispersers, and they soon become the front of the invasion. When they breed and produce even faster offspring, the cycle continues, and the front moves more quickly every year. That's spatial sorting, "evolution through space, not time," Shine says. In other words, it's survival of the fastest, not the fittest, when it comes to cane toads.

Spatial sorting potentially has implications beyond invasion biology—species move all the time, driven by changes in climate or the opening of landscapes. And evidence of spatial sorting can be seen in other species; wood butterflies at the edge of their range expansion in England, for example, have stronger flight muscles.

CREDIT: PETER HARLOW

Not all evolutionary biologists are convinced that spatial sorting is a novel concept in their field; "I'd just call it gene flow," says Mark McPeek of Dartmouth College. But some say it does appear to have been largely forgotten until Shine's work on cane toads. "Spatial sorting is a new component of evolution that people had ignored," Endler contends. "It's a fundamental additional process of evolution."

Toxic backlash

Understanding why cane toads have become such a problem is all well and good, but spatial sorting doesn't offer an obvious way to stop their spread across northern Australia. Farmers, volunteer groups, and government scientists have tried to get rid of the toads by manually removing eggs from ponds or physically killing adults, but both tactics have proved woefully inadequate. Attempts to identify or create a virus or other biocontrol agent that would wipe out the whole cane toad population have not borne fruit yet, either. Shine's group, for example, is still looking into using parasitic lungworms for cane toad control.

Given the cane toad's toxic payload, Australians have long assumed that the amphibian's native predators were doomed, but it turns out that's not necessarily the case. The cane toad's toxins are "devastating for a small number of species," Shine says, "and really no big deal for most of the others."

Raptors, for instance, have figured out how to avoid the majority of the toad's toxins by eating only their tongues. And Australia's native frogs have quickly learned that cane toads aren't tasty and now avoid them. Shine even taught young captive quolls, native catlike marsupials, that the toads taste bad by feeding them a nonlethal dead toad laced with a nausea-inducing chemical; when released into the wild, those quolls taught their offspring to avoid the amphibians.

This may help native predators to survive, but it can't do too much to slow the toads. "If they can have 30,000 kids a year, then really, you're not going to have too much impact just removing the adults," Shine notes. "It's more like dealing with an insect pest than it is like dealing with the average vertebrate."

That's why an unexpected discovery by Shine's team—that cane toads are sometimes cannibals, with tadpoles of the species consuming cane toad eggs—finally has Shine and others hopeful. What some might have dismissed as a quirk of nature, Shine has turned into a plan to get rid of the toads.

It all started with the observation that native frog tadpoles would munch on cane toad eggs and soon die. When Shine, postdoc

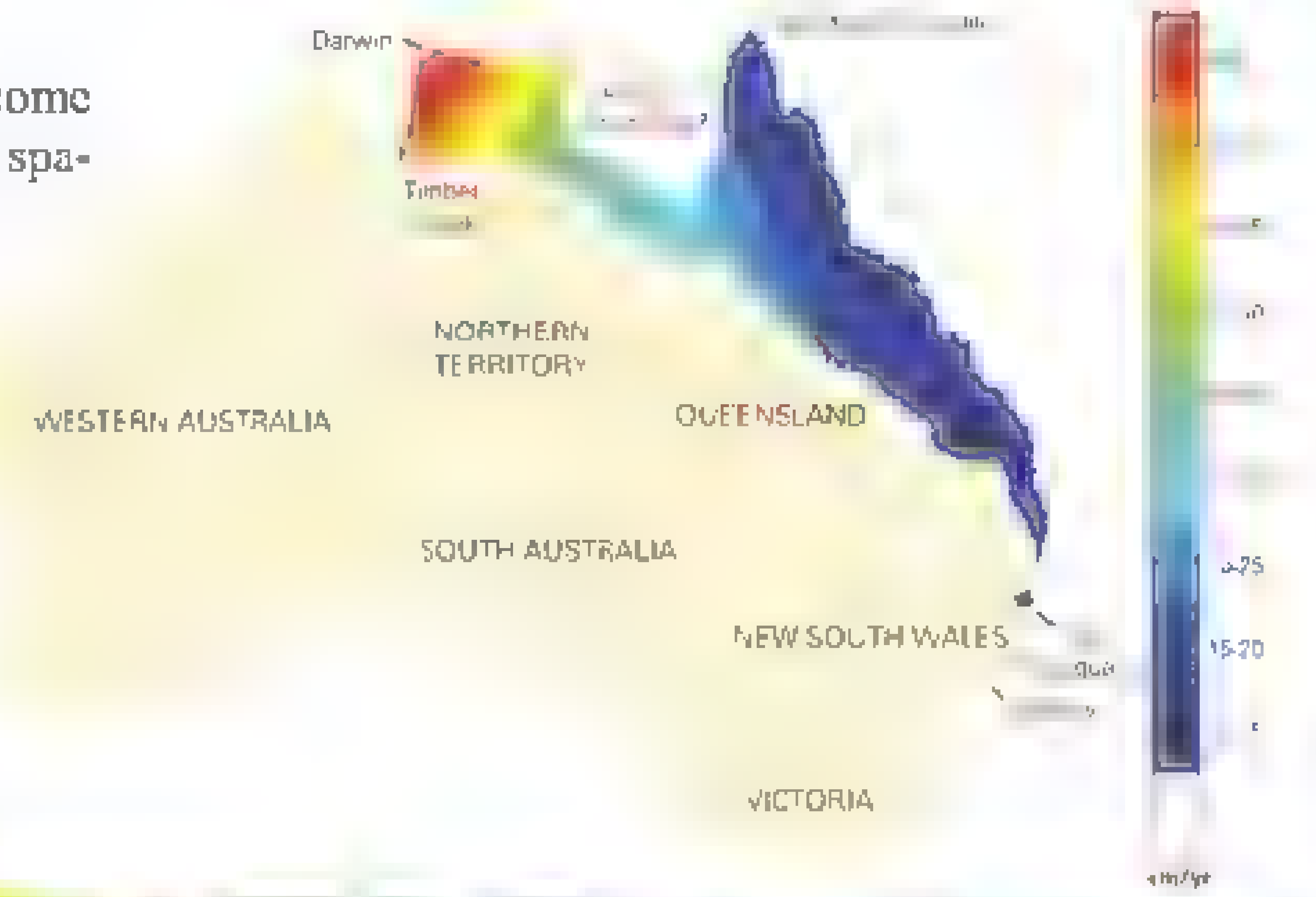

Speedy toads. As cane toads have spread from Queensland, their invasion front has quickened (*top*) and local groups aiming to slow the toads (*bottom*) have had limited success.

CREDITS (TOP TO BOTTOM): ADAPTED FROM URBAN ET AL. THE AMERICAN NATURALIST MARCH 2008; K. M. HAND

Michael Crossland, and their colleagues used those eggs as bait in traps, they found cane toad, not frog, tadpoles by the dozen. Unexpectedly, they found that the toad tadpoles were lured to the eggs by the same toxins the adult toads use to deter and poison predators. Crossland and Shine then used those attractants as bait in funnel traps in ponds and caught tens of thousands of toad tadpoles in just a few days, removing nearly all that were living in a pond, with very few native frog tadpoles, fish, or insects as by-catch.

This "is a testament to the value of pure research," Phillips says. Shine "discovered something that is a chink in the toad's armor and discovered that it can be exploited."

Crossland and Shine have tried the toad toxin-laden traps in a half-dozen ponds so far, including one in Sydney, at the edge of the cane toad's Australian range, and the traps have been a success each time. Shine's team presents the trap results this week in the *Proceedings of the Royal Society B*.

Shine envisions a day when the community groups that currently carry out toad kills are instead enlisted to collect the animals, harvest their toxins, and build tadpole traps. It's still only a local solution, but it could prove invaluable in places such as nature reserves. The trap strategy "seems like it could be very promising at that level," says ecologist David Skelly of Yale University.

But, Skelly adds, "I'm not sure this is something that could knock the invasion wave back." Others say that shouldn't be the key goal. "People always think in terms of 'Wouldn't it be nice if we had some sort of biological control [for cane toads] and knock them all out,'" says invasion biologist Peacock. "Rick is working beyond that. ... We should be concentrating on those areas and those ecosystems where the toads do the most damage," such as where they interact with the northern quoll, the species most likely to be driven extinct by the toad invasion.

Shine himself acknowledges that the toxin traps aren't the ultimate toad killers. "We won't have a magic bullet to get rid of cane toads from Australia," he says, "but we now have an approach that can massively reduce their numbers."

That may disappoint some cane toad-busting groups, but it's a hallmark of Shine's "pragmatic" and "clear-eyed" approach to this research, according to Skelly. And even if Shine hasn't found the Holy Grail of cane toad control, he's certainly brought Australia hope. "We really have a much better idea of how one of the classic, textbook invasive species influences environments," Skelly says, "because [Shine has] been willing ... and been productive enough to tell the whole story about this species." **–SARAH ZIELINSKI**

Sarah Zielinski is a freelance writer based in Washington, D.C.

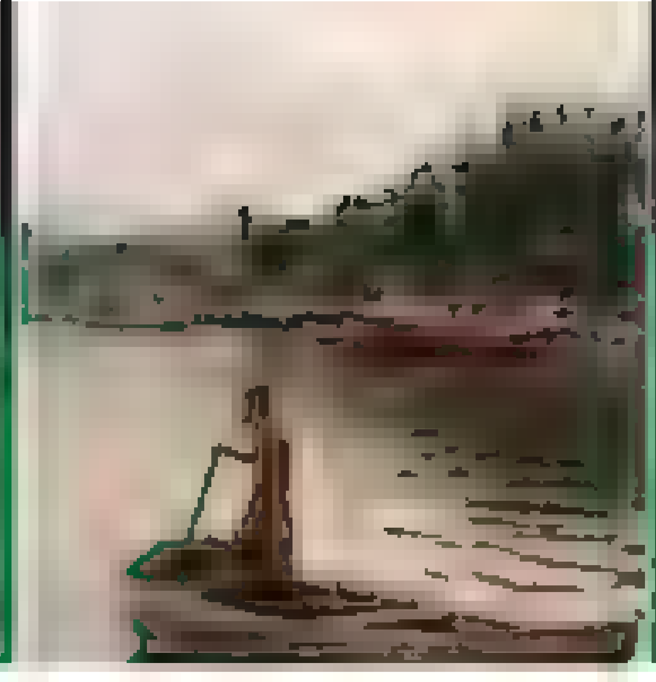

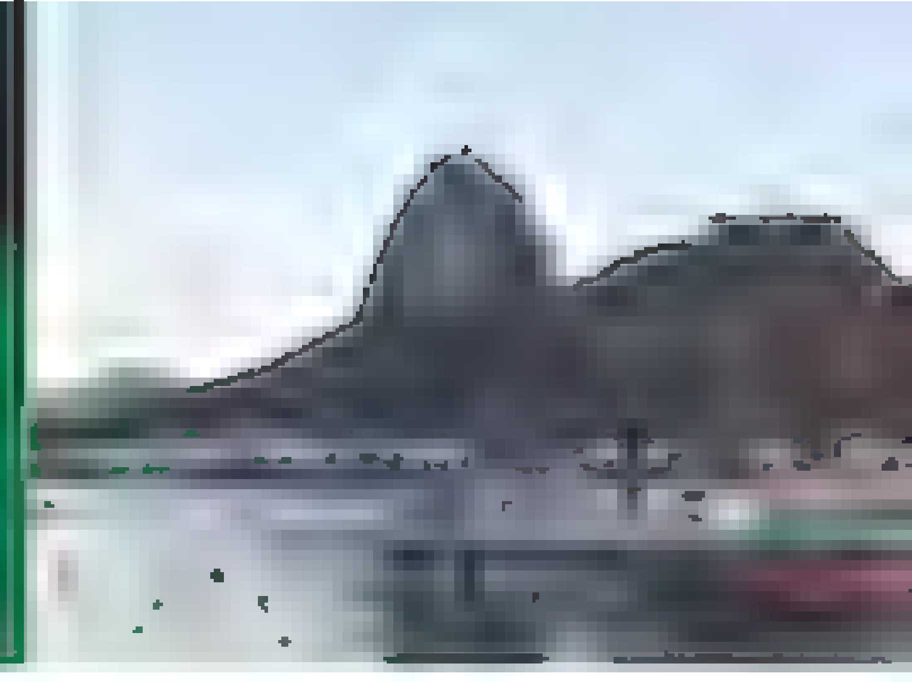

LETTERS

edited by Jennifer Sills

Forgotten Biodiversity in Desert Ecosystems

AS THE WORLD'S GOVERNMENTS CONGREGATE FOR THE UNITED NATIONS CONFERENCE ON Sustainable Development (Rio+20), we call on them to address one of the greatest oversights in conservation in recent years: the neglect of desert ecosystems. Deserts cover 17% of the world's land mass and harbor surprisingly high biodiversity (*1*), including some of the most endangered species in the world (*2*). They are also home to 6% of the world's population (*3*), including some of the poorest and most marginalized people in the world (*4*), who depend on deserts to deliver sustainable ecosystem services in a changing climate. Deserts and other dryland ecosystems currently harbor almost one-third of terrestrial global carbon stock (*5*), with further potential for carbon sequestration through improved land management. Furthermore, desert genetic biodiversity is key to improving dryland agricultural productivity (*6*).

Deserted land. The Ahaggar Cultural Park, Algeria, is home to overlooked biodiversity.

Over the past two decades, however, conservationists have argued that targeting funding at tropical forests and other "biodiversity hotspots" maximizes the number of species conserved per conservation dollar and contributes to climate change mitigation by reducing greenhouse gas emissions from forest loss and degradation (*7*, *8*). Consistent with these goals, between 1992 and 2008 only 1% of Darwin Initiative funding went to projects in deserts, compared with 24% to forests (*9*). Similarly, between 1991 and 2009 only 11% of Global Environment Facility funding to Africa went to Saharan nations (*10*). Lack of financial support is mirrored by lack of scientific information. Between 2000 and 2011, most scientific publications in ecology focused on forest biomes (67%) compared with deserts (9%) (*11*).

We call on governments to reverse the historic neglect of deserts and include them with forests at the top of the agenda at Rio+20; to support the UN Convention on Combating Desertification minimum target of halting land degradation; and to set a clear target for restoration of desert ecosystems to benefit biodiversity and people.

S. M. DURANT,[1,2*] N. PETTORELLI,[1] S. BASHIR,[3] R. WOODROFFE,[1] T. WACHER,[4] P. DE ORNELLAS,[4] C. RANSOM,[4] T. ABÁIGAR,[5] M. ABDELGADIR,[6] H. EL ALQAMY,[7] M. BEDDIAF,[8] F. BELBACHIR,[1,9] A. BELBACHIR-BAZI,[9] A. A. BERBASH,[10] R. BEUDELS-JAMAR,[11] L. BOITANI,[12] C. BREITENMOSER,[13] M. CANO,[5] P. CHARDONNET,[14] B. COLLEN,[1] W. A. CORNFORTH,[1] F. CUZIN,[15] P. GERNGROSS,[16] B. HADDANE,[17] M. HADJELOUM,[18] A. JACOBSON,[19,20] A. JEBALI,[21] F. LAMARQUE,[22] D. MALLON,[23] K. MINKOWSKI,[24] S. MONFORT,[25] B. NDOASSAL,[26] J. NEWBY,[27] B. E. NGAKOUTOU,[26] B. NIAGATE,[28] G. PURCHASE,[4,2] S. SAMAÏLA,[29] A. K. SAMNA,[29] C. SILLERO-ZUBIRI,[30] A. E. SOULTAN,[7] M. R. STANLEY PRICE,[30,31] J. E. M. BAILLIE[4]

[1]Institute of Zoology, Zoological Society of London, London NW1 4RY, UK. [2]Wildlife Conservation Society, Bronx Zoo, Bronx, NY 10460, USA. [3]4 Brizay Park, 279947, Singapore. [4]Conservation Programmes, Zoological Society of London, London NW1 4RY, UK. [5]Estación Experimental de Zonas Áridas (EEZA), CSIC, Carretera de Sacramento s/n, 04120-La Cañada de San Urbano, Almería, Spain. [6]Department of Biology, University of Hail, Kingdom of Saudi Arabia. [7]St. Katherine Protectorate, Nature Conservation Sector, Egyptian Environmental Affairs Agency, EEAA, Cairo, Egypt. [8]Office National du Parc Culturel du Tassili n Ajjer, B.P. 11, Djanet 33100, Algeria. [9]Laboratoire d'Ecologie et Environnement, Faculté des Sciences de la Nature et de la Vie, Université de Béjaïa, Route Targa Ouzemmour, 06000, Bejaïa, Algeria. [10]Nature Conservation Department, Environment General Authority (EGA), Tripoli, Libya. [11]Royal Belgian Institute of Natural Sciences, 1000 Bruxelles, Belgium. [12]Department of Biology and Biotechnologies, Università La Sapienza, 00185 Roma, Italy. [13]IUCN/SSC Cat Specialist Group, c/o KORA, 3074 Muri, Switzerland. [14]GF Foundation, 75003 Paris, France. [15]Bab Agnaw, 40 000 Marrakech, Morocco. [16]BIOGEOMAPS, Umwelt-PR Gerngross e.U., Neubaugasse 4/7-9, A-1070 Vienna, Austria. [17]Fondation Mohamed VI pour la Protection de l'Environnement, Temara 12 000, Morocco. [18]Direction Generale des Forêts, Direction de la Protection de la Faune et de la Flore, Chef de Bureau de la Gestion et de la Preservation de la Faune, B.P. 232, Ben Aknoun Alger, Algeria. [19]Nicholas School of the Environment, Duke University, Durham, NC 27708, USA. [20]Big Cats Initiative, National Geographic Society, Washington, DC 20036–4688, USA. [21]Tunisia Wildlife Conservation Society (TWCS), Departement de Biologie, Faculté des Sciences de Tunis, Campus Universitaire 2092 Tunis, Tunisia. [22]Ministère de l'Ecologie, du Développement Durable et de l'Energie, Sous-direction de la protection et de la valorisation des espèces et de leur milieu, Grande Arche de La Defense 92055, La Défense CEDEX, France. [23]Division of Biology and Conservation Ecology, Manchester Metropolitan University, Manchester M1 5GD, UK. [24]Santa Cruz, CA 95060, USA. [25]Smithsonian Conservation Biology Institute, National Zoological Park, Front Royal, VA 22630, USA. [26]Direction des Parcs Nationaux Reserves de Faune et de la Chasse, B.P. 905, N'djamena, Tchad. [27]Sahara Conservation Fund, 1148 L'Isle, Switzerland. [28]Directeur du Parc National et Réserve de Biosphère de la Boucle du Baoulé, B.P. 275 Bamako, Mali. [29]Direction de la Faune, de la Chasse et des Aires Protégée, B.P. 578, Niamey, Niger. [30]Wildlife Conservation Research Unit, Department of Zoology, University of Oxford, The Recanati-Kaplan Centre, Tubney House, Tubney OX13 5QL, UK. [31]Al Ain Zoo, Abu Dhabi, United Arab Emirates

*To whom correspondence should be addressed. E-mail sdurant@wcs.org

References and Notes

1. J. Safriel *et al.*, in *Millennium Ecosystem Assessment*, R. M. Hassan, R. Scholes, N. Ash, Eds. (Island Press, Washington, DC, 2005), ch. 22.
2. IUCN, *The IUCN Red List of Threatened Species, Version 2011.2* (www.redlist.org).
3. M. Mortimore *et al.*, "Dryland opportunities: A new paradigm for people, ecosystems and development" (IUCN, Gland, Switzerland; IIED, London; UNDP, New York, 2009).
4. N. Middleton, L. Stringer, A. Goudie, D. Thomas, "The forgotten billion: MDG achievement in the drylands" (United Nations Development Programme, New York, 2011).
5. K. Trumper, C. Ravilious, B. Dickson, "Carbon in drylands

Desertification, climate change, and carbon finance" (UNEP-UNDP-UNCCD Technical Note for Discussions, Istanbul, Turkey, 2008).
6. M. B. K. Darkoh, *J Arid Env.* 54, 261 (2003)
7. N. Myers, R. A. Mittermeier, C. G. Mittermeier, G. A. B. da Fonseca, J. Kent, *Nature* **403**, 853 (2000)
8. K. L. Denman *et al.*, in *IPCC Climate Change 2007: The Physical Science Basis*, S. Solomon *et al.*, Eds. (Cambridge Univ. Press, Cambridge, 2007), pp. 499–587
9. P. D. Hardcastle, "Thematic review of Darwin Initiative projects related to forest biodiversity" (Department for Environment, Food, and Rural Affairs, London, 2008); http://darwin.defra.gov.uk
10. Global Environmental Facility, "OPS4 progress towards impact: Fourth overall performance study of the GEF" (Global Environmental Facility Evaluation Office, Washington, DC, 2010); www.gefonline.org
11. On 9 February 2012, we searched the ISI Web of Science (http://wok.mimas.ac.uk) for scientific articles under the subject area ecology that included the terms "desert" and "forest," as well as other major biomes. We found 29,318 publications on forests and 4114 on deserts

Predatory Publishers and Plagiarism Prevention

M. BALTER ("REVIEWER'S DÉJÀ VU, FRENCH science sleuthing uncover plagiarized papers," News & Analysis, 9 March, p. 1157) describes how a scientist recently published at least nine articles that largely or entirely duplicated papers written by others and was exposed only after we found one of our papers integrally copied in a manuscript that both of us coincidentally received for review. What is remarkable here is not only the flagrant fraud, but the fact that six of these papers were published in scholarly journals only last year. Publishers can easily prevent publishing plagiarism by systematically running submitted manuscripts through software such as CrossCheck and eBlast (*1*, *2*) or by running strings of words that are unlikely to be repeated by chance through search engines (*3*). It is evident that not all publishers systematically use these tools, despite the fact that plagiarism is common (*1*, *2*). It is also noteworthy that these six 2011 papers—as well as the manuscript for review—are all from journals of publishers that Beall (*4*) lists as "predatory open-access scholarly publishers." Such publishers "exploit the author-pays, Open-Access model for their own profit" and do not invest in quality control (*4*, *5*). In this light, it is less surprising that papers escape plagiarism detection today. We argue that publishers that do not systematically use anti-plagiarism tools consciously take the risk of copyright infringement and of being accomplices in plagiarism. We encourage copyright holders to sue publishers of plagiarism for these offenses. When fines become a realistic threat, plagiarism prevention will become valuable even for predatory publishers.

PATRICK A. JANSEN[1,2,*] AND PIERRE-MICHEL FORGET[3]

[1]Department of Environmental Sciences, Wageningen University, Wageningen, Netherlands. [2]Smithsonian Tropical Research Institute, Balboa, Ancon, Republic of Panama. [3]Museum National d'Histoire Naturelle, Brunoy, France

*To whom correspondence should be addressed. E-mail: patrick.jansen@wur.nl

References
1. H. Y. Zhang, *Learned Pub.* **23**, 9 (2010)
2. J. Couzin-Frankel, J. Grom, *Science* **324**, 1004 (2009)
3. M. Errami *et al.*, *Bioinformatics* **26**, 1453 (2010).
4. Scholarly Open Access, Beall's list of predatory open-access publishers (2012) (http://scholarlyoa.com/publishers)
5. J. Beall, *Charleston Advisor* **11.4**, 10 (2010)

LIFE IN SCIENCE

Potato Pedagogy

When I was in ninth grade, my class did a common experiment: We stained the starch in a potato with iodine. We found that the area of the potato exposed to the iodine-containing solution turns dark purple. I remember dejectedly staring at my purple potato and wondering what happened to the grand vision of science promised to me in television, films, and comic books. A scientist was supposed to go into a laboratory, mix some things together, generate a small fire (or at least some smoke), and end up with a cure for cancer.

Little did I know, I was indeed participating in this mythical idea of science: The simple iodine-staining reaction can be used to detect cervical cancer. The staining works because the normal cells of the cervix contain glycogen, a starch-like molecule, whereas cancerous cells do not. Iodine stains the normal cells brown but leaves the glycogen-deficient cancer cells white. Once exposed, the malignant cells can be excised. If the detected tumor is localized and accessible, it can be surgically removed in its entirety, curing the patient.

Understanding the real-world implications of the simple potato experiment would have transformed my science experience as a student. With this in mind, I committed my time to The Providence Alliance of Clinical Educators (*1*), an organization dedicated to connecting important health topics to basic science concepts covered in high school. Science lessons that put scientific concepts in context allow students to appreciate their relevance immediately. These students won't have to wait 16 years like I did to realize that one purple potato is more impressive than any puff of smoke.

BILL BRUCKER

Providence Alliance of Clinical Educators, Providence, RI 02906, USA. E-mail: william_brucker@brown.edu

Reference
1. More examples of these connections can be found at www.pacescience.org.

EDITOR'S NOTE
This is an occasional feature highlighting some of the day-to-day humorous realities that face our readers. Can you top this? Submit your best stories at www.submit2science.org.

CORRECTIONS AND CLARIFICATIONS

News Focus: "Researchers set course to blockade ballast invaders" by D. Strain (11 May, p. 664). The article incorrectly referred to the Asian clam by an obsolete Latin name, *Potamocorbula amurensis*. It is currently cited in literature as *Corbula amurensis*.

News & Analysis: "First spinoff of African math institute takes root in Senegal" by M. Enserink (4 May, p. 533). Neil Turok was quoted as saying that a network of AIMS institutes across Africa would cost $100 million over the next 10 years, or about 0.003% of Africa's aid budget. Actually, $100 million is about 0.03% of that budget.

News Focus: "New lens offers scientist a brighter outlook" by A. Saini (30 March, p. 1562). The second sentence in the fourth paragraph stated that the Mesolens can image up to 0.22 micrometers below the surface of a specimen. The correct figure is 0.22 millimeters.

News Focus: "Partners prepare to pick a site for world's biggest telescope" by D. Clery (30 March, p. 1564). To clarify, the images on pages 1564 and 1565 show artists' conceptions of antennas planned for the proposed Square Kilometre Array; the actual antennas have not been built yet.

EDUCATION

Let's Finnish Schooling

Henrik Saalbach

Imagine you are placed in charge of reforming your country's educational system in order to increase students' academic performance. What would you do? Ideas that come to mind likely include the following: lower the age for starting school, give students more instructions, require more homework, establish a prescribed curriculum for teachers with high performance standards for students, increase competition among schools, provide merit-based pay for teachers, and increase accountability of schools through regular standardized, census-based tests and school inspections. All of these tactics for educational reform have been applied in multiple countries. However, one small country in northern Europe did not follow the global trends when reforming its educational system—and it has done best: Finland, the primus of the Program for International Student Assessment studies.

Trusted with the task. A teacher conducting a lesson at a high school in Helsinki.

Pasi Sahlberg's *Finnish Lessons* provides an insightful account of how, within recent decades, the Finns managed to shift their educational system from mediocre to top-performing. Sahlberg, a teacher and educational reformer currently at the Finnish Ministry of Education and Culture, sketches the history of the Finnish reforms and points out its key elements. His account helps us understand why the Finnish school system is among the best not only for the performance of its students but also for its equality.

The Finnish strategy for educational change can be summarized in these points: professionalism, trust, and shared responsibility. Teachers are considered "esteemed professionals similar to medical doctors, engineers, or economists," and they are trained accordingly. Earlier than others, the Finns realized that high-quality teaching (on both primary and secondary levels) requires expertise in three domains: content, content-specific pedagogy, and general learning sciences. Furthermore, teaching is seen as an ill-defined problem. Dealing skillfully with such problems requires adaptive expertise that enables people to rapidly retrieve and accurately apply appropriate knowledge and skills in order to best respond to changing situations. Teacher-education programs thus need to instill deep understanding and easy enactment of key concepts from the three aforementioned knowledge domains.

The Finnish teacher-education system has high academic requirements and provides practical training from early on. All teachers from primary school level upward must hold a master's degree. Research methodology forms an integral part of their curriculum, which prepares them to conduct studies on educationally relevant questions in their thesis. Their program repeatedly requires practice of teaching skills, which is carried out in special teacher training schools that are governed by the universities. The high professional requirements for the teachers who supervise the student-teachers in these schools are crucial for the quality of the training on the whole. Careful supervision of the practice teaching concurrent with coursework improves the student-teachers' success at putting into practice what they are learning. Furthermore, the initial classroom experience of student-teachers is a good predictor of their later teaching effectiveness.

Successful educational systems, however, require more than just well-trained teachers. Sahlberg rightly points out: "[I]t is not enough to establish world-class teacher education programs or pay teachers well. … [T]he true Finnish difference is that teachers in Finland may exercise their professional knowledge and judgment both widely and freely in their schools." Here, trust comes into play. In contrast to their peers in many other countries, Finnish teachers have a very high degree of autonomy that includes control of curriculum, student assessment, and school improvement. Instead of implementing standards, prescribing curricula, and conducting frequent tests, Finnish educational authorities (and lay people) trust in the professionalism of teachers and schools and do not patronize them with regulations. Shared responsibility—instead of competition among teachers, schools, and municipalities—helped drive educational reform in Finland. Implementing innovation in school requires all levels of the "nested" educational system to participate in a responsible way: researchers, policy-makers, administrators, and teachers.

Sahlberg notes: "Many factors have contributed to Finland's educational system's current fame, such as its 9-year comprehensive school (*peruskoulu*) for all children, modern learning-focused curricula, systematic care for students with diverse special needs, and local autonomy and shared responsibility. However, research and experience suggest that one factor trumps all others: the daily contributions of excellent teachers." Professionalism, trust, and shared responsibility are certainly fundamental, but there is another important factor contributing to the excellence of teachers in Finland: the students who go into teaching. Whereas in many countries, teaching ranks far lower in popularity than other professions, the most talented Finnish students often want to become school teachers. The high prestige of becoming a teacher can mainly be traced back to the features

Finnish Lessons
What Can the World Learn from Educational Change in Finland?
by Pasi Sahlberg
Teachers College Press, New York, 2011. 191 pp. Paper, $34.95.
ISBN 9780807752579.

The reviewer is at the ETH Zürich Institute for Behavioral Sciences, Research on Learning and Instruction, Universitätsstrasse 41, CH-8092 Zürich, Switzerland. E-mail: henrik.saalbach@ifv.gess.ethz.ch

of the profession and the training program. In particular, given the high degree of freedom, work at school is perceived as highly autonomous and independent. Furthermore, the high academic requirements of a master's degree enable graduates to also take positions outside school or to continue their academic career at some point. Nonetheless, there are also culture-specific reasons involved—teaching has always been a highly regarded career in Finland. Other countries may find that adopting the Finnish system doesn't rapidly result in attracting the most talented students to teaching.

Sahlberg's book contains important lessons for a broad range of academics, educators, politicians, and the public. I especially appreciated its demonstration that top academic performance can be achieved with low inequality, comprehensive school for all students, low dropout rates, low school-related anxiety, and a high degree of freedom for teachers. In fact, Finland teaches that all these aspects need to be considered when giving directions for effective and sustainable educational reform.

10.1126/science.1222314

SCIENCE PRACTICE

Known Unknowns

Moran Cerf

The back dust jacket of Stuart Firestein's *Ignorance* includes a silhouette of a black cat. It is very easy to miss the cat, though, as the jacket itself is also black. The design image reflects one of the book's main themes: "It is very difficult to find a black cat in a dark room. Especially when there is no cat." According to Firestein, this proverb aptly describes the way science proceeds: not as a puzzle with a certain answer in the end, but rather by stumbling in dark rooms, looking for content that might not even be there. The book, however, doesn't promote a gloomy view of scientific discovery. Rather Firestein celebrates its ultimate success: generating more ignorance. According to him, ignorance—not knowledge—is the key driver of science.

Firestein (a neurobiologist at Columbia University) takes us outside of the lab meetings, popular-science books, journal papers, and public talks where scientists promote what they already know and invites us into the bars and the diners where researchers sit after the talk is over. There scientists discuss not what they have already mastered but rather the things they wish they knew—the questions that are still open, thoughts that keep them up at night, results that do not support their hypotheses, and methods they wish they could use to settle matters. Delving behind the scenes of science, Firestein unveils the parts of the journey that, he argues, are the more interesting aspects of research: the yet unknowns.

The author writes like a father trying to teach his kids how to view the world. Although the book focuses, as its title suggests, on how ignorance drives science, one can find more between the lines. We basically get Firestein's advice to young investigators and to those who shape these researchers' ways of work: peers, collaborators, mentors, and the lay audience. To all, he recommends: Learn to communicate what you do not know and to inquire about others' ignorance. As he describes it, the job of a scientist importantly includes finding ways to communicate the science such that the knowns and, even more so, the ignorance will be accessible to everyone.

Ignorance
How It Drives Science
by Stuart Firestein
Oxford University Press, New York, 2012. 207 pp. $21.95, £14.99. ISBN 9780199828074.

The book demonstrates its author's own communication skills, which may be grounded in the 15-plus years he spent in the theater as a stage manager and director before beginning his undergraduate studies in science. In an autobiographical section, Firestein discusses how his education in science was shaped by helpful mentors, intentional decisions, and serendipitous events (with recurring roles for ignorance). Among the crucial factors seems to be the fact that memorizing scripts for a living provided a preadaptation for the organic chemistry course required of biology majors.

For the past several years, Firestein has run a "course devoted to, and titled, Ignorance." It features sessions in which guest scientists talk for a couple hours about their work, focusing on "the current state of their ignorance." Firestein presents examples from the course in a series of case histories that he takes us through in the second half of the book. There and elsewhere, he incorporates stories from his own experiences and from those of his colleagues (including cognitive psychologist Diana Reiss, astronomer David Helfand, and neuroscientist Larry Abbott). These anecdotes showcase the questions that baffle the researchers. Deploying the term made famous by Donald Rumsfeld (former U.S. secretary of defense), Firestein urges us to ask scientists about their known unknowns, the things that they know they do not know.

In the Acknowledgments at the beginning of the book, Firestein recounts his "response to the inevitable questions about grades" at the start of his course. He warns "the students ... that they should consider carefully what grade they would actually like to appear on their records. After all, the transcript will read 'SNC3429 *Ignorance*'—and do they want the grade that appears after this to be an A ... or an F?" But within a few pages Firestein convinces us that getting an A in ignorance should be our ultimate goal. Science is risky, he notes. After months, or even years, of work, one may end up finding nothing, knowing nothing, and achieving nothing. Yet this is in fact good, because ignorance is the true essence of science. Echoing George Bernard Shaw's dictum, "Science ... never solves a problem without creating ten more," Firestein argues that ignorance works as the engine of science because it is essentially unbounded, and that makes science much more expansive.

Through his musings and the case studies, Firestein advocates for the virtue of ignorance, teaches about the different types of ignorance, and educates us on how to talk about ignorance. The book is full of questions that are worth asking ourselves and others whenever encountering ignorance. These include queries we should address to any scientist we find ourselves talking to: Are there things that are unknowable in your field? What are the current technology limits in your work? Can you see solutions? Are there data from labs that don't agree with yours? What was the thrust of your last grant application? As in the lab, the well-formed question can lead to surprising answers.

An excellent read, *Ignorance* would be a fine companion text for potential scientists at the beginning of their studies. The book reminds us that although we are repeatedly given the impression our world contains an endless amount of knowledge, most of that is inaccessible to us, and it is the absence of knowledge that should concern us. Firestein's short account may even make you embrace your ignorance, wearing it like a badge of honor. You may gradually become more and more ignorant as you read, and you will enjoy the journey. Ignorance in this telling is truly bliss.

10.1126/science.1222943

The reviewer is at the Department of Neurosurgery, University of California, Los Angeles, and the Stern School of Business, New York University. E-mail: moran@morancerf.com

OCEANS

Avoiding Empty Ocean Commitments at Rio+20

To improve sustainability of ocean ecosystems, implementation of existing commitments should be prioritized.

Liane Veitch,[1]* Nicholas K. Dulvy,[2] Heather Koldewey,[1] Susan Lieberman,[3] Daniel Pauly,[4] Callum M. Roberts,[5] Alex D. Rogers,[6] Jonathan E. M. Baillie[1]

The principles of sustainable management of marine capture fisheries and the protection of biodiversity are established by the United Nations Convention on the Law of the Sea (UNCLOS) and its implementing agreement (*1*). Building on these, Agenda 21, released after the UN "Earth Summit" in 1992 in Rio de Janeiro, and the Johannesburg Plan of Implementation (JPOI) from the 2002 summit, set quantitative and qualitative targets relating to the marine environment (see the table). Unfortunately, implementation of many of these commitments has been difficult, ineffective, or practically nonexistent.

In June 2012, heads of state and government will meet at the UN Conference on Sustainable Development ("Rio+20") to renew political commitments to sustainable development and to identify gaps from previous Earth Summits. Oceans are one of ten "critical issues" at Rio+20; therefore, it is timely to revisit existing fisheries commitments and to review evidence of their implementation and success (*2*). We discuss fisheries-related actions to evaluate progress across five areas: improving fisheries management; decreasing harmful subsidies; eliminating illegal, unreported, and unregulated (IUU) fishing; increasing marine protection; and decreasing biodiversity loss.

Sustainable management

Fishing capacity has declined in some countries (*3*), although, globally, fishing capacity has increased since the JPOI target was set from 4.02 billion kilowatt days in 2002 to 4.35 billion in 2010 (*4*), which indicates that the target to reduce overcapacity by 2005 was not achieved. Global fisheries catches are between 17 and 112% higher than what could be sustainably appropriated from shelf ecosystems on the basis of estimates of primary production (*5*), and the proportion of assessed stocks classified as overexploited, depleted, or recovering from depletion reached 30% in 2009 (*6*). These findings suggest that, in general, both unilaterally and acting through regional fisheries management organizations and agreements, governments will fail to meet their commitments to maintain or restore stocks to maximum sustainable yield (MSY) (*7*) either regionally [e.g., (*8*)] or globally by 2015 (*9*). Although a few countries have improved management of their domestic stocks (*10*), there are concerns that in some cases this has displaced overfishing to less well regulated fisheries in distant waters (often of developing countries) or led to the sourcing of fish from harmful forms of aquaculture (*11*).

The Ecosystem Approach to Fisheries (EAF) was adopted as a policy goal before the availability of a tested framework for implementation (*12*, *13*); therefore, development of the EAF has proven challenging and contentious (*14*). Even where relatively sophisticated management systems exist, consensus is generally lacking regarding the metrics or tools to apply the EAF (*15*). One indicator that we are not achieving even a minimal EAF within the target time frame is the low proportion of stocks managed by using precautionary reference points and inadequate implementation of even nonbinding national plans of actions, such as that for sharks (*16*). Nonetheless, progress has been made in the past decade on the meaning and practical use of the EAF [e.g., (*13*, *17*)], and initiatives such as the European Union's Marine Strategy Framework Directive are beginning to show promise (*18*).

Subsidies

Awareness of harm caused by subsidies has increased, and the issue is now on the agenda of international institutions such as the World Trade Organization (WTO) and major nongovernmental organizations (NGOs). Even so, a decade after being tasked with reducing global capacity-enhancing subsidies, worth U.S. $16.2 billion in 2003 (*19*), the WTO has failed to achieve the required consensus (*20*), despite intense advocacy by environmental NGOs and the support of numerous countries. Harmful subsidies should be phased out by a set date or redirected into beneficial fisheries management plans by governments that choose to continue to provide subsidies.

IUU fishing

The International Plan of Action (IPOA) on IUU fishing continues to be voluntary and has not halted illegal fishing (*21*), which continues to be worth up to U.S. $23 billion per year (*22*, *23*). Ubiquitous IUU fishing undermines fisheries management; increases risks to target and by-catch species, steals profits from legitimate fishers and governing bodies (*21*); and is especially pervasive where chances of detection or penalty are low and benefits are high, e.g., along West Africa's coast (*24*). Focus on the "I" of IUU, has obscured the "UU"; the bulk of fisheries catches, at least in developing countries, are landed by small-scale fisheries that remain unreported and unregulated, and their true value in national

[1]Zoological Society of London, London NW1 4RY, UK. [2]Simon Fraser University, Burnaby, British Columbia V5A 1S6, Canada. [3]Pew Environment Group, Washington, DC 20004, USA. [4]University of British Columbia, Vancouver, British Columbia V6T 1Z4, Canada. [5]University of York, York YO10 5DD, UK. [6]University of Oxford, Oxford OX1 3PS, UK.

*Author for correspondence: E-mail. liane.veitch@zsl.org

accounting and poverty alleviation goes unrecognized (*25*).

Initiatives such as the Food and Agriculture Organization of the United Nations (FAO) Port State Measures to Prevent, Deter and Eliminate Illegal, Unreported and Unregulated Fishing to monitor vessels where they land fish (*26*) and the Partnership for African Fisheries to fight IUU at the regional level are encouraging developments In addition, widespread monitoring, control, surveillance, and enforcement of vessels at sea and increased uptake of catch and trade documentation schemes are required (*27*).

OUTCOMES RELEVANT TO OC[illegible] AND FISHERIES MANAGEMENT

Agenda 21 and the agreement on the CBD (168 signatories), from the 1992 UN Conference on Environment and Development (attended by 172 governments)

Implement strategies for sustainable use of living marine resources through legal and regulatory frameworks, including small-scale artisanal fisheries.

Maintain biological diversity and productivity of marine habitats under national jurisdiction.

Protect critical habitat areas and highly biologically diverse and productive habitats, where appropriate.

JPOI from the 2002 World Summit on Sustainable Development (WSSD) (attended by 192 governments)

Sustainable management: Implement the FAO IPOA for the Management of Fishing Capacity by 2005 to address overcapacity; maintain or restore depleted fish stocks so they can produce MSY by 2015; eliminate destructive fishing practices and facilitate the use of the ecosystem approach to fisheries by 2012.

Subsidies: Eliminate harmful subsidies that contribute to overcapacity or IUU fishing.

IUU fishing: Implement the FAO IPOA to prevent, deter, and eliminate IUU fishing by 2004

MPAs: Develop and implement a network of representative MPAs by 2012.

Biodiversity: Substantially reduce the rate of biodiversity loss at national, regional, and global levels by 2010; maintain the productivity and biodiversity of important and vulnerable areas within and beyond national jurisdiction.

Outcomes relevant to ocean conservation and fisheries management from the 1992 and 2002 UN Earth Summits. The desired state of the system was described in 1992, whereas targets for achieving this state were agreed in 2002 (which we sort according to the themes discussed in this paper)

Marine protected areas

Marine protected areas (MPAs), particularly strict "no-take" zones, confer multiple ecosystem and societal benefits, such as rebuilding fish stocks and improving fisheries yields, restoring biodiversity and habitat quality, improving resilience to environmental or human pressures, and contributing to local poverty alleviation (*28–31*). In 2010, about 7.2% of territorial waters and 1.6% of the total ocean was classified as protected (*32*). The strength of protection for many designated areas is questionable, however, and needs improvement (*33*). The recent creation of very large marine reserves around remote unpopulated islands, such as the Chagos Archipelago, the Northwestern Hawaiian Islands, and South Orkney Islands are encouraging developments, although beyond territorial waters there is presently little or no protection (*34*).

Despite the commendable increase in MPA designation, at the current rate, the 2012 target will not be met. As suitable places for very large MPAs are scarce, the rate of progress may decline as these "low-hanging fruit" become protected. Encouragingly, no-take reserves have increased markedly since the late 1990s (*9*), and although current coverage remains insufficient [e.g., (*35*)], we are moving in the right direction. For example, the Convention on Biological Diversity (CBD) has committed to protect 10% of marine areas by 2020 (extended from 2012 as that deadline passed) and the World Parks Congress has set the target of 30% by 2030.

Protection of marine biodiversity

Many populations have shown promising recovery at the local level after changes to management practices, often including the establishment of MPAs or changes to fishing practices (*11*). However, global assessments of marine biodiversity [e.g., (*36*)] paint a bleak picture for many taxa; even the most cared for and most closely watched species such as turtles, sharks, and coral reef fishes are not safe. A substantial fraction (16%) of these charismatic marine animals is threatened with an elevated risk of extinction (*37*)

There has been progress in the protection of some groups of threatened marine birds, particularly albatrosses and petrels. Species such as wandering, black-browed, and gray-headed albatrosses and white-chinned petrels were in decline as a result of incidental mortality associated with long-line and trawl fishing. International collaboration (*38*) has resulted in technical mitigation measures and changes to fishing practices that have dramatically reduced by-catch in many fisheries (*39*), sometimes to almost zero [e.g., (*40*)] Nevertheless, it is estimated that globally some 160,000 seabirds a year are still being killed as a result of by-catch from long-line fisheries alone (*41*), and the implementation of measures to protect seabirds is still far from adequate in many areas (*42*)

Because of the growing numbers of exploited fish stocks and other marine species classified as Threatened or Endangered on the International Union for the Conservation of Nature (IUCN) Red List (*43*), it is widely acknowledged that the commitment to maintain biodiversity and productivity in vulnerable areas both within and beyond national jurisdiction and to reduce the rate of biodiversity loss has not been achieved [e.g., (*44*, *45*)]. However, there is some good news. For example, a campaign for a global moratorium on high-seas bottom trawl fishing, which can destroy fragile habitats (*46*) and deplete slow-growing and long-lived species that are highly vulnerable to overexploitation (*47*) achieved a UN resolution in 2006 to ban the method in sensitive sea-bed areas by 2008 (*48*, *49*) Although promising, this resolution has yet to be implemented widely and the future trajectory of high-seas protection remains unclear (*50*, *51*). Unless implementation improves, ocean biodiversity risks enduring an extended phase of marine population crashes and species extinctions that has already begun (*52*).

Future commitments and action

Although many of the fisheries commitments made at previous Earth Summits will not be met by target dates, we are making progress in some areas, and solutions do exist. Public engagement is increasing governmental mandate through initiatives such as "Hugh's Fish Fight" in Europe and awareness-raising movies like "The End of the Line," "Finding Nemo," and "Sharkwater" Still, agreeing on, implementing, and enforcing science-based quotas and the use of sustainable fishing gear has proven difficult within individual countries, and getting many to agree at the multilateral level has caused significant delays. Obstacles such as strong interest-group opposition to commitments, including subsidy redirection and increased MPA coverage, have made it politically difficult to make necessary changes, especially as the benefits are unlikely to be felt before the next electoral cycle. Negotiating capacity reduction is particularly complicated, "everyone" agrees that capacity should be reduced, as long as it is from other countries' fleets.

The complexity of problems and the politics of cooperation have been greater than anticipated Targets and implementation

strategies need to be more nuanced and context-specific to be realistic and achievable. Overcoming current barriers to coordinated and large-scale implementation of targets should be a priority at Rio+20 (*53–56*).

We are calling on governments to honor their long-standing commitments to a sustainable marine environment, through (i) implementing a program to deliver the target of reducing global fishing effort to bring capacity in line with resources, both in domestic waters and in areas beyond national jurisdiction; (ii) redirecting harmful subsidies toward improved management and protection, for example, through allocating more resources to fight IUU and to establish MPA networks; and (iii) implementing even a minimal EAF that protects vulnerable species, while increasing the use of necessary single-species targets.

Rio+20 is also a real opportunity for governments to launch a negotiation process for a new implementing agreement under UNCLOS, seen as a key element for the protection and conservation of biodiversity on the high seas. Following the adage of what gets monitored gets managed, development of surveillance indicators for marine ecosystems must go hand in hand with and enhance implementation of these societal aspirations. Increased participation of fishers and other industry stakeholders is also a necessary and desirable objective in the process to achieve sustainable management. Continued failure to address these problems will incur greater environmental and socioeconomic risk and costs in the near future (*52*, *57*).

Finally, numerous new ecological surprises have emerged in the last two decades that will further hinder progress toward achieving our goals. Ocean acidification, mass coral bleaching, disease outbreaks, invasive species, expanding marine dead zones, and dangerous climate change were not considered serious issues at the previous Earth Summits, although we now know they will increasingly threaten sustainable marine management (*52*, *57*). Emerging ecological challenges such as these provide even greater incentive to avoid empty ocean commitments at Rio+20. The livelihoods of millions, the food security of billions, and the safe functioning of our planet's oceans are at stake.

References and Notes

1. UN Agreement for the Implementation of the Provisions of the UN Convention on the Law of the Sea of 10 December 1982 relating to the Conservation and Management of Straddling Fish Stocks and Highly Migratory Fish Stocks (UNFSA).
2. A number of other commitments have been made through different international political processes, such as the FAO Code of Conduct for Responsible Fisheries; FAO International Plan of Action for Managing Fishing Capacity; FAO International Plan of Action for the Conservation and Management of Sharks; FAO International Plan of Action to Prevent, Deter, and Eliminate Illegal, Unreported and Unregulated Fishing; FAO International Plan of Action for Reducing Incidental Catch of Seabirds in Longline Fisheries; UN Millennium Development Goals (MDGs); and CBD.
3. FAO, *The State of the World Fisheries and Aquaculture 2010* (FAO, Rome, 2010).
4. J. A. Anticamara, R. Watson, A. Gelchu, D. Pauly, *Fish. Res.* **107**, 131 (2011).
5. E. Chassot *et al.*, *Ecol. Lett.* **13**, 495 (2010).
6. Y. Ye, K. L. Cochrane, in *Review of the State of Marine Fishery Resources* (FAO Fisheries and Aquaculture Department, Rome, 2011), pp. 3–18.
7. Also disturbing is the growing consensus among fisheries scientists that the MSY bar was set too low and that the exploitation rate that achieves MSY should be seen as an upper limit rather than a management target, lending more support to the general need to reduce exploitation levels.
8. R. Froese, A. Proelß, *Fish Fish.* **11**, 194 (2010).
9. Y. Ye *et al.*, *Fish Fish.* 10.0000/j.1467-2979.2012.00460.x (2012).
10. R. Hilborn, *Ecosystems (N. Y.)* **10**, 1362 (2007).
11. B. Worm *et al.*, *Science* **325**, 578 (2009).
12. S. M. Garcia, K. L. Cochrane, *ICES J. Mar. Sci.* **62**, 311 (2005).
13. H. Tallis *et al.*, *Mar. Policy* **34**, 340 (2010).
14. J. Rice, *Mar. Ecol. Prog. Ser.* **300**, 265 (2005).
15. M. Ruckelshaus, T. Klinger, N. Knowlton, D. P. DeMaster, *Bioscience* **58**, 53 (2008).
16. E. J. Techera, N. Klein, *Mar. Policy* **35**, 73 (2011).
17. S. L. Ellis *et al.*, *PLoS ONE* **6**, e18997 (2011).
18. S. Jennings, J. Rice, *Fish Fish.* **12**, 125 (2011).
19. U. R. Sumaila *et al.*, *J. Bioeconomics* **12**, 201 (2010).
20. U. R. Sumaila, *Nature* **481**, 265 (2012).
21. FAO–UN Environment Programme (UNEP) *Report of the FAO/UNEP Expert Meeting on Impacts of Destructive Fishing Practices, Unsustainable Fishing, and Illegal, Unreported and Unregulated Fishing on Marine Biodiversity and Habitats* (FAO Fisheries and Aquaculture, FAO, Rome, 2010).
22. MRAG–Fisheries Ecosystem Restoration Research (FERR), *The Global Extent of Illegal Fishing* (MRAG Ltd. and FERR, University of British Columbia Fisheries Centre, Vancouver 2008).
23. S. Flothmann *et al.*, *Science* **328**, 1235 (2010).
24. D. J. Agnew *et al.*, *PLoS ONE* **4**, e4570 (2009).
25. D. Pauly, R. Froese, *Mar. Policy* **36**, 746 (2012).
26. Agreement on Port State Measures to Prevent, Deter and Eliminate Illegal, Unreported and Unregulated Fishing, www.fao.org/Legal/treaties/037s-e.htm
27. A. Fabra, V. Gascón, M. Marrero, S. Lieberman, K. Sack, *Closing the Gap: Comparing Tuna RFMO Port State Measures with the FAO Agreement on Port State Measures* (Pew Environment Group, Philadelphia, 2011).
28. Human Development Report Office, UN Development Programme (UNDP), Sub-saharan Africa—The human costs of the 2015 'business-as-usual' scenario (Human Development Report Office, UNDP, New York, 2005).
29. C. Toropova, I. Meliane, D. Laffoley, E. Matthews, M. Spalding, Eds., *Global Ocean Protection: Present Status and Future Possibilities* [Agence des aires marines protegees, Brest, France; IUCN, Gland, Switzerland; IUCN World Commission on Protected Areas, Washington DC and New York, USA; UNEP–World Conservation Monitoring Center (WCMC), Cambridge, UK; The Nature Conservancy, Arlington, VA; United Nations University, Tokyo, Japan; World Conversation Society, New York, 2010].
30. H. E. Fox *et al.*, *Conserv. Lett.* **5**, 1 (2012).
31. G. R. Russ, A. C. Alcala, *Ecol. Appl.* **21**, 241 (2011).
32. IUCN, UNEP-WCMC, *The World Database on Protected Areas* (UNEP-WCMC, Cambridge, 2011).
33. L. Burke, K. Reytar, M. Spalding, C. Perrings, Eds., *Reefs at Risk: Revisited* (World Resources Institute, Washington, DC, 2011).
34. B. C. O'Leary *et al.*, *Mar. Policy* **36**, 598 (2012).
35. C. J. Edgar, *Aquat. Conserv. Marine Freshw. Ecosys.* **21**, 313 (2011).
36. IUCN, Global Marine Species Assessment project; http://sci.odu.edu/gmsa/.
37. L. McClenachan, A. B. Cooper, K. E. Carpenter, N. K. Dulvy, *Conserv. Lett.* **5**, 73 (2012).
38. Coordinated through the Agreement on the Conservation of Albatrosses and Petrels program.
39. L. S. Bull, *Fish Fish.* **10**, 408 (2009).
40. J. P. Croxall, *Bird Conserv. Int.* **18**, (S1), S13 (2008).
41. O. R. J. Anderson *et al.*, *Endanger. Species Res.* **14**, 91 (2011).
42. J. P. Croxall *et al.*, *Bird Conserv. Int.* **22**, 1 (2012).
43. IUCN, Red List Version 2011.2. (IUCN, Gland, Switzerland, 2011).
44. S. H. M. Butchart *et al.*, *Science* **328**, 1164 (2010).
45. G. M. Mace *et al.*, *Curr. Opin. Environ. Sustain.* **2**, 3 (2010).
46. R. H. Thurstan, S. Brockington, C. M. Roberts, *Nature Commun.* **1**, 1 (2010).
47. UN General Assembly (UNGA), Actions taken by States and regional fisheries management organizations and arrangements to give effect to paragraphs 83 to 90 of General Assembly resolution 61/105 on sustainable fisheries, including through the 1995 Agreement for the Implementation of the Provisions of the UN Convention on the Law of the Sea of 10 December 1982 relating to the Conservation and Management of Straddling Fish Stocks and Highly Migratory Fish Stocks, and related instruments (64th Session of UNGA, A/64/305, 2009).
48. UNGA, Actions taken by States and regional fisheries management organizations and arrangements in response to paragraphs 80 and 83 to 87 of General Assembly resolution 61/105 and paragraphs 113 to 117 and 119 to 127 of General Assembly resolution 64/72 on sustainable fisheries, addressing the impacts of bottom fishing on vulnerable marine ecosystems and the long-term sustainability of deep-sea fish stocks (66th Session of UNGA, A/66/307, 2011).
49. O. K. L. Drammeh, in *Illegal, Unreported and Unregulated Fishing in Small Scale Marine and Inland Capture Fisheries* (FAO, Rome, 2000), pp. 135–144.
50. Many conservation organizations and governments are calling for negotiation of a new implementing agreement under UNCLOS for the protection and conservation of high seas biodiversity. In December 2011, the UN GA, through its annual Oceans Omnibus Resolution, endorsed progress on this issue, and a number of governments are working to ensure progress on this agreement at Rio+20.
51. A. D. Rogers, M. Gianni, *The Implementation of UNGA Resolutions 61/105 and 64/72 in the Management of Deep-Sea Fisheries on the High Seas: Report Prepared for the Deep-Sea Conservation Coalition, International Programme on the State of the Ocean (IPSO)* (IPSO, London, 2010).
52. A. D. Rogers, D. A. Laffoley, *International Earth System Expert Workshop on Ocean Stresses and Impacts: Summary Report* (IPSO, Oxford, 2011).
53. B. Cicin-Sain, M. Balgos, J. Appiott, K. Wowk, G. Hamon, *Oceans at Rio+20: How Well Are We Doing in Meeting the Commitments from the 1992 Earth Summit and the 2002 World Summit on Sustainable Development? Summary for Decision Makers* (Global Ocean Forum, University of Delaware, Newark, DE, 2011).
54. Intergovernmental Oceanographic Commission of UNESCO (IOC-UNESCO), International Marine Organization, FAO, UNDP, *A Blueprint for Ocean and Coastal Sustainability* (IOC-UNESCO, Paris, 2011).
55. Pew Environment Group, *Rio+20: Time to Turn Back the Tide* (Pew Environment Group, Philadelphia, 2011).
56. U. R. Sumaila *et al.*, in *Green Economy Report* (UNEP, 2011), chap. 3; www.unep.org/greeneconomy
57. C. M. Roberts, *Ocean of Life: How Our Seas Are Changing* (Allen Lane, London, 2012).

Acknowledgments: We thank L. McRae and three anonymous reviewers for thoughtful and constructive input and acknowledge the support of all our institutions and funders including Selfridges' Project Ocean, the Natural Science and Engineering Research Council of Canada, and the Pew Charitable Trusts.

10.1126/science.1223009

PHYSIOLOGY

COX-2 Inhibitors and Cardiovascular Risk

The vascular location of an enzyme accounts for the cardiovascular hazards associated with its inhibition.

Christopher P. Cannon[1] and Paul J. Cannon[2]

Nonsteroidal anti-inflammatory drugs (NSAIDs) are used by millions of people worldwide to reduce pain and inflammation. They exert their pharmacologic effect by inhibiting the cyclooxygenase-1 (COX-1) and COX-2 enzymes, thereby blocking conversion of arachidonic acid to prostaglandin E_2 (PGE_2) and PGI_2 (prostacyclin), which mediate pain (see the figure). However, because COX enzymes exist throughout the body, NSAIDs have many physiological effects, including complications, such as development of gastric ulcers and gastrointestinal bleeding. In 2004, the blockbuster drug rofecoxib (sold commercially as Vioxx) was withdrawn from the U.S. market when a study linked a selective COX-2 inhibitor with a higher rate of heart attack and stroke. However, studies on COX inhibitors have shown varying risk profiles, fueling a debate about their association with cardiovascular risk. A recent study by Yu *et al.* (*1*) now provides a biochemical explanation for the increased cardiovascular risk associated with COX-2 inhibitors, closing this part of the long-standing discussion.

COX enzymes convert arachidonic acid to prostaglandins in the gastric lining, where they protect the gastric mucosa, and in vascular endothelial and smooth muscle cells of blood vessels, where they lead to vasodilation and inhibition of platelet aggregation. In platelets, prostaglandins are further converted by thromboxane synthase to thromboxane A_2 (TxA_2) which, when released, stimulates platelet aggregation and vasoconstriction (*2*). However, because pain and inflammation are mediated by COX-2, and gastric protection by COX-1, COX-2 selective inhibitors can avoid the gastrointestinal complications of nonselective NSAIDs (which inhibit both COX-1 and COX-2), while still reducing pain and inflammation. Several COX-2 inhibitors (e.g., celecoxib, rofecoxib, etoricoxib) were developed and approved for clinical use in some countries.

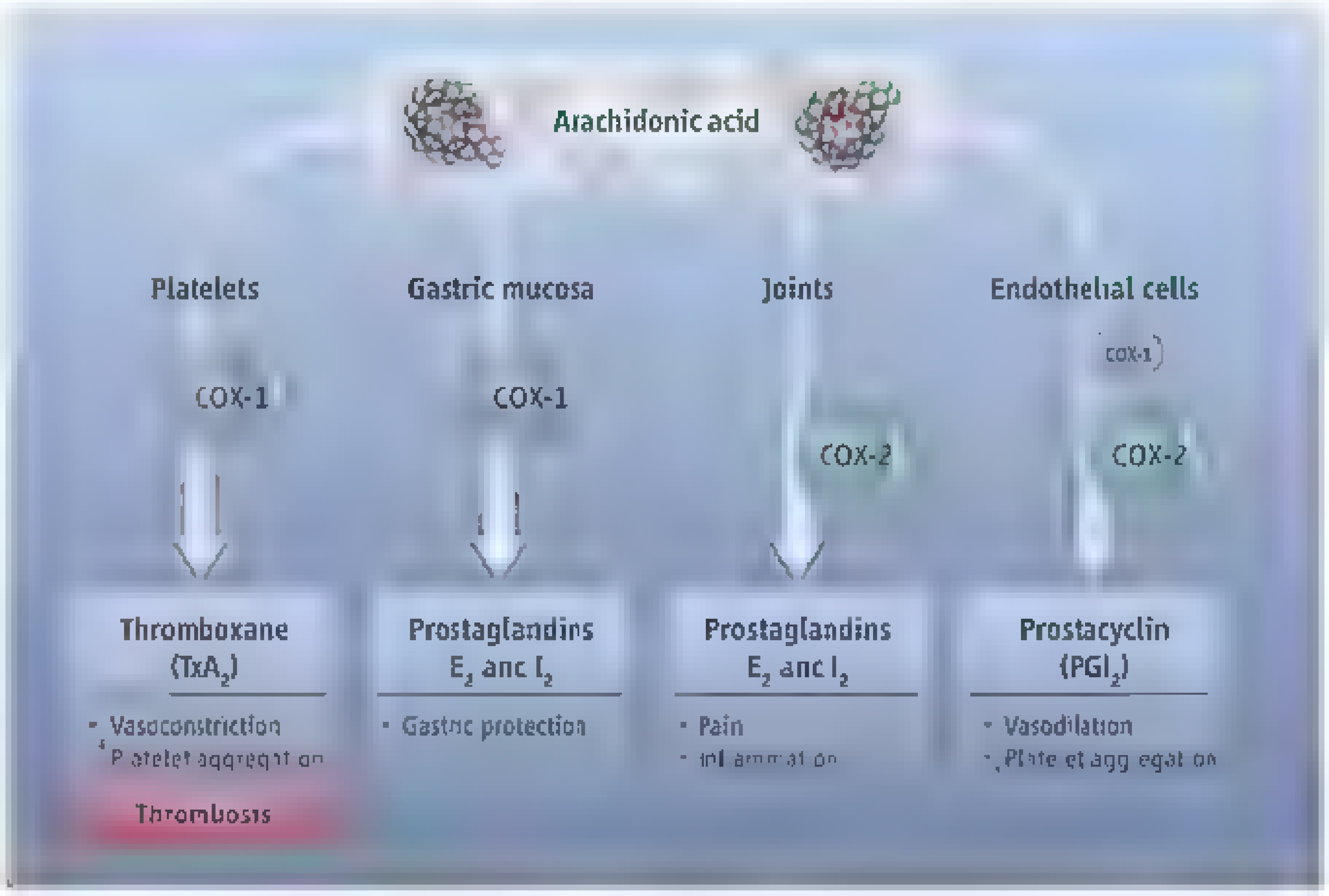

COX enzyme effects. COX-1 and COX-2 enzymes convert arachidonic acid to various prostanoids in different tissues. Inhibition of COX-2 reduces pain and inflammation but also blocks the vasodilatory and antiplatelet effects in the vascular wall. Blocking COX-1 reduces the risk of thrombosis, but also inhibits the gastroprotective effects of PGE_2 and PGI_2, thereby predisposing to gastric ulcers and bleeding.

Trials have shown equal pain efficacy and reduced gastrointestinal complications (*3*, *4*).

However, large clinical studies identified an increased risk of developing cardiovascular conditions, including myocardial infarction and stroke, with the use of selective COX-2 inhibitors (*3*–*7*). One of these studies found that the COX-2 inhibitor rofecoxib had a higher rate of cardiovascular events than the older nonselective NSAID (naproxen) (*3*). Subsequent studies similarly reported a higher risk with the COX-2–selective agent celecoxib (*6*, *7*). No large trials with a placebo comparator were available for older nonselective NSAIDs; however, observational studies have found higher risks of cardiovascular events with all such agents, with the exception of naproxen (*8*). One large randomized trial directly comparing selective and nonselective NSAIDs demonstrated a similar risk profile for the COX-2–selective agent etoricoxib and the traditional NSAID diclofenac, reporting nearly identical rates of thrombotic cardiovascular events (*9*). In addition, higher rates of hypertension and heart failure were seen with all NSAIDS.

A mechanistic explanation has been long sought to explain these observations. NSAIDs and COX-2 inhibitors were found to decrease production of PGI_2, as measured by its urinary metabolite 2,3-dinor-6-keto $PGF_1\alpha$ (PGI-M) in humans (*10*, *11*). But the source of the PGI_2 (whether vascular cells or other tissue in the body) was unclear. Because PGI_2 prevents platelet aggregation and vasoconstriction, Yu *et al.* postulated a balance between vasoconstriction and vasodilation in the vascular system. On one hand, TxA_2 formed in platelets can lead to vasoconstriction and platelet aggregation. This is offset by the production of PGI_2, which restrains platelet activation and promotes vasodilation. Inhibiting PGI_2 and PGE_2 in the blood vessel wall by COX-2–selective agents, without the concomitant inhibition of TxA_2, could promote hypertension and thrombosis, and increase cardiovascular risk.

Yu *et al.* provide evidence supporting and expanding upon this hypothesis. In a mouse model (*1*), they demonstrate that deletion of the gene encoding COX-2 in vascular

[1]Thrombolysis in Myocardial Infarction Study Group, Cardiovascular Division, Brigham and Women's Hospital, Harvard Medical School, 75 Francis Street, Boston, MA 02115, USA. [2]Columbia Presbyterian Medical Center, Division of Cardiology, New York, NY 10032, USA. E-mail: cpcannon@partners.org

CREDIT: C. BICKEL/SCIENCE

smooth muscle cells and vascular endothelial cells lowered the urinary excretion of the PGI_2 metabolite and predisposed to the development of thrombosis and hypertension. Furthermore, deletion of *COX2* gene in vascular endothelial cells and vascular smooth muscle cells decreased the synthesis and release of nitric oxide (NO), a powerful vasodilator, thereby reducing vascular relaxation. This was accompanied by a heightened predisposition toward both hypertension and thrombosis. Thus, by genetically engineering mice that lack COX-2 in the vasculature, Yu *et al.* show that the mechanism of increased cardiovascular risk from COX inhibition results from specifically blocking COX-2 in the blood vessels and not from other tissues in the body.

The implications of the work by Yu *et al.* are that the increased cardiovascular risk is not an individual drug side effect but is rather a direct pharmacologic consequence of inhibition of COX-2. Furthermore, these risks apply to all COX-2 inhibitors—both selective and nonselective NSAIDs (*3*–*9*) [Naproxen is the only NSAID that has not shown increased cardiovascular risk, likely due to its sustained inhibition of COX-1, which provides an antiplatelet effect (*12*).] The findings of Yu *et al.* thus support the clinical advice from the American Heart Association, which recommends minimizing the dose and duration of NSAIDS as much as possible, as a means of reducing the cardiovascular risk associated with COX-2 inhibition (*13*).

References

1. Y. Yu *et al.*, *Sci. Transl. Med.* **4**, 132ra54 (2012).
2. Y. Cheng *et al.*, *Science* **296**, 539 (2002).
3. C. Bombardier *et al.*, *N. Engl. J. Med.* **343**, 1520, 2, 1528 (2000).
4. R. S. Bresalier *et al.*, *N. Engl. J. Med.* **352**, 1092 (2005).
5. D. Mukherjee, S. E. Nissen, E. J. Topol, *JAMA* **286**, 954 (2001).
6. M. M. Bertagnolli *et al.*, *N. Engl. J. Med.* **355**, 873 (2006).
7. S. D. Solomon *et al.*, *Circulation* **117**, 2104 (2008).
8. L. A. García Rodríguez, A. González-Pérez, *BMC Med.* **3**, 17 (2005).
9. C. P. Cannon *et al.*, *Lancet* **368**, 1771 (2006).
10. B. F. McAdam *et al.*, *Proc. Natl. Acad. Sci. U.S.A.* **96**, 272 (1999).
11. F. Catella-Lawson *et al.*, *J. Pharmacol. Exp. Ther.* **289**, 735 (1999).
12. T. Grosser, S. Fries, G. A. FitzGerald, *J. Clin. Invest.* **116**, 4 (2006).
13. E. M. Antman *et al.*, *Circulation* **115**, 1634 (2007).

10.1126/science.1224398

ANTHROPOLOGY

Absolute Dating of Cave Art

Use of uranium-thorium dating shows that cave art in Spain is older than expected.

John Hellstrom

Paleolithic cave art is one of the most striking visual reminders of tens of millennia of human prehistory. Found throughout the world, it is fundamental for understanding the earliest human culture and artistic endeavor. Yet, despite great advances in dating technologies, it remains extremely difficult to determine the age of a thin layer of pigment on a cave or rock shelter wall. Researchers are often limited to reconstructing relative chronology by comparing drawing styles and, where available, creating sometimes tenuous links to other dated human remains or artifacts (*1*, *2*). Mass-spectrometric radiocarbon dating has arguably been the most successful technique for dating cave art, in the rare cases where it is possible to directly date charcoal or other pigments containing carbon (*2*). On page 1409 of this issue, Pike *et al.* report an ambitious study of paleolithic cave art sites from Spain in which they have applied the previously underused uranium-thorium (U-Th) dating method (*3*).

U-Th dating measures the ingrowth of radioactive thorium-230 in a geological or biogenic material, through decay of uranium incorporated within it at its time of formation. When it was first applied almost 50 years ago, this technique required samples of 100 g or more in the case of cave formations such as those now dated by Pike *et al.* In 1987, Edwards *et al.* showed that U-Th dating could be conducted by mass spectrometric analysis (*4*). Through this and subsequent advances, the efficiency of measurement has increased by more than four orders of magnitude, enabling hypersensitive techniques like that used by Pike *et al.* to operate on milligrams of such material (*5*, *6*) (see the figure).

Cave art is typically found in carbonate terrains, where the majority of caves have developed worldwide. The stalagmites, stalactites, and similar formations that grow in such caves, collectively known as speleothems, all contain trace amounts of uranium and are thus amenable to U-Th dating. Very thin sheets or drapes of this material can sometimes be found grown over the top of Paleolithic cave art, and in some cases may also underlie or even sandwich it (*7*, *8*).

U-Th sampling of calcite overgrowths. Since U-Th dating was first introduced in the 1960s, sample size requirements have fallen continually. Large jumps in efficiency occurred with the introduction of mass spectrometric analysis and with advances in mass spectrometric technology and can now often lead to sample sizes of less than 10 mg, or 4 mm^3. As shown by Pike *et al.*, a 1 mm-thick speleothem from overlying a cave art panel can now be dated by removing a few square millimeters of overgrowth, minimizing impact on the artwork.

School of Earth Sciences, The University of Melbourne, VIC 3010 Australia. E-mail: j.hellstrom@unimelb.edu.au

As long as large amounts of material were required for dating, its sampling could only be condoned in very rare circumstances. The greatly reduced sample size required for analysis allows subtle removal of small volumes of speleothem directly associated with cave art, from which precise absolute ages may be determined.

Coatings of speleothem calcite do not directly date the cave art itself, but give robust and reliable determinations of the minimum age for the underlying art. Any one calcite overgrowth has a relatively low probability of approaching the age of the underlying art. Studies of overlying calcite layers that consider a small number of examples of cave art in isolation may therefore return ages that do not advance understanding of the age of that art (*2*). By undertaking a broad regional study of many examples of cave art, Pike *et al.* have transcended this problem. The scope of their study has allowed them to unambiguously identify a number of examples that challenge and overturn the previous understanding of that art's origin. In particular, 3 of the 50 examples dated show art to have been created in Spain at around (or indeed possibly before) the time of the arrival of modern humans, bringing current ideas of the prehistory of human art in southern Europe into question.

U-Th dating, particularly of speleothems, has mostly been used to reconstruct climatic change over the past several hundreds of thousands of years (*9*, *10*). The techniques developed for this field now allow archaeological applications to be revisited. Human remains, artifacts, and other evidence of habitation are sometimes coated with calcium carbonate coatings and may thus be dated in the same way as the cave art of Pike *et al.*'s study. Sample material can be collected using micromachining strategies developed for high-resolution climate change chronologies (*6*, *11*), such that growth intervals and durations may be determined, even within a single thin film of carbonate. Other applications include the dating of cave sediments (and any archaeological horizons that they contain) using fragile incorporated fragments of soda straw stalactites (*12*).

All geochronological technologies available for dating prehistorical remains have improved greatly over recent decades. In the case of particularly important or irreplaceable human artifacts, a question has been whether to attempt to date them with available technologies or to wait until less destructive capabilities become available. U-Th dating has become more than 10,000 times more efficient since its invention, and in the case of the technique used by Pike *et al.*, there is little room for further spectacular gains. Now allowing cave art and other human artifacts found in caves to be dated based on a few milligrams of speleothem calcite, the U-Th technique can be considered mature enough for widespread use in this field.

Pike *et al.*'s findings push the earliest evidence of cave art in Europe back by several thousand years to at least 40,800 years before the present and raise the question of whether such art was the exclusive domain of modern humans. Further large-scale U-Th studies of cave art in Europe and elsewhere may prove similarly illuminating.

References

1. M. Aubert, *J. Archaeol. Sci.* **39**, 573 (2012).
2. P. Pettitt, A. Pike, *J. Archaeol. Method Theory* **14**, 27 (2007).
3. A. W. G. Pike *et al.*, *Science* **336**, 1409 (2012).
4. R. L. Edwards, J. H. Chen, G. J. Wasserburg, *Earth Planet. Sci. Lett.* **81**, 175 (1987).
5. J. Hellstrom, *J. Anal. At. Spectrom.* **18**, 1346 (2003).
6. D. L. Hoffmann, C. Spötl, A. Mangini, *Chem. Geol.* **259**, 253 (2009).
7. P. S. C. Taçon *et al.*, *J. Archaeol. Sci.* **39**, 492 (2012).
8. A. W. G. Pike *et al.*, *J. Archaeol. Sci.* **32**, 1649 (2005).
9. H. Cheng *et al.*, *Science* **326**, 248 (2009).
10. R. N. Drysdale *et al.*, *Science* **325**, 1527 (2009).
11. R. N. Drysdale *et al.*, *Geology* **35**, 77 (2007).
12. E. St Pierre, J.-X. Zhao, Y.-X. Feng, E. Reed, *J. Archaeol. Sci.* **39**, 922 (2012).

10.1126/science.1224185

CANCER

Cancer and Telomeres— An ALTernative to Telomerase

Finding ways to target the alternative (ALT) telomere lengthening pathway found in some cancer cells could complement telomerase inhibitors currently in clinical trials

Jerry W. Shay,[1] Roger R. Reddel,[2] Woodring E. Wright[1]

To grow indefinitely, human cancer cells must counteract the progressive loss of telomeric DNA that universally accompanies cell division. To do this, about 85 to 90% of cancers use telomerase (*1*–*3*), an enzyme that synthesizes the tandem 5′-TTAGGG-3′ hexanucleotide repeats of telomeric DNA by reverse transcription using its own RNA subunit as a template. Because telomerase is not expressed in most normal human cells, telomerase inhibition is considered an almost universal oncology target, and several clinical trials are under way (*4*). However, the future success of inhibiting telomerase to treat cancer is far from assured. Indeed, ~10 to 15% of human cancers lack detectable telomerase activity (*3*), and many of these use an alternative lengthening of telomeres (ALT) mechanism (*5*). These ALT-expressing tumors would not be expected to respond to anti-telomerase therapies, and telomerase-expressing tumors could become resistant by switching to an ALT mechanism, as has recently been shown in mice (*6*). Here we present a brief history of ALT research, outline what is left to learn about the pathway, and propose it as a valuable drug target both alone and in combination with telomerase as a dual-targeted anticancer strategy.

Because of the semiconservative mechanism whereby DNA is replicated, all cellular proliferation is accompanied by progressive telomere shortening. When telomeres become short, they elicit a DNA damage response that leads to the irreversible cell cycle arrest known as replicative senescence, which is a potent anticancer protection mechanism (*7*). Occasionally human cells acquire mutations that permit bypass of senescence to prolong proliferation. This results in telomeres that are so short that chromosome ends fuse together, leading to increased genomic instability, aneuploidy, and cell death. Rarely, the ensuing genomic changes result in engagement of a telomere maintenance mechanism (telomerase or ALT) and therefore unlimited proliferative potential, which contributes indirectly to the development of cancer (*7*).

In 1993 it was reported that yeast cells that survive deletion of telomerase activ-

[1]Department of Cell Biology, University of Texas Southwestern Medical Center, Dallas, TX 75390, USA and CEGMR, KAU, Jeddah, Saudi Arabia. [2]Cancer Research Unit, Children's Medical Research Institute, Westmead, NSW 2145 and Sydney Medical School, University of Sydney, NSW 2006, Australia. E-mail: jerry.shay@utsouthwestern.edu

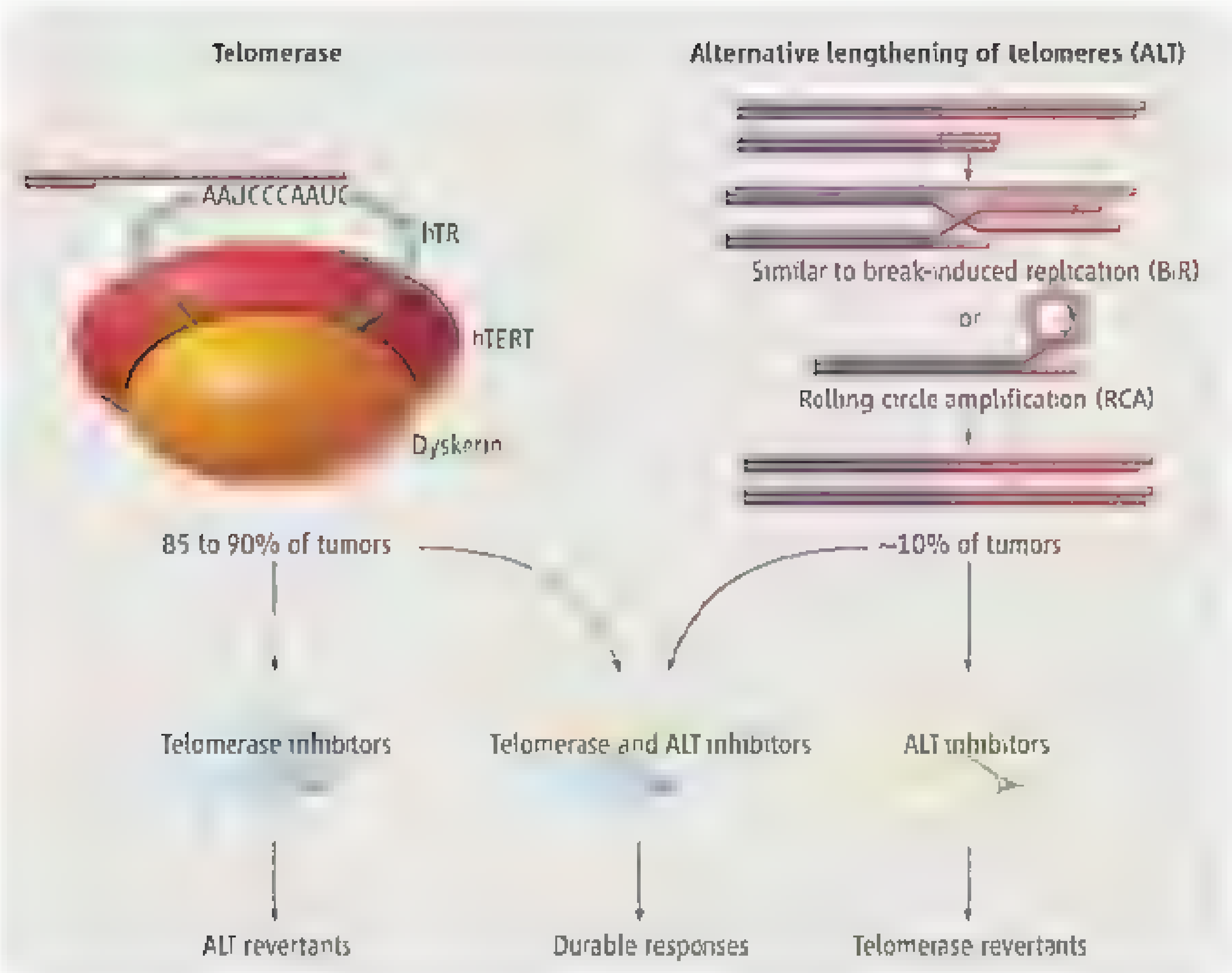

Telomerase and ALT In cancer cells, telomeres (red) may be lengthened by telomerase, which reverse transcribes the template region of its RNA subunit (hTR), or by ALT, in which a telomeric DNA template is copied. The template may be the telomere of a nonhomologous chromosome, or it could include extrachromosomal telomeric DNA in circular (illustrated) or linear form, another region of the same telomere via loop formation, or the telomere of a sister chromatid (*11*). A combination of telomerase and ALT inhibitors is predicted to be an effective strategy for treating cancer.

ity are dependent on genes required for homologous recombination (*8*). In the following year, a small subset of human primary tumors (*2*) and immortalized cell lines (*2*, *9*) was found to be telomerase-negative. Based on the yeast cell findings that telomere length can be maintained in the absence of telomerase, it was deduced that one or more alternative, telomerase-independent mechanisms exist in human cells (*10*). ALT involves copying of a telomeric template DNA via homologous recombination (see the figure). Cells that use ALT to overcome telomere shortening have many unusual characteristics (*5*, *10*, *11*), such as highly heterogeneous telomere lengths and abundant extrachromosomal telomeric DNA. Although we are beginning to understand some of the molecular details of ALT, there has not been any progress in developing anticancer therapeutics targeting the pathway. Moreover, the possibility of more than one ALT mechanism in human cells has not yet been ruled out.

ALT occurs in a wide range of tumor types, and is a common telomere-lengthening mechanism in tumors such as osteosarcomas, undifferentiated pleomorphic sarcomas, leiomyosarcomas, astrocytic tumors grades 2 and 3, and pancreatic neuroendocrine tumors (*11*, *12*). The clinical consequences of ALT require more detailed study, but appear to be highly dependent on tumor type, with a notably worse outcome for individuals who have ALT-positive liposarcomas and a better outcome for adults with ALT-positive glioblastoma multiforme (*11*). Presumably, the prognosis is dictated by the sum total of genetic changes associated with activation of ALT in a particular tumor type, rather than the telomere-lengthening mechanism alone. Future work will require the development of simple blood tests, such as the C-circle assay (*13*), to identify ALT-expressing cancers to better determine the prognostic value of ALT in a variety of cancers.

ALT is relatively rare in the most common types of cancers, carcinomas, which are derived from epithelia. One reason could be that some highly proliferative epithelial tissues normally express regulated levels of telomerase, which partially compensates for telomere shortening to permit the cellular proliferation required over a human lifetime. Therefore, during oncogenesis these cells may be more likely to maintain their telomeres by up-regulating telomerase expression than by engaging ALT. However, these cells could still engage ALT if telomerase is inhibited by drugs during cancer therapy.

How is ALT activated in some cancer cells? It was recently observed that ALT-positive pancreatic neuroendocrine tumors and tumors of the central nervous system have mutations in or lose normal expression of the ATRX or DAXX proteins, and/or histone H3.3 (*14*, *15*). Because ATRX and DAXX act together to deposit H3.3 and remodel telomeric chromatin, it was proposed that this may block telomeric recombination and repress ALT, and that loss of function of these three proteins contributes to derepression of ALT (*14*, *15*). It will be important to determine whether these changes are sufficient for activation of ALT or whether additional changes are required.

Telomerase is expressed in the great majority of malignant tumors (*2*, *3*) and thus holds great promise as a critical and cancer cell specific drug target. Indeed, there are several telomerase therapies in clinical trials, all of which are effective in the preclinical setting. These include the enzymatic activity inhibitor imetelstat (non–small cell lung cancer, multiple myeloma, and breast cancer, phase 2); an immunotherapy targeting telomerase epitopes expressed only on cancer cells (pancreatic cancer, phase 3); and a virotherapy that includes the hTERT promoter regulating critical adenoviral genes and thus only kills telomerase-positive cells (*4*). However, as with any targeted cancer therapy, the development of resistance is a potential threat, and malignancies that initially have only telomerase activity (i.e., the great majority) could become resistant to telomerase inhibitors by activating the ALT mechanism. In vitro experiments suggest that this is relatively uncommon, but the likelihood of resistance by this mechanism cannot be dismissed because the number of cells in typical cell culture experiments is many orders of magnitude lower than in clinically important tumors. In support of this conclusion, telomerase-positive T cell lymphomas arising in mice engineered to have telomeres of limiting length and from which telomerase activation was subsequently withdrawn entered a period of slow growth and then emerged with features of ALT (*6*). Another factor that will complicate treatment with telomerase inhibitors is that some tumors may have both telomerase and ALT activity (*5*, *11*). This is at least in part due to intratumoral heterogeneity, and whether both telomere-lengthening mechanisms are sometimes spontaneously activated within the same cells is unknown. Continued growth of ALT-positive cells would likely make these tumors rapidly resistant to telomerase inhibitors.

While there continues to be high enthusiasm for developing better telomerase inhibitors, there appears to be less interest in academia and industry for targeting ALT. This is perhaps because it is much less common, and there is limited information about activation of ALT in telomerase-positive cancer cells treated with telomerase inhibitors (*16*). As more studies focus on the molecular details of ALT and the mechanism(s) involved in its engagement, specific molecular targets and vulnerabilities may be identified that lead to the development of ALT inhibitors. These, similar to telomerase inhibitors, could be effective targeted therapies for specific cancer subtypes. Strategies combining inhibitors of both telomerase and ALT may then prove to be the most powerful and durable anticancer approach (see the figure).

References

1. C. W. Greider, E. H. Blackburn, *Cell* **43**, 405 (1985).
2. N.-W. Kim *et al.*, *Science* **266**, 2011 (1994).
3. J. W. Shay, S. Bacchetti, *Eur. J. Cancer* **33**, 787 (1997).
4. M. M. Ouellette, W. E. Wright, J. W. Shay, *J. Cell. Mol. Med.* **15**, 1433 (2011).
5. T. M. Bryan, A. Englezou, L. Dalla-Pozza, M. A. Dunham, R. R. Reddel, *Nat. Med.* **3**, 1271 (1997).
6. J. Hu *et al.*, *Cell* **148**, 651 (2012).
7. J. W. Shay, W. E. Wright, *Carcinogenesis* **26**, 867 (2005).
8. V. Lundblad, E. H. Blackburn, *Cell* **73**, 347 (1993).
9. J. P. Murnane, L. Sabatier, B. A. Marder, W. F. Morgan, *EMBO J.* **13**, 4953 (1994).
10. T. M. Bryan, A. Englezou, J. Gupta, S. Bacchetti, R. R. Reddel, *EMBO J.* **14**, 4240 (1995).
11. J. D. Henson, R. R. Reddel, *FEBS Lett.* **584**, 3800 (2010).
12. C. M. Heaphy *et al.*, *Am. J. Pathol.* **179**, 1608 (2011).
13. J. D. Henson *et al.*, *Nat. Biotechnol.* **27**, 1181 (2009).
14. C. M. Heaphy *et al.*, *Science* **333**, 425 (2011).
15. J. Schwartzentruber *et al.*, *Nature* **482**, 226 (2012).
16. O. E. Bechter, Y. Zou, W. Walker, W. E. Wright, J. W. Shay, *Cancer Res.* **64**, 3444 (2004).

10.1126/science.1222394

PLANETARY SCIENCE

Fragments of the Lunar Cataclysm

Meteorite samples returned from the Moon may reveal processes involved in the evolution of the early solar system.

Alan E. Rubin

The flux of extraterrestrial materials impacting the Earth is not representative of potential source bodies in the solar system. Except for the Moon and Mars, chunks of planets and moons are absent from our meteorite collections. And aside from tiny interplanetary dust particles, comets are also missing; they strike Earth at high relative velocities and do not leave identifiable remains. Although asteroidal fragments face a less harrowing journey to Earth, they have to endure launch from their parent body by hypervelocity collisions, impacts by micrometeorites in interplanetary space, and frictional stresses involved in passing through Earth's atmosphere. Major collisions on asteroids are stochastic events; for example, an asteroid-shattering impact 470 million years ago on a particular chondritic body (*1*) disgorged a clutch of material so massive that numerous fossil meteorites from that body have been found in Ordovician sedimentary rocks (*2*). The flux of material that reaches the top of Earth's atmosphere is the same as that impacting the lunar surface. Although we cannot identify intact meteoritic debris in terrestrial rocks that are billions of years old, there is a chance that such material would survive on the Moon. On page 1426 in this issue, Joy *et al.* (*3*) identify ancient projectile fragments in Apollo 16 lunar rocks that were consolidated sometime between 3.8 and 3.4 billion years ago (Ga). This time interval corresponds to the tail end of the epoch when large lunar impact basins like Imbrium were being formed (*4*) (see the figure).

Image of an impact. The Imbrium Basin, with a diameter of 1160 km, is the largest basin on the lunar nearside. It was formed by a giant impact event ~3.85 Ga and was subsequently filled with basaltic lava. Image taken by NASA's Lunar Orbiter 4 in 1967.

In the lunar samples examined by Joy *et al.*, projectile material occurs as rare ultramagnesian clasts tens to hundreds of micrometers in size. The clasts are similar in texture and mineralogy to chondrule fragments from primitive carbonaceous chondritic meteorites. The compositions of these clasts differ dramatically from those of the much-more-ferroan Moon rocks; they are also richer in Mg and poorer in Ni than terrestrial igneous rocks, indicating that they are not contaminants introduced during curation and processing.

Meteoritic materials that have been identified in younger lunar soils include carbonaceous chondrites (*5*), enstatite chondrites (*6*), mesosiderites (*7*), and irons (*8*). Although only a handful of samples are involved, their diversity roughly resembles that of modern meteorite falls on Earth. In contrast, the relative uniformity and magnesian compositions of the meteoritic material preserved in the ancient lunar regolith suggest that the flux of materials pelting the Earth and Moon ≥3.4 Ga ago was different from the modern flux.

Many researchers think that this difference was due to some catastrophic event that resulted in a shift of the abundance and types

Institute of Geophysics and Planetary Physics, University of California, Los Angeles, CA 90095–1567, USA. E-mail: aerubin@ucla.edu

CREDIT: NASA

of materials flooding the inner solar system. The fairly sharp cut-off at ~3.8 Ga in the formation of the giant lunar impact basins is often attributed to a lunar cataclysm or late heavy bombardment—a spike between 4.1 and 3.8 Ga ago in the impact rate (*9*, *10*). Such a spike, if it occurred, should also have affected Earth. Indeed, the oldest terrestrial crustal rocks are 3.8 to 4.0 Ga old (*11*), consistent with the hypothesis that older rocks were destroyed during such a bombardment. Several meteorite groups derived from asteroids also have degassing ages that cluster around 3.8 Ga (*12*, *13*), suggesting that the flux of projectiles whizzing around the solar system was higher at that time.

The possible cause of this enhanced flux is addressed in the so-called Nice model; researchers affiliated with the Observatoire de la Côte d'Azur in the French city of Nice advanced a dynamical evolution model of the solar system involving migration of the giant planets (*14*). In this model (and its subsequent refinements), the giant planets were formed relatively close together, and then, due to gravitational perturbations involving the scattering of planetesimals, began to migrate with respect to each other and to the Sun. These movements led to the formation of the Kuiper belt of icy planetesimals (one of the principal reservoirs of comets, located ~30 to 50 astronomical units from the Sun) and to destabilization of the asteroid belt. Collisions increased throughout the solar system; asteroids crashed into one another, large bodies hit the Moon and formed the large basins, and tens of thousands of large bodies struck Earth (*15*) and Mars (*16*). Because the earliest isotopic evidence for life comes from 3.85-billion-year-old terrestrial sedimentary rocks (*17*), it seems plausible that this bombardment also influenced the origin of life on Earth.

The identification of the ultramagnesian clasts in rocks derived from ancient lunar regolith materials by Joy *et al.* may offer the first clues to the identities of these cataclysm-inducing impactors.

References

1. E. V. Korochantseva *et al.*, *Meteorit. Planet. Sci.* **42**, 113 (2007).
2. B. Schmitz, M. Tassinari, B. Peucker-Ehrenbrink, *Earth Planet. Sci. Lett.* **194**, 1 (2001).
3. K. H. Joy *et al.*, *Science* **336**, 1426 (2012); 10.1126/science.1219633.
4. F. Tera, D. D. Papanastassiou, G. J. Wasserburg, *Earth Planet. Sci. Lett.* **22**, 1 (1974).
5. M. E. Zolensky, *Meteorit. Planet. Sci.* **32**, 15 (1997).
6. A. E. Rubin, *Meteorit. Planet. Sci.* **32**, 135 (1997).
7. J. A. Wood, U. B. Marvin, B. N. Powell, J. S. Dickey, *Smithsonian Astrophysical Observatory Special Report* #307 (1970).
8. W. Quaide, T. Bunch, *Proc. Lunar Sci. Conf.* **1**, 711 (1970).
9. T. Kirsten, P. Horn, J. Kiko, *Proc. Lunar Sci. Conf.* **4**, 1757 (1973).
10. G. Ryder, *Eos* **71**, 322 (1990).
11. S. A. Bowring, I. S. Williams, *Contrib. Mineral. Petrol.* **134**, 3 (1999).
12. D. A. Kring, B. A. Cohen, *J. Geophys. Res.* **107**, 4-1 (2002).
13. T. D. Swindle, C. E. Isachsen, J. R. Weirich, D. A. Kring, *Meteorit. Planet. Sci.* **44**, 747 (2009).
14. K. Tsiganis, R. Gomes, A. Morbidelli, H. F. Levison, *Nature* **435**, 459 (2005).
15. W. K. Hartmann, G. Ryder, L. Dones, D. Grinspoon, in *Origin of the Earth and Moon*, R. M. Canup, K. Righter, Eds. (Univ. of Arizona Press, Tucson, 2000), pp. 493–512.
16. G. Turner, S. F. Knott, R. D. Ash, J. D. Gilmour, *Geochim. Cosmochim. Acta* **61**, 3835 (1997).
17. S. J. Mojzsis, T. M. Harrison, *GSA Today* **10**, 1 (2000).

Published online 17 May 2012
10.1126/science.1224184

MOLECULAR BIOLOGY

All Packed Up and Ready to Go

Gene silencing depends on the higher-order structure of heterochromatin as well as repressive biochemical modifications.

Yannick Jacob and Rob Martienssen

In eukaryotes, the two states of chromatin were first distinguished cytologically according to their different levels of condensation. Euchromatin has an open conformation that correlates with an active state of gene expression, whereas the transcriptionally silent heterochromatin is tightly packaged. On page 1448 of this issue, Moissiard *et al.* describe the identification of proteins that are specifically required for the condensed structure of heterochromatin in flowering plants (*1*). And on page 1445 of this issue, Qian *et al.* (*2*) identify a plant protein that binds to biochemically modified DNA and itself modifies histones to generate a chromatin state that allows active DNA demethylation (and gene expression).

Heterochromatin can be facultative or constitutive. Facultative heterochromatin is associated with repressed genes that can be turned on and off during development (*3*). By contrast, constitutive heterochromatin is a more permanent state and is associated with repetitive sequences and transposons that need to be continually silenced to protect the integrity of the genome. Constitutive heterochromatin is readily distinguishable cytologically as densely stained structures characteristic of condensed chromatin. Many epigenetic marks (DNA methylation, histone posttranslational modifications, and histone variants) have now been identified that uniquely localize to constitutive heterochromatin and functionally contribute to its specification (*4*). In terms of chromatin compaction, how do these epigenetic marks make some regions of the chromatin more or less likely to interact and condense to form heterochromatin? Epigenetic marks do this in several ways, such as by affecting the physical properties of the chromatin (*3*) and by serving as signals for the recruitment of chromatin-remodeling proteins (*5*).

Through a screen for genes required to suppress the activity of a promoter containing tandem repeats, Moissiard *et al.* have found two homologous proteins that are involved in heterochromatin condensation and transposon silencing in the model plant *Arabidopsis thaliana*. AtMORC1 [also called COMPROMISED RECOGNITION OF TCV-1 (CRT1)] and AtMORC6 [also called CRT1 HOMOLOG-6 (CRH6)/DEFECTIVE IN MERISTEM SILENCING 11 (DMS11)] both contain a GHKL (gyrase, Hsp90, histidine kinase, MutL)–type adenosine triphosphatase (ATPase) domain. Eukaryotic proteins containing this domain were hypothesized to be involved in large-scale chromatin remodeling through detection of epigenetic marks (*6*). This information implies that heterochromatin decondensation is likely to be the primary defect in *atmorc1* and *atmorc6* mutant plants, and that transcriptional reactivation of transposons can be construed as a secondary effect of the loss of heterochromatin structure. Moissiard *et al.* found support for this idea by applying chromatin conformation capture technology, which indicated that close interactions within condensed heterochromatic regions were disrupted in the mutants. Future work will focus on the subsequent interactions with euchromatin in *atmorc1* and *atmorc6* mutant plants.

Interestingly, Moissiard *et al.* show that

Cold Spring Harbor Laboratory, Cold Spring Harbor, NY 11724, USA. E-mail: martiens@cshl.edu

two repressive epigenetic marks—histone H3 lysine 9 dimethylation (H3K9me2) and DNA methylation—are maintained genome-wide in *atmorc1* and *atmorc6* mutants. This is an important finding, as it suggests that the process of compacting heterochromatin is directly responsible for the loss of gene silencing. It is possible, therefore, that AtMORC1 and AtMORC6 function downstream of H3K9me2 and DNA methylation, but they must be recruited to heterochromatin indirectly, as these proteins do not contain known methylation binding domains. Both *atmorc1* and *atmorc6* single and double mutants have near-identical phenotypes, suggesting that they both function in the same pathway (see the figure), but their impact on the silencing of transposons is relatively modest relative to mutants of the genes coding for the chromatin remodeler DECREASE IN DNA METHYLATION 1 (DDM1) and the maintenance DNA methyltransferase MET1, which also lose heterochromatin condensation (*7*).

In an independent study, Lorković *et al.* found that a mutation in *AtMORC6* impairs RNA-directed DNA methylation by partially affecting DNA methylation in the CHH (where H is A, C, or T) sequence context—a hallmark of this pathway in plants (*8*). Thus, AtMORC6 might have local effects on DNA methylation, and in support, Lorković *et al.* show that AtMORC6 interacts with DEFECTIVE IN MERISTEM SILENCING 3 (DMS3) when both proteins are coexpressed in bacteria. DMS3 is an integral part of the DDR complex (which also contains the proteins DRD1 and RDM1), required for RNA-directed DNA methylation, although AtMORC6 was not previously found in this complex purified from plants (*9*). Interestingly, DDR interacts with the plant-specific RNA polymerase Pol V, and plants with inactive Pol V or DRD1 also have defects in heterochromatin condensation (*10*). This indicates that AtMORC6 could control large-scale structural organization of heterochromatin in a complex with DDR and Pol V. It will be important to assess whether the DDR complex or only DRD1 is involved in heterochromatin condensation. As RNA-directed DNA methylation is not required for heterochromatin condensation (*10*), AtMORC6 would play another role in the DNA methylation pathway. Alternatively, it is possible that the effect of AtMORC6 on CHH DNA methylation is a consequence of its role in structurally organizing heterochromatin.

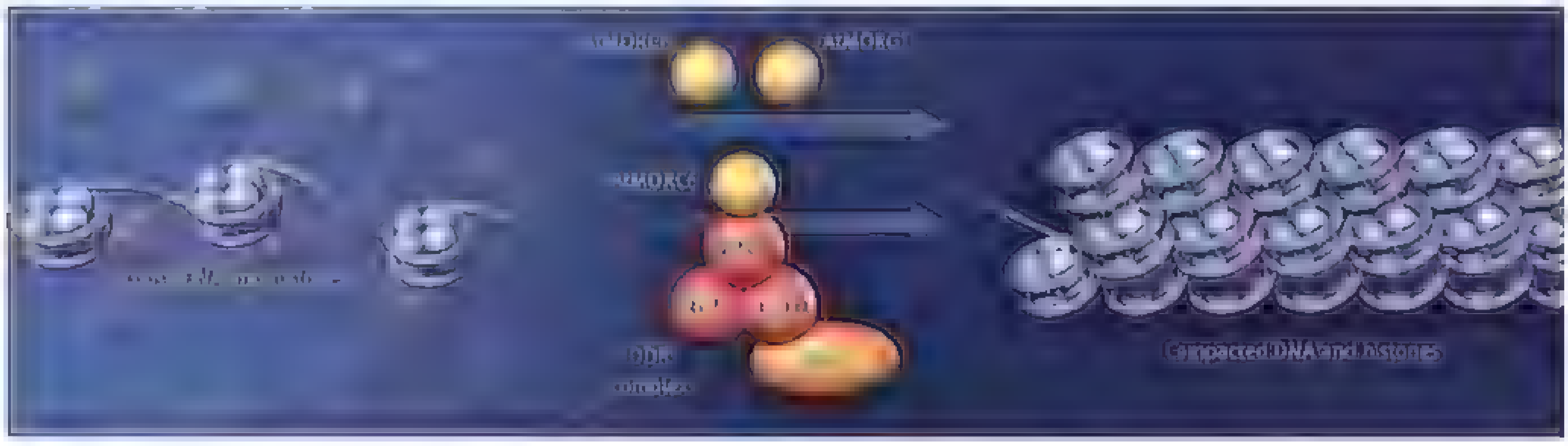

Heterochromatin condensation. AtMORC1 and AtMORC6 function similarly in heterochromatin condensation, and both colocalize to the same regions in the nucleus, which suggests that they are in the same pathway and may interact. Recombinant AtMORC6 protein interacts with DMS3, an integral part of the DDR complex. The DDR complex protein DRD1 also regulates chromatin compaction with Pol V independently of their role in RNA-directed DNA methylation.

AtMORC1 and AtMORC6 proteins are part of a seven-member family in *Arabidopsis*, and homologs are also present in animals. Deletion of the mouse gene homolog *Microrchidia* (*Morc1*) produces mice with defects in meiosis and spermatogenesis, closely resembling mice lacking either the *Miwi2* or *Dnmt3L* gene, which also have defects in RNA interference–guided DNA methylation (*11*–*14*). Moissiard *et al.* show that the single ortholog of *MORC1* in the worm *Caenorhabditis elegans* (*morc-1*) is also required for gene silencing, although it still remains to be tested whether this is due to heterochromatin decondensation. The mouse protein SMCHD-1 has N-terminal and C-terminal domains related to AtMORC6 and DMS3, respectively (*8*). Heterozygous mice engineered to lack one allele of *SMCHD-1* have defects in heterochromatic gene silencing, but homozygous female embryos lacking both alleles are lethal because of defects in X inactivation—a dramatic example of chromosome condensation in mammals (*15*). Because it occurs only upon cellular differentiation, X inactivation is considered a paradigm for facultative heterochromatin (*3*). The fact that facultative and constitutive heterochromatin rely on related proteins suggests that they may have more in common than previously supposed.

Little is known about how active demethylation of DNA is regulated. In *Arabidopsis*, it is carried out in a base excision repair process that involves DNA glycosylases. Qian *et al.* identify an *Arabidopsis* protein called IDM1 (in mutant plants, it causes increased DNA methylation 1) that functions as a histone acetyltransferase, which may promote or even guide demethylation via DNA glycosylases (such as Repressor of Silencing 1) in plants. IDM1 contains domains that recognize a combination of epigenetic marks on DNA and histones. Determining how it activates glycosylases should further clarify the relationship among histone modifications, active demethylation of DNA, and protection from gene silencing.

References

1. G. Moissiard *et al.*, *Science* **336**, 1448 (2012); 10.1126/science.1221472
2. W. Qian *et al.*, *Science* **336**, 1445 (2012).
3. P. Fraser, W. Bickmore, *Nature* **447**, 413 (2007).
4. M. Rigal, O. Mathieu, *Biochim. Biophys. Acta* **1809**, 452 (2011).
5. S. Feng, S. E. Jacobsen, *Curr. Opin. Plant Biol.* **14**, 179 (2011).
6. L. M. Iyer, S. Abhiman, L. Aravind, *Biol. Direct* **3**, 8 (2008).
7. R. K. Slotkin, R. Martienssen, *Nat. Rev. Genet.* **8**, 272 (2007).
8. Z. J. Lorković, U. Naumann, A. J. M. Matzke, M. Matzke, *Curr. Biol.* **22**, 933 (2012).
9. J. A. Law *et al.*, *Curr. Biol.* **20**, 951 (2010).
10. O. Pontes, P. Costa-Nunes, P. Vithayathil, C. S. Pikaard, *Mol. Plant* **2**, 700 (2009).
11. A. A. Aravin *et al.*, *Mol. Cell* **31**, 785 (2008).
12. D. Bourc'his, T. H. Bestor, *Nature* **431**, 96 (2004).
13. M. A. Carmell *et al.*, *Dev. Cell* **12**, 503 (2007).
14. M. L. Watson *et al.*, *Proc. Natl. Acad. Sci. U.S.A.* **95**, 14361 (1998).
15. M. E. Blewitt *et al.*, *Nat. Genet.* **40**, 663 (2008).

Acknowledgments: R.M. is a Howard Hughes Medical Institute (HHMI)–Gordon and Betty Moore Foundation (GBMF) Investigator in Plant Biology.

10.1126/science.1224272

CREDIT: C. BICKEL/SCIENCE

ECOLOGY

The Heartbeat of Ecosystems

Which indicators of ecosystem structure and function must be measured to assess ecosystem health?

Margaret A. Palmer[1,2,3] and Catherine M. Febria[1,2]

People generally equate health with a long and active life, but when it comes to ecosystems there is no agreement on what it means to be healthy. On page 1438 of this issue, Woodward *et al.* (*1*) show that different conclusions on the health of stream ecosystems can be reached depending on which combinations of metrics are used to assess them. The work points to an urgent need for a general framework for assessing ecosystem health.

An increasingly popular way to assess ecosystems is to evaluate the level of goods and services they provide to humans, such as water for drinking or irrigation (*2*). However, using ecosystem services as an indicator of ecosystem health is an oversimplification of the ecosystems services concept (*3*) and does not provide sufficient information on the extent to which those services can be provided sustainably (*4*–*6*). A second, older approach bases ecosystem health on its similarity to a least-impacted, reference, or historical state. This is the main approach in use today by water resource managers and typically involves measurements of what ecologists call ecosystem structure (*7*).

Ecosystem structure refers to attributes that can be evaluated with point-in-time measurements and that are assumed to reflect the existing status or condition of an ecosystem. Structural attributes may be easy to measure, but they do not capture the dynamic properties of an ecosystem that represent its actual performance. Functional measurements, on the other hand, attempt to capture system dynamics through repeated measurements that quantify key biophysical processes (see the table).

Structure and function both contribute to ecosystem status and to the provision of goods and services, but what combination of measurements should be used to evaluate ecosystems is a matter of current scientific debate. Woodward *et al.* (*1*) evaluate river health on a continental scale using measurements or "health metrics": the taxonomic composition of aquatic biota (structural), the eutrophication status based on nitrogen concentration (structural), and the decomposition rate of organic material in the form of leaf litter (functional). Their work suggests that management efforts to reduce nitrogen pollution may not lead to recovery of desired species or efficient processing of organic matter. The data show that the functional metric of decomposition can be quite variable even at some fixed level of water quality. Other factors known to influence the measurements they used, such as river geomorphology and land use, were not reported.

On the surface, the results might seem unsatisfying, but in fact they clearly demonstrate why it is important to use multiple metrics. Ecosystem components interact in complex ways, and ecological processes are context dependent (*8*); interpretation of measurements thus requires multiple types of data. For example, the rate of organic matter decomposition in rivers and streams is well-known to be influenced by the species and size of aquatic insects that tear apart decomposing leaves while feeding. Other key players that influence decomposition—microbes—increase their activity when nutrients are elevated and, like insects, also respond to other factors that typically change as rivers become eutrophic (*9*).

Recent studies have started to elucidate how these factors influence microbial production and community structure at large spatial and temporal scales (*10*). Such work is essential for understanding how to interpret and use metrics such as decomposition rate. Exploring patterns like those reported by Woodward *et al.* (*1*), coupled with clever natural and manipulative experiments (*11*, *12*), is also an important step to take if ecologists hope to link suites of metrics to the desired future state of ecosystems. A review of more than 250 studies in the mid-Atlantic United States found that data are currently insufficient to identify which metrics will best reflect whether an ecosystem is on a clear trajectory toward improvement, because of the paucity of studies that couple functional measures with routine quantification of ecosystem structure (*13*).

METRICS FOR EVALUATING THE HEALTH OF RIVER AND STREAM ECOSYSTEMS

Structural [illegible]	[illegible]
Biological diversity or species of interest	Productivity/reproduction, migration, trophic status
Native riparian vegetation width	Pollutant removal rates
Floodplain presence/width	Hydraulic retention
Canopy cover	Photosynthetic active radiation
Oxygen level	Biochemical oxygen demand, whole stream metabolism
Nitrogen, phosphorus concentrations	Nutrient cycling or flux rates
Pollutant concentrations	Pollutant removal or sequestration
Organic matter	Decomposition rate
Temperature	Thermal regime (magnitude, duration and timing)
Mean annual flow and depth	Flow regime (magnitude, duration and timing)
Turbidity	Sediment flux
Channel morphology	Channel migration, erosion rate
Streambed substrate	Streambed mobility

Ecosystem structure and function. The components of an ecosystem (structure) interact with dynamic biophysical processes (functions) to produce goods and services that people reply on from rivers and streams (e.g., fisheries, drinking water, irrigation, flood mitigation, recreation). Structural measurements (**left**) may be easier to make but provide less information than related functional measurements (**right**). In practice, these metrics vary widely. For example, nitrogen processing, commonly measured as denitrification potential, varies with organic matter by several orders of magnitude (*21*). Metabolism varies by two to three orders of magnitude (*15*, *17*), as does decomposition rate depending on leaf type (*1*, *14*). As Woodward *et al.* show, combinations of structural and functional measurements may be required to predict the state of an ecosystem or availability of a good or service.

PHOTO CREDIT: ALAN ECKERT PHOTOGRAPHY

[1]Chesapeake Biological Laboratory, University of Maryland Center for Environmental Science, Solomons, MD 20688, USA. [2]Department of Entomology, University of Maryland, College Park, MD 20742, USA. [3]National Socio-Environmental Synthesis Center, 1 Park Place, Suite 300, Annapolis, MD 21401, USA. E-mail: mpalmer@sesync.org

Structural measures, such as the presence or absence of an iconic species like salmon, can indicate that something is wrong with an ecosystem, but typically not why. Thus, reliance on structure alone makes it difficult to prescribe ecosystem management or restoration actions. After all, doctors will routinely measure a sick patient's heart rate and blood pressure, rather than just their height, weight, and temperature. Human health metrics are based on long-term research that links metabolic processes to longevity and disease risk across highly diverse populations. Analogous studies for river and stream ecosystems are now accumulating (*14*–*17*).

To move river science into the realm of effective health diagnosis before ecosystems collapse, researchers must work with natural resource managers to compile regionally specific data on how functional metrics vary over time and space—particularly in rivers considered to be least impacted. Knowledge of the range of natural variability, the factors that drive changes in ecosystem functions, and how these functions respond to management actions will generate a framework for sound prescriptions to improving ecosystem health.

Such an understanding could help to address several pressing questions: Which ecosystem functions should be the target of management efforts, given desired outcomes? Is temporal variation in ecological processes itself an important driver of ecosystem states, much like annual cycles of high and low flows are thought to influence species composition in rivers (*18*)? Which metrics can be used as early indicators of degradation or recovery, and how do they vary with each stressor? Can we predict the ecological consequences of managing for a specific ecosystem service?

The recently launched Intergovernmental Platform on Biodiversity and Ecosystem Services (*19*) and other large-scale efforts will have these questions to address. Given worldwide declines in species, and growing evidence that biodiversity may control and not just respond to ecological processes (*20*), more data such as those provided by Woodward *et al.* (*1*) on how ecosystem structure and function vary across a large range of conditions are urgently needed. Only then will ecologists have enough information to determine which set of metrics, under which contexts, best equates to the human heartbeat for ecosystems.

References

1. G. Woodward *et al.*, *Science* **336**, 1438 (2012).
2. A. Paetzold *et al.*, *Ecol. Complex.* **7**, 273 (2010).
3. G. C. Daily *et al.*, *Front. Ecol. Environ* **7**, 21 (2009).
4. M. A. Palmer, S. Filoso, *Science* **325**, 575 (2009).
5. R. B. Norgaard, *Ecol. Econ.* **69**, 1219 (2010).
6. R. A. Holland *et al.*, *Ecol. Appl.* **21**, 2034 (2011).
7. M. A. Palmer *et al.*, *J. Appl. Ecol.* **42**, 208 (2005).
8. M. E. Power *et al.*, *Bioscience* **46**, 609 (1996).
9. J. R. Webster, E. F. Benfield, *Annu. Rev. Ecol. Syst.* **17**, 567 (1986).
10. T. J. Battin *et al.*, *Nat. Geosci.* **1**, 95 (2008).
11. F. T. Maestre *et al.*, *Science* **335**, 214 (2012).
12. B. J. Cardinale, *Nature* **472**, 86 (2011).
13. K. G. Sellner *et al.*, *Metrics and Protocols for Progress Assessment in Chesapeake Bay Stewardship Fund Grants. Final Report to the National Fish and Wildlife Foundation* Chesapeake Research Consortium (CRC) Publ. No. 12-174 (CRC, Edgewater, MD, 2012).
14. M. O. Gessner, E. Chauvet, *Ecol. Appl.* **12**, 498 (2002).
15. M. J. Bernot *et al.*, *Freshw. Biol.* **55**, 1874 (2010).
16. B. O. L. Demars *et al.*, *Freshw. Biol.* **56**, 1106 (2011).
17. R. G. Young *et al.*, *J. N. Am. Benthol. Soc.* **27**, 605 (2008).
18. N. L. Poff *et al.*, *Bioscience* **47**, 769 (1997).
19. Intergovernmental Platform on Biodiversity and Ecosystem Services, www.ipbes.net.
20. P. B. Reich *et al.*, *Science* **336**, 589 (2012).
21. S. E. G. Findlay *et al.*, *Biogeochem.* **104**, 381 (2011).

10.1126/science.1223250

CHEMISTRY

A Boron-Boron Triple Bond

A complex with a boron-boron triple bond expands the range of genuine triple bonds known to chemists.

Gernot Frenking and Nicole Holzmann

Although carbon readily forms double and even triple bonds, such bonds are much rarer between the heavier elements of the same group or between atoms of other main groups of the periodic system. Chemists have succeeded in creating some such molecules, such as double-bonded silicon compounds, although they are usually highly reactive. On page 1420 of this issue, Braunschweig *et al.* (*1*) report the synthesis of one such highly unusual chemical compound, which has a boron-boron triple bond.

In 2008, Robinson and co-workers reported the isolation of a compound with the formula L→Si=Si←L, where L is an N-heterocyclic carbene (NHC) that stabilizes diatomic silicon (Si_2) in an unprecedented way (*2*). Subsequent efforts to synthesize further members of this class of molecules, with the general formula (NHC)→E_2←(NHC), led to the synthesis of the group 14 species (NHC)→Ge_2←(NHC) (*3*) and the group 15 species (NHC)→P_2←(NHC) (*4*) and (NHC)→As_2←(NHC) (*5*). However, experimental attempts to isolate group 13 homologs, with E = B, Al, Ga, and In, were not successful. Quantum chemical calculations suggested that the complexes of the heavier group 13 atoms (Al, Ga, and In) have a double bond, (NHC)→E=E←(NHC), and a trans-bent arrangement of the central atoms (*6*). For the boron homolog, the calculations predicted a linear form with a boron-boron triple bond, (NHC)→B≡B←(NHC). Braunschweig *et al.* now provide the experimental verification of this structure.

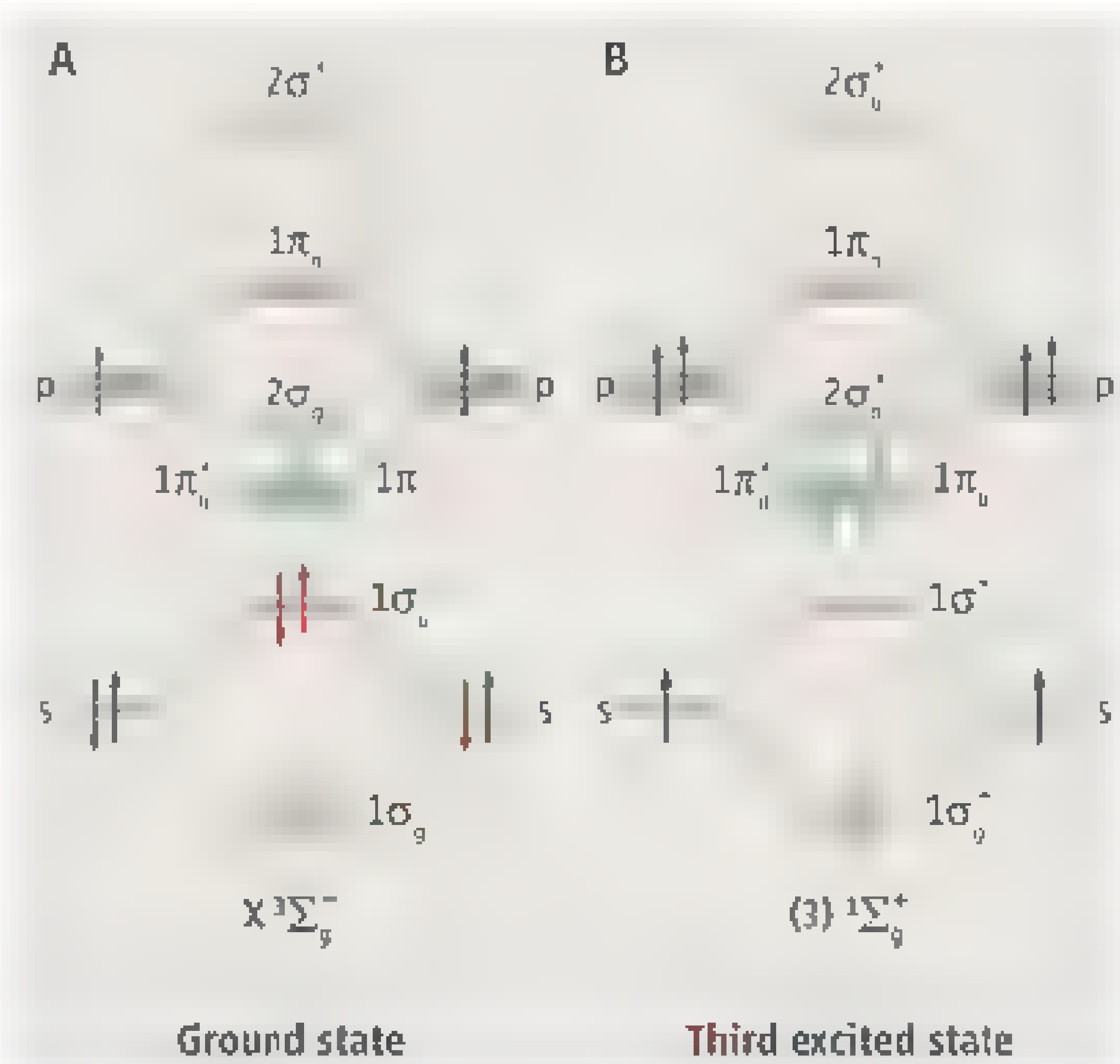

Toward explaining the triple bond. Schematic representation of **(A)** the ground state and **(B)** the third excited state of B_2 in the (NHC)→B≡B←(NHC) molecule reported by Braunschweig *et al.* The ground state, seen in ligand-free B_2, has two doubly occupied bonding orbitals (blue) but one doubly occupied antibonding orbital (red), giving a bond order of 1 and hence a single bond. In contrast, the third excited state observed in (NHC)→B≡B←(NHC) has three doubly occupied bonding orbitals and hence a triple bond.

Fachbereich Chemie, Philipps-Universität Marburg, Hans-Meerwein Strasse, D-35039 Marburg, Germany. E-mail: frenking@chemie.uni-marburg.de

There are two ways in which the synthesis of the (NHC)→B≡B←(NHC) complex constitutes a breakthrough in main-group chemistry. First, it shows that a group 13 dimer can be stabilized, isolated, and structurally characterized in a L→E_2←L complex. A related boron compound, L→B≡B←L with L = CO, has previously been identified in low-temperature matrix experiments (*7*). The doubly charged anion L→B≡B←L with L = BO^- (which is isoelectronic to CO) has been observed in the gas phase by means of photoelectron spectroscopy (*8*). Both compounds have a boron-boron triple bond (*9*). However, neither is stable in a condensed phase under normal laboratory conditions, and they cannot be used in synthetic chemistry. In contrast, the (NHC)→B≡B←(NHC) complex has a surprising thermal stability, opening the door to experimental exploration of its reactivity.

Second, the (NHC)→B≡B←(NHC) complex has a hitherto unknown homoatomic triple bond between two main-group atoms. Very few classes of known stable compounds have a genuine triple bond, which consists of a σ bond and a doubly degenerate π bond. These are the alkynes, RC≡CR, which have a carbon-carbon triple bond, and dinitrogen N≡N. Triple bonds between heavier atoms have a trans-bent structure (*10*) and a different bonding character (*11*). Thus, the diboron L→B≡B←L complexes are only the second class of stable main-group compounds with genuine homoatomic triple bonds that can be modified experimentally by changing the nature of the ligand L.

How does the NHC ligand enforce a boron-boron triple bond in (NHC)→B≡B←(NHC) while at the same time stabilizing the complex strongly enough to allow its isolation? The answer can be found with the help of qualitative molecular orbital (MO) diagrams (see the first figure). In the electronic ground state of the ligand-free B_2 molecule, only two of the doubly occupied MOs ($1\sigma_g^+$ and $1\pi_u/1\pi_u'$) are bonding, whereas one MO ($1\sigma_u$) is antibonding, giving an effective bond order value of 1 and hence a B-B single bond (see the first figure, panel A). The NHC ligands push one electron pair from the antibonding $1\sigma_u^+$ MO into the bonding $1\pi_u/1\pi_u'$ MOs, resulting in the third excited state (see the first figure, panel B). The latter state has three doubly occupied bonding MOs ($1\sigma_g^+$, $1\pi_u$, and $1\pi_u'$) and hence a B≡B triple bond.

The energy required for the electronic excitation from the ground state to the third excited state comes from the very strong donor-acceptor bonds between the NHC donors and B_2 in the third excited state. The latter state has two vacant orbitals ($1\sigma_u^+$ and $2\sigma_g^+$), which are perfectly suited for accepting electronic charge from the NHC ligands. Because the $1\sigma_u^+$ and $2\sigma_g^+$ MOs are antibonding and bonding, respectively, the net bond order for the boron-boron bond remains 3.

The B-B bond length in Braunschweig *et al.*'s compound is much shorter (1.449 Å) than in the electronic ground state of B_2 (1.590 Å) (*12*), supporting the assignment of a higher bond order in the complex. The much larger donor strength of NHC relative to CO makes (NHC)→B≡B←(NHC) stable enough to be isolated under normal laboratory conditions, whereas OC→B≡B←CO can only be prepared in a low-temperature matrix (*8*).

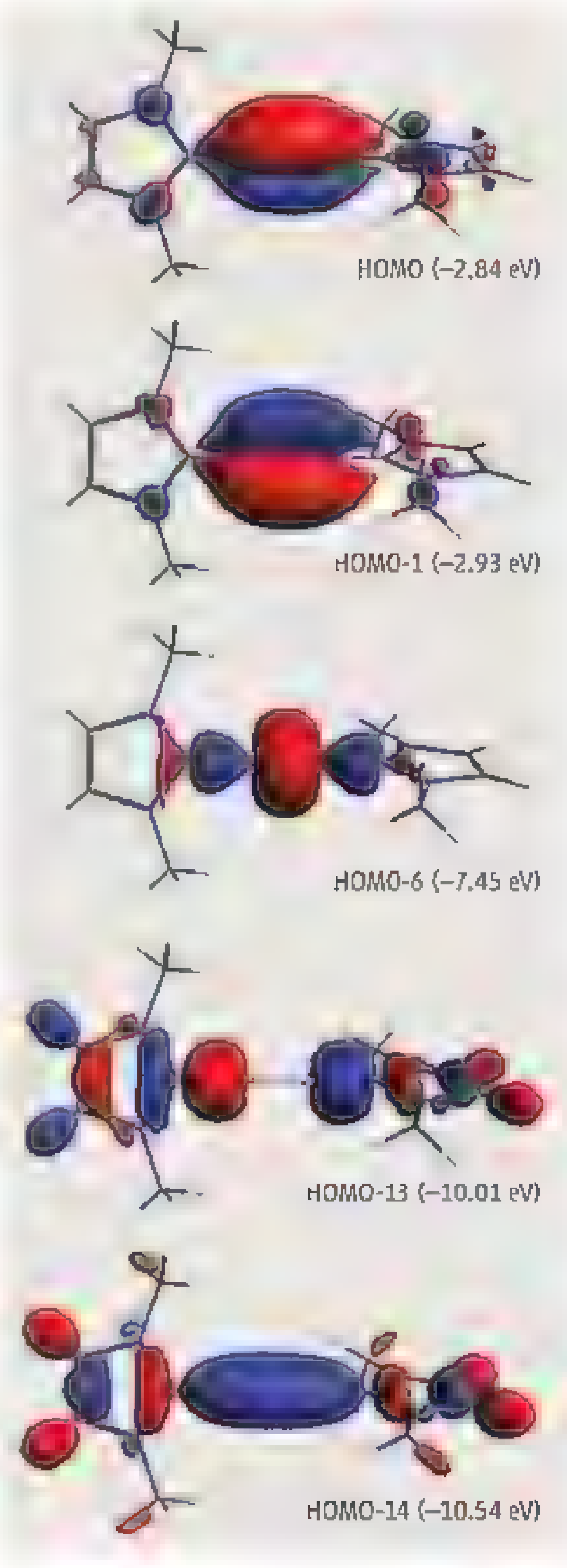

Bonding in the (NHC)→B≡B←(NHC) complex. The five occupied valence orbitals of (NHC)→B≡B←(NHC) show that the five lowest lying orbitals in the third excited state of B_2 (first figure, panel B) are occupied.

CREDIT: NICOLE HOLZMANN/PHILIPPS-UNIVERSITÄT MARBURG

The exceptional donor strength of NHC ligands has also been exploited in the synthesis of the related borylene complex (CAAC)→(BH)←(CAAC). The CAAC (cyclic alkyl amino carbene) ligand has only one nitrogen atom in the donor moiety (*13*), instead of two in NHC, making the CAAC ligand a slightly stronger donor. It may therefore also be possible to isolate a (CAAC)→B≡B←(CAAC) complex.

The MOs of (NHC)→B≡B←(NHC) (see the second figure) further elucidate the bonding in the complex (*5*). Four highest occupied MOs are B-B bonding (HOMO, HOMO-1, HOMO-6, HOMO-14), whereas HOMO-13 is B-B antibonding. The net bond order is thus 3. HOMO-13 and HOMO-14 nicely show the donation of the electrons from the NHC ligands into the vacant $1\sigma_u^+$ and $2\sigma_g^+$ orbitals of the third excited state of B_2. The $2\sigma_g^+$ orbital becomes lower in energy than the $1\pi_u$ and $1\pi_u'$ orbitals as a result of charge donation from the ligands.

The synthesis of the (NHC)→B≡B←(NHC) complex is a remarkable achievement in the chemistry of main-group compounds with multiple bonds. It is a striking example for the donor strength of the NHC ligand, which may stabilize very reactive species in complexes that can be isolated and structurally characterized by x-ray analysis. Future studies are likely to explore the chemical reactivity of the boron-boron triple bond in addition reactions. The reactivity of the complexes may be modulated by changing the ligands at the nitrogen atoms. Finally, the search for donor ligands other than NHC to stabilize L→B≡B←L complexes is a challenge for inventive chemists.

References

1. H. Braunschweig *et al.*, *Science* **336**, 1420 (2012).
2. Y. Wang *et al.*, *Science* **321**, 1069 (2008).
3. A. Sidiropoulos, C. Jones, A. Stasch, S. Klein, G. Frenking, *Angew. Chem. Int. Ed.* **48**, 9701 (2009).
4. Y. Wang *et al.*, *J. Am. Chem. Soc.* **130**, 3298 (2008).
5. M. Y. Abraham *et al.*, *Chem. Eur. J.* **16**, 432 (2010).
6. N. Holzmann, A. Stasch, C. Jones, G. Frenking, *Chem. Eur. J.* **17**, 13517 (2011).
7. M. Zhou *et al.*, *J. Am. Chem. Soc.* **124**, 12936 (2002).
8. S. D. Li, H. J. Zhai, L. S. Wang, *J. Am. Chem. Soc.* **130**, 2573 (2008).
9. L. C. Ducati, N. Takagi, G. Frenking, *J. Phys. Chem. A* **113**, 11693 (2009).
10. P. P. Power, *Chem. Rev.* **99**, 3463 (1999).
11. M. Lein, A. Krapp, G. Frenking, *J. Am. Chem. Soc.* **127**, 6290 (2005).
12. K. P. Huber, G. Herzberg, *Molecular Spectra and Molecular Structure IV. Constants of Diatomic Molecules* (Van Nostrand-Reinhold, New York, 1979).
13. R. Kinjo, B. Donnadieu, M. A. Celik, G. Frenking, G. Bertrand, *Science* **333**, 610 (2011).

10.1126/science.1224003

RIO+20

Science for Sustainable Development

The United Nations Conference on Sustainable Development takes place in Rio de Janeiro, Brazil, on 20 to 22 June. Dubbed "Rio+20," the conference comes 20 years after the 1992 UN Conference on Environment and Development, also held in Rio. That '92 "Earth Summit" produced 27 guiding principles and the adoption of Agenda 21, all focused on sustainable development. *Science* invited experts from different countries, institutions, and fields to reflect on progress thus far, anticipate challenges and opportunities ahead, and highlight the roles that science and technology can play. **–Brad Wible**

Analyzing Sustainable Development Goals

Lidia Brito
Director, Division of Science Policy and Capacity-Building, United Nations Educational, Scientific and Cultural Organization (UNESCO), 75352 Paris, France

The Rio+20 agenda has grown from two uninspiring, but essential, foci, the green economy and institutional framework for sustainable development, into a chaotic catchall for the world's woes. Neither approach offers much hope of attracting the attention of world leaders needed to make the conference a success. In recent months, though, one promising idea has emerged:

... [sustainable development goals] deserve deeper analysis of interconnections and synergies ...

universal sustainable development goals (SDGs). Proposed by Colombia and Guatemala, SDGs have gained momentum and could provide a much-needed "big idea." Much work, including early engagement from science, needs to be done to ensure success.

The new goals would likely expand on the United Nations Millennium Development Goals (MDGs) due to end in 2015. But several key differences must mark SDGs. First, MDGs centered around seven social goals and just one environmental goal. Long-term social and economic improvement will need closer attention to be paid to the environment. Second, whereas MDGs focused on developing countries, SDGs need buy-in from all nations. Third, MDGs were hastily assembled without thorough analysis. In spite of this, there have been successes, particularly those with quantitative targets such as universal primary education (MDG 2) and access to safe drinking water (MDG 7). SDGs deserve deeper analysis of interconnections and synergies between goals, trade-offs, and indicators and targets.

The March conference, Planet Under Pressure, held the first major science-policy dialogue on SDGs, jointly organized with the team set up to direct the post-2015 MDGs. The resulting State of the Planet Declaration endorsed the SDG proposal, but the conference concluded that rushing to identify goals without in-depth dialogue with all stakeholders would be a grave mistake. Given that we have 3 years left to run on MDGs, there is no excuse to sidestep such a deep analysis. The global scientific community is ready to participate in the codesign of the SDGs and related measures. The launching of the 10-year Future Earth initiative focusing on global sustainability solutions is an example of their commitment and that of their funders.

The Urban Challenge

David Fisk
Director, Laing O'Rourke Centre for Systems Engineering and Innovation, Imperial College London, London SW7 2AZ UK.

"The Urban Challenge" was a chapter in the 1987 Brundtland report, *Our Common Future*. The issues remain depressingly familiar for Rio+20. Urbanization has continued around the world, sometimes diminishing rather than enhancing social and environmental capital. Urban populations then 2 billion are estimated to have reached 3.5 billion. But three unforeseen new factors have changed the world's urban landscape since the 1980s: globalization of transportation, information technology, and clean energy. Globalization could only have taken place with adaption of cities (and their ports) on a scale without precedence. Driving that change have been leaps in logistics and transport technology. Modern cities have become inseparable from the means with which they link to each other. The scale of production and consumption in modern cities is awesome, not least for the problems created in waste and pollution. At the heart of these issues is continued availability of clean energy that is affordable for all and less dependent on fossil fuel. The race is on to reconfigure urban processes and land-use patterns to extract the most from waste streams of matter and energy and to minimize the resource overhead of transport.

Finding optimal solutions for the complexity of the growing modern city is beyond the reach of conventional pencil-and-paper city master planning. Cities are turning to increasingly sophisticated software decision-support tools both to minimize internal transportation needs and to optimize the locational opportunity to recover high-grade waste energy and material flows to lower-grade uses. At the moment, even the powerful optimizers used in process industries are hard pressed to tackle the formidable "integer programming" problem presented by the myriad of possible networks of resource flows of a modern city.

Nevertheless, the prospect is a possible halving of primary resource use, and it will have to be achieved. One study of global data for cities sounds the warning, as urban population grows, major innovation cycles have had to be generated at a continually accelerating rate to sustain growth and so avoid stagnation or collapse. The urban citizen is running with no time to take breath.

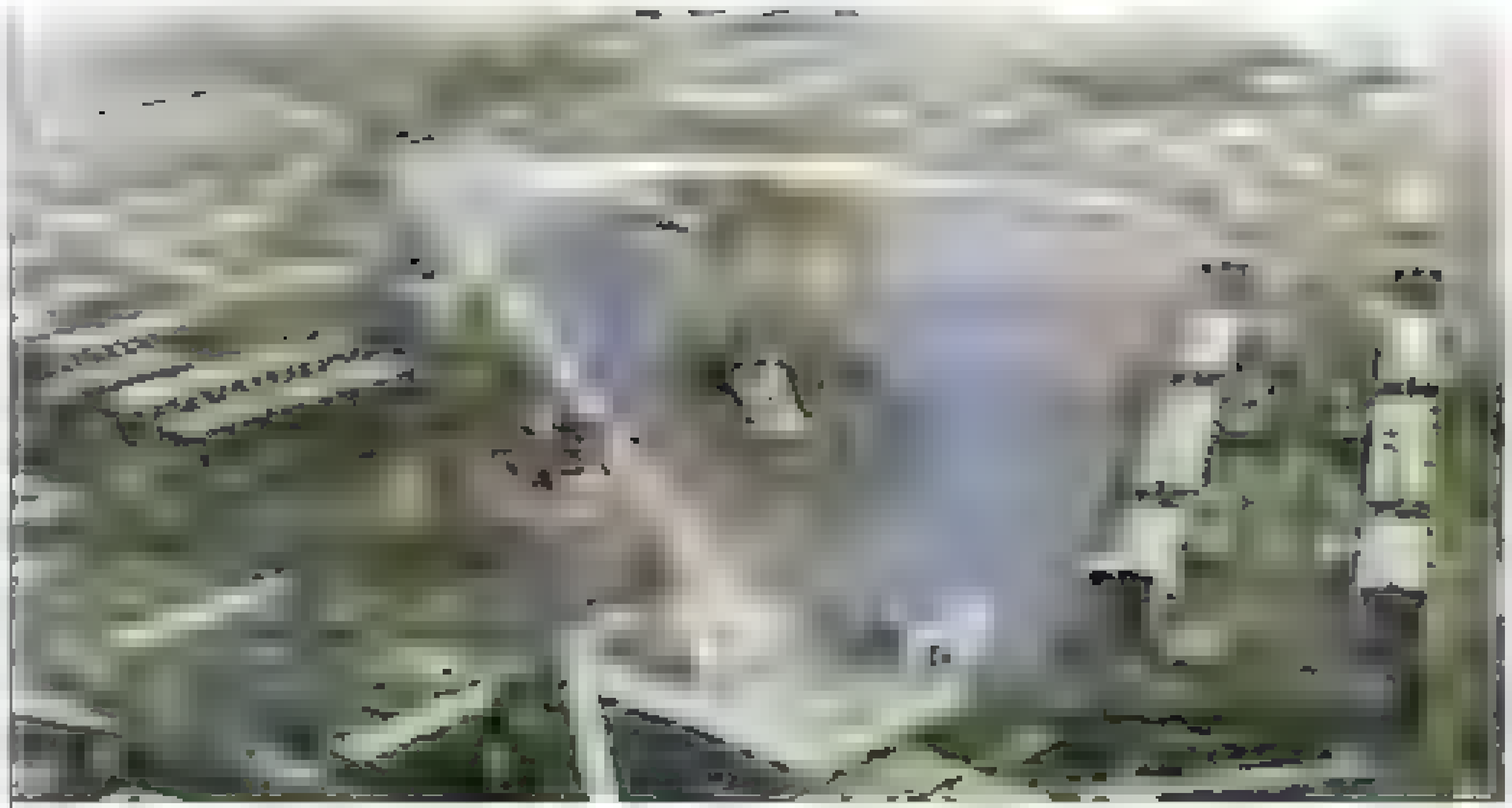

Harnessing New Scientific Capacity

Alice Abreu

Emeritus Professor, Federal University of Rio de Janeiro, Rio de Janeiro, 21941 Brazil; Regional Coordinator for Rio+20, International Council for Science (ICSU)

There is worldwide recognition that progress on Agenda 21, the result of the 1992 Earth summit, has been woefully insufficient. Rio+20 must start a process where all countries, North and South, commit to sustainable development and the "greening" of their economic systems. But there will be no green economy without clean technology, innovation, and sound science. For the proposed Sustainable Development Goals to be effective, they should include a call for a mechanism for international scientific cooperation and coordinated research on major sustainable development challenges—building on, and working with, existing programs. Recent decades saw the development of a robust research community in many developing countries. They should be part from the start of an effort that would gather existing knowledge and coordinate research on key sustainable development and green economy issues—working with the private, public, and nonprofit sectors—and would enhance collaboration with policy-makers, funders, and other stakeholders in designing, implementing, and communicating research. Another important aspect of this mechanism would be promoting and coordinating capacity-building in science and technology where needed. To promote progress toward these goals, ICSU and its partners will launch, during Rio+20, a new, 10-year global initiative, Future Earth: Research for global sustainability—a voluntary commitment from the scientific and technological community. Such initiatives should allow a more effective transition to the sustainable development we want.

From Industrial Toward Ecological in China

Jiahua Pan

Director, Research Center for Sustainable Development, Chinese Academy of Social Sciences, Beijing, China

Since the 1992 Rio summit, China has been on the fast track to industrialize and urbanize, having transitioned from a low-income developing country into the second-largest economy in the world. But many, including President Hu Jintao, have admitted that the current conventional path to industrialization and urbanization is unsustainable. Although China has met the millennium goals for poverty reduction, there have been increasing disparities between rich and poor, rural and urban, and coastal and inland regions. Concerns are growing over water availability and pollution, land degradation, depletion of exhaustible resources, and so on.

China has no choice but to lead the way for a new paradigm of sustainable development. In 2007, China called for shifting from traditional models of production and consumption to more environmentally friendly and resource-saving models. Among 17 mandatory targets in the 12th 5-year (2011–2015) plan, 12 are related to the protection of natural resources and the environment, with the rest for social welfare improvement and with none for economic growth. Although progress has been slow, actions are being taken: progressive pricing for electricity consumption introduced; energy consumption quota and emission targets disaggregated for implementation and monitored, emissions trading schemes experimented; initiatives for eco-cities and low-carbon cities developed and implemented; and building codes upgraded and enforced. Moreover, the rate of GDP growth is no longer considered the primary indicator for evaluating the performance of local government officials. The official target is set at 7% per year as compared with two-digit figures in the past decades. In many aspects, China is accelerating the transition from industrial to ecological civilization. Looking beyond Rio+20, although the road will be difficult and will require intensified international cooperation, there is reason to believe that sustainable development is not simply a slogan or vision but a real ongoing process in China.

Creating the New Development Ecosystem

Alex Dehgan

Science & Technology Adviser to the Administrator of the U.S. Agency for International Development (USAID), Washington, DC 20523, USA.

Twenty years after the Earth summit, we continue to face tremendous challenges to ecological, human, and national security. Development is the frontline defense, but traditional approaches are no longer sufficient. Development interventions have been dominated by a handful of bilateral and multilateral institutions that defined the problems and implemented a narrow set of solutions. Although there have been tremendous successes, this has not been enough to reverse the continued degradation of our environment or to overcome entrenched problems. To turn grand chal-

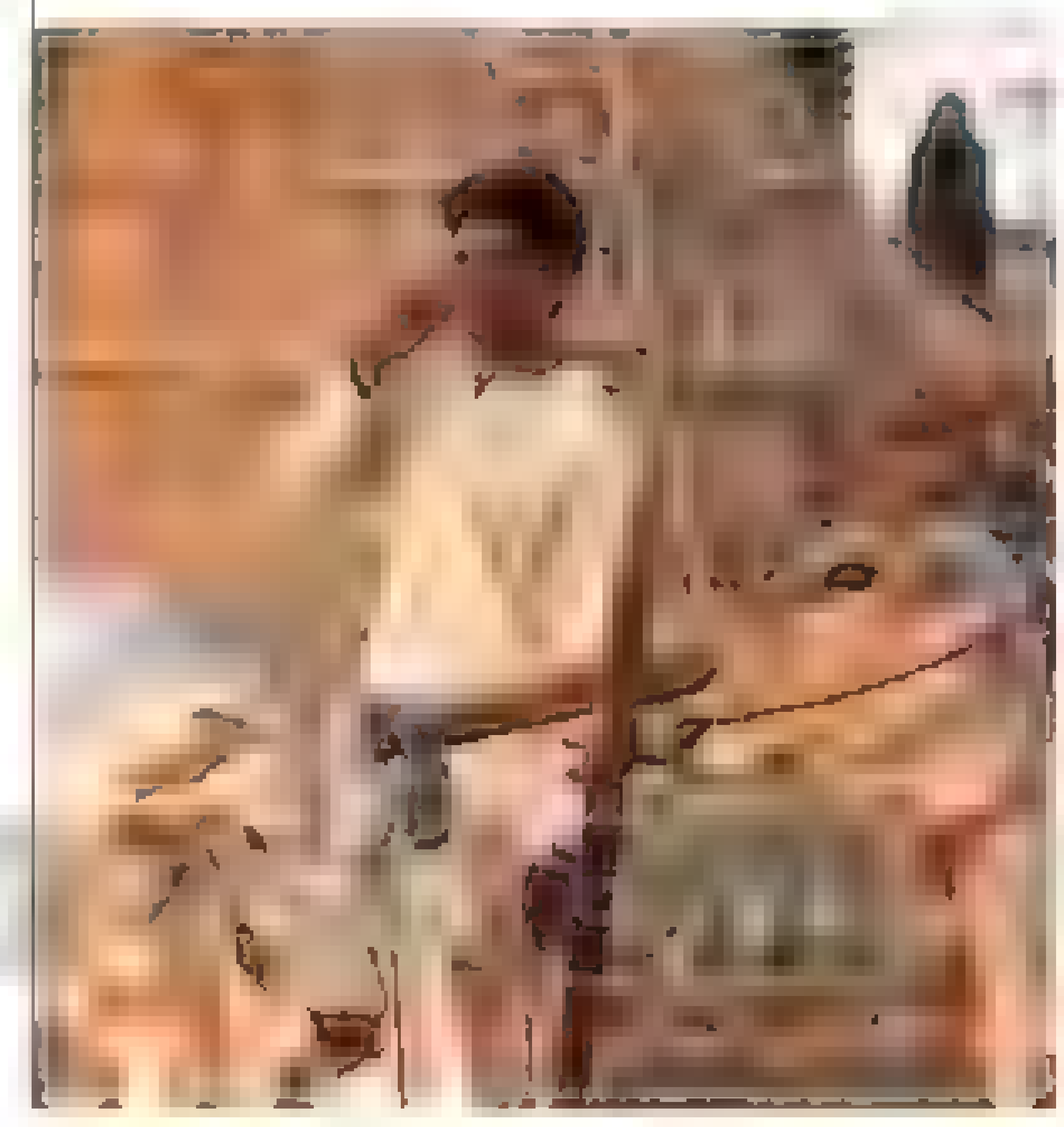

CREDITS (TOP TO BOTTOM): MCT VIA GETTY IMAGES; AFP/GETTY IMAGES; ADRIAN POPE/GETTY IMAGES

lenges into grander opportunities, we must harness the entire planet's creativity to contribute novel solutions.

The USAID and its partners have crowd-sourced the world to apply science, technology, and innovation against seemingly intractable barriers to solving the Grand Challenges for Development (GCDs) and to catalyze global action to achieve scale, sustainability, and impact. Between 25 and 50% of the proposed solutions to the first two GCDs (Saving Lives at Birth and All Children Reading) have come from developing countries. A new partnership between USAID and the U.S. National Science Foundation (NSF), Partnerships for Enhanced Engagement in Research, generated 488 proposals from 63 of the 79 eligible countries with a USAID presence to partner developing-country scientists with NSF-funded American scientists on shared global development problems. These programs, and others like Open-Source Drug Discovery, recognize that developing countries are sources of solutions and ideas as much as developed countries. Constraints of low-resource settings allow for creation of efficacious world-class products that can cost less and have a smaller environmental impact.

Democratization of science and technology, increases in global connectivity, and greater availability of data will facilitate a movement from a handful of traditional global development agencies toward 7 billion development agents. Cell phones, for example, have been tools of transformation that moved societies beyond traditional infrastructure barriers, serving as platforms for services and learning, providing remote diagnostics for medical treatment, identifying centers of corruption, and serving as distributed sensors of communities and their ecosystems. Our planet's future, driven largely by developing countries, will depend on whether we can work collaboratively to leapfrog 200 years of industrialization and to harness the power of science and technology to create a new revolution based on knowledge.

Systems Science for Policy Evaluation

Pavel Kabat

Director and Chief Executive Officer, International Institute for Applied Systems Analysis (IIASA), 2361 Laxenburg, Austria; Professor, Earth System Science & Climate Change Group, Wageningen University and Research Centre, 6700 AA Wageningen, Netherlands

Narrowly focused, single-disciplinary science alone cannot adequately underpin policies and solutions to resolve major sustainability challenges. For science to play a pivotal role in addressing the green growth and sustainability challenges of Rio+20, or the UN MDGs, we must rapidly refocus intellectual and economic investments toward multiscale, integrated, interdisciplinary approaches that consider social, economic, and environmental aspects, that look across and between borders and sectors, and that identify feedbacks or the cobenefits of a policy or management decision, before it is made.

... academic merit should value and reward integrated, multidisciplinary "systems science,"...

One example of this "systems" approach is the Global Energy Assessment (GEA), a multiyear, multidisciplinary study (coordinated by IIASA), whose findings will be released during Rio+20. The GEA links energy to climate, air quality, human health and mortality, economic growth, urbanization, water, land use, and other factors. The GEA scenarios find that energy access for all (by 2050) is possible with cobenefits of limiting warming to 2°C, improving air quality and human health, and stimulating economic growth within a green economy framework. A similar analysis on water resources will be undertaken by IIASA, UN Water, and the World Water Council.

On the basis of our experience with the GEA, realizing the sustainability goals of Rio+20 will require investment in integrated analyses to fully understand the Earth system (human and natural). This must be enabled by substantial growth in public-private partnerships that stimulate and fund activities that encourage collaboration between social and natural scientists and that engage key stakeholders in the user community at all stages of the research cycle—from inception to implementation. In addition, academic merit should value and reward integrated, multidisciplinary "systems science," with scholarships and tenure no longer dominated by single disciplines. Above all else, success requires clear leadership and defined objectives.

Rigorous Evaluation of Human Behavior

Esther Duflo

Director, Abdul Latif Jameel Poverty Action Lab, Cambridge, MA 02142; Professor of Poverty Alleviation and Development Economics, Massachusetts Institute of Technology, Cambridge, MA 02139, USA

Scientific and technological advances, combined with an internationally coordinated effort to help the diffusion of those technologies to poor countries, have had important impacts on the quality of life for millions of poor people. For example, antibiotics and vaccinations have dramatically increased life expectancy. New seeds have promoted a "green revolution," making several Asian countries self-sufficient for their food needs. Some current development challenges undoubtedly would benefit from new technologies. The world still needs vaccines for malaria and HIV, as well as crops better suited to Africa.

The contribution of science to development and poverty alleviation, however, should not be limited to facilitating the development of new products. For there are numerous technologies that are known to be effective but have not been widely adopted, from bed nets to chlorine to iron pills. And others

have yet to prove their effectiveness in the real world, despite their promise in the lab, such as cheap laptop computers in schools. The missing part is often recognizing human behaviors that are barriers to adoption or correct use and designing appropriate policies to address them. A recent experiment on improved cookstoves, for example, showed that the stoves were not properly used or maintained. This was sufficient to override the encouraging effects of stoves on health that were found in more controlled conditions.

In the last 15 years, social scientists have adopted the method of randomized controlled trials (RCTs), one of the key tools of scientific practice, to evaluate development policy. RCTs allow researchers and policy-makers to rigorously evaluate the impact of an intervention. Once very rare in social science, they are now widely used: Hundreds of RCTs are currently being run to evaluate the impact of policies ranging from police reform to the health impacts of fortified foods. Beyond the obvious value of finding out what works and what does not, RCTs can also shed light on the reasons for individuals' behavior, by incorporating insights from economics, psychology, and sociology into the design and analysis of experiments. This makes for good science; these experiments make it possible to test scientific hypotheses with a degree of rigor that was not available before. It is also essential to the design of policies that take our human nature into account. This is the new frontier for the collaboration between science and development policy.

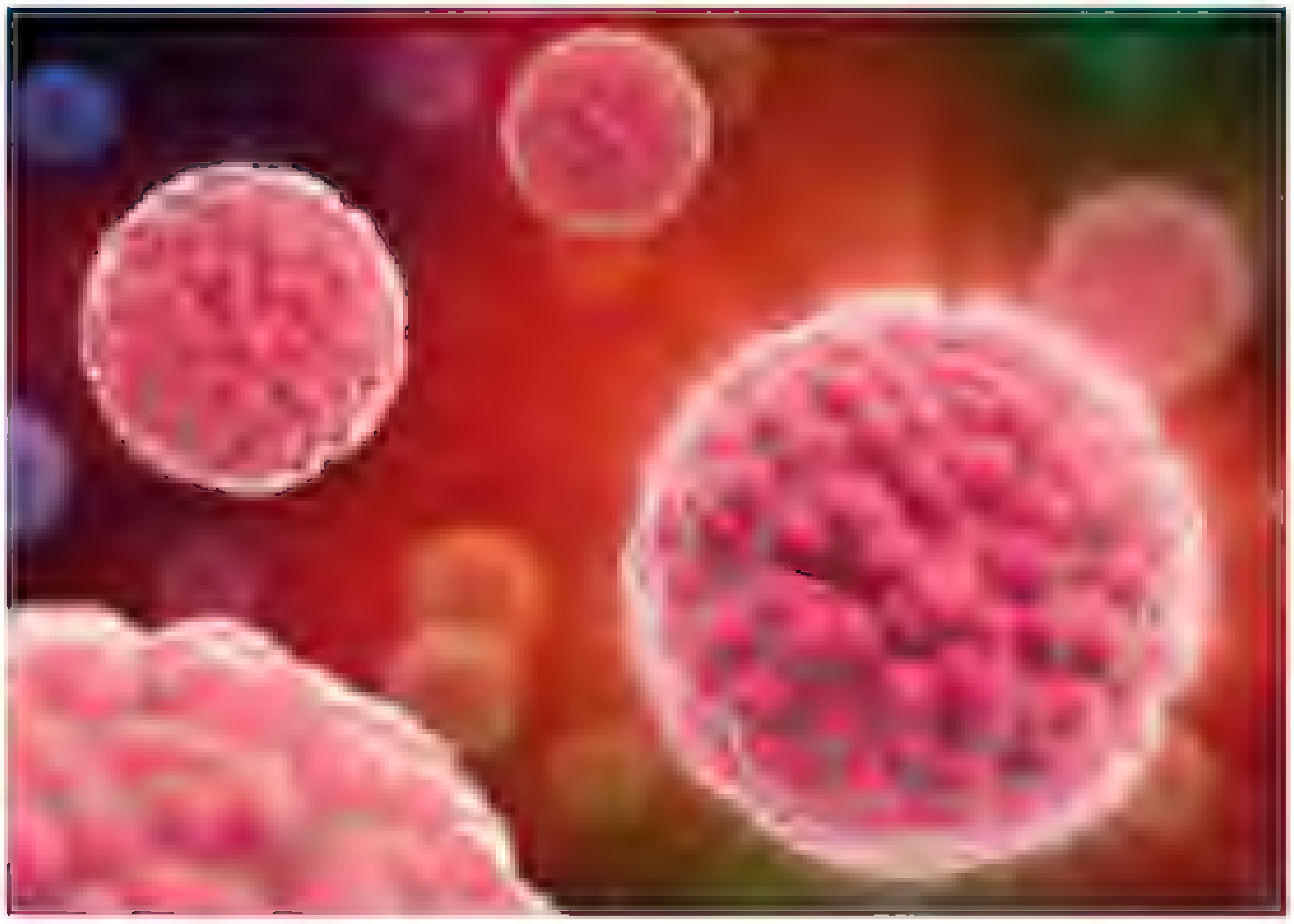

Cell division: The Research Institute of Molecular Pathology researches into the weaknesses of human cancer cells.

Photo: istockphoto

Research for life

Competence in the fight against cancer: the German group Boehringer Ingelheim carries out most of its oncology research in Austria. What makes the business location so attractive.

They are small and unpredictable, aggressive and destructive. Scientists around the world have been searching for their weak spots for decades. Research into cancer cells is a basic feature of the life science sector. A particularly strong business location in this field is Austria. Not only pharmaceutical giants such as Baxter, Sandoz and GlaxoSmithKline, but also small, innovative companies such as AFFiRiS find optimal conditions there. "Customized R&D funding programs as well as a research premium of ten percent are only two ways in which Austria supports the life science sector", says René Siegl, Managing Director of the national investment promotion agency ABA Invest in Austria, which consults companies free of charge and provides consulting services for firms setting up business operations in Austria. In addition, Austria offers numerous tax advantages. German companies such as Boehringer Ingelheim are also represented in Austria with research facilities. Boehringer Ingelheim operates its global oncology research center here, and coordinates its entire clinical research for the region of Central and Eastern Europe. For 25 years the company has been the main sponsor of the Research Institute of Molecular Pathology (IMP) at the Campus Vienna Biocenter, where scientists are trying to find the weaknesses of leukemia cells, amongst other things.

SUCCESSFUL CANCER RESEARCH. The objective is to "reprogram" these cells by blocking certain genes. Initial attempts have shown that the approach is successful. An immediate stop to cell division occurs after a specific gene is deactivated. This means that the cancer cells no longer reproduce or even die off. Moreover, researchers also hope to be able to use appropriate drugs in the fight against other types of cancer.

www.investinaustria.at

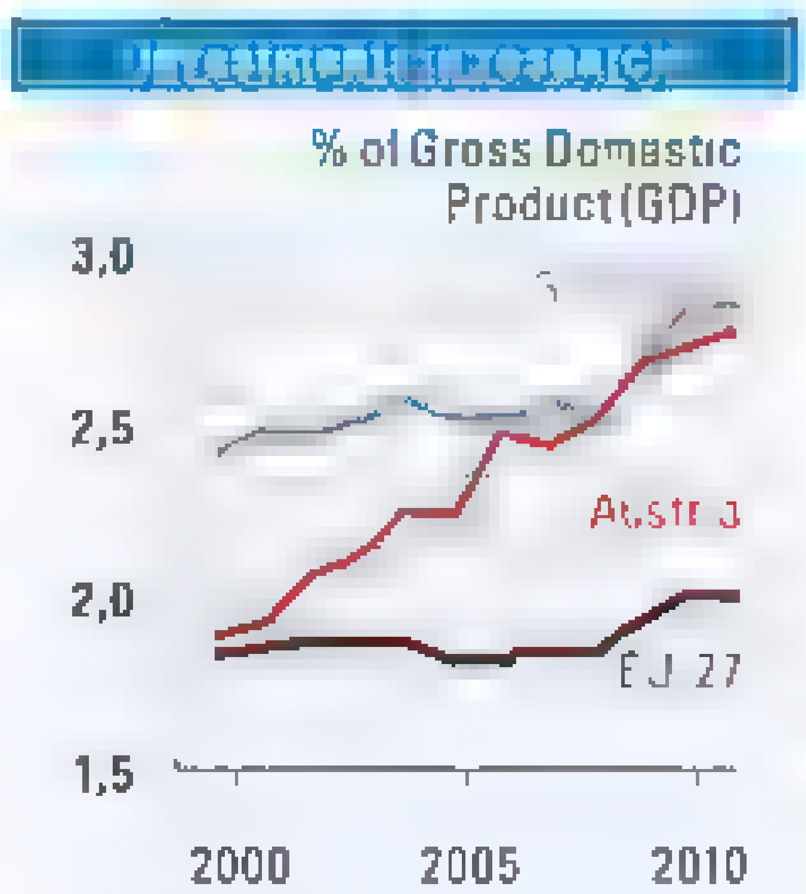

Development of R&D expenditures in Austria, Germany* and the EU 27

Source: Eurostat *2010 estimate

The Functions of Biological Diversity in an Age of Extinction

Shahid Naeem,[1]* J. Emmett Duffy,[2] Erika Zavaleta[3]

Ecosystems worldwide are rapidly losing taxonomic, phylogenetic, genetic and functional diversity as a result of human appropriation of natural resources, modification of habitats and climate, and the spread of pathogenic, exotic, and domestic plants and animals. Twenty years of intense theoretical and empirical research have shown that such biotic impoverishment can markedly alter the biogeochemical and dynamic properties of ecosystems, but frontiers remain in linking this research to the complexity of wild nature, and in applying it to pressing environmental issues such as food, water, energy, and biosecurity. The question before us is whether these advances can take us beyond merely invoking the precautionary principle of conserving biodiversity to a predictive science that informs practical and specific solutions to mitigate and adapt to its loss.

The biological organisms that are the engines of Earth's biogeochemistry, which strongly influences environmental conditions from local to global scales, also provide our food, biomaterials, biofuels, pollination, biocontrol, genetic resources, cultural values, and many other benefits. At a basic level, it is the cumulative mass of these organisms and their collective biological processes that fundamentally govern an ecosystem's biogeochemistry, but this mass often comprises a staggering diversity of organisms. Whereas the biological processes underlying biogeochemistry are generally well characterized, understanding the relationship of life's extraordinary diversity to biogeochemical or ecosystem functioning poses a fundamental challenge of modern science: Is biodiversity necessary to the functioning of ecosystems, or is it essentially an epiphenomenon of long- and short-term evolutionary and ecological processes?

The question of biodiversity's role in the functioning of ecosystems has been under intense investigation for two decades. Three volumes, one documenting the beginning, another the maturation, and the most recent the current state of the discipline, have been published; two consensus papers have addressed debates that dogged its early years; and numerous meta-analyses have quantitatively assessed central findings (*1*). From this rapidly expanding literature, we review three scientific frontiers that shape current research. Here, we focus primarily on the science, but given that we are living in an age of extinction (*2*) due to multiple anthropic drivers of biodiversity loss (Fig. 1)—with potentially profound implications for our future—we also touch on environmental insights gained from these two decades of research.

[1]Department of Ecology, Evolution, and Environmental Biology, Columbia University, New York, NY 10027, USA. [2]Virginia Institute of Marine Science, College of William and Mary, Gloucester Point, VA 23062, USA. [3]Environmental Studies Department, University of California, Santa Cruz, CA 95064, USA.

*To whom correspondence should be addressed. E-mail: sn2121@columbia.edu

The Frontier of Integrative Biodiversity

The first generation of studies on biodiversity's influence over ecosystem functioning asked simply whether the production of biomass (a commonly studied ecosystem function) varies predictably with species richness. Biodiversity, however, has many dimensions, species richness being only a measure of the taxonomic dimension (Box 1). Functional diversity, assessed as the number of functional groups, was recognized early on as a dimension that was a better predictor of ecosystem functioning; a proliferation of more objective trait-based measures of functional diversity followed (*3*). Working with multiple rather than single dimensions of biodiversity, of course, increases the complexity of current research. For example, Mouillot *et al.* (*4*) explored two measures of taxonomic diversity and six measures of functional diversity (based on five plant traits) to explain four independent ecosystem functions in an experimental manipulation of plant species richness in Germany—a far cry from simply comparing species richness to biomass production.

Adding functional diversity to taxonomic diversity in single studies was just a first step. Among several additional components of biodiversity, phylogenetic diversity has emerged as the best predictor of ecosystem functioning in several systems (*5–7*). Within species, genetic or genomic diversity is also proving to be an important dimension of biodiversity in governing ecosystem function (*8–11*). In experimental grassland plots, for example, increasing genetic diversity (one to eight genotypes) of a single species of primrose (*Oenothera biennis*) had the same positive effect on production as increasing taxonomic diversity from one to eight plant species, excluding primrose (*9*). Going further still, taxonomic diversity has been linked to interaction diversity, the complex web of interactions among species in a system. For example, in a grassland experiment, low-diversity plots (four plant species) produced lower interaction diversity among the 427 resident arthropod species than did high-diversity plots (16 plant species) (*12*). Taken to the extreme, the next step might seem to require conducting an experiment that examines the effects of taxonomic, functional, phylogenetic, genetic, spatial, temporal, landscape, and interaction diversity (all the dimensions we list in Box 1) to explain multiple ecosystem functions.

But such an additive progression—in which biodiversity and ecosystem function research steadily increases the number of dimensions of biodiversity it investigates—is not integrative nor likely tractable. Additive approaches primarily pit different dimensions of biodiversity against one another to identify the best predictor. In contrast, an integrative approach would seek the mechanistic underpinnings of ecosystem responses to biodiversity loss by focusing on the relationships among genes, traits, phylogeny, the biotic and abiotic factors that affect these relationships, and how all these ultimately explain ecosystem functioning.

The data requirements and statistical complexity involved in such an approach are daunting, but new technologies offer means by which they might be addressed. One promising example examined the functional genetics of how below-ground microbial diversity mediated ecosystem responses to elevated CO_2 by using 454 pyrosequencing of polymerase chain reaction amplicons and the GeoChip functional gene array containing more than 27,000 probes of more than 57,000 gene sequences in more than 250 gene families (*13*). This tool was used to quantify CO_2-induced changes in the composition of microbial functional genes associated with metabolic pathways in C, N, P, and S cycling, and related these responses to ecosystem functions such as soil C, soil N, and aboveground biomass production. This study illustrates our developing ability to integrate across relatively unexplored dimensions of biodiversity, such as microbial genetic and functional diversity, to explain ecosystem responses to key global change factors including biodiversity loss.

New technologies and newly accessible dimensions of biodiversity are currently shifting the field's goals. Once focused on simply examining which dimension of biodiversity was the better predictor of ecosystem functioning, the goals are now to better understand why and how multiple dimensions of biodiversity simultaneously influence ecosystem functioning.

Ecological Structure

Ecosystems are not random assemblages of species engaged in a hodgepodge of biogeochemical

processes. Rather, they are highly structured around two related elements. First, communities are structured by networks of interactions, in which species are the nodes and biotic interactions are the links (Fig. 2, lower panel). These links reflect exchanges or transfers of energy (in the form of organic compounds) and material (nutrients, water, biochemicals, and their elemental constituents) among interacting organisms. Second, ecosystems are structured by a network of biogeochemical pathways (Fig. 2, upper panel). Neither interaction networks nor biogeochemical pathways exist independently of the other: Organisms are pools of elements in biogeochemical pathways. This is a core idea in biodiversity and ecosystem functioning research, and is the basis of the unified theoretical framework recently developed by Loreau (*14*).

A growing body of work illustrates the key importance of this ecological structure to ecosystem functioning, operating through a multiplicity of effects of biodiversity change. Zavaleta *et al.* (*15*), for example, found that changes in plant species diversity in experimental grassland plots more strongly affected ecosystem functions and properties as more functions were considered together. Other experiments similarly highlight how ecological structure mediates complex effects on functioning, showing that loss of plant diversity cascades "upward" to trophic levels above ground and in the soil (*16*), that changes in plant diversity influence the stability of multiple insect trophic levels (*17*), that manipulations of arthropod trophic structure cascade "downward" to plants and ecosystem functions (*18*), and that manipulating fish biodiversity in freshwater systems influences ecosystem properties (*19*).

The influence of ecological structure on different dimensions of stability has been a mainstay of community ecological research since the late 1950s, but biodiversity and ecosystem functioning research has brought functional stability into sharper focus. Of particular note is that populations of individual species in diverse communities often fluctuate more in the face of environmental heterogeneity than ecosystem functions that are generally aggregate properties of all populations, although the particular outcome is dependent on the degree of interspecific interactions and demographic synchrony (*20*) among species. For example, the relative abundance of grassland species in Inner Mongolia fluctuates with precipitation over time, yet overall primary production of the system is less variable where diversity is high (*21*). Similarly, wild salmon populations in individual tributaries at Bristol Bay, Alaska, fluctuate considerably, but total production of salmon biomass through the whole system is much more constant (*22*). In these and other studies, it is the complementarity of species' responses to environmental heterogeneity that allows increased functional stability. Greater biodiversity can also allow for greater species turnover and compensatory growth as environments change, lowering system variability (*23*–*25*). These effects are variously known as statistical averaging, biological insurance, or the portfolio effect [see (*26*) for a review].

The impacts of biodiversity change on ecosystem function are clearly far richer than our historical focus on predominantly monotrophic,

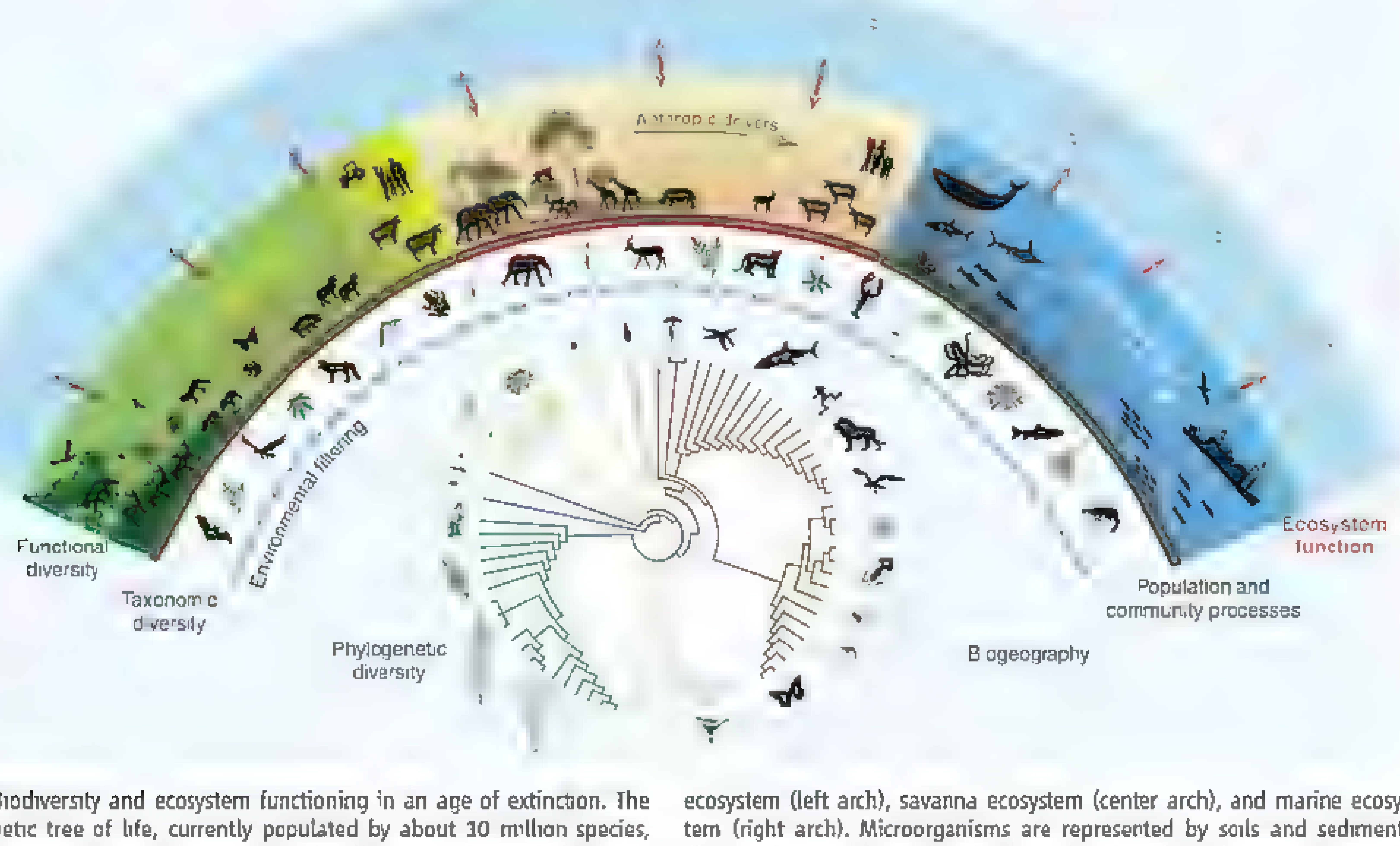

Fig. 1. Biodiversity and ecosystem functioning in an age of extinction. The phylogenetic tree of life, currently populated by about 10 million species, ranges from microscopic to enormous multicellular organisms, of which only a few representative phyla and divisions are shown as icons at the tips of the branches. Where species from the global phylogenetic pool are found is largely determined by environmental filters, represented here as a barrier with pores (dashed arch). Here we show only phylogenetic and taxonomic diversity, but biogeography, population processes, biotic interactions, metagenomic and intragenomic variation, and functional traits contribute to different dimensions of biodiversity (Box 1) that characterize the biota of each ecosystem. Three representative ecosystems are illustrated: a forested ecosystem (left arch), savanna ecosystem (center arch), and marine ecosystem (right arch). Microorganisms are represented by soils and sediments, illustrated as a dark band at the base of each arch. Each ecosystem contributes to ecosystem functioning, shown here primarily as biogeochemical processes (chemical exchanges between the atmosphere and biosphere shown in the outermost arch). Widespread extinction attributable to anthropic drivers (human transformations of ecosystems going from left to right in each arch) lead to biotic impoverishment (reductions in local biodiversity) and biotic homogenization (increasing dominance by domestic species). For clarity, the complexity of biogeochemical pathways and interaction networks (Figs. 2 and 3) is not shown.

Box 1. Dimensions of Biodiversity

Since 1988, when the term biodiversity was first published, its use has risen exponentially. Currently, as indexed by *Biological Abstracts*, more than 66,300 journal articles have used the term. Definitions, however, vary widely from the all-encompassing "diversity of life on Earth" to the enigmatic definition adopted by the UN Convention on Biological Diversity, "the variability among living organisms from all sources including, inter alia, terrestrial, marine and other aquatic ecosystems and the ecological complexes of which they are part; this includes diversity within species, between species and of ecosystems."

Connecting biodiversity to ecosystem functioning entails locating ecosystems in a multivariate space defined by dimensions that describe different ways of relating organisms to one another. Examples of these dimensions include:

- Taxonomic diversity: the number and relative abundance of taxa (e.g., species, genera, families, and onward) defined by a hierarchical, evolutionary classification
- Phylogenetic diversity: relationships among taxa based on elapsed time since divergence (e.g., sum of the branch lengths linking species in a phylogeny)
- Genetic diversity: nucleotide, allelic, chromosomal, genotypic, or other aspects of genomic variability
- Functional diversity: variation in the degree of expression of multiple functional traits
- Spatial or temporal diversity: rates of turnover of species through space or time
- Interaction diversity: characteristics of the network of linkages defined by biotic interactions, such as competition, predation, parasitism, or facilitation, with other species (food web and trophic networks are subsets of biotic networks)
- Landscape diversity: number, relative abundance, and distribution of different habitat types within a landscape

By these definitions, one community may be called more diverse than another if it has any combination of more species (taxonomic diversity), greater cumulative phylogenetic distance among its species (phylogenetic diversity), greater genotypic diversity within species (genetic diversity), greater distance among species in multivariate functional trait space (functional diversity), higher species turnover across a unit of space (spatial diversity), greater numbers of links per species in the interaction network (network diversity), and more habitat types within the landscape (landscape diversity). In practice, because the necessary data are often lacking, such a comprehensive assessment is untenable. Assessments are further complicated by the fact that the dimensions are not orthogonal (e.g., taxonomic, phylogenetic, and functional diversity correlate with one another) and may need to be differently weighted for particular applications (e.g., network diversity may be more important than taxonomic diversity when assessing biodiversity's influence over system stability).

monofunctional, monodimensional biodiversity studies has revealed. Such studies generally lacked the ecological structure inherent to ecosystems, which we increasingly realize is key to their functioning. The emphasis now is on discovering why increased biodiversity has mixed effects on stability and how to scale findings up to larger levels such as those of the Inner Mongolia and Alaska studies.

External Validity

In much of experimental ecological research, nature is seen as the complex, species-rich reference against which treatment effects are measured. In contrast, biodiversity and ecosystem functioning experiments often simply compare replicate ecosystems that differ in biodiversity, without any replicate serving as a reference to nature. Consequently, it has often been difficult to evaluate the external validity of biodiversity and ecosystem functioning research, or how its findings map onto the "real" worlds of conservation and decision making. Put another way, what light can be shed on the stewardship of nature by microbial microcosms that have no analogs in nature, or by experimental grassland studies in which some plots have, by design, no grass species?

The quest for external validation or generalizability has resulted in a steady increase in the diversity of taxa, ecosystems, and ecosystem functions and properties investigated. Such studies have dealt with bacteria [e.g., (*27*)], phytoplankton [e.g., (*28*)], marine angiosperms (*29*), trees [e.g., (*30*)], birds (*31*), and more. The generally positive influence of biodiversity on production and resource use efficiency has proven robust in studies that go beyond the traditional monotrophic approach [e.g., (*32*)] and that articulate with other ecological processes such as succession (*33*), metacommunity interactions (*34*), emigration and immigration (*35*), and assembly (*36*) and disassembly (*37*). Finally, longer-term studies that use higher levels of diversity, measure simultaneous effects on multiple functions (*15*, *38*), and measure emergent functions such as reliability (*24*) all suggest that the importance of biodiversity increases as research incorporates increasing complexity to better approximate nature.

Spatial scale is central in assessing the external validity of biodiversity and ecosystem functioning research because, relative to nature, typical experiments have less biodiversity and are smaller in size, shorter in duration, and much simpler in ecological structure. At large scales, in the absence of experimental manipulation, it can be difficult to determine the relationship between biodiversity and ecosystem functioning. The relationship between primary production and plant species richness is a classic example that has not yet been resolved despite more than 30 years of research (*39*). Observational studies can solve some of these problems by using statistical methods to partition the effects of biodiversity from other factors in large ecosystems subject to complex environmental forcing. For example, Maestre *et al.* (*40*) examined the influence of plant species richness—relative to climatic, geopositional, and edaphic factors—on ecosystem multifunctionality (a measure incorporating 14 ecosystem functions) across 224 dryland ecosystems. They found that plant species richness was positively associated with ecosystem multifunctionality, although it explained less than 3% of the variation. Other observational studies that used structural equations modeling to partition covariation among variables in complex causal models have found that biodiversity's effects vary but can be quite strong relative to other environmental drivers [e.g., compare (*30*, *41*)].

Another challenge to evaluating external validity is that theoretical, simulation, observational, and experimental studies often provide seemingly different answers to the same question, making it difficult to identify generalities and achieve consensus. Meta-analyses and integrative studies can help to address this issue. Meta-analyses have identified central tendencies in biodiversity and ecosystem functioning's diverse arrays of studies [e.g., (*42*–*46*)].

An emerging approach of much promise is to manipulate or simulate more realistic scenarios of biodiversity loss, rather than the randomized loss typical of past studies (*47*–*51*); these scenario-based approaches often find quite different impacts on ecosystem functioning than random losses, emphasizing the sensitivity of ecosystem functioning to specific stressors, such as pollution or overharvesting, or perturbations, such as fire or drought. For example, McIntyre *et al.* (*50*) found that simulated random extinctions (typical of traditional approaches in biodiversity and ecosystem functioning research) of freshwater fish species in Rio Las Marias, Venezuela, resulted in linear declines of N cycling rates, but if rare species had a higher probability of extinction due to greater sensitivity to fishing pressures (a more realistic scenario for species loss), then declines were asymptotic.

Although it is not easy to gauge when an ecological discipline has validated itself by showing

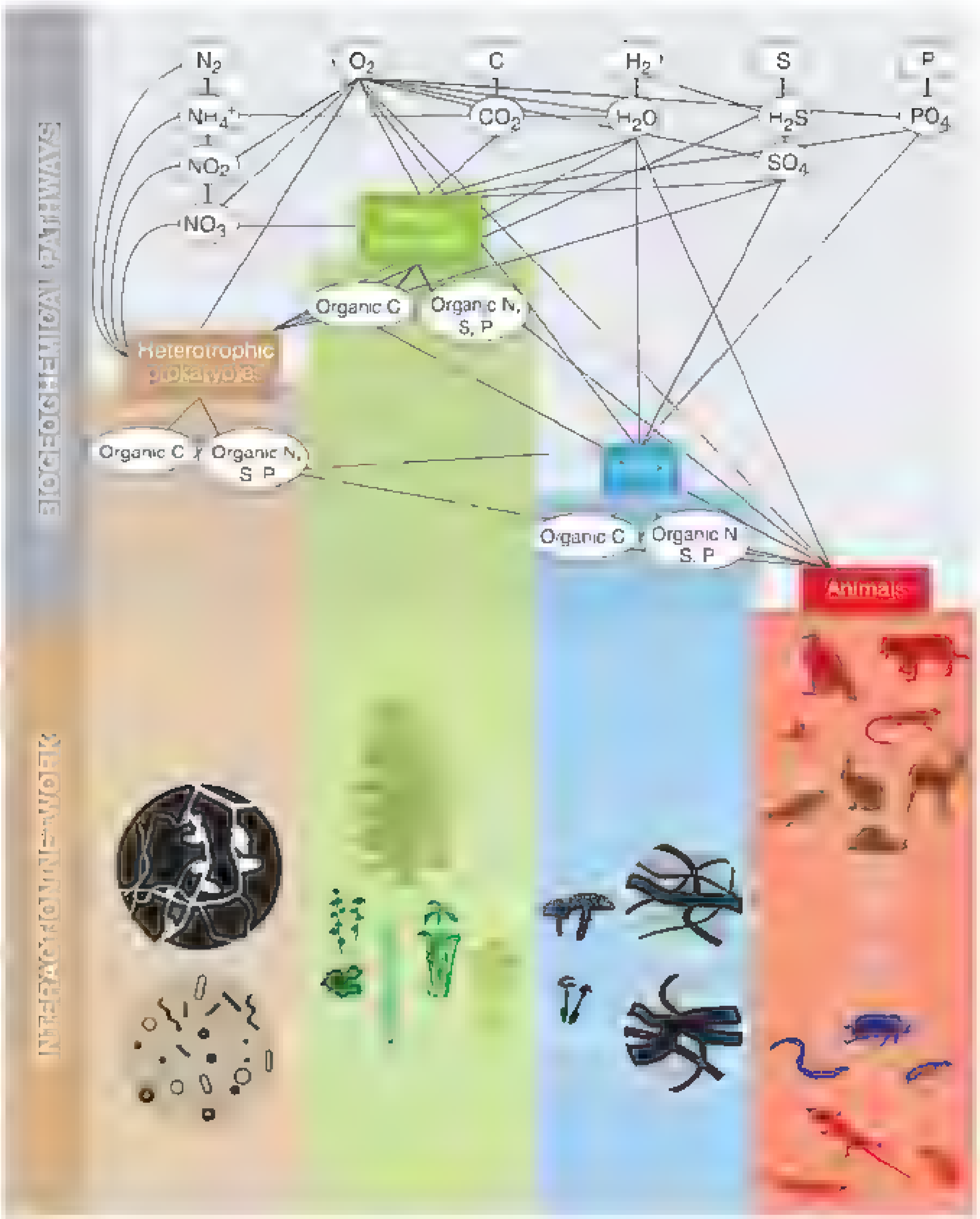

Fig. 2. Ecological structure in terrestrial systems. Biodiversity and ecosystem functioning research couples biogeochemical pathways (upper panel) with interaction networks (lower panel). Biogeochemical pathways, or elemental and material fluxes, are illustrated for C, H, N, O, P, and S. Biological contributions are collected into four groups defined by major taxa: heterotrophic prokaryotes, photoautotrophs (plants), fungi, and animals. Interaction networks are illustrated for each group, with animals organized from top to bottom (by color) as carnivores, herbivores, microbivores and detritivores, and detrital carnivores. We show only two fungal and two heterotrophic prokaryote trophic groups: decomposers and plant uptake facilitators such as rhizobia bacteria living in the nodulated roots of legumes (upper circle of heterotrophic prokaryotes), or fungal mycorrhizal associates (hyphal masses in upper circle and mushrooms in fungi). Colored vertical bars link sources of mass for each species in the lower panel to the biogeochemical group where the mass is produced. The figure shows all organisms, whether above or below ground, as pools of elements and all interactions as pathways of energy and material transfer among organisms.

one-to-one correspondence with all the complexity inherent in nature, hundreds of studies over the past two decades have examined many individual facets of nature's complexity. Collectively, the emerging picture is compelling. Few ecological disciplines have been as thoroughly scrutinized as biodiversity and ecosystem functioning, but there are still many issues to be addressed and gaps to fill. To illustrate, Fig. 3 shows a landscape consisting of a freshwater ecosystem (such as a lake) located within a forested ecosystem, with the many elements of biodiversity and ecosystem function that characterize such an idealized landscape. Most of the elements shown in Fig. 3 have been explored by biodiversity and ecosystem functioning research, although some of these themes would benefit from closer study, such as (i) how the effects of apex species loss ripple through biotic networks and biogeochemical pathways, (ii) how changes in genetic and interaction diversity influence ecosystem functioning, and (iii) how landscape connections are affected by changes in biodiversity.

Although some disagreement remains, the collective results of biodiversity and ecosystem functioning studies offer growing confidence that the general findings of early biodiversity and ecosystem functioning studies are robust and may even underestimate diversity's role in nature (*52*). The frontier now consists of exploring the impacts of realistic loss of multiple biodiversity components on ecological structure and how this affects the dynamics of ecosystem functioning, rather than repeating existing studies with different species in different ecosystems.

Current Challenges

Twenty years of research has answered the initial confirmatory questions in biodiversity and ecosystem functioning research, yielding a field today that is complex, broad in scope, and able to provide important insights into the ecosystem consequences of biodiversity change. The field now grapples with four specific challenges.

1. In order for biodiversity and ecosystem functioning to become a strongly predictive science, it needs efficient ways to extrapolate information about key functional traits of known species to estimate the traits of poorly known species, which number in the millions, especially microbial species.

2. Biodiversity and ecosystem functioning research needs to embrace the challenge of extracting order from complexity. The greater the focus on the multifunctionality and multiple integrated dimensions of biodiversity characteristic of wild nature, the more useful the conclusions that can be drawn concerning how ecological structure shapes the influence of biodiversity changes on the functioning of real ecosystems. Meeting this challenge is particularly important in light of increasing concerns over environmental tipping points and safe planetary boundaries.

3. Ecological research needs to better integrate advanced technologies. The use of such technologies as pyrosequencing and remote sensing will better enable measurement of the impact of changes in functional diversity (at the level of genes and traits of individual organisms) on ecosystem functions at local and global levels.

4. Similarly, research on biodiversity and ecosystem functioning must take advantage of increasingly powerful statistical methodologies and observatory systems such as the recently commissioned National Ecological Observatory Network (NEON), the Global Biodiversity Information Facility (GBIF), and the Global Earth Observation System of Systems (GEOSS). These facilities offer both promise and challenges for more accurately parsing the effects

of biodiversity and biodiversity change from other factors controlling ecosystem functions at larger scales.

The Environmental Implications of Biodiversity and Ecosystem Functioning Research

The chief contribution of research on biodiversity and ecosystem functioning has been to articulate, and provide compelling scientific support for, the idea that maintaining a high proportion of biological diversity leads to efficient and stable levels of ecosystem functioning. Although this review's focus has been on scientific issues, biodiversity and ecosystem functioning research has also contributed to environmental science by linking biodiversity to ecosystem services that benefit humans. This construct formed the foundation of the Millennium Ecosystem Assessment's framework (*53*), is central to the 2020 targets of the Convention on Biological Diversity (*54*), and is also the foundation for the new United Nations Intergovernmental Platform on Biodiversity and Ecosystem Services, signed by 90 member states on 23 April 2012.

The straightforward environmental message of biodiversity and ecosystem functioning is essentially a statement of the precautionary principle: that biodiversity conservation ensures ecosystem functions that in turn ensure ecosystem services benefiting humanity. A number of studies have examined the connections between biodiversity and ecosystem services in the form of food provision, disease resistance, and economic benefits. For example, a detailed survey showed that greater diversity of bird hosts in the eastern United States is associated with lower incidence of West Nile virus in humans (*31*). Higher diversity of wildlife has also been shown to increase economic benefits to human communities in Namibia (*55*). Planting more diverse varieties of rice in Yunnan Province in China improved resistance to fungal pathogens so strongly that fungicides were

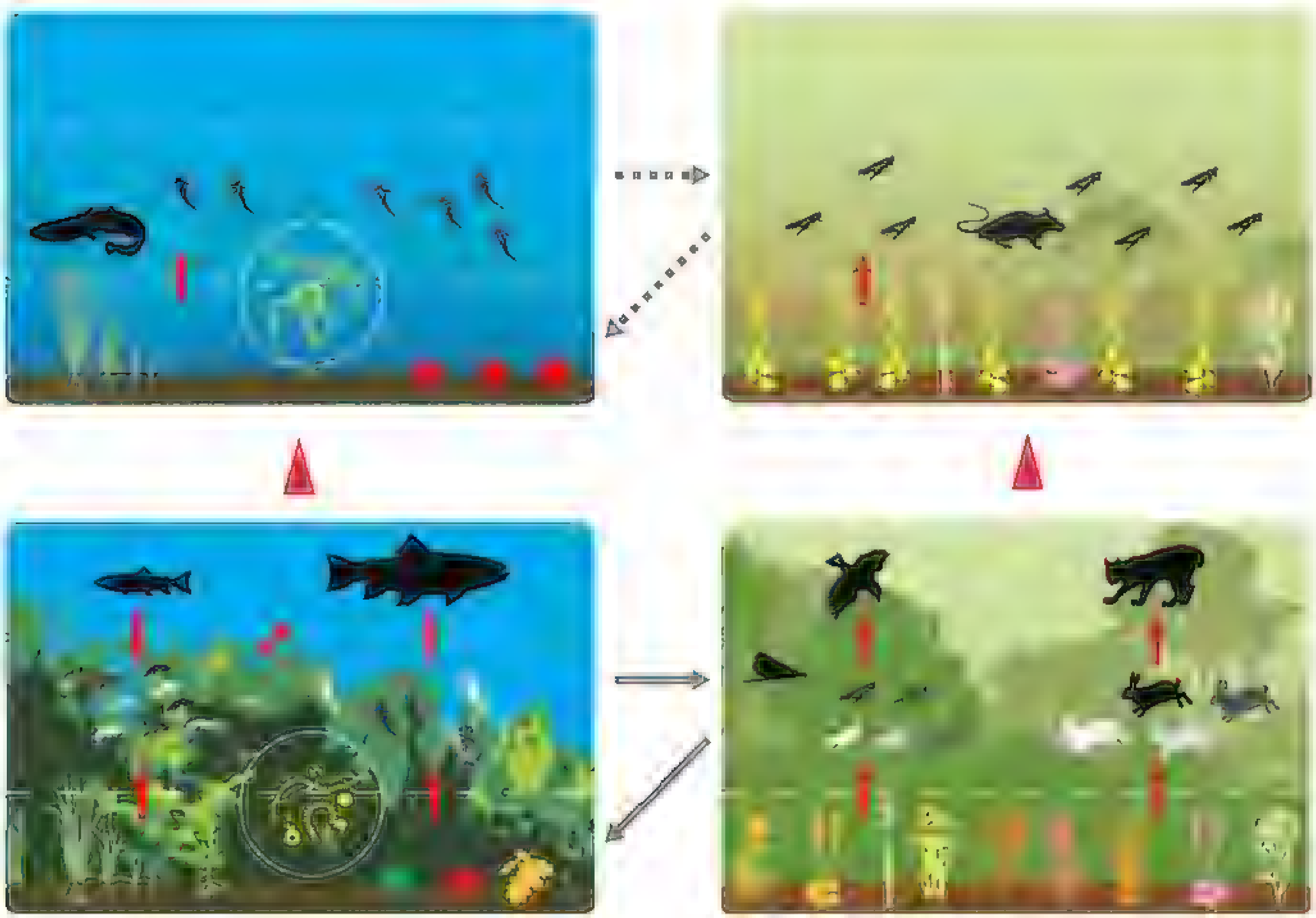

Fig. 3. External validation. Ecosystems are characterized by a complex set of organisms, biogeochemical pathways, energy and nutrient fluxes, and many other elements of ecological structure (Fig. 2), but most biodiversity and ecosystem functioning studies examine only one or a few of these elements, making it difficult to know whether their findings are valid. This figure illustrates several of these elements for a landscape comprising a freshwater aquatic ecosystem within a forested terrestrial ecosystem. Interaction diversity is shown as a three-level trophic network in which species in one level feed on species below them. Taxonomic and functional diversity are shown as different colors and forms within levels. Genetic diversity is shown as different shades of gray among the amphipods and mayfly larvae in the middle level of the freshwater system and for the grasshoppers and rabbits in the terrestrial system. Red arrows within panels indicate the transfer of nutrients and energy between organisms among levels. Gray arrows between lower panels represent how habitat diversity influences nutrient and energy flow within a landscape: The freshwater system receives terrestrial inputs (shown as different tree leaves on the sediment surface) and the terrestrial system receives inputs from the freshwater system (shown as a mayfly entering the terrestrial system). Human impacts on biodiversity are illustrated by the change in each of these elements from the bottom panels to the top panels. Both systems have lost apex predators and their top trophic level is empty, representing a decline in "vertical diversity." Human-mediated gain in biodiversity is shown as an exotic catfish having entered the freshwater system and an exotic rat and plant having entered the terrestrial system. Microorganisms are represented by the brown bands at the base of each panel and also as plankton (in the white circle in the water) in the freshwater system.

not needed in the intercropped system (*56*). A promising frontier in this arena is quantifying the influence of biodiversity on multiple services, to reduce the tendency for single-service analyses to miss important trade-offs (*57*).

After two decades of research, we now appreciate more keenly that biodiversity is one of multiple factors that govern ecosystem properties, and that changes in both the number and identity of species, genes, and functional types imposed by human actions can yield ecosystem effects that vary from small to far-reaching and cascading. The theoretical emphasis of inquiry into biodiversity and ecosystem functioning has also helped to build first principles and new theory for understanding how the natural world works at fundamental levels. That is, we have mechanistic theories, refined through substantial empirical testing across taxa and systems, that we can now carry forward and apply to other systems, including the human-dominated, domesticated ecosystems that already dominate much of the world (*58*).

The Future in an Age of Extinction

The frontiers of biodiversity and ecosystem functioning research are rapidly expanding as new approaches and technologies, and a rapidly growing database, allow researchers to address questions at levels of precision and scale not possible in 1992 when the field formally began. There is no question that we need new data, tools, and approaches to understand how growing biotic impoverishment and biotic homogenization will influence ecosystem functioning and the environmental and economic fates of nations. The Millennium Ecosystem Assessment (*59*), guided in part by advances in biodiversity and ecosystem functioning research, moved us beyond the state of affairs in 1992, when the precautionary principle was the chief message that helped to shape biodiversity policy, by linking biodiversity to human well-being in a range of systems around the world. What biodiversity and ecosystem functioning can continue to contribute includes theory, understanding, and practical tools to tell us when, where, and what kinds of biodiversity changes are likely to have far-reaching and cascading effects on ecosystem properties. An increasingly robust implication of this research for a wide array of ecologically dependent practices and businesses—such as habitat restoration, conservation, public health management, biosecurity, agriculture, agroforestry, aquaculture, and environmental monitoring—is that their short- and long-term goals are often better met by increasing biodiversity and focusing on multiple rather than single functions. But time is short; the next decade will be an important period for testing these implications in the real world, outside the domain of theoretical, laboratory, and field-based experimental studies that dominate present research.

The central environmental message of biodiversity and ecosystem functioning research, to conserve biodiversity to improve human well-being, has historically been essentially utilitarian in its reasoning. This focus is sometimes understandably seen as contrary to widespread and urgent conservation efforts to save species and ecosystems from extinction for non-utilitarian, cultural reasons (*60*). Indeed, species targeted for conservation, reserves, and protected areas represent a tiny fraction of the biosphere and are therefore not likely to strongly influence biogeochemically derived ecosystem services such as carbon sequestration and food production. Yet the cultural values of biological diversity can themselves be construed as ecosystem services, and their preservation is fully coherent with non-utilitarian conservation efforts and arguably no less important. Nothing in biodiversity and ecosystem functioning research should dissuade conservation from its efforts to bring our age of extinction to a halt.

Biodiversity and ecosystem functioning research is now maturing; it has advanced sufficiently to move beyond simply invoking the precautionary principle as it has done throughout its history. This research has helped to clarify why protecting biodiversity is a goal of fundamental importance and can support efforts to safeguard the intrinsic capacity of ecosystems for self-renewal, adaptive dynamics, and supporting humanity now and for generations to come.

References and Notes

1. S. Naeem, D. E. Bunker, A. Hector, M. Loreau, C. Perrings, Eds., *Biodiversity, Ecosystem Functioning, and Human Wellbeing: An Ecological and Economic Perspective* (Oxford Univ. Press, Oxford, 2009).
2. A. D. Barnosky *et al.*, *Nature* **471**, 51 (2011).
3. D. Schleuter, M. Daufresne, F. Massol, C. Argillier, *Ecol. Monogr.* **80**, 469 (2010).
4. D. Mouillot, S. Villéger, M. Scherer-Lorenzen, N. W. H. Mason, *PLoS ONE* **6**, e17476 (2011).
5. D. F. B. Flynn, N. Mirotchnick, M. Jain, M. I. Palmer, S. Naeem, *Ecology* **92**, 1573 (2011).
6. M. W. Cadotte, J. Cavender-Bares, D. Tilman, T. H. Oakley, *PLoS ONE* **4**, e5695 (2009).
7. J. Connolly *et al.*, *Ecology* **92**, 1385 (2011).
8. L. Latta *et al.*, *Evol. Ecol.* **25**, 1107 (2011).
9. S. C. Cook-Patton, S. H. McArt, A. L. Parachnowitsch, J. S. Thaler, A. A. Agrawal, *Ecology* **92**, 915 (2011).
10. M. W. Cadotte, K. Carscadden, N. Mirotchnick, *J. Appl. Ecol.* **48**, 1079 (2011).
11. C. W. Hargrave, K. D. Hambright, L. J. Weider, *Ecology* **92**, 1226 (2011).
12. M. Rzanny, W. Voigt, *J. Anim. Ecol.* (2012).
13. Z. He *et al.*, *Ecol. Lett.* **13**, 564 (2010).
14. M. Loreau, *From Populations to Ecosytems: Theoertical Foundations for a New Ecological Synthesis* (Princeton Univ. Press, Princeton, NJ, 2010).
15. E. S. Zavaleta, J. R. Pasari, K. B. Hulvey, G. D. Tilman, *Proc. Natl. Acad. Sci. U.S.A.* **107**, 1443 (2010).
16. C. Scherber *et al.*, *Nature* **468**, 553 (2010).
17. N. M. Haddad, G. M. Crutsinger, K. Gross, J. Haarstad, D. Tilman, *Ecol. Lett.* **14**, 42 (2011).
18. O. J. Schmitz, *Ecology* **90**, 2339 (2009).
19. M. P. Carey, D. H. Wahl, *Oikos* **120**, 84 (2011).
20. M. Loreau, C. de Mazancourt, *Am. Nat.* **172**, E48 (2008).
21. Y. Bai, X. Han, J. Wu, Z. Chen, L. Li, *Nature* **431**, 181 (2004).
22. D. E. Schindler *et al.*, *Nature* **465**, 609 (2010).
23. E. Allan *et al.*, *Proc. Natl. Acad. Sci. U.S.A.* **108**, 17034 (2011).
24. A. Hector *et al.*, *Ecology* **91**, 2213 (2010).
25. N. R. Franssen, M. Tobler, K. B. Gido, *Oikos* **120**, 582 (2011).
26. J. N. Griffin *et al.*, in *Biodiversity, Ecosystem Functioning, and Human Wellbeing*, S. Naeem, D. E. Bunker, A. Hector, M. Loreau, C. Perrings, Eds. (Oxford Univ. Press, Oxford, 2009), pp. 78–93.
27. T. Bell, J. A. Newman, B. W. Silverman, S. L. Turner, A. K. Lilley, *Nature* **436**, 1157 (2005).
28. M. Striebel, S. Behl, S. Diehl, H. Stibor, *Am. Nat.* **174**, 141 (2009).
29. C. Gustafsson, C. Boström, *Oikos* **120**, 1037 (2011).
30. A. Paquette, C. Messier, *Glob. Ecol. Biogeogr.* **20**, 170 (2011).
31. J. P. Swaddle, S. E. Calos, *PLoS ONE* **3**, e2488 (2008).
32. J. E. Duffy, J. P. Richardson, K. E. France, *Ecol. Lett.* **8**, 301 (2005).
33. E. Maggi, I. Bertocci, S. Vaselli, L. Benedetti-Cecchi, *Ecology* **92**, 1399 (2011).
34. M. Loreau, N. Mouquet, A. Gonzalez, *Proc. Natl. Acad. Sci. U.S.A.* **100**, 12765 (2003).
35. K. E. France, J. E. Duffy, *Nature* **441**, 1139 (2006).
36. T. Fukami *et al.*, *Ecol. Lett.* **13**, 675 (2010).
37. E. Zavaleta *et al.*, *Ann. N.Y. Acad. Sci.* **1162**, 311 (2009).
38. F. Isbell *et al.*, *Nature* **477**, 199 (2011).
39. P. B. Adler *et al.*, *Science* **333**, 1750 (2011).
40. F. T. Maestre *et al.*, *Science* **335**, 214 (2012).
41. E. Weiher, S. Forbes, T. Schauwecker, J. B. Grace, *Oikos* **106**, 151 (2004).
42. B. J. Cardinale *et al.*, *Nature* **443**, 989 (2006).
43. B. Worm *et al.*, *Science* **314**, 787 (2006).
44. B. Schmid *et al.*, in *Biodiversity, Ecosystem Functioning, and Human Wellbeing*, S. Naeem, D. E. Bunker, A. Hector, M. Loreau, C. Perrings, Eds. (Oxford Univ. Press, Oxford, 2009), pp. 14–29.
45. D. K. Letourneau, J. A. Jedlicka, S. G. Bothwell, C. R. Moreno, *Annu. Rev. Ecol. Evol. Syst.* **40**, 573 (2009).
46. B. J. Cardinale *et al.*, *Am. J. Bot.* **98**, 572 (2011).
47. F. I. Isbell, D. A. Losure, K. A. Yurkonis, B. J. Wilsey, *Oikos* **117**, 996 (2008).
48. M. E. Bracken, S. E. Friberg, C. A. Gonzalez-Dorantes, S. L. Williams, *Proc. Natl. Acad. Sci. U.S.A.* **105**, 924 (2008).
49. P. C. Selmants, E. S. Zavaleta, J. R. Pasari, D. L. Hernandez, *J. Ecol.* **100**, 723 (2012).
50. P. B. McIntyre, L. E. Jones, A. S. Flecker, M. J. Vanni, *Proc. Natl. Acad. Sci. U.S.A.* **104**, 4461 (2007).
51. S. Naeem, *Trends Ecol. Evol.* **23**, 414 (2008).
52. J. E. Duffy, *Front. Ecol. Environ* **7**, 437 (2009).
53. Millennium Ecosystem Assessment, *Ecosystems and Human Well-Being: A Framework for Assessment* (Island, Washington, DC, 2003); pdf.wri.org/ecosystems_human_wellbeing.pdf.
54. C. Perrings *et al.*, *Front. Ecol. Environ* **9**, 512 (2011).
55. R. Naidoo, L. C. Weaver, G. Stuart-Hill, J. Tagg, *J. Appl. Ecol.* **48**, 310 (2011).
56. Y. Zhu *et al.*, *Nature* **406**, 718 (2000).
57. I. A. Dickie *et al.*, *J. Appl. Ecol.* **48**, 926 (2011).
58. P. Kareiva, S. Watts, R. McDonald, T. Boucher, *Science* **316**, 1866 (2007).
59. Millennium Ecosystem Assessment, *Ecosystems and Human Well-Being: Synthesis* (Island, Washington, DC, 2005); www.millenniumassessment.org/documents/document.356.aspx.pdf.
60. D. S. Srivastava, M. Vellend, *Annu. Rev. Ecol. Evol. Syst.* **36**, 267 (2005).

Acknowledgments: We thank two anonymous reviewers for their comments and suggestions. Supported by NSF grants OCE-1031061 (J.E.D.), DEB-0639161 (S.N.), and DEB-0918715 (E.Z.).

10.1126/science.1215855

Massive Phytoplankton Blooms Under Arctic Sea Ice

Kevin R. Arrigo,*† Donald K. Perovich, Robert S. Pickart, Zachary W. Brown, Gert L. van Dijken, Kate E. Lowry, Matthew M. Mills, Molly A. Palmer, William M. Balch, Frank Bahr, Nicholas R. Bates, Claudia Benitez-Nelson, Bruce Bowler, Emily Brownlee, Jens K. Ehn, Karen E. Frey, Rebecca Garley, Samuel R. Laney, Laura Lubelczyk, Jeremy Mathis, Atsushi Matsuoka, B. Greg Mitchell, G. W. K. Moore, Eva Ortega-Retuerta, Sharmila Pal, Chris M. Polashenski, Rick A. Reynolds, Brian Schieber, Heidi M. Sosik, Michael Stephens, James H. Swift

The seasonal sea ice and snow cover in the Arctic Ocean strongly reflect and attenuate incoming solar radiation. Consequently, current estimates of pan-Arctic primary productivity assume that the growth and biomass of phytoplankton, free-floating single-celled photosynthetic organisms at the base of the marine food web, are negligible in waters beneath ice because of insufficient light (*1*). However, during the 2011 ICESCAPE (Impacts of Climate on EcoSystems and Chemistry of the Arctic Pacific Environment) cruise, we observed a massive phytoplankton bloom that had developed beneath the 0.8- to 1.3-m-thick first-year sea ice on the Chukchi Sea continental shelf.

From 4 to 8 July, we sampled (*2*) along two 250-km transects extending from open water far into the ice pack (fig. S1). Depth-integrated phytoplankton biomass beneath the ice was extremely high (Figs. 1, A and B), about fourfold greater than in open water. This massive under-ice bloom extended for >100 km into the ice pack. Peak particulate organic carbon biomass (28.7 to 32.5 g C m^{-2}) was located far within the pack in the vicinity of the shelf break where ice was thickest and nutrient upwelling had been driven by easterly winds. Biomass was greatest (>1000 mg C m^{-3}) near the ice/seawater interface and was associated with nutrient depletion to depths of 20 to 30 m (Fig. 1, C and D), indicative of phytoplankton, rather than ice algal, growth. Species composition of the bloom was distinct from that in the overlying ice and was overwhelmingly (>80% by cell cross-sectional area) dominated by healthy pelagic diatoms of the genera *Chaetoceros*, *Thalassiosira*, and *Fragilariopsis*. Furthermore, rates of phytoplankton growth (0.83 to 1.44 day^{-1}) and carbon fixation (1.2 to 2.0 mg C mg^{-1} chlorophyll *a* hour^{-1}), and the maximum efficiency of photosystem II (>0.5), were high to depths of >50 m within the under-ice bloom.

In contrast, phytoplankton biomass in open waters was markedly lower than that beneath the ice and was greatest at depths of 20 to 50 m (Fig. 1, A and B) because of nutrient depletion near the surface (Fig. 1, C and D). The high oxygen (480 µmol l^{-1}) and low dissolved inorganic carbon (2020 µmol l^{-1}) relative to the low phytoplankton concentrations (~150 mg C m^{-3}) in these nutrient-depleted waters suggest that they had recently supported high rates of phytoplankton growth. Thus, the ice-free portions of both transects likely harbored remnant under-ice blooms that had developed near the surface weeks earlier, when the region was ice-covered.

The light required by the under-ice bloom had to penetrate the fully consolidated ice pack to reach the upper ocean. Light transmission through ice was enhanced by a recent increase in the fraction of first-year ice, which is much thinner (0.5 to 1.8 m) than the historically dominant multiyear ice pack (2 to 4 m), and especially by a high surface melt pond fraction (25 to 50%). Optical measurements showed that the ice beneath these melt ponds transmitted fourfold more incident light (47 to 59%) than adjacent snow-free ice (13 to 18%). Although the under-ice light field was less intense than in ice-free waters, it was sufficient to support the blooms of under-ice phytoplankton, which grew twice as fast at low light as their open ocean counterparts.

The Arctic Ocean has an enormous, mostly ice-covered continental shelf, ~50% of which has surface nitrate concentrations >10 µmol l^{-1} in early spring (*3*), making these potential sites for under-ice phytoplankton blooms. Previous reports hinted at similar blooms in the Barents Sea, Beaufort Sea, and Canadian Arctic Archipelago (*4*–*6*), suggesting that under-ice blooms are widespread. If so, current rates of annual net primary production on Arctic continental shelves, based only on open water measurements, may be drastic underestimates, being 10-fold too low in our study area. Work is still required to determine the timing and spatial distribution of under-ice phytoplankton blooms across the Arctic Ocean, the extent to which they are controlled by thinning sea ice and proliferating melt pond fractions, and how they affect marine ecosystems. This is particularly important if we are to understand and predict the biological and biogeochemical impacts of ongoing and future changes in the Arctic Ocean physical environment.

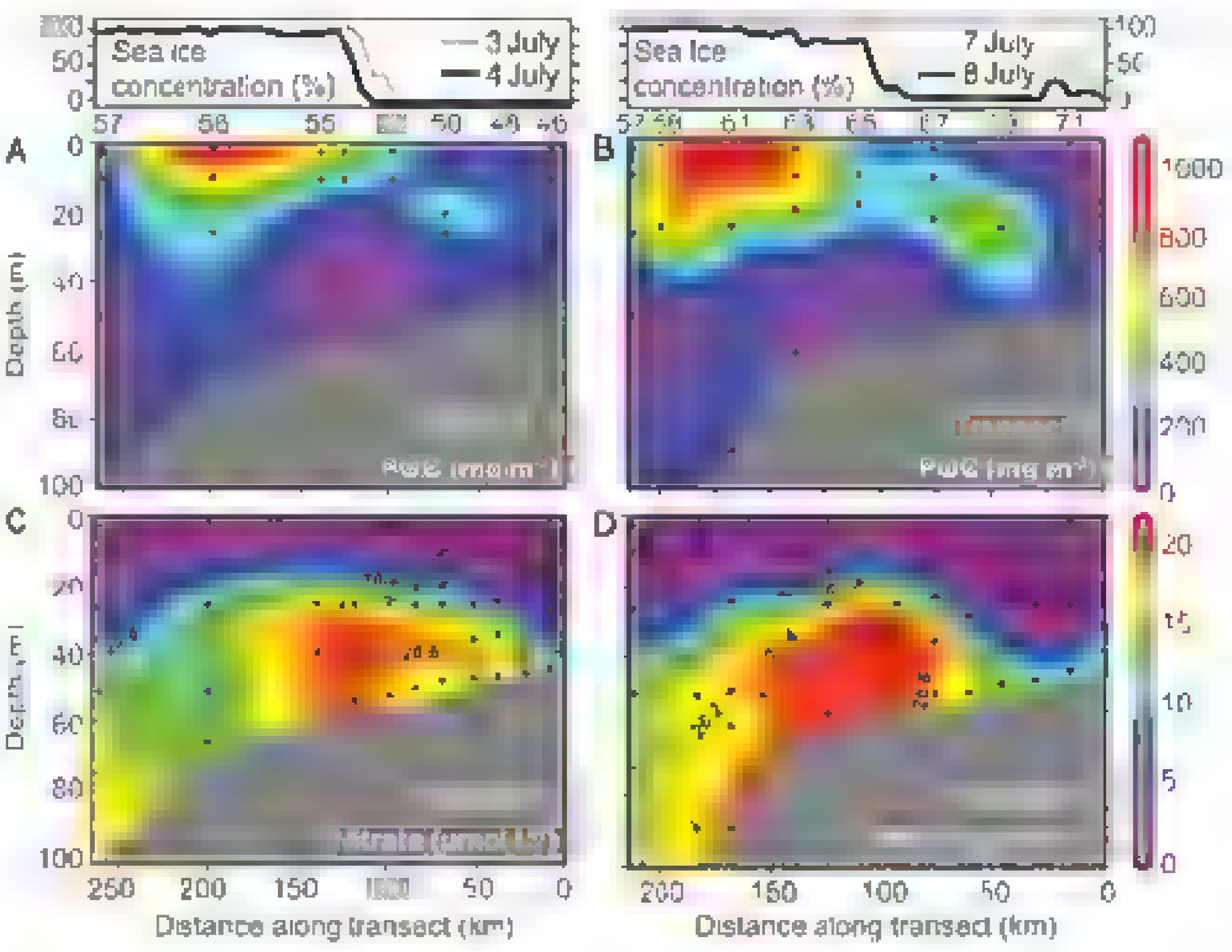

Fig. 1. Under-ice phytoplankton bloom observed during ICESCAPE 2011. **(A)** Particulate organic carbon (POC) and **(C)** nitrate from transect 1. **(B)** POC and **(D)** nitrate from transect 2. Sea ice concentrations and station numbers are shown above (A) and (B); black dots represent sampling depths; black lines denote potential density.

References and Notes

1. K. R. Arrigo, G. L. van Dijken, *J. Geophys. Res.* **116**, C09011 (2011).
2. Materials and methods are available as supplementary materials on *Science* Online.
3. J. Zhang *et al.*, *J. Geophys. Res.* **115**, C10015 (2010).
4. V. H. Strass, E.-M. Nöthig, *Polar Biol.* **16**, 409 (1996).
5. C. J. Mundy *et al.*, *Geophys. Res. Lett.* **36**, L17601 (2009).
6. M. Fortier, L. Fortier, C. Michel, L. Legendre, *Mar. Ecol. Prog. Ser.* **225**, 1 (2002).

Acknowledgments: We thank the crew of the U.S. Coast Guard Cutter *Healy* for their dedication. This research was supported by the Ocean Biology and Biogeochemistry and the Cryospheric Sciences programs of NASA. Data deposited in the Dryad Repository: http://dx.doi.org/10.5061/dryad.4dn793t6. R. J. Olson and H.M.S. have U.S. Patent Application 20090109432.

Supplementary Materials
www.sciencemag.org/cgi/content/full/336/6087/1408/DC1
Materials and Methods
Fig. S1
References (*7*–*15*)

10 October 2011; accepted 7 March 2012
10.1126/science.1215065

*The full list of author affiliations can be found in the supplementary materials.

†To whom correspondence should be addressed. E-mail: arrigo@stanford.edu

U-Series Dating of Paleolithic Art in 11 Caves in Spain

A. W. G. Pike,[1*] D. L. Hoffmann,[2,3] M. García-Diez,[4] P. B. Pettitt,[5] J. Alcolea,[6] R. De Balbín,[6] C. González-Sainz,[7] C. de las Heras,[8] J. A. Lasheras,[8] R. Montes,[8] J. Zilhão[9]

Paleolithic cave art is an exceptional archive of early human symbolic behavior, but because obtaining reliable dates has been difficult, its chronology is still poorly understood after more than a century of study. We present uranium-series disequilibrium dates of calcite deposits overlying or underlying art found in 11 caves, including the United Nations Educational, Scientific, and Cultural Organization (UNESCO) World Heritage sites of Altamira, El Castillo, and Tito Bustillo, Spain. The results demonstrate that the tradition of decorating caves extends back at least to the Early Aurignacian period, with minimum ages of 40.8 thousand years for a red disk, 37.3 thousand years for a hand stencil, and 35.6 thousand years for a claviform-like symbol. These minimum ages reveal either that cave art was a part of the cultural repertoire of the first anatomically modern humans in Europe or that perhaps Neandertals also engaged in painting caves.

European Upper Paleolithic cave painting and engraving are among some of the earliest examples of art and human symbolic behavior, although there is considerable uncertainty in when they began and how styles and practices developed. Accurate dating would help determine whether they arrived with the earliest populations of anatomically modern humans by 35 to 40 thousand years ago, were a by-product of their interaction with Neandertals, or developed later (*1*–*4*). Distinct phases are recognized in the art, based on technique, theme, style, and superimposition (*5*), but it is unclear whether these overlapped or evolved. Engravings and, in many cases, paintings lack organic pigments or binders suitable for accelerator mass spectrometry radiocarbon dating (*6*). Where suitable material exists (e.g., charcoal pigments), only small samples can be dated so as to minimize damage to the art, magnifying the effects of contamination and resulting in larger uncertainties. Discrepancies between multiple ^{14}C determinations on a single painted motif have been common, as are discrepancies between the dates of different chemical (e.g., humic/humin) fractions of the same sample (*7*).

[1]Department of Archaeology and Anthropology, University of Bristol, 43 Woodland Road, Bristol BS8 1UU, UK. [2]Bristol Isotope Group, School of Geographical Sciences, University of Bristol, University Road, Bristol BS8 1SS, UK. [3]Centro Nacional de Investigación sobre la Evolución Humana (CENIEH), Paseo Sierra de Atapuerca s/n, 09002 Burgos, Spain. [4]Department of Geography, Prehistory and Archaeology, University of Basque Country (UPV/EHU), c/ Tomas y Valiente s/n, 01006 Vitoria, Spain. [5]Department of Archaeology, University of Sheffield, Northgate House, West Street, Sheffield S1 4ET, UK. [6]Prehistory Section, University of Alcalá de Henares, c/ Colegios 2, 28801 Alcalá de Henares, Madrid, Spain. [7]Department of Historic Sciences, University of Cantabria, Avenida Los Castros s/n, 39005 Santander, Spain. [8]Museo Nacional y Centro de Investigación de Altamira, 39330 Santillana del Mar, Cantabria, Spain. [9]University of Barcelona/Institució Catalana de Recerca i Estudis Avançats (ICREA), Departament de Prehistòria, Història Antiga i Arqueologia (SERP), c/ Montalegre 6, 08001 Barcelona, Spain.

*To whom correspondence should be addressed. E-mail: alistair.pike@bristol.ac.uk

We used uranium-series disequilibrium to date the formation of thin calcite flowstone growths that formed on the surfaces of paintings and engravings in 11 caves in Asturias and Cantabria, northwestern Spain. This approach circumvents the problems related with radiocarbon dating (*6*) and yields minimum ages for the art. In some cases where paint has been applied atop a flowstone or a flowstone has been engraved, maximum ages can also be obtained (*8*). Uranium-series isotopes can be measured in samples as small as 10 mg (*9*, *10*), which makes it possible to acquire samples whose stratigraphic relationship with the art is robust.

Results

We obtained 50 calcite samples that overlay paintings or engravings from the 11 cave sites in Asturias and Cantabria in northwest Spain (Fig. 1). Samples of between 10 and 150 mg were extracted by scraping with a blade or with an electric drill. We sampled calcite covering a variety of art and representing a range of styles. The samples were processed and U-series isotopes measured by using the method of Hoffmann *et al.* (*9*–*11*). Where sampling allowed a second aliquot to be taken, we tested the integrity of the calcite by comparing the dates of the upper layers of the calcite to those closer to the painting. In all cases, the date from the deeper sample was older, supporting the reliability of our method (*11*).

Our U-series ages ranged from 0.164 to 40.8 ky [corresponding to radiocarbon ages of near modern to 35,500 radiocarbon years before the present (^{14}C yr B.P.)]. Figure 2 shows calculated uranium series dates, from calcite on top of paintings, arranged in ascending order (also table S1). A painting cannot be younger than the calcite that formed on top of it, but there is an unknown delay between the execution of the painting and the formation of the calcite, so we present the data as the cumulative proportion, p, of paintings we have dated that cannot be younger than the date, T (Fig. 2 and table S1).

For context in discussing the ages of the paintings, the earliest reported ^{14}C date for the Proto-Aurignacian culture in northern Spain, assumed to represent the arrival of *Homo sapiens*, is from the site of Morín at 36,590 ± 770 ^{14}C yr B.P., yielding (*12*) a 2-σ calibrated age of 40,037 to 42,778 calendar years before the present (cal yr B.P.). This has been thought to be followed by the Aurignacian I at about 40,000 cal yr B.P. and the Aurignacian II culture at about 37,000 cal yr B.P. (*13*). In France and Iberia, the latest Aurignacian dates from 37,000 to 34,500 cal yr B.P. (*14*). In Cantabria, the latest Aurignacian is possibly represented at Cuco and dated to 30,020 ± 160 ^{14}C yr B.P. (34,490 to 35,032 cal yr B.P.) (*15*). The earliest Gravettian levels in northern Spain are around 27,400 ^{14}C yr B.P. at Antoliñako and Almada; the most precise age is from Antoliñako at 27,390 ± 320 ^{14}C yr B.P. or 31,145 to 32,487 cal yr B.P. (*16*). The latest Gravettian is represented by a date of 20,124 ± 340 ^{14}C yr B.P. (23,275 to 24,975 cal yr B.P.), again from Morín (*16*), which is within error of the earliest date on Solutrean levels from La Riera (20,970 ± 620 ^{14}C yr B.P., 23,578 to 26,921 cal yr B.P.). In light of other ages from southwest Europe (*17*, *18*), the

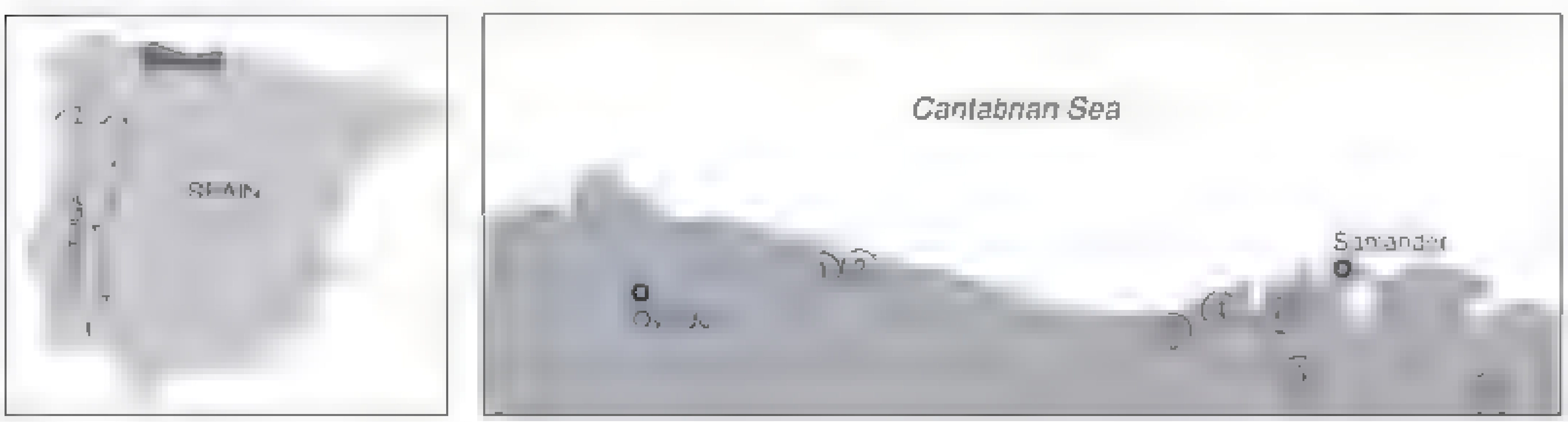

Fig. 1. Locations of the caves sampled: 1, Pedroses; 2, Tito Bustillo; 3, Las Aguas; 4, Altamira; 5, Santián and El Pendo; 6, El Castillo, La Pasiega, and Las Chimeneas; 7, Covalanas and La Haza.

latter date is a more reliable indicator of the timing of the Gravettian-Solutrean transition in northern Spain.

Nearly 20% of our dates on cave paintings fall into pre-Magdalenian times (i.e., before 21,000 cal yr B.P.), and of these four are pre-Gravettian. This distribution is not meant to represent relative intensity of artistic activity over time because of sampling bias, including those caused by cave settings and the influence of climate on calcite growth (*19*), but the dates indicate that early painting was not a one-off activity. Below and in Table 1 and Fig. 3, we focus on several of the more interesting (pre-Magdalenian) dates.

Altamira. Altamira cave, on the northern coast of Spain, contains numerous paintings, including of human hands and animals. The chronology of the art has been debated since its discovery, particularly since Breuil developed a scheme based on the superimpositions of several paintings (*20, 21*). Although there is general agreement that several phases are recognizable in the cave's 10 main decorated zones, these have been suggested to span either a relatively short period of time that corresponds broadly to the cave's known archeology—that is, the Solutrean and the Magdalenian, Leroi-Gourhan's styles III and IV (*22, 23*)—or considerably longer (*21*). We obtained a minimum age of 22.0 thousand years (ky) for the red dot outline horse on the ceiling of the polychrome chamber (O-53); thus, it is at least Solutrean in age. A second minimum age of 35.6 ky was obtained for the large claviform-like symbol (O-50) in the

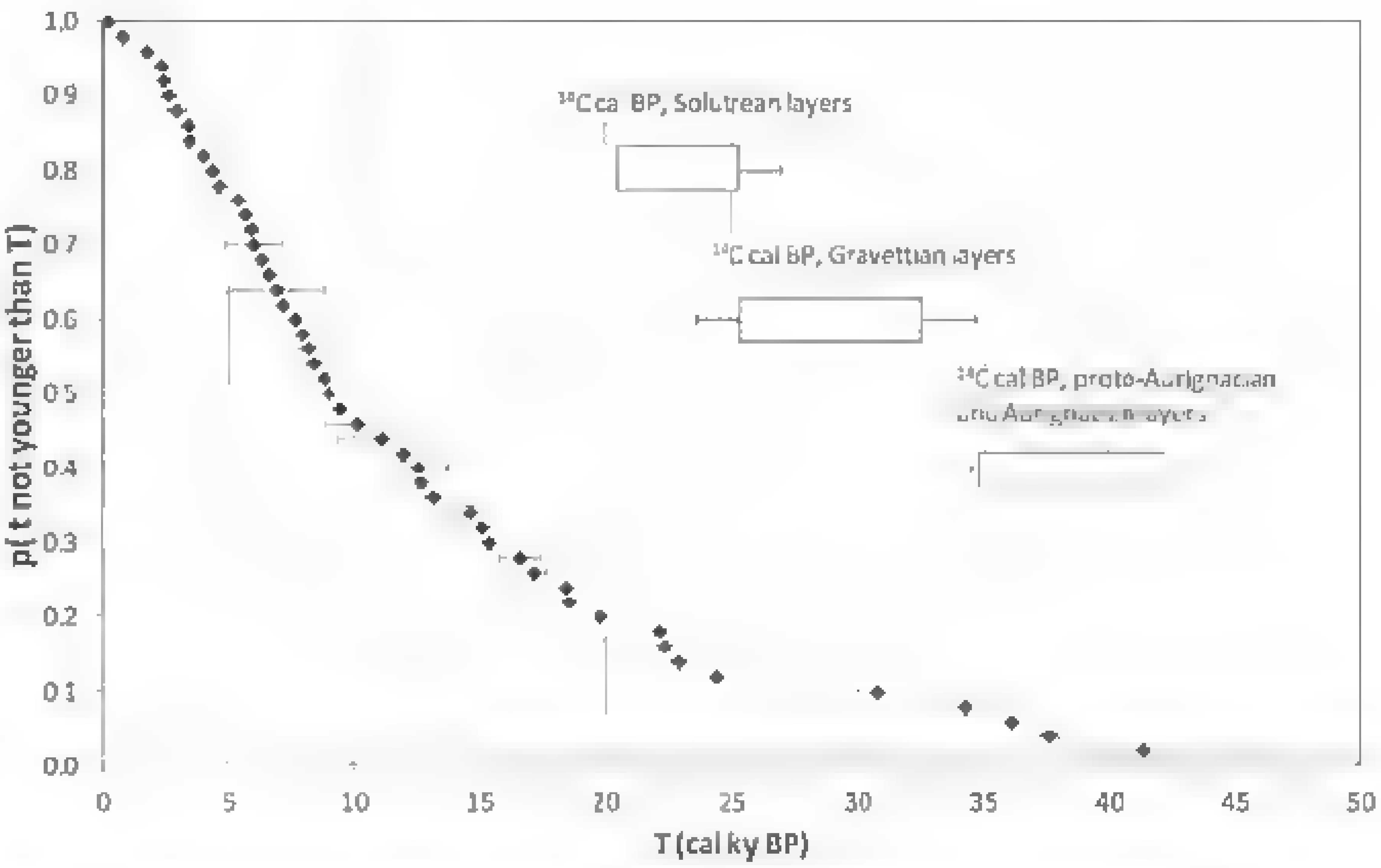

Fig. 2. U-series ages representing minimum ages for the cave art that we have sampled. Also shown is the pre-Magdalanian radiocarbon chronology from excavated cultural horizons in northern Spain (with arbitrary *y*-axis offsets for clarity).

Table 1. Results of U-series disequilibrium dating for samples mentioned in the text. All isotopic ratios are activity ratios; errors are at 2σ. Ages are corrected for detritus by using an assumed $^{232}Th/^{238}U$ activity of 1.250 ± 0.625 and $^{230}Th/^{238}U$ and $^{234}U/^{238}U$ at equilibrium, except age marked with an asterisk, which is corrected by using measured values on insoluble residue $^{230}Th/^{232}Th = 0.8561 \pm 0.0039$, and age marked with a dagger, which is corrected by using measured values on insoluble residue $^{230}Th/^{232}Th = 0.9390 \pm 0.0077$.

Sample BIG-UTh-	Site	Description	$^{230}Th/^{238}U$	$^{234}U/^{238}U$	$^{230}Th/^{232}Th$	Uncorrected age (ky)	Corrected age (ky)
			Minimum ages				
O-53	Altamira	Overlays red spotted outline horse of *Techo de los Polícromos* chamber	0.2884 ± 0.0013	1.5471 ± 0.0026	107.07 ± 0.20	22.26 ± 0.11	22.11 ± 0.13
O-80	El Castillo	Overlays black outline drawing of indeterminate animal of corridor of *Techo de las Manos*	0.7879 ± 0.0047	3.9828 ± 0.0073	30.01 ± 0.15	23.43 ± 0.16	22.88 ± 0.27
O-58	El Castillo	Overlays red stippled negative hand stencil of *Techo de las Manos*	0.5272 ± 0.0020	2.5774 ± 0.0049	222.70 ± 0.49	24.42 ± 0.11	24.34 ± 0.12
O-21	Tito Bustillo	Red pigment associated with anthropomorphic figure of *Galería de los Antropomorfos*	0.6252 ± 0.0031	1.8038 ± 0.0037	2.17 ± 0.01	44.94 ± 0.29	30.8 ± 5.6 29.65 ± 0.55*
O-69	El Castillo	Large red disk of *Galería de los Discos*	0.7512 ± 0.0029	2.7072 ± 0.0051	788.2 ± 5.5	34.28 ± 0.17	34.25 ± 0.17
O-50	Altamira	Large red claviform-like symbol of *Techo de los Polícromos*	0.4933 ± 0.0024	1.6594 ± 0.0030	17.473 ± 0.068	37.60 ± 0.23	36.16 ± 0.61
O-82	El Castillo	Sample overlays red negative hand stencil, and underlies yellow outline bison of *Panel de las Manos*	0.5112 ± 0.0029	1.6970 ± 0.0035	48.81 ± 0.49	38.15 ± 0.27	37.63 ± 0.34
O-83	El Castillo	Overlays large red stippled disk of *Panel de las Manos*	0.3573 ± 0.0022	1.1048 ± 0.0020	28.64 ± 0.29	42.38 ± 0.33	41.40 ± 0.57
			Maximum ages				
O-87	El Castillo	Underlies large red disk of *Galería de los Discos* (same panel as O-69)	0.7969 ± 0.0038	2.7432 ± 0.0051	61.24 ± 0.61	36.11 ± 0.21	35.72 ± 0.26
O-48	Tito Bustillo	Underlies red anthropomorph figure of *Galería de los Antropomorfos* (see also O-21)	0.5281 ± 0.0038	1.6895 ± 0.0042	7.260 ± 0.047	39.85 ± 0.36	36.2 ± 1.5 35.54 ± 0.39†

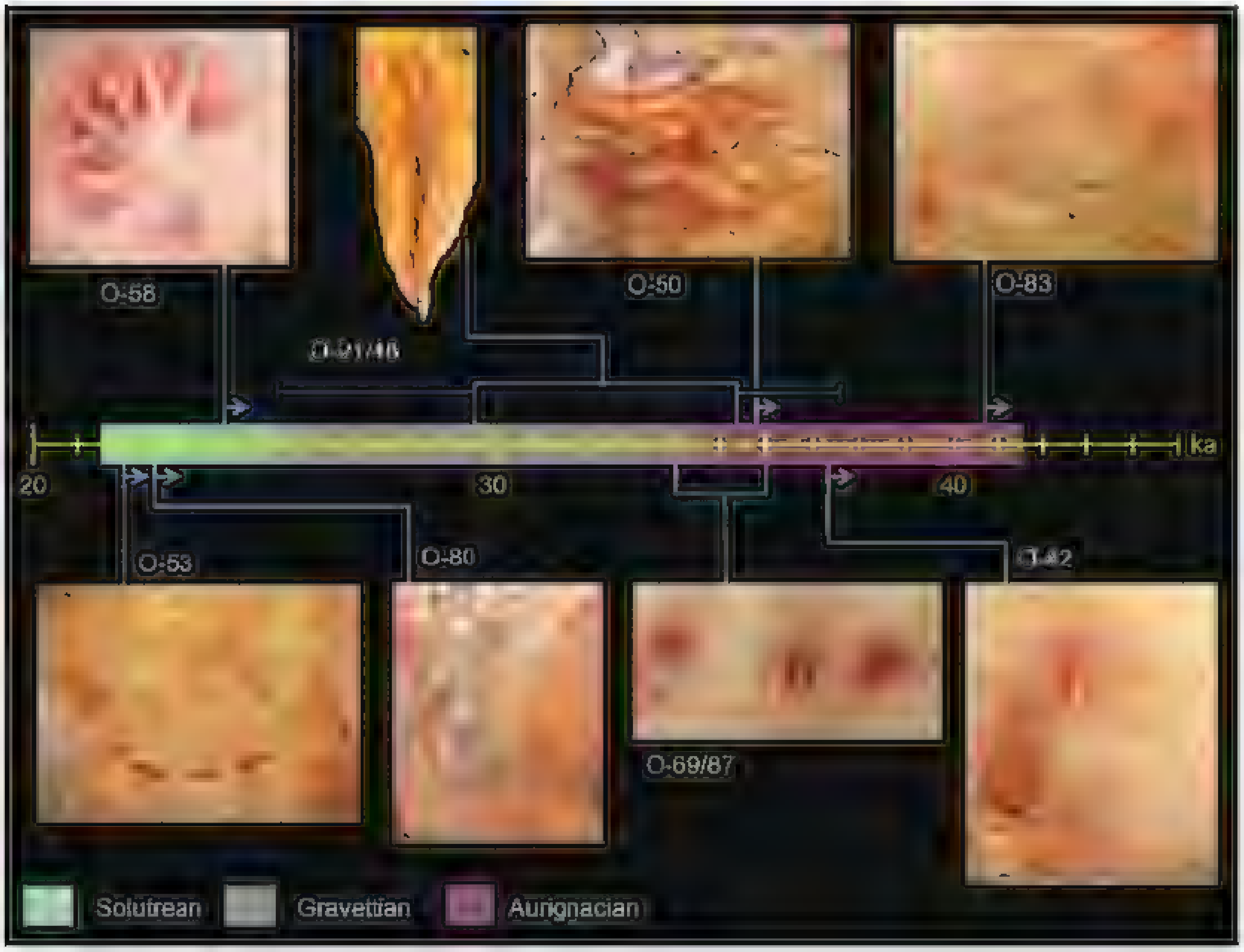

Fig. 3. A time line of the cave art dated. A single arrow represents a minimum age, but, where two dates are indicated, both maximum and minimum ages have been obtained. The error bars for O-21 reflect the variation resulting from the two different methods of detrital correction (*11*). Larger versions of these images showing sample locations are available in the supplementary materials, figs. S2 to S12.

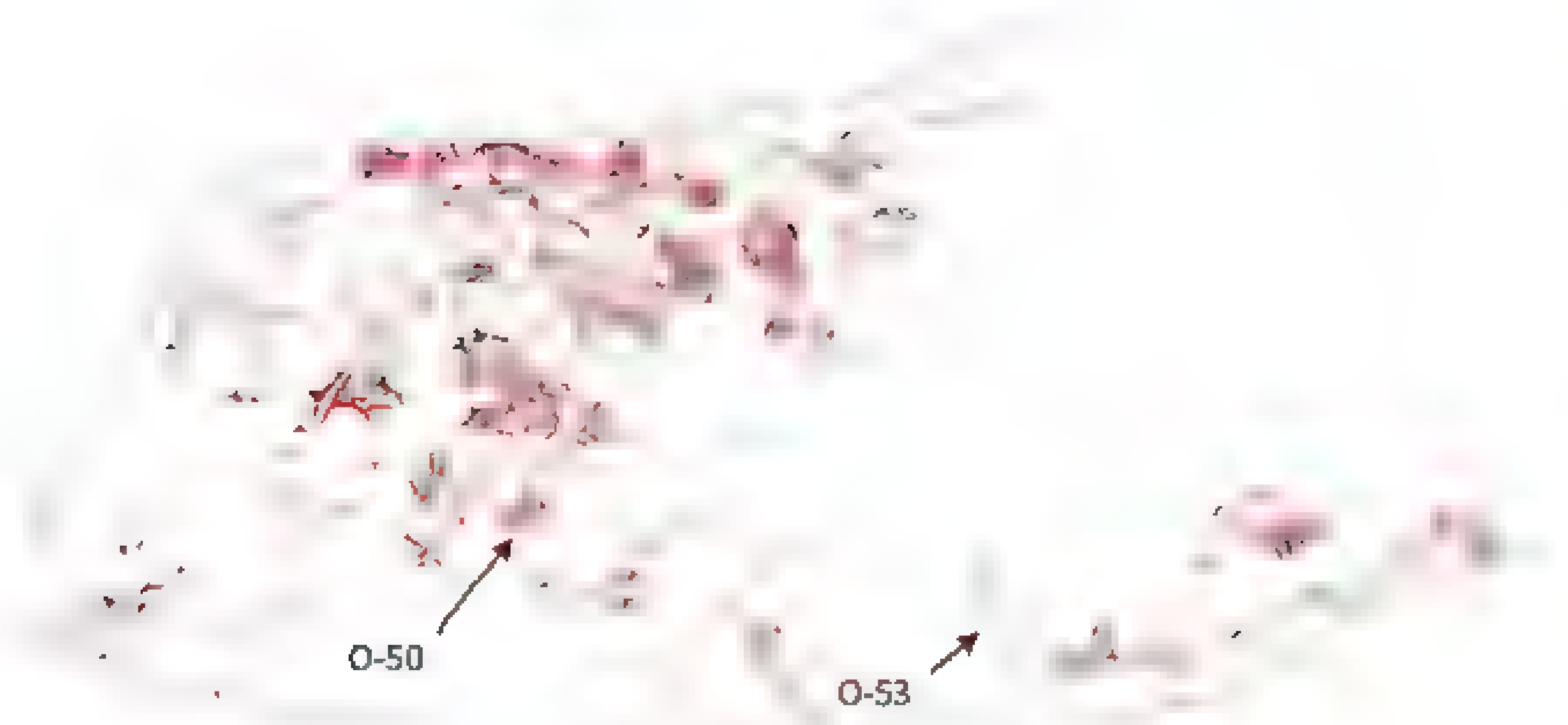

Fig. 4. The *Techo de los Polícromos*, Altamira Cave, showing the red spotted outline horse (sample O-53) and the larger red claviform-like symbol (sample O-50). [Tracing credit: National Museum and Research Centre of Altamira/Pedro Saura]

famous *Techo de los Polícromos* (Fig. 4); thus, it must be considerably older and at least Aurignacian in age. The previous chronological schemes all placed the panel's polychrome images later, in the Magdalenian (*5*). Our date thus indicates earlier use of the cave and support, and may extend, the long chronology. Although a few small claviforms on the same panel are superimposed on the polychromes and thus were painted afterward, our result for the larger version of the sign confirms Breuil's suggestion that red claviforms (or claviform-like symbols) originated before the Solutrean and probably in the Aurignacian and had a long chronological currency (*24*).

El Castillo. The caves of El Castillo, along the Pas river in northern Spain, also contain more than 100 images in multiple chambers. We obtained an age of >22.6 ky (O-80) for the black outline drawing of an indeterminate animal, which demonstrates that it was painted at least during the Solutrean. Traditional chronological schemes attribute most of the black animal figures to Magdalenian times (*25*) as a succession to the earlier red figures. This result suggests an earlier chronology for at least some of the black figures.

We also dated calcite overlying one red disk in the *Corredor de los Puntos* (fig. S7) and underneath another one, providing a minimum age of 34.1 ky (O-69) and a maximum age of 36.0 ky (O-87). Given the homogeneity in technique and location of the various large disks, it seems reasonable to assume they represent a single episode of painting. If so, the dates constrain the paintings to the latest part of the Aurignacian.

Hand stencils (O-58 and -82) are found in numerous caves in France and Spain. They are thought to have been made by blowing pigment onto the hand placed against the cave wall. They are usually assumed to be mainly or exclusively Mid Upper Paleolithic (Gravettian) in age, and, where available, direct radiocarbon measurements support this notion (ages range from ~29,000 to 22,000 ^{14}C yr B.P. for paintings at Gargas, Cosquer, Labattut, Fuente de Salín, and Paglicci) (*26*–*28*). We dated two hand stencils at El Castillo. One date of >24.2 ka for O-58, close to the Solutrean/Gravettian boundary, is consistent with the stylistic attribution of hand stencils to the Gravettian. But the other date from a hand stencil from the *Panel de las Manos* (O-82) is older,

>37.3 ka, and from the Aurignacian period or earlier. This date considerably increases the antiquity of this motif and implies that depictions of the human hand were among the oldest art known from Europe. One of several large red disks (O-83) nearby, also made by using a blowing technique, has a minimum age of 40.8 ky, supporting this interpretation. Because the disk and hand stencil are in the same panel (Fig. 5), it is possible that the older age of 40.8 ky is the minimum age of the entire composition, including rectangular and oval signs, about 40 hand stencils, and dozens of large disks, indicating intense artistic activity in pre-Gravettian times.

Tito Bustillo. The *Galeria de los Antropomorfos* in the cave of Tito Bustillo (Ribadesella) contains a scarf stalactite, about 3 m above the present ground surface, painted on two sides with two anthropomorphic figures and red pigment along the vertices of the stalactite. We dated calcite on top of this red pigment, providing minimum ages with two different methods of detrital correction (*11*) of 29.6 and 25.2 ky, and a sample drilled into a recent break, providing maximum ages of 35.5 and 37.7 ky, (samples O-21 and -48). These results put the possible age of the painting from the Gravettian (either early or late) to the Late Aurignacian. Excavation in the *Galeria de los Antropomorfos* yielded charcoal radiocarbon dated to 32,990 ± 450 ^{14}C yr B.P. (38,729 to 36,665 cal yr B.P.) (*29*) associated with a short-lived and nondomestic human occupation as far back as the Aurignacian, represented by pigment, crushed bones, and deliberately selected flat stones. Our result confirms that this cave hosts a long artistic tradition. These results may imply an old age for early paintings that are partly covered in the *Panel de los Policromos*, elsewhere in the cave, which is thought to have been painted in the Magdalenian (*7*, *29*).

Fig. 5. The *Panel de las Manos*, El Castillo Cave, showing the location of samples O-82 overlaying a negative hand stencil, and O-83 overlaying a large red stippled disk. The tracing is taken from (*35*).

Discussion

Our dates show that artistic activity began at least in the Aurignacian period, in two distinct caves, and in one case at least as far back as 40.8 ka. The large red disk from El Castillo (O-83) currently represents the earliest dated example of European cave art. Its age is ~4000 years earlier than the claimed age of the art at Grotte Chauvet, France. The oldest radiocarbon date there is 32,410 ± 720 ^{14}C yr BP (35,300 to 38,827 cal yr B.P.), although others cluster around 35,000 cal yr B.P. (*30*, *31*).

Pre-Gravettian cave painting should be evident elsewhere in Europe. Blocks presumed to be a former cave wall, with red pigment (one interpreted as an anthropomorphic figure), have been found in Aurignacian layers in Fumane Cave, Italy (*32*), and in several rockshelters of the Vezere River, Dordogne (*33*). The pre-Gravettian signs (large dots, disks, and the claviform-like symbol) and hand stencils that we dated are similar to many found in other caves across Europe, although use of particular symbols may differ regionally (*34*). The apparent lack of further pre-Gravettian examples elsewhere in Europe is more likely the result of targeting charcoal-based black pigments with radiocarbon dating and the resulting ambiguities than a genuine absence of pre-Gravettian images.

Our results are consistent with the notion that there was a gradual increase in technological and graphic complexity over time, as well as a gradual increase in figurative images. Our earliest dates (pre-Gravettian) are for art that is nonfigurative and monochrome (red), supporting the notion that the earliest expression of art in Western Europe was less concerned with animal depictions and characterized by red dots, disks, lines, and hand stencils. If the earliest cave paintings appeared in the region shortly before 40.8 ka, this would, assuming that the Proto-Aurignacian cultural complex was made exclusively by *Homo sapiens*, support the notion that cave art coincided with their arrival in western Europe ~41.5 ka and that the exploration and decorating of caves was part of their cultural package. However, because the 40.8-ky date for the disk is a minimum age, it cannot be ruled out that the earliest paintings were symbolic expressions of the Neandertals, which were present in Cantabrian Spain until at least 42 ka (*13*, *15*).

References and Notes

1. A. Sinclair, *Nature* **426**, 774 (2003).
2. J. Zilhão, *J. Archaeol. Res.* **15**, 1 (2007).
3. N. J. Conard, *Proc. Natl. Acad. Sci. U.S.A.* **107**, 7621 (2010).
4. J. Fortea, in *Pitture Paleolitiche nelle Prealpi venete Grotta di Fumane e Riparo Dalmeri*, A. Broglio, G. Dalmeri, Eds. (Museo Civico di Storia Naturale di Verona, Verona, 2005), pp. 89–99.
5. A. Leroi-Gourhan, B. Delluc, G. Delluc, *Préhistoire de l'art occidental* (Mazenod, Paris, 1995).
6. P. B. Pettitt, A. W. G. Pike, *J. Archaeol. Method Theory* **14**, 27 (2007).

7. F. J. Fortea Pérez, *Bull. Soc. Préhistorique Ariège Pyrénées* **LVII**, 7 (2002).
8. A. W. G. Pike *et al.*, *J. Archaeol. Sci.* **32**, 1649 (2005).
9. D. L. Hoffmann, *Int. J. Mass Spectrom.* **275**, 75 (2008).
10. D. L. Hoffmann *et al.*, *Int. J. Mass Spectrom.* **264**, 97 (2007).
11. Materials and methods are available as supplementary materials on *Science* Online.
12. P. J. Reimer *et al.*, *Radiocarbon* **51**, 1111 (2009).
13. J. Zilhão, *Pyrenae* **37**, 7 (2006).
14. J. Zilhão *et al.*, *PLoS ONE* **5**, e8880 (2010).
15. J. Maroto *et al.*, *Quat. Int.* **247**, 15 (2012).
16. L. G. Straus, *Evol. Anthropol.* **14**, 145 (2005).
17. J. Zilhão, T. Aubry, F. Almeida, in *Les faciès leptolithiques du nord-ouest méditerranéen: milieux naturels et culturels. XXIV^e Congrès Préhistorique de France. Carcassonne, 26–30 Septembre 1994*, D. Sacchi, Ed. (Société Préhistorique Française, Paris, 1999), pp. 165–183.
18. C. Renard, *World Archaeol.* **43**, 726 (2011).
19. I. J. Fairchild, S. Frisia, A. Borsato, A. F. Tooth, in *Geochemical Sediments and Landscapes*, D. J. Nash, S. J. McLaren, Eds. (Blackwell, Oxford, 2007), pp. 200–245.
20. A. Beltran, *The Cave of Altamira* (Harry Abrams, New York, 1999).
21. C. González-Sainz, R. Cacho Toca, R. Fukazawa, *Arte Paleolítico en la Región Cantábrica* (Universidad de Cantabria, Cantabria, Spain, 2003).
22. F. Bernaldo de Quirós, *Proc. Prehistoric Soc.* **57**, 81 (1991).
23. C. Heras Martín, R. Montes Barquín, J. A. Lasheras, P. Rasines, P. Fatás Monforte, *Cuadernos de Arte Rupestre de Moratalla* **4**, 117 (2008).
24. H. Breuil, E. Cartailhac, H. Obermaier, M. E. Boyle, *The Cave of Altamira at Santillana del Mar, Spain* (Tip. de Archivos, Madrid, 1935).
25. H. Breuil, *Quatre cents siècles d'art pariétal. Les cavernes ornées de l'âge du renne* (Centre d'Études de Documentation Préhistoriques, Montignac, Paris, 1952).
26. M. Lorblanchet, *Les Grottes Ornées de la Préhistoire. Nouveaux Regards* (Editions Errance, Paris, 1995).
27. F. Djindjian, in *Art Mobilier Paléolithique Supérieur en Europe Occidental*, A-C. Welté, E. Ladier, Eds. [Actes du Colloque 8.3, Congrès de l'UISPP (Union Internationale des Sciences Préhistoriques et Protohistoriques), Université de Liège, Liège, Belgium, 2004], pp. 249–256.
28. J. Clottes, J. Courtin, *The Cave Beneath the Sea: Paleolithic Images at Cosquer* (H. N. Adams, New York, 2006).
29. R. de Balbín, J. J. Alcolea, M. A. González, in *El Arte Prehistórico Desde Los Inicios del s. XXI. Primer Symposium Internacional de Arte Prehistórico de Ribadesella*, R. de Balbín, P. Bueno, Eds. (Asociación Cultural de Amigos de Ribadesella, Ribadesella, Spain, 2003).
30. J. Clottes, *Return to Chauvet Cave: Excavating the Birthplace of Art* (Thames & Hudson, London, 2003).
31. P. B. Pettitt, P. Bahn, C. Züchner, in *An Enquiring Mind: Studies in Honor of Alexander Marshack*, P. Bahn, Ed. (American School of Prehistoric Research Monograph Series, Oxbow Books, Oxford, UK, 2009), pp. 239–262.
32. A. Broglio, M. de Stefani, F. Gurioli, M. Peresani, *Int. Newsl. Rock Art* **44**, 1 (2006).
33. B. Delluc, G. Delluc, *L'Art Pariétal Archaïque en Aquitaine* (Gallia Préhistoire XXVIII supplement, CNRS, Paris, 1991).
34. M. García-Diez, J. A. Mujika Alustiza, M. Sas, eta, J. Arruabarrena, J. Aiberdi, *Int. Newsl. Rock Art* **60**, 13 (2011).

Acknowledgments: This research was funded by a grant to A.W.G.P. from the Natural Environmental Research Council (NE/F000510/1). C. Taylor performed the sample preparation and assisted in collecting samples in the field along with C. Hinds, S. White, and S. Paine. We thank the governments of Asturias and Cantabria for granting permission to sample the cave art and B. Hanson for editorial guidance. The data described are presented in the supplementary materials.

Supplementary Materials
www.sciencemag.org/cgi/content/full/336/6087/1409/DC1
Materials and Methods
Figs. S1 to S12
Table S1
References (35–39)

1 February 2012; accepted 25 April 2012
10.1126/science.1219957

REPORTS

Spin-Orbit Echo

N. Sugimoto[1,2] and N. Nagaosa[1,2]*

Preserving and controlling the quantum information content of spins is a central challenge of spintronics. In solids, the relativistic spin-orbit interaction (SOI) leads to a finite spin lifetime. Here, we show that spin information is preserved by the hidden conserved "twisted spin" and survives elastic disorder scatterings. This twisted spin is an adiabatic invariant with respect to a slow change in the SOI. We predict an echo phenomenon, spin-orbit echo, which indicates the recovery of the spin moment when the SOI is tuned off adiabatically, even after spin relaxation has occurred; this is confirmed by numerical simulations. A concrete experiment in two-dimensional semiconductor quantum wells with Rashba-Dresselhaus SOI is proposed to verify our prediction.

For the manipulation of spin and spin current by electric fields in spintronics, the relativistic spin-orbit interaction (SOI) is essential because it connects the orbital motion and the spin of an electron (*1*). This interaction, however, destroys the rotational symmetry in the spin space and the consequent spin conservation law. In the presence of the SOI, there are several mechanisms to relax the spins by changing their direction at and between impurity scatterings (Fig. 1A) (*2–8*); spins decay with a (phenomenological) spin lifetime τ_s, which is typically on the order of (or less than) 1 ns [(Fig. 1B, (i) to (iv)]. This is a serious issue for applications because the transfer and storage of information for a long time/distance is a crucial requirement for device function.

It has long been recognized that the SOI is closely related to the parallel transport and rotating frame comoving with the electron in the context of Thomas precession (*9*). This naturally leads to the formulation of the SOI in terms of the SU(2) spin gauge field $\hat{A}_\mu$ ($\mu = t, x, y, z$) connecting the neighboring frames in the nonrelativistic approximations to the Dirac equation (*10–12*). Based on this idea, there have been many attempts to find a conserved quantity by generalizing the spin (*11–17*). It has been known (*11, 12, 18*) that the electronic spin is only covariantly conserved as $D_0 s_a + \boldsymbol{D}\cdot\boldsymbol{j}_a = 0$, a spin density s_a, and a spin current density $\boldsymbol{j}_a$ ($a = x, y, z$), i.e., the continuity equation where the usual derivative ∂_μ is replaced by the covariant derivative $D_\mu := (D_0, \mathbf{D})$ holds. This means that the conservation law is satisfied in the comoving spin frame with the electron's motion but not in the laboratory frame. In a notable recent advance related to this concept, experiments were performed in semiconductor quantum wells with Rashba (α) and Dresselhaus (β) SOIs described by $H_{RD} = \frac{p^2}{2m} + \alpha(p_y\sigma_x - p_x\sigma_y) + \beta(p_x\sigma_x - p_y\sigma_y)$, where H_{RD} is the Rashba-Dresselhaus Hamiltonian, $\boldsymbol{p}$ is the momentum, m is the mass of an electron, σs are the Pauli matrices, and $\hbar = 1$. In this system, the lifetime of a Fourier component of the spin S_q for $\boldsymbol{q} = (2\sqrt{2}m\alpha, 2\sqrt{2}m\alpha)$ [persistent spin helix (PSH)] is observed to be enhanced when the condition $\alpha = \beta$ is satisfied (*19, 20*). In this case, the SU(2) gauge field strength $\hat{F}_{\mu\nu} \propto (\alpha^2 - \beta^2)\sigma_z$ is zero; that is, the SOI vanishes in the rotated spin frame.

We explicitly construct a conserved twisted spin in a generic situation when the electric field is regarded as a background static field (Fig. 1A). Furthermore, we study the adiabatic invariance of this twisted spin and predict a phenomenon called the spin-orbit echo [Fig. 1B, (iv) to (vii)]. The twisted spin preserves the information on the spin, and as the SOI is switched off adiabatically, the spin is recovered to coincide with the conserved twisted spin.

We consider a noninteracting electron system whose Hamiltonian is given by (*10–12*)

$$H = \frac{1}{2m}\left(\boldsymbol{p} - \frac{e}{mc^2}\hat{\boldsymbol{A}}\right)^2 + V(\boldsymbol{x}) \qquad (1)$$

where $\hat{\boldsymbol{A}} = \sum_{i,a} A_i^a \mathbf{e}_i \sigma_a/2$, where $A_i^a := \sum_l \epsilon^{ial} E^l$ describes the SOI, $\mathbf{e}_i$ is the unit vector, and $V(\boldsymbol{x})$ is a scalar potential that includes the periodic crystal potential and the disorder potential. Here, $-e$ represents the charge of an electron; c is the velocity of

[1]Department of Applied Physics, University of Tokyo, Tokyo 113-8656, Japan. [2]Cross-Correlated Materials Research Group and Correlated Electron Research Group, RIKEN, Saitama 351-0198, Japan.

*To whom correspondence should be addressed. E-mail: nagaosa@ap.t.u-tokyo.ac.jp

light; ε^{ijl} denotes the totally antisymmetric tensor; and E^l is an electric field. Note that this Hamiltonian describes the SOI quite generally. The periodic part of $V(x)$ leads to band formation, and multiband effects are fully taken into account. Therefore, the SOI for an effective low-energy Hamiltonian that cannot be necessarily expressed through $\vec{\lambda}$ can also be described by Eq. 1 in the multiband formulation.

The definition of the twisted spin density s^t_a for the generic Hamiltonian in Eq. 1 is given in eq. S11 (*21*, *22*); for concreteness, we consider here the Rashba-Dresselhaus Hamiltonian

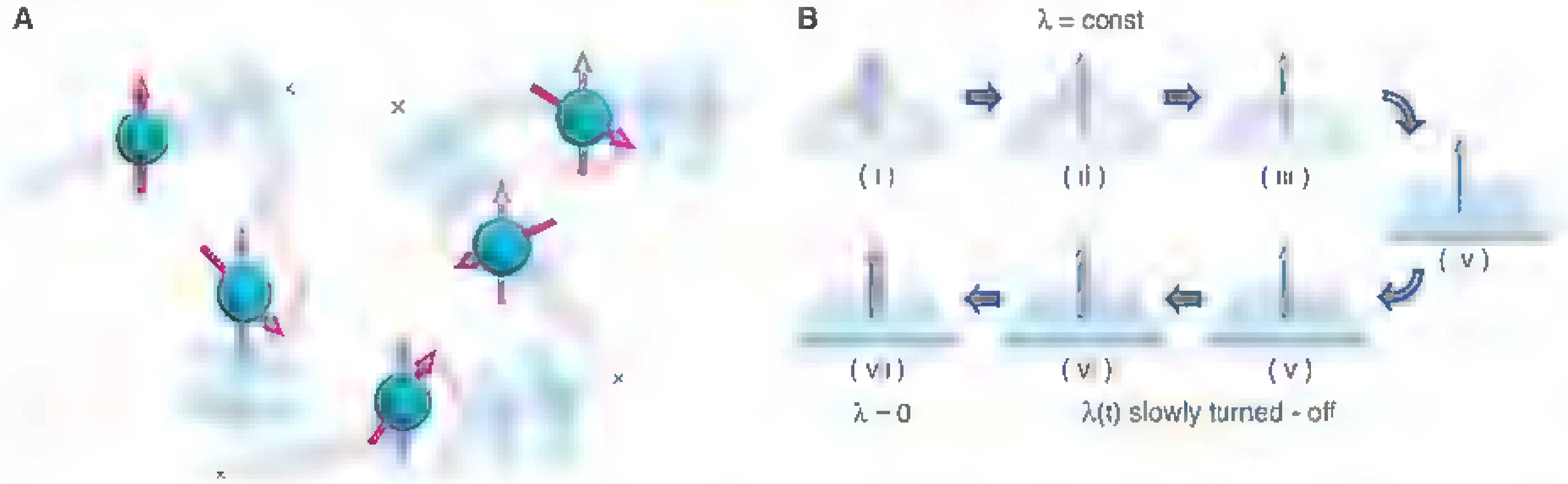

Fig. 1. (**A**) The electron spin (red arrows) changes its direction at and between scatterings by impurities (x symbols) in the presence of the SOI; the twisted spin (blue arrows) does not change. (**B**) Spin-orbit echo. Multiple impurity scatterings cause the diffusive motion of the electron, and the total spin (red arrows) decays in the presence of a constant SOI λ [stages (i) to (iv)]. As λ is reduced slowly to zero in (v) to (vii), the total spin is recovered and eventually coincides with the total twisted spin (blue arrows), which has remained constant during the whole process.

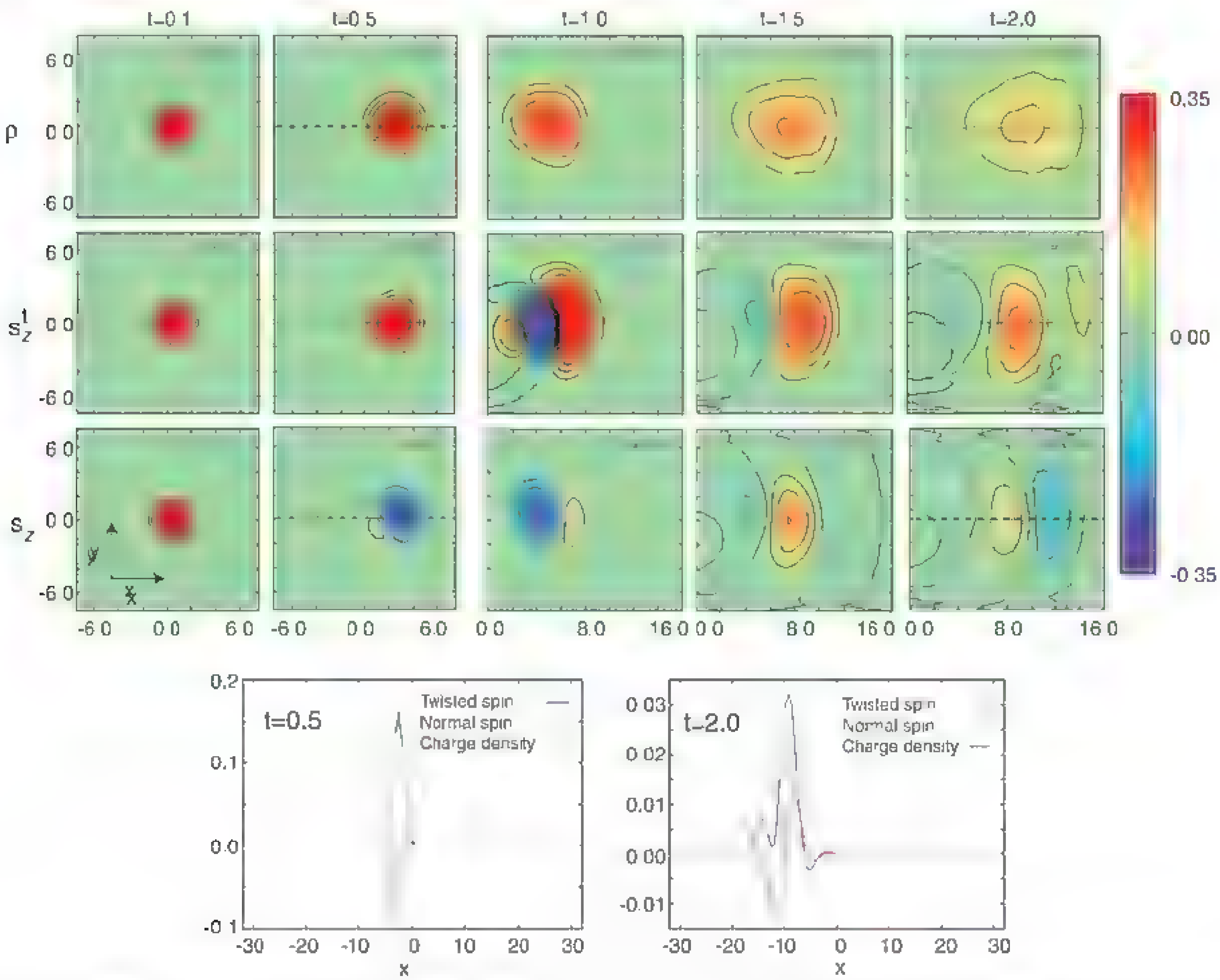

Fig. 2. Contour maps of charge density ρ (first row), twisted spin density s^t_z (second row), and spin density s_z (third row) at t = 0.1, 0.5, 1.0, 1.5, and 2.0, where the Rashba SOI α = 0.8. The center of the initial wave function is at (x, y) = (0.0, 0.0) with the initial velocity (v_x, v_y) = (5.0, 0.0). The size of the sample is 64.0 by 16.0. The two bottom panels are the cross sections of the contour maps at t = 0.5 and 2.0 along the dashed lines. ρ, s^t_z, and s_z are shown in green, blue, and red, respectively.

H_{RD}. The twisted spin density is given by $s_a^t = \frac{\hbar}{2}\psi^\dagger Y^\dagger \sigma_a Y \psi$, where ψ is the spinor, and the operator Y is given by

$$Y = \lim_{x' \to x} \frac{1}{2} e^{\frac{i}{2}m(\alpha+\beta)\sigma_- x_+} \cdot \Big\{ e^{[illegible]} \ldots [illegible] \ldots e^{[illegible]} + 2\sin^2\left[\frac{i(\overleftarrow{\partial}_x - \overleftarrow{\partial}_y)}{8\sqrt{2}m(\alpha+\beta)}\right] \Big\} \quad (2)$$

with $\alpha > 0$ and $\beta > 0$. Here, $\sigma_\pm = \sigma_x \pm \sigma_y$, $x_\pm = x \pm y$, and $\overleftarrow{\partial}$ represents the differential operator acting only to the left. The usual conservation law $\partial_0 s_a^t + \nabla \cdot j_a^t = 0$ is satisfied, where j_a^t is the twisted spin current density from eq. S11 (*21*, *22*). An important property of the twisted spin density is that it obeys the same transformation law as the usual spin density with respect to gauge transformation; by the SU(2) local gauge transformation $U_\alpha(x)$, the spinor, the gauge potential, and spin and twisted spin densities are transformed into $\chi'(x) = U_\alpha(x)\chi(x)$, $\hat{A}'_\mu(x) = U(x)\hat{A}_\mu(x)U^\dagger(x) + U(x)\partial_\mu U^\dagger(x)$, $s'(x) = R(x)s(x)$, and $(s^t)'(x) = R(x)s^t(x)$, respectively. Here, $R(x)$ is an orthogonal 3-by-3 matrix; $U_\alpha^\dagger(x)\sigma_b U_\alpha(x) = \sum_c R_{bc}(x)\sigma_c$. Note that Y is not a unitary operator for the SU(2) local gauge transformation, except for in the case of $\alpha = \beta$, because it includes a derivative operator. In the limit $\alpha \to \beta$, the factor $1/(\alpha^2 - \beta^2)$ in the exponent does not lead to a divergence because the x' dependence vanishes in this limit, leading to a finite result as $Y \to U_\alpha = e^{im\alpha(\sigma_x - \sigma_y)(x+y)}$. The gauge potential is transformed into zero [i.e., $\hat{A}'_\mu(x) = 0$], and s_a^t becomes the persistent spin helix component S_q by this unitary transformation (*19*, *20*). Therefore, the twisted spin can be regarded as the generalization of the persistent spin helix.

From the continuity equation, the integral S_a^t of the twisted spin density s_a^t is constant; i.e., $dS_a^t/dt = 0$, even for the case of $\alpha \neq \beta$. The twisted spin conservation law can be regarded as the mapping of the covariant conservation law in the comoving frame to the laboratory frame for the generic case of nonzero $\hat{F}_{\mu\nu}$. The twisted spin conservation law means that some information related to spin is preserved, even after spin relaxation. We prove that dS_a^t/dt does not contain terms linear in $d\lambda/dt$, where λ is the SOI coupling constant (*21*, *22*); the leading order term is $\propto (d\lambda/dt)^2$ for a slow change in a spatially uniform $\lambda(t)$. Therefore, S_a^t remains constant in the adiabatic limit $d\lambda/dt \to 0$, whereas the total change in $\lambda(t)$ is finite; S_a^t is an adiabatic invariant. Therefore, the spin will be recovered completely when the SOI is switched off adiabatically within the inelastic lifetime—a phenomenon we term the spin-orbit echo. This is analogous to the spin echo in which the spin decaying within the elastic lifetime (T_2) can be recovered by a π-pulse within the inelastic lifetime (T_1).

The spin-orbit echo in disordered Rashba and Rashba-Dresselhaus models can be demonstrated by numerically solving the time-dependent Schrödinger equation for the Hamiltonian in Eq. 1 with a random potential $V(x)$ (*21*). The initial condition is taken to be a Gaussian wave packet $\psi(x, t = 0) = \exp(-x^2/2\xi^2 - im\mathbf{v}\cdot x)/\pi\xi^2$ with $\mathbf{v} = (5.0, 0.0)[1/m\xi]$, where the length unit is 2ξ. The energy unit is $E_0 = 1/2m\xi^2$, the estimated kinetic energy of the initial wave packet for $\mathbf{v} = 0$. Figure 2 shows the time evolution of the charge wave packet, the z component of spin (s_z), and twisted spin (s_z^t) densities for the Rashba model with $\alpha = 0.8[1/4m\xi]$. The center of mass of the charge density ρ moves toward the right and in a downward direction corresponding to the anomalous Hall effect, whereas the positive and negative spin densities split, as in the spin Hall effect (*23*, *24*), and decay. In contrast, the twisted spin density s_z^t is positive everywhere for $t \leq 0.5$, similar to the charge density (Fig. 2). For the period $0.5 < t < 2.0$, s_z^t obtains some features of s_z and eventually becomes spatially uniform.

Figure 3A shows the numerically obtained time evolution of the z component of the total (integrated) spin $S_z(t)$ (red) and the total twisted spin $S_z^t(t)$ (blue) as $\alpha(t)$ is reduced according to $\alpha(t) = 0.8 \times \tanh(\tau_\alpha^2/t^2)[\hbar/4m\xi]$, with $\tau_\alpha = 40$ (green). $\beta = 0$ is fixed. The total spin $S_z(t)$ first relaxes in an oscillating fashion, whereas the total twisted spin $S_z^t(t)$ is conserved while α is constant. $S_z(t)$ recovers gradually from zero as the SOI is reduced, demonstrating the spin-orbit echo. Note that the recovery is not complete due to the finite rate of the decrease in $\alpha(t)$. This recovery will increase as the change in $\alpha(t)$ gets slower and slower and will eventually become perfect because S_z^t is an adiabatic invariant.

In realistic cases, the Dresselhaus SOI still remains, even if the Rashba contribution can be tuned to zero. In this case, the SU(2) gauge invariant point $\alpha = \beta$ can be regarded to have no SOI in the rotated frame, and the total spin is interpreted as the PSH component S_q^{PSH}. Figure 3B shows the time evolution of S_q^{PSH} as $\alpha(t)$ evolves from 0 to reach the SU(2) invariant point $\alpha(t = \infty) = \beta = 0.8[\hbar/4m\xi]$; i.e., $\alpha(t) = 0.8 \times [1 - \tanh(\tau_\alpha^2/t^2)][\hbar/4m\xi]$ with $\tau_\alpha = 40$. The recovery of S_q^{PSH} is seen as expected. Because the electric control of the Rashba SOI is established in GaAs quantum well systems (*25*), the spin-orbit echo is now realistic in the PSH system. In the experiment in (*25*), the Fermi wave number is $k_F \sim 10^8$ m^{-1}, the momentum lifetime is $\tau/\hbar \sim 0.5 \times 10^5$ eV^{-1}, and the spin splitting energy is $\Delta_\alpha \simeq 10^{-3}$ eV. On the other hand, the parameters used in our simulations correspond to $k_F \simeq 10^8$ m^{-1}, $\tau/\hbar \simeq 0.3 \times 10^4$ eV^{-1}, $\Delta_\alpha \cong 2 \times 10^{-3}$ eV, and $t_{max} \sim 400$ ps.

In metals and semiconductors, four spin-relaxation mechanisms have been identified; the Elliott-Yafet (EY) (*2*, *3*), D'yakonov-Perel'(DP) (*4*, *5*), and Bir-Aronov-Pikus (BAP) (*6*) mechanisms, as well as hyperfine coupling with the nuclear spins. Inelastic scattering by phonons and electron/hole-electron interaction, such as the BAP mechanism, and magnetic scattering, such

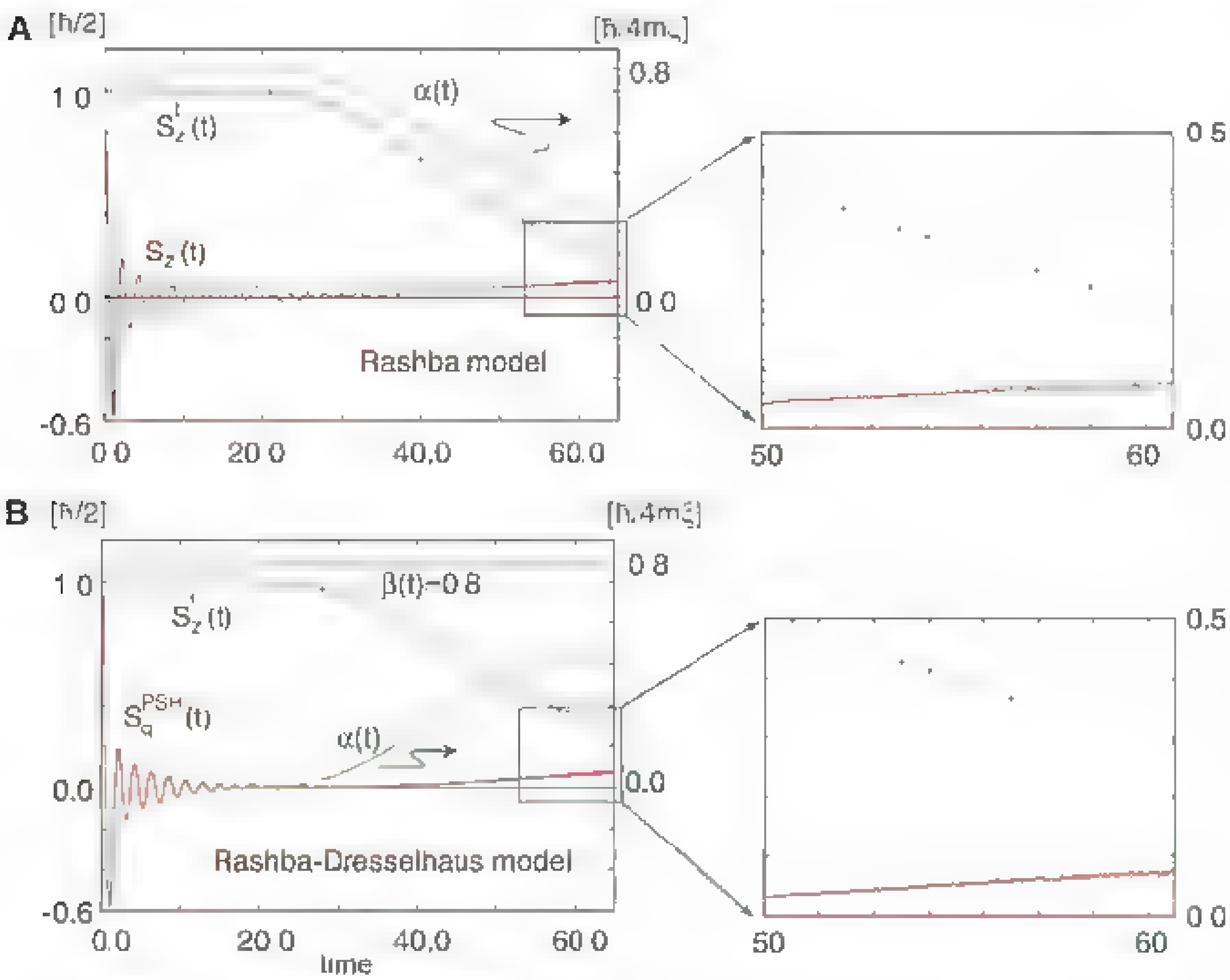

Fig. 3. Numerical simulations of spin-orbit echo. **(A)** Time evolution of the z component of the total spin [$S_z(t)$, red curve] and total twisted spin [$S_z^t(t)$, blue dotted curve] for the Rashba SOI $\alpha(t) = 0.8 \times \tanh(\tau_\alpha^2/t^2)[\hbar/4m\xi]$ with $\tau_\alpha = 40$ (green curve) without the Dresselhaus SOI. **(B)** Spin-orbit echo of PHS S_q^{PSH} in a Rashba-Dresselhaus system where the Rashba SOI varies as $\alpha(t) = 0.8 \times (1 - \tanh(\tau_\alpha^2/t^2))[\hbar/4m\xi]$ with $\tau_\alpha = 40$ ($t = 0 - 65$), and the Dresselhaus SOI $\beta = 0.8$ [$\hbar/4m\xi$] is fixed.

as hyperfine interaction mechanism, will probably destroy the conservation of the twisted spin. However, the relevant inelastic lifetime increases as $\sim T^{-1}$ (T, temperature) and eventually becomes on the order of a nanosecond at $T \sim 0.1$ K (*26*, *27*); the BAP mechanism is absent in n-type materials. Additionally, the typical time scale of the spin lifetime resulting from hyperfine coupling is estimated at ~1 ns in n-type GaAs (i.e., longer than 400 ps). The cubic Dresselhaus SOI β_3 of $GaAs/Al_{0.3}Ga_{0.7}As$ quantum well samples is the dominant term causing the relaxation of the PSH, which is regarded as the nonpure gauge potential giving finite $\hat{F}_{\mu\nu}$, and gives the elastic EY and DP mechanisms (*20*). The enhanced spin lifetime on the order of 0.8 ns obtained in (*20*) is already long enough for the purpose of the spin-orbit echo discussed above. Therefore, it is anticipated that the spin-orbit echo can be tested at $T \sim 0.1$ K with the Rashba SOI tuned by electric field with the help of the optical grating method, as in (*20*).

References and Notes

1. S. A. Wolf *et al.*, *Science* **294**, 1488 (2001).
2. R. J. Elliott, *Phys. Rev.* **96**, 266 (1954).
3. Y. Yafet, in *Solid State Physics*, F. Seitz, D. Turnbull, Eds. (Academic, New York, 1963), vol. 14, p. 2.
4. M. I. D'yakonov, V. I. Perel, *Sov. Phys. JETP* **33**, 1053 (1971).
5. M. I. D'yakonov, V. I. Perel, *Sov. Phys. Solid State* **13**, 3023 (1971).
6. G. L. Bir, A. G. Aronov, G. E. Pikus, *Sov. Phys. JETP* (Engl. transl.) **42**, 705 (1975) [transl. from *Zh. Eksp. Teor. Fiz.* **69**, 1382 (1975)].
7. J. M. Kikkawa, D. D. Awschalom, *Phys. Rev. Lett.* **80**, 4313 (1998).
8. R. I. Dzhioev *et al.*, *Phys. Rev. B* **66**, 245204 (2002).
9. L. H. Thomas, *Nature* **117**, 514 (1926).
10. J. Fröhlich, U. M. Studer, *Rev. Mod. Phys.* **65**, 733 (1993).
11. P.-Q. Jin, Y.-Q. Li, F.-C. Zhang, *J. Phys. Math. Gen.* **39** 7115 (2006).
12. B. W. A. Leurs, Z. Nazario, D. Santiago, J. Zaanen, *Ann. Phys.* **323**, 907 (2008).
13. T.-W. Chen, C.-M. Huang, G. Y. Guo, *Phys. Rev. B* **73**, 235309 (2006).
14. Y. Wang, K. Xia, Z. B. Su, Z. Ma, *Phys. Rev. Lett.* **96**, 066601 (2006).
15. R. Shen, Y. Chen, Z. D. Wang, D. Y. Xing, *Phys. Rev. B* **74**, 125313 (2006).
16. D. Culcer *et al.*, *Phys. Rev. Lett.* **93**, 046602 (2004).
17. J. Shi, P. Zhang, D. Xiao, Q. Niu, *Phys. Rev. Lett.* **96**, 076604 (2006).
18. C. N. Yang, R. L. Mills, *Phys. Rev.* **96**, 191 (1954).
19. B. A. Bernevig, J. Orenstein, S.-C. Zhang, *Phys. Rev. Lett.* **97**, 236601 (2006).
20. J. D. Koralek *et al.*, *Nature* **458**, 610 (2009).
21. For details, see the supplementary materials on *Science* Online.
22. N. Sugimoto, N. Nagaosa, http://arxiv.org/abs/1205.6629
23. S. Murakami, N. Nagaosa, S.-C. Zhang, *Science* **301**, 1348 (2003).
24. J. Sinova *et al.*, *Phys. Rev. Lett.* **92**, 126603 (2004).
25. T. Koga, J. Nitta, T. Akazaki, H. Takayanagi, *Phys. Rev. Lett.* **89**, 046801 (2002).
26. B. J. F. Lin, M. A. Paalanen, A. C. Gossard, D. C. Tsui, *Phys. Rev. B* **29**, 927 (1984).
27. F. E. Meijer, A. Morpurgo, T. Klapwijk, T. Koga, J. Nitta, *Phys. Rev. B* **70**, 201307(R) (2004).

Acknowledgments: We thank K. Richter, V. Krueckl, and S. Onoda for fruitful discussion. This work is supported by Grant-in-Aid for Scientific Research from the Ministry of Education, Culture, Sports, Science and Technology of Japan; Strategic International Cooperative Program (Joint Research Type) from Japan Science and Technology Agency; and the Funding Program for World-Leading Innovative Research and Development on Science and Technology, Japan.

Supplementary Materials
www.sciencemag.org/cgi/content/full/336/6087/1413/DC1
Supplementary Text
Fig. S1
References (*28*–*30*)

1 December 2011; accepted 27 April 2012
10.1126/science.1217346

Dipolar Antiferromagnetism and Quantum Criticality in $LiErF_4$

Conradin Kraemer,[1,2] Neda Nikseresht,[1] Julian O. Piatek,[1] Nikolay Tsyrulin,[1] Bastien Dalla Piazza,[1] Klaus Kiefer,[3] Bastian Klemke,[3] Thomas F. Rosenbaum,[4] Gabriel Aeppli,[5] Ché Gannarelli,[5] Karel Prokes,[3] Andrey Podlesnyak,[6] Thierry Strässle,[2] Lukas Keller,[2] Oksana Zaharko,[2] Karl W. Krämer,[7] Henrik M. Rønnow[1]*

Magnetism has been predicted to occur in systems in which dipolar interactions dominate exchange. We present neutron scattering, specific heat, and magnetic susceptibility data for $LiErF_4$, establishing it as a model dipolar-coupled antiferromagnet with planar spin-anisotropy and a quantum phase transition in applied field $H_{c\parallel} = 4.0 \pm 0.1$ kilo-oersteds. We discovered non–mean-field critical scaling for the classical phase transition at the antiferromagnetic transition temperature that is consistent with the two-dimensional XY/h_4 universality class; in accord with this, the quantum phase transition at H_c exhibits three-dimensional classical behavior. The effective dimensional reduction may be a consequence of the intrinsic frustrated nature of the dipolar interaction, which strengthens the role of fluctuations.

The dipolar force between magnetic moments—a consequence of Maxwell's fundamental laws for electromagnetism—is present in all magnetic systems, from classical to quantum magnets, from bulk materials to nanoparticles. More than a half century ago, Luttinger and Tisza (*1*) discussed whether a polarized state of matter can be induced by classical dipole-dipole interactions alone and in the absence of short-range forces such as exchange interactions. They conjectured that both ferromagnetic (FM) and antiferromagnetic (AFM) order can arise, depending on the geometrical arrangement of the dipoles. When the modern theory of critical phenomena was developed, dipolar-coupled ferromagnets—in which the dipoles are atomic magnetic moments—presented material realizations on which concepts could be tested. Being three-dimensional (3D) systems, they were at the upper marginal dimension for the applicability of mean-field (MF) theory. This resulted in logarithmic corrections, which could be calculated exactly and agreed with the measured behavior around the classical phase transition (*2*). In the context of quantum phase transitions (QPTs), anisotropic dipolar systems are excellent realizations of, for example, the Ising model in a transverse field. In dipolar systems, the anisotropy ratio for the dipolar interaction scales as the square of the anisotropy ratio for response to an external magnetic field, and as a consequence, even for modest single-ion anisotropy the dipolar interaction along the hard axis is much smaller than along the easy axis. This hierarchy of scales is much harder to achieve in exchange-coupled systems in which the moment-carrying electron wave functions are responsible for both the exchange and single-ion anisotropies.

An excellent testing ground for the physics of dipolar-coupled systems are the lithium rare earth (*RE*) tetrafluorides, $LiREF_4$, in which tightly bound 4*f* electrons are far enough apart for the dipolar interactions to dominate exchange interactions. Another major advantage of the $LiREF_4$ family is the possibility of isostructural dilution with nonmagnetic yttrium, $LiRE_xY_{1-x}F_4$—permitting experiments from isolated dipoles (*3*) through disordered interacting dipoles forming spin glass states (*4*–*6*)—to the undiluted limit $LiREF_4$. To date, activity has centered on the Ising-like ferromagnets $LiTbF_4$ (*2*) and $LiHoF_4$ (*7*) and their respective dilution series (*8*). Here, we focus on an AFM member of the family $LiErF_4$ and address the magnetic order, the classical phase transition, and the transition and fluctuations about the quantum critical point.

Known as *RE*:YLF, very dilute ($x < 1\%$) $LiRE_xY_{1-x}F_4$ is used commercially in laser technology because of the long lifetimes of the crystal field energy levels of isolated RE^{3+} ions. The crystal field also sets the stage for low-temperature collective properties. The electric field from neighboring ions act differently on the orbital wave-

[1]Laboratory for Quantum Magnetism, Ecole Polytechnique Fédérale de Lausanne (EPFL), 1015 Lausanne, Switzerland. [2]Laboratory for Neutron Scattering, Paul Scherrer Institute, 5232 Villigen, Switzerland. [3]Helmholtz-Zentrum Berlin, 14109 Berlin Wannsee, Germany. [4]James Franck Institute and Department of Physics, University of Chicago, Chicago, IL 60637, USA. [5]London Centre for Nanotechnology and Department of Physics and Astronomy, University College London, London WC1E 6BT, UK. [6]Oak Ridge National Laboratory, Spallation Neutron Source, Oak Ridge, TN 37831, USA. [7]Department of Chemistry and Biochemistry, University of Bern, 3000 Bern 9, Switzerland.

*To whom correspondence should be addressed. E-mail: henrik.ronnow@epfl.ch

functions and, restricted by the local symmetry, gives the following crystal field Hamiltonian

$$\mathcal{H}_{CF} = \sum_{l=2,4,6} B_l^0 \mathbf{O}_l^0 + \sum_{l=4,6} B_l^4(c)\mathbf{O}_l^4(c) + B_6^4(s)\mathbf{O}_6^4(s) \quad (1)$$

$\mathbf{O}_l^m$ are the Stevens operators with amplitudes B_l^m [see (9) for definitions]. The dominant crystal field component is $\mathbf{O}_2^0 = 3J_z^2 - J(J+1)$, where the operator J_z is the component of the electronic angular momentum (J) along the z axis. In $LiHoF_4$, a negative B_2^0 leads to strong z axis Ising anisotropy, whereas a positive B_2^0 leads to planar XY anisotropy in $LiErF_4$.

The full magnetic Hamiltonian for $LiREF_4$ contains crystal field, external field (H), and hyperfine coupling to the nuclear spins, as well as dipolar and exchange interactions

$$\mathcal{H} = \sum_i [\mathcal{H}_{CF}(\mathbf{J}_i) - g_L\mu_B \mathbf{J}_i \cdot \mathbf{H} + A\mathbf{J}_i \cdot \mathbf{I}_i] - \frac{1}{2}\sum_{ij}\sum_{\alpha\beta} \mathcal{J}_D D_{ij}^{\alpha\beta} J_{i\alpha}J_{j\beta} - \frac{1}{2}\sum_{ij,n.n} \mathcal{J}_{ex}\mathbf{J}_i \cdot \mathbf{J}_j \quad (2)$$

where $\mathbf{J}_i$ and $\mathbf{I}_i$ are the electronic and nuclear angular momentum operators at site i. The electronic dipole moment is given by the angular momentum multiplied by the Bohr magneton μ_B and the Landé factor $g_L = 1.2$. The strength of hyperfine, exchange, and dipolar couplings are defined by A, $\mathcal{J}_{ex}$, and $\mathcal{J}_D$, respectively. The dipole interaction is the tensor

$$D_{ij}^{\alpha\beta} = \frac{3(r_{i\alpha} - r_{j\alpha})(r_{i\beta} - r_{j\beta}) - |\mathbf{r}_i - \mathbf{r}_j|^2\delta_{\alpha\beta}}{|\mathbf{r}_i - \mathbf{r}_j|^5} \quad (3)$$

where $\mathbf{r}_i$ is the position of the ith ion. Its peculiar spatial anisotropy is illustrated in (Fig. 1). In $LiHoF_4$, the moments point along z, and nearest neighbors (NNs) are coupled ferromagnetically. In $LiErF_4$, in which the moments reside in the ab plane, half the NN couplings are AFM, the other half FM, and rotating the moments by 90° switches between FM and AFM interactions. In $LiHoF_4$, the exchange coupling is very small, on the order of 2% of the effective coupling at zero wave vector (10). Given the similar wave functions for Ho and Er, we also expect $\mathcal{J}_{ex}$ to be negligible in $LiErF_4$. The hyperfine coupling $A = 0.5(1)$ μeV for ^{167}Er (11) is weaker than $A = 3.36$ μeV in $LiHoF_4$ (10) and tunable because crystals can be prepared by using ^{168}Er without or ^{167}Er with nuclear moments. Our sample contained natural Er with 23% nuclear moments.

Limited data exist on the magnetic properties of $LiErF_4$. Electron paramagnetic resonance (EPR) (12, 13), susceptibility, ^7Li nuclear magnetic resonance (NMR) (14), and optical spectroscopy (15) show planar XY anisotropy, but considerable variation in the reported anisotropy ratio and the lack of a globally consistent set of crystal field parameters prevented predictions of low-temperature properties. Susceptibility (16) and specific heat (17) show a transition around 380 mK. The shape of the specific heat anomaly differs from that of $LiHoF_4$ and 3D exchange-coupled XY materials, but the implied short-range correlations were discussed in terms of unlikely large exchange coupling. Susceptibility suggested AFM order (18), but the magnetic structure has not been determined. To this end, we have undertaken comprehensive neutron scattering, specific heat, and magnetic susceptibility studies.

The crystal field was determined by using neutron spectroscopy on a single crystal, providing not only the position of the energy levels but also the matrix elements of the angular momentum operators, more accurately defining the effective model (fig. S1). The ground state is a Kramers doublet isolated by a $\Delta = 2.25$ meV gap (tables S1 and S2). Within this subspace, an effective Hamiltonian for the low-temperature properties can be used in future theoretical work

$$\mathcal{H}_{eff} = \sum_{ij\alpha\beta} \mathcal{J}_{ij}^{\alpha\beta}\sigma_i^\alpha\sigma_j^\beta + g_\perp(\sigma_i^x B^x + \sigma_i^y B^y) + g_\parallel \sigma_i^z B^z \quad (4)$$

where σ_i denotes the Pauli operators and $\mathcal{J}_{ij}^{\alpha\beta} = (\mu_B g_L)^2 C_\alpha C_\beta D_{ij}^{\alpha\beta}$, the magnetic coupling tensor between the effective $S = 1/2$ spins $S^\alpha = C_\alpha\sigma^\alpha$, with parameters calculated from the crystal field refinement: $C_x = C_y = 3.480$, $C_z = 0.940$, $g_\perp$

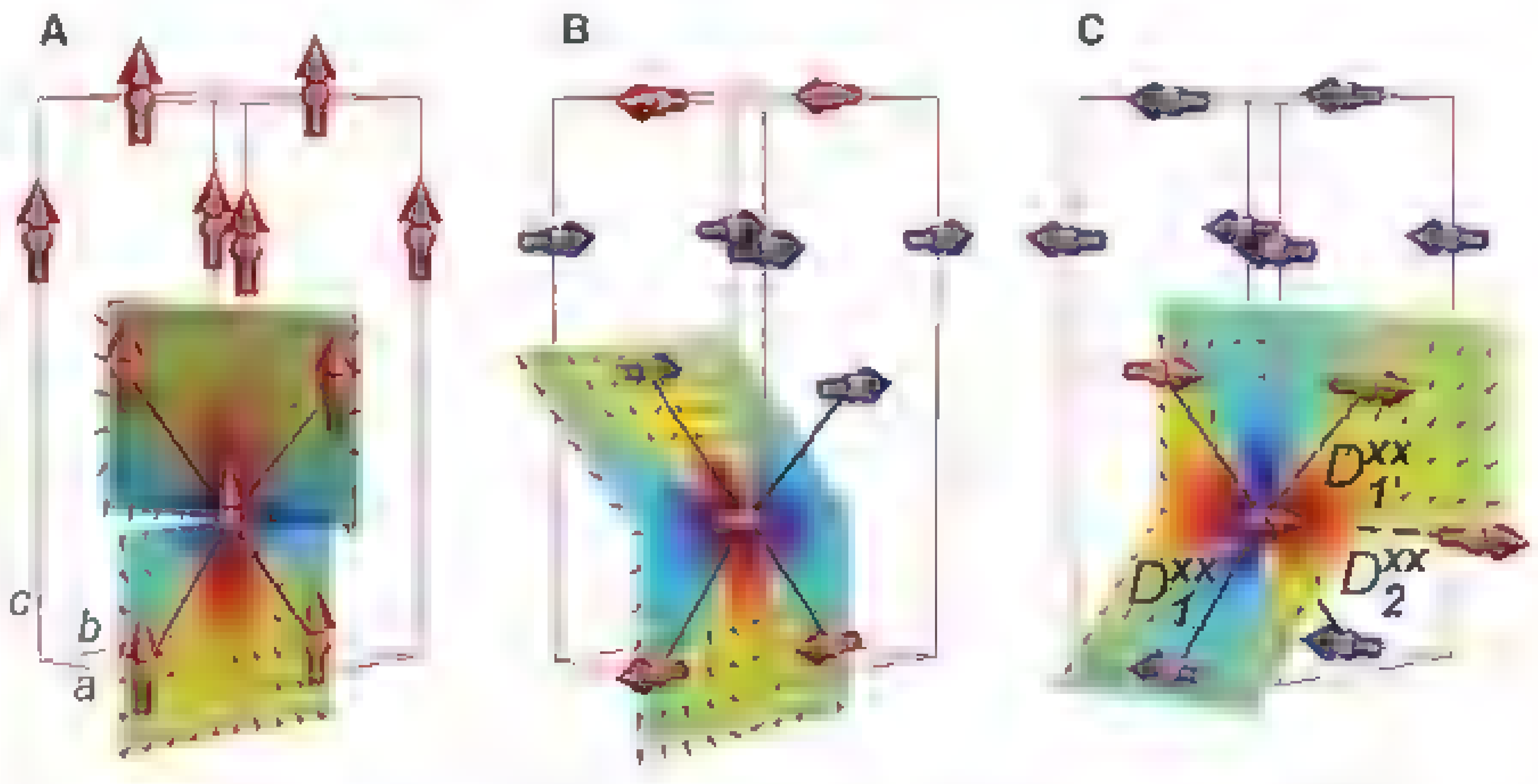

Fig. 1. Magnetic structures of $LiREF_4$. **(A)** Ferromagnetic c axis order in $LiHoF_4$, and BLAFM order with moments along **(B)** x or **(C)** y axis in $LiErF_4$. The dipole field from the central moment yields FM (red scale) and AFM (blue scale) coupling. Sign and strengths of the coupling depends on the direction of the moments. In the BLAFM structure, nearest and next-nearest couplings are $vD_1^{xx} = -5.5$ (AFM), $vD_{1'}^{xx} = 2.5$ (FM), and $vD_2^{xx} = 4.2$, $v = a^2c$. The crystal structure is tetragonal, space group $I4_1/a$ with $a = b = 5.162$ Å and $c = 10.70$ Å.

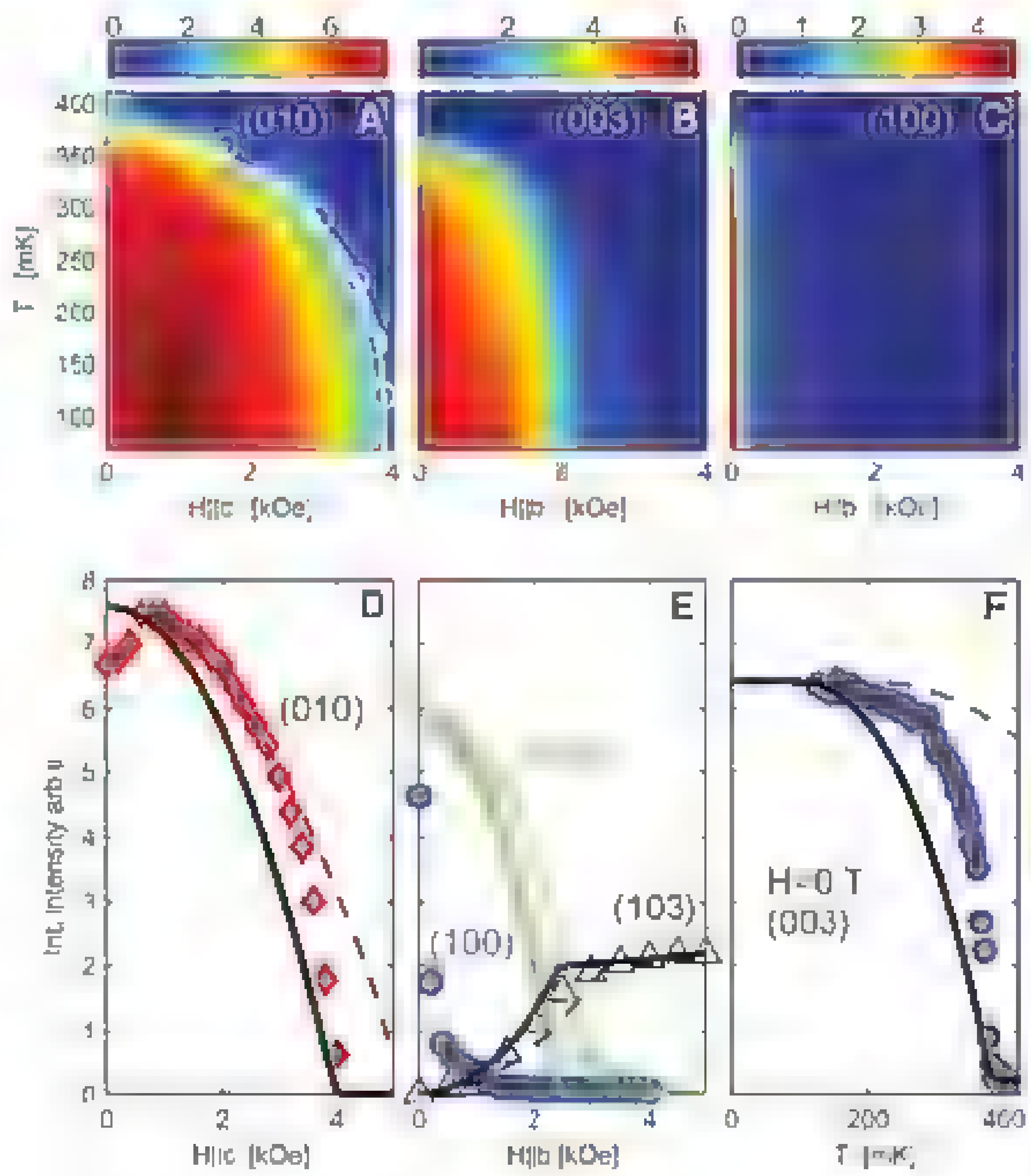

Fig. 2. (A to C) Field-temperature phase diagrams from the intensity of magnetic Bragg peaks: (010) with $H_{c||}$, (003) and (100) with $H_{b||}$, respectively. **(D and E)** Field dependence of peak intensities at $T = 100$ mK for field along c: (010) and along b: (100), (103), (003), respectively. **(F)** Temperature dependence of the (003) intensity. In (D) to (F), dashed lines are mean-field predictions, also shown in solid with temperature and field axes scaled by 0.52 and 0.76, respectively, to match the measured T_N and H_c.

$2g_L C_x$ 8.35, and $g_{\|}$ $2g_L C_z$ 2.25 Albeit the anisotropy ratio of the response to a magnetic field $g_{\perp}/g_{\|}$ = 3.7 is modest, the anisotropy ratio of the dipolar coupling $(g_{\perp}/g_{\|})^2$ 13.8 becomes large, which is what causes the XY anisotropy.

The magnetic structure was determined by means of single-crystal and powder neutron diffraction (fig. S2). Magnetic Bragg peaks at ($h + k + l$ = odd)—distinct from the structural peaks ($h + k + l$ = even)—prove explicitly AFM order. The single-crystal Bragg peak intensities are consistent with the bilayered antiferromagnetic (BLAFM) structure depicted in Fig. 1, and also verified by powder diffraction. The BLAFM has two equivalent configurations with moments along the a axis or b axis, respectively. A very small field of 300 Oe along the b axis suppresses the (100) reflection (Fig. 2E), populating a single a axis domain. Hence, the zero-field structure is a distribution of spatially separated domains with moments along a and b, respectively. Full powder refinement yielded an ordered moment $\langle J^x \rangle$ = 2.2 ± 0.1, reduced from the value $\langle J^x \rangle_{MF}$ = 3.0 predicted by a MF calculation.

The phase diagram as function of temperature and fields along the c and b axes is shown in Fig. 2. The transition temperature T_N 373 ± 5 mK agrees with previous reports. For fields along c, the intensity at (010), corresponding to the order parameter squared, disappears in a sharp QPT at $H_{c\|}$ 4.0 ± 0.1 kOe. For fields along b, the (100) peak disappears owing to mono-domain formation. The (003) peak, which is independent of ab domains, decreases toward $H_{c\perp} \cong$ 2.1 kOe, but a long tail remains to 4 kOe. The (103) peak, measuring the uniform FM component, grows toward a kink at $H_{c\perp}$, corresponding to maximal polarization of the ground-state doublet. Above $H_{c\perp}$, a weak linear increase, achieved by mixing-in higher lying crystal field levels, is well reproduced by the MF prediction.

A MF calculation yields the correct BLAFM ordered and a qualitatively correct phase diagram (supplementary materials). In $LiHoF_4$, a MF treatment accounts for most of the phase diagram except close to T_C, which is overestimated by 37% (*10*). In $LiErF_4$, T_N^{mf} = 728 mK, $H_{c\|}^{mf}$ = 5.25 kOe, and $H_{c\perp}^{mf}$ = 3.25 kOe are all dramatically overestimated. Unlike $LiHoF_4$, any NN exchange interaction cancels in the BLAFM and cannot fine-tune the phase boundary. Including hyperfine coupling has little effect: $H_{c\|}$ = 5.75 kOe and T_N 735 mK.

Scaling the temperature and field to match T_N and H_c, the $T_N(H)$ curve is well described (Fig. 2A), but the onset of order is more abrupt than the MF prediction (Fig. 2, D and E). Deep in the ordered phase, the unscaled MF calculation works (except for the low-field dip in Fig. 2D, which requires further investigation), but around the transition, fluctuations gain importance. We measured simultaneously the strength of the critical scattering, whose divergences independently determine T_N and H_c (Fig. 3, inset), increasing the precision of the extracted critical exponents: β_T = 0.15 ±

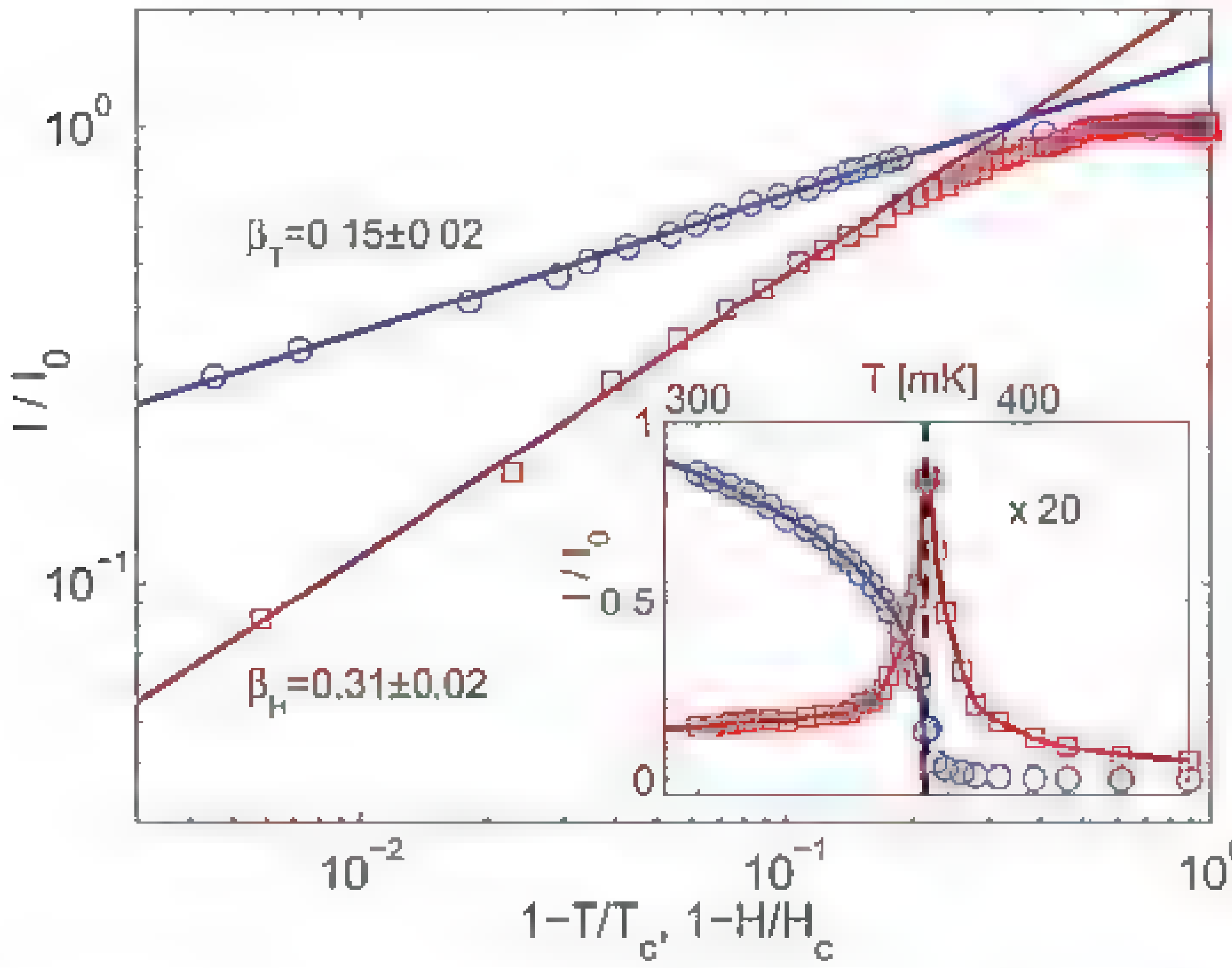

Fig. 3. (010) intensity as a function of temperature at H = 0 (blue circles) and a c axis field at T = 80 mK (red squares). Lines are power law fits. (Inset) Intensity of Bragg peak (blue circles) and critical scattering (red squares) extracted by fitting a resolution-corrected sum of a delta function and a Lorentzian to crystal rotation scans.

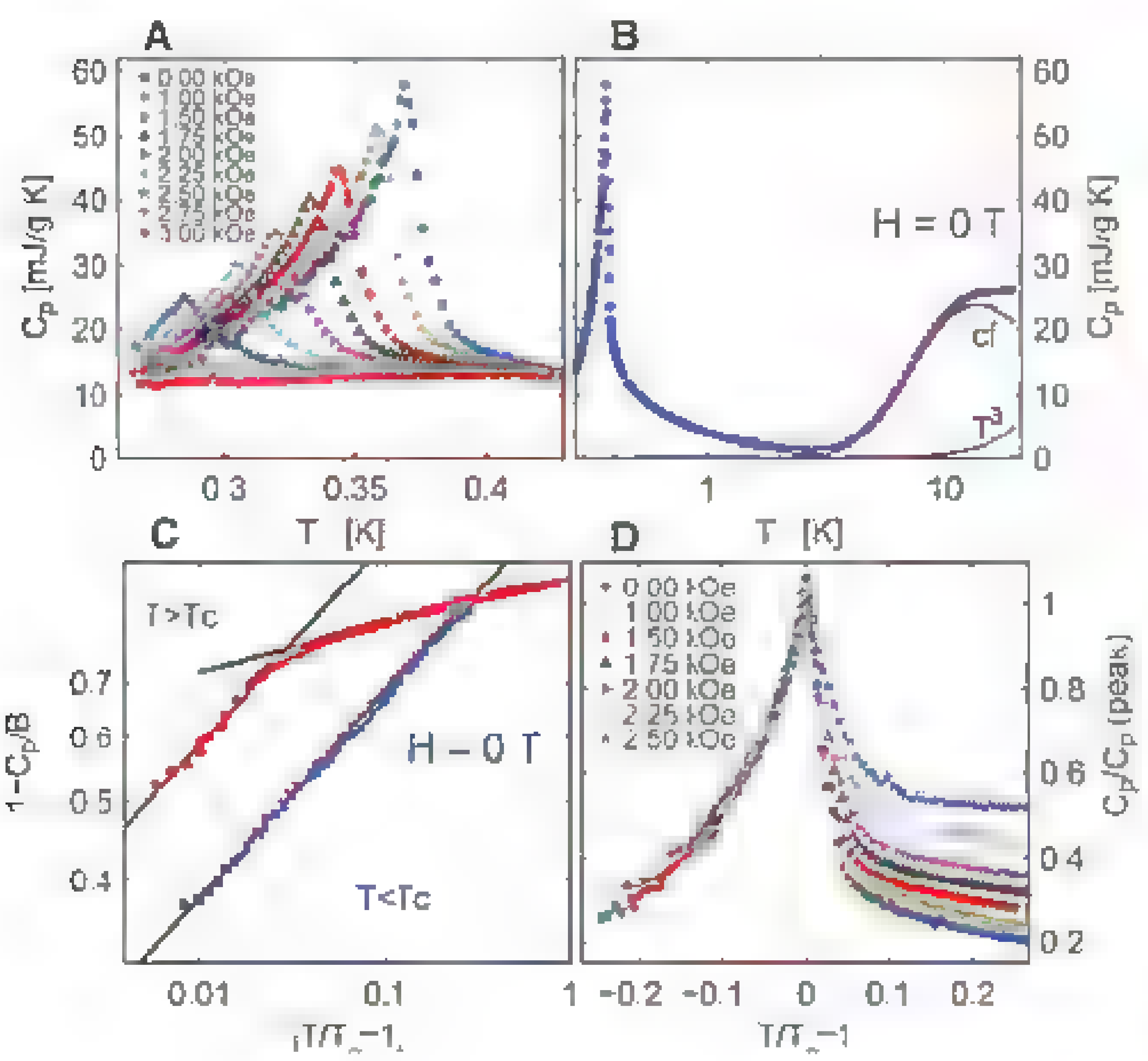

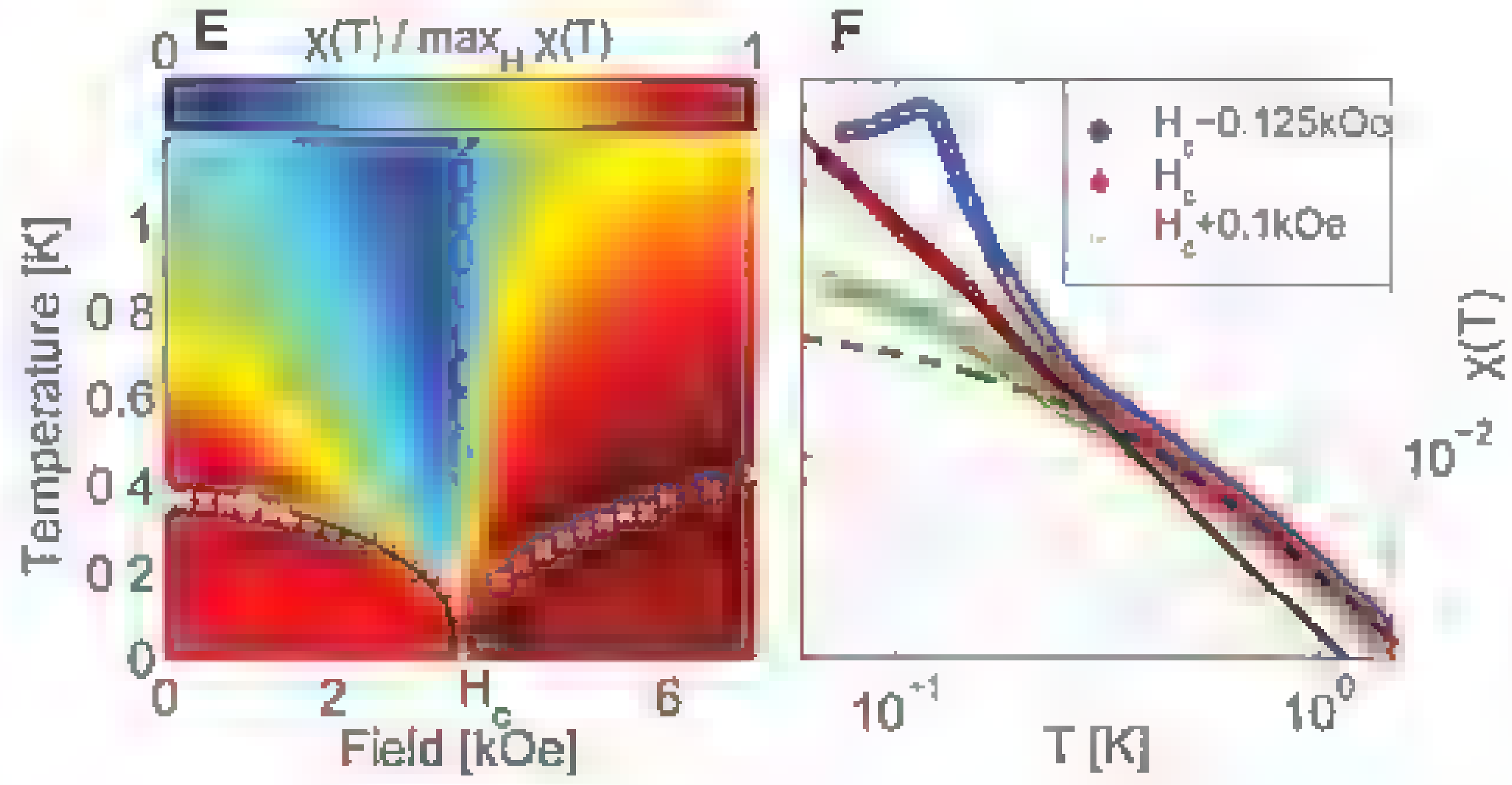

Fig. 4. **(A)** Specific heat versus temperature for several fields along the c axis **(B)** Above 2K, specific heat is described by the sum (red line) of the crystal field Shottky anomaly (cf) and a very weak T^3 phonon contribution. **(C)** Power law behavior of specific heat at H = 0 T determines critical exponents. **(D)** Curves measured at different field values shifted to the same peak center and normalized by peak height to compare the evolution of peak shape. Below T_N, the data collapse onto a unique curve. **(E)** Susceptibility $\chi(T)$ normalized for each field. Peak positions are marked by crosses [$\chi(T)$] and diamonds [$C_p(T)$]. Black line is power law fit to $T_N(H)$. **(F)** $\chi(T)$ just below, at, and just above H_c. At H_c, $\chi(T)$ displays quantum critical scaling with exponent 0.70 ± 0.03 (solid line), up to a crossover around 250 mK, above which regular Curie-Weiss behavior $C/(T - \theta_{CW})$ with θ_{CW} = −0.55 ± 0.01 K describes the data (dashed line).

0.02 for the thermal transition at $H = 0$ T and $\beta_H = 0.31 \pm 0.02$ for the QPT at $H_{c\parallel}$ (Fig. 3). Both exponents considerably deviate from the MF expectation ($\beta^{mf} = 1/2$).

The specific heat shows a pronounced ordering anomaly (Fig. 4), which is in good accordance with the phase diagram established by neutrons (figs. S3 and S4). The broad bump around 12 K is exactly described by our crystal field Hamiltonian. The phonon contribution ρT^3 with $\rho = (6.6 \pm 0.1) \times 10^{-7}$ J/gK^4 is much lower than previously reported for Li*RE*F_4 (17), where the crystal field contribution was not subtracted. The tail above T_N is much more pronounced than in the FM cases of $LiHoF_4$ and $LiTbF_4$ (17, 19, 20). Around T_N, the specific heat follows a universal power law

$$C_p = A|t|^{-\alpha} + B \qquad t = T/T_c - 1 \tag{5}$$

where $\alpha = -0.28 \pm 0.04$ below and above the transition, while $A_+/A_- = 1.68 \pm 0.04$ (A_+ and A_- are the values of the parameter A above and below the transition temperature, respectively). Subtracting B reveals a crossover to $\alpha = -0.07 \pm 0.05$ for $t > 0.03$ (Fig. 4C). Scaling to peak height and temperature, $C_p(T)$ curves for different fields collapse to a single unique curve below T_N (Fig. 4D).

For the classical phase transition, the exponent $\beta_T = 0.15 \pm 0.02$ is far from the $\beta = 0.3$ to 0.35 of standard 3D universality classes and instead falls in the window $\beta = 0.125$ to 0.23 for 2D XY criticality (21). Furthermore, the specific heat exponent $\alpha = -0.28 \pm 0.04$ is more negative than is the $\alpha = -0.13$ to -0.198 predicted for classical, dipolar, and quantum 3D Heisenberg models. Both exponents are consistent with recent Monte Carlo data on a dipolar 2D bilayer square lattice finding $\beta = 0.18 \pm 0.02$ and $\alpha \simeq -0.4 \pm 0.2$ (22). Combining the Rushbrooke and Widom relations yields the exponent $\delta = (2-\alpha)/\beta - 1$, which describes the critical behavior of the (antiferromagnetic) order parameter versus (staggered) field $M \propto H^{1/\delta}$ at the transition. Together with $\eta = 2 - d(\delta - 1)/(\delta + 1)$, δ is super-universal, depending only on the spatial dimension: $\delta = 4.7$, $\eta = 0.03$ for 3D (Ising, XY, and Heisenberg), and $\delta = 15$, $\eta = 0.25$ for 2D (Ising and XY/h_4). The exponent $\delta = 14.2$ for $LiErF_4$ is close to the 2D values. If the anomalous scaling dimension η of the spatial correlation function $\langle S_0 S_r \rangle \propto r^{-d+2-\eta}$ at the critical point is zero, the critical properties can be derived with straightforward dimensional analysis—assuming 2D fluctuations in $LiErF_4$ yields $\eta = 0.26$, signaling strong fluctuations which is consistent with the large reduction in transition temperature compared with the MF prediction.

The Mermin-Wagner theorem excludes long-range order in pure 2D XY models, but even infinitesimal fourfold (h_4) anisotropy leads to conventional order slightly above the Kosterlitz-Thouless transition. Weak h_4 anisotropy results in the effective exponents $\eta \simeq 0.35$ and $\beta \simeq 0.23$ (21), which on increasing h_4 approach $\eta = 0.25$ and $\beta = 0.125$—the Onsager solution for 2D Ising magnets. The Onsager solution also predicts a transition temperature reduced from the MF expectation by a factor of $T_c/T_c^{mf} = 1/2\log(1+\sqrt{2}) = 0.56$ for a NN square lattice model. This is close to our experimental value of $T_N/T_N^{mf} = 0.52$ in $LiErF_4$, but a theoretical effort is needed to generalize the Onsager solution to dipolar compounds.

It is surprising that we obtain 2D quasi-Ising-like exponents for a system whose two-dimensionality is not apparent from simple inspections of the direct and reciprocal crystal lattices and where the local symmetry was believed to be XY-like. For our data to be related to these models, two ingredients are needed: (i) reduction of spatial dimensionality from three to two and (ii) reduction of spin space dimensionality from one (XY) to zero (Ising). We leave the origins of these dimensional reductions as a topic for future theoretical efforts, noting here only that quantum fluctuations acting in concert with the tensorial nature of the dipolar interaction could give rise to (ii) through the phenomenon of order-by-disorder (23, 24). Indeed, an estimate of the h_4 anisotropy due to order-by-disorder is of the correct order of magnitude to yield $\beta = 0.15$ (details available in the supplementary materials). The long history of theoretical studies of the 2D dipolar-coupled rotor model was recently revived through advances in microfabricated artificial nanomagnet arrays, which are pursued both as model systems for fundamental physics (25) and for ultrahigh-density magnetic storage technology (26, 27). $LiErF_4$, which we see falls into this universality class, now provides a bulk material with a fully determined Hamiltonian with which theoretical predictions can be guided and tested.

Turning to the quantum phase transition, we observed an order parameter exponent $\beta_H = 0.31 \pm 0.02$ consistent with classical 3D scaling, thus confirming the long-standing Hertz result that a QPT in a d-dimensional system (2D XY/h_4 in our case) scales as a classical system in $d + 1$ dimensions (28). The detailed shape of the phase boundary was determined from susceptibility measurements (Fig. 4, E and F). Above 2 kOe, $T_N(H)$ scales as a power law with exponent 0.34 ± 0.01. At H_c, $\chi(T)$ exhibits quantum critical scaling, following a power-law exponent 0.70 ± 0.03 up to 250 mK, above which it crosses over to classical Curie-Weiss behavior. This behavior around the QCP is in stark contrast to the MF behavior observed in FM $LiHoF_4$. The exponent is close to the 0.75 reported for the heavy Fermion metal $CeCu_{6-x}Au_x$ near quantum criticality (29).

For $LiHo_xY_{1-x}F_4$, much recent theoretical interest focused on random fields, off-diagonal terms of the dipole interaction, and the emergence of glassiness (30–32). We expect $LiErF_4$ to show dramatic effects of dilution with nonmagnetic ions, or enhancement of off-diagonal terms via substitution of Ho for Er ions. An added benefit of Er is the existence of isotopes with and without nuclear spins, allowing comparative exploration of decoherence and mixing effects (33, 34). Compared with other insulating or itinerant systems, $LiErF_4$ has the advantage of a simple, well-characterized Hamiltonian and of being available in large, high-quality single crystals; it promises insights into the fundamental science of quantum dipolar antiferromagnetism.

References and Notes

1. J. M. Luttinger, L. Tisza, *Phys. Rev.* **70**, 954 (1946).
2. J. Als-Nielsen, *Phys. Rev. Lett.* **37**, 1161 (1976).
3. R. Giraud, W. Wernsdorfer, A. M. Tkachuk, D. Mailly, B. Barbara, *Phys. Rev. Lett.* **87**, 057203 (2001).
4. W. Wu, B. Ellman, T. F. Rosenbaum, G. Aeppli, D. H. Reich, *Phys. Rev. Lett.* **67**, 2076 (1991).
5. P. E. Jönsson, R. Mathieu, W. Wernsdorfer, A. M. Tkachuk, B. Barbara, *Phys. Rev. Lett.* **98**, 256403 (2007).
6. J. A. Quilliam, S. Meng, C. G. A. Mugford, J. B. Kycia, *Phys. Rev. Lett.* **101**, 187204 (2008).
7. D. Bitko, T. F. Rosenbaum, G. Aeppli, *Phys. Rev. Lett.* **77**, 940 (1996).
8. D. H. Reich *et al.*, *Phys. Rev. B* **42**, 4631 (1990).
9. J. Jensen, A. R. Mackintosh, *Rare Earth Magnetism* (Clarendon, Oxford, 1991).
10. H. M. Rønnow *et al.*, *Phys. Rev. B* **75**, 054426 (2007).
11. J. P. Sattler, J. Nemarich, *Phys. Rev. B* **4**, 1 (1971).
12. M. R. Brown, K. G. Roots, W. A. Shand, *J. Phys. C Solid State Phys.* **2**, 593 (1969).
13. J. Magariño, J. Tuchendler, P. Beauvillain, I. Laursen, *Phys. Rev. B* **21**, 18 (1980).
14. P. E. Hansen, T. Johansson, R. Nevald, *Phys. Rev. B* **12**, 5315 (1975).
15. H. P. Christensen, *Phys. Rev. B* **19**, 6564 (1979).
16. P. Beauvillain, J. P. Renard, P. E. Hansen, *J. Phys. Chem.* **10**, L709 (1977).
17. G. Mennenga, L. J. de Jongh, W. J. Huiskamp, *J. Magn. Magn. Mater.* **44**, 48 (1984).
18. K. S. Mura, J. Felsteiner, *Phys. Rev. B* **15**, 4309 (1977).
19. G. Ahlers, A. Kornblit, H. J. Guggenheim, *Phys. Rev. Lett.* **34**, 1227 (1975).
20. J. Nikkel, B. Ellman, *Phys. Rev. B* **64**, 214420 (2001).
21. A. Taroni, S. T. Bramwell, P. C. W. Holdsworth, *J. Phys. Condens. Matter* **20**, 275233 (2008).
22. L. A. S. Mól, B. V. Costa, *Phys. Rev. B* **79**, 054404 (2009).
23. J. Villain, R. Bidaux, J. P. Carton, R. Conte, *J. Phys. (Paris)* **41**, 1263 (1980).
24. C. L. Henley, *Phys. Rev. Lett.* **73**, 2788 (1994).
25. R. F. Wang *et al.*, *Nature* **439**, 303 (2006).
26. J. I. Martín, J. Nogués, K. Liu, J. L. Vicent, K. Ivan Schuller, *J. Magn. Magn. Mater.* **256**, 449 (2003).
27. M. V. Lubarda, S. Li, B. Livshitz, E. E. Fullerton, V. Lomakin, *Appl. Phys. Lett.* **98**, 012513 (2011).
28. A. J. Hertz, *Phys. Rev. B* **14**, 1165 (1976).
29. A. Schröder, G. Aeppli, E. Bucher, R. Ramazashvili, P. Coleman, *Phys. Rev. Lett.* **80**, 5623 (1998).
30. D. M. Silevitch *et al.*, *Nature* **448**, 567 (2007).
31. M. Schechter, N. Laflorencie, *Phys. Rev. Lett.* **97**, 137204 (2006).
32. S. M. A. Tabei, M. J. P. Gingras, Y. J. Kao, P. Stasiak, J. Y. Fortin, *Phys. Rev. Lett.* **97**, 237203 (2006).
33. N. V. Prokof'ev, P. C. E. Stamp, *Rep. Prog. Phys.* **63**, 669 (2000).
34. H. M. Rønnow *et al.*, *Science* **308**, 389 (2005).

Acknowledgments: We gratefully acknowledge fruitful discussions with J. Mesot, J. Jensen, A. J. Fisher, S. T. Bramwell, and S. Sachdev; support from Swiss National Science Foundation and Materials with Novel Electronic Properties; and neutron beam access at the Berlin Neutron Scattering Center, Helmholtz-Zentrum Berlin, and the Swiss Spallation Neutron Source, Paul Scherrer Institut. Work at the University of Chicago was supported by the U.S. Department of Energy Basic Energy Sciences, the NSF Materials Research Science and Engineering Center, and the London Centre for Nanotechnology by the UK Engineering and Physical Sciences Research Council.

Supplementary Materials

www.sciencemag.org/cgi/content/full/336/6087/1416/DC1
Materials and Methods
Figs. S1 to S4
Tables S1 to S3

13 March 2012; accepted 19 April 2012
10.1126/science.1221878

Ambient-Temperature Isolation of a Compound with a Boron-Boron Triple Bond

Holger Braunschweig,* Rian D. Dewhurst, Kai Hammond, Jan Mies, Krzysztof Radacki, Alfredo Vargas

Homoatomic triple bonds between main-group elements have been restricted to alkynes, dinitrogen, and a handful of reactive compounds featuring trans-bent heavier elements of groups 13 and 14. Previous attempts to prepare a compound with a boron-boron triple bond that is stable at ambient temperature have been unsuccessful, despite numerous computational studies predicting their viability. We found that reduction of a bis(N-heterocyclic carbene)-stabilized tetrabromodiborane with either two or four equivalents of sodium naphthalenide, a one-electron reducing agent, yields isolable diborene and diboryne compounds. Crystallographic and spectroscopic characterization confirm that the latter is a halide-free linear system containing a boron-boron triple bond.

Stable compounds with homoatomic triple bonds, although well known for carbon and nitrogen, are particularly rare for the heavier main-group elements (groups 13 to 15) and are unknown for boron (*1–3*). The difficulties involved in synthesizing molecules with homoatomic triple bonds of the heavier main-group elements are well documented: Low-valent main-group centers are typically highly reactive in the absence of extreme steric protection by inert groups. In cases where these daunting synthetic difficulties have been overcome, such compounds of the heavier main-group elements are often severely trans-bent, reducing their triple-bond character (*1*).

For the first-row main-group element boron, which resists multiple bonding in general and forms triple bonds to other elements only very rarely (*4–7*), the synthetic challenge of preparing a stable B-B triple bond has thus far been prohibitive. In 2002 the molecule OCBBCO, ostensibly a B_2 molecule stabilized by two Lewis bases, was isolated in an argon matrix at 8 K by the reaction of laser-vaporized boron atoms with CO (*8*). This finding prompted a flurry of theoretical studies of molecules with B-B triple bonds from the groups of Mavridis, Jones, Frenking, and Michalak (*9–13*), considering L→E–E←L (E = B, Al, Ga, In) systems in which the donors L were diatomic molecules (CO, CS, N_2, BO⁻), noble gases (Ar, Kr), phosphines (PCl_3, PMe_3), N-heterocyclic carbenes (NHCs), or tetracoordinate germylenes. In marked contrast to the heavier Al, Ga, and In analogs, NHC-stabilized L→B≡B←L compounds were predicted to be linear, to have very short B-B distances, and to possess, in effect, true boron-boron triple bonds.

Successful attempts at creating stable molecules with homoatomic multiple bonding between group 13 elements have been based on populating the empty π-bonding orbital between the atoms. Most often this has been accomplished by reduction, whereby the groups of Berndt and Power accessed mono- and dianionic diboranes(4) [e.g., $(R_2BBR_2)^{-}$, **1**; $(R_2BBR_2)^{2-}$, **2**, Fig. 1] with one- and two-electron π bonds (*14–19*). Similarly, Power and co-workers reported dialuminyne and digallyne dianions of the form $[REER]^{2-}$ (E = Al, Ga), which, although trans-bent, show some triple-bond character (*20–22*). A second strategy, used by Robinson's group, involved Lewis base stabilization of the boron atoms by NHC donors, allowing boron's own valence electrons to fill the π-bonding orbital of an "HBBH" unit. Thereby, they were able to isolate the bis(carbene)-stabilized diborene **3** (Fig. 1) by reduction of an NHC-BBr_3 adduct (*23*). Were it not for the opportunistic abstraction of hydrogen, presumably from the reaction solvent, this reaction might have resulted in a triply bound species of the form L→B≡B←L. The stability and triple-bond character of such a compound was subsequently predicted computationally by the groups of Mitoraj, Jones, and Frenking (*11, 12*).

The hydrogen abstraction implicit in Robinson's diborene synthesis led us to assume that during the reduction a boron-based radical intermediate was being formed, perhaps as the result of a slow boron-boron coupling step. If so, we reasoned that the synthesis of a triply bound L→B≡B←L compound could be promoted by the reduction of a molecule with a preformed B-B bond. After

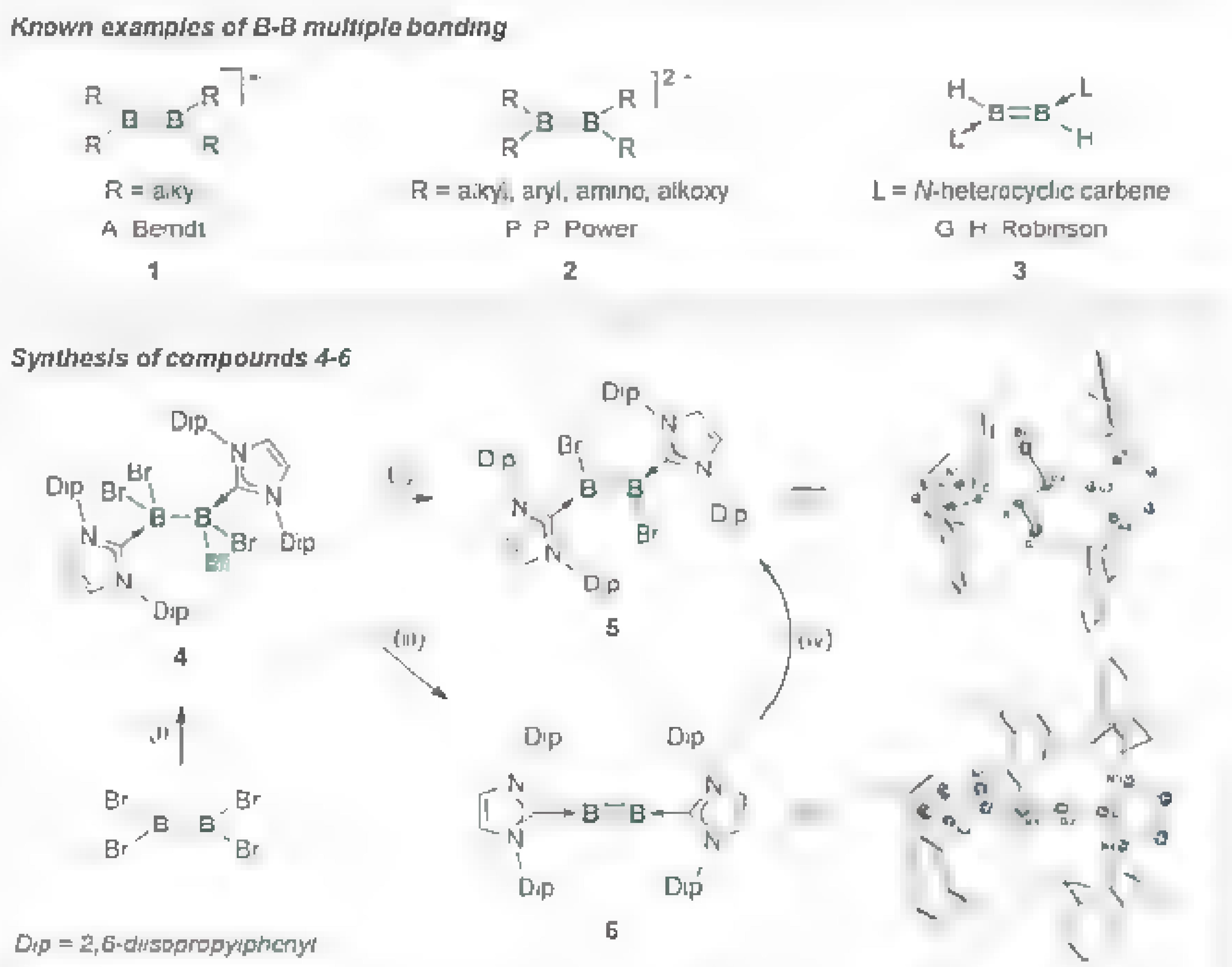

Fig. 1. Top: Previously published examples of B-B multiple bonding. Bottom: Synthesis of compounds **4** to **6** and crystallographic molecular structures of **5** and **6**. Reaction conditions: (i) 2 equiv. 1,3-bis-(2,6-diisopropylphenyl)imidazol-2-ylidene (IDip), pentane, −78°C; (ii) 2 equiv. sodium naphthalenide, tetrahydrofuran (THF), −78°C; (iii) 4 equiv. sodium naphthalenide, THF, −78°C; (iv) 1 equiv. compound **4**, C_6D_6, room temperature. Thermal ellipsoids in the structures at right depict the 50% probability level. For clarity, hydrogen atoms have been removed and the nitrogen substituents have been simplified. Selected bond lengths and angles for **5**: B1-B2, 1.546 ± 0.006 Å; B1-C1, 1.569 ± 0.006 Å; B1-Br1, 2.030 ± 0.004 Å; B2-C2, 1.586 ± 0.007 Å; B2-Br2, 2.046 ± 0.004 Å; B2-B1-C1, 128.6 ± 0.4°; B2-B1-Br1, 120.2 ± 0.3°; B1-B2-C2, 132.0 ± 0.7°; B1-B2-Br2, 116.2 ± 0.3°. Selected bond lengths and angles for **6**: B1-B2, 1.449 ± 0.003 Å; B1-C1, 1.487 ± 0.003 Å; B2-C2, 1.495 ± 0.003 Å; B2-B1-C1, 173.0 ± 0.2°; B1-B2-C2, 173.3 ± 0.2°.

Institut für Anorganische Chemie, Julius-Maximilians-Universität Würzburg, Am Hubland, 97074 Würzburg, Germany

*To whom correspondence should be addressed. E-mail: h.braunschweig@uni-wuerzburg.de

preparing tetrabromodiborane(4) (*24*, *25*), simple addition of two equivalents of the free NHC 1,3-bis-(2,6-diisopropylphenyl)imidazol-2-ylidene (IDip) furnished the bis(carbene)-stabilized diborane(4), **4** (Fig. 1) (*26*). By treating **4** with either two or four equivalents of a tetrahydrofuran solution of the one-electron reducing agent sodium naphthalenide [$Na(C_{10}H_8)$], we were able to controllably generate and isolate the bis(NHC)-stabilized dibromodiborene **5** (48% yield) and bis(NHC)-stabilized diboryne **6** (57% yield) as green solids after removal of by-product naphthalene under high vacuum and extraction of the neutral compounds into pentane.

The ^{11}B nuclear magnetic resonance (NMR) signals of **4** (δ = −4.8 ppm), **5** (δ = 20 ppm), and **6** (δ = 39 ppm) show a clear progression toward low field, as expected for the stepwise decrease in the coordination number at boron. The ^{11}B NMR chemical shift of **6** matches those calculated using the gauge-independent atomic orbital density functional theory [GIAO-DFT (*27*–*31*)] method at the B3LYP/6-311G* level and referenced to BF_3 (δ = 36.54 and 36.01 ppm). The identity and purity of complexes **4** to **6** were confirmed by ^1H and $^{13}C\{^1H\}$ NMR spectra and elemental analyses. Further support for the connectivity of compounds **5** and **6** was provided by a comproportionation reaction, in which mixing of an equimolar amount of tetrabromodiborane(4) **4** and diboryne **6** resulted in full conversion (monitored by ^{11}B NMR) to the dibromodiborene **5**. Compound **6** exhibits impressive thermal stability, decomposing only at 234°C.

Molecular structures of compounds **5** and **6** derived from single-crystal x-ray crystallography are shown in Fig. 1. The diborene **5** has a planar structure similar to that of dihydrodiborene **1** (Fig. 1, top; L = IDip) prepared by Robinson, and their B-B distances are also comparable (**5**, 1.546 ± 0.006 Å; **1**, 1.561 ± 0.018 Å) (*23*). These distances compare well with calculated values from the groups of Mitoraj (1.57 to 1.60 Å) and Jones and Frenking (1.618 and 1.594 Å) for diborene systems (*11*, *12*). The B-B distances of neutral, base-stabilized diborenes are slightly shorter than the corresponding distances of dianionic diboranes(4) containing B-B double bonds (1.623 to 1.706 Å). The structure of **6** shows an effectively linear C→B≡B←C core, as predicted by theory (*11*, *12*), with a B-B distance of 1.449 ± 0.003 Å and very slight bending at the boron atoms (173.0 ± 0.2°, 173.3 ± 0.2°). The B-B distance of **6** fits very well with the calculated values for the highly comparable bis(carbene)- and bis(phosphine)-stabilized diborynes [1.45 to 1.46 Å in (*11*); 1.470 Å in (*12*)] and surprisingly well with both measured (1.453 to 1.468 Å) (*8*) and calculated (1.439 Å) (*9*) values of OCBBCO, as well as calculated values of SCBBCS (1.482 Å) (*9*), N_2BBN_2 (1.460 Å) (*9*), and $[OBBBBO]^{2-}$ (1.481 to 1.504 Å) (*10*, *13*). The difference in the B-B bond distances of the doubly (**5**) and triply bonded (**6**) species is statistically significant (0.097 Å) and corresponds to a contraction of ~6%.

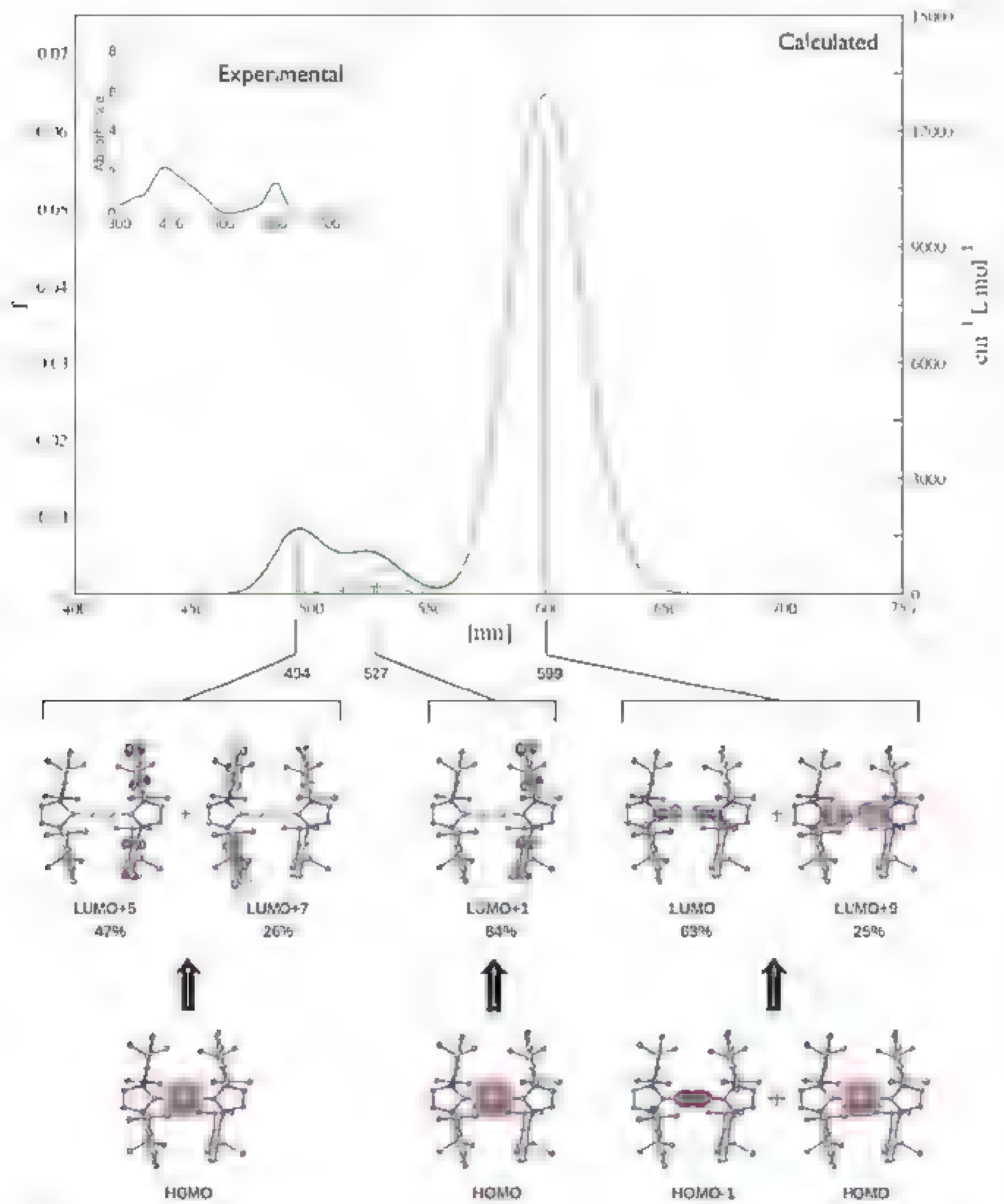

Fig. 2. Top: Simulated UV-vis absorption spectrum of **6** derived from TD-DFT, with calculated oscillator strengths shown as black vertical lines. Inset: Experimental UV-vis spectrum of **6**. Bottom: Electronic transitions corresponding to the individual bands of the calculated spectrum, along with their percent contributions to the absorption.

A solid-state infrared spectrum of diboryne **6** showed a number of strong bands at 1467, 1386, 1363, and 1328 cm^{-1}. Although we expect these bands to be somewhat associated with the B_2 unit of **3**, we calculated the true B≡B stretch of the molecule to be at 1339 cm^{-1}. This mode is highly symmetrical and is calculated to be infrared-inactive (see figs. S4 and S5). The color of both **5** and **6** can be explained by low absorption in the green region of their ultraviolet-visible (UV-vis) absorption spectra (**5**, ~530 nm; **6**, 510 nm). Diborene **5** has absorption bands centered at 380 nm (extinction coefficient: 134,965 L mol^{-1} cm^{-1}) and 695 nm (317,819 L mol^{-1} cm^{-1}) (fig. S1), whereas diboryne **6** has a weak band at 335 nm (9852 L mol^{-1} cm^{-1}) and intense bands at 385 nm (26,426 L mol^{-1} cm^{-1}, with relatively strong shoulder peak) and 600 nm (17,685 L mol^{-1} cm^{-1}) (Fig. 2).

The unusual color of diboryne **6** prompted us to turn to computation in order to find an explanation. Our computational results on the geometry and structure of the electronic ground state of diboryne **6** show no notable differences from those determined by Jones and Frenking (*12*) for a comparable analog; thus, our discussion focuses only on computational studies related to the spectral properties of **6**. We sought to identify the states that are responsible for the observed absorption bands in the UV-vis spectrum. Dipole-allowed electronic excitation calculations were carried out on gas-phase optimized structures within the adiabatic local density approximation (ALDA) of time-dependent DFT (TD-DFT) at the B3LYP/6-311G* level.

Figure 2 shows the stick plot of the calculated oscillator strengths and the simulated spectra. The overall absorption profile (shape) of the

bands is well reproduced; however, there are some small discrepancies. The narrow nonabsorbing domain centered at 510 nm in the experimental spectrum (which gives the compound its green color) is shifted some 40 nm to the red on an absolute energy scale; moreover, the relative intensity of the higher-energy band is somewhat lower than what is observed experimentally. DFT is well known to underestimate the highest occupied molecular orbital (HOMO)–lowest unoccupied molecular orbital (LUMO) gap of molecules, and thus tends to provide excitations that are too low in energy. Nonetheless, the calculations predict a green-yellow coloration for diboryne **6**. The absorption band observed experimentally at 380 nm is not fully symmetrical and probably incorporates a side peak, making it appear steeply cambered in the 410- to 510-nm region. This effect is fully explained by calculations: The stronger band (494.2 nm) is a result of an excitation from the HOMO to the LUMO+5 and the LUMO+7, whereas the neighboring shoulder (527.9 nm) is a transition from the HOMO to the LUMO+1. All three of these transitions involve electronic promotion into orbitals centered on the aryl substituents. The calculated spectra also predict a very intense band at 599.2 nm. The high intensity of this signal is not surprising in light of the seemingly high overlap between the occupied B≡B-centered π system and the empty B-C π-like orbitals of **6**. This signal is attributed to the HOMO→LUMO+9 and HOMO-1→LUMO transitions. The three major absorption bands in the UV-vis region all involve excitation of electrons from one or the other of the π bonds of the B≡B unit.

Compound **3** is stable at room temperature in the absence of air and water. The chromophore properties and robustness of **5** and **6** offer exciting possibilities for the further study of the reactivity and optical properties of B-B double and triple bonds, in line with the recent interest in boron-based functional materials (*32*, *33*).

References and Notes

1. R. C. Fischer, P. P. Power, *Chem. Rev.* **110**, 3877 (2010).
2. Y. Wang, G. H. Robinson, *Chem. Commun.* **2009**, 5201 (2009).
3. Y. Wang, G. H. Robinson, *Inorg. Chem.* **50**, 12326 (2011).
4. P. Paetzold, A. Richter, T. Thijssen, S. Würtenberg, *Chem. Ber.* **112**, 3811 (1979).
5. P. Paetzold, C. von Plotho, *Chem. Ber.* **115**, 2819 (1982).
6. H. Braunschweig, K. Radacki, D. Rais, K. Uttinger, *Angew. Chem. Int. Ed.* **45**, 162 (2006).
7. H. Braunschweig, K. Radacki, A. Schneider, *Science* **328**, 345 (2010).
8. M. Zhou *et al.*, *J. Am. Chem. Soc.* **124**, 12936 (2002).
9. A. Papakondylis, E. Miliordos, A. Mavridis, *J. Phys. Chem. A* **108**, 4335 (2004).
10. L. C. Ducati, N. Takagi, G. Frenking, *J. Phys. Chem. A* **113**, 11693 (2009).
11. M. P. Mitoraj, A. Michalak, *Inorg. Chem.* **50**, 2168 (2011).
12. N. Holzmann, A. Stasch, C. Jones, G. Frenking, *Chem. Eur. J.* **17**, 13517 (2011).
13. S.-D. Li, H.-J. Zhai, L.-S. Wang, *J. Am. Chem. Soc.* **130**, 2573 (2008).
14. H. Klusik, A. Berndt, *Angew. Chem. Int. Ed. Engl.* **20**, 870 (1981).
15. A. Moezzi, R. A. Bartlett, P. P. Power, *Angew. Chem. Int. Ed. Engl.* **31**, 1082 (1992).
16. A. Moezzi, M. M. Olmstead, P. P. Power, *J. Am. Chem. Soc.* **114**, 2715 (1992).
17. P. P. Power, *Inorg. Chim. Acta* **198–200**, 443 (1992).
18. W. J. Grigsby, P. P. Power, *Chem. Commun.* **1996**, 2235 (1996).
19. W. J. Grigsby, P. P. Power, *Chem. Eur. J.* **3**, 368 (1997).
20. R. J. Wright, M. Brynda, P. P. Power, *Angew. Chem. Int. Ed.* **45**, 5953 (2006).
21. N. J. Hardman, R. J. Wright, A. D. Phillips, P. P. Power, *J. Am. Chem. Soc.* **125**, 2667 (2003).
22. N. J. Hardman, R. J. Wright, A. D. Phillips, P. P. Power, *Angew. Chem. Int. Ed.* **41**, 2842 (2002).
23. Y. Wang *et al.*, *J. Am. Chem. Soc.* **129**, 12412 (2007).
24. W. Keller, L. G. Sneddon, W. Einholz, A. Gemmler, *Chem. Ber.* **125**, 2343 (1992).
25. H. Nöth, H. Pommerening, *Chem. Ber.* **114**, 398 (1981).
26. See supplementary materials on *Science* Online.
27. F. London, *J. Phys. Radium* **8**, 397 (1937).
28. R. McWeeny, *Phys. Rev.* **126**, 1028 (1962).
29. R. Ditchfield, *Mol. Phys.* **27**, 789 (1974).
30. K. Wolinski, J. F. Hinton, P. Pulay, *J. Am. Chem. Soc.* **112**, 8251 (1990).
31. J. R. Cheeseman, G. W. Trucks, T. A. Keith, M. J. Frisch, *J. Chem. Phys.* **104**, 5497 (1996).
32. C. D. Entwistle, T. B. Marder, *Angew. Chem. Int. Ed.* **41**, 2927 (2002).
33. A. Steffen, R. M. Ward, W. D. Jones, T. B. Marder, *Coord. Chem. Rev.* **254**, 1950 (2010).

Acknowledgments: Supported by Deutsche Forschungsgemeinschaft grant BR 1149/13-1. Crystallographic data have been deposited with the Cambridge Crystallographic Data Centre as supplementary publication nos. 868974 (5) and 868975 (6). These data can be obtained free of charge via www.ccdc.cam.ac.uk/data_request/cif.

Supplementary Materials

www.sciencemag.org/cgi/content/full/336/6087/1420/DC1
Materials and Methods
Figs. S1 to S5
Tables S1 and S2
References (34–45)

27 February 2012; accepted 25 April 2012
10.1126/science.1221138

Reticulated Nanoporous Polymers by Controlled Polymerization-Induced Microphase Separation

Myungeun Seo and Marc A. Hillmyer*

Materials with percolating mesopores are attractive for applications such as catalysis, nanotemplating, and separations. Polymeric frameworks are particularly appealing because the chemical composition and the surface chemistry are readily tunable. We report on the preparation of robust nanoporous polymers with percolating pores in the 4- to 8-nanometer range from a microphase-separated bicontinuous precursor. We combined polymerization-induced phase separation with in situ block polymer formation from a mixture of multifunctional monomers and a chemically etchable polymer containing a terminal chain transfer agent. This marriage results in microphase separation of the mixture into continuous domains of the etchable polymer and the emergent cross-linked polymer. Precise control over pore size distribution and mechanical integrity renders these materials particularly suited for various advanced applications.

Mesoporous metals, ceramics, and polymers are tremendously useful in the fields of catalysis, templating, and separations (*1*). Those containing both a percolating pore structure and a continuous matrix structure (i.e., bicontinuous structures) are highly desirable from the standpoint of pore accessibility and structural isotropy. Although metal and ceramic nanoporous materials of this type have dominated the landscape (*2*, *3*), nanoporous polymers (*4*, *5*) have received attention due to the exquisite synthetic control of their functional attributes using contemporary polymerization mechanisms and functionalization protocols (*6*).

Block polymers are an intriguing class of self-assembling hybrid macromolecules that are versatile precursors to nanoporous polymers with well-defined pore structures, sizes, and surface functionality (*7*). However, there are three key issues that currently limit the utility of nanoporous materials from block polymers in separation applications (*8*). The straightforward preparation of large-area samples with a bicontinuous pore structure has only been achieved in a few cases (*9*–*12*). The drive to smaller and smaller pore sizes (e.g., below ~10 nm) has been challenging due to fundamental block polymer thermodynamic issues and high Laplace pressures that can lead to pore collapse (*13*). In addition, the typically poor mechanical properties of nanoporous polymers generated from block polymers limit how they can be implemented in practice (*10*). Here, we present a new block polymer-based strategy for the preparation of nanoporous

Department of Chemistry, University of Minnesota, Minneapolis, MN 55455, USA.

*To whom correspondence should be addressed. hillmyer@umn.edu

polymers that simultaneously address all three of these issues.

We combined polymerization-induced phase separation with in situ block polymer formation (*14*, *15*) by polymerizing a mixture of multifunctional monomers in the presence of a macromolecular chain transfer agent (macro-CTA) that is initially soluble in the monomer mixture but incompatible with the emergent cross-linked polymer. Covalent connection of the macro-CTA to the polymerizing mixture of monomers favors the formation of structured materials with length scales that are restricted by the macromolecular dimensions of the block polymers formed. Importantly, the reversible addition-fragmentation chain transfer (RAFT) polymerization process (*16*) allows for linear increases in molar mass. Thus, the majority of the growing block polymers reach the point of becoming incompatible in the polymerizing monomer medium and microphase-separate over a small time interval, giving a homogeneous cross-linked, mechanically robust, and nanostructured composite. The resultant bicontinuous structure is prevented from coarsening by virtue of the cross-linking of the matrix. By employing a chemically etchable block as the macro-CTA, nanoporous monoliths with a percolating pore structure can be generated. Relying on microphase separation of a block polymer obtained by controlled polymerizations, this strategy is distinguished from other polymerization-induced phase separation methods that result in the formation of bicontinuous but macrophase-separated monoliths (*5*, *17*) or that generate microphase-separated conetworks by uncontrolled polymerization mechanisms (*15*, *18*). A schematic of the overall process is given in Fig. 1.

Polylactide (PLA) with a trithiocarbonate chain transfer agent at one terminus (PLA-CTA) was chosen as the chemically etchable macro-CTA, and styrene (S)/divinylbenzene (DVB) was selected as the cross-linkable monomer mixture. Importantly, PLA and poly(styrene) (PS) are characterized by a large Flory-Huggins interaction parameter and thus their block polymers should form well-segregated structures with sharp interfaces in the ordered state (*19*). The number-average molar masses of the PLA-CTA samples were 11, 22, and 41 kg mol^{-1} and are labeled PLA-CTA-11, PLA-CTA-22, and PLA-CTA-41, respectively (fig. S1) (*20*). Similar PLA-CTA agents are effective for controlled RAFT polymerization of S, yielding well-defined PLA-PS block polymers (*21*, *22*). Initiation of the S/DVB mixture leads to rapid incorporation of the PLA-CTA due to the high chain transfer constant for the trithiocarbonate group. Continued growth of the S/DVB copolymer results in the formation of a PLA-P(S/DVB) block polymer in the presence of the remaining unreacted S/DVB. Because of pendant double bonds stemming from the DVB incorporation, this growing P(S/DVB) block is ultimately incorporated into a cross-linked network, and microphase separation of the PLA block from this emergent cross-linked matrix occurs. We posit that as the S/DVB mixture continues to polymerize, the S and DVB in the swollen PLA-rich regions of the mixture migrates to the growing matrix, ultimately leading to relatively pure PLA domains.

In an exemplary case, 30 weight percent (wt %) PLA-CTA-22 was dissolved in a 4/1 molar mixture of S/DVB to give a homogeneous solution that was optically transparent. Heating to 120°C (with or without added radical initiator) for 5 hours results in a transparent, insoluble monolithic solid, as shown in Fig. 2. When hydroxyl-terminated PLA (PLA-OH) or a mixture of PLA-OH with CTA was used instead of PLA-CTA, macrophase separation was evident (fig. S2). Consistent with related cross-linked PS/DVB resins, the monolith exhibited an ultimate tensile strength of 38 MPa, an ultimate elongation of ~14%, and a Young's modulus of 560 MPa (fig. S3). Small-angle x-ray scattering (SAXS) analysis of the sample gave a single broad reflection centered at a scattering vector $q = 0.3$ nm^{-1}, consistent with a microphase-separated, but disorganized, structure with compositional heterogeneities on a ~21-nm-length scale (fig. S4). Observation of the fractured surface after coating with Pt (~1 nm) by scanning electron microscopy (SEM) did not reveal obvious nanostructuring. However, selective staining of the PS domain with RuO_4 gave images that support the presence of a nanostructure consistent with the SAXS data (fig. S5). Differential scanning calorimetry (DSC) analysis of this and all other samples indicated a single thermal transition attributed to the glass transition of PLA plasticized with residual unreacted S/DVB (fig. S6). Similar samples prepared with PLA-CTA-11 and PLA-CTA-41 gave cross-linked monoliths with nearly identical physical characteristics. However, SAXS analysis revealed principal domain dimensions of 15 nm and 27 nm, respectively.

To remove the PLA, the monolithic samples were immersed in 0.5 M methanol (40% by volume)/water solution of NaOH. Complete PLA removal was indicated by a mass loss corresponding to the initial weight fraction of PLA used in the synthesis, absence of the PLA C=O vibration in the infrared spectrum, and disappearance of glass transition corresponding to PLA in the DSC thermogram (figs. S6 and S7). An image of a monolith synthesized using PLA-CTA-11 after PLA etching is shown in Fig. 2. The change in sample dimension upon etching was minimal, and the transparency post-etching is consistent with retention of a nanostructured material. A related sample prepared from PLA-CTA-22 exhibited an ultimate tensile strength of 6.4 MPa, an ultimate elongation of ~9%, and a Young's modulus of ~170 MPa, indicating robust mechanical properties after PLA removal (fig. S3).

Elimination of PLA in all samples resulted in dramatically increased SAXS intensity compared with the precursor material, but no change

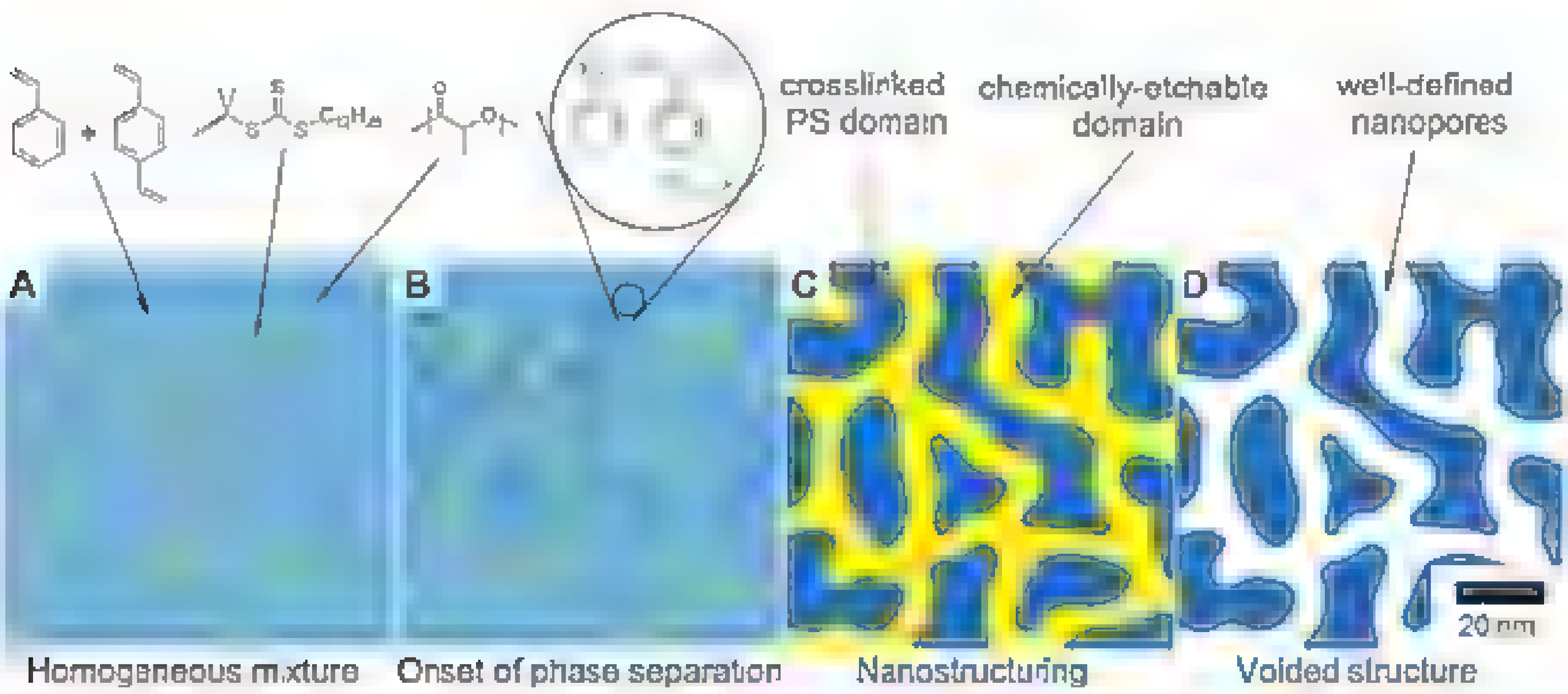

Fig. 1. Schematic depiction of nanoporous monolith generation by a controlled polymerization-induced microphase separation process. (**A**) Initially, a macro-CTA containing the etchable polymer (yellow) is dissolved in the mixture (light blue) of a monomer and a cross-linker. RAFT copolymerization allows controlled growth of chains (dark blue) generating a block polymer structure; the growing chains are also being cross-linked in situ (**B**). At a critical conversion, microphase separation occurs over a small time interval, and cross-linking arrests the emergent bicontinuous structure with a nanoscopic length scale (**C**). Subsequent removal of the etchable polymer produces percolating nanopores in a cross-linked and mechanically robust matrix (**D**).

Fig. 2. Image of the cross-linked precursor (left) and the nanoporous monolith (right) generated from PLA-CTA-11 (32 wt %) and azobisisobutyronitrile (0.16 equivalents relative to PLA-CTA) in a 4/1 S/DVB mixture that was heated to 120°C for 5 hours.

in the position of the principal peak was observed (fig. S4). These data strongly support generation of a porous structure similar to the nanostructured morphology present in the as-synthesized monoliths. An SEM image of a cryofractured surface of a cross-linked, nanoporous material prepared using PLA-CTA-22 revealed that interconnected nanopores were evenly distributed through the material (Fig. 3). The structure is similar to inorganic nanoporous structures such as Vycor glass, where bicontinuous structures are produced by a spinodal decomposition process that is kinetically restricted from coarsening due to the viscosity of the medium; subsequent selective leaching results in nanopore formation (*3*). Characteristics of the scattering data from the nanoporous materials described here were consistent with other materials formed by spinodal decomposition processes (fig. S8) (*23*, *24*). Image analysis of Fig. 3 gave an estimate of average pore diameter ≈ 9 ± 2 nm (after accounting for a ~1-nm Pt coating). This is in contrast to conventional porous P(S/DVB) and its analogs that adopt macroporous structures consisting of a network of agglomerated microgel particles (*17*)

SEM images of the nanoporous materials indicated that the pore diameter could be controlled by the molar mass of PLA-CTA used (fig. S9); pores down to 6 nm were evident in voided monoliths derived from PLA-CTA-11. Nitrogen adsorption experiments were consistent with these observations and provided more information on the average pore size and distribution (Fig. 4, A and B, and fig. S10). All the

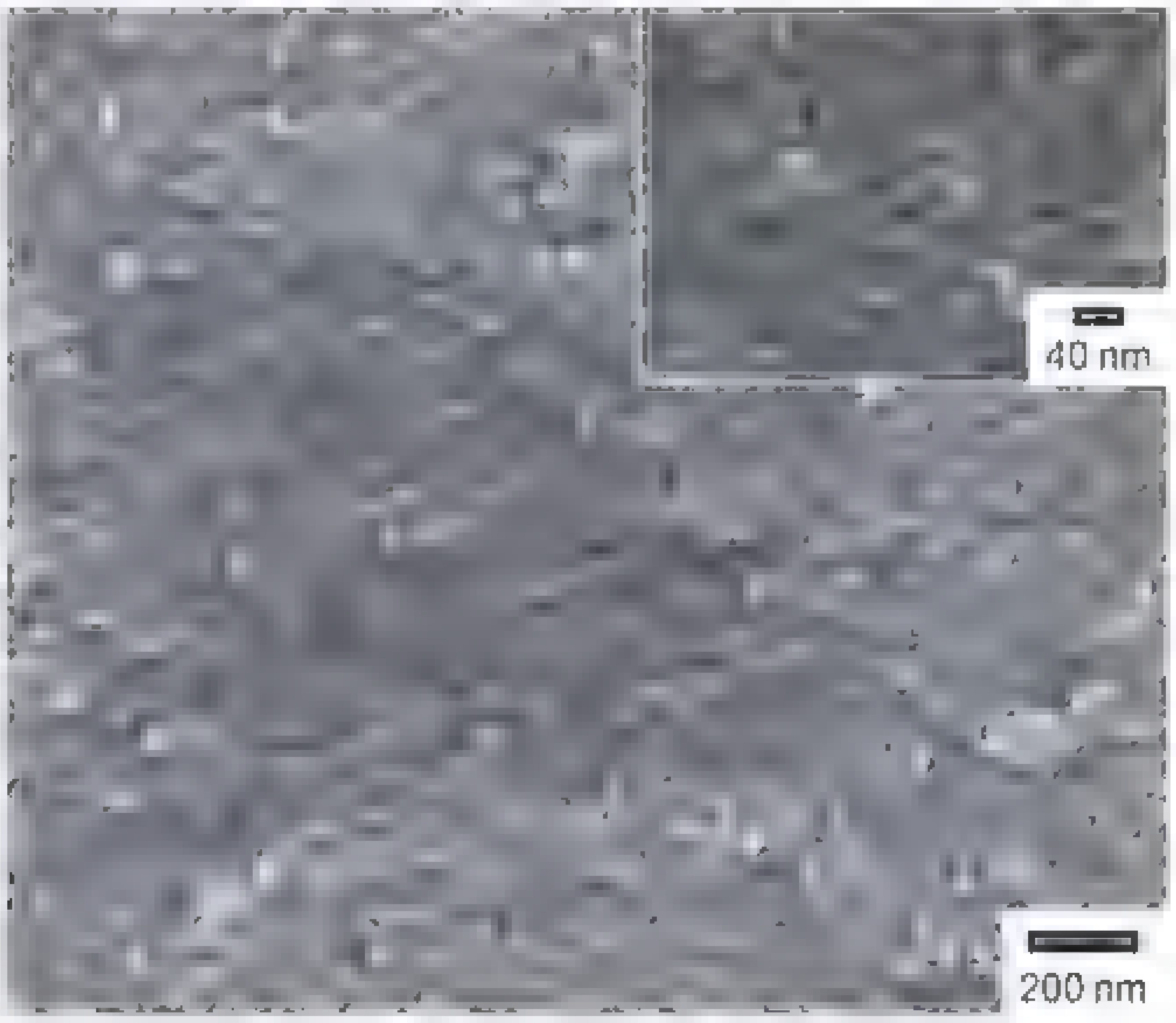

Fig. 3. A representative SEM image of the nanoporous monolith. The sample was coated with ~1 nm of Pt. The sample was derived from 32 wt % of PLA-CTA-22 in a 4/1 S/DVB mixture that was heated to 120°C for 5 hours and etched in a basic solution.

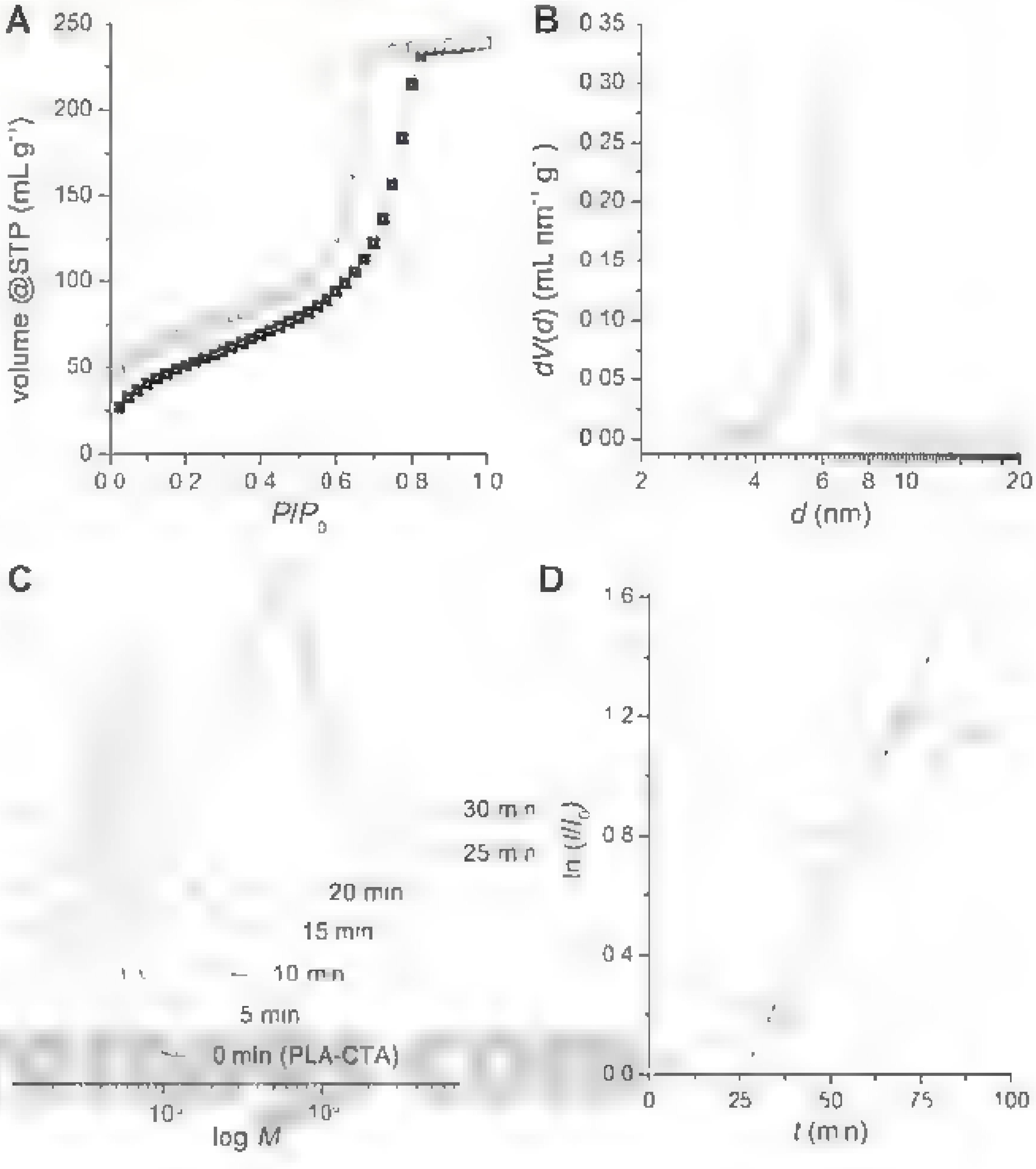

Fig. 4. (**A**) Nitrogen adsorption isotherm of the nanoporous monolith at 77.3 K. The sample was derived from 32 wt % of PLA-CTA-22 in a 4/1 S/DVB mixture that was heated to 120°C for 5 hours and etched in a basic solution. Filled squares, adsorption branch; empty circles, desorption branch. (**B**) Pore size distribution as a function of pore diameter (d) based on BJH analysis of the desorption branch in Fig. 4A. (**C**) Evolution of SEC traces for the first 30 min of polymerization of S and DVB (4/1) in the presence of PLA-CTA-22 (32 wt %) at 120°C. Intensities were obtained by refractive index detector responses, and molar masses were relative to polystyrene standards. (**D**) Evolution of SAXS peak intensity (I) over polymerization time (t) during the polymerization of S and DVB (4/1) in the presence of PLA-CTA-22 (31 wt %) at 120°C. The peak intensity at $q = 0.3$ nm^{-1} was normalized by the intensity at $t = 0$. The dashed line indicates exponential increase of I at the onset of phase separation obtained by linear least-square fitting of data points from 35 to 70 min.

nanoporous materials produced H2-type hysteresis curves very similar to the adsorption isotherms observed for Vycor glass, supporting the presence of a three-dimensionally connected porous network (fig. S11). At low relative pressures, the desorption branch was not coincident with the adsorption branch and thus resulted in an "open" isotherm. One possible explanation for this behavior is that nitrogen remains dissolved within the polymer matrix (*25*). Pore size distributions based on Barrett-Joyner-Halenda (BJH) (*26*) analysis of the desorption branch gave a mean pore diameter of 6 nm when 32 wt % of PLA-CTA-22 was used (Fig. 4B). A total pore volume of 0.37 mL g^{-1} was estimated from these data. Using densities of PLA and P(S/DVB) of 1.25 g cm^{-3} and 1.05 g cm^{-3}, respectively, the initial volume of PLA in the cross-linked monolith was estimated to be 0.38 mL g^{-1}, in a good agreement with the pore volume in the nanoporous version (fig. S12). The surface area for the sample generated using PLA-CTA-22 was determined to be 210 m^2 g^{-1} by Brunauer-Emmett-Teller (BET) analysis (*27*). Nanoporous samples prepared using PLA-CTA-11 and PLA-CTA-41 gave pore diameters of 4 and 8 nm, and surface areas of 250 and 170 m^2 g^{-1}, respectively (table S1). Based on the Flory-Huggins interaction parameter for PLA-PS (*19*), we estimate that pore diameters as low as 2 nm will be accessible. The nanoporous monoliths were more thermally stable compared with non-cross-linked nanoporous polystyrene that collapsed above 94°C with a coincident exothermic transition in the DSC thermogram (*19*). No such exothermic transition was found for these cross-linked materials up to 150°C (fig. S6). The thermal stability was further supported by 83% retention of the pore volume for the sample derived from a PLA-CTA-41 sample after heating for 1 hour at 100°C (fig. S13).

The microphase separation during the polymerization was investigated by combination of reaction kinetics and in situ SAXS studies (Fig. 4, C and D, and figs. S14 to S16). When a 4/1 S/DVB mixture in the presence of 32 wt % PLA-CTA-22 was heated to 120°C, soluble polymers were obtained for the first 30 min of the polymerization. The apparent molar masses of the polymers generated over the first 20 min, as characterized by size exclusion chromatography (SEC), gradually shifted to higher values, suggesting controlled growth of P(S/DVB) from PLA-CTA by the RAFT process (Fig. 4C). Shoulders at high molar mass were consistent with dimerized and trimerized PLA-P(S/DVB) molecules with low P(S/DVB) content. Over the next 5 min, coupling reactions produced very high molar mass species (~10^3 kg mol^{-1}). ^{1}H nuclear magnetic resonance spectra of the soluble polymers supported formation of PLA-P(S/DVB) with pendent vinyl groups (fig. S15 and tables S2 and S3) (*28*). The mixture gelled after 40 min (70% gel fraction) and solidified after 90 min (90% gel fraction).

In situ SAXS analysis of a similar polymerization mixture at 120°C (31 wt % of PLA-CTA-22 in a 4/1 S/DVB mixture) showed the appearance and subsequent growth of a scattering peak at $q \approx 0.3$ nm^{-1} after 35 min that saturated after 80 min, indicating microphase structuring of the emergent PLA-P(S/DVB) block polymer (fig. S16, A and B). The position of the scattering peak was essentially constant throughout the polymerization as cross-linking arrested further coarsening of the microphase-separated structure. The scattering intensity increased exponentially at early times, reminiscent of early-stage spinodal decomposition (Fig. 4D), and further analysis of this data supports microphase separation driven by in situ block polymer formation (fig. S16C) (*29*, *30*).

Bicontinuity of the nanoporous monolith was also supported by gas and liquid transport measurements. Gas permeation profiles of methane, nitrogen, and carbon dioxide through a nanoporous monolith synthesized using PLA-CTA-41 were consistent with Knudsen diffusion, assuming 8-nm pores (from BJH analysis) and incorporating a tortuosity factor of 1.7 (fig. S17 and table S4). This tortuosity value was consistent with the literature value for other bicontinuous materials (*31*). In addition, water was able to pass through a similarly produced 310-μm-thick nanoporous sample with a permeability of 0.45 L h^{-1} m^{-2} bar^{-1}. Using the data obtained from the nitrogen adsorption experiment, we deduced a similarly valued tortuosity of 1.4 (fig. S18).

Nanoporous polymers with sub-10-nm pores were prepared by a controlled polymerization-induced microphase separation method. Although the specific combination of PLA-CTA with S and DVB was presented, similar nanoscopic bicontinuous structures should be accessible if controlled cross-linking polymerization can induce microphase separation. Considering the utility of bicontinuous phases in various applications, the versatility of block polymer self-assembly, and the chemical tunability of block structures and interfacial functionality, this strategy can find even broader application because of the added advantages of simple synthesis, processability, and precise domain size control.

References and Notes

1. G. Q. Lu, X. S. Zhao, Eds., *Nanoporous Materials, Science and Engineering* (Imperial College Press, London, 2004).
2. J. Erlebacher, M. J. Aziz, A. Karma, N. Dimitrov, K. Sieradzki, *Nature* **410**, 450 (2001).
3. P. Levitz, G. Ehret, S. K. Sinha, J. M. Drake, *J. Chem. Phys.* **95**, 6151 (1991).
4. N. Zhou, F. S. Bates, T. P. Lodge, *Nano Lett.* **6**, 2354 (2006).
5. K. Kanamori, K. Nakanishi, T. Hanada, *Adv. Mater.* **18**, 2407 (2006).
6. C. J. Hawker, K. L. Wooley, *Science* **309**, 1200 (2005).
7. D. A. Olson, L. Chen, M. A. Hillmyer, *Chem. Mater.* **20**, 869 (2008).
8. E. A. Jackson, M. A. Hillmyer, *ACS Nano* **4**, 3548 (2010).
9. H. Uehara *et al.*, *Macromolecules* **39**, 3971 (2006).
10. L. Chen, W. A. Phillip, E. L. Cussler, M. A. Hillmyer, *J. Am. Chem. Soc.* **129**, 13786 (2007).
11. L. M. Pitet, M. A. Amendt, M. A. Hillmyer, *J. Am. Chem. Soc.* **132**, 8230 (2010).
12. L. Li *et al.*, *ACS Nano* **5**, 7754 (2011).
13. V. Muralidharan, C.-Y. Hui, *Macromol. Rapid Commun.* **25**, 1487 (2004).
14. R. Motokawa, Y. Iida, Y. Zhao, T. Hashimoto, S. Koizumi, *Polymer J.* **39**, 1312 (2007).
15. K. Yamamoto, E. Ito, S. Fukaya, H. Takagi, *Macromolecules* **42**, 9561 (2009).
16. G. Moad, E. Rizzardo, S. H. Thang, *Acc. Chem. Res.* **41**, 1133 (2008).
17. O. Okay, *Prog. Polym. Sci.* **25**, 711 (2000).
18. T. Arai, M. Nakajima, T. Otsu, U.S. Patent 6,559,234 (2003).
19. A. S. Zalusky, R. Olayo-Valles, J. H. Wolf, M. A. Hillmyer, *J. Am. Chem. Soc.* **124**, 12761 (2002).
20. Materials and methods are available as supplementary materials on *Science* Online.
21. J. Rzayev, M. A. Hillmyer, *J. Am. Chem. Soc.* **127**, 13373 (2005).
22. M. J. Stanford, A. P. Dove, *Macromolecules* **42**, 141 (2009).
23. F. S. Bates, P. Wiltzius, *J. Chem. Phys.* **91**, 3258 (1989).
24. T. Koga, K. Kawasaki, M. Takenaka, T. Hashimoto, *Physica A* **198**, 473 (1993).
25. J. Weber, L. Bergstrom, *Macromolecules* **42**, 8234 (2009).
26. E. P. Barrett, L. G. Joyner, P. P. Halenda, *J. Am. Chem. Soc.* **73**, 373 (1951).
27. S. Brunauer, P. H. Emmett, E. Teller, *J. Am. Chem. Soc.* **60**, 309 (1938).
28. M. L. Koh, D. Konkolewicz, S. Perrier, *Macromolecules* **44**, 2715 (2011).
29. T. Hashimoto, *Macromolecules* **20**, 465 (1987).
30. J. G. Connell, R. W. Richards, A. R. Rennie, *Polymer* **32**, 2033 (1991).
31. H.-Y. Chen, Y. Kwon, K. Thornton, *Scr. Mater.* **61**, 52 (2009).

Acknowledgments: The authors thank Dow Chemical Company for financial support. Partial support for this work was also provided by the National Science Foundation (DMR-1006370). We acknowledge E. L. Cussler, J. Rzayev, and M. Schulze for helpful input, M. Soma for tensile testing, and C. Frethem and F. Zhou for SEM imaging of the cross-linked precursor. Parts of this work were carried out in the College of Science and Engineering Characterization Facility, University of Minnesota, a member of the NSF-funded Materials Research Facilities Network. Synchrotron SAXS data were acquired at the DuPont-Northwestern-Dow Collaborative Access Team (DND-CAT) located at Sector 5 of the Advanced Photon Source (APS). DND-CAT is supported by E. I. DuPont de Nemours & Co., The Dow Chemical Company, and Northwestern University. Use of the APS, an Office of Science User Facility operated for the U.S. Department of Energy (DOE) Office of Science by Argonne National Laboratory, was supported by the U.S. DOE under contract DE-AC02-06CH11357. The authors are declared to be inventors on a patent filed by the University of Minnesota and the Dow Chemical Company related to the work presented here.

Supplementary Materials

www.sciencemag.org/cgi/content/full/336/6087/1422/DC1
Materials and Methods
Figs. S1 to S18
Tables S1 to S4
References (*32*–*37*)

2 March 2012; accepted 18 April 2012
10.1126/science.1221383

Direct Detection of Projectile Relics from the End of the Lunar Basin–Forming Epoch

Katherine H. Joy,[1,2]* Michael E. Zolensky,[2,3] Kazuhide Nagashima,[4] Gary R. Huss,[4] D. Kent Ross,[3,5] David S. McKay,[2,3] David A. Kring[1,2]

The lunar surface, a key proxy for the early Earth, contains relics of asteroids and comets that have pummeled terrestrial planetary surfaces. Surviving fragments of projectiles in the lunar regolith provide a direct measure of the types and thus the sources of exogenous material delivered to the Earth-Moon system. In ancient [>3.4 billion years ago (Ga)] regolith breccias from the Apollo 16 landing site, we located mineral and lithologic relics of magnesian chondrules from chondritic impactors. These ancient impactor fragments are not nearly as diverse as those found in younger (3.4 Ga to today) regolith breccias and soils from the Moon or that presently fall as meteorites to Earth. This suggests that primitive chondritic asteroids, originating from a similar source region, were common Earth-Moon–crossing impactors during the latter stages of the basin-forming epoch.

All lunar basins were formed before 3.7 billion years ago (Ga) (*1*) during an interval of high-impact flux that may have extended over the entire first 700 million years (My) of solar system history (*2*) or may have been concentrated in one or more cataclysmic impact bursts (*3*) that affected the whole inner solar system (*3*–*6*). Competing models of the basin-forming epoch (*7*) imply that the projectiles were dominated by either asteroids (*5*, *8*), comets (*9*), relatively even mixtures of the two populations (*10*, *11*), or the breakup of a single large asteroid or protoplanet (*12*). To test those models, we initiated a search for impactor relics in the lunar regolith that were produced during the basin-forming epoch. A key component of our strategy is to use regolith samples whose ages have been recently calibrated (*13*).

Chemical signatures of material accreting to the Moon have been detected in the past, generally in the form of highly siderophile elements (HSEs). Mature lunar regoliths exposed to space for tens to hundreds of millions of years have ~2 weight % (wt %) added siderophile-rich material with average CI/CM-like chondritic compositions (*14*). HSE analyses of individual lunar basin impact melts imply projectile compositions similar to both chondritic and differentiated bodies that are interpreted to be asteroids rather than comets or Kuiper belt objects (*5*, *15*–*19*). The size-frequency of impact craters on the lunar surface has also been used to implicate main-belt asteroids in the basin-forming epoch (*8*).

A more direct measure, however, would be the detection of mineralogical and lithological fragments of impacting objects. Such remnants have been found on Earth, ranging in kind from iron meteorites surrounding the ~1-km-diameter, 50,000-year-old Meteor Crater (*20*) to a chondritic fragment found at the 65-million-year Cretaceous-Tertiary boundary, which is inferred to be part of the projectile that formed the ~180-km-diameter Chicxulub basin (*21*). Six meteoritic fragments have also been described in relatively young lunar regolith (*22*–*27*), implying the survival of similar debris on the Moon. To determine whether previously undetected impactor remnants exist on the Moon and, in particular, to determine whether they were different during the basin-forming epoch, we examined regolith samples with ages ranging from 3.8 Ga to the present day.

We used (supplementary materials text S1.2) field emission scanning electron microscope techniques to chemically map the samples and electron microprobe analyses to identify mineral and lithic fragments that are texturally and/or chemically distinct from lunar material (such as mafic minerals with high MgO/FeO ratios and nonlunar FeO/MnO ratios; concentrations of meteoritic metal and sulphide; and refractory, ferric, phyllosilicate or amphibole minerals). Our study was not biased toward any particular type of impactor debris (cometary, chondritic, achondritic silicate, or iron), although it may have overlooked any impactor fragments with major element compositions similar to lunar minerals.

Ancient regolith at the Apollo 16 collection landing site (*28*) was produced on top of the Cayley Plains Formation, which was emplaced by the Imbrium basin-forming impact event 3.85 (*1*) to 3.92 Ga (*29*). Those soils were exposed to space for only a few million years (*28*) before being consolidated into rocks between ~3.8 and 3.4 Ga (*13*). Impactor relics (Fig. 1, A and B) were detected in five ancient regolith breccias (10 particles in sample 61135, 13 particles

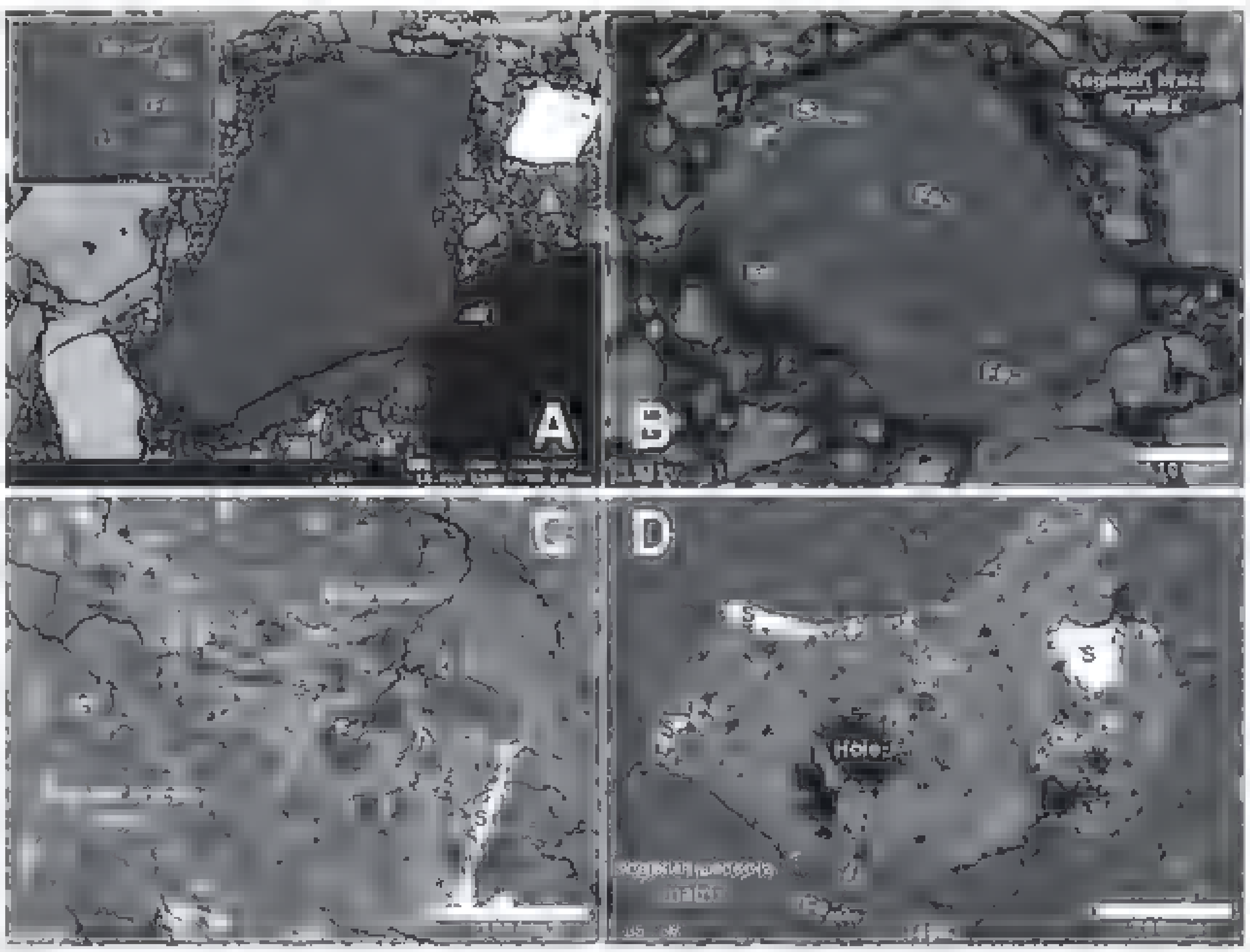

Fig. 1. Backscattered electron images of representative projectile fragments found in ancient and younger lunar regolith breccias (see also figs. S2 to S6). **(A)** Cryptocrystalline UMMF in 60016,83; the inset shows a close-up of mineral intergrowth. **(B)** POP fragment in 60016,93. **(C)** Olivine-phyric melt in 60255,110. **(D)** Chondrule fragment within lunar meteorite PCA 02007 [see also (*27*)]. Abbreviations: Fo, forsteritic olivine; En, enstatitic pyroxene; IS, interstitial area; P, plagioclase; S, sulphide-metal intergrowth.

[1]Center for Lunar Science and Exploration, Lunar and Planetary Institute, Universities Space Research Association, 3600 Bay Area Boulevard, Houston, TX 77058, USA. [2]NASA Lunar Science Institute. [3]ARES, NASA Johnson Space Center, Houston, TX 77058 USA. [4]Hawai'i Institute of Geophysics and Planetology, School of Ocean and Earth Science and Technology, University of Hawai'i at Manoa, Honolulu, HI 96822, USA. [5]Engineering and Science Contract Group, Jacobs Technology, 2224 Bay Area Boulevard, Houston, TX 77058, USA.

*To whom correspondence should be addressed. E-mail joy@lpi.usra.edu

in 60016, 1 particle in 66035, 4 particles in 66075, and 2 particles in 60019; text S1.1 and fig. S1). All 30 analyzed particles are small (20 to 225 μm) ultramagnesian mafic fragments (UMMFs) that make up 0.01% (samples 60016,93; 66075,58; 60019,176; and 61135,36) to 0.25% (sample 66035,14) of the surface area of the fine-fraction (<2 mm) regolith component in each thin section (text S1.1).

The fragments have igneous textures similar to those in chondrules of primitive chondrites: cryptocrystalline, porphyritic olivine (PO), porphyritic olivine-pyroxene (POP), and radial and barred olivine (BO) assemblages (Fig. 1, A and B, and figs. S2 to S6). None exhibit shock-metamorphic features. Microcrystalline varieties include forsteritic olivine grains (Fo_{93-98} and FeO/MnO 40 to 192: Fig. 2A and fig. S7), surrounded by near end-member enstatite pyroxene ($Mg\#_{97-98}$ and $En_{94-96}Fs_{2-3}Wo_{0-5}$; fig. S8) [Mg#, molar MgO/(MgO+FeO)] that are not in chemical equilibrium with the lunar regolith. Some fragments have rims with more ferroan olivine (Fo_{78-90} and FeO/MnO = 87 to 115, Fig. 2A). All fragments have bulk compositions (Fig. 2B) that are highly magnesian (Mg# = 93 to 99 and FeO/MnO 76 to 165), reflective of forsterite ($MgSi_2O_4$), and enstatite ($MgSiO_3$), and a minor felsic component. UMMF olivine and pyroxene are more magnesian than any lunar indigenous mafic minerals (Fo_{80-95}) (*30*) and are distinct from experimentally produced and theoretically calculated minerals from early mantle cumulates of the lunar magma ocean (olivine: $Fo_{<96}$) (*31*), suggesting that they do not represent lunar mantle lithologies (Fig. 2B). UMMF particles are texturally and compositionally distinct (with higher MgO and FeO/MnO ratios) from seven ultra-Mg# Apollo 16 impact glasses (*32*, *33*). UMMF olivine is also more magnesian (fig. S7 and table S2), and more Ni-poor (<0.008 wt % Ni), than terrestrial olivine from mafic and ultramafic rocks (*34*), indicating that the fragments are not terrestrial material. The FeO/MnO values are unlike those in differentiated asteroids (such as the parent bodies of howardite-eucrite-diogenite or aubrite meteorites) (fig. S7B). Low MnO concentrations in UMMF forsterite and pyroxene (<0.08 wt %, typically <0.03 wt %) (tables S2 and S3) indicate that the fragments are compositionally different from chondrule-like crystalline lithics seen in Comet Wild 2 (olivine: Fo_{79-95}, FeO/MnO = 4 to 26, and MnO = 0.2 to 2 wt %) (*35*) and from interplanetary dust particle like material (olivine: Fo_{95-100}, FeO/MnO < 2.5, and MnO typically >0.5 wt %) (*36*), also probably sourced from comet-like objects. However, the olivine and bulk compositions of the UMMFs are as magnesian and MnO-poor [olivine typically <0.5 wt % MnO (*35*, *36*)] as some type 1 chondrules in carbonaceous chondrite (CC) meteorites (fig. S9).

Oxygen isotope compositions of UMMF fragments are within the ranges exhibited by ordinary chondrite and CC chondrite (Fig. 3 and text S2.3). Because of the large uncertainties associated with analyses of such small particles (text S1.2), however, the error bars statistically overlap the terrestrial fractionation line (TFL) at ($\Delta^{17}O$) 0 and compositions of lunar rocks, achondritic meteorites, and enstatite chondrites. The Mg-rich UMMF compositions imply that those isotope compositions were established in a region of the solar nebula with near-solar redox conditions (*37*), similar to carbonaceous and enstatite chondrites, and was more reducing than the region where ordinary chondrite material was processed.

Collectively, textural, chemical (such as Mg# and FeO/MnO), and isotope compositions indicate that UMMF fragments are remnants of primitive chondritic asteroids delivered to the lunar surface in the final stages of the basin-forming epoch (Fig. 4), surviving either as material ejected from projectiles such as those at Meteor Crater and Chicxulub (*20*, *21*) or as smaller debris delivered from the same source region at the same time when asteroids of all sizes were being delivered to the Moon (*8*). The fragments could represent a component common to the Cayley Plains Formation, or alternatively they may represent several distinct impacts of primitive projectiles delivered to the Moon after the Cayley Plains Formation was emplaced at ~3.85 Ga (*1*) but before 3.4 Ga (the time when the youngest ancient regolith breccia studied here was consolidated into a rock) (*13*) (Fig. 4).

The post-basin-forming projectile record is represented by regolith breccias 60275 (~2.3 Ga, with a glassy coat that is <2.3 Ga), 60255 (~1.7 Ga), and PCA 02007 (<3.85 Ga), and by soils 60014 (<3.85 Ga), 12037 (~1.7 Ga), 10084/5 (~0.65 Ga), and 15601 (~present day) (Fig. 4 and text S1.2). The parent regoliths of these samples have higher maturity levels than the ancient regolith breccia collection (*28*), suggesting that they were exposed to space for many millions of years.

The projectile relics in these younger samples are more diverse and include (i) a fragment (in the glassy coat of breccia 60275; fig. S10), which, although it is Fe,Ni-metal-bearing, is the only particle texturally and compositionally similar to UMMFs (Fig. 2); (ii) a magnesian assemblage (in breccia 60255) (fig. S11) and a forsterite (Fo_{96-97} and FeO/MnO 11 to 15), enstatite ($En_{94-96}Fs_{2-3}Wo_{1-3}$), and sulphide-rich assemblage (in breccia 60255) (fig. S12), in which the mafic phases are compositionally similar to those in type 1 chondrules and both of which have much lower FeO/MnO values than UMMFs (Fig. 2); (iii) an olivine-phyric melt (Fig. 1C and fig. S13) (in breccia 60255) with a porphyritic texture and phenocrysts of olivine (Fo_{86-90}; Fig. 2A) that plot along the TFL with isotopically heavier compositions [$\delta^{18}O$ ~14 to 18 per mil (‰)

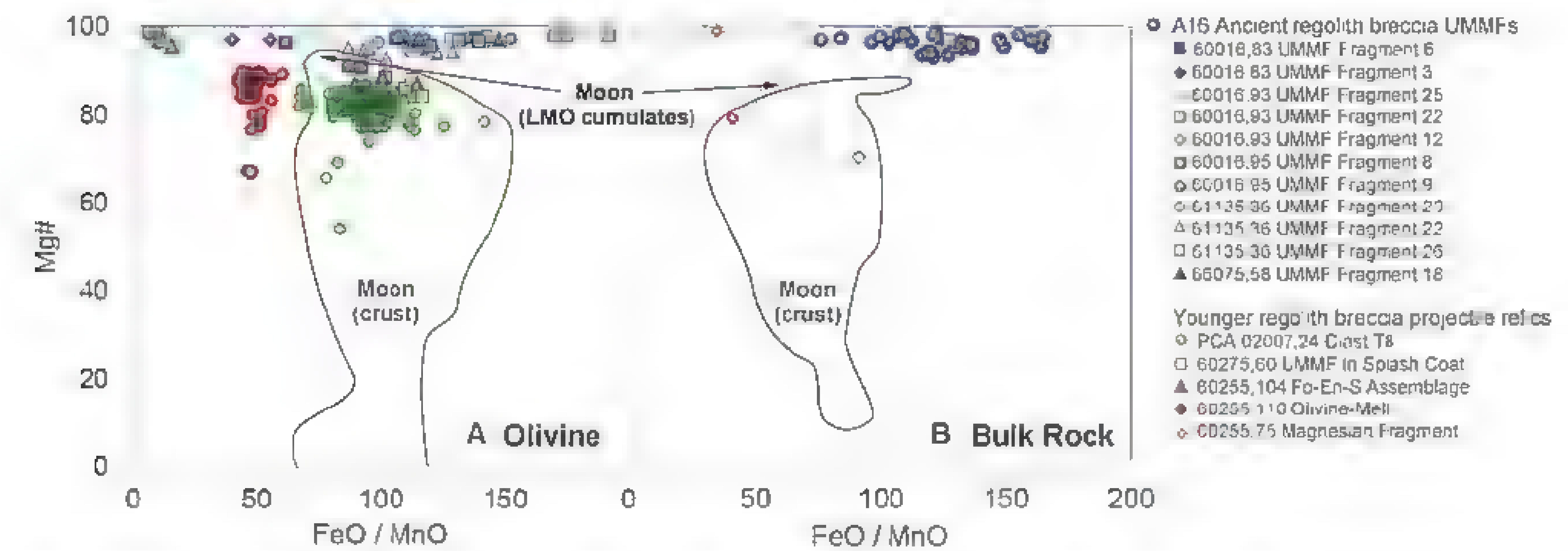

Fig. 2. Composition in Mg# of (**A**) olivine and (**B**) the bulk of projectile fragments investigated in this study. Data are compared with data from lunar minerals and rocks, where the dashed field labeled LMO depicts the results of magma ocean crystallization experiments (*31*). Apollo and lunar meteorite bulk rock compositions and Apollo olivine compositions are taken from literature data (see fig. S9 for details). The PCA 02007 bulk rock composition is taken from (*27*). All other data are from this study (tables S1 and S2).

and $\delta^{17}O$ ~7.9 to 9.8‰; table S6) similar to bulk-rock CI meteorites (Fig. 3); (iv) a carbonaceous chondrite (Bench Crater meteorite in soil 12037) (*26*); (v) an enstatite chondrite (Hadley Rille meteorite in soil 15601) (*25*); (vi) a mesosiderite fragment (in soil 10084) (*22*); (vii) iron meteorite fragments (in soils 10085 and 60014) (*23*, *24*); and (viii) a plagioclase-rich chondrule fragment (Fig. 1D and fig. S14 and S15) in lunar meteorite regolith breccia Pecora Escarpment (PCA 02007) (*27*). Our oxygen isotope analyses (Fig. 3 and table S6) of both relict forsterite and groundmass ferroan olivine in this latter fragment show that it is debris from a CC projectile.

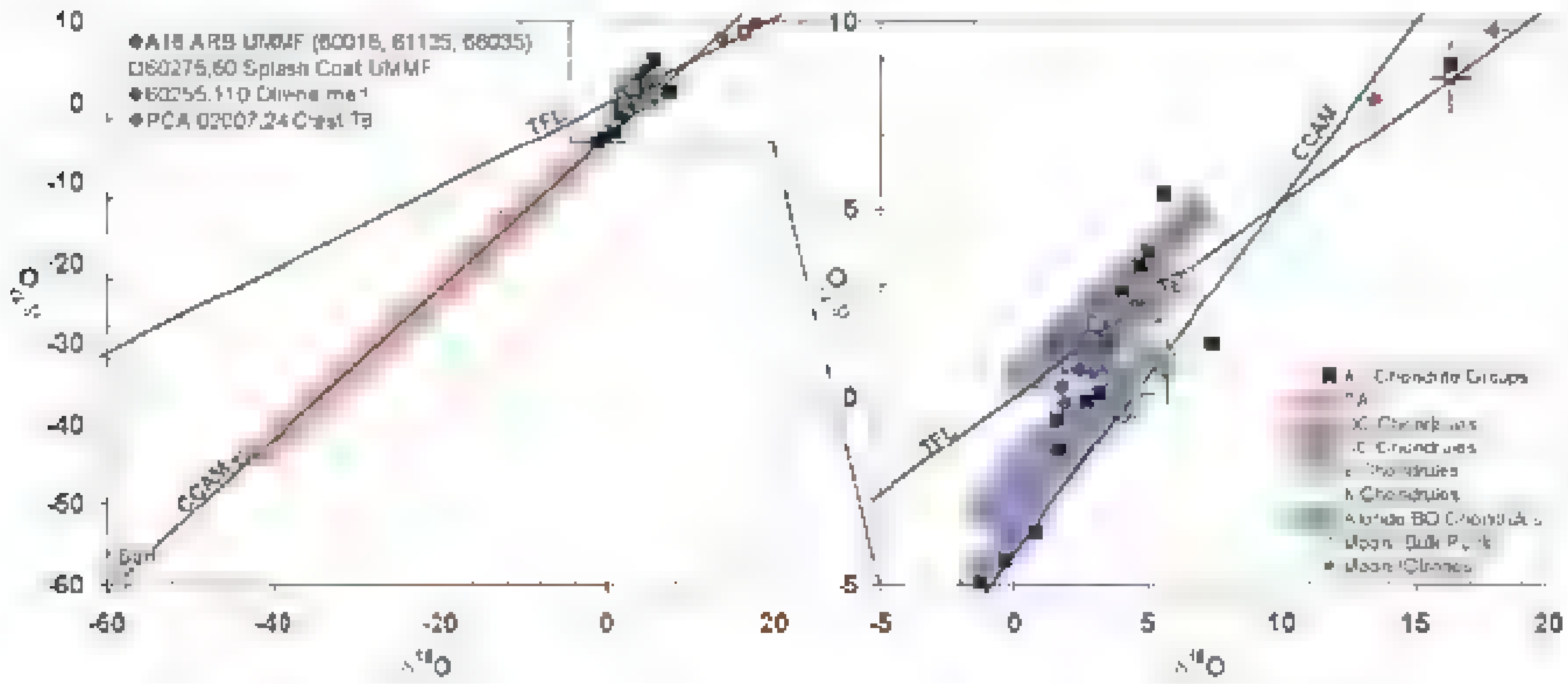

Fig. 3. Mean three–oxygen isotope compositions of projectile fragments found in lunar breccias and soils [see text S1.2 for methods, (*40*), and tables S4 to S6)]. The left panel shows solar and planetary context, and the right panel shows a close-up view of most impactor fragment data. Shown are the TFL, the carbonaceous chondrite anhydrous minerals (CCAM) mixing line, lunar olivine oxygen isotope compositions, and bulk rock oxygen isotope compositions (figs. S19 and S20). The average composition of bulk chondritic meteorites is shown as black symbols (*41*); also shown are the solar oxygen isotope composition (*42*) and the bulk fields for different components of meteorites (figs. S19 and S20). Error bars represent 2σ.

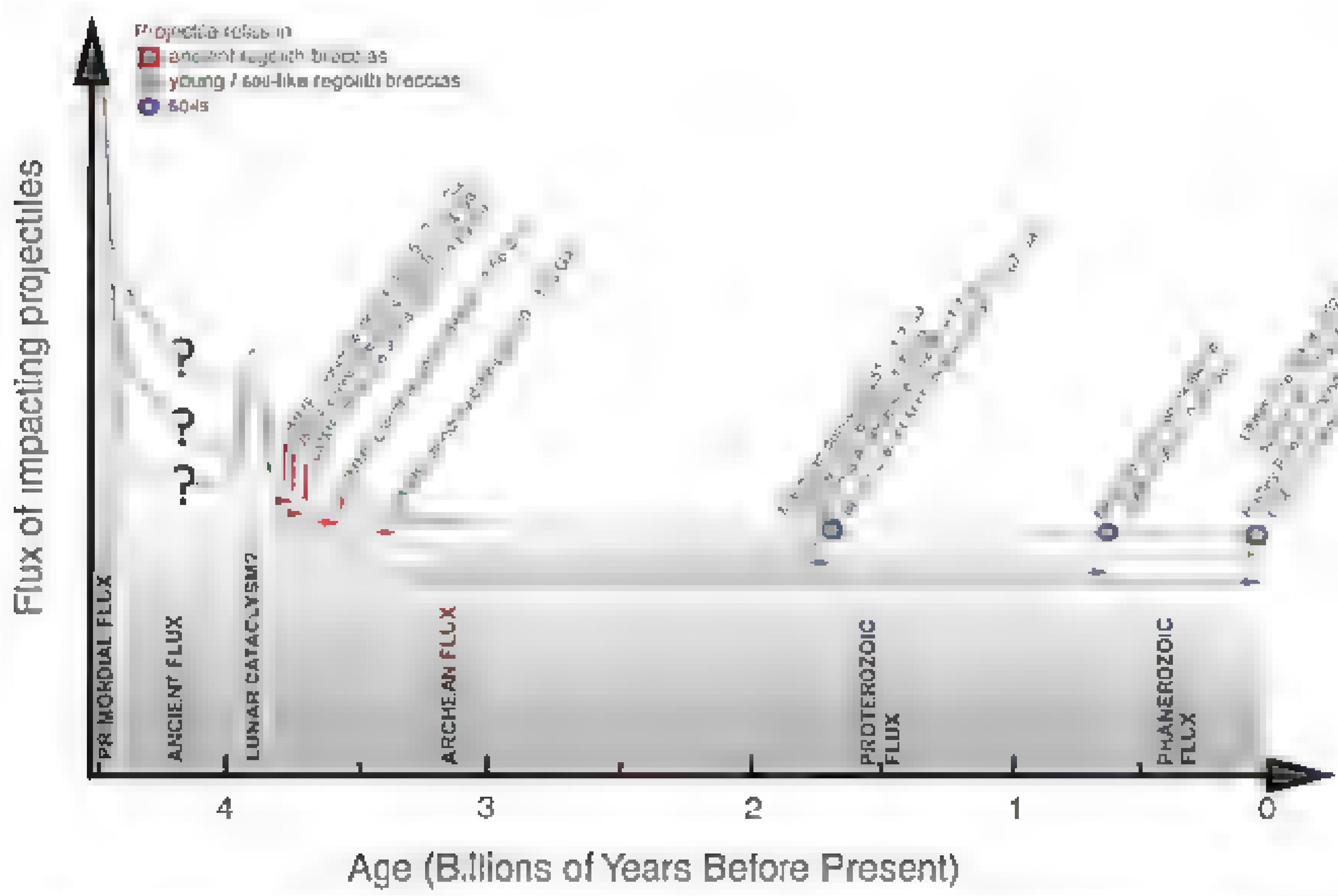

Fig. 4. Schematic diagram illustrating the variation among models of the early impact cratering of the Earth-Moon system. Although it is generally agreed that there was a decrease in the impact rate after 3.8 Ga, it is still unsettled (*1*–*3*, *5*, *7*) whether (i) there was an anomalously high flux ~3.9 Ga; (ii) if there was a high flux ~3.9 Ga, how long it lasted; and (iii) whether the impact rate between ~4.4 and ~4.0 Ga was relatively high or low. Impact flux curves are not numerically quantified, because the flux rate for the pre–4-Ga part of the flux curve is highly speculative and currently poorly constrained (*13*). Arrows indicate the possible range of projectile fragment delivery, where the upper limit is constrained by the age of the geological surface where the sample was collected, and the lower limit is constrained by the modeled closure ages [(*13*) and text S1.2] of regolith breccias and soils that contain projectile debris. Fragments of poorly constrained delivery age (PCA 02007 and 60014) are not depicted.

Thus, there appear to be two distinct populations of impacting objects. In ancient regolith breccias, which were closed to input toward the end of the basin-forming epoch (Fig. 4), the projectiles have similar, highly magnesian compositions. Although the textures, mineralogy, and compositions of the UMMFs point to chondritic precursors, they appear to be from planetesimals that are sparsely or not at all found in the current meteorite collection. This is consistent with HSE analyses of basin impact melts formed by unknown types of chondritic impactors (*16*, *19*). The UMMFs, therefore, provide direct evidence of asteroids that differ from meteoritic material currently being delivered from resonances to the Earth-Moon system. After the basin-forming epoch, there is a larger diversity of projectiles responsible for cratering on the lunar surface (Fig. 4).

The direct detection of primitive chondritic projectile relics in ancient regolith breccias confirms indirect observations (HSE analysis and crater size-frequency distributions) that asteroid-type projectiles (*5*, *8*, *15*–*19*) were delivered to the Moon in the latter stages of the basin-forming epoch (Fig. 4) and therefore favors models involving asteroid collisions rather than comets. Previous studies of the size distribution of lunar craters suggest that the asteroid belt was sampled in a size-independent fashion during the basin-forming epoch (*8*), implying that resonances swept through the asteroid belt when Jupiter's orbit moved (*8*, *11*). If comets were involved in the basin-forming epoch, remnants of them elude us. Hydrocode simulations imply that a larger fraction of comets than of asteroids would be ejected from the Moon with escape velocities. For impact trajectories of 45°, 86% of cometary debris escapes in an expanding high-velocity ejecta plume, whereas only 42% of asteroid debris escapes (*38*). Integrated over reasonable impact velocities, 93.5% of comets and 83.5% of asteroid debris entrained in the plume may have been lost (*39*). Thus, there is a small retention factor (~2 to 4) that favors asteroids. If taken at face value, these results imply that at least 1 particle out of a population of 30 (the number analyzed thus far in ancient regolith breccias) would be from a comet, if comets were responsible for ≥5 to 17% of the impactors. Thus, the impactor relics described here indicate that asteroids were the dominant objects hitting the Earth-Moon system at the end of the basin-forming epoch and that the flux of comets was small.

References and Notes

1. D. E. Wilhelms, J. F. McCauley, N. J. Trask, *The Geologic History of the Moon* (U.S. Geological Survey Professional Paper 1348, U.S. Department of the Interior, Washington, DC, 1987).
2. W. K. Hartmann, *Meteorit. Planet. Sci.* **38**, 579 (2003).
3. G. Ryder, *EOS* **71**, 313 (1990).
4. D. Bogard, *Meteorit. Planet. Sci.* **30**, 244 (1995).
5. D. A. Kring, B. A. Cohen, *J. Geophys. Res.* **107**, 4-1 (2002).
6. T. D. Swindle, C. E. Isachsen, J. R. Weirich, D. A. Kring, *Meteorit. Planet. Sci.* **44**, 747 (2009).

7. W. K. Hartmann, G. Ryder, L. Dones, D. Grinspoon, in *Origin of the Earth and Moon*, R. Canup, K. Righter, Eds. (Univ. of Arizona Press, Tucson, AZ, 2000), pp. 805–826.
8. R. G. Strom, R. Malhotra, T. Ito, F. Yoshida, D. A. Kring, *Science* **309**, 1847 (2005).
9. U. G. Jørgensen *et al.*, *Icarus* **204**, 368 (2009).
10. H. F. Levison, L. Dones, C. R. Chapman, S. A. Stern, *Icarus* **151**, 286 (2001).
11. R. S. Gomes, H. F. Levison, K. Tsiganis, A. Morbidelli, *Nature* **435**, 466 (2005).
12. V. Zappala, A. Cellino, B. J. Gladman, S. Manley, F. Migliorini, *Icarus* **134**, 176 (1998).
13. K. H. Joy, D. A. Kring, D. D. Bogard, D. S. McKay, M. E. Zolensky, *Geochim. Cosmochim. Acta* **75**, 7208 (2011).
14. J. J. Papike, L. A. Taylor, S. B. Simon, in *Lunar Sourcebook—A Users Guide to the Moon*, G. Heiken, D. Vaniman, B. French, Eds. (Cambridge Univ. Press, Cambridge, 1991), pp. 121–181.
15. J. W. Morgan, R. Ganapathy, H. Higuchi, U. Krahenbuhl, E. Anders, *Proc. Lunar Sci. Conf.* **5**, 1703 (1974).
16. I. S. Puchtel, R. J. Walker, O. B. James, D. A. Kring, *Geochim. Cosmochim. Acta* **72**, 3022 (2008).
17. P. H. Warren, J. T. Wasson, *Lunar Planet. Sci. Conf.* **9**, 185 (1978).
18. M. D. Norman, V. C. Bennett, G. Ryder, *Earth Planet. Sci. Lett.* **202**, 217 (2002).
19. J. G. Liu, M. G. Galenas, I. S. Puchtel, R. J. Walker, *Lunar Planet. Sci.* **XLIII**, abstr. 2366 (2012).
20. D. M. Barringer, *Proc. Acad. Nat. Sci. Phila.* **57**, 861 (1905).
21. F. T. Kyte, *Nature* **396**, 237 (1998).
22. J. A. Wood, U. B. Marvin, B. N. Powell, J. S. Dickey Jr., *Smithsonian Astrophysical Observatory Special Report 307* (Smithsonian Astrophysical Observatory, Cambridge, MA, 1970).
23. W. Quaide, T. Bunch, *Proc. Lunar Sci. Conf.* **1**, 711 (1970).
24. B. L. Jolliff, R. L. Korotev, L. A. Haskin, *Lunar Planet. Sci. Conf.* **24**, 729 (1993).
25. A. E. Rubin, *Meteorit. Planet. Sci.* **32**, 135 (1997).
26. M. E. Zolensky, *Meteorit. Planet. Sci.* **32**, 15 (1997).
27. J. M. D. Day, C. Floss, L. A. Taylor, M. Anand, A. D. Patchen, *Geochim. Cosmochim. Acta* **70**, 5957 (2006).
28. D. S. McKay *et al.*, *Proc. Lunar Planet. Sci. Conf.* **16**, D277 (1986).
29. D. Liu *et al.*, *Earth Planet. Sci. Lett.* **319-320**, 277 (2012).
30. C. K. Shearer, J. J. Papike, *Geochim. Cosmochim. Acta* **69**, 3445 (2005).
31. S. M. Elardo, D. S. Draper, C. K. Shearer Jr., *Geochim. Cosmochim. Acta* **75**, 3024 (2011).
32. S. J. Wentworth, D. S. McKay, *Proc. Lunar Planet Sci. Conf.* **18**, 67 (1988).
33. C. K. Shearer, J. J. Papike, K. C. Galbreath, S. J. Wentworth, N. Shimizu, *Geochim. Cosmochim. Acta* **54**, 1851 (1990).
34. PetDB database, www.petdb.org/
35. T. Nakamura *et al.*, *Science* **321**, 1664 (2008).
36. W. Klock, K. Thomas, D. McKay, H. Palme, *Nature* **339**, 126 (1989).
37. D. A. Kring, thesis, Harvard University, Cambridge, MA (1988).
38. N. A. Artemieva, V. V. Shuvalov, *Sol. Syst. Res.* **42**, 329 (2008).
39. L. Ong, E. I. Asphaug, D. Korycansky, R. F. Coker, *Icarus* **207**, 578 (2010).
40. K. Makide *et al.*, *Geochim. Cosmochim. Acta* **73**, 5018 (2009).
41. D. W. Mittlefehldt, R. N. Clayton, M. J. Drake, K. Righter, *Rev. Mineral. Geochem.* **68**, 399 (2008).
42. K. D. McKeegan *et al.*, *Science* **332**, 1528 (2011).

Acknowledgments: The data reported in this paper are tabulated in the supplementary materials. This research was funded by NASA Lunar Science Institute contract NNA09DB33A (D.A.K.), NASA Cosmochemistry grant NNX11AG78G (G.R.H.), and NASA Cosmochemistry grant NNX08AH77G (K.N.). This is Lunar and Planetary Institute contribution number 1665. We thank the three reviewers for helpful comments and D. Mittlefehldt, J. Berlin, R. Jones and H. McSween for sharing meteorite data sets.

Supplementary Materials
www.sciencemag.org/cgi/content/full/science.1219633/DC1
Materials and Methods
Supplementary Text
Figs. S1 to S21
Tables S1 to S6
References (*43–132*)

25 January 2012; accepted 2 May 2012
Published online 17 May 2012;
10.1126/science.1219633

Sparse Pre-Columbian Human Habitation in Western Amazonia

C. H. McMichael,[1]* D. R. Piperno,[2] M. B. Bush,[1] M. R. Silman,[3] A. R. Zimmerman,[4] M. F. Raczka,[1] L. C. Lobato[5]

Locally extensive pre-Columbian human occupation and modification occurred in the forests of the central and eastern Amazon Basin, but whether comparable impacts extend westward and into the vast terra firme (interfluvial) zones, remains unclear. We analyzed soils from 55 sites across central and western Amazonia to assess the history of human occupation. Sparse occurrences of charcoal and the lack of phytoliths from agricultural and disturbance species in the soils during pre-Columbian times indicated that human impacts on interfluvial forests were small, infrequent, and highly localized. No human artifacts or modified soils were found at any site surveyed. Riverine bluff areas also appeared less heavily occupied and disturbed than similar settings elsewhere. Our data indicate that human impacts on Amazonian forests were heterogeneous across this vast landscape.

The Amazon Basin, an area approximately the size of the continental United States, is an important reservoir of biodiversity. A major recent question is the degree to which humans settled and modified Amazonian landscapes before European contact. It was initially thought that prehistoric Amazonia supported mainly small and highly mobile human populations, who exerted little impact on their environments (*1*, *2*), but recent work has documented dense and complex human settlements in eastern Amazonia and on the river bluffs of the central Amazon. The evidence includes the presence of highly modified soils such as terra pretas (anthropogenic "black earth") (*3*) and large-scale landscape alterations (Fig. 1) (*4*, *5–10*). The evidence is impressive, but comes largely from riverine environments with abundant natural resources, especially river bluffs, or the driest parts of the eastern Amazon (Fig. 1).

[1]Department of Biological Sciences, Florida Institute of Technology, Melbourne, FL 32901, USA. [2]Program in Human Ecology and Archaeobiology, Department of Anthropology, Smithsonian National Museum of Natural History, Washington, DC 20560, USA, and Smithsonian Tropical Research Institute, Balboa, Panama. [3]Department of Biology, Wake Forest University, Winston-Salem, NC 27106, USA, and Center for Energy, Environment and Sustainability, Winston-Salem, NC 27106, USA. [4]Department of Geological Sciences, University of Florida, Williamson Hall, Gainesville, FL 32611, USA. [5]Núcleo de Ciência e Tecnologia, Laboratório de Geografia Humana e Planejamento Ambiental, Universidade Federal de Rondônia, Porto Velho, Rondônia, Brazil.

*To whom correspondence should be addressed. E-mail: cmcmicha@my.fit.edu

The extent of this impact on terra firme settings has been uncertain. The terra firme forests of the interfluvial zone occupy 95% of Amazonia and have less-fertile soils and poorer-quality resources (*11*). Available data from several regions suggest that the prehistoric impacts on interfluvial landscapes were heterogeneous and highly localized (*12*, *13*). Here we reconstruct histories of fire, vegetation, and soil modification from charcoal, phytolith, and geochemical data recovered from 247 soil cores collected from 55 locations, including sites with known impacts, across 3,000,000 km^2 in western Amazonia (Fig. 1 and table S1) (*14*). We sampled soils from sites where the probability of past disturbances was high, such as river bluffs with known archaeological histories and nearby terra pretas, including Tefe, Barcelos, and Iquitos; from a previously unstudied river bluff at Los Amigos; and from terra firme sites, including Acre, Iquitos, Tefe, and a transect from Porto Velho to Manaus (PVM).

Natural fires in Amazonia are rare today (*15–17*), but fire was a mainstay of prehistoric land use in the tropics (*11*, *18*, *19*). Consequently, charcoal recovered from soils can provide evidence of past human disturbances, and phytoliths, which document mature and disturbed vegetation, reflect the intensity of those occupations. In our samples, charcoal was most common in soils from riverine bluffs, especially in the central basin (Fig. 2, C to F). At Barcelos and Tefe, charcoal was present in many intervals in most cores, especially from 0 to 40 cm (Fig. 2, D and F). Charcoal dates ranged from ca. 500 to 2700 calendar years before the present (cal yr B.P.) at Tefe and from ca. 1200 to 1300 cal yr B.P. at Barcelos (table S2). The vegetation at Tefe appears to have been more heavily affected than that at Barcelos, which is in agreement with the

longer span of documented occupation. In riverine settings, Tefe soil phytoliths contained elevated amounts of early successional herbaceous taxa (ESH, such as grasses, *Heliconia*, and sedges) and some grass phytoliths that were burned. These patterns probably reflect forest clearing and other human disturbances (see phytolith analyses in the supplementary materials and fig. S1). However, neither site yielded crop phytoliths. Arboreal-dominated phytolith assemblages and relatively sparse charcoal from riverine Iquitos sites indicate that the forest remained relatively undisturbed there, and nutrients and black carbon concentrations in soils from these sites were low. At Los Amigos, the charcoal dates ranged from 1000 to 4000 cal yr B.P. (table S2), but the soils were not enriched in nutrients and arboreal taxa dominated phytolith assemblages, which is consistent with a light and shifting human impact (table S4, Fig. 2E, and fig. S1).

We recovered little charcoal from soils at Acre or interfluvial Iquitos sites, indicating a lack of recurrent or extensive fires over the past several thousand years (Fig. 2, A and C, and table S2). Similar results were obtained from the phytolith records, which were dominated by forest taxa; ESH phytoliths were absent or rare (0 to 1%). No evidence for crops or burned phytoliths was found (fig. S1). Charcoal was more common in soils of the PVM transect than in the western interfluvial Iquitos or Acre sites (Fig. 2, A to C). However, phytolith records showed no signs of a significant human presence at most sites. ESH phytoliths were absent or scarce (0 to 6%), and burned tree phytoliths were nearly absent (Fig. 2B and fig. S1); forest taxa dominated in all samples. Site 121 contained evidence of maize cultivation and elevated frequencies of grass and *Heliconia* phytoliths, many of which were burned. No other crops, including squash (*Cucurbita* spp.), manioc (*Manihot esculenta*), arrowroot (*Maranta arundinacea*), and leren (*Calathea allouia*), were found. Because manioc produces fewer phytoliths than many other crops, we cannot state with the same confidence that it was not grown nearby.

We found no prehistoric ceramics, stone tools, or terra pretas in any of the 247 soil cores, and none of 184 samples analyzed for phytoliths contained evidence of intensive or persistent forest clearing. In many soil levels, no ESH phytoliths were observed in scans of >500 to 1000 additional phytoliths, underscoring the lack of disturbance that took place in these interfluvial forests. Together, the data suggest that human population densities in the sampled regions were low and highly localized, and were not consistent with major population centers with associated areas of widespread, extensive agriculture (*20*). Our data support the idea that humans had much less impact on interfluvial forests than on riverine environments (*21*) or in the drier eastern forests (*22*). However, even regions with known human sites and terra pretas (such as Barcelos and Tefe) were not subjected to continuous or large-scale forest clearing or intensive agriculture (Fig. 2), and show a lesser disturbance signature than found in modern slash-and-burn systems (see phytolith analyses in the supplementary materials). Forest clearings were probably small and short-lived, and the interior forests were apparently not permanently or intensively occupied by humans in prehistory. We found little indication that repeated fire, vegetational disturbance, and/or agriculture extended more than 5 km into the terra firme forests of the Tefe, PVM, Acre, and Iquitos regions (Fig. 2).

Our data imply that the disturbance signature was stronger in both riverine and interfluvial forests of the central basin than in the western basin (Fig. 2). Even in the PVM transect, however, evidence for disturbances was patchy and localized, despite being located 20 to 50 km from the Madeira River and within 100 to 200 km of dense concentrations of terra pretas (*23*) (Fig. 1). The frequency and distribution of terra pretas documented along the Madeira River (*24*) may have continued southward, parallel to our interfluvial transect. The resulting contrasting pattern of highly concentrated terra preta soils along the river, with localized and patchy disturbance 20 to 50 km into the uplands, illustrates how even in the central Amazon, intensive landscape modifications appear to be confined to near-riverine locations.

We interpret the charcoal presence along with low frequencies of burned tree phytoliths, and the dominance of forest over grass phytoliths, to mean that fires were mainly confined to the forest floor. The apparently infrequent and low-intensity fires do not appear to have penetrated canopies and altered forest structure substantially at most sites. Therefore, soil charcoal alone should not be taken to mean that fires were of sufficient intensity and duration to cause canopy disruption and major forest alteration [see also (*12*)].

It is likely that in some forests, edible or other useful fruit trees were planted or managed, resulting in an enrichment of those species (*25*). Palms such as peach palm (*Bactris gasipaes*) and *Astrocaryum* are economic mainstays in the Amazon and are prolific phytolith producers. We found no evidence for these species in most samples from every site studied (fig. S1 and palm distributions in the supplementary materials). There was no association between palm phytolith frequencies and other evidence of vegetation disturbance, and palm frequencies were never so high that they implied that a local grove was present. These data suggest that humans were not cultivating or selectively managing palms at most of our study sites. There was also no indication that many noneconomic species were selectively removed (*26*), because little change in forest composition was seen from the bottom to the top of the soil cores, including when early successional herbaceous taxa and/or charcoal were present.

Our data imply that the terra firme forests we studied in the western Amazon Basin were

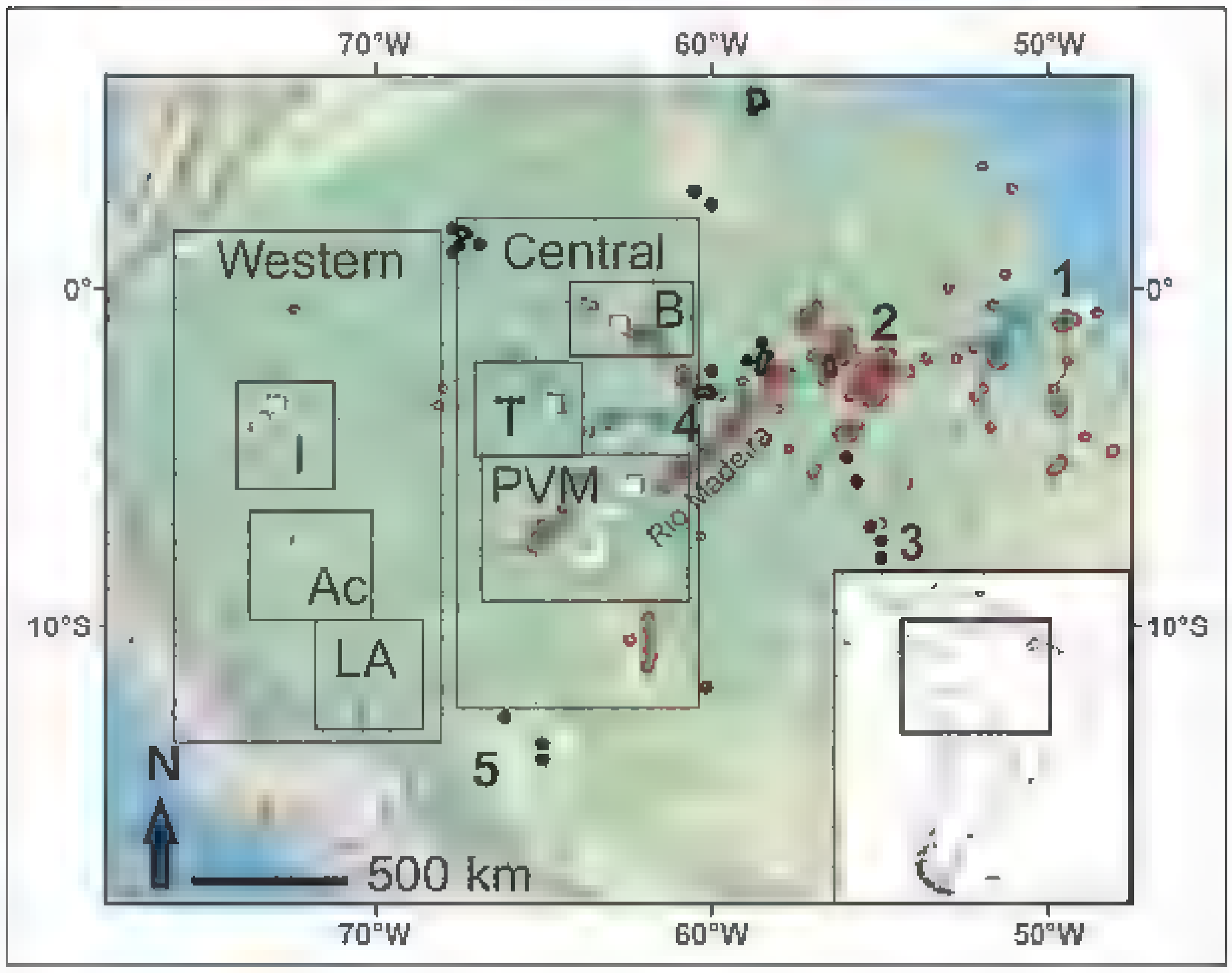

Fig. 1. Sampled locations within western Amazonia (white squares) in relation to major pre-Columbian archaeological sites (1, Marajó Island; 2, Santarém; 3, Upper Xingu; 4, Central Amazon Project; 5, Bolivian Beni), known terra preta locations (brown circles) (*3*, *32*, *33*), and soil charcoal survey locations (black circles) (*12*, *22*). Charcoal and phytolith data are presented from regions outlined in black (B, Barcelos; T, Tefe; PVM, Porto Velho-Manaus transect; I, Iquitos; Ac, Acre; LA, Los Amigos). The locations of Rio Madeira and associated terra pretas are shown. Here we define Amazonia as the region drained by the Amazon River and its tributaries.

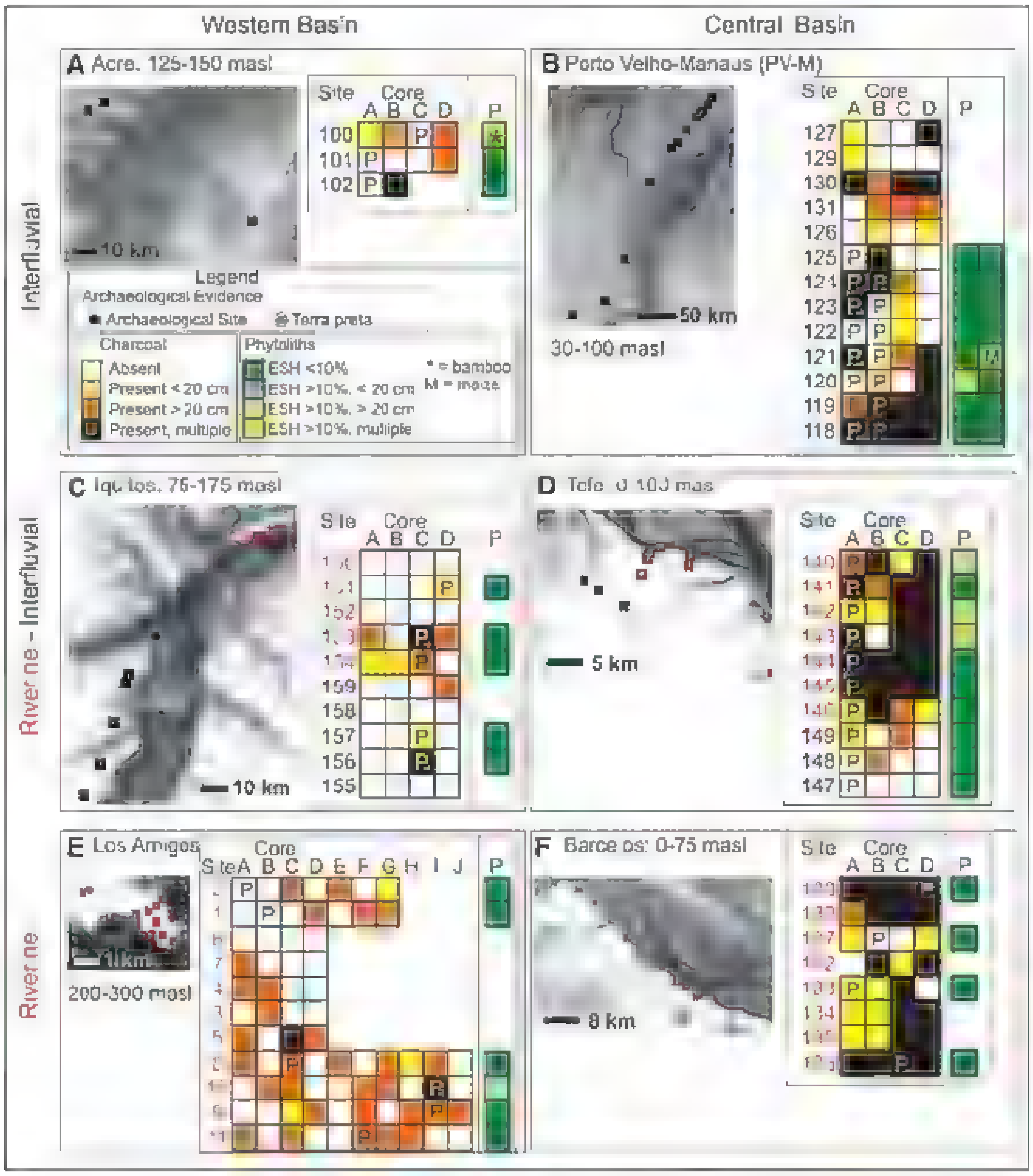

Fig. 2. Regional maps, soil charcoal distributions, and phytolith percentages for soil cores from riverine (red squares and text) and interfluvial (black squares and text) sites in each region: Acre (**A**), PVM (**B**), Iquitos (**C**), Tefe (**D**), Los Amigos (**E**), and Barcelos (**F**). Areas of lower (darker) and higher (lighter) elevations illustrate drainage and rivers (from 90-m–resolution data from the Shuttle Radar Topography Mission) on each regional map. Colored boxes indicate charcoal results for each core within each site (see legend). Sites are listed in a north-to-south orientation. Soil cores with accompanying phytolith data are denoted with P. Phytolith percentages (column P) are listed to the right of the charcoal results. Geographic coordinates of all sites are provided in table S3.

predominantly occupied by relatively small and shifting human populations during the pre-Columbian era. This has many implications for hypotheses about human effects on Amazonian forests. First, humans may have augmented the alpha-diversity of some Amazonian landscapes, but the hyperdiverse floras and faunas are more a product of long-term evolutionary and ecological processes (*27*) than anthropic landscape alteration (*4*, *26*, *28*–*30*). Second, to the extent that prehistoric deforestation occurred, it was apparently primarily in the eastern Amazon, and this may have limited the proposed impact of post-Columbian population collapse and reforestation on atmospheric CO_2 and CH_4 levels (*18*, *31*). Third, we cannot assume that Amazonian forests were resilient in the face of heavy pre-Columbian disturbance, because vast areas were probably never heavily disturbed. Prehistoric peoples settled most densely in habitats where resources were abundant and easily captured, fertile soils were available, and transportation routes were nearby, making ecological factors important in pre-Columbian settlement patterns.

References and Notes

1. B. J. Meggers, *Amazonia: Man and Culture in a Counterfeit Paradise; Worlds of Man: Studies in Cultural Ecology* (Aldine-Atherton, Chicago, 1971).
2. B. J. Meggers, *Rev. Archaeol.* **25**, 31 (2004).
3. J. Lehmann, D. C. Kern, B. Glaser, W. I. Woods *Amazonian Dark Earths: Origin, Properties, Management* (Kluwer Academic, Dordrecht, Netherlands, 2003).
4. C. L. Erickson, in *Time and Complexity in Historical Ecology*, W. Balee, C. L. Erickson, Eds. (Columbia Univ. Press, New York, 2006), pp. 235–278.
5. M. J. Heckenberger, J. C. Russell, J. R. Toney, M. J. Schmidt, *Philos. Trans. R. Soc. London Ser. B* **362**, 197 (2007).
6. B. J. Meggers, C. Evans, *Archeological Investigations at the Mouth of the Amazon* (Bureau of American Ethnology, Washington, DC, 1957).
7. E. Neves, J. Petersen, in *Time and Complexity in Historical Ecology: Studies in the Neotropical Lowlands*, W. Balee, C. L. Erickson, Eds. (Columbia Univ. Press, New York, 2006), pp. 279–310.
8. A. C. Roosevelt, *Moundbuilders of the Amazon. Geophysical Archaeology on Marajo Island, Brazil* (Academic Press, San Diego, CA, 1991).
9. A. C. Roosevelt, R. A. Housley, M. I. DA Silveira, S. Maranca, R. Johnson, *Science* **254**, 1621 (1991).
10. M. J. Heckenberger *et al.*, *Science* **301**, 1710 (2003).
11. D. R. Piperno, D. M. Pearsall, *The Origins of Agriculture in the Lowland Neotropics* (Academic Press, San Diego, CA, 1998).
12. C. McMichael *et al.*, *Holocene* **22**, 131 (2012).
13. D. R. Piperno, P. Becker, *Quat. Res.* **45**, 202 (1996).
14. Site descriptions and materials and methods are available as supplementary materials on *Science* Online.
15. L. Aragão *et al.*, *Geophys. Res. Lett.* **34**, L07701 (2007).
16. Y. Malhi *et al.*, *Proc. Natl. Acad. Sci. U.S.A.* **106**, 20610 (2009).
17. D. Nepstad *et al.*, *Glob. Change Biol.* **10**, 704 (2004).
18. R. A. Dull *et al.*, *Ann. Assoc. Am. Geogr.* **100**, 755 (2010).
19. D. R. Piperno, in *Tropical Rainforest Response to Climatic Change*, M. B. Bush, J. R. Flenley, Eds. (Springer, Chichester, UK, 2007), pp. 185–212.
20. R. Nevle, D. Bird, W. Ruddiman, R. Dull, *Holocene* **21** 853 (2011).
21. W. M. Denevan, *Ann. Assoc. Am. Geogr.* **86**, 654 (1996).
22. M. B. Bush, M. R. Silman, C. McMichael, S. Saatchi, *Philos. Trans. R. Soc. London Ser. B* **363**, 1795 (2008).
23. M. Heckenberger, E. G. Neves, *Annu. Rev. Anthropol.* **38**, 251 (2009).
24. J. Fraser, A. Junqueira, N. Kawa, C. Moraes, C. Clement, *Hum. Ecol.* **39**, 395 (2011).
25. C. R. Clement, in *Time and Complexity in Historical Ecology: Studies in the Neotropical Lowlands*, W. Balee, C. L. Erickson, Eds. (Columbia Univ. Press, New York, 2006), pp. 165–186.
26. C. L. Erickson, in *The Handbook of South American Archaeology*, H. Silverman, W. H. Isbell, Eds. (Springer, New York, 2008), pp. 157–183.
27. E. G. Leigh Jr., *et al.*, *Biotropica* **36**, 447 (2004).
28. W. Balee, C. L. Erickson, *Time, Complexity, and Historical Ecology* (Columbia Univ. Press, New York, 2006).
29. C. L. Erickson, *Diversity* **2**, 618 (2010).
30. C. C. Mann, *1491: New Revelations of the Americas Before Columbus* (Knopf, New York, 2005).
31. R. J. Nevle, D. K. Bird, W. F. Ruddiman, R. A. Dull, *Holocene* **21**, 853 (2011).
32. B. Glaser, W. I. Woods, *Amazonian Dark Earths: Explorations in Space and Time* (Springer-Verlag, Berlin, 2004).
33. S. P. Aldrich, A. M. G. A. WinklerPrins, *J. Latin Am. Geogr.* **9**, 33 (2010).

Acknowledgments: Field work and ^{14}C dating of charcoal fragments were funded by the NSF Ecology Program (awards DEB 0742301 and DEB 0743666). Other funding was provided by the Florida Institute of Technology; the Smithsonian National Museum of Natural History, including a Restricted Endowment and Small Grant Award; and the Smithsonian Tropical Research Institute. All data will be deposited in the Neotoma Database (www.neotomadb.org/). We thank B. McMichael, A. Correa-Metrio, J. Hernandez, T. Harrison, and B. Rado for field assistance.

Supplementary Materials

www.sciencemag.org/cgi/content/full/336/6087/1429/DC1
Materials and Methods
Supplementary Text
Fig. S1
Tables S1 to S4
References (*34*–*65*)

2 February 2012; accepted 16 April 2012
10.1126/science.1219982

A Three-Stage Symbiosis Forms the Foundation of Seagrass Ecosystems

Tjisse van der Heide,[1*] Laura L. Govers,[2] Jimmy de Fouw,[3] Han Olff,[1] Matthijs van der Geest,[3] Marieke M. van Katwijk,[2] Theunis Piersma,[3,4] Johan van de Koppel,[5] Brian R. Silliman,[6] Alfons J. P. Smolders,[7] Jan A. van Gils[3]

Seagrasses evolved from terrestrial plants into marine foundation species around 100 million years ago. Their ecological success, however, remains a mystery because natural organic matter accumulation within the beds should result in toxic sediment sulfide levels. Using a meta-analysis, a field study, and a laboratory experiment, we reveal how an ancient three-stage symbiosis between seagrass, lucinid bivalves, and their sulfide-oxidizing gill bacteria reduces sulfide stress for seagrasses. We found that the bivalve–sulfide-oxidizer symbiosis reduced sulfide levels and enhanced seagrass production as measured in biomass. In turn, the bivalves and their endosymbionts profit from organic matter accumulation and radial oxygen release from the seagrass roots. These findings elucidate the long-term success of seagrasses in warm waters and offer new prospects for seagrass ecosystem conservation.

Seagrass meadows are important ecological and thus economic components of coastal zones worldwide (*1*, *2*). In many areas, coral reefs and seagrass meadows are tightly linked habitats that form the basis for marine biodiversity (*3*). Seagrasses serve as a keystone habitat for migrating coral reef species as well as thousands of other animals, including waterbirds, fish, dugongs, manatees, and turtles; are important carbon and nutrient sinks; and are important to fisheries and coastline protection (*1*–*3*). Dense seagrass meadows attenuate currents and waves and trap pelagic and benthic organic matter in the sediment (*2*, *4*, *5*). Owing to a lack of oxygen in many coastal marine sediments, an important fraction of organic matter is decomposed by bacteria that use the abundant sulfate in seawater as an electron acceptor instead of oxygen and produce toxic sulfide as a metabolic end product (*6*). Although seagrasses transport oxygen into their roots and the surrounding rhizosphere (radial oxygen release) (*2*, *7*), sulfide production outpaces oxygen release under warmer conditions, resulting in sulfide accumulation and seagrass mortality (*2*, *7*, *8*). Seagrass beds tend to accumulate organic matter, and so it is expected that seagrass beds would build up toxic sulfides and hence have a limited productivity and diversity (*2*). But this is not the observed case, and the underlying reason for the long-term persistence of seagrass ecosystems is an enigma (fig. S1A).

We tested the hypothesis that a three-stage symbiosis between seagrasses, associated burrowing lucinid bivalves, and their symbiotic gill bacteria contribute to reducing the cyclic build-up of sulfide (fig. S1, B to D). Paleo records suggest that the Lucinidae and their endosymbiotic relation date back to the Silurian (*9*–*11*), but that they increasingly diversified since the evolutionary emergence of seagrasses in the late Cretaceous (*2*, *12*, *13*). Seagrass communities later became widespread in the Eocene, and lucinid remains frequently occur in association with their deposits since (*13*, *14*). Lucinids and their gill-inhabiting bacteria have a symbiosis in which the bivalves transport sulfide and oxygen to their gills (fig. S1D), where the bacteria oxidize sulfide for synthesizing sugars that fuel growth of both organisms (*15*–*19*). We hypothesized that seagrass meadows may provide an optimal habitat for these bivalves and their symbionts by indirectly stimulating sulfide production through high organic matter input and by providing oxygen through radial oxygen release from the roots. In turn, lucinids remove sulfide, which could relieve any stress caused to seagrass growth by sulfide accumulation as organic matter is degraded (fig. S1, A and B).

Indirect support for our hypothesis was provided by a worldwide meta-analysis of 84 studies describing the fauna of seagrass beds in 83 sites covering the entire climatic distribution of seagrasses, combined with a 110-point field survey

[1]Community and Conservation Ecology Group, Centre for Ecological and Evolutionary Studies (CEES), University of Groningen, Post Office Box 11103, 9700 CC Groningen, Netherlands. [2]Department of Environmental Science, Institute for Water and Wetland Research, Radboud University Nijmegen, Faculty of Science, Heyendaalseweg 135, 6525 AJ Nijmegen, Netherlands. [3]Department of Marine Ecology, NIOZ Royal Netherlands Institute for Sea Research, Post Office Box 59, 1790 AB Den Burg, Texel, Netherlands. [4]Animal Ecology Group, CEES, University of Groningen, Post Office Box 11103, 9700 CC Groningen, Netherlands. [5]Centre for Estuarine and Marine Ecology, NIOZ Royal Netherlands Institute for Sea Research, Post Office Box 140, 4400 AC Yerseke, Netherlands. [6]Department of Biology, University of Florida, Gainesville, FL 32611, USA. [7]Department of Aquatic Ecology and Environmental Biology, Institute for Water and Wetland Research, Radboud University Nijmegen, Faculty of Science, Heyendaalseweg 135, 6525 AJ Nijmegen, Netherlands.

*To whom correspondence should be addressed. E-mail: t.van.der.heide@rug.nl

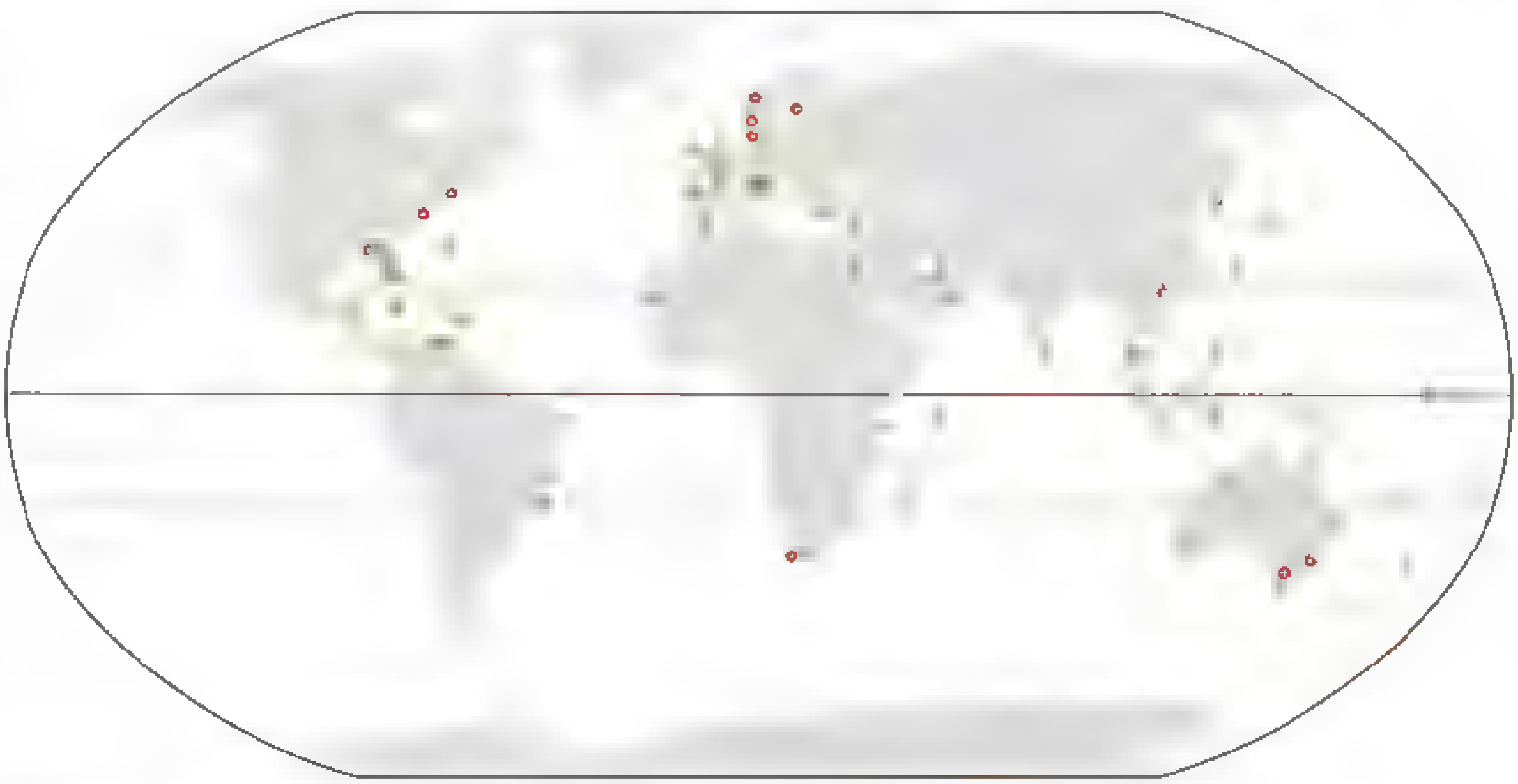

Fig. 1. Presence (green; dark points are quantitative, light points are qualitative) and absence (red) of lucinids in seagrass ecosystems based on our meta-analysis. The bivalves were present in 97% (93% of the quantitative sites) of all tropical seagrass beds, 90% (83% of the quantitative sites) of the subtropical beds, and 56% (50% of the quantitative sites) of the temperate seagrass meadows. The seagrass-lucinid association spans six out of seven continents, at least 18 genera of lucinids, and 11 out of 12 seagrass genera (and *Ruppia* spp.). Only meadows of *Phyllospadix* spp., a seagrass genus that grows on bare rock, did not contain Lucinidae. The analyzed ecosystems generally contained high (~100 individuals per square meter) to extremely high densities (>1000 individuals per square meter) of lucinids (table S1).

that we conducted at Banc d'Arguin, Mauritania (*20*). The meta-analysis reveals a relationship that covers 11 out of 12 seagrass genera (and *Ruppia* spp.) and at least 18 genera of Lucinidae (Fig. 1 and table S1). Only meadows of *Phyllospadix* spp., a seagrass genus that grows on bare rock, do not associate with Lucinidae. The association spans six out of seven continents, with bivalve densities ranging from 10 to over 1000 individuals per square meter. The bivalves were present in 97% of the tropical seagrass sites, 90% of the subtropical meadows, and 56% of the temperate seagrass beds surveyed, indicating that the association may be dependent on temperature-related sulfide production (*8*). Furthermore, results from our field study showed a positive correlation between seagrasses and lucinids that explained 42% of their respective variation [Pearson's correlation coefficient (r) = 0.65] (fig. S2).

To experimentally test our hypothesis (fig. S1B), we investigated the effects of sulfide oxidation by the lucinid bivalve *Loripes lacteus* on the production of the seagrass species *Zostera noltii* and the potential reciprocal benefits for *Loripes* in a full factorial experiment under controlled conditions (*20*). We set up *Zostera*, *Loripes*, *Zostera-Loripes*, and bare sediment treatments in the top sections of 40 two-compartment columns (fig. S3), which were placed in a large seawater basin. The lower compartment of each column contained anaerobic seawater and an injection tube through which sulfide was added twice a week in half of the columns. The injected sulfide was allowed to diffuse into the top section through a porous membrane.

The presence of *Loripes*, and to a lesser extent of *Zostera*, decreased sediment sulfide levels. After 5 weeks, pore water sulfide concentrations in the top sections of the sediment controls reached about 400 µM, whereas the semiweekly addition of sulfide caused levels to increase to nearly 2700 µM (Fig. 2A). The presence of *Zostera* decreased sulfide levels to ~200 µM in the controls and 2200 µM in the sulfide addition treatments. In contrast, sulfide levels remained low when *Loripes* was present (~15 µM), even in the sulfide addition treatments. As expected, the oxygen detection depth was reduced when sulfide was added but increased when only *Loripes*, but not *Zostera*, was present because of sulfide-oxidation and intake of surface water (Fig. 2B). *Zostera* alone did not significantly affect sediment oxygen conditions. The joint presence of *Zostera* and *Loripes* enhanced oxygen detection depth beyond that of their separate effects.

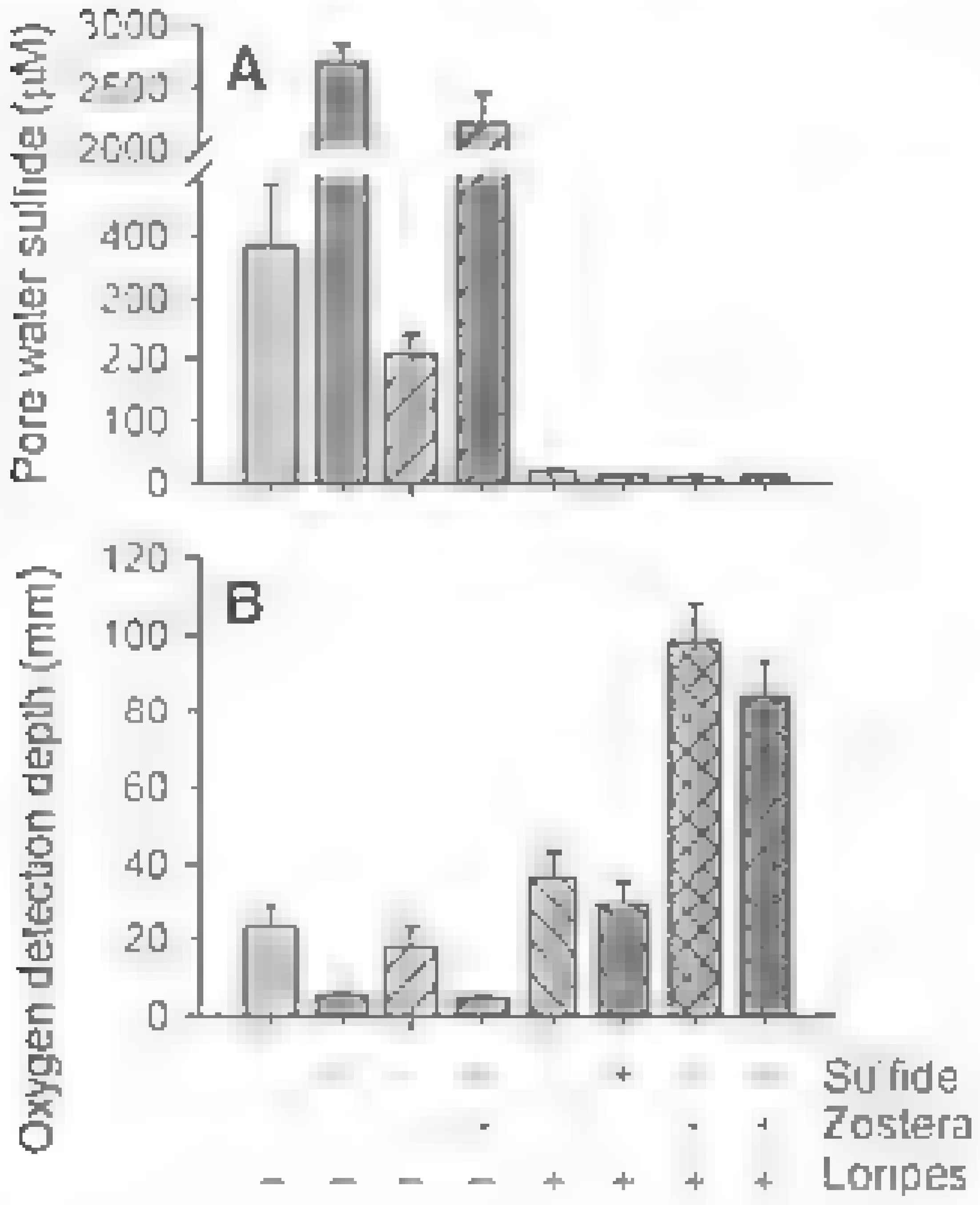

Fig. 2. (**A**) Pore water sulfide concentrations and (**B**) oxygen detection depth after 5 weeks; error bars represent SEM (n = 5 replicates). Oxygen detection depth decreased as sulfide was added [analysis of variance (ANOVA) $F_{1,32} = 8.9$, $P < 0.006$]. The presence of *Loripes* reduced sulfide levels (repeated measures ANOVA: $F_{1,32} = 268.8$, $P < 0.001$) and increased oxygen detection depth ($F_{1,32} = 125.0$, $P < 0.001$). Reduction of the sulfide concentration by *Zostera* alone was less, but still significant ($F_{1,32} = 6.8$, $P = 0.014$). That interactions occurred between *Zostera* and *Loripes* was apparent in the oxygen measurements ($F_{1,32} = 48.3$, $P < 0.001$) but was also significant in the sulfide data ($F_{1,32} = 7.8$, $P = 0.009$). The interaction between *Loripes* and sulfide was significant for the sulfide measurements ($F_{1,32} = 102.7$, $P < 0.001$) but not for the oxygen data ($F_{1,32} = 0.3$, $P = 0.578$).

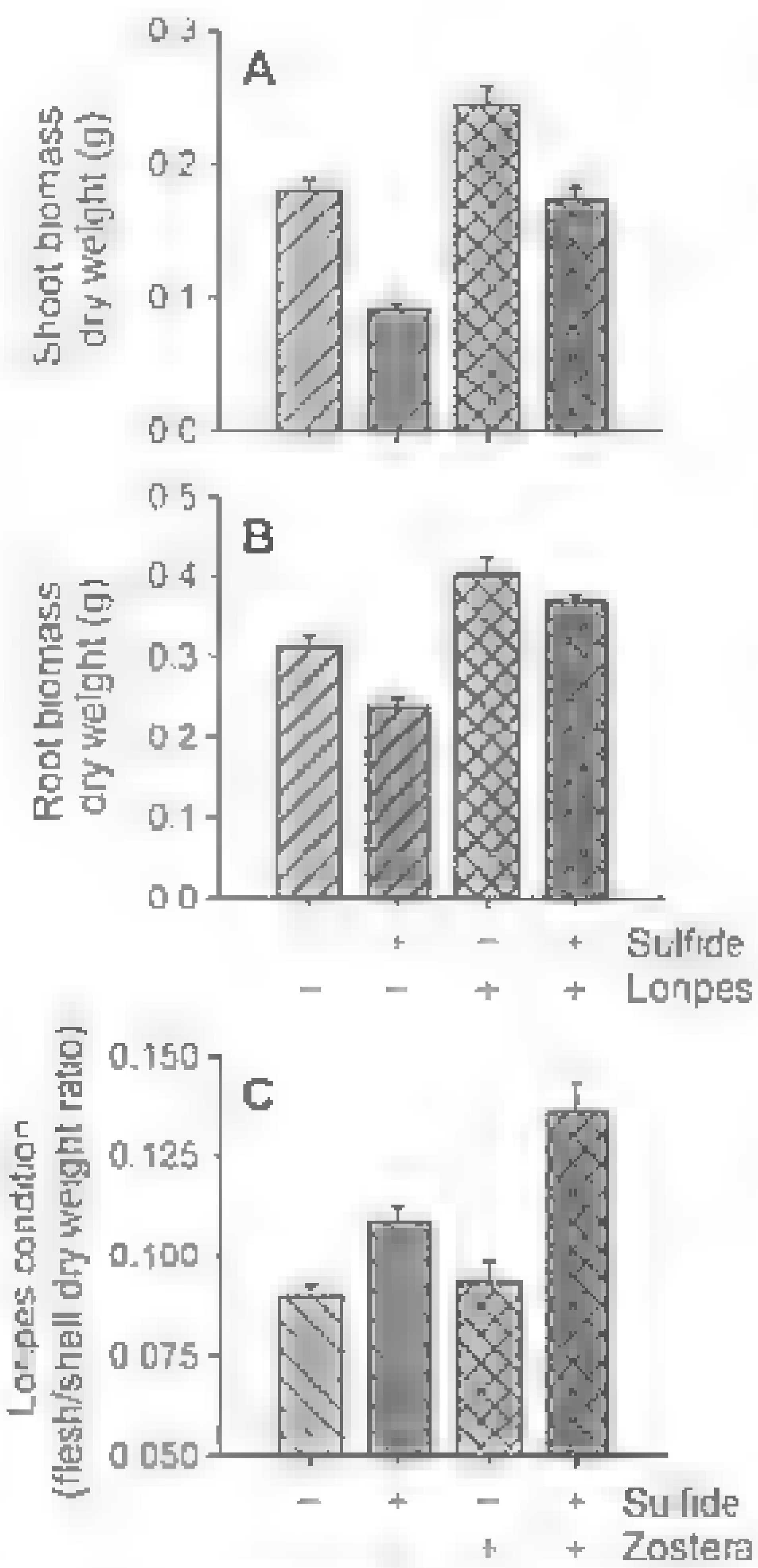

Fig. 3. (**A**) *Zostera* shoot and (**B**) root dry weight biomass per column and (**C**) *Loripes* condition expressed as the dry weight flesh/shell ratio after 5 weeks; error bars represent SEM (n = 5 replicates). *Zostera* biomass was reduced by means of sulfide addition (ANOVA: shoots $F_{1,16} = 72.6$, $P < 0.001$; roots $F_{1,16} = 12.0$, $P = 0.003$), whereas the presence of *Loripes* had a positive effect on both shoot ($F_{1,16} = 61.3$, $P < 0.001$) and root biomass ($F_{1,16} = 50.2$, $P < 0.001$). We found no significant effects on rhizome biomass. *Loripes* condition was positively affected by both sulfide addition (ANOVA: $F_{1,16} = 37.3$, $P < 0.001$) and *Zostera* presence ($F_{1,16} = 9.0$, $P = 0.008$). We also found a significant positive combined effect of the presence of *Zostera* and sulfide on *Loripes* condition ($F_{1,16} = 5.4$, $P = 0.034$).

Our experiment showed that *Zostera* production is facilitated by *Loripes*, both in the control and in the sulfide-addition treatments. In the treatments without *Loripes*, sulfide addition reduced *Zostera* shoot biomass to 50% of the controls (Fig. 3A). Reduced shoot biomass was accompanied by decreased root biomass (Fig. 3B) and impaired phosphate uptake (*20*). In contrast, the addition of *Loripes* increased *Zostera* shoot biomass 1.9-fold and root weight 1.5-fold, as seen in the sulfide-addition treatments. In the treatments without additional sulfide, the presence of *Loripes* increased both shoot and root weight by 1.4-fold and 1.3-fold, respectively.

Loripes condition, expressed as the flesh/shell dry weight ratio, was positively affected by sulfide addition (Fig. 3C). Furthermore, the addition of *Zostera* did not affect *Loripes* in the units to which no sulfide was added but improved the bivalve's condition in the sulfide treatments. As hypothesized, the positive effect of *Zostera* on *Loripes* seems to result from radial oxygen release from the seagrass roots (fig. S1B). Although sulfide was almost completely removed in all *Loripes* treatments (Fig. 2A), the bivalve was less able to profit from the addition of sulfide in the absence of *Zostera* (Fig. 3C). This indicates that at least in the *Loripes* units without seagrass, sulfide was not completely oxidized by the symbiotic bacteria because of oxygen limitation.

Overall, our results confirm our hypothesis that a three-stage symbiosis between seagrass, lucinids, and sulfide-oxidizing bacteria reduces sulfide stress in seagrass meadows. Even though radial oxygen release by *Zostera noltii* and of seagrasses in general is limited (*21*, *22*), *Loripes* in our experiment clearly benefitted from the increased oxygen input in the sediment. In the field, the positive effects of seagrasses on lucinids are not confined to sediment oxygenation alone but also by indirectly stimulating sulfide production and releasing dissolved organic molecules (*2*, *18*). The positive effects of *Loripes* on *Zostera* in our experiment could not be explained by differences in nutrient availability (*20*). Plants were not nutrient-limited, but both *Zostera* and *Loripes* significantly lowered dissolved ammonium and phosphorus in the sediment pore water, whereas sulfide addition increased nutrient availability (fig. S4). We found that in our experiment, the negative effects of sulfide addition on *Zostera* biomass could not fully be prevented by *Loripes* addition (Fig. 3A), despite the removal of almost all sulfide by *Loripes* after 3 days. As the observed experimental effects could not be attributed to differences in nutrient availability, this is

most likely caused by the pulsed nature of our sulfide supply. This may have led to short periods of exposure of *Zostera* to toxic sulfide levels.

Coastal ecosystems, and seagrass meadows in particular, are currently declining at an alarming and increasing rate worldwide, leading to loss of biodiversity (*1*). Extensive restoration efforts have had little success so far (<30%), despite their extremely high costs (±\$100,000 per hectare) (*23*). Similar to the function of mycorrhizae, pollinators, or seed dispersers in terrestrial systems (*24–26*), our findings indicate that restoration efforts should not only focus on environmental stressors such as eutrophication, sediment runoff, or high salinity as a cause of decline but should also consider internal ecological interactions, such as the presence and vigor of symbiotic or mutualistic relations. Breakdown of symbiotic interactions can affect ecosystem functioning, with bleaching events in coral reefs as a clear example (*27*). Similar to the well-known symbiosis between corals and their unicellular algal endosymbionts (*28*), we conclude that symbioses, rather than one defining species, forms the foundation of seagrass ecosystems.

References and Notes

1. M. Waycott *et al.*, *Proc. Natl. Acad. Sci. U.S.A.* **106**, 12377 (2009).
2. A. W. D. Larkum, R. J. Orth, C. M. Duarte, *Seagrasses: Biology, Ecology, and Conservation* (Springer, Berlin, 2006).
3. I. Nagelkerken, *Ecological Connectivity Among Tropical Coastal Ecosystems* (Springer Science and Business Media, Dordrecht, 2009).
4. T. van der Heide *et al.*, *Ecosystems (N.Y.)* **10**, 1311 (2007).
5. T. van der Heide, E. H. van Nes, M. M. van Katwijk, H. Olff, A. J. P. Smolders, *PLoS ONE* **6**, e16504 (2011).
6. B. B. Jorgensen, *Nature* **296**, 643 (1982).
7. M. L. Calleja, N. Marba, C. M. Duarte, *Estuar. Coast. Shelf Sci.* **73**, 583 (2007).
8. M. S. Koch, S. Schopmeyer, C. Kyhn-Hansen, C. J. Madden, *J. Exp. Mar. Biol. Ecol.* **341**, 91 (2007).
9. J. D. Taylor, E. A. Glover, in *The Evolutionary Biology of the Bivalvia*, E. M. Harper, J. D. Taylor, J. A. Crame, Eds. (Geological Society of London, London, 2000), pp. 207–225.
10. L. Liljedahl, *Palaeontology* **34**, 219 (1991).
11. D. L. Distel, *Bioscience* **48**, 277 (1998).
12. S. M. Stanley, in *Patterns of Evolution as Illustrated by the Fossil Record*, A. Hallam, Ed. (Elsevier, Amsterdam, Netherlands, 1977), pp. 209–250.
13. J. D. Taylor, E. A. Glover, L. Smith, P. Dyal, S. T. Williams, *Zool. J. Linn. Soc.* **163**, 15 (2011).
14. G. J. Vermeij, *Proc. R. Soc. B Biol. Sci.* **278**, 2362 (2011).
15. C. M. Cavanaugh, *Nature* **302**, 58 (1983).
16. J. J. Childress, P. R. Girguis, *J. Exp. Biol.* **214**, 312 (2011).
17. M. Johnson, M. Diouris, M. Lepennec, *Symbiosis* **17**, 1 (1994).
18. L. K. Reynolds, P. Berg, J. C. Zieman, *Estuaries Coasts* **30**, 482 (2007).
19. A. E. Anderson, *Am. Zool.* **35**, 121 (1995).
20. Materials and methods are available as supplementary materials on *Science* Online.
21. K. Sand-Jensen, O. Pedersen, T. Binzer, J. Borum, *Ann. Bot. (Lond.)* **96**, 613 (2005).
22. J. M. Caffrey, W. M. Kemp, *Aquat. Bot.* **40**, 109 (1991).
23. M. S. Fonseca, W. J. Kenworthy, B. E. Julius, S. Shutler, S. Fluke, in *Handbook of Ecological Restoration*, M. R. Perrow, Ed. (Cambridge Univ. Press, Cambridge, 2002), pp. 149–170.
24. M. G. A. van der Heijden *et al.*, *Nature* **396**, 69 (1998).
25. J. Bascompte, P. Jordano, *Annu. Rev. Ecol. Evol. Syst.* **38**, 567 (2007).
26. U. Bastolla *et al.*, *Nature* **458**, 1018 (2009).
27. K. E. Carpenter *et al.*, *Science* **321**, 560 (2008).
28. A. C. Baker, *Annu. Rev. Ecol. Evol. Syst.* **34**, 661 (2003).

Acknowledgments: We thank G. Quaintenne and H. Blanchet for their help with the collection of *Loripes*; J. Eygensteyn and E. Pierson for technical assistance; and G. J. Vermeij, H. de Kroon, T. J. Bouma, E. J. Weerman, and C. Smit for their comments on the manuscript. T.v.d.H. was financially supported by the "Waddenfonds" program; M.v.d.G. and T.P. by the Nederlandse Organisatie voor Wetenschappelijk Onderzoek (NWO)–WOTRO Integrated Programme grant W.01.65.221.00 awarded to T.P.; and J.d.F. and J.v.G. by the NWO–VIDI grant 864.09.002 awarded to J.v.G. B.S. was supported by an NSF CAREER award, the Andrew Mellon Foundation, and the Royal Netherlands Academy Visiting Professorship. The authors declare no conflicts of interest. A detailed description of all materials and methods, sources, as well as supplementary information are available as supplementary materials. The data are deposited in DRYAD at http://dx.doi.org/10.5061/dryad.210mp.

Supplementary Materials

www.sciencemag.org/cgi/content/full/336/6087/1432/DC1
Materials and Methods
Supplementary Text
Figs. S1 to S4
Tables S1 and S2
References (*29–119*)

2 February 2012; accepted 27 April 2012
10.1126/science.1219973

Fear of Predation Slows Plant-Litter Decomposition

Dror Hawlena,[1,2]* Michael S. Strickland,[1,3] Mark A. Bradford,[1] Oswald J. Schmitz[1]

Aboveground consumers are believed to affect ecosystem functioning by regulating the quantity and quality of plant litter entering the soil. We uncovered a pathway whereby terrestrial predators regulate ecosystem processes via indirect control over soil community function. Grasshopper herbivores stressed by spider predators have a higher body carbon-to-nitrogen ratio than do grasshoppers raised without spiders. This change in elemental content does not slow grasshopper decomposition but perturbs belowground community function, decelerating the subsequent decomposition of plant litter. This legacy effect of predation on soil community function appears to be regulated by the amount of herbivore protein entering the soil.

The quantity and quality of detrital inputs to soil regulate the rate at which microbial communities perform ecosystem processes such as decomposition, nitrogen (N) mineralization, and carbon (C) sequestration (*1, 2*). Because uneaten plant litter makes up the majority of detritus (*3*), it is assumed that these belowground ecosystem processes are only marginally influenced by biomass inputs from higher trophic levels in aboveground food webs, such as herbivores themselves (*4*). We provide evidence here, however, that predators may influence the decomposition of plant litter via a legacy effect of predation risk. Specifically, a physiological stress response to the risk of predation changes the elemental content of herbivore biomass. In turn, the decomposition of these stressed herbivores alters the function of belowground communities, leading to an overall decrease in the decomposition of plant litter.

Our work addresses whether food web structure (especially the existence of predators) influences ecosystem functioning via changes in the nutritional contents of prey (*5, 6*). The prevailing view is that food web structure does not influence prey body C-to-N (C:N) contents, because to survive and reproduce, prey must maintain relatively constant body C:N ratios (*7*). However, this view assumes that predator effects on prey are entirely consumptive (*5*). Instead the presence of predators generates fear, leading to physiological stress responses in prey, such as elevated metabolism and the synthesis of heat shock proteins (*8*). Together, these stress responses increase basal energy demands (*9–12*) that, in nutrient-limited systems, reduce the energy available for the competing demands of production (that is, reproduction and growth) (*13*). Thus, to meet heightened maintenance-energy demands, stressed herbivores divert energy from production, as well as increase their consumption of energy-rich carbohydrates (*12*). Given that the amount of energy used for production correlates positively with N demand, and that herbivores have limited ability to store excess nutrients, stressed herbivores should also excrete more N (*8, 14*). N excretion is further enhanced because chronically heightened stress hormone levels increase the breakdown of body proteins to produce glucose (*15*). Ultimately, prey stressed by predation risk should increase their body C:N ratio (*8*), and this is observed in field and laboratory experiments (*12, 16*).

In this study we asked whether predators can regulate plant-litter decomposition through

[1]School of Forestry and Environmental Studies, Yale University, 370 Prospect Street, New Haven, CT 06511, USA. [2]Department of Ecology, Evolution and Behavior, The Alexander Silberman Institute of Life Sciences, The Hebrew University of Jerusalem, Givat-Ram, Jerusalem 91904, Israel. [3]Department of Biological Sciences, Virginia Polytechnic Institute and State University, Blacksburg, VA 24061, USA.

*To whom correspondence should be addressed. E-mail: dror.hawlena@mail.huji.ac.il

indirect influences on the elemental stoichiometry of their prey. Our working hypothesis is that the C:N content (quality) of herbivore biomass entering soils as detritus induces changes in how soil communities process other resource inputs such as plant litter. Such legacy effects of resource quality have been observed in litter-decomposition studies (*17*). Moreover, simple organic compounds may prime soil communities in ways that enhance the decomposition of more-complex organic compounds (*18*).

Using a combination of laboratory and field experiments, our work built on examinations of food web effects on prey physiological stress and elemental stoichiometry in a well-studied grassland ecosystem including the spider predator *Pisuarina mira*, a dominant grasshopper herbivore (*Melanoplus femurrubrum*), and a variety of grasses and forbs (*12*). We reared grasshoppers in the field with the risk of spider predation (stress treatment) and without (control) (*19*). The body C:N content of stressed grasshoppers (mean ± SE, 4.00 ± 0.03; N = 11.62 ± 0.12%) was significantly higher (Wilcoxon signed-rank test $z = -2.023$; $P < 0.05$) than that of nonstressed grasshoppers (3.85 ± 0.04; N = 12.11 ± 0.16%). We then used carcasses of these grasshoppers in laboratory microcosm experiments to test whether the difference in body elemental composition altered the decomposition of the grasshoppers and subsequent plant litter inputs. We added a small amount (3.5 mg) of either stressed or nonstressed grasshopper biomass to microcosms containing soil collected from our grassland ecosystem. Carbon mineralization rates of grasshopper biomass were monitored until rates did not differ from reference microcosms containing only soil. At this time (42 days), there was little difference in cumulative C mineralization (that is, the total amount of C respired as CO_2 across the entire incubation) between stressed and stress-free grasshopper treatments (Fig. 1A). This was not unexpected, given that both stressed and stress-free grasshoppers represent high-quality resources to belowground communities. More interesting was how small elemental changes in these inputs might affect the subsequent functioning of soil communities, especially the decomposition of lower-quality substrates such as plant litter (*18*).

To test the functional implications of slight nutrient differences in high-quality resource inputs, we added grass litter (500 mg) to the microcosm soils previously amended with stressed or stress-free grasshopper carcasses and then measured C mineralization. After 118 days, mineralization of the grass litter in soils previously amended with stressed grasshoppers was 62% lower ($F_{1,4} = 13.9$, $P < 0.05$) than that of the same litter in soils amended with nonstressed grasshoppers (Fig. 1B). Thus, the small input of herbivore biomass (~140 times less than the added litter mass), coupled with a 4% difference in the C:N ratio between stressed and nonstressed grasshopper carcasses, caused a threefold difference in the mineralization of plant-litter inputs. These results suggest a causative link between predation-induced changes in prey body chemistry and altered soil community function. The most plausible explanation for why such a small shift in prey C:N ratio might

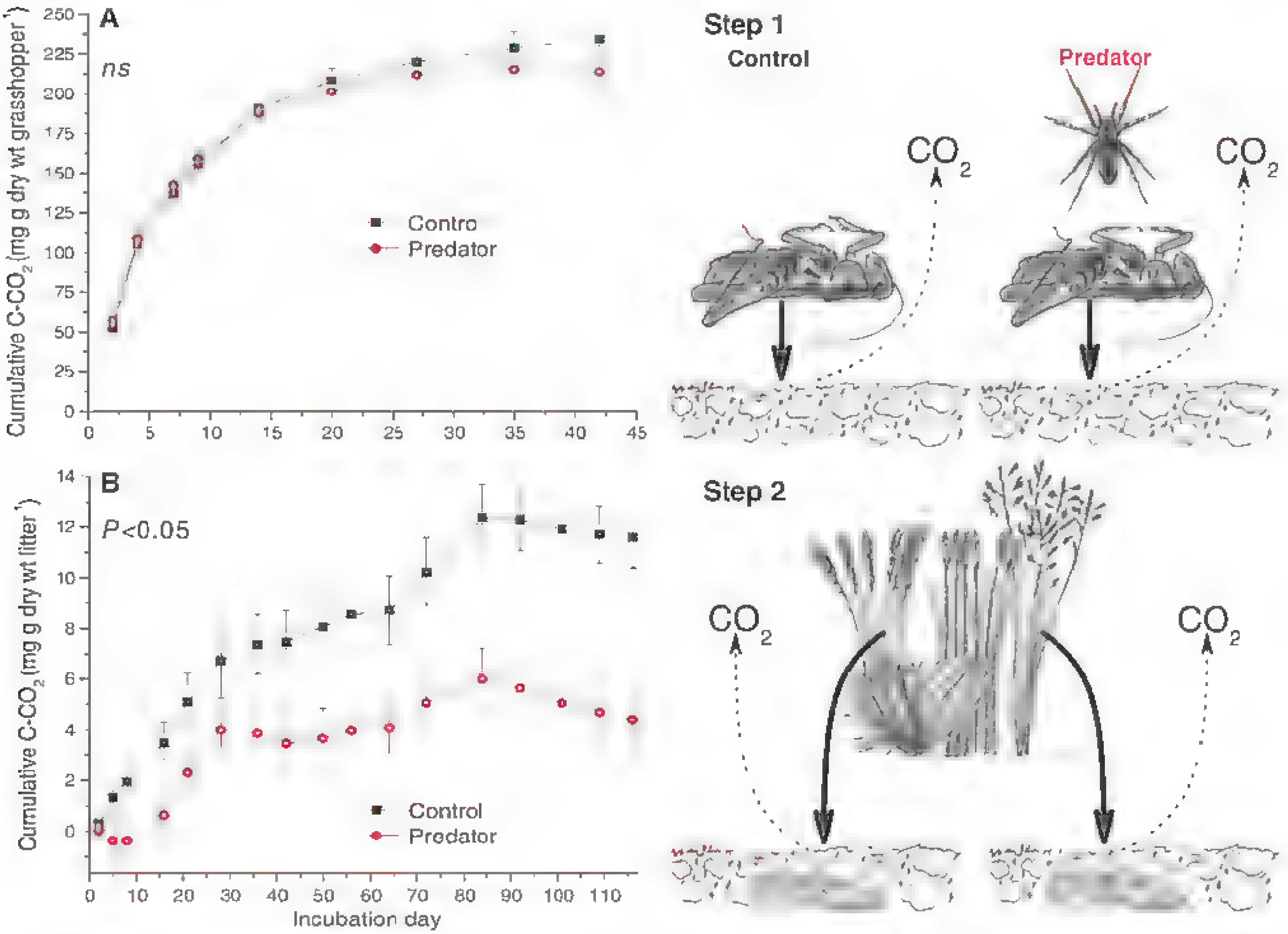

Fig. 1. Cumulative C mineralization (mean ± 1 SE, $n = 5$ microcosms) during decomposition of (**A**) nonstressed grasshoppers versus those stressed by predators (step 1); and (**B**) grass litter added to the same microcosms (step 2) after the completion of the grasshopper decomposition experiment shown in step 1. Although control and stressed grasshoppers were mineralized at similar rates ($P > 0.05$), the addition of grasshopper carcasses reared with disarmed predators led to subsequent reductions in plant-litter decomposition rates ($P < 0.05$). Rates are differences from microcosms not amended with grasshoppers, so cumulative values can be negative.

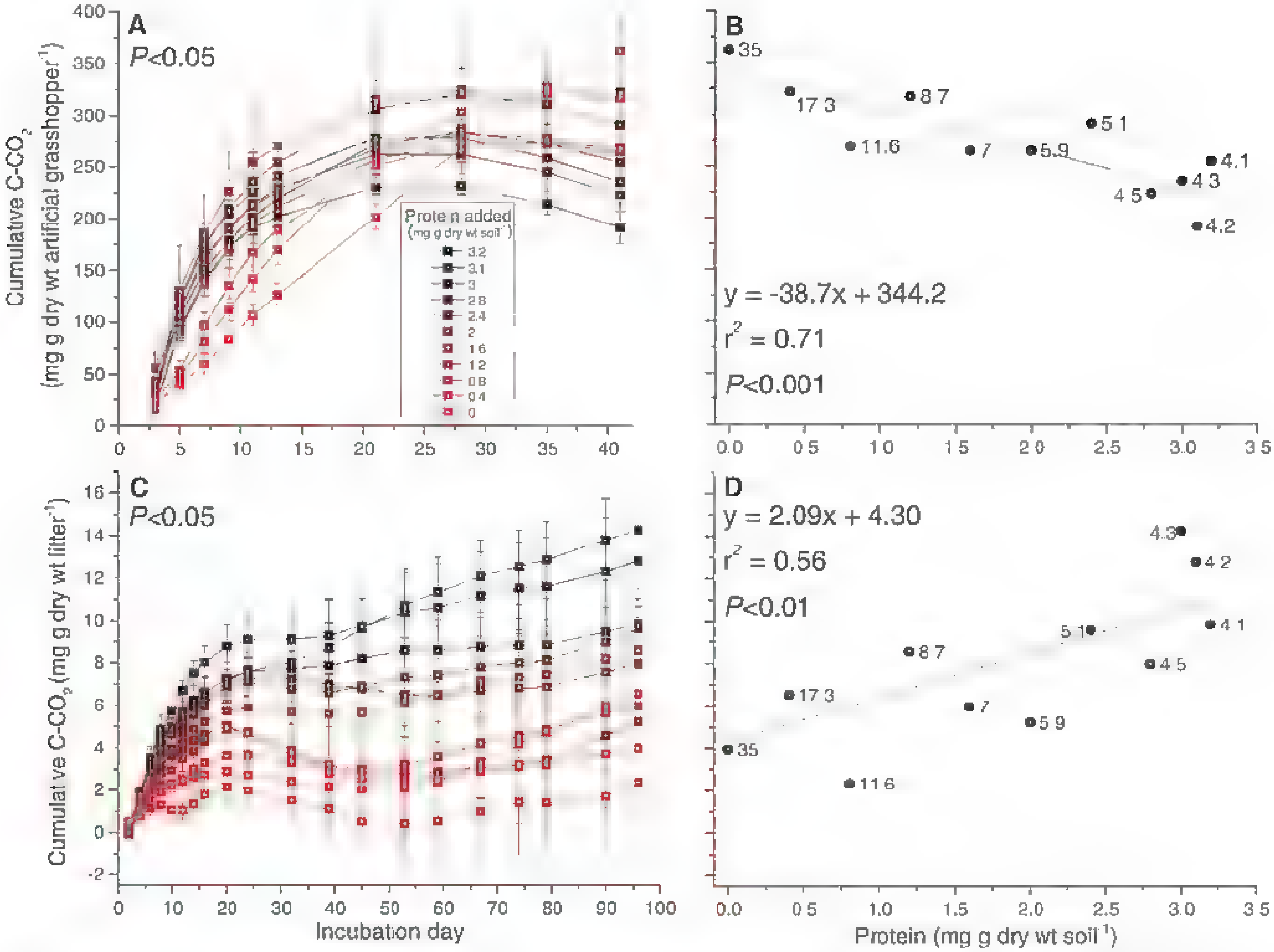

Fig. 2. (**A**) Cumulative C mineralization (mean ± 1 SE, $n = 6$ microcosms) during decomposition of artificial grasshoppers with varying C:N ratios and protein contents and (**B**) the relationship between the amount of protein added and the cumulative mineralization associated with these artificial grasshoppers. (**C**) The cumulative C mineralization (mean ± 1 SE) of grass litter added to the same microcosms after completion of artificial grasshopper decomposition and (**D**) the relationship between the amount of protein added and subsequent grass-litter mineralization. Rates are differences from microcosms not amended with artificial grasshoppers, so cumulative values can be negative [as in (C)]. The C:N ratios associated with the different artificial grasshoppers are shown next to their respective points.

translate to such a large shift in litter mineralization rates is that small increases in N availability can prime the activities of decomposer microorganisms and hence accelerate litter mineralization (*20*). We next examined whether the observed effects on litter mineralization were probably attributable to the variation in the C:N content of prey tissue being linked to N availability and hence priming of microbial activity.

To test whether prey body C:N content influenced plant-litter decomposition, we again used a laboratory microcosm approach, but this time manipulated C:N ratios by creating "artificial grasshoppers" (*19*). To simulate grasshopper tissue, we used 4-mg organic matter mixtures of 20% chitin and varying proportions of carbohydrates (0 to 80%) and proteins (0 to 80%), generating C:N ratios that spanned more than the observed variation. Carbon mineralization of the artificial grasshoppers was measured (for 40 days)

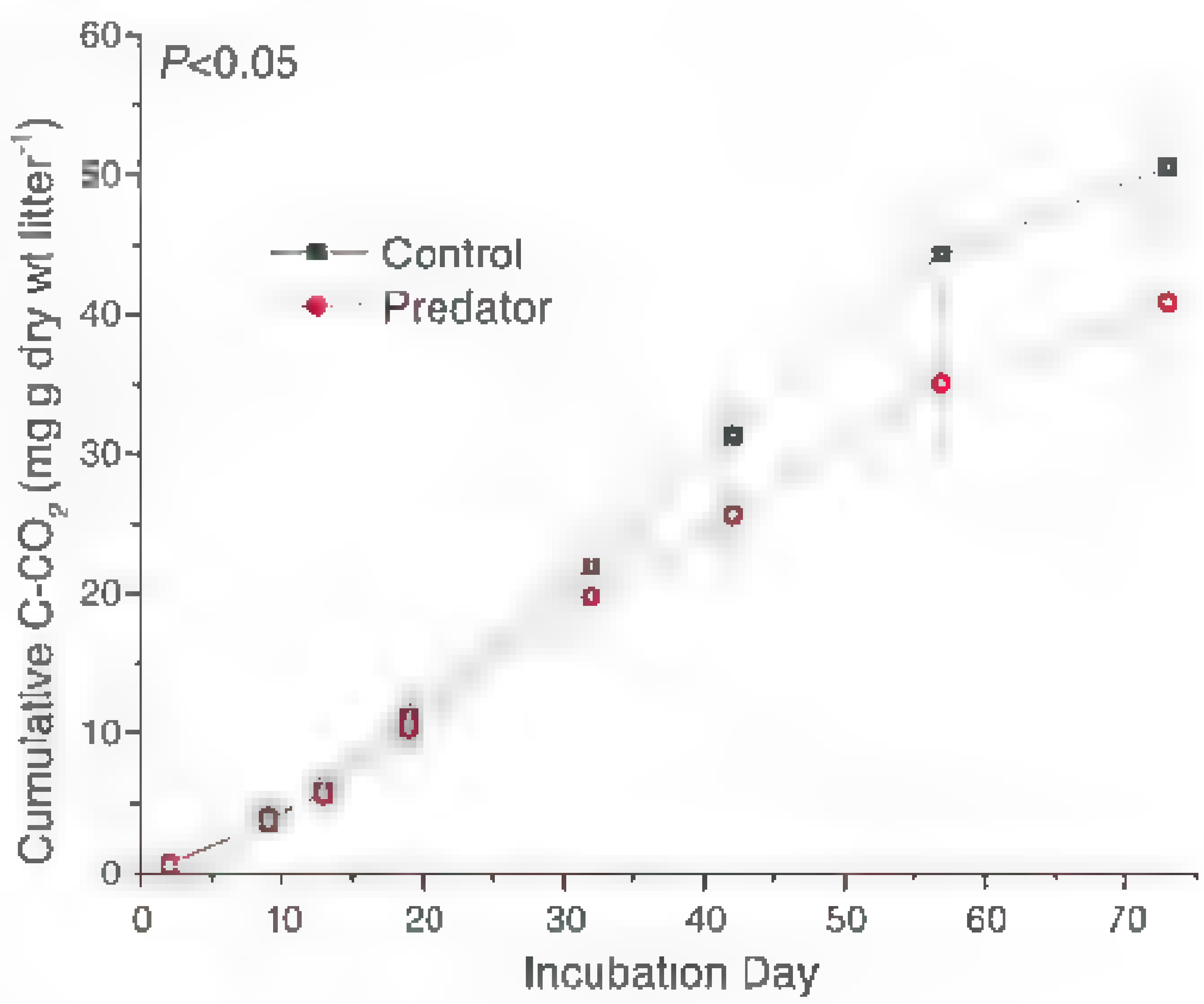

Fig. 3. Cumulative C mineralization (mean ± 1 SE, $n = 7$ field plots) of ^{13}C-labeled grass litter decomposed in blocked field plots, first amended with control grasshoppers or those stressed by predator presence.

until it approximated rates in reference microcosms containing only soil. Cumulative C mineralization varied by up to twofold across the artificial grasshopper treatments ($F_{10,55}$ 2.15, $P < 0.05$; Fig. 2A). Notable, given the broad range in C:N across treatments, is the positive relationship between the C:N of artificial grasshoppers and the cumulative C-mineralization, as well as the negative relationship between mineralization and amount of protein (Fig. 2B). These observations are most likely explained by higher growth efficiencies of soil organisms. This might be expected because organisms consuming resource inputs with lower C:N ratios and consequently higher protein levels will favor production over waste respiration and hence reduce total C mineralization (*20*).

The availability of protein N is essential both for microbial production and for facilitating the decomposition of organic matter, because it is used to produce extracellular enzymes that catalyze the degradation of complex C compounds (*20–22*). It then follows that the carcasses of stressed grasshoppers, which have higher biomass C:N, probably because of lower body protein levels (*23*), provide less available N and thus should retard plant-litter decomposition. Further support for this interpretation came when we added grass litter (500 mg) to the microcosms previously amended with artificial grasshoppers. Across 96 days, the mineralization rates of grass litter diverged by as much as sixfold ($F_{10,55} = 2.34$, $P < 0.05$; Fig. 2C), despite the only twofold difference in the cumulative mineralization of artificial grasshoppers. These results mirror, qualitatively, our first experiment with real grasshoppers, in which lower available N led to reductions in the decomposition of plant litter (Fig. 2, C and D). These results also show that varying C:N ratios only partially explain altered plant-litter mineralization. Specifically, the protein content of artificial grasshoppers, for which the C:N ratio is a common but indirect index (*23*), has over twice the power [coefficient of determination-explained variance (R^2) = 0.56, $F_{1,10} = 13.5$, $P < 0.01$; Fig. 2D] of the C:N ratio (R^2 0.23, F_1 4.0, P 0.08) to explain plant-litter decomposition rates. This is probably because the C:N ratio is influenced by both labile and recalcitrant N-bearing compounds. Consequently, a small difference in the C:N ratio may reflect much larger variation in protein N content. Together, the laboratory experiments reveal a potentially important general mechanism (*8*) by which predators regulate soil ecosystem processes through stress-induced changes to herbivore nutrient content. It remained uncertain whether this mechanism explains variation in belowground community function in nature.

To test for predator-induced regulation of decomposition variation in mineralization rates under natural conditions, we added intact carcasses of grasshoppers reared either with predation risk (stress treatment) or without (control) to field plots. After 40 days, we added ^{13}C-labeled grass litter (550 g m^{-2}) to the same plots and measured ^{13}C mineralization in situ, using cavity ring-down spectroscopy, a highly sensitive form of laser absorption spectrometry that quantifies the stable isotope composition of C in CO_2 (*19*). Using ^{13}C labeling meant that we could separate the contribution of mineralization of the added litter from total soil respiration. After 73 days, mineralization of the grass litter, in plots amended with stressed grasshoppers, was 19% lower ($F_{1,6}$ 9.06, $P < 0.05$) than in plots that received stress-free grasshoppers (Fig. 3). This mechanism is not mutually exclusive of other mechanisms that regulate soil communities (*4*, *21*, *24*). Nonetheless, in our experiments, the effect of predation on litter decomposition had a measureable impact through changes in the nutrient content of herbivore carcasses. These results highlight the potential for this mechanism to influence decay rates of organic matter inputs and hence ecosystem C and N cycling.

A key remaining question is whether predator-induced changes persist when multiple aboveground and belowground pathways act simultaneously. We examined this question by rearing grasshoppers in field plots where predation risk was absent (no spiders) or present (spiders with glued mouthparts) (*19*). Toward the end of the growing season and 1 month after the grasshopper adults had reproduced, died, and been allowed to decompose, we transferred surface soil from the field plots to laboratory microcosms. We found no difference in soil pH between risk and risk-free field mesocosms ($F_{1,6} = 0.761$, $P = 0.417$). To test for legacy effects of fear, we then added grass litter to the microcosms and measured C mineralization for 93 days. Cumulative mineralization of grass litter, amended to soil communities developed under the predator treatment, was ~200% lower than litter mineralization from communities developed without spider predators ($F_{1,6} = 6.23$, $P < 0.05$; Fig. 4). Collectively, our experiments suggest that cascading effects of predation risk are measurable on litter decomposition in the field and laboratory and occur through predator-induced changes in prey chemical composition.

Traditional concepts of trophic pyramids in ecosystems highlight the idea that inputs of plant-derived materials to soils are more important for regulating belowground processes than are inputs from other trophic levels, because plant inputs are dominant (*4*). Accordingly, predators are presumed to regulate ecosystem processes mainly by altering the quality and quantity of plant-derived materials entering belowground systems, through the control of herbivore density (that is, through trophic cascades) and/or by altering herbivore foraging behavior (*4*, *5*). Our work instead suggests that predators can regulate ecosystem processes more directly through stress-induced changes in the chemical composition of prey body tissue. We find that small additions of high-quality herbivore biomass influence the decomposition of much larger inputs of recalcitrant plant litter, with effects lasting for at least the duration of a normal growing season (80 to 110 days). Indeed, we show that predator-induced changes in the nutritional composition of herbivore biomass dramatically slow the decomposition of plant litter through legacy effects on soil communities. Our work suggests that the mechanism governing these effects is the amount of animal protein that enters the soil. Our work adds to the body of recent work (*5*, *25*) showing that predators exert top-down control, through multiple mechanisms, on ecosystem processes. Evaluating the importance of these newly identified roles of predators in ecosystems is made all the more urgent because we are losing them from ecosystems at disproportionately higher rates than other species (*25*, *26*).

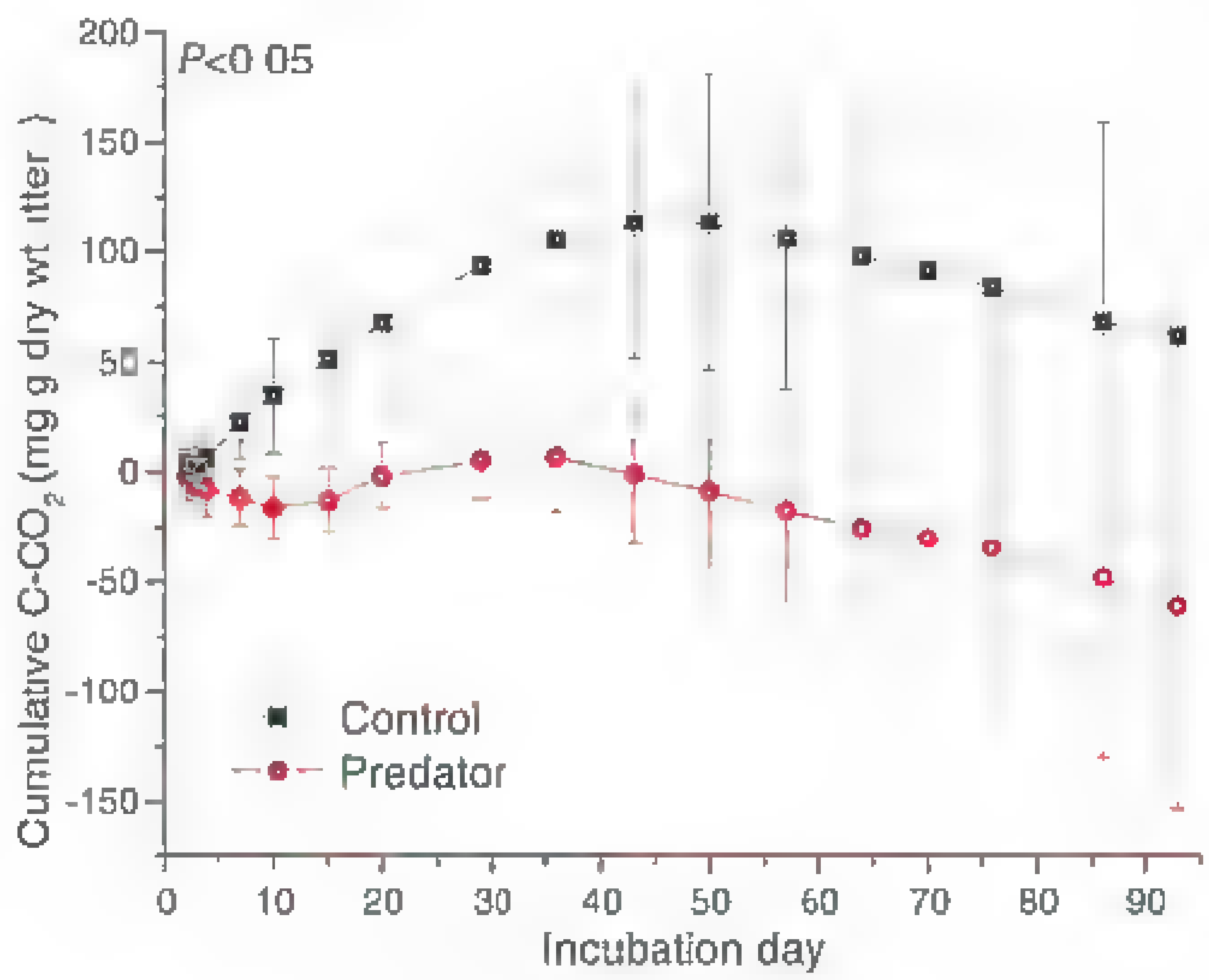

Fig. 4. Cumulative C mineralization (mean ± 1 SE, $n = 7$ microcosms) of grass litter on soil collected from blocked field plots with or without predation risk. Rates are differences from reference soils, so cumulative values can be negative.

References and Notes

1. D. A. Wardle *et al.*, *Science* **304**, 1629 (2004).
2. S. Hättenschwiler, A. V. Tiunov, S. Scheu, *Annu. Rev. Ecol. Syst.* **36**, 191 (2005).
3. J. Cebrian, *Ecol. Lett.* **7**, 232 (2004).
4. R. D. Bardgett, D. A. Wardle, Eds., *Aboveground-Belowground Linkages* (Oxford Univ. Press, Oxford, 2010).
5. O. J. Schmitz, D. Hawlena, G. C. Trussell, *Ecol. Lett.* **13**, 1199 (2010).
6. J. J. Elser *et al.*, *Nature* **408**, 578 (2000).

7. J. J. Elser *et al.*, *Ecol. Lett.* **3**, 540 (2000).
8. D. Hawlena, O. J. Schmitz, *Am. Nat.* **176**, 537 (2010).
9. F. Rovero, R. N. Hughes, G. Chelazzi, *J. Anim. Ecol.* **69**, 683 (2000).
10. K. Pauwels, R. Stoks, L. de Meester, *J. Evol. Biol.* **18**, 867 (2005).
11. U. K. Steiner, J. Van Buskirk, *PLoS ONE* **4**, e6160 (2009).
12. D. Hawlena, O. J. Schmitz, *Proc. Natl. Acad. Sci. U.S.A.* **107**, 15503 (2010).
13. S. E. DuRant, W. A. Hopkins, L. G. Talent, *Comp. Biochem. Physiol. C Toxicol. Pharmacol.* **145**, 442 (2007).
14. R. W. Sterner, *Freshw. Biol.* **38**, 473 (1997).
15. R. Stoks, M. De Block, M. A. McPeek, *Ecol. Lett.* **8**, 1307 (2005).
16. D. Hawlena, K. M. Hughes, O. J. Schmitz, *Funct. Ecol.* **6**, 1223 (2011).
17. M. S. Strickland, C. Lauber, N. Fierer, M. A. Bradford, *Ecology* **90**, 441 (2009).
18. S. Fontaine, G. Bardoux, L. Abbadie, A. Mariotti, *Ecol. Lett.* **7**, 314 (2004).
19. Materials and methods are available as supplementary materials on *Science* Online.
20. J. P. Schimel, M. N. Weintraub, *Soil Biol. Biochem.* **35**, 549 (2003).
21. J. Schimel, T. C. Balser, M. Wallenstein, *Ecology* **88**, 1386 (2007).
22. S. D. Allison *et al.*, *Soil Biol. Biochem.* **41**, 293 (2009).
23. R. W. Sterner, J. J. Elser, *Ecological Stoichiometry* (Princeton Univ. Press, Princeton, NJ, 2002).
24. M. A. Bradford *et al.*, *Ecol. Lett.* **11**, 1316 (2008).
25. J. A. Estes *et al.*, *Science* **333**, 301 (2011).
26. J. E. Duffy, *Ecol. Lett.* **6**, 680 (2003).

Acknowledgments: We thank P. Raymond, A. Genin, C. Burch, and the anonymous reviewers for their comments and suggestions on earlier versions of this manuscript and K. Hughes and K. McLean for field assistance. This research was supported by a grant from the Yale Climate and Energy Institute to O.J.S. and M.A.B. and by NSF grant DEB-0816504 to O.J.S. Data used in this study are available at http://dx.doi.org/10.5061/dryad.2cm3h1q7.

Supplementary Materials
www.sciencemag.org/cgi/content/full/336/6087/1434/DC1
Materials and Methods
References (*27*, *28*)

6 February 2012; accepted 2 May 2012
10.1126/science.1220097

Continental-Scale Effects of Nutrient Pollution on Stream Ecosystem Functioning

Guy Woodward,[1,2]*† Mark O. Gessner,[3,4,5,6]*† Paul S. Giller,[1] Vladislav Gulis,[7]‡ Sally Hladyz,[1]§ Antoine Lecerf,[8,9] Björn Malmqvist,[10] Brendan G. McKie,[10]‖ Scott D. Tiegs,[3,4,11] Helen Cariss,[12]¶ Mike Dobson,[12]# Arturo Elosegi,[13] Verónica Ferreira,[7] Manuel A.S. Graça,[7] Tadeusz Fleituch,[14] Jean O. Lacoursière,[15] Marius Nistorescu,[16] Jesús Pozo,[13] Geta Risnoveanu,[16] Markus Schindler,[3,4] Angheluta Vadineanu,[16] Lena B.-M. Vought,[15] Eric Chauvet[8,9]†

Excessive nutrient loading is a major threat to aquatic ecosystems worldwide that leads to profound changes in aquatic biodiversity and biogeochemical processes. Systematic quantitative assessment of functional ecosystem measures for river networks is, however, lacking, especially at continental scales. Here, we narrow this gap by means of a pan-European field experiment on a fundamental ecosystem process—leaf-litter breakdown—in 100 streams across a greater than 1000-fold nutrient gradient. Dramatically slowed breakdown at both extremes of the gradient indicated strong nutrient limitation in unaffected systems, potential for strong stimulation in moderately altered systems, and inhibition in highly polluted streams. This large-scale response pattern emphasizes the need to complement established structural approaches (such as water chemistry, hydrogeomorphology, and biological diversity metrics) with functional measures (such as litter-breakdown rate, whole-system metabolism, and nutrient spiraling) for assessing ecosystem health.

Nutrient enrichment from organic inputs and agricultural run-off is placing the world's vulnerable fresh waters in a precarious position (*1*–*4*). Far-reaching environmental legislation has been introduced to redress human impacts on aquatic communities (*5*, *6*), yet the consequences of nutrient loading for stream ecosystem functioning remain poorly understood (*4*, *7*, *8*). This is worrying because key ecosystem services (such as maintenance of viable fisheries as a provisioning service, and organic matter decomposition as a supporting service) ultimately depend on ecosystem processes, such as leaf-litter breakdown and other processes involved in nutrient cycling (*3*, *9*).

Many aquatic ecosystems are supported by plant litter inputs (*10*–*12*). This includes streams, where terrestrial leaf breakdown—which is driven by resource quality; the abundance, diversity, and activity of consumers; and environmental factors—is a key ecosystem process (*10*, *13*, *14*). Moderate nutrient enrichment of streams can accelerate breakdown by stimulating microbial conditioning and invertebrate consumption (*15*, *16*). However, a wide range of responses along nutrient gradients has been reported in field studies, suggesting environmental drivers beyond elevated nutrient supply. For instance, wastewater discharge can induce anoxia, mobilize heavy metals, and physically smother benthic organisms (*17*, *18*). Litter breakdown by invertebrates (*19*) appears especially sensitive to nutrient pollution relative to that mediated by microbes (*20*) and, because invertebrates often attain their highest densities in moderately enriched streams, a hump-shaped breakdown rate response might be expected along long nutrient gradients (*5*).

We hypothesized that breakdown rates are constrained by microbial nutrient limitation at the low end of nutrient pollution gradients and by the effects of environmental degradation on invertebrates at the high end. Most studies, however, have been unable to detect this pattern because they have been conducted over relatively short nutrient gradients and small spatial scales (*5*, *7*). Here, we report a field experiment in 100 European streams spanning 1000-fold differences in nutrient concentrations, as proxy measures of nutrient loading by direct and indirect inputs (*21*). The validity of this approach is highlighted by the positive relationship between biochemical oxygen demand (BOD_5) and nutrient concentrations in more than 8000 European streams, and the comparable frequency distributions of nutrient concentrations between these and our sites (fig.

[1]Department of Zoology, Ecology and Plant Science, University College Cork, National University of Ireland, Cork, Enterprise Centre, Distillery Fields, Cork, Ireland. [2]Queen Mary University of London, School of Biological and Chemical Sciences, London E1 4NS, UK. [3]Department of Aquatic Ecology, Eawag: Swiss Federal Institute of Aquatic Science and Technology, 6047 Kastanienbaum, Switzerland. [4]Institute of Integrative Biology (IBZ), ETH Zurich, 8092 Zurich, Switzerland. [5]Leibniz Institute of Freshwater Ecology and Inland Fisheries (IGB), Alte Fischerhütte 2, 16775 Stechlin, Germany. [6]Department of Ecology, Berlin Institute of Technology (TU Berlin), Ernst-Reuter-Platz 1, 10587 Berlin, Germany. [7]Institute of Marine Research (IMAR) and Department of Life Sciences, University of Coimbra, 3001-401 Coimbra, Portugal. [8]Université de Toulouse; INP, UPS; Laboratoire Ecologie Fonctionnelle et Environnement (EcoLab), 118 Route de Narbonne, 31062 Toulouse, France. [9]CNRS, EcoLab, 31062 Toulouse, France. [10]Department of Ecology and Environmental Science, Umeå University, 90187 Umeå, Sweden. [11]Department of Biological Sciences, Oakland University, Rochester, MI 48309–4401, USA. [12]Department of Environmental and Geographical Sciences, Manchester Metropolitan University, Chester Street, Manchester M15 6BH, UK. [13]Department of Plant Biology and Ecology, Faculty of Science and Technology, University of the Basque Country, Post Office Box 644, 48080 Bilbao, Spain. [14]Institute of Nature Conservation, Polish Academy of Sciences, Mickiewicza 33, 31-120 Krakow, Poland. [15]School of Education and Environment, Kristianstad University, 29188 Kristianstad, Sweden. [16]Department of Systems Ecology and Sustainability, University of Bucharest, Splaiul Independentei 91-95, 050095 Bucharest, Romania.

*These authors contributed equally to this work.
†To whom correspondence should be sent. E-mail: g.woodward@qmul.ac.uk (G.W.); gessner@igb-berlin.de (M.O.G.); eric.chauvet@univ-tlse3.fr (E.C.)
‡Present address: Department of Biology, Coastal Carolina University, Post Office Box 261954, Conway, SC 29528–6054, USA.
§Present address: Monash University, Australian Centre for Biodiversity and School of Biological Sciences, Clayton, Victoria 3800, Australia.
‖Present address: Department of Aquatic Sciences and Assessment, Swedish University of Agricultural Sciences, 75007 Uppsala, Sweden.
¶Present address: Forestry Commission Wales, Rhodfa Padarn, Llanbadarn Fawr, Aberystwyth, Ceredigion SY23 3UR, UK.
#Present address: Freshwater Biological Association, the Ferry Landing, Far Sawrey, Ambleside, Cumbria LA22 0LP, UK.

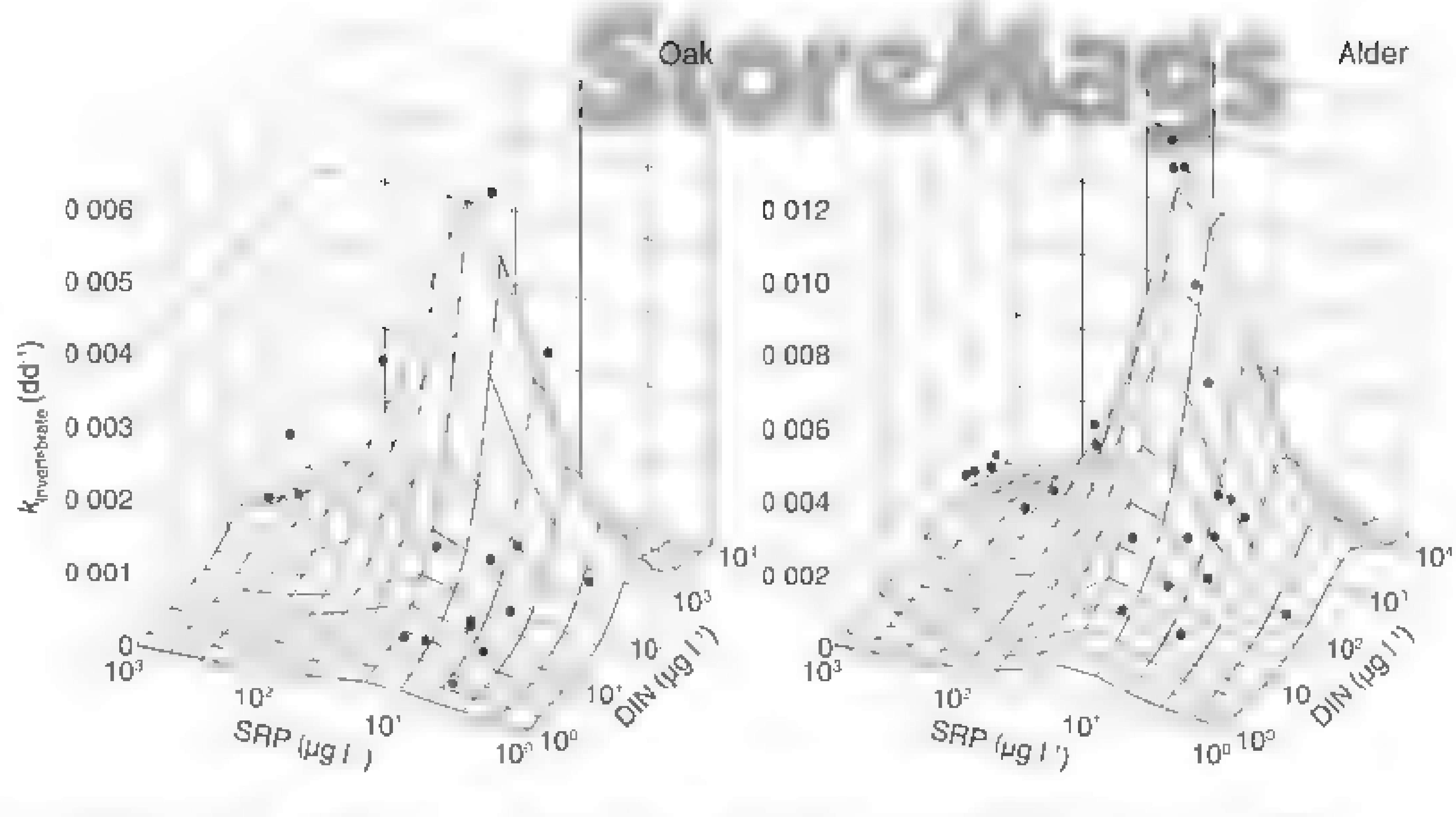

Fig. 1. Rates of invertebrate-mediated breakdown as a function of SRP and DIN concentrations for oak (**Left**) and alder (**Right**) leaves. Each data point represents a temperature-corrected rate [expressed in degree days^{-1} (dd^{-1})] for a single stream. Three-dimensional volume-filling relationships between nutrient gradients and breakdown rates with unimodal Lorentzian surfaces are fitted as bounding envelopes to maxima within categories of nutrient concentrations (per 0.5 $\log_{10}$ division of SRP and DIN in μg l^{-1}); R^2 values of the fits to these maxima are 0.85 for oak and 0.77 for alder, respectively (randomization tests were carried out to rule out any potential influence of different sample sizes setting the bounding envelopes along the nutrient gradients) (figs. S4 and S5) (*21*). Data points above and below unimodal Lorentzian surfaces are displayed in black and gray, respectively.

S1). We deployed 2400 experimental litter bags made with fine or coarse mesh to determine total, microbially mediated, and invertebrate-driven breakdown rates of litter from two common tree species: slow-decomposing pedunculate oak (*Quercus robur L.*) and fast-decomposing black alder (*Alnus glutinosa* [L.] Gaertn.), both widespread across Europe and with closely related species that are common throughout the Holarctic region.

Both litter types exhibited hump-shaped responses for invertebrate-driven breakdown rates as a function of soluble reactive phosphorus (SRP) and dissolved inorganic nitrogen (DIN) concentrations (Fig. 1 and figs. S2 and S3). Rates were always low at the extremes, but low-to-high at intermediate nutrient concentrations. Within a given range of nutrient concentrations, the spread of breakdown rates was almost equal to the maximum (there was an upper, but not a lower, limit) (figs. S4 and S5), supporting the idea that factors beyond nutrients alone modulated consumer activity (*14*). Although a similar pattern emerged for total breakdown with highest rates at intermediate enrichment levels, this response was not as clear as for invertebrate-mediated breakdown (fig. S2).

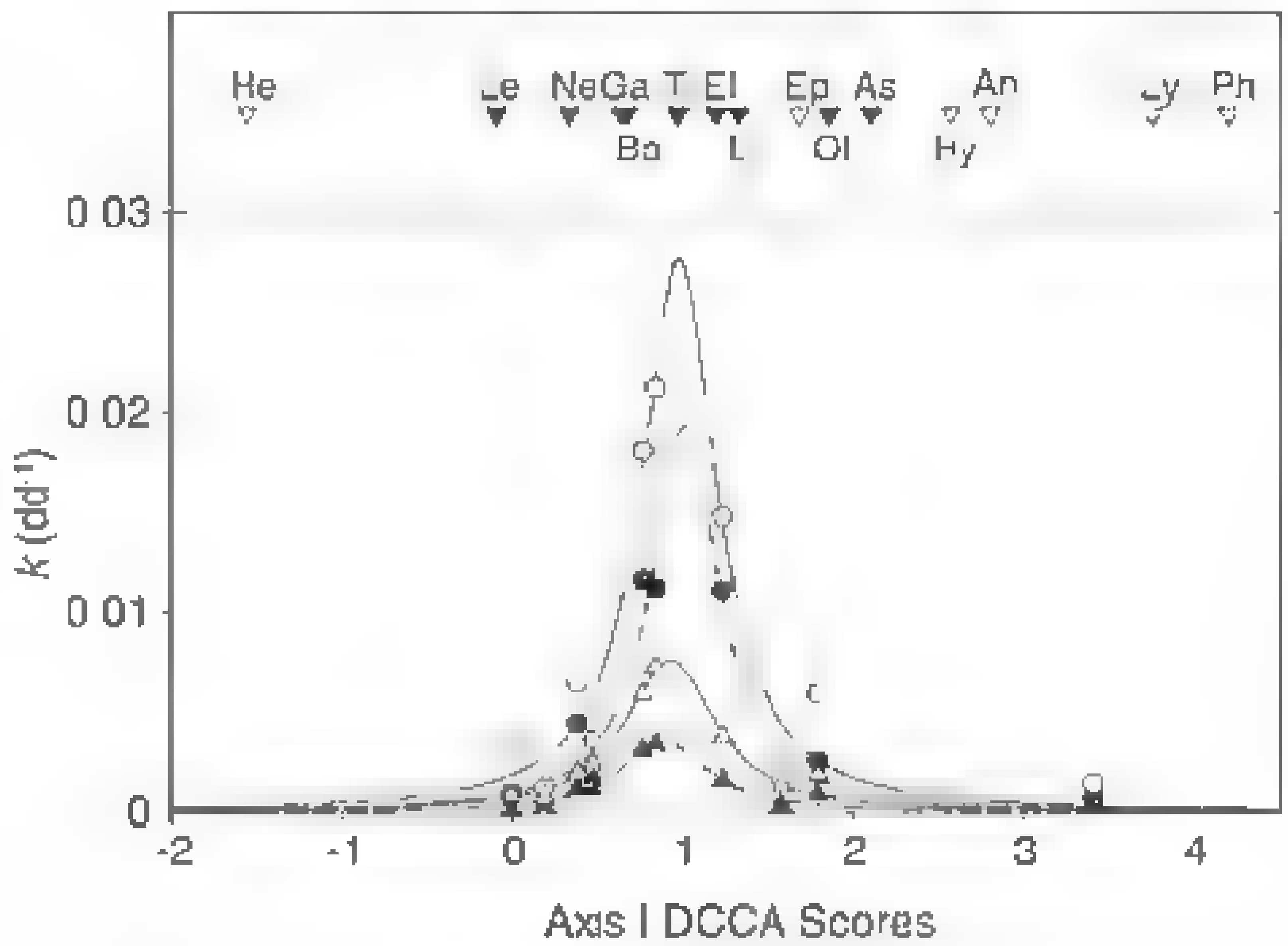

Fig. 2. Axis I sample scores from a DCCA on communities of primary consumers in alder (circles) and oak (triangles) leaf bags at 10 streams in Ireland, plotted against total (white symbols) and invertebrate-mediated (black symbols) breakdown rate (expressed in degree days^{-1}). Unimodal Lorentzian curves have been fitted to the data (alder k_{total}: R^2 = 0.93; P < 0.0001; alder $k_{invertebrate}$: R^2 = 0.88; P = 0.0006; oak k_{total}: R^2 = 0.97, P < 0.0001; oak $k_{invertebrate}$: R^2 = 0.96; P = 0.0001). Scores of individual invertebrate taxa depicted as letters at the top of the graph show that the largest litter-consuming detritivores, gammarid shrimps and limnephilid caddisfly larvae, are close to the peak of the curves. An, Ancylidae; As, Asellidae; Ba, Baetidae; El, Elmidae; Ep, Ephemerellidae; Ga, Gammaridae; He, Heptageniidae; Hy, Hydrobiidae; Le, Leuctridae; Li, Limnephilidae; Ly, Lymnaeidae; Ne, Nemouridae; Ol, Oligochaeta; Ph, Physidae; Ti, Tipulidae.

In addition to our Europe-wide measures of breakdown rates, we characterized the structure of invertebrate communities in 10 Irish streams that spanned the entire continental nutrient gradient (*21*). Condensing the principal gradient of invertebrate primary consumer relative abundance across these sites into a single ordination axis, via detrended canonical correspondence analysis (DCCA) (*22*), revealed the typical community response to pollution, from indicators of clean water (such as heptagenid mayflies) to those typical of polluted conditions (such as physid snails) (Fig. 2). This enabled us to plot invertebrate community structure against breakdown rate. The moderately enriched sites exhibited the fastest breakdown and were characterized by the largest consumer taxa (Fig. 2), whose abundance was a strong predictor of breakdown rate (fig. S6). This integrated community gradient yielded clearer unimodal relationships to our functional measure (R^2 all > 0.88, P < 0.001) (Fig. 2) than to either nutrient alone (SRP, R^2 = 0.66 to 0.79, P = 0.04 to 0.004; DIN, not significant).

The rising part of the unimodal curve likely resulted from nutrient stimulation of microbes and subsequent increased consumption of leaf litter by invertebrates. In contrast, the falling portion probably reflects deteriorating environmental conditions suppressing invertebrate-mediated breakdown (for example, chemical and habitat conditions associated with high BOD_5) (fig. S1), suggesting that increases in detrimental pollution syndromes (such as oxygen depletion, smothering, or disappearance of sensitive invertebrate taxa) might counteract the stimulating effects of nutrients (*23*). Because breakdown at moderately enriched sites was released from constraints of both nutrient limitation and stressors accompanying excess nutrient supply, other drivers, including biological community structure (*24, 25*), clearly assume importance here. This poses challenges—and also provides opportunities—to stream assessment and management because most European streams and rivers lie in this zone of

maximum uncertainty (Fig. 1 and fig. S1). For example, increased breakdown rates in slightly enriched streams would indicate altered ecosystem functioning, although most managers would consider such streams ecologically intact on the basis of traditional assessment criteria. Conversely, low breakdown rates at moderately enriched sites are no guarantee that streams are unaffected, requiring comprehensive assessments based on a range of indicators in order to draw conclusions about ecosystem impairment.

Our results raise fundamental questions about how to determine ecosystem health. First, naturally low-nutrient conditions are the desired state that water resource managers aspire to, and yet breakdown rates in such systems were indistinguishable from those in heavily polluted streams. This suggests that ensuring both low-nutrient water and effective resource use in stream food webs (from leaf litter to detritivores to fish) coupled with high process rates might be irreconcilable goals in stream management. Second, stream managers currently rely primarily on structural measures to assess stream ecosystem health. In particular, changes in biological community structure (invertebrates, fish, and algae) have long underpinned stream bioassessment schemes because they provide a reliable time-integrated response to stressors such as organic pollution or acidification (*5*), but biogeographical constraints make this approach difficult to standardize at large scales (*10*). Litter breakdown can help here because biogeography is a minor issue (for example, black alder or similar species of the genus are common throughout most of Europe and the Holarctic), and marked changes in breakdown rate occurred in the rising portion of the pollution gradient, in which established structural measures (such as water chemistry, hydromorphology, and metrics based on fish, invertebrate, or algal communities) are typically least sensitive. Consequently, litter breakdown—and potentially other functional measures such as whole-ecosystem metabolism, nutrient spiraling, or primary production (*26*–*28*)—can be used to complement, not replace, established procedures to assess stream ecosystem health. This highlights the need for differential diagnoses in environmental assessment, as is standard practice in medicine. Importantly, litter breakdown and some other functionally based methods can be implemented at relatively little cost or resource input (*29*) in order to assess effects of pollution and other ecosystem impacts that are of concern to environmental managers and stakeholders.

Increasing human pressure is accelerating environmental change throughout the world, threatening water security for humans and aquatic biodiversity (*2*). Large stretches of the landscape in Europe and other parts of the world are characterized today by highly industrialized, intensively managed agriculture and the large-scale application of fertilizers. This, in combination with other nutrient sources such as atmospheric deposition, has resulted in widespread nutrient pollution of aquatic ecosystems (*2*, *5*, *8*). Our study reveals that along with biodiversity losses, as fresh waters drift away from their natural conditions, ecosystem processes are profoundly changed, too. Impacts on stream functioning may go beyond the effects on litter breakdown because changing litter dynamics can have strong effects on nutrient retention and transformations (*27*), invertebrate productivity (*12*, *30*), and other functional ecosystem attributes. Given these complexities and large uncertainties surrounding human environmental impacts (*5*, *24*), a critical objective for the future will be to improve concepts and implementation tools to simultaneously manage surface waters sustainably and meet the demands of biodiversity conservation and environmental legislation.

References and Notes

1. A. M. Helton *et al.*, *Front. Ecol. Environ* **9**, 229 (2011)
2. C. J. Vorosmarty *et al.*, *Nature* **467**, 555 (2010)
3. E. S. Bernhardt *et al.*, *Science* **308**, 636 (2005)
4. P. H. Gleick, *Science* **302**, 1524 (2003)
5. N. Friberg *et al.*, *Adv. Ecol. Res* **44**, 2 (2011).
6. D. Hering *et al.*, *Sci. Total Environ.* **408**, 4007 (2010)
7. M. O. Gessner, E. Chauvet, *Ecol. Appl.* **12**, 498 (2002)
8. J. Hilton, M. O'Hare, M. J. Bowes, J. I. Jones, *Sci. Total Environ.* **365**, 66 (2006)
9. C. Perrings *et al.*, *Science* **330**, 323 (2010).
10. M. O. Gessner *et al.*, *Trends Ecol. Evol.* **25**, 372 (2010).
11. J. C. Moore *et al.*, *Ecol. Lett.* **7**, 584 (2004)
12. J. B. Wallace, S. L. Eggert, J. L. Meyer, J. R. Webster, *Science* **277**, 102 (1997)
13. J. L. Tank, E. J. Rosi-Marshall, N. A. Griffiths, S. A. Entrekin, M. L. Stephen, *J. N. Am. Benthol. Soc.* **29**, 118 (2010)
14. J. R. Webster, E. F. Benfield, *Annu. Rev. Ecol. Syst.* **17**, 567 (1986)
15. V. Gulis, K. Suberkropp, *Freshw. Biol.* **48**, 123 (2003)
16. A. D. Rosemond, C. M. Pringle, A. Ramirez, M. J. Paul, J. L. Meyer, *Limnol. Oceanogr.* **47**, 278 (2002)
17. C. F. Mason, *Biology of Freshwater Pollution* (Prentice-Hall, Upper Saddle River, NJ, ed. 4, 2002), p. 391
18. M. Bundschuh, T. Hahn, M. O. Gessner, R. Schulz, *Environ. Toxicol. Chem.* **28**, 197 (2009)
19. M. Hieber, M. O. Gessner, *Ecology* **83**, 1026 (2002)
20. C. Pascoal, M. Pinho, F. Cassio, P. Gomes, *Freshw. Biol* **48**, 2033 (2003)
21. Materials and methods are available as supplementary materials on *Science* Online.
22. C. J. F. ter Braak, P. Smilauer, *CANOCO Reference Manual and User's Guide to CANOCO for Windows: Software for Canonical Community Ordination* (Microcomputer Power, Ithaca NY, 1998)
23. A. Lecerf *et al.*, *Arch. Hydrobiol.* **165**, 105 (2006)
24. L. Boyero *et al.*, *Ecol. Lett.* **14**, 289 (2011)
25. S. Hladyz *et al.*, *Adv. Ecol. Res* **44**, 211 (2011)
26. R. G. Young, K. J. Collier, *Freshw. Biol.* **54**, 2155 (2009)
27. P. J. Mulholland, J. R. Webster, *J. N. Am. Benthol. Soc.* **29**, 100 (2010)
28. P. J. Mulholland *et al.*, *Nature* **452**, 202 (2008)
29. M. J. Feio, T. Alves, M. Boavida, A. Medeiros, M. A. S. Graça, *Freshw. Biol.* **55**, 1050 (2010)
30. W. F. Cross, J. B. Wallace, A. D. Rosemond, S. L. Eggert, *Ecology* **87**, 1556 (2006).

Acknowledgments: We thank the European Commission and the Swiss State Secretariat for Research and Education for funding the RivFunction research project (European Union contract EVK1-CT 2001-00088), which was supported under the Fifth Framework Programme. The constructive comments by three anonymous reviewers, which substantially improved the paper, are greatly appreciated. All basic data are available in the supplementary materials. This paper is dedicated to the memory of our colleague Björn Malmqvist, who sadly passed away in 2010.

Supplementary Materials
www.sciencemag.org/cgi/content/full/336/6087/1438/DC1
Materials and Methods
Figs. S1 to S6
Table S1
Reference (*31*)
Databases S1 and S2

23 January 2012; accepted 26 April 2012
10.1126/science.1219534

p53 Dynamics Control Cell Fate

Jeremy E. Purvis, Kyle W. Karhohs, Caroline Mock, Eric Batchelor,* Alexander Loewer,† Galit Lahav‡

Cells transmit information through molecular signals that often show complex dynamical patterns. The dynamic behavior of the tumor suppressor p53 varies depending on the stimulus; in response to double-strand DNA breaks, it shows a series of repeated pulses. Using a computational model, we identified a sequence of precisely timed drug additions that alter p53 pulses to instead produce a sustained p53 response. This leads to the expression of a different set of downstream genes and also alters cell fate: Cells that experience p53 pulses recover from DNA damage, whereas cells exposed to sustained p53 signaling frequently undergo senescence. Our results show that protein dynamics can be an important part of a signal, directly influencing cellular fate decisions.

Cells use molecular signaling networks to sense, interpret, and respond to stimuli. Recent advances in time-lapse microscopy have revealed that many signaling molecules show complex dynamical behaviors (*1*–*13*). In some instances, dynamical properties such as oscillation frequency or signal duration, have been shown to alter gene expression (*1*, *3*, *6*, *8*, *11*, *13*–*16*) or to control cellular differentiation (*7*, *12*, *17*). These examples point to a rich mode of regula-

tion that is largely unexplored for most biological pathways. We developed a mathematically designed perturbation of p53 dynamics in response to DNA damage and have shown experimentally that p53 dynamics determine cellular responses.

p53 is a tumor suppressor activated in response to cellular stress (*18*, *19*). Induction of p53 triggers multiple cellular programs ranging from transient responses, such as DNA repair and cell cycle arrest, to terminal fates such as cell death (apoptosis) and permanent cell cycle arrest (senescence) (Fig. 1A). Recently, it was shown that different stresses evoke different dynamic patterns of p53 protein levels (Fig. 1B) (*20*). In response to DNA breaks caused by γ-irradiation, the levels of p53 exhibit a series of pulses with fixed amplitude and frequency (*4*, *21*). Higher radiation doses increase the number of pulses without affecting their amplitude or duration.

Department of Systems Biology, Harvard Medical School, Boston, MA 02115, USA.

*Present address: Laboratory of Pathology, National Cancer Institute, National Institutes of Health, Bethesda, MD 20892, USA.

†Present address: Berlin Institute for Medical Systems Biology, Max Delbrueck Center for Molecular Medicine, Berlin-Buch 13125, Germany.

‡To whom correspondence should be addressed. E-mail: galit@hms.harvard.edu

These p53 pulses were observed in a live mouse model (*22*) and in various transformed and nontransformed human cell lines (*23*–*25*). In contrast, ultraviolet (UV) radiation triggers a single p53 pulse with a dose-dependent amplitude and duration (*20*). Although much insight has been gained into the molecular mechanisms that control these differential p53 dynamics in response to γ and UV radiation (*20*, *25*, *26*), the effect of p53 dynamics on downstream responses remains unknown. UV and γ radiation activate distinct targets of p53 (*27*) and lead to different cellular outcomes (Fig. 1B), suggesting that downstream elements in the p53 network may respond to the dynamic profiles of p53. However, γ and UV radiation also lead to many p53-independent events in cells, which could contribute to the differential outcomes. A definitive conclusion about the role of p53 dynamics on cellular outcomes may come from experimentally perturbing p53 dynamics in response to the same stress and observing the effect on downstream responses.

We developed a method for altering p53 dynamics after γ-irradiation. Our goal was to switch p53 natural pulses into a sustained p53 signal held at the peak pulse amplitude (Fig. 1C). We used the small molecule Nutlin-3, which binds to the p53 inhibitor Mdm2, inhibiting degradation of the p53 protein (*28*). Nutlin-3 is selective for p53 because p53$^{-/-}$ cells show no change in genome-wide expression profiling upon Nutlin-3 treatment (*29*). Achieving a sustained signaling response with a single Nutlin-3 treatment proved to be difficult: *MDM2* is activated by p53, and therefore, addition of Nutlin-3 not only stabilizes p53 but also causes an increase in Mdm2 levels that eventually overcomes Nutlin-3 inhibition, resulting in down-regulation of p53 (fig. S1). Treatment with a higher dose of Nutlin-3 led to prolonged induction of p53 but also to an overshoot in p53 levels (fig. S1). To overcome this obstacle, we trained our model of p53 dynamics (*26*) to predict the optimal sequence of Nutlin-3 additions necessary to sustain p53 at a constant level (Fig. 1D, fig. S2, and tables S1 and S2). The model predicted that three sequential treatments of Nutlin-3 at 2.5 hours (0.75 μM), 3.5 hours (2.25 μM), and 5.5 hours (4 μM) after γ-irradiation would produce a sustained p53 response with an amplitude equal to p53 natural pulses. This prediction was validated experimentally in both cell populations and single cells (Fig. 1E and fig. S3). These two dynamical "inputs"—naturally pulsed and pharmacologically sustained p53 signaling (hereafter, "pulsed" and "sustained")—were then used to study the downstream effects of p53 dynamics on target gene expression and cellular outcome.

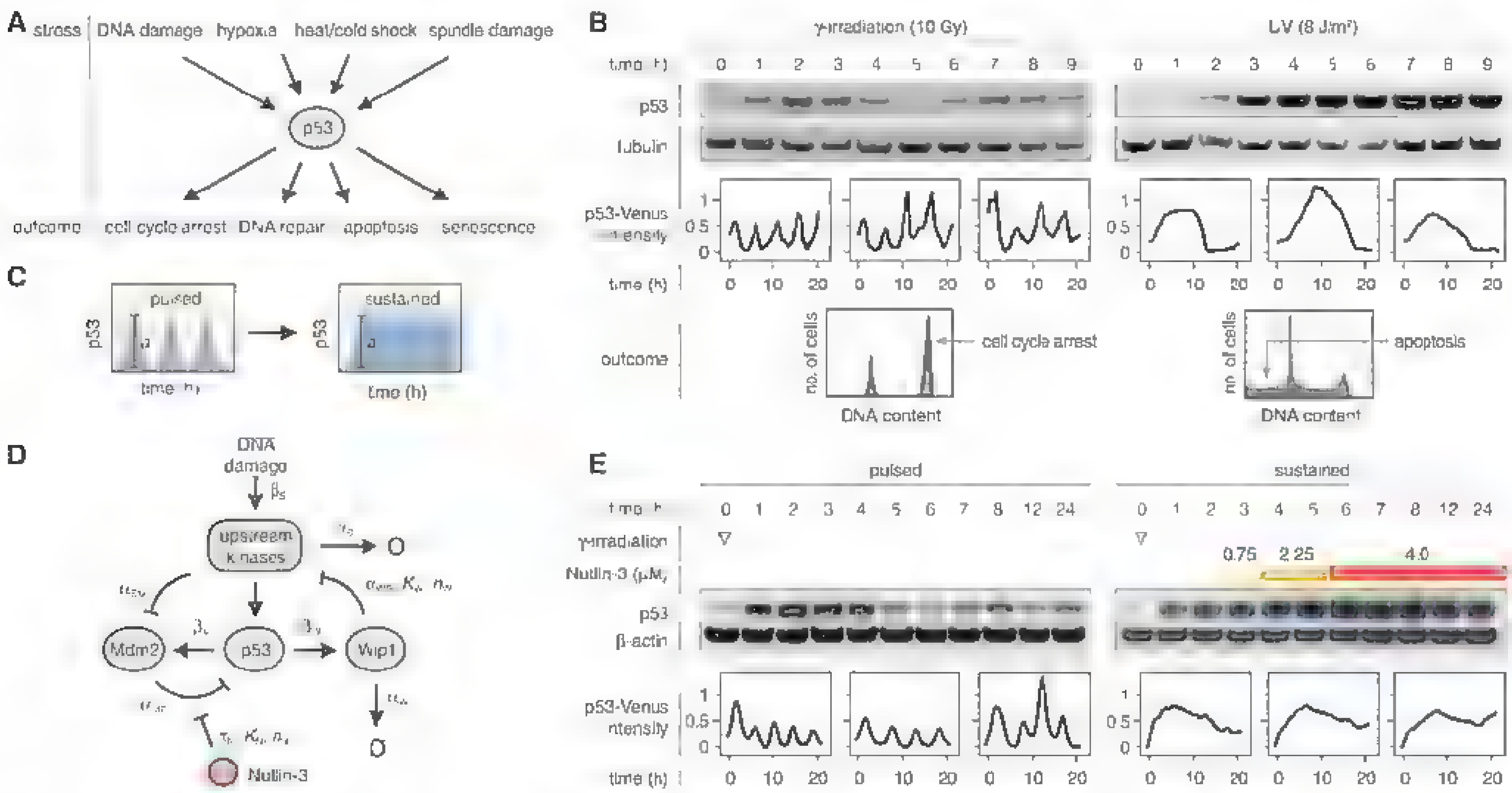

Fig. 1. Perturbation of p53 dynamics. (**A**) p53 mediates the response to multiple cellular stresses and evokes diverse cellular outcomes. (**B**) γ-irradiation leads to p53 pulses and cell cycle arrest; UV radiation induces a single prolonged pulse and leads to apoptosis. (**C**) p53's natural pulses were perturbed to produce a sustained response with equal amplitude, *a*. (**D**) A diagram capturing the main species and parameters in the mathematical model of p53 dynamics after DNA damage (*26*). This model was used to predict the optimal sequence of Nutlin-3 additions needed to generate a sustained p53 response after γ-irradiation (supplementary materials). (**E**) p53 dynamics under (left) naturally pulsed or (right) pharmacologically sustained conditions. The sequence of Nutlin-3 treatments is denoted by differently colored bars. Pulses in immunoblots appear as damped oscillations because of the asynchronous responses of single cells. Representative single-cell traces show average nuclear p53-Venus intensities that were normalized to the median value and zeroed to the minimum value. Sequential Nutlin-3 treatment did not alter the amplitude of p53 (fig. S3).

To understand how p53 dynamics control gene expression, we selected a panel of well-studied p53 target genes representing different functional pathways and cellular outcomes (*30*). A subset of genes showed a clear oscillatory response that mirrored p53 protein dynamics (Fig. 2, A and B, and table S3). This group included genes involved in cell cycle arrest and DNA repair (*CDKN1A*, *GADD45A*, and *XPC*), as well as genes known to regulate p53 levels (*MDM2* and *PPM1D*). In contrast, transcripts encoding apoptotic proteins (*APAF1*, *BAX*, and *TP53AIP*) or involved in p53-dependent senescence (*PML* and *YPEL3*) (*31*, *32*) were not induced by p53 pulses (Fig. 2, C and D).

We next measured expression of these transcripts using our dynamic drug treatment (Fig. 1E) to sustain p53 signaling. Oscillating genes (such as *MDM2* and *CDKN1A*) showed sustained increases in expression. Genes involved in apoptosis or senescence—which were not induced by p53 pulses—showed either no induction (*APAF1* and *TP53AIP1*) or a delayed increase in expression (*BAX*, *PML*, and *YPEL3*) under sustained p53 signaling. These trends were p53-dependent (fig. S4). Taken together, these results indicate that p53 pulses selectively activate genes involved in transient responses to DNA damage, whereas sustained p53 signaling allows induction of genes associated with terminal fates.

We next asked whether changes in p53 dynamics lead to different cell fates—specifically, whether sustained p53 will trigger irreversible fates such as apoptosis or senescence, whereas pulsed p53 will allow recovery and growth. DNA content analysis by means of flow cytometry revealed only a small amount of cell death under both pulsed and sustained p53 conditions (fig. S5). We therefore pursued the alternate possibility that sustained p53 signaling promotes cellular senescence, a state of permanent cell cycle arrest (*33*, *34*). Cells were subjected to pulsed or sustained p53 signaling at several γ-irradiation doses and then assayed for senescence-associated β-galactosidase (β-gal) activity and their ability to proliferate in fresh growth media (fig. S6). At lower doses of γ-irradiation [2.5 and 5 grays (Gy)], sustained p53 signaling led to large increases in β-gal–positive cells (Fig. 3, A and B). At these levels of DNA damage, the majority of cells exposed to pulsed p53 were able to undergo multiple rounds of growth and division after recovery (Fig. 3, C to E, and fig. S7), whereas sustained p53 signaling reduced this fraction substantially, leading to a characteristically flattened morphology and an apparent inability to divide (Fig. 3C). These differences were most pronounced after 5 Gy of γ-irradiation—a dose at which nearly all cells showed a permanent arrest after sustained p53 signaling (Fig. 3, D and E). Sustained p53 signaling at 2.5 Gy led to a greater fraction of senescent cells than did pulsed p53 at 5 Gy (Fig. 3, B and E), suggesting that it is not the extent of DNA damage that induces senescence, but rather the dynamics of p53 signaling.

We did not observe a large difference in β-gal activity or in proliferative ability at the highest dose of γ-irradiation (10 Gy). This suggested that prolonged p53 pulsing (*4*, *21*, *25*) caused by extensive DNA damage might eventually lead to expression of senescence genes. Indeed, we found that after 3 days under pulsed conditions, the p53-dependent senescence genes were induced to similar levels reached under sustained conditions after 1 day (Fig. 3F). *CDKN1A*, which is involved in both cell cycle arrest and p53-dependent senescence (*33*, *34*), showed the most dramatic increase in expression (>100-fold) under sustained p53 signaling.

Thus, sustained p53 signaling appears to accelerate the expression of senescence genes, whereas pulsed p53 delays gene expression and so protects cells from prematurely committing to an irreversible fate. However, by the time a cell commits to senescence the total amount of p53 accumulated over time ("cumulative p53") is

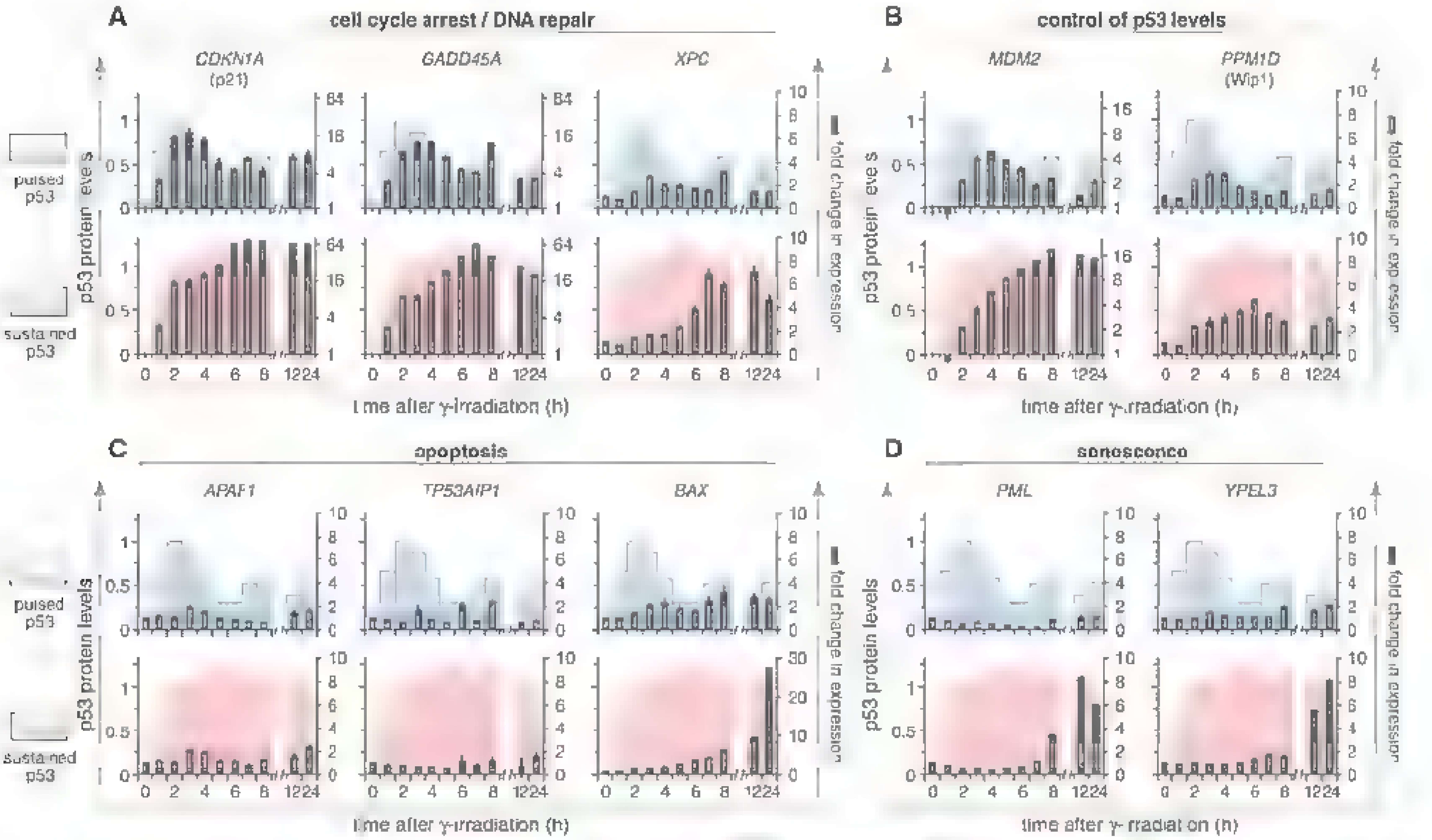

Fig. 2. Pulsed and sustained p53 signaling activate different sets of target genes. Expression of p53 target genes was measured under pulsed or sustained conditions after γ-irradiation. Genes are grouped according to function: **(A)** cell cycle arrest and DNA repair, **(B)** control of p53 levels, **(C)** apoptosis, and **(D)** senescence. For reference, p53 protein levels are shown in the background as light blue (pulsed) or red (sustained) bars. p53 levels are normalized to the peak ($t = 2$ hours) p53 concentration. A base-2 logarithmic scale is used for *CDKN1A*, *GADD45A*, and *MDM2*. Data are mean ± SD. Significance of correlation between target genes and p53 protein levels under pulsed conditions is reported in table S3.

much higher under sustained conditions than in pulsing cells. To determine whether this change in cell fate is due to p53 dynamics or merely to an increase in cumulative p53, we compared expression of senescence genes between pulsed and sustained p53 at equivalent levels of cumulative p53 (Fig. 4A). We found that even for similar cumulative p53, sustained p53 signaling led to higher expression of its target genes than pulsed p53, suggesting that it is the dynamics of p53 rather than its accumulated levels that control gene expression.

We further tested this in single cells. We first showed that individual senescent cells have significantly higher levels of *CDKN1A* and *PML* transcripts than those of proliferating cells (fig. S8), confirming that these transcripts are reliable markers for the induction of senescence. We then quantified p53 dynamics under pulsed and sustained conditions and used fluorescence in situ hybridization (FISH) to compare the level of *CDKN1A* and *PML* (Fig. 4, B and C). To achieve comparable cumulative p53 levels between pulsed and sustained p53, we terminated pulsed p53 21 hours after irradiation (t_1) and sustained p53 12 hours after irradiation (t_2) (Fig. 4D). We found that expression of both *CDKN1A* and *PML* was significantly higher under sustained p53 than under pulsed p53 even at similar cumulative p53 levels (Fig. 4, E and F). These results suggest that the decision of whether and when to enter senescence is communicated to cells through the temporal pattern of p53 (Fig. 4G).

It is well established that different posttranslational modifications of p53 or different cofactors that bind p53 affect the choice of downstream gene programs (*35*). Here, we have shown another mechanism for specificity in this network: the dynamics of p53. Our work suggests that p53 dynamics are important but do not act alone: p53 signaling produced by γ-irradiation and Nutlin-3 leads to senescence, whereas a comparable dynamical profile in response to UV radiation leads to apoptosis (Fig. 1B). Future studies are required to explore the combined effect of p53 dynamics and modifications on cellular outcomes.

What molecular mechanism may decode p53 dynamics to determine cell fate? One hypothesis is that p53 pulses periodically exceed a threshold concentration for transcriptional activation of senescence genes. In this scenario, sustained p53 or a greater number of p53 pulses increases the probability that p53 will activate downstream targets that are involved in the induction of senescence. A similar mechanism was previously reported (*14*), in which the frequency of calcium oscillations controls specificity for activation of proinflammatory transcription factors. Another plausible mechanism involves a feed-forward loop motif that discriminates transient and persistent p53 signaling. This type of mechanism was identified in the extracellular signal-related kinase (ERK) signaling pathway, in which the early gene product c-Fos functions as a sensor for sustained ERK levels (*17*). By analogy, an early gene induced by p53 and essential for activating senescence with p53 may decay with a time scale close to the time scale of p53 pulses and therefore accumulates slowly during p53 pulses, but more rapidly during a sustained p53 response. It is also possible that expression of senescence genes is initially repressed, for example, by epigenetic silencing or antisense RNA, and that these factors are deactivated by persistent p53 signaling.

Other signaling pathways have been shown to encode information through the dynamics of their signaling molecules (*1–3*, *5–13*), suggesting that varying protein dynamics may offer a functional advantage in certain contexts. For example, information encoded in the dynamics, rather than the absolute concentration of a signaling molecule, may be less sensitive to spontaneous fluctuations in the cellular environment. In addition, certain dynamical patterns may allow neighboring cells to synchronize their responses to produce emergent multicellular behaviors. A better understanding of how signaling dynamics are regulated and how they affect cellular responses will provide new insights for manipulating them in a controlled way. In addition, targeted perturbation of protein dynamics, such as the one illustrated in this study, may enable new pharmacological strategies for altering cell fate in a range of diseases.

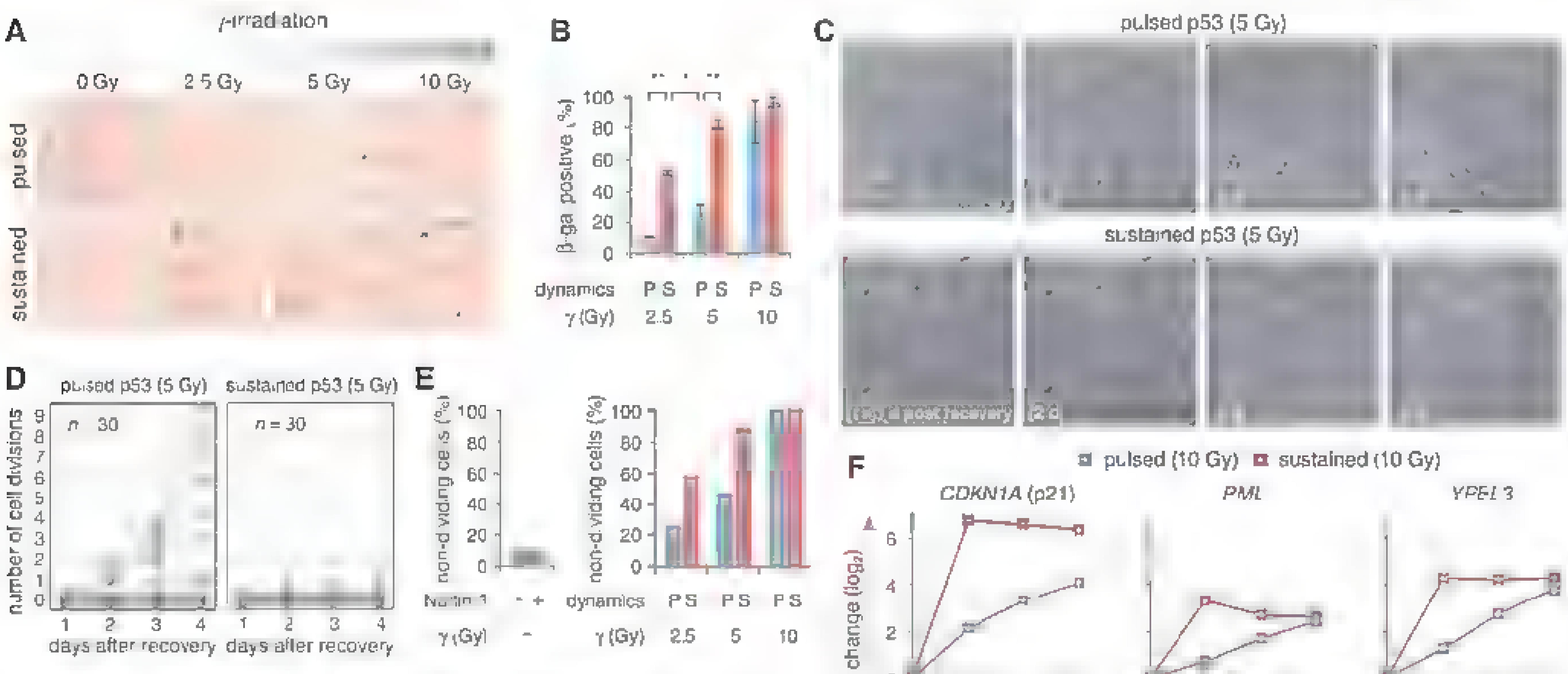

Fig. 3. Pulsed and sustained p53 signaling lead to different cell fates. **(A)** Cells were subjected to pulsed (top) or sustained (bottom) conditions for 3 days and then stained for β-gal activity 1 day after recovery. Blue color and flattened morphology are indicative of senescence. **(B)** Percentage of β-gal-positive cells under pulsed (P) or sustained (S) p53 signaling at various γ-irradiation doses. $n \geq 100$ cells per condition per experiment. $^{*}P < 0.05$, $^{**}P < 0.01$. **(C)** Typical images of single cells that were recovered after 3 days of pulsed (top) or sustained (bottom) p53 signaling at 5 Gy γ-irradiation. White boxes are drawn to show the fate of an individual cell. **(D)** Number of cell divisions for single cells after recovery from pulsed or sustained p53 signaling at 5 Gy. **(E)** (Left) Percentage of cells that did not divide under resting conditions or sequential Nutlin-3 treatment alone (no γ-irradiation). (Right) Percentage of nondividing cells under pulsed (P) or sustained (S) p53 signaling. **(F)** Fold change in expression of *CDKN1A*, *PML*, and *YPEL3* after 24, 48, and 72 hours under pulsed (blue) or sustained (red) p53 signaling (10 Gy γ-irradiation). Expression levels were normalized to *ACTB*. Data are mean ± SD.

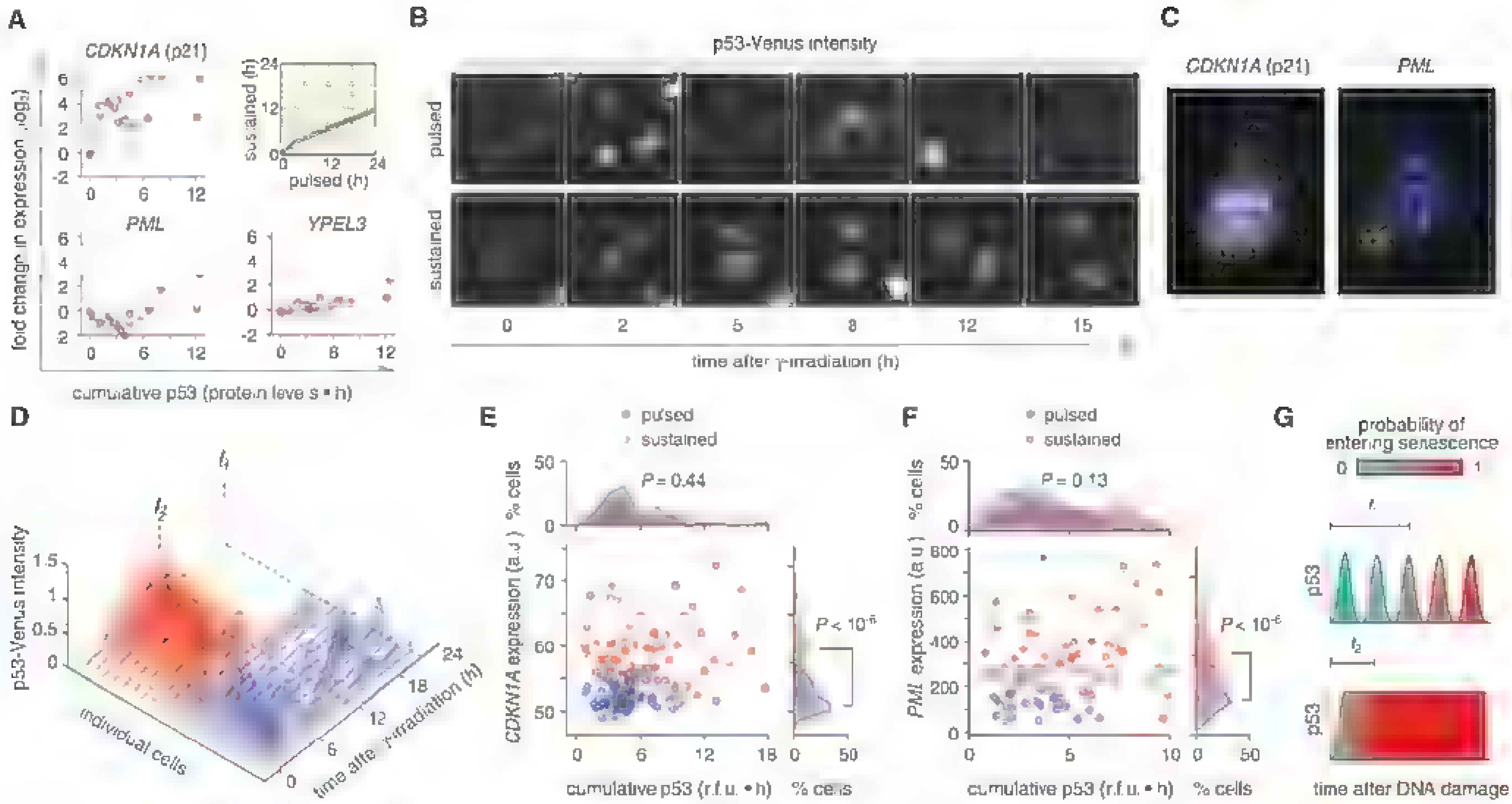

Fig. 4. p53 dynamics, and not its cumulative level, control cell fate. **(A)** (Inset) Time points for which pulsed and sustained p53 signaling show equivalent cumulative p53 levels [$\int p53(t)dt$] lie along the gray line. Gene expression under pulsed (blue dots) or sustained (red dots) p53 signaling are plotted as a function of cumulative p53 by using the data presented in Fig. 1E. The time integral of p53 protein levels was computed by using trapezoidal integration of p53 levels over time. Gene expression was normalized to *ACTB*. The last time point in sustained conditions (24 hours) was omitted because there is no comparable data point under pulsed conditions. **(B)** p53 dynamics were recorded by means of live-cell microscopy under pulsed and sustained conditions. **(C** and **D)** Representative single-cell traces of p53 levels under (blue) pulsed or (red) sustained conditions. Time-lapse imaging was terminated by fixing cells 21 hours after irradiation (pulsed conditions, t_1) or 12 hours after irradiation (sustained conditions, t_2) and probing for expression of *CDKN1A* or *PML* by means of FISH. **(E)** *CDKN1A* and **(F)** *PML* expression versus cumulative p53 in individual cells. a.u., arbitrary units; r.f.u., relative fluorescence units (supplementary materials). **(G)** Model for p53 dynamics controlling cell fate. Transient damage encountered under low-radiation dose or physiological conditions is repaired quickly and generates a small number of p53 pulses, allowing the cell to continue dividing. Persistent damage—whether from a large number of initial DNA lesions or a small number of irreparable breaks—generates repeated p53 pulses that ultimately trigger cellular senescence. t_1 and t_2 represent time points in which the cumulative level of p53 is equal between pulsed and sustained conditions. However, the probability of entering senescence differs between these two types of dynamics. Pulsed p53 allows more time for recovery from DNA damage, whereas sustained p53 accelerates this process.

References and Notes

1. L. Cai, C. K. Dalal, M. B. Elowitz, *Nature* **455**, 485 (2008).
2. N. Hao *et al.*, *Mol. Cell* **30**, 649 (2008).
3. A. Hoffmann, A. Levchenko, M. L. Scott, D. Baltimore, *Science* **298**, 1241 (2002).
4. G. Lahav *et al.*, *Nat. Genet.* **36**, 147 (2004).
5. J. T. Mettetal, D. Muzzey, C. Gómez-Uribe, A. van Oudenaarden, *Science* **319**, 482 (2008).
6. D. E. Nelson *et al.*, *Science* **306**, 704 (2004).
7. G. M. Suel, J. Garcia-Ojalvo, L. M. Liberman, M. B. Elowitz, *Nature* **440**, 545 (2006).
8. S. Tay *et al.*, *Nature* **466**, 267 (2010).
9. J. J. Ventura *et al.*, *Mol. Cell* **21**, 701 (2006).
10. T. K. Lee *et al.*, *Sci. Signal.* **2**, ra65 (2009).
11. S. L. Werner, D. Barken, A. Hoffmann, *Science* **309**, 1857 (2005).
12. S. D. Santos, P. J. Verveer, P. I. Bastiaens, *Nat. Cell Biol.* **9**, 324 (2007).
13. L. Ashall *et al.*, *Science* **324**, 242 (2009).
14. R. E. Dolmetsch, K. Xu, R. S. Lewis, *Nature* **392**, 933 (1998).
15. M. H. Sung *et al.*, *PLoS ONE* **4**, e7163 (2009).
16. N. Hao, E. K. O'Shea, *Nat. Struct. Mol. Biol.* **19**, 31 (2012).
17. L. O. Murphy, S. Smith, R. H. Chen, D. C. Fingar, J. Blenis, *Nat. Cell Biol.* **4**, 556 (2002).
18. H. F. Horn, K. H. Vousden, *Oncogene* **26**, 1306 (2007).
19. B. Vogelstein, D. Lane, A. J. Levine, *Nature* **408**, 307 (2000).
20. E. Batchelor, A. Loewer, C. Mock, G. Lahav, *Mol. Syst. Biol.* **7**, 488 (2011).
21. N. Geva-Zatorsky *et al.*, *Mol. Syst. Biol.* **2**, 2006.0033 (2006).
22. D. A. Hamstra *et al.*, *Cancer Res.* **66**, 7482 (2006).
23. W. Hu *et al.*, *Cancer Res.* **67**, 2757 (2007).
24. R. Lev Bar-Or *et al.*, *Proc. Natl. Acad. Sci. U.S.A.* **97**, 11250 (2000).
25. A. Loewer, E. Batchelor, G. Gaglia, G. Lahav, *Cell* **142**, 89 (2010).
26. E. Batchelor, C. S. Mock, I. Bhan, A. Loewer, G. Lahav, *Mol. Cell* **30**, 277 (2008).
27. R. Zhao *et al.*, *Genes Dev.* **14**, 981 (2000).
28. L. T. Vassilev *et al.*, *Science* **303**, 844 (2004).
29. C. Tovar *et al.*, *Proc. Natl. Acad. Sci. U.S.A.* **103**, 1888 (2006).
30. T. Riley, E. Sontag, P. Chen, A. Levine, *Nat. Rev. Mol. Cell Biol.* **9**, 402 (2008).
31. E. de Stanchina *et al.*, *Mol. Cell* **13**, 523 (2004).
32. K. D. Kelley *et al.*, *Cancer Res.* **70**, 3566 (2010).
33. J. Campisi, F. d'Adda di Fagagna, *Nat. Rev. Mol. Cell Biol.* **8**, 729 (2007).
34. F. d'Adda di Fagagna, *Nat. Rev. Cancer* **8**, 512 (2008).
35. A. M. Bode, Z. Dong, *Nat. Rev. Cancer* **4**, 793 (2004).

Acknowledgments: We thank R. Agami for the MCF7/p53shRNA cell line; B. Fang for the MCF7/Casp3 cell line; A. Raj and Z. Waks for help with mRNA FISH; R. Kishony, R. Ward, W. Forrester, E. O'Shea, T. Mitchison, A. Klein, J. Orth, and U. Alon for comments and discussions; and the Nikon Imaging Center at Harvard Medical School for help with light microscopy. This research was supported by the Novartis Institutes for Biomedical Research, the National Institutes of Health grant GM083303 and fellowship F32GM095168 (J.E.P.), a National Science Foundation graduate fellowship (K.W.K.), the American Cancer Society, California Division, Pamela and Edward Taft Postdoctoral Fellowship (E.B.), and fellowships from the German Research Foundation and the Charles A. King Trust (A.L.). J.E.P. and G.L. conceived the study, designed the experiments, and wrote the paper. J.E.P. modeled and designed perturbation experiments and performed gene expression and cell fate assays, live-cell microscopy, single-cell mRNA detection, and image analysis. K.W.K. performed live-cell microscopy, single-cell mRNA detection, and image analysis. C.M. characterized p53 and p53-Venus dynamics under radiation and various drug treatments. E.B. and A.L. performed UV treatment experiments and provided preliminary results and foundational concepts.

Supplementary Materials

www.sciencemag.org/cgi/content/full/336/6087/1440/DC1
Materials and Methods
Figs. S1 to S8
Tables S1 to S5
References (*36*, *37*)

22 December 2011; accepted 1 May 2012
10.1126/science.1218351

A Histone Acetyltransferase Regulates Active DNA Demethylation in *Arabidopsis*

Weiqiang Qian,[1,2]* Daisuke Miki,[1]* Heng Zhang,[1,2] Yunhua Liu,[2,3] Xi Zhang,[4] Kai Tang,[2] Yunchao Kan,[5] Honggui La,[1,2] Xiaojie Li,[6] Shaofang Li,[7] Xiaohong Zhu,[2] Xiaobing Shi,[4] Kangling Zhang,[8] Olga Pontes,[9] Xuemei Chen,[7] Renyi Liu,[7] Zhizhong Gong,[6] Jian-Kang Zhu[1,2]†

Active DNA demethylation is an important part of epigenetic regulation in plants and animals. How active DNA demethylation is regulated and its relationship with histone modification patterns are unclear. Here, we report the discovery of IDM1, a regulator of DNA demethylation in *Arabidopsis*. IDM1 is required for preventing DNA hypermethylation of highly homologous multicopy genes and other repetitive sequences that are normally targeted for active DNA demethylation by Repressor of Silencing 1 and related 5-methylcytosine DNA glycosylases. IDM1 binds methylated DNA at chromatin sites lacking histone H3K4 di- or trimethylation and acetylates H3 to create a chromatin environment permissible for 5-methylcytosine DNA glycosylases to function. Our study reveals how some genes are indicated by multiple epigenetic marks for active DNA demethylation and protection from silencing.

Epigenetic control of gene expression involves dynamic regulation of DNA methylation and histone modification marks (*1*, *2*). A DNA repair–based mechanism functions in active DNA demethylation in plants and possibly in animals as well (*3*). In plants, active DNA demethylation is initiated by a family of 5-methylcytosine DNA glycosylases that includes ROS1, DME, DML2, and DML3 (*3*). Although a large body of literature concerns the regulation of DNA methylation by histone modification patterns (*1*, *2*), little is known about the regulation of active DNA demethylation.

[1]Shanghai Center for Plant Stress Biology and Shanghai Institute of Plant Physiology and Ecology, Shanghai Institutes of Biological Sciences, Chinese Academy of Sciences, China. [2]Department of Horticulture and Landscape Architecture, Purdue University, West Lafayette, IN 47906, USA. [3]College of Plant Sciences and Technology, Huazhong Agricultural University, Wuhan, and Shanghai Agrobiological Gene Center, Shanghai 201106, China. [4]Department of Biochemistry and Molecular Biology, The University of Texas M. D. Anderson Cancer Center, Houston, TX 77030, USA. [5]China-UK-NYNU-RRes Joint Laboratory of Insect Biology, Nanyang Normal University, Henan, China. [6]State Key Laboratory of Plant Physiology and Biochemistry, College of Biological Sciences, China Agricultural University, Beijing 100193, China. [7]Department of Botany and Plant Science, University of California, Riverside, CA 92521, USA. [8]Department of Biochemistry, School of Medicine, Loma Linda University, Loma Linda, CA 92350, USA. [9]Department of Biology, University of New Mexico, Albuquerque, NM 87131, USA.

*These authors contributed equally to this work.

†To whom correspondence should be addressed. E-mail: jkzhu@purdue.edu

We developed a polymerase chain reaction (PCR)–based marker for reporting DNA methylation status at the 3′ region of *At1g26400* (also referred to as *DT-77*) (*4*). This marker suggests that the *At1g26400* region is hypermethylated in *ros1* mutant alleles (Fig. 1A). We screened a population of homozygous transferred DNA (T-DNA) insertion lines of *Arabidopsis* for DNA hypermethylation mutants. Two of the identified mutants (Fig. 1A), referred to as *idm1* (for increased DNA methylation 1), have T-DNA insertions in the gene *At3g14980* (fig. S1A). Bisulfite sequencing showed that, compared to the Col wild-type control, the *idm1* and *ros1-4* mutants have higher levels of DNA methylation in all sequence contexts at *DT-77* (Fig. 1B). There is also increased CG and CHG (where H is C, A, or T) methylation at the *At4g18650* gene promoter, which was previously shown to be targeted for demethylation by ROS1 (*5*) (Fig. 1C). ROS1 was originally identified because it is required for preventing the *RD29A-LUC* and *35S-NPTII* transgenes from transcriptional silencing (*6*). From an independent genetic screen for mutants impaired in the prevention of silencing of the *35S-NPTII* transgene, we found the *idm1-3* mutation that changes glutamic acid-451 to a premature stop codon and causes the silencing of *35S-NPTII* but not the *RD29A-LUC* transgene (fig. S2).

Double-mutant analysis indicated that the DNA hypermethylation phenotypes of *ros1-4* and *idm1-1* are not additive (Fig. 1, B and C, and fig. S3A). These results suggest that IDM1 and ROS1 may function in the same genetic pathway to prevent DNA hypermethylation. Quantitative reverse transcription PCR analysis showed that *ROS1* or *ROS3* expression is not reduced in the *idm1* mutants (fig. S4A). In addition, like *ROS1* (*3*), *IDM1* expression level was reduced in RNA-directed DNA methylation (RdDM) pathway mutants (fig. S4B), which suggests that *IDM1* expression is sensitive to non-CG methylation. The hypermethylation in *idm1-1* at CHG and CHH sequence contexts could be suppressed by the *nrpd1-3* mutation (*7*), suggesting that the methylation at both *DT-77* and *At4g18650* promoter is caused by RdDM (Fig. 1, B and C).

Southern blot analysis showed that *idm1* does not affect the DNA methylation at *5S* or *45S* ribosomal DNA or at the 180–base pair centromeric repeat (fig. S5). We compared the genome-wide DNA methylation profiles of *idm1-1* and wild-type plants. There was no significant difference between *idm1-1*, *ros1-4*, or *ros1-3dml2-1dml3-1* (*rdd*) (*8*) and wild-type plants in their overall genome methylation patterns (fig. S6). We identified 1098, 4991, and 9290 loci where DNA methylation levels are increased significantly in *idm1-1*, *ros1-4*, and *rdd*, respectively (tables S1 to S3). In contrast, only 75, 106, and 1052 loci were found to have a decreased DNA methylation in *idm1-1*, *ros1-4*, and *rdd*, respectively (tables S4 to S6). Out of the 1098 hypermethylated loci in *idm1-1* (referred herein as DT loci for demethylation target loci), seven were selected for validation by individual locus bisulfite sequencing and were all confirmed to be hypermethylated in *idm1-1* as well as *ros1-4* or

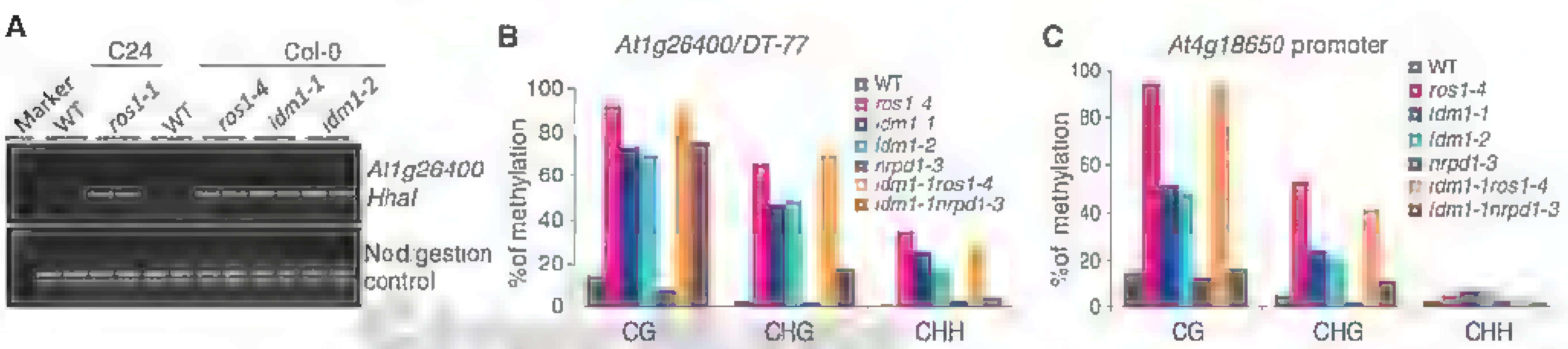

Fig. 1. Identification and characterization of the *idm1* mutants. (**A**) Analysis of DNA methylation level at the *At1g26400* locus by chop-PCR (*4*). Undigested DNA is shown as a control. (**B** and **C**) Bisulfite sequencing data showing the effects of *idm1* mutations on *At1g26400* (B) and *At4g18650* (C) DNA methylation in different sequence contexts and genetic interactions with *ros1* or *nrpd1*. WT, wild type.

rdd (fig. S3). The DT loci are distributed across the five chromosomes (fig. S7A), are enriched in small RNAs (fig. S7B), and the majority of them overlap with repeats (table S1 and fig. S8). Genic loci account for ~80% of the DT loci in *idm1-1* (fig. S7C). The hypermethylation in genic regions in *idm1-1* mutant plants is not restricted to CGs (Fig. 1, B and C, and fig. S3). More than half of these hypermethylated genic loci in *idm1-1* are in multigene families where the member genes are highly homologous.

About 52% and 63% of the 1098 hypermethylated loci in *idm1-1* are also hypermethylated in the *ros1-4* and *rdd* mutants, respectively, based on the methylome analysis (table S1 and fig. S7D). As a comparison, the same analysis showed that ~81% (as opposed to a theoretical 100%) of the hypermethylated loci in *ros1-4* overlap with those in *rdd* (table S2 and fig. S7D). Three loci that were identified as hypermethylated in *idm1-1* but not *ros1-4* or *rdd* were analyzed by individual locus bisulfite sequencing (fig. S3B). The analysis shows that all of them are hypermethylated in *ros1* or *rdd* as well as in *idm1*. In addition, four other loci that were identified as hypermethylated in the *rdd* mutant but not in *idm1-1* in the DNA methylome study were tested by individual locus bisulfite sequencing and found hypermethylated in *idm1-1* (Fig. 1C and fig. S3). These results suggest that the actual number of hypermethylated loci in *idm1-1* is larger and the percentage of overlap with the hypermethylated loci in the *rdd* mutant is likely higher. It thus appears that the majority of the loci hypermethylated in *idm1* are also hypermethylated in the *rdd* mutant. This is consistent with the *idm1ros1* double-mutant analysis that indicated that IDM1 and ROS1 (and DML2 and DML3) function in the same DNA demethylation pathway.

The expression levels of 15 genes that have increased DNA methylation in or near the genes in *idm1-1* and *ros1-4* mutants were examined. We found that seven of the tested genes show a substantial reduction in their transcript levels in the mutants (fig. S8). Our results suggest that, like ROS1, IDM1 is critical for preventing the transcriptional silencing of some transgenes and endogenous genes.

The tissue pattern of *IDM1* expression is similar to those of *DML2* and *ROS1* (fig. S9). IDM1 is predicted to have a MBD domain, a PHD finger domain and an N-acetyltransferase domain (fig. S1D). We found that the PHD finger of IDM1 specifically binds the N-terminal tail of histone H3 and that the binding is inhibited by H3K4 di- or trimethylation (fig. S10A). H3R2 methylation also appears to inhibit the binding (fig. S10A). In vitro affinity pull-down assays confirmed that the PHD finger of IDM1 recognizes H3 N-terminal tail and that the recognition is prevented by H3K4 di- or trimethylation (Fig. 2A). In contrast, H3K9 methylation does not inhibit the interaction (Fig. 2A and fig. S10A). C732W or C740W mutation (fig. S11A) abolishes the binding of IDM1 to histone H3 (Fig. 2A). Expression of the wild-type but not the C732W or C740W mutant version of *IDM1* under its native promoter could complement the DNA hypermethylation phenotype of the *idm1-1* mutant (Fig. 2B and fig. S10B). The results suggest that histone H3 binding is important for IDM1 function in vivo.

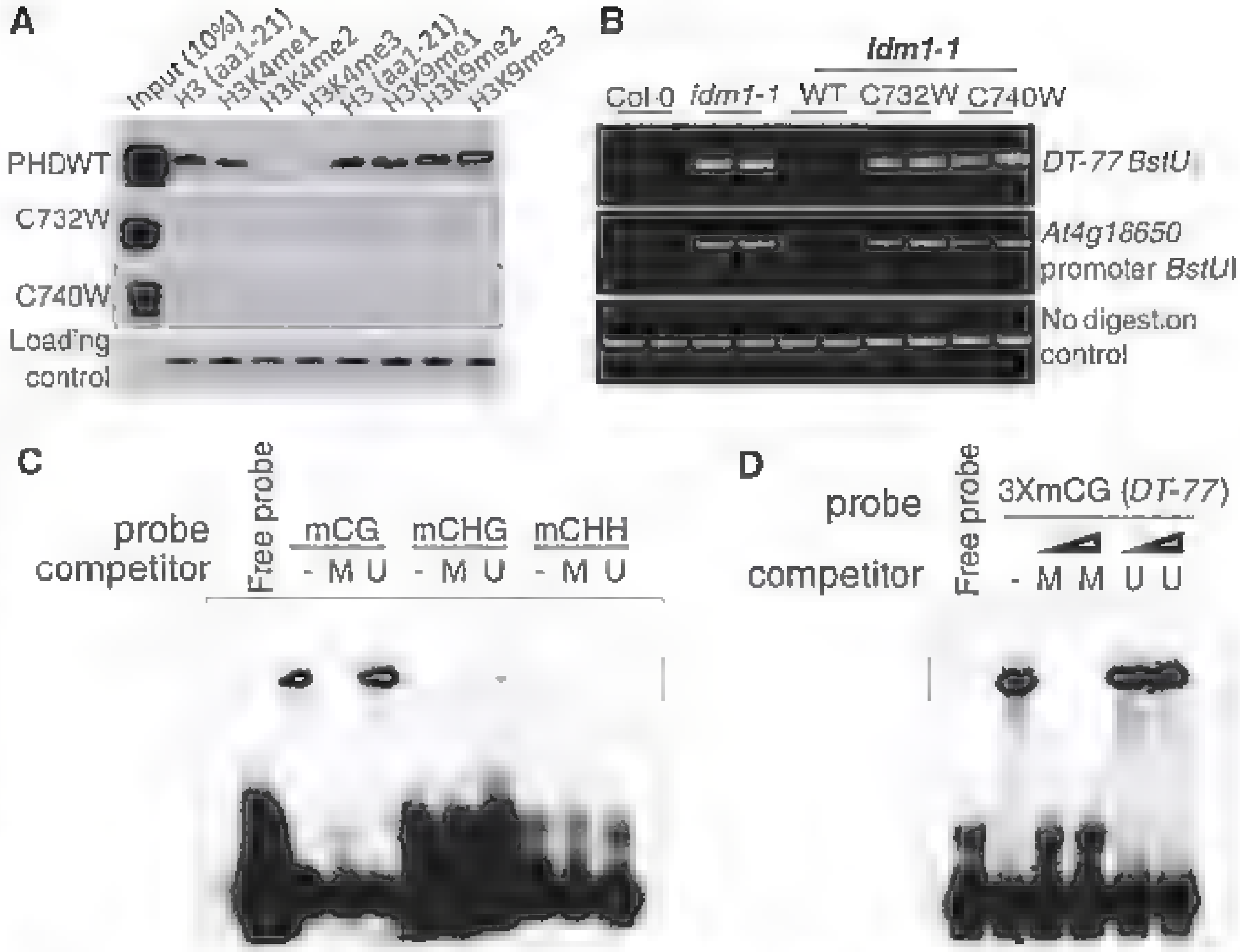

Fig. 2. Functional analysis of the PHD finger and MBD domains of IDM1. **(A)** Western blot analysis of the PHD finger of IDM1 in a peptide pull-down assay. Coomassie blue–stained biotinylated histone peptides are shown as a loading control. **(B)** DNA hypermethylation phenotypes of *idm1-1* plants transformed with WT or mutant forms of *IDM1*. **(C)** Electrophoretic mobility shift assay (EMSA) of IDM1-N (amino acids 1 to 400) binding to methylated oligonucleotides (fig. S12). -, no competitor; M, methylated; U, unmethylated. **(D)** EMSA showing IDM1-N (amino acids 1 to 400) binding to a methylated oligonucleotide probe corresponding to the *DT-77* locus.

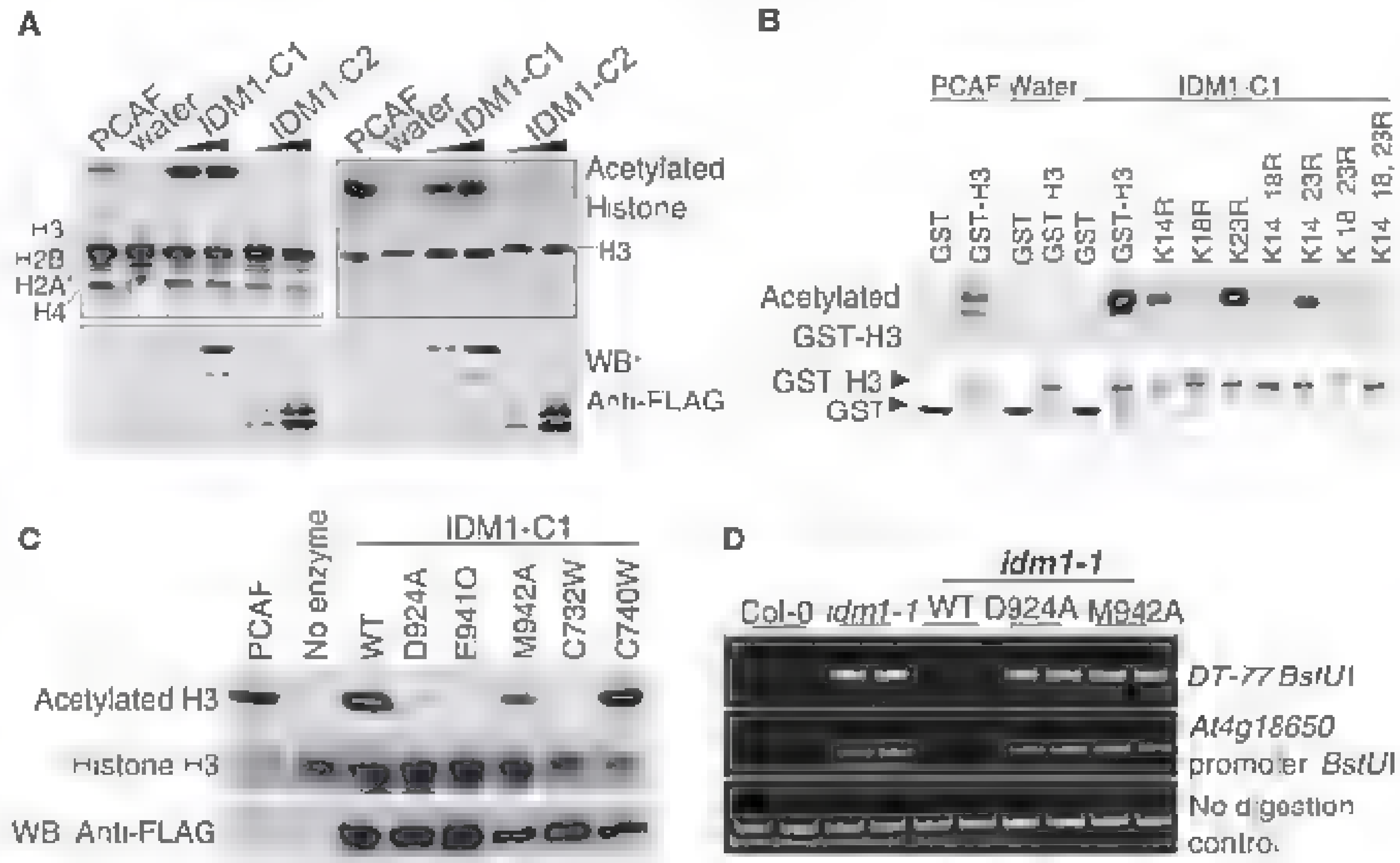

Fig. 3. Histone acetyltransferase activity of IDM1. **(A)** HAT assays. (Top) Autoradiograph for acetylated histone. (Middle) Coomassie blue–stained membrane picture. (Bottom) Western blot detection of IDM1 with antibody to FLAG. p300-CBP-associated factor (PCAF) was used as a positive control. **(B)** HAT assay results using recombinant histone H3 mutated at different lysine positions as substrates. **(C)** HAT assay results using histone H3 as substrate and using WT and mutated forms of IDM1-C1 proteins as enzymes. **(D)** DNA hypermethylation phenotypes of *idm1-1* plants transformed with WT or mutant forms of IDM1.

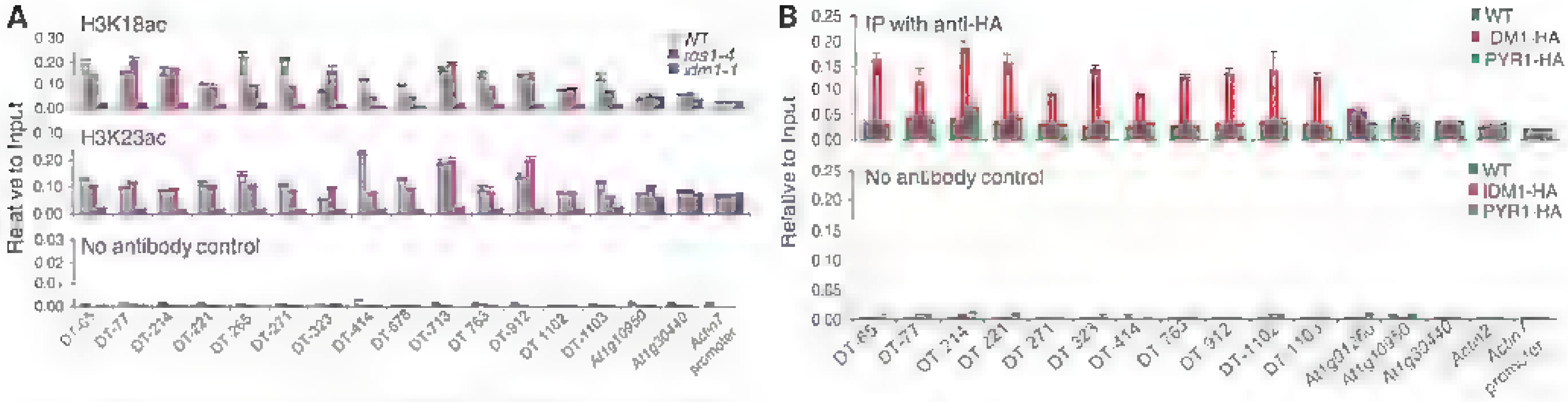

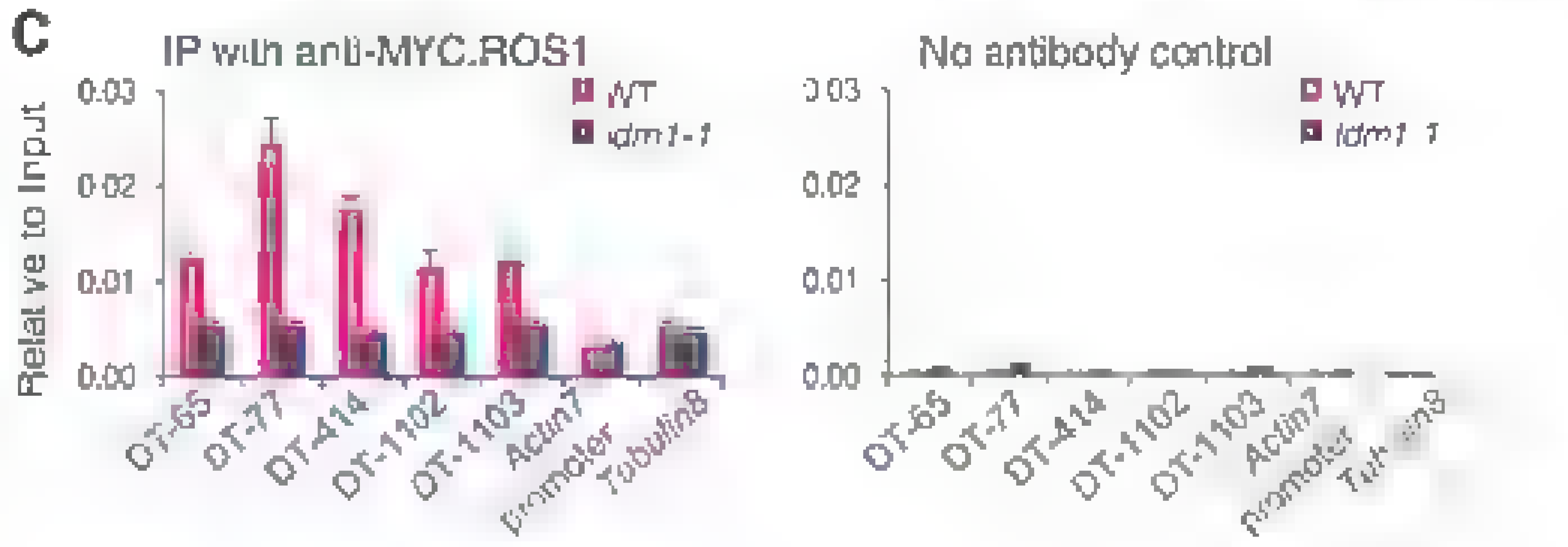

Fig. 4. Histone acetylation marks and IDM1 and ROS1 association with chromatin. **(A)** H3K18 acetylation (ac) and H3K23ac levels at the DT loci and control regions. ChIP was performed with antibodies to H3K18ac and H3K23ac. **(B)** Association of IDM1 protein with DT loci. ChIP was performed in WT, PYR1:3HA, and IDM1:3HA:YFP transgenic plants with antibody to hemagglutinin. **(C)** Effect of *idm1* on ROS1 protein association with DT loci. ChIP was performed in MYC:ROS1/*ros1-4* (WT) and MYC:ROS1/*idm1-1* plants using antibody to MYC. The ChIP signal was quantified as relative to input DNA. The no-antibody precipitates served as a negative control. Standard errors were calculated from three technical repeats.

IDM1 binds to the DNA containing CG methylation, and the binding is competitively blocked by unlabeled methylated, but not unmethylated, DNA of the same sequence (Fig. 2C and fig. S12). We also tested DNA with CG methylation corresponding to the *DT-77* locus and found that IDM1 binds specifically to methylated *DT-77* DNA (Fig. 2D).

We expressed and purified IDM1 fragments containing the putative HAT and PHD domains (IDM1-C1) or the HAT domain only (IDM1-C2) (fig. S13, A and B) from insect cells. Using core histones, histone H3 (Fig. 3A) and oligonucleosome (fig. S13C) as substrates, we found that IDM1-C1, but not IDM1-C2, has an acetyltransferase activity on histone H3. K14, K18, and K23 of H3 are acetylated by IDM1-C1 in vitro (Fig. 3B). Mass spectrometry analysis of the in vitro acetylated histone H3 confirmed that K18 and K23, as well as K14, are acetylated and K18 and K23 are the main targets of acetylation by IDM1-C1 (fig. S13, D and E). D924A, E941Q, or M942A mutation in conserved residues in the HAT domain abolished or diminished the in vitro acetyltransferase activity of IDM1-C1 (Fig. 3C). Expression of the D924A or M942A mutated *IDM1* under its native promoter failed to complement the DNA hypermethylation phenotypes of the *idm1-1* mutant (Fig. 3D and fig. S10B). The results suggest that the histone H3 acetylation activity is necessary for IDM1 function in preventing DNA hypermethylation in plants. The C732W, but not the C740W, mutation in the PHD domain required for H3 interaction also abolished the acetyltransferase activity of IDM1-C1 (Fig. 3C), suggesting that the PHD domain can affect the acetyltransferase activity of IDM1 independently of its role in binding histone H3. Chromatin immunoprecipitation (ChIP) assays showed that acetylated histone H3K18 and H3K23 marks are reduced considerably in *idm1-1* mutant plants specifically at the DT loci (Fig. 4A), suggesting that IDM1 is critical for H3K18 and H3K23 acetylation in vivo.

ChIP assays also indicated that IDM1 is enriched at all of the DT loci tested (Fig. 4B). The DT loci have CG methylation (Fig. 1, B and C, fig. S3, and table S1), and several of them were found to have low levels of H3K4 dimethylation by ChIP assays (fig. S14). In contrast, IDM1 is not enriched in the highly expressed *At1g01260*, *At1g10950*, and *At1g30440* genes (Fig. 4B) that have abundant CG methylation (*9*) and a high level of H3K4 dimethylation. DT loci in general correspond to sequences with low H3K4 mono-, di-, and trimethylation, relative to a comparison group of CG methylated and expressed genes (*10*) (fig. S15). The results are consistent with the notion that IDM1 binds to methylated DNA through its MBD domain but, because of its PHD finger domain, the binding is prevented at loci where there is a high level of H3K4 di- or trimethylation. Transposons are characterized by high CG methylation and low H3K4 di- or trimethylation (*10*). However, IDM1 does not affect the methylation status of most transposons, which are associated with heterochromatin (fig. S7C). This discrimination against heterochromatic regions could potentially be explained by the inhibition of IDM1 interaction with histone H3 by H3R2 methylation (fig. S10A), which is known to be associated with heterochromatin in yeast (*11*). The DNA hypermethylation phenotypes of *idm1* mutants and the HAT activity and DNA- and histone-binding characteristics suggest that IDM1 may be important in selectively binding to the DT loci and creating a permissible chromatin environment for DNA demethylation enzymes. Consistent with this notion, ChIP results show that ROS1 protein is enriched at the DT loci in wild-type plants but that the enrichment is reduced to basal levels of nonspecific binding in *idm1* mutant plants (Fig. 4C).

Active DNA demethylation in plants is achieved through a base excision repair pathway that is initiated by the ROS1 subfamily of 5-methylcytosine DNA glycosylases (*3*). Our results here suggest that IDM1 controls the DNA methylation levels of a subset of loci targeted by the 5-methylcytosine DNA glycosylases. It is critical for preventing DNA hypermethylation and transcriptional silencing of some transgenes and endogenous genes with repetitive sequences or highly homologous genes in multigene families. We showed that IDM1 is a histone H3 acetyltransferase that is capable of recognizing methylated DNA through its MBD domain and recognizing unmethylated histone H3K4 through its PHD domain. Thus, IDM1 can recognize multiple epigenetic features at some demethylation target loci and create acetylated H3K18 and H3K23 marks, which then may be recognized by DNA demethylation enzymes or their interacting partner proteins (fig. S16) because IDM1 does not appear to colocalize with ROS1 (fig. S17).

References and Notes

1. M. Tariq, J. Paszkowski, *Trends Genet.* **20**, 244 (2004).
2. J. A. Law, S. E. Jacobsen, *Nat. Rev. Genet.* **11**, 204 (2010).
3. J. K. Zhu, *Annu. Rev. Genet.* **43**, 143 (2009).
4. Materials and methods are available as supplementary materials on *Science* Online.
5. J. Zhu, A. Kapoor, V. V. Sridhar, F. Agius, J. K. Zhu, *Curr. Biol.* **17**, 54 (2007).
6. Z. Gong *et al.*, *Cell* **111**, 803 (2002).

7. Y. Onodera *et al.*, *Cell* **120**, 613 (2005).
8. J. Pentterman *et al.*, *Proc. Natl. Acad. Sci. U.S.A.* **104**, 6752 (2007).
9. R. Lister *et al.*, *Cell* **133**, 523 (2008).
10. X. Zhang, Y. V. Bernatavichute, S. Cokus, M. Pellegrini, S. E. Jacobsen, *Genome Biol.* **10**, R62 (2009).
11. A. Kirmizis *et al.*, *Nature* **449**, 928 (2007).

Acknowledgments: This work was supported by National Institutes of Health grants R01GM070795 and R01GM059138 to , K.Z. and by the Chinese Academy of Sciences (CAS), China. We thank B. Stevenson for technical assistance and X. Zhang for the gift of glutathione S-transferase H3 (amino acids 1 to 57) construct. Sequence data are available in the Gene Expression Omnibus database (GEO accession GSE33071).

Supplementary Materials
www.sciencemag.org/cgi/content/full/336/6087/1445/DC1
Materials and Methods
Figs. S1 to S17
Tables S1 to S7
References (*12*–*20*)

20 January 2012; accepted 26 April 2012
10.1126/science.1219416

MORC Family ATPases Required for Heterochromatin Condensation and Gene Silencing

Guillaume Moissiard,[1] Shawn J. Cokus,[1] Joshua Cary,[1] Suhua Feng,[1] Allison C. Billi,[2] Hume Stroud,[1] Dylan Husmann,[1] Ye Zhan,[3] Bryan R. Lajoie,[3] Rachel Patton McCord,[3] Christopher J. Hale,[1] Wei Feng,[4] Scott D. Michaels,[4] Alison R. Frand,[5] Matteo Pellegrini,[1,6] Job Dekker,[3] John K. Kim,[2] Steven E. Jacobsen[1,5,6,7]*

Transposable elements (TEs) and DNA repeats are commonly targeted by DNA and histone methylation to achieve epigenetic gene silencing. We isolated mutations in two *Arabidopsis* genes, *AtMORC1* and *AtMORC6*, which cause derepression of DNA-methylated genes and TEs but no losses of DNA or histone methylation. AtMORC1 and AtMORC6 are members of the conserved *Microrchidia* (*MORC*) adenosine triphosphatase (ATPase) family, which are predicted to catalyze alterations in chromosome superstructure. The *atmorc1* and *atmorc6* mutants show decondensation of pericentromeric heterochromatin, increased interaction of pericentromeric regions with the rest of the genome, and transcriptional defects that are largely restricted to loci residing in pericentromeric regions. Knockdown of the single MORC homolog in *Caenorhabditis elegans* also impairs transgene silencing. We propose that the MORC ATPases are conserved regulators of gene silencing in eukaryotes.

Gene silencing in the *Arabidopsis* genome is highly correlated with DNA methylation, which is found in three different cytosine contexts. Methylation of symmetric CG and CHG sites (in which H is A, T, or C) are mediated by DNA METHYLTRANSFERASE1 (MET1) and CHROMOMETHYLASE3 (CMT3), respectively, whereas CHH methylation is mainly catalyzed by DOMAINS REARRANGED METHYLTRANSFERASE2 (DRM2) (*1*). Silent loci are also enriched in the repressive histone H3 lysine 9 dimethylation mark (H3K9me2) (*2*, *3*).

Suppressor of drm2 cmt3 (*SDC*) is a gene whose repression in most tissues depends on the redundant activities of DRM2 and CMT3 (*4*, *5*). Hence, a loss of *SDC* silencing is observed in the *drm2 cmt3* double mutant but not in *drm2* or *cmt3*

[1]Department of Molecular, Cell, and Developmental Biology, University of California at Los Angeles, Terasaki Life Sciences Building, 610 Charles Young Drive East, Los Angeles, CA 90095–723905, USA. [2]Life Sciences Institute and Department of Human Genetics, University of Michigan, Ann Arbor, MI 48109, USA. [3]Lazare Research Building 570N, Program in Systems Biology and Gene Function and Expression, University of Massachusetts Medical School, 364 Plantation Street, Worcester, MA 01605, USA. [4]Department of Biology, Indiana University, Bloomington, IN 47405, USA. [5]Department of Biological Chemistry, David Geffen School of Medicine, University of California Los Angeles, Los Angeles, CA 90095, USA. [6]Eli and Edythe Broad Center of Regenerative Medicine and Stem Cell Research, University of California Los Angeles, Los Angeles, CA 90095, USA. [7]Howard Hughes Medical Institute, University of California Los Angeles, Los Angeles, CA 90095, USA.

*To whom correspondence should be addressed. E-mail: jacobsen@ucla.edu

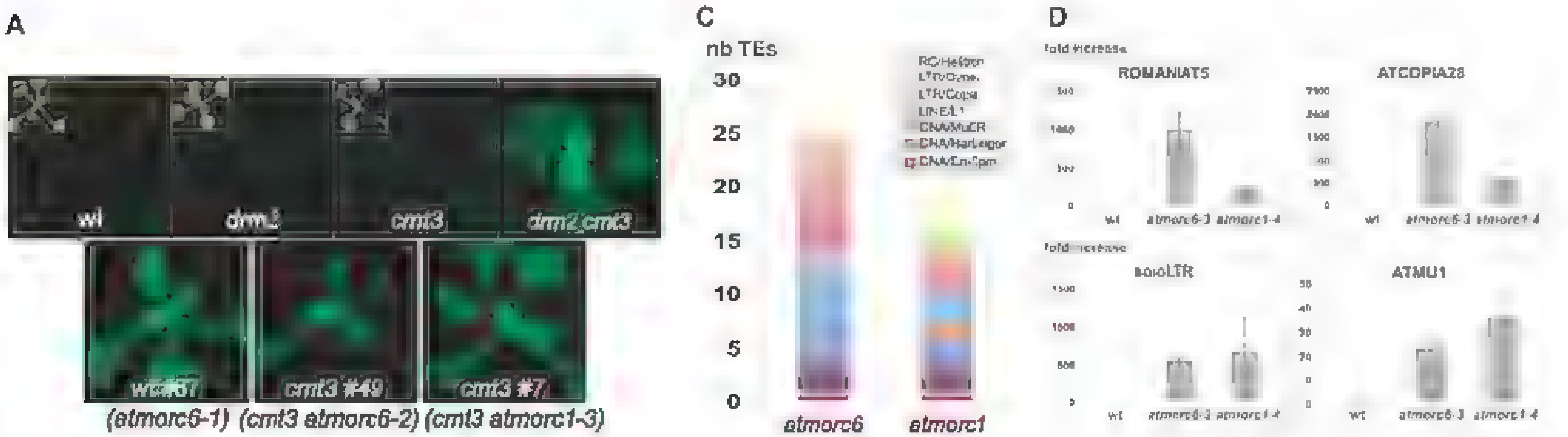

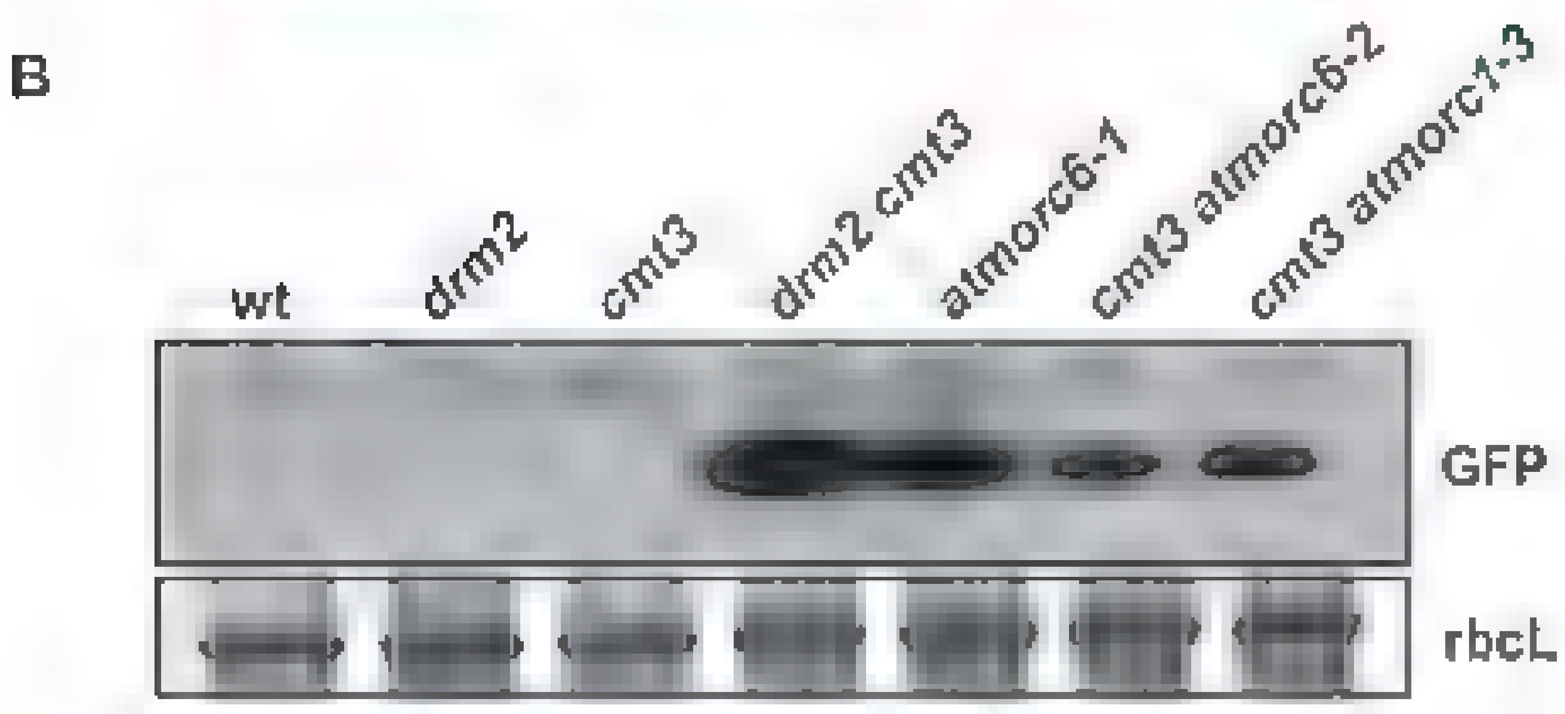

Fig. 1. Mutations of two MORC homologs induce *SDC::GFP* and TE overexpression. (**A**) wt, *drm2* mutant, and *cmt3* mutant plants carrying *SDC::GFP* showed no GFP fluorescence under ultraviolet (UV) light (insets show each plant under white light), and *drm2 cmt3* double mutant and EMS-mutagenized lines wt #67, *cmt3* #49, and *cmt3* #7 plants showed strong GFP fluorescence. (**B**) Western blot using antibody against GFP (anti-GFP) confirms *SDC::GFP* overexpression in the EMS mutants. Coomassie staining of the large Rubisco subunit (rbcL) is used as loading control. (**C**) Number of TEs overexpressed in *atmorc1* and *atmorc6* mutants and classified by superfamily. For each mutant, only TEs with at least a fourfold increase in both the EMS and T-DNA alleles over wt and with a $P < 0.05$ are represented. (**D**) Relative fold increase of four TE transcripts in *atmorc1-4* and *atmorc6-3* over wt assayed by real-time quantitative polymerase chain reaction (RT-qPCR) and normalized to *ACTIN7*. Errors bars indicate standard deviation based on three independent biological replicates.

single mutants. The *SDC* promoter carries seven tandem repeats, which recruit the DNA methylation machinery and cause transcriptional gene silencing. We engineered a green fluorescent protein (GFP)–based sensor construct controlled by the *SDC* promoter (fig. S1A). The *SDC::GFP* transgene behaves similarly to endogenous *SDC*, and GFP fluorescence is not detectable in wild-type, *drm2*, or *cmt3* plants but is highly expressed in *drm2 cmt3* double mutant (Fig. 1A).

We carried out ethyl methanesulfonate (EMS) mutagenesis screens in wild-type (wt) or *cmt3* backgrounds for mutants showing *SDC::GFP* overexpression and identified the wt #67, *cmt3* #7, and *cmt3* #49 mutants (Fig. 1, A and B). Mapping experiments using bulk segregant analysis coupled to deep genome resequencing indicated that *cmt3* #7 contained a mutation in *At4g36290* (*AtMORC1*), previously also named *COMPROMISED RECOGNITION OF TCV-1* (*CRT1*) (*6*, *7*), whereas wt #67 and *cmt3* #49 both contained mutations in *At1g19100* (*AtMORC6*) (*7*) (figs. S1B, S2, and S3A). An *atmorc1* allele was previously reported to show reduced resistance to

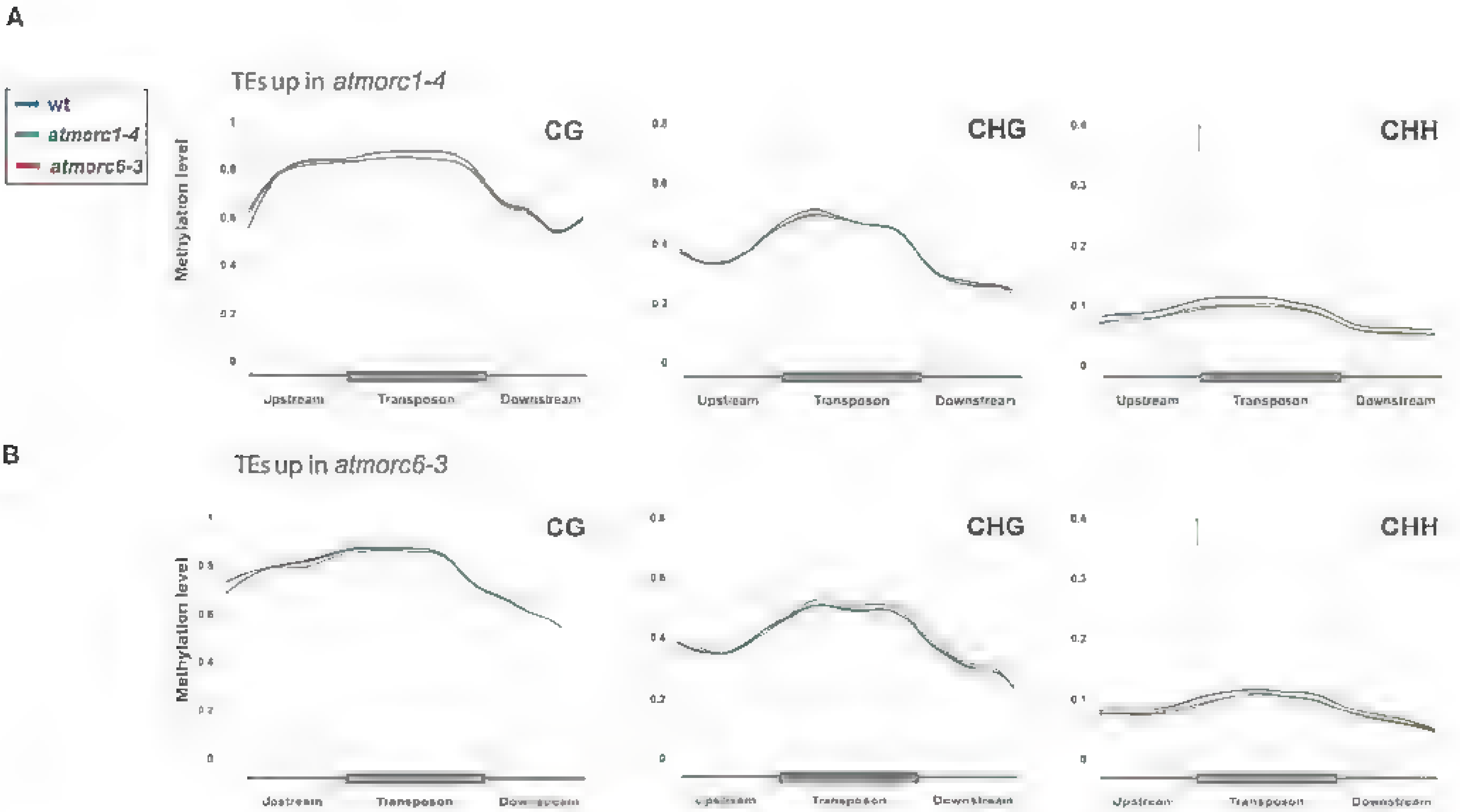

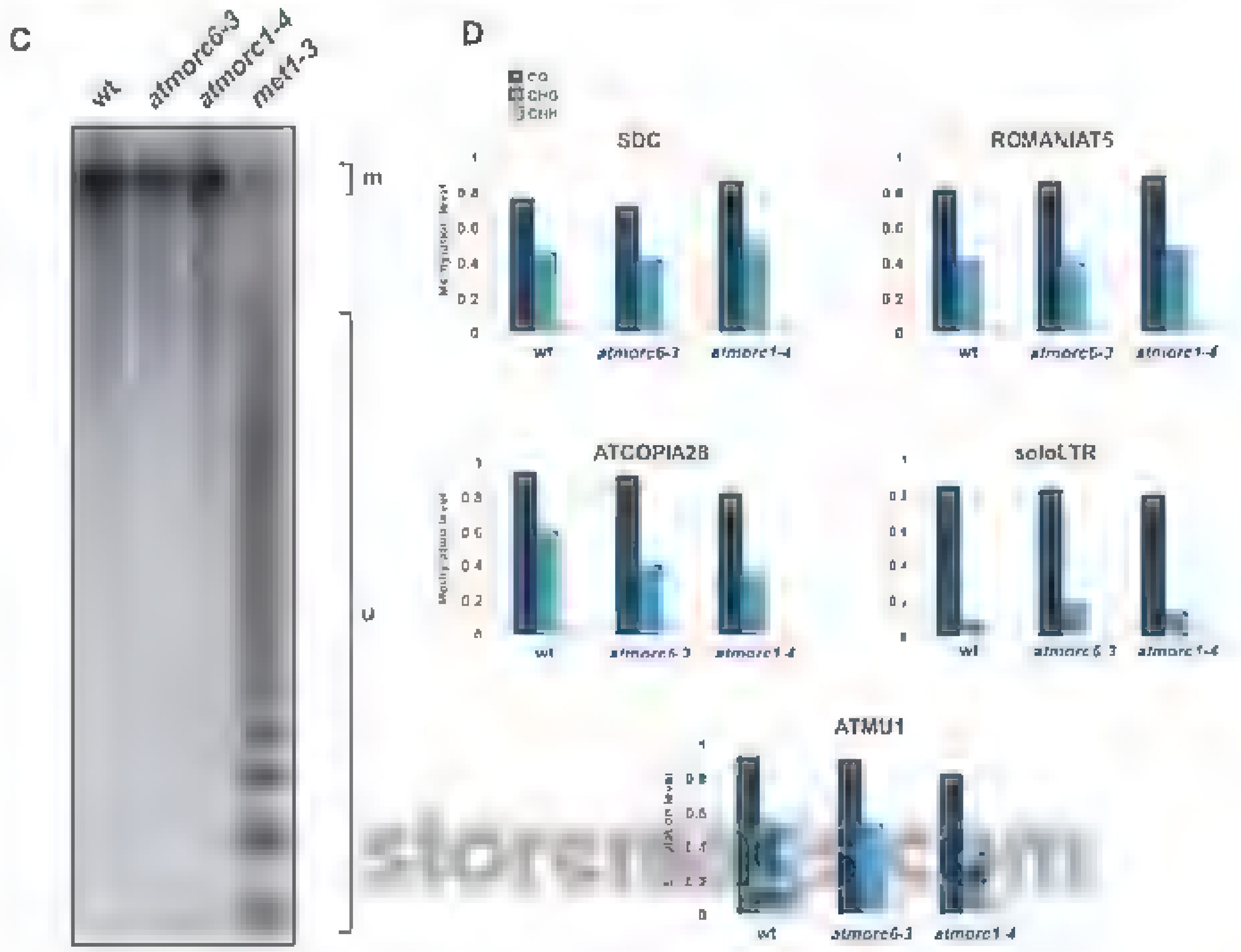

Fig. 2. DNA methylation is not impaired in *atmorc1* and *atmorc6* mutants. (**A** and **B**) Metaplot analyses show DNA methylation level in *atmorc1-4*, *atmorc6-3*, and wt for the set of TEs up-regulated in *atmorc1-4* (A) and *atmorc6-3* (B). The gray vertical lines mark the boundaries between 1 kilobase upstream and downstream regions of TEs. (**C**) Southern blot analyses assayed CG methylation level at CEN180 repeats by using *Hpa*II-treated genomic DNAs. m, methylated; u, unmethylated. *met1-3* genomic DNA is used as positive control for loss of CG methylation (*23*). (**D**) Percent DNA methylation at *SDC* and four TEs overexpressed in *atmorc1-4* and *atmorc6-3* mutants assayed by bisulfite sequencing. Twenty-four clones were analyzed for each individual analysis.

the turnip crinkle virus (TCV) (*6*, *7*), suggesting that AtMORC1 is involved in viral resistance in addition to its role in gene silencing described in this study, whereas mutations in *AtMORC6* have not been described. To ensure that *atmorc1* and *atmorc6* mutations were those responsible for the loss of *SDC* silencing, we isolated knock-out transferred DNA (T-DNA) insertion lines *atmorc1-4* and *atmorc6-3* and confirmed *SDC* overexpression in these two mutant alleles (fig. S3, B to D). Genetic complementation crosses between the recessive EMS and T-DNA mutants confirmed *AtMORC1* and *AtMORC6* as the mutated genes responsible for *SDC::GFP* activation in the three EMS lines (fig. S3E). Therefore, #7, #67, and #49 were renamed *atmorc1-3*, *atmorc6-1*, and *atmorc6-2*, respectively.

By using RNA sequencing (RNA-seq) (*8*), we found that the majority of RNAs significantly affected in the *atmorc1* and *atmorc6* mutants showed up-regulation, and many of these were transposable elements (TEs) belonging to various transposon superfamilies, including, among others, the LTR/Gypsy, LTR/Copia, DNA/MuDR, and DNA/Harbinger families (Fig. 1, C and D; fig. S4A, table S1). The expression defects in the *atmorc1* and *atmorc6* mutants were very similar, with all but two of the transposons up-regulated in *atmorc1* also up-regulated in *atmorc6* (fig. S4B). Protein-coding genes overexpressed in the *atmorc1* and *atmorc6* EMS and T-DNA mutants included endogenous *SDC* (table S2). There was a high degree of overlap between the genes up-regulated in *atmorc1* and *atmorc6* (fig. S4C), most of them corresponding to DNA-methylated and silenced loci (fig. S4, D and E). We also performed RNA-seq in the *atmorc1 atmorc6* double mutant and found a very similar set of genes and transposons up-regulated, with only a few genes up-regulated in the double mutant that were not up-regulated in each of the single mutants (table S3), suggesting that AtMORC1 and AtMORC6 may act together to enforce gene silencing.

Whole-genome bisulfite sequencing (BS-seq) (*9*) revealed that DNA methylation levels in all sequence contexts were unaltered in *atmorc1* or *atmorc6* relative to wild type at TEs up-regulated in *atmorc1* or *atmorc6* (Fig. 2, A and B), nor were there any bulk alterations in protein-coding genes or TEs in the genome (fig. S5, A and B). In addition, analyses at the pericentromeric satellite CEN180 repeats and five loci up-regulated in *atmorc1* and *atmorc6* showed that the DNA methylation patterns in *atmorc1-4* and *atmorc6-3* were similar to those of wild type (Fig. 2, C and D). Chromatin immunoprecipitation sequencing (ChIP-seq) analyses of H3K9me2 also did not reveal any changes in the *atmorc1* or *atmorc6* mutants at *SDC* or other up-regulated locations (fig. S6, A and B). Lastly, small RNA sequencing analyses showed that elements up-regulated in *atmorc1* and *atmorc6* mutants were enriched in small interfering RNAs (siRNAs), but these siRNA levels did not change in the mutants (fig. S7). Thus, *AtMORC1* and *AtMORC6* are not required to maintain DNA methylation, H3K9me2, or siRNAs, suggesting that AtMORC1 and AtMORC6 are likely to either act downstream of DNA methylation or enforce silencing by a novel mechanism.

AtMORC1 and *AtMORC6* are homologs of mouse *Microrchidia1* (*MORC1*) (*10*, *11*) and contain gyrase, Hsp90, histidine kinase, and MutL (GHKL) and S5 domains, together comprising an adenosine triphosphatase (ATPase) module (*6*) in addition to a putative C-terminal coiled-coil domain (fig. S1B). The EMS mutations found in *atmorc1-3*, *atmorc6-1*, and *atmorc6-2* alleles all introduced premature stop codons within the GHKL domain (fig. S1B).

Because of the similarity of AtMORC1 and AtMORC6 to ATPases involved in manipulating chromatin superstructure (*12*), these proteins may affect gene silencing through higher-order compaction of methylated and silent chromatin. In wild-type nuclei, pericentromeric heterochromatin forms densely staining nuclear bodies called chromocenters that localize to the nuclear periphery

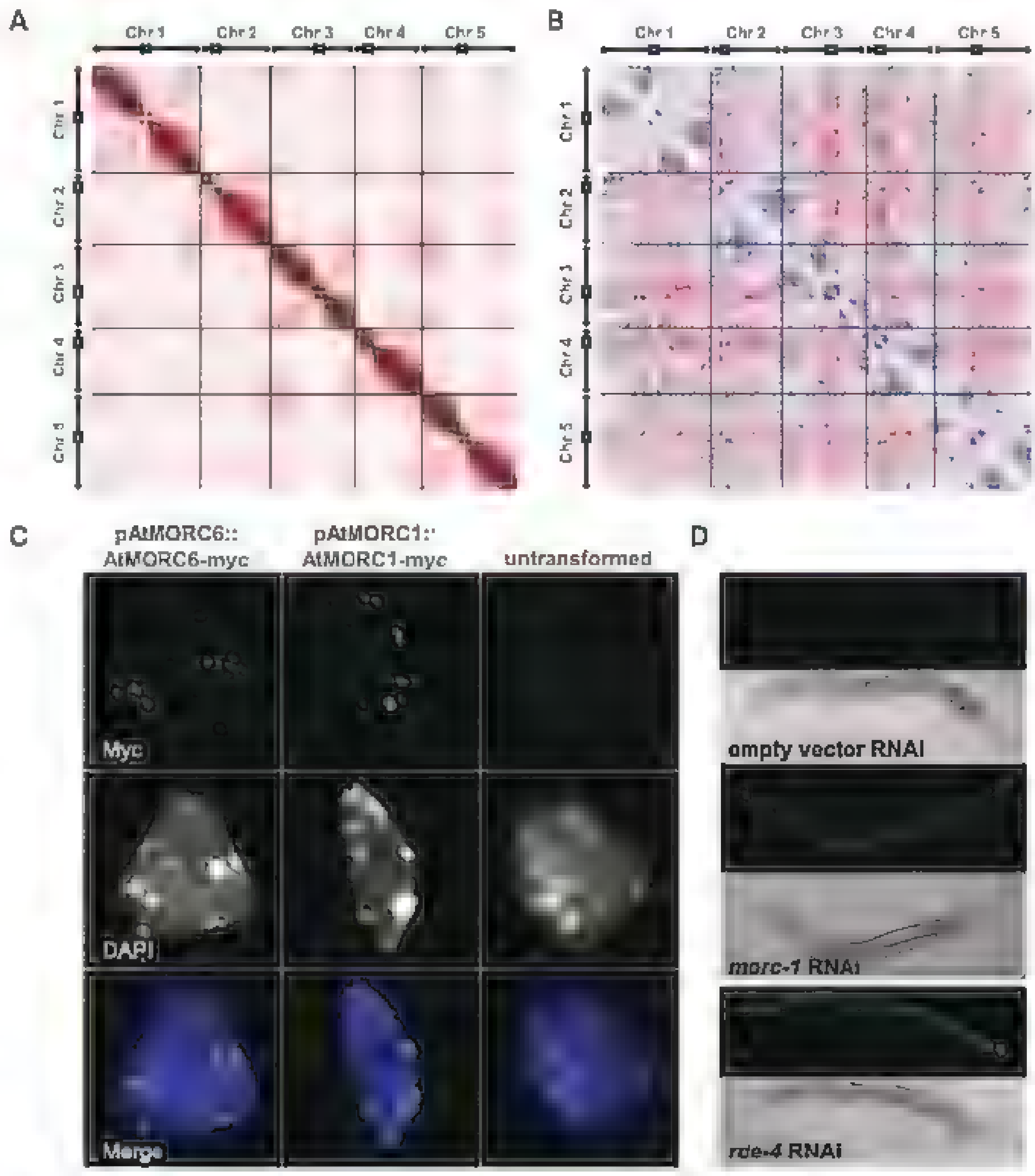

Fig. 3. AtMORC1 and AtMORC6 are required for maintenance of chromatin architecture and form nuclear bodies near chromocenters, and *morc-1* is involved in gene silencing in *C. elegans*. **(A)** Interaction matrix of the wt *Arabidopsis* genome from Hi-C analysis. Positions along the five chromosomes are shown from left to right and top to bottom, and each pixel represents interactions from uniquely mapping paired end reads in 200-kilobase bins. Black bars and circles mark the positions of the pericentromeric and telomeric regions, respectively. Light gray regions represent areas masked out because of problematic mapping. Black bars show separation between chromosomes. **(B)** Difference plot shows enrichment of Hi-C interactions in *atmorc6-1* in red and interactions depleted in *atmorc6-1* in blue. **(C)** Anti-Myc immunostaining showing localization of pAtMORC6::AtMORC6-Myc and pAtMORC1::AtMORC1-Myc in nuclear bodies adjacent to chromocenters. AtMORC1 and AtMORC6 showed 2.0 ± 1.0 (average ± standard deviation) and 2.5 ± 1.2 bodies per chromocenter, respectively. DAPI (4′,6-diamidino-2-phenylindole) staining shows chromocenter location. Bottom images are merges. **(D)** A silenced seam cell–specific GFP transgene in the *eri-1* (*mg366*) sensitized background is overexpressed in worms fed with bacteria expressing double-stranded RNA targeting *morc-1* or *rde-4* but not in worms fed with bacteria expressing a control empty vector. Results are representative of five independent replicates.

(*13*). We observed decondensation of chromocenters in the *atmorc1* and *atmorc6* mutants (as well as in *atmorc1 atmorc6* double mutant) (figs. S8 to S11) and found that loci transcriptionally derepressed in the mutants mostly localized to pericentromeric heterochromatin (fig. S12 and tables S1 and S3). To directly examine whole-genome chromatin interactions, we performed Hi-C analyses in wild type and *atmorc6-1* (*14*). Consistent with previous cytological studies (*13*), the wild-type genome showed interactions between telomeres as well as between euchromatic regions on the same chromosome arm (Fig. 3A). In contrast, pericentromeric heterochromatin regions interacted very weakly with the rest of the genome, consistent with their compaction in chromocenters (Fig. 3A). Although *atmorc6-1* showed a roughly similar chromatin architecture (fig. S13), plotting the differences between mutant and wild type showed that *atmorc6-1* shows an increase in interactions between the pericentromeric regions of all chromosomes with the euchromatic arms of all chromosomes and a corresponding depletion of interactions of euchromatic arms with themselves. Because the analysis reports relative changes with the sum of differences set to zero, the most likely interpretation of these findings is that pericentromeric regions interact more strongly with the euchromatic arms in *atmorc6-1*, although we cannot exclude that the mutant also has effects on the euchromatic arms (Fig. 3B). This interpretation is consistent with the cytological observations showing that chromocenters expand out into a larger area of the nucleus in the mutants (fig. S8). We also found, by using complementing myc-tagged transgenes, that AtMORC1 and AtMORC6 proteins formed small nuclear bodies that were usually adjacent to but not within chromocenters (Fig. 3C and figs. S14 and S15). These results are all consistent with a model in which AtMORC1 and AtMORC6 enforce compaction and gene silencing of pericentromeric heterochromatin, although it is also possible that changes in chromatin and gene expression in the mutant secondarily lead to the observed changes in chromatin compaction. Mutation of the plant-specific *MOM1* gene has also been shown to affect gene silencing but not DNA methylation in *Arabidopsis*; however, *mom1* mutants do not show chromocenter decondensation and therefore are likely to act via a different mechanism (*15*, *16*).

A single MORC homolog, *morc-1*, is present in the worm *Caenorhabditis elegans*, which is devoid of DNA methylation (*17*). To test whether the *C. elegans morc-1* (ZC155.3) is involved in gene silencing, we performed RNA interference (RNAi)–mediated knockdown of *morc-1* in the *eri-1* sensitized background, in which a GFP transgene is silenced in most of the worm seam cells (Fig 3D) (*18*). *morc-1*–depleted worms showed GFP reactivation similar to worms depleted of *rde-4*, an essential component of gene silencing in *C. elegans* (Fig. 3D) (*19*). These results suggest that MORCs may play an ancient and conserved role in gene silencing. In addition, the observation that *morc-1* is required for gene silencing in *C. elegans* reinforces our view that MORCs in *Arabidopsis* are enforcing silencing by a mechanism that may not be directly linked with DNA methylation. It is interesting to note that the phenotype of the *Morc1*-knockout mouse resembles *Miwi2*- and *Dnmt3L*-knockout mouse phenotypes, showing male-specific meiotic defects during spermatogenesis (*10*, *20*–*22*). Miwi2 and Dnmt3L are both required for TE silencing, and it is possible that Morc1 might be involved in transposon silencing in mammals as well. We propose that MORC family ATPases act to regulate chromatin architecture and gene silencing in a wide variety of eukaryotes.

References and Notes

1. J. A. Law, S. E. Jacobsen, *Nat. Rev. Genet.* **11**, 204 (2010).
2. J. P. Jackson, A. M. Lindroth, X. Cao, S. E. Jacobsen, *Nature* **416**, 556 (2002).
3. F. Malagnac, L. Bartee, J. Bender, *EMBO J.* **21**, 6842 (2002).
4. X. Zhang *et al.*, *Cell* **126**, 1189 (2006).
5. I. R. Henderson, S. E. Jacobsen, *Genes Dev.* **22**, 1597 (2008).
6. H. G. Kang, J. C. Kuhl, P. Kachroo, D. F. Klessig, *Cell Host Microbe* **3**, 48 (2008).
7. H. G. Kang *et al.*, *Plant Cell* **22**, 918 (2010).
8. Z. Wang, M. Gerstein, M. Snyder, *Nat. Rev. Genet.* **10**, 57 (2009).
9. S. J. Cokus *et al.*, *Nature* **452**, 215 (2008).
10. M. L. Watson *et al.*, *Proc. Natl. Acad. Sci. U.S.A.* **95**, 14361 (1998).
11. N. Inoue *et al.*, *Hum. Mol. Genet.* **8**, 1201 (1999).
12. L. M. Iyer, S. Abhiman, L. Aravind, *Biol. Direct* **3**, 8 (2008).
13. P. Fransz, J. H. De Jong, M. Lysak, M. R. Castiglione, I. Schubert, *Proc. Natl. Acad. Sci. U.S.A.* **99**, 14584 (2002).
14. E. Lieberman-Aiden *et al.*, *Science* **326**, 289 (2009).
15. P. Amedeo, Y. Habu, K. Afsar, O. Mittelsten Scheid, J. Paszkowski, *Nature* **405**, 203 (2000).
16. A. V. Probst, P. F. Fransz, J. Paszkowski, O. Mittelsten Scheid, *Plant J.* **33**, 743 (2003).
17. V. J. Simpson, T. E. Johnson, R. F. Hammen, *Nucleic Acids Res.* **14**, 6711 (1986).
18. S. Kennedy, D. Wang, G. Ruvkun, *Nature* **427**, 645 (2004).
19. H. Tabara *et al.*, *Cell* **99**, 123 (1999).
20. M. A. Carmell *et al.*, *Dev. Cell* **12**, 503 (2007).
21. D. Bourc'his, T. H. Bestor, *Nature* **431**, 96 (2004).
22. A. A. Aravin *et al.*, *Mol. Cell* **31**, 785 (2008).
23. M. W. Kankel *et al.*, *Genetics* **163**, 1109 (2003).

Acknowledgments: We thank M. Akhavan for sequencing, L. Goddard and L. Iruela-Arispe for assistance with confocal microscopy, and P. Fransz and I. Schubert for helpful discussions. S.F. is a Special Fellow of the Leukemia and Lymphoma Society. J.C. is supported by the Ruth L. Kirschstein National Research Service Award GM007185. R.P.M. is supported by the National Institute of General Medical Sciences (grant F32GM100617), and J.D. is supported by a W. M. Keck Foundation Distinguished Young Scholar in Medical Research Award. Research in the Jacobsen, Kim, Michaels, and Dekker laboratories was supported by NIH grants GM60398, GM088565, GM075060, and HG003143, respectively. Sequencing files have been deposited at Gene Expression Omnibus (GEO) (accession code GSE37644). The authors declare no competing financial interests. S.E.J. is an investigator of the Howard Hughes Medical Institute. Correspondence and requests for materials should be addressed to S.E.J.

Supplementary Materials

www.sciencemag.org/cgi/content/full/science.1221472/DC1
Materials and Methods
Figs. S1 to S15
Tables S1 to S4
References (*24*–*44*)

5 March 2012; accepted 24 April 2012
Published online 3 May 2012;
10.1126/science.1221472

The Structures of COPI-Coated Vesicles Reveal Alternate Coatomer Conformations and Interactions

Marco Faini,[1] Simone Prinz,[1] Rainer Beck,[2] Martin Schorb,[1] James D. Riches,[1*] Kirsten Bacia,[3] Britta Brügger,[2] Felix T. Wieland,[2†] John A. G. Briggs[1,4†]

Transport between compartments of eukaryotic cells is mediated by coated vesicles. The archetypal protein coats COPI, COPII, and clathrin are conserved from yeast to human. Structural studies of COPII and clathrin coats assembled in vitro without membranes suggest that coat components assemble regular cages with the same set of interactions between components. Detailed three-dimensional structures of coated membrane vesicles have not been obtained. Here, we solved the structures of individual COPI-coated membrane vesicles by cryoelectron tomography and subtomogram averaging of in vitro reconstituted budding reactions. The coat protein complex, coatomer, was observed to adopt alternative conformations to change the number of other coatomers with which it interacts and to form vesicles with variable sizes and shapes. This represents a fundamentally different basis for vesicle coat assembly.

Cellular transport vesicles are formed by conserved protein coats (*1*–*3*). Detailed structural information about vesicle coats assembled on a membrane bilayer has remained elusive. The clearest insights into the architecture of vesicle coats have been obtained by applying electron microscopy (EM) to coat protein complex COPII and clathrin protein cages, assembled in vitro from outer coat protein components in the absence of membranes (*1*, *4*, *5*). The cages have point group symmetries and discrete size distributions (*6*), whereas in vivo formed clathrin-

coated vesicles are surrounded by cages that can deviate from point group symmetry (7). In both cases, each cage subunit makes the same set of interactions with the same number of partners. The clathrin cage vertex consists of three-fold triskelions, whose arms intertwine to form two-fold symmetrical edges with some flexibility; in COPII, four rodlike edges of the cage converge at each two-fold vertex (fig. S1, A and B).

In the COPI system, which transports cargo within the Golgi and from the Golgi to the endoplasmic reticulum (ER) (8), the membrane-binding inner coat components are recruited to the membrane en bloc with the outer coat components as a single heptameric complex, called coatomer (9). Cytosolic coatomer is a highly flexible complex, precluding high-resolution structural study (10). To obtain structural information on the COPI coat, we studied COPI-coated membrane vesicles.

COPI-coated vesicles were formed by reconstituting budding in vitro with giant unilamellar vesicles (GUVs) as donor membranes together with recombinantly expressed heptameric coatomer complex (11), the small guanosine triphosphatase Arf1, a guanine nucleotide exchange factor, and guanosine 5′-*O*-(3′-thiotriphosphate). The budding reaction was plunge-frozen without further purification and analyzed by cryoelectron tomography. Large numbers of coated vesicles were formed, ranging in shape from spherical to slightly elliptical (Fig. 1, A and B). Vesicle membranes were covered with a fuzzy coat ~14 nm thick. The mean vesicle diameter at the membrane was 45 nm ± 6 nm (n = 244) (Fig. 1C), comparable with observations carried out in vivo (12) and in vitro (13, 14). In control incubations in the presence of guanosine diphosphate, no coated vesicles were produced.

The variable size and shape of the vesicles precluded averaging of whole vesicles to obtain a high-resolution three-dimensional (3D) structure. We thus applied subtomogram averaging to analyze the repetitive unit of the coat. Subvolumes were extracted at vesicle surfaces and were iteratively aligned and averaged in an unbiased, reference-free manner (15–17). This procedure was performed on two independent budding reactions, converging to the same structure: a three-fold symmetrical arrangement of leaf-shaped densities surrounding a central platform (Fig. 2A and fig. S2, A to C). Three leaves form a triad, which is ~32 nm across. Subtomogram averaging of further data sets yielded a 3D structure of the triad at 26 Å resolution (Fig. 2, B to D; fig. S3; and movie S1). The triad contacts the membrane below each leaf (Fig. 2C, black arrowhead) and below the central platform (Fig. 2C, white arrowhead).

The size of one leaf matched the expected mass of one coatomer-Arf1 complex (17), whereas its shape was comparable to that of the cytosolic yeast coatomer complex (10) (fig. S4). The crystal structure of the adaptor protein 2 (AP2) trunk domain (18), which is homologous to the βδ/γζ-COP subcomplex (19), did not fit as a rigid body into the leaf, which indicated conformational differences between crystallized AP2 and the assembled form of βδ/γζ-COP (17) (fig. S5, A and B). Upon automated docking of the triskelion-like crystal structure of an αβ′-COP fragment (20) into the triad, parts of αβ′-COP protruded from the density (17) (fig. S5, C and D). This suggested that, within the assembled coat, either the triskelion does not represent the structural form of αβ′-COP or that the triskelion arms are differently oriented. Upon automated docking of a single copy of αβ′-COP, the two highest-scoring solutions were found within the leaf of the triad such that the α-COP α-solenoid of one solution superimposes on the homologous α-solenoid in β′-COP from the other solution, and vice versa, consistent with the described pseudo-two-fold interaction between α- and β′-COP (17, 20) (fig. S5, E and F).

To generate "lattice maps" showing the arrangement of triads on individual coated vesicles, we placed triangles at the positions and rotational orientations to which triad subtomograms aligned (15, 17) (Fig. 3, A to D). This showed that the corners and edges of triads are arranged around local three-fold symmetry axes in a triangular lattice (Fig. 3, A and B). All vesicles also had local positions at which the corners of two, instead of three, triads met, either singly (Fig. 3C) or paired (Fig. 3D). Because a triangular lattice is geometrically flat, such two-corner positions are required for assembly of a curved lattice. A relative increase in number of three-corner over two-corner positions, or of paired two-corner over single two-corner positions, increases the diameter of the resulting shell in any curved triangular lattice. The relative numbers of triad patterns found on vesicles of different sizes were consistent with these geometrical principles. For example, two-corner positions were more prevalent relatively to three-corner positions in smaller vesicles with higher membrane curvature (fig. S6A).

The distribution of triads over the vesicle surface did not consistently conform to any point group symmetry. Vesicle coats also contained gaps in the triangular lattice (Fig. 3E). In some cases, the triad arrangement around such gaps precluded the addition of further triads, making it unlikely that gaps resulted from disassembly, prematurely arrested assembly, or unidentified triads; instead, the arrangement suggested that gaps formed during assembly and budding. Electron density seen at most gaps indicated that they contained disordered protein density. Lattice maps of COPI-coated buds that had not completed scission were incomplete at the bud neck (Fig. 3F), which suggested that the gap represents a "budding scar" and that formation of a complete, closed protein coat is not required to mediate vesicle formation in the in vitro budding reaction. Quantitative fluorescence microscopy shows that, under certain conditions, a partially complete clathrin coat can also internalize vesicles from the plasma membrane (21, 22).

To derive structural information about the interactions between triads, we calculated the positional and rotational coordinates of all positions where the corners of three triads met (Fig. 3A), positions where the edges of three triads met (Fig. 3B), single two-corner positions (Fig. 3C), and paired two-corner positions (Fig. 3D). Structures derived by averaging subtomograms extracted at these positions (Fig. 3, G to N, and fig. S6B), revealed that the central platform of the triad and the cores of the leaves were consistent in all structures, whereas the parts of leaves forming corners and edges of the triad adopted different conformations (Fig. 3, K to O). Where three triad corners met, leaves formed a raised three-fold

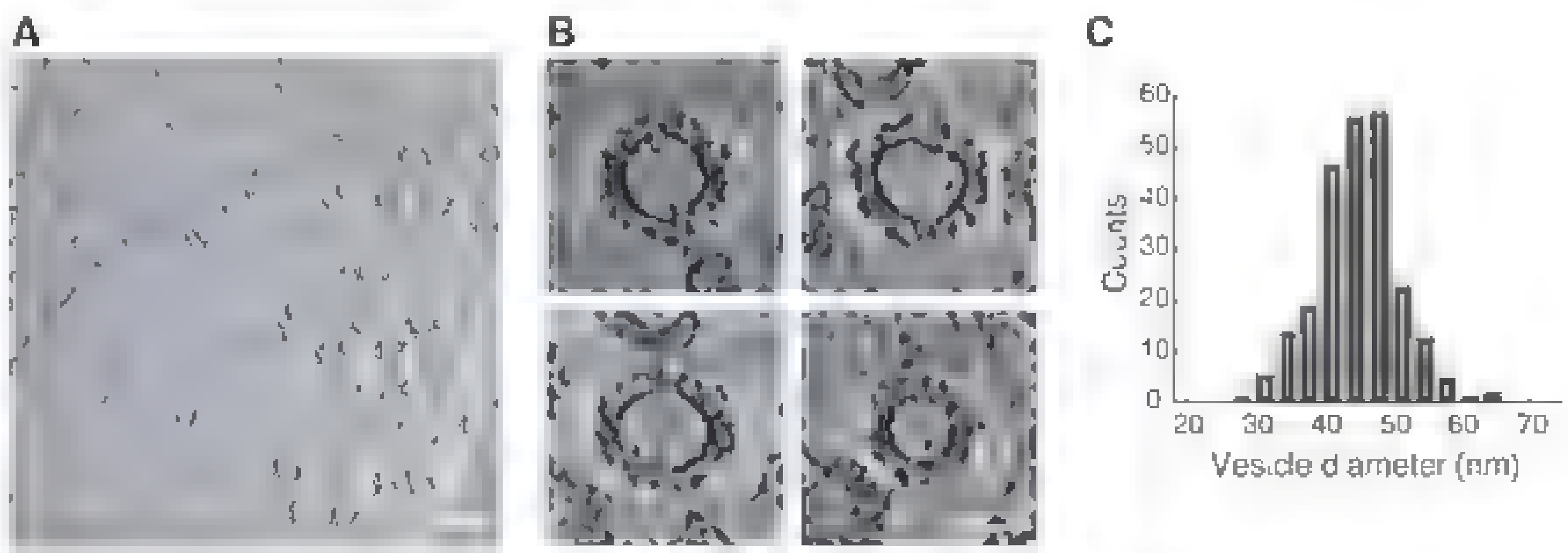

Fig. 1. COPI-coated vesicle budding reconstituted from giant unilamellar vesicles. **(A)** Section through a cryoelectron tomogram of COPI-coated vesicles from an in vitro budding reaction. Scale bar, 100 nm. **(B)** Central sections of vesicles showing variable size and ellipticity, and a fuzzy ~14-nm-thick coat. Scale bar, 50 nm. (A) and (B) were Gaussian filtered to ease visualization. **(C)** Average vesicle diameter measured at the membrane. Distribution mean is 45 nm (n = 244).

[1]Structural and Computational Biology Unit, European Molecular Biology Laboratory, Meyerhofstrasse 1, 69117 Heidelberg, Germany. [2]Heidelberg University Biochemistry Center, Heidelberg University, Im Neuenheimer Feld 328, 69120 Heidelberg, Germany. [3]HALOmem, University of Halle, Kurt-Mothes-Strasse 3, 06120 Halle, Germany. [4]Cell Biology and Biophysics Unit, European Molecular Biology Laboratory, Meyerhofstrasse 1, 69117 Heidelberg, Germany.

*Present address: Analytical Electron Microscopy Facility, Queensland University of Technology, Brisbane, Australia.
†To whom correspondence should be addressed. E-mail: john.briggs@embl.de (J.A.G.B.); felix.wieland@bzh.uni-heidelberg.de (F.T.W.)

connection (Fig. 3K, arrow). At single and paired two-corner positions, the corner of the triad adopted a different conformation (Fig. 3, M and N, arrows). The connections between triad edges can link three (Fig. 3L, arrowhead) or two triads (Fig. 3, M and N, arrowheads). Hence, dependent on its position within the lattice, coatomer can form homotrimeric or dimeric interactions. This variable valency of interaction is achieved through substantial conformational variability (Fig. 3O).

Structures of triads and linkages were placed at the positions and orientations where they were

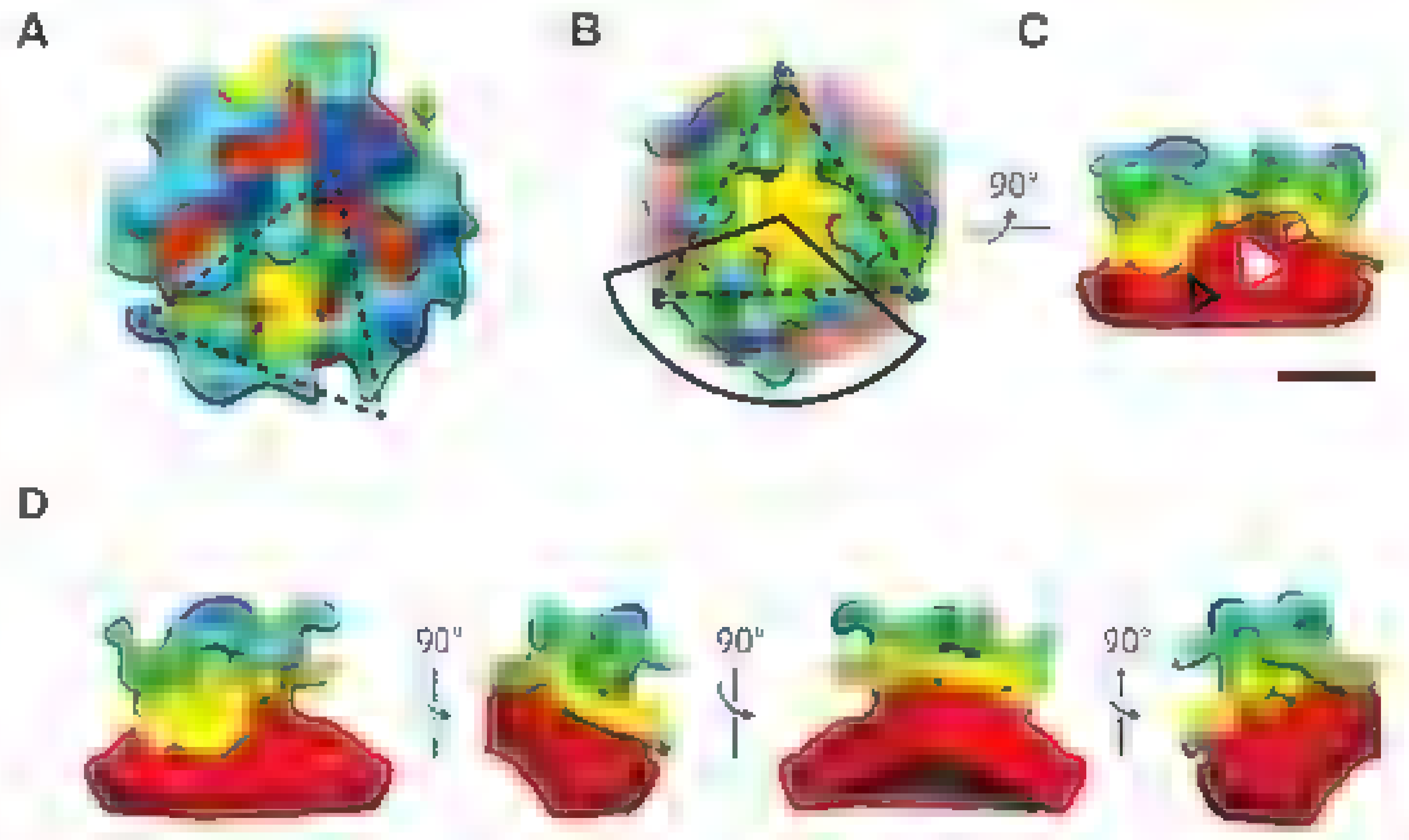

Fig. 2. Structure of a COPI triad. **(A)** Isosurface representation of a reference-free reconstruction of a COPI-coated vesicle subvolume (fig. S2). Coat density is colored from yellow to blue according to radial distance from the membrane (red). A triad consists of three leaflike coatomer densities, arranged in a pseudo–three-fold fashion (dotted triangle) around a central platform (yellow). **(B)** Top view, 26 Å resolution isosurface representation of a triad after three-fold symmetrization. Dotted triangle highlights three-fold symmetry. Black outline indicates one leaf. Transparent surfaces indicate density from adjacent triads. **(C)** Side view of the triad, showing contacts with the membrane below the platform (white arrowhead), and below the leaf (black arrowhead). Scale bar, 10 nm. **(D)** Side views of the leaf outlined in (B).

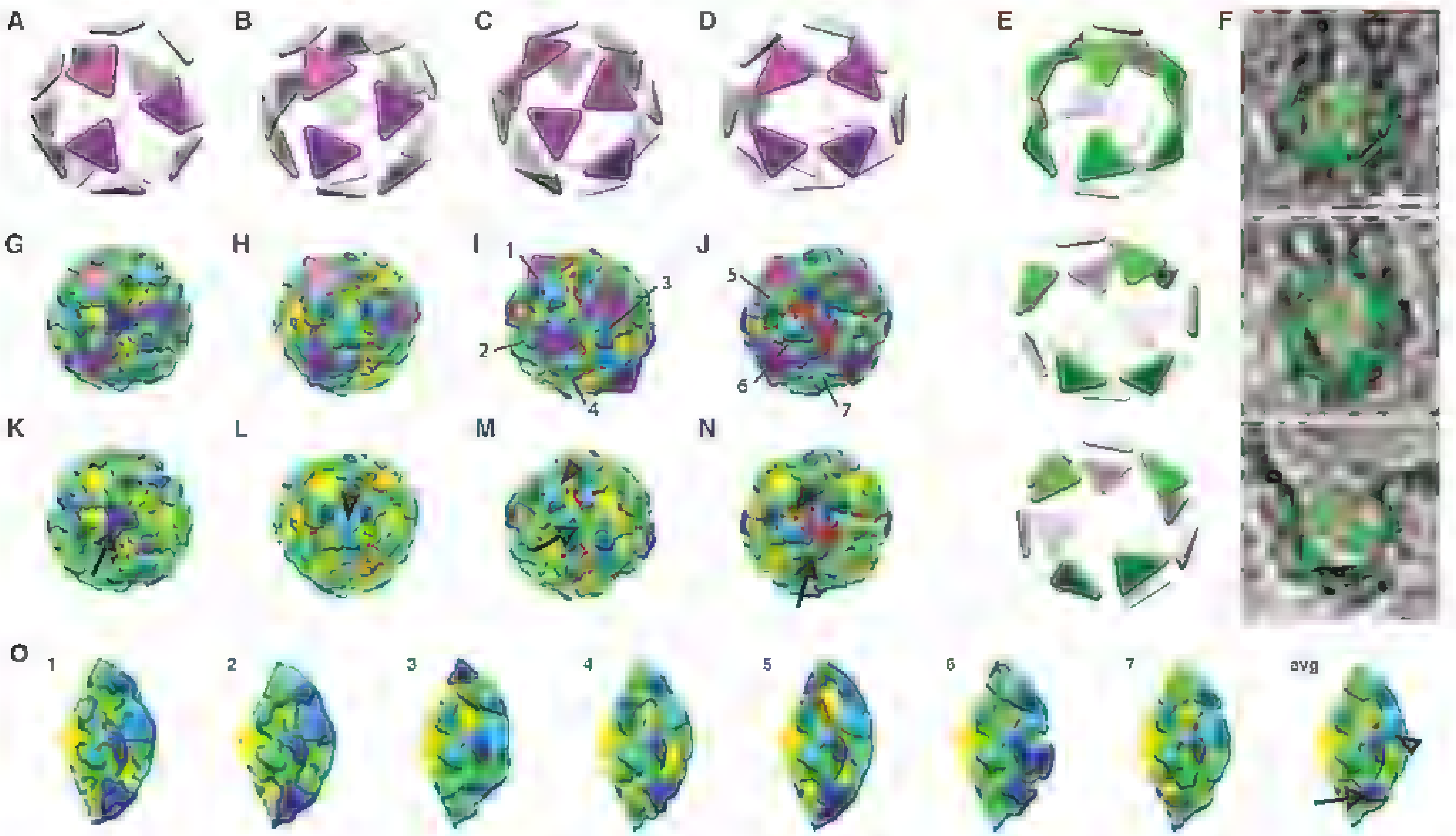

Fig. 3. Arrangement of triads in the vesicle coat and structures of triad patterns. **(A to D)** Lattice maps where each triangle represents the position and orientation of a triad identified during subtomogram averaging. Purple triangles indicate characteristic triad arrangements: (A) where the corners of three triads met, (B) where the edges of three triads met, (C) a single two-corner position, and (D) a paired two-corner position. **(E)** Three coated vesicle lattice maps with the budding scar oriented toward the reader. The triad arrangement around the gap (green) precludes closing the gap by placing further triads into the lattice. **(F)** Lattice maps of COPI vesicle buds, superimposed on tomogram slices to show the shape of the membrane. The only gap found is at the bud neck (oriented toward the top). Scale bar, 30 nm. **(G to J)** Isosurface representations of structures corresponding to characteristic triad patterns, superimposed on the purple triangles. Numbers in (I) and (J) indicate the seven unique leaf conformations relative to the two-corner positions. **(K to N)** As in (G) to (J) without superimposed triangles. Arrows and arrowheads indicate triad corners and edges, respectively, where different conformations are seen in different linkages. **(O)** Isosurface representations of each of the different leaf conformations, these are averages of all leaves found at equivalent positions indicated in (I) and (J). Leaf number 2 is the conformation at the three-corner position. The leaf marked "avg" is the weighted average of leaves 1 to 7. Densities are cut as in the black sector of Fig. 2B. The inner region of the leaves, facing the platform (left side), is constant, whereas the connections with other triads (arrow and arrowhead in avg) show substantial structural variability. Densities are colored as in Fig. 2.

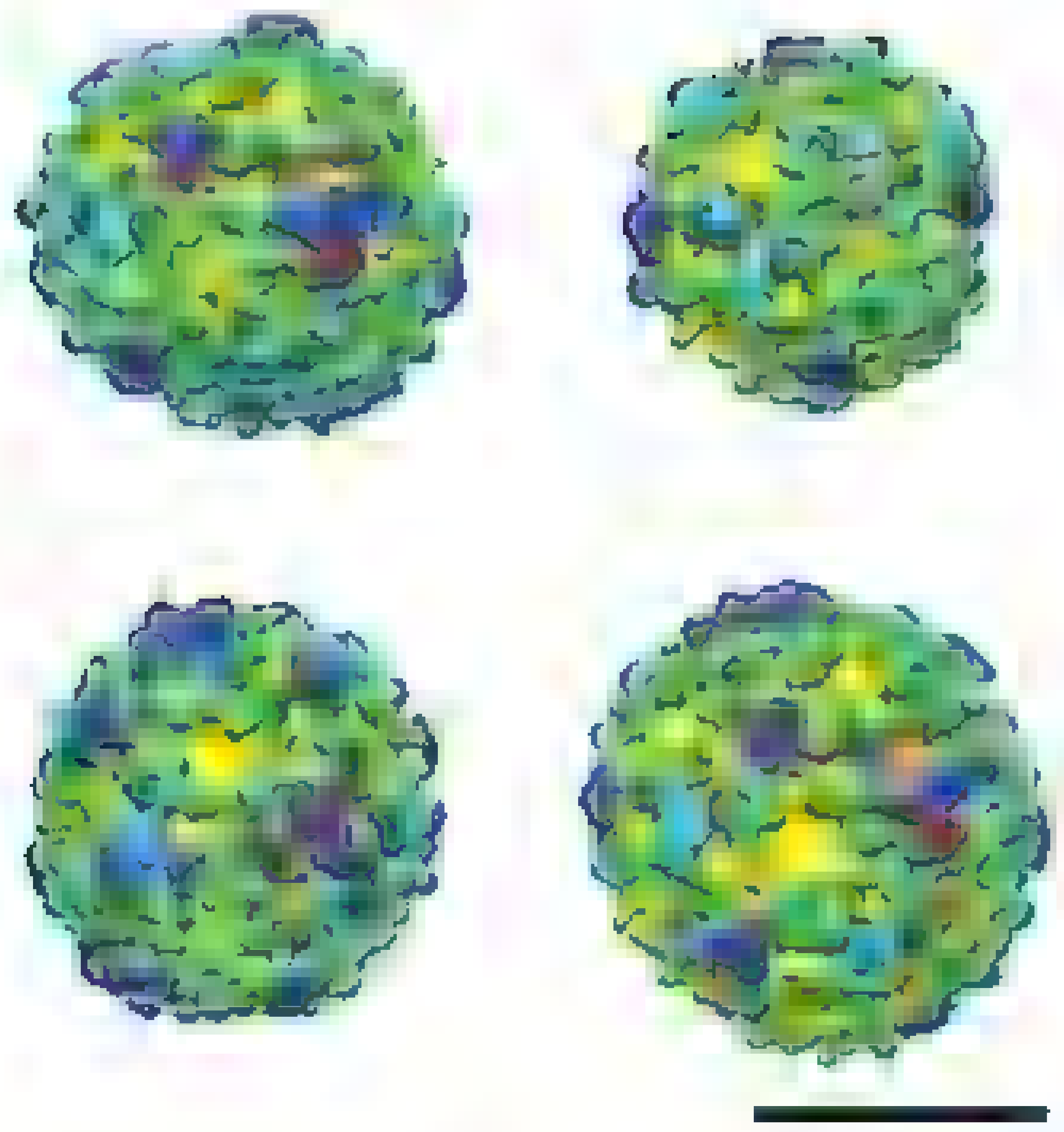

Fig. 4. The structures of COPI-coated vesicles. Isosurface representations of four COPI-coated vesicles produced by positioning reconstructions of triads and triad patterns (Figs. 2 and 3, K to N) at the positions and orientations in space at which they were identified during subtomogram averaging. Densities are colored as in Fig. 2. Scale bar, 50 nm.

found in each vesicle and were merged to create continuous density models of individual vesicles (Fig. 4 and movie S2). These models suggest that the COPI coat contains only small apertures (Fig. 4 and fig. S1). Sufficient membrane access for fusion with a target membrane could only be achieved after coat disassembly or through budding scars. In contrast, clathrin and COPII cages form lattices with larger apertures (fig. S1).

In existing models for clathrin and COPII vesicle coats, multiple identical subunits each make the same set of interactions with the same number of neighbors (*1*). Structural flexibility allows formation of vesicles from different total numbers of subunits. Based on these principles, both clathrin-like (*20*) and COPII-like (*23*) models have been proposed for the assembled COPI coat. We found instead that assembled coatomer can adopt different conformations to interact with different numbers of neighbors. By regulating the relative frequencies of different triad patterns in the COPI coat during assembly—for example, by stabilizing particular coatomer conformations—the cell would have a mechanism to adapt vesicle size and shape to cargoes of different sizes.

References and Notes

1. S. C. Harrison, T. Kirchhausen, *Nature* **466**, 1048 (2010).
2. H. T. McMahon, I. G. Mills, *Curr. Opin. Cell Biol.* **16**, 379 (2004).
3. K. Schledzewski, H. Brinkmann, R. R. Mendel, *J. Mol. Evol.* **48**, 770 (1999).
4. A. Fotin *et al.*, *Nature* **432**, 573 (2004).
5. S. M. Stagg *et al.*, *Nature* **439**, 234 (2006).
6. S. M. Stagg, P. LaPointe, W. E. Balch, *Curr. Opin. Struct. Biol.* **17**, 221 (2007).
7. Y. Cheng, W. Boll, T. Kirchhausen, S. C. Harrison, T. Walz, *J. Mol. Biol.* **365**, 892 (2007).
8. R. Beck, M. Rawet, F. T. Wieland, D. Cassel, *FEBS Lett.* **583**, 2701 (2009).
9. S. Hara-Kuge *et al.*, *J. Cell Biol.* **124**, 883 (1994).
10. C. K. Yip, T. Walz, *J. Mol. Biol.* **408**, 825 (2011).
11. M. C. Sahlmüller *et al.*, *Traffic* **12**, 682 (2011).
12. G. Griffiths, R. Pepperkok, J. K. Locker, T. E. Kreis, *J. Cell Sci.* **108**, 2839 (1995).
13. M. Bremser *et al.*, *Cell* **96**, 495 (1999).
14. L. Orci, B. S. Glick, J. E. Rothman, *Cell* **46**, 171 (1986).
15. J. A. Briggs *et al.*, *Proc. Natl. Acad. Sci. U.S.A.* **106**, 11090 (2009).
16. F. Förster, O. Medalia, N. Zauberman, W. Baumeister, D. Fass, *Proc. Natl. Acad. Sci. U.S.A.* **102**, 4729 (2005).
17. Materials and methods are available as supplementary materials on *Science* Online.
18. L. P. Jackson *et al.*, *Cell* **141**, 1220 (2010).
19. X. Yu, M. Breitman, J. Goldberg, *Cell* **148**, 530 (2012).
20. C. Lee, J. Goldberg, *Cell* **142**, 123 (2010).
21. D. K. Cureton, R. H. Massol, S. Saffarian, T. L. Kirchhausen, S. P. Whelan, *PLoS Pathog.* **5**, e1000394 (2009).
22. V. Sirotkin, J. Berro, K. Macmillan, L. Zhao, T. D. Pollard, *Mol. Biol. Cell* **21**, 2894 (2010).
23. K. C. Hsia, A. Hoelz, *Proc. Natl. Acad. Sci. U.S.A.* **107**, 11271 (2010).

Acknowledgments: We thank M. Beck, J. Ellenberg, M. Kaksonen, and S. Welsch for critically reading the manuscript and F. Thommen, T. Bharat, and A. de Marco for technical assistance. This work was funded by the Deutsche Forschungsgemeinschaft within SFB638 (A16) to J.A.G.B. and F.T.W., by Bundesministerium für Bildung und Forschung to K.B., and was technically supported by use of the European Molecular Biology Laboratory EM Core Facility and Information Technology Services. EM maps are deposited in the Electron Microscopy Data Bank (EMDB) (accession codes from EMD-2084 to EMD-2088). J.A.G.B. and F.T.W. conceived and administered the study. S.P., M.F., and R.B. reconstituted budding reactions, supported by K.B. and B.B. S.P., R.B., and K.B. prepared reagents. M.F., S.P., and J.D.R. collected data. M.F., M.S., and J.A.G.B. developed image processing routines. M.F. and J.A.G.B. analyzed data. M.F., F.T.W. and J.A.G.B. interpreted data. M.F. and J.A.G.B. wrote the paper, supported by all authors.

Supplementary Materials
www.sciencemag.org/cgi/content/full/science.1221443/DC1
Materials and Methods
Figs. S1 to S6
References (*24*–*31*)
Movies S1 and S2

5 March 2012; accepted 2 May 2012
Published online 24 May 2012;
10.1126/science.1221443

Awake Hippocampal Sharp-Wave Ripples Support Spatial Memory

Shantanu P. Jadhav, Caleb Kemere, P. Walter German, Loren M. Frank*

The hippocampus is critical for spatial learning and memory. Hippocampal neurons in awake animals exhibit place field activity that encodes current location, as well as sharp-wave ripple (SWR) activity during which representations based on past experiences are often replayed. The relationship between these patterns of activity and the memory functions of the hippocampus is poorly understood. We interrupted awake SWRs in animals learning a spatial alternation task. We observed a specific learning and performance deficit that persisted throughout training. This deficit was associated with awake SWR activity, as SWR interruption left place field activity and post-experience SWR reactivation intact. These results provide a link between awake SWRs and hippocampal memory processes, which suggests that awake replay of memory-related information during SWRs supports learning and memory-guided decision-making.

Animals use past experience to guide decisions, an ability that requires storing memories for the events of daily life and retrieving those memories as needed. This storage and retrieval depends on the hippocampus and associated structures in the medial temporal lobe (*1*–*5*), but the specific patterns of neural activity that support these memory functions remain poorly understood. We know that during exploration, individual neurons fire in specific regions of space (*5*, *6*) known as place fields. In contrast, during periods of slow movement, immobility, and slow-wave sleep, groups of neurons are active during sharp-wave ripple (SWR) events (*7*, *8*). This activity frequently represents a replay of a past experience on a rapid time scale (*9*–*13*). SWRs that occur during sleep contribute to memory consolidation of preceding experiences (*14*–*18*), and both changes in place fields and the intensity of awake memory reactivation have been correlated with memory performance (*19*). Awake SWRs in particular can reactivate sets of place fields encoding forward and reverse paths associated with both current and past locations (*9*–*13*). This reactivation has been hypothesized to contribute to multiple functions including learning, retrieval, consolidation, and trajectory planning (*19*–*23*). To investigate the role of awake hippocampal SWRs and to determine whether awake replay can be functionally dissociated from place field activity, we selectively disrupted awake SWRs in rats learning a hippocampus-dependent W-track task (*24*). We have previously shown that the hippocampus frequently replays memories of past experience while animals learn this task (*11*).

Animals are rewarded on the W-track each time they visit the end of one of the three maze arms in the correct task sequence (center-left-center-right-center…, Fig. 1A). This task consists

Department of Physiology and Center for Integrative Neuroscience, University of California, San Francisco, CA 94143, USA.

*To whom correspondence should be addressed. E-mail: loren@phy.ucsf.edu

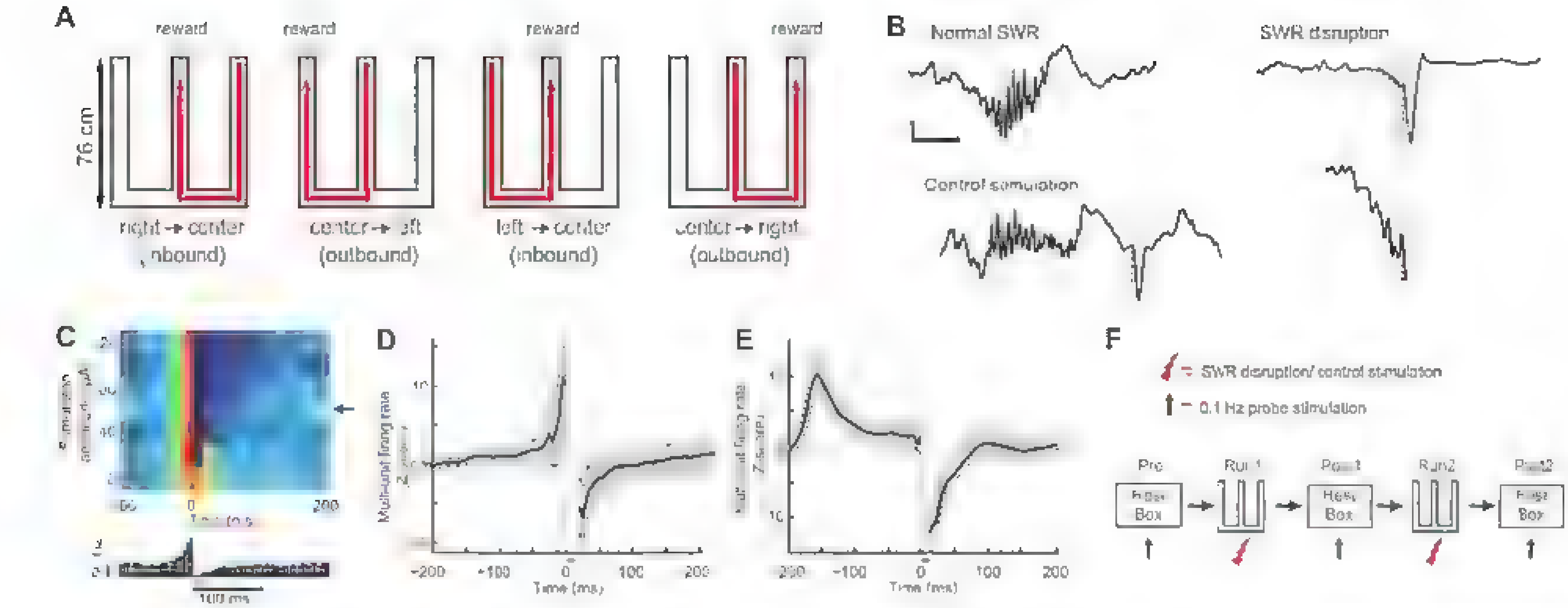

Fig. 1. Experimental design and SWR disruption during behavior. **(A)** Schematic illustrating the W-track task. **(B)** Example of a normal SWR (top left), disrupted SWR (right), and control stimulation after SWR (bottom left). Each panel shows an online detected SWR in the broadband local field potential (1 to 400 Hz). Cyan lines denote time of SWR detection; red lines denote time of vHC stimulation. The region in the gray box for the disrupted SWR is expanded below. Scale bars, 50 ms and 200 μV. **(C)** Top: Mean normalized multiunit activity (5-ms bins) versus stimulation intensity during calibration. Arrow denotes chosen amplitude. Bottom: Corresponding histogram for chosen amplitude; cyan line denotes baseline firing rate. Gray bar denotes spiking obscured by stimulation artifacts and fPSPs. **(D** and **E)** *Z* scores of multiunit firing rate aligned to stimulation for all sessions for the SWR disruption group (D) and the control stimulation group (E). Vertical red lines show the time of stimulation; horizontal cyan lines denote mean firing rates. **(F)** Sequence of rest and run sessions for each day.

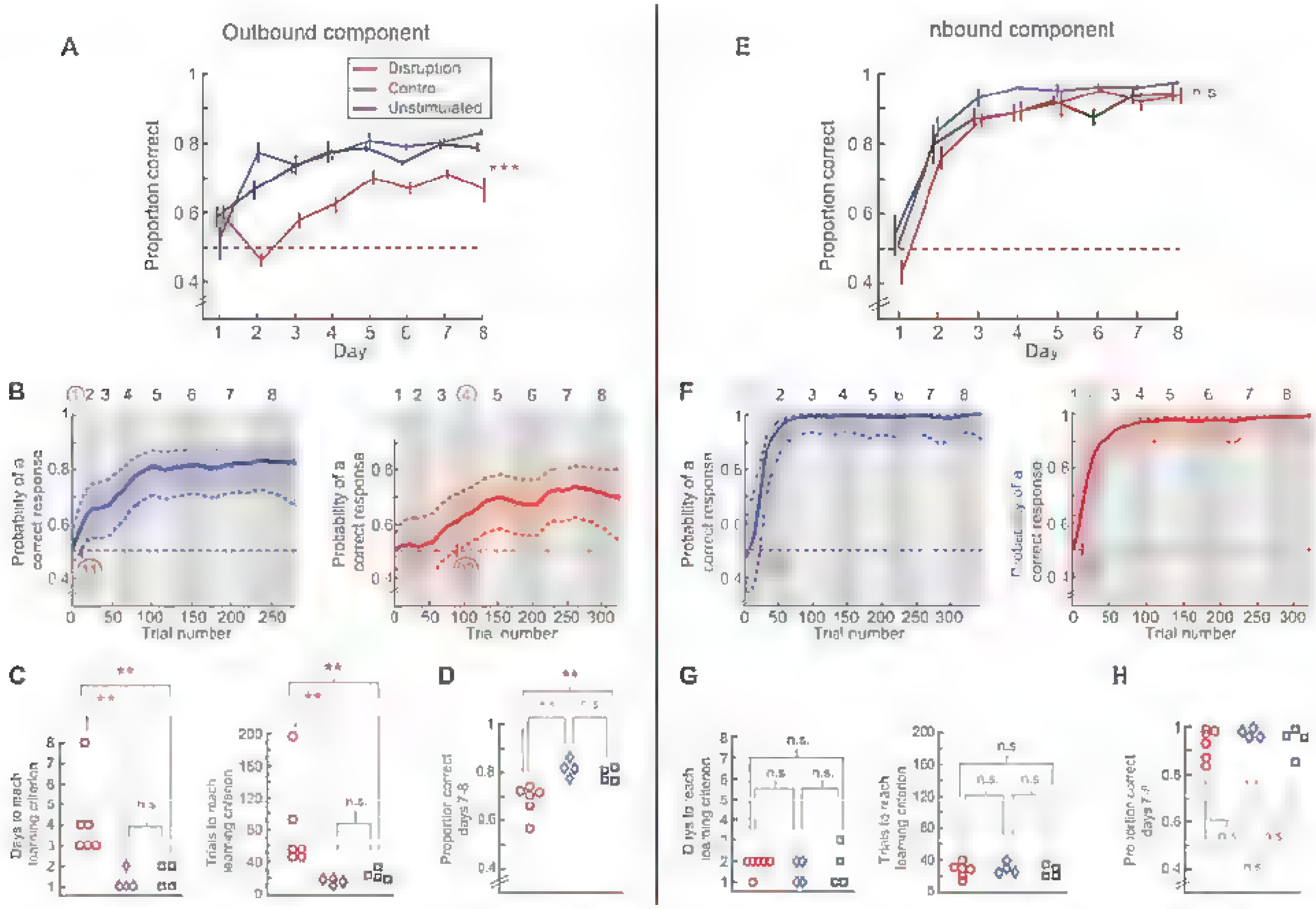

Fig. 2. SWR disruption causes a specific impairment in the outbound, spatial working memory component of the W-track task. **(A)** Proportion correct versus day number for outbound trials. Horizontal dotted line represents chance-level performance of 0.5. **(B)** Outbound learning curves with 90% confidence intervals for a control stimulation animal (left) and a SWR disruption animal (right). Background shaded areas denote days (numbers on top). Learning trial and learning day are highlighted in red. **(C)** Outbound learning day (left) and learning trial (right) for each animal. **(D)** Average outbound performance on the last 2 days of testing (days 7 and 8). **(E** to **H)** Corresponding plots for inbound performance. **P* < 0.05, ***P* < 0.01, ****P* < 0.001; error bars represent SEM.

of two components: (i) an "outbound" alternation component that specifies that when the animal is in the center arm, the next correct outer arm is the one opposite to the outer arm it most recently visited, and (ii) an "inbound" return-to-center component that specifies that when the animal is in an outer arm, it must then proceed to the center arm. Hippocampal damage impairs the rapid learning of both components, although hippocampal-lesion animals eventually learn the task (*24*), which suggests that other structures such as the basal ganglia and prefrontal cortex can support task performance after extended training.

We disrupted awake hippocampal SWRs on the W-track across 8 days of learning with the use of an online feedback system similar to that used in previous studies that disrupted SWRs during post-behavior sleep (*17*, *18*). SWRs in CA1 were detected by monitoring power in the ripple band (*25*) simultaneously across multiple tetrodes. Online detection of a SWR event triggered calibrated single-pulse electrical stimulation of CA3 afferents to CA1 delivered through a bipolar stimulation electrode in the ventral hippocampal commissure (vHC, fig. S1). This terminated the ripple oscillation within 25 ms of SWR onset and transiently inhibited CA1 spiking (Fig. 1, B to E, and fig. S2) (*25*). We calibrated the stimulation magnitude for each animal to find the minimum current that inhibited multiunit spiking activity in CA1 for ~100 ms (Fig. 1, C to E, and fig. S2). To ensure that any observed effects were due to disruption of activity during SWRs, we used the same online detection protocol in a control group of animals, but delayed stimulation by 150 to 200 ms after detection (*17*) (Fig. 1, B and E, and fig. S2). This control stimulation left SWR-associated spiking activity intact while still inhibiting a temporally equivalent period of hippocampal activity (Fig. 1E).

Animals in three groups—SWR disruption, control stimulation, and an unimplanted, unstimulated group (n = 6, 4, and 4, respectively)—ran

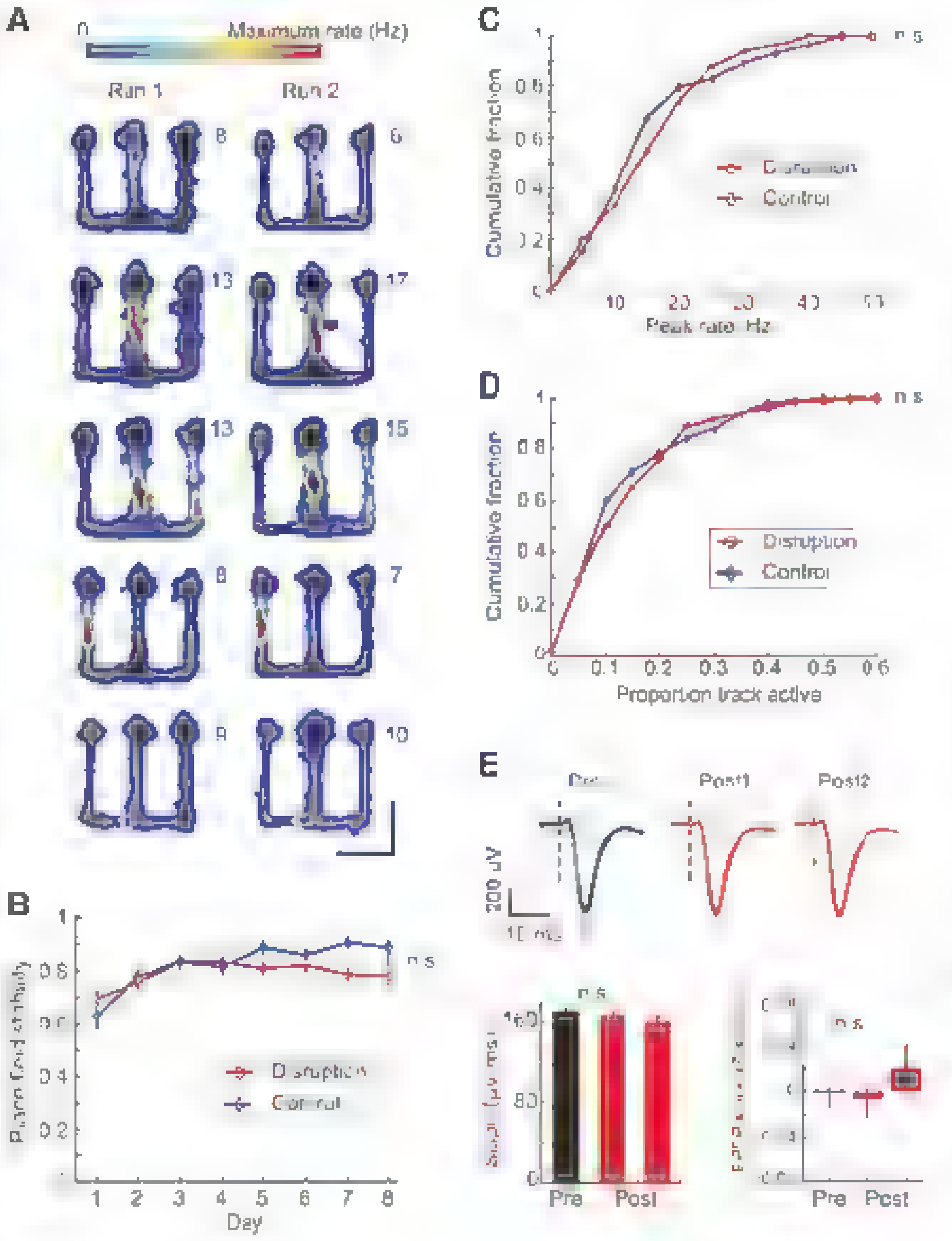

Fig. 3. Intact place-field representations and unchanged PSPs in SWR disruption animals. **(A)** Place fields from SWR disruption animals across run sessions within a day. Color plots represent occupancy-normalized firing rates of place cells. Numbers on top right of each plot denote peak spatial firing rate. Cells are from days 2, 3, 4, 6, and 8 (top to bottom), respectively. **(B)** Place field stability across days. **(C)** Cumulative distribution function (CDF) of place field peak rates. **(D)** CDF of place field sizes. **(E)** Evoked field responses during rest sessions. Top: Example showing mean evoked field PSPs during rest sessions in a single day in a SWR disruption animal. Shaded areas represent SEM. Dotted black lines indicate time of stimulation. Slopes of field PSPs were measured in the 1.5- to 2-ms window illustrated by cyan area in the left panel. Bottom: Slopes for the example above (left), and Z scores of field PSP slopes in the pre and post rest sessions for the SWR disruption group (right).

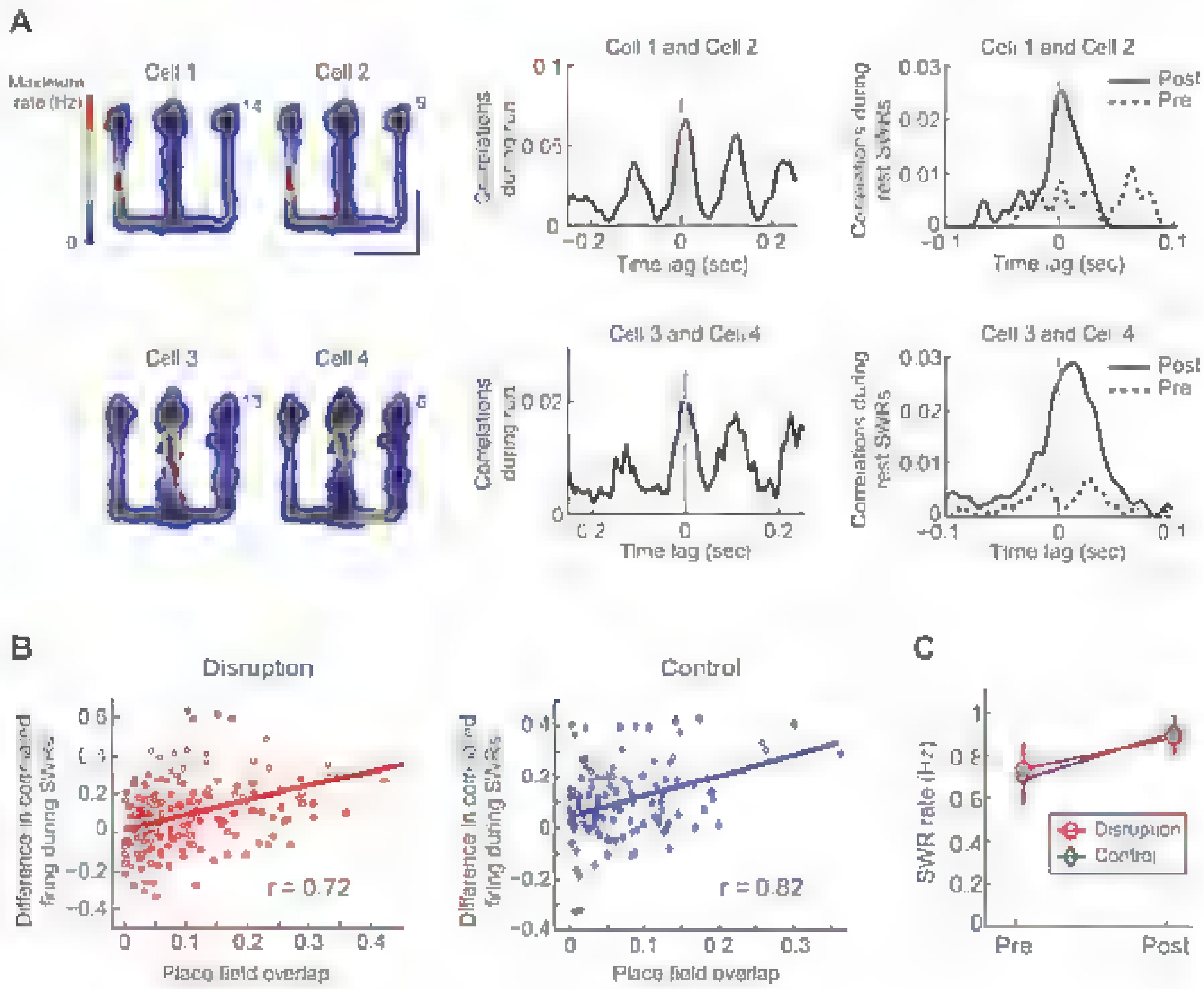

Fig. 4. Reactivation during SWRs in rest periods after behavior is intact. **(A)** Examples of reactivation from SWR disruption animals. Left: Place fields for cells during run sessions. Center: Cross-correlations for the cell pairs during run. Right: Cross-correlations during SWRs in rest periods. **(B)** Reactivation strength versus place field overlap for all cell pairs in the two groups (n = 183 pairs for the SWR disruption group; n = 145 pairs for the control stimulation group). Line represents best linear fit corresponding to the r value. **(C)** Mean SWR rate during the pre and post rest sessions. Error bars represent SEM.

two 15-min sessions on the W-track with interleaving 15-min rest sessions (one "pre" rest session before behavior and two "post" rest sessions after behavior) each day (Fig. 1F) for a total of 8 days. Spiking activity in CA1 was monitored during all run and rest sessions in the SWR disruption and control stimulation groups. To control for the possibility that vHC stimulation could lead to changes in the synaptic strength of CA3 input to CA1, we also measured evoked field responses to 0.1-Hz probe stimulation in the intervening rest periods (Fig. 1F) (*25*).

SWR disruption animals were impaired on the outbound component of the task as compared to controls (Fig. 2, A to D). SWR disruption animals performed a lower proportion of correct outbound trials than the control animals across all eight days of learning (Fig. 2A; $n = 6$, 4, and 4 animals, repeated-measures ANOVA, main effect of group, $P < 0.001$, group × day interaction, $P < 0.01$; no differences between control and unstimulated group, $Ps > 0.4$). We also used a state-space model to estimate the trial and day on which performance was above chance for each animal (*24–26*) (Fig. 2B and figs. S3 to S5). SWR disruption animals learned later than controls in terms of both trials and days to criterion (Fig. 2C, rank-sum test, $Ps < 0.01$). SWR disruption animals also had significantly lower performance levels on the final 2 days (Fig. 2D, rank-sum test, $P < 0.01$). Further, all SWR disruption animals learned more slowly than all eight control animals, and all SWR disruption animals had lower performance on days 7 and 8 than all eight control animals. These perfect separations in the rank order of learning rates and final performance would occur by chance with a probability < 0.0007. Similar statistical results were obtained with the two control groups combined (*25*).

In contrast, SWR disruption animals performed normally in the inbound component of the task (Fig. 2E; $n = 6$, 4, and 4 animals, repeated-measures ANOVA, main effect of group, $P > 0.33$, group × day interaction, $P > 0.5$) and had similar learning rates as compared to controls (Fig. 2F and figs. S6 to S8). Learning trial and day were similar among the SWR disruption and control groups (Fig. 2G, rank-sum tests, $Ps > 0.5$), and the final performance levels achieved by the animals in the last 2 days were also similar (Fig. 2H, rank-sum test, $P > 0.48$). The distinction between learning on the outbound and inbound tasks remained clear when learning curves were aligned by trial number for the three groups (fig. S9).

SWR disruption effectively suppressed hippocampal activity during SWRs but had no discernible effect on place cell representations. We examined the stability of CA1 place fields in run sessions (Fig. 3A and fig. S10) and computed the correlation between linearized place fields (*11*, *25*, *27*) of each cell across the two run sessions within each day (Fig. 3, A and B, and fig. S11). We found no difference in place field stability between place cells from the two groups (SWR disruption: $n = 108$ place cells, mean correlation $= 0.80 \pm 0.02$; control stimulation: $n = 96$ cells, mean correlation $= 0.81 \pm 0.02$; t test, $P > 0.5$) across all days (Fig. 3B; two-way ANOVA, main effect of group, $P > 0.16$, group × day interaction, $P > 0.5$; within-day comparisons, n.s.; Bonferroni post hoc tests). The distributions of peak rates and place field sizes for the two groups were also similar (Fig. 3, C and D, KS test, $Ps > 0.5$). We also found no evidence that stimulation induced synaptic plasticity. We found no difference in field postsynaptic potential (PSP) slopes in response to 0.1-Hz probe stimulation between the pre rest period before behavior and the post rest periods after behavior compared on each day for all animals (example and Z scores across all days in Fig. 3E, n.s., t test, $P > 0.43$). Further, differences in other behavior or stimulation parameters could not account for the learning deficit in the SWR disruption group (figs. S12 to S17).

The deficit on outbound but not inbound trials suggests that loss of awake SWRs did not cause a global deficit in memory consolidation. Consistent with this, we found no evidence for alteration of the rest/sleep SWR activity associated with consolidation. Pairs of cells with overlapping place fields had theta-modulated correlations during run periods and showed increased correlations during SWRs in post relative to pre rest periods (Fig. 4A), as has been observed in animals with intact hippocampal activity (*14*, *16*, *28*). For both SWR disruption and control stimulation groups, reactivation strength (Fig. 4B) was significantly correlated with place field overlap (linear regression, $Ps < 0.001$) and with correlations during run (fig. S18, linear regression, $Ps < 0.001$). SWR rates in the rest periods were also similar for the SWR disruption and control stimulation groups (Fig. 4C and fig. S18).

Our observation of intact place fields, intact reactivation during rest SWRs, and intact inbound performance suggests that place fields and post-experience reactivation are sufficient to support learning and performance of the inbound trials. As hippocampal lesions disrupt learning on the inbound component, place cell activity may be important for learning and applying the inbound rule. More broadly, place cell activity could provide information about current position that promotes rapid learning and application of location-specific rules (fig. S19).

The specific performance deficit observed in SWR disruption animals provides a causal link between awake hippocampal SWRs and the spatial memory requirements of outbound trials. Learning of the outbound rule requires linking immediate and more remote past experience to reward (fig. S19), and the observed replay of both recent and remote experiences during awake SWRs (*11–13*) is well suited to contribute to this learning. Applying the outbound rule in the center arm requires knowledge of current location, memory for immediate past outer arm location, and the ability to use that memory to plan and execute a movement to the opposite outer arm. This memory-guided decision-making process has been referred to as "spatial working memory" (*2*, *4*). Impaired outbound performance in the SWR disruption group on later days (Fig. 2), even after most animals performed above chance, suggests a spatial working memory impairment. Additional evidence for this was provided by a decline in performance in three of the animals from the control stimulation group that were switched to SWR disruption on days 9 and 10 (fig. S20). Forward and backward replay of both past and possible future trajectories during SWRs (*9–13*, *21*) may therefore contribute to outbound performance. Conversely, we would predict that manipulations that cause selective spatial working memory deficits, such as the removal of parvalbumin-positive interneurons in CA1 and GluR1 knockout animals at the CA3-CA1 synapse (*29*, *30*), have their impact primarily as a result of disrupting awake replay processes. Thus, we hypothesize that the forward and reverse replay of local and spatially remote paths seen during awake replay provides information about past locations and possible future options (fig. S19) to structures such as the prefrontal cortex that use this information to learn the outbound alternation rule and to subsequently apply the learned rule to guide behavior.

References and Notes

1. L. R. Squire, *Psychol. Rev.* **99**, 195 (1992).
2. H. Eichenbaum, N. J. Cohen, *From Conditioning to Conscious Recollection* (Oxford Univ. Press, New York, 2001).
3. G. Riedel *et al.*, *Nat. Neurosci.* **2**, 898 (1999).
4. D. S. Olton, J. T. Becker, G. E. Handelmann, *Behav. Brain Sci.* **2**, 313 (1979).
5. J. O'Keefe, L. Nadel, *The Hippocampus as a Cognitive Map* (Oxford Univ. Press, London, 1978).
6. M. A. Wilson, B. L. McNaughton, *Science* **261**, 1055 (1993).
7. G. Buzsáki, *Brain Res.* **398**, 242 (1986).
8. J. O'Neill, T. Senior, J. Csicsvari, *Neuron* **49**, 143 (2006).
9. D. J. Foster, M. A. Wilson, *Nature* **440**, 680 (2006).
10. K. Diba, G. Buzsáki, *Nat. Neurosci.* **10**, 1241 (2007).
11. M. P. Karlsson, L. M. Frank, *Nat. Neurosci.* **12**, 913 (2009).
12. T. J. Davidson, F. Kloosterman, M. A. Wilson, *Neuron* **63**, 497 (2009).
13. A. S. Gupta, M. A. van der Meer, D. S. Touretzky, A. D. Redish, *Neuron* **65**, 695 (2010).
14. M. A. Wilson, B. L. McNaughton, *Science* **265**, 676 (1994).
15. G. Buzsáki, *Cereb. Cortex* **6**, 81 (1996).
16. H. S. Kudrimoti, C. A. Barnes, B. L. McNaughton, *J. Neurosci.* **19**, 4090 (1999).
17. G. Girardeau, K. Benchenane, S. I. Wiener, G. Buzsáki, M. B. Zugaro, *Nat. Neurosci.* **12**, 1222 (2009).
18. V. Ego-Stengel, M. A. Wilson, *Hippocampus* **20**, 1 (2010).
19. D. Dupret, J. O'Neill, B. Pleydell-Bouverie, J. Csicsvari, *Nat. Neurosci.* **13**, 995 (2010).
20. J. O'Neill, B. Pleydell-Bouverie, D. Dupret, J. Csicsvari, *Trends Neurosci.* **33**, 220 (2010).
21. M. F. Carr, S. P. Jadhav, L. M. Frank, *Nat. Neurosci.* **14**, 147 (2011).
22. A. C. Singer, L. M. Frank, *Neuron* **64**, 910 (2009).
23. S. Cheng, L. M. Frank, *Neuron* **57**, 303 (2008).
24. S. M. Kim, L. M. Frank, *PLoS ONE* **4**, e5494 (2009).

25. See supplementary materials on *Science* Online.
26. A. C. Smith *et al.*, *J. Neurosci.* **24**, 447 (2004).
27. G. Dragoi, K. D. Harris, G. Buzsáki, *Neuron* **39**, 843 (2003).
28. J. O'Neill, T. J. Senior, K. Allen, J. R. Huxter, J. Csicsvari, *Nat. Neurosci.* **11**, 209 (2008).
29. D. Reise, *et al.*, *Nat. Neurosci.* **5**, 868 (2002).
30. A. J. Murray *et al.*, *Nat. Neurosci.* **14**, 297 (2011).

Acknowledgments: Supported by a Wheeler Center Fellowship (S.P.J.), a Helen Hay Whitney Foundation grant (C.K.), and NIH grant R01 MH080283. The authors declare no competing financial interests.

Supplementary Materials
www.sciencemag.org/cgi/content/full/science.1217230/DC1
Materials and Methods
Supplementary Text
Figs. S1 to S20
References (31–35)

29 November 2011; accepted 16 April 2012
Published online 3 May 2012;
10.1126/science.1217230

Segregation of Axonal and Somatic Activity During Fast Network Oscillations

Tamar Dugladze,[1] Dietmar Schmitz,[2,3,4] Miles A. Whittington,[5] Imre Vida,[4] Tengis Gloveli[1,3]*

In central neurons, information flows from the dendritic surface toward the axon terminals. We found that during in vitro gamma oscillations, ectopic action potentials are generated at high frequency in the distal axon of pyramidal cells (PCs) but do not invade the soma. At the same time, axo-axonic cells (AACs) discharged at a high rate and tonically inhibited the axon initial segment, which can be instrumental in preventing ectopic action potential back-propagation. We found that activation of a single AAC substantially lowered soma invasion by antidromic action potential in postsynaptic PCs. In contrast, activation of soma-inhibiting basket cells had no significant impact. These results demonstrate that AACs can separate axonal from somatic activity and maintain the functional polarization of cortical PCs during network oscillations.

In response to synaptic inputs, action potentials (APs) are generated at the axon initial segment (AIS) and propagate along the axon to provide an output signal (*1*, *2*). However, APs can also be initiated in the distal axon under certain conditions (*3*–*7*), but it is unknown how back-propagation of such ectopic APs (EAPs) to the somatodendritic compartment is controlled.

We performed patch-clamp recordings from the soma or axon of hippocampal CA3 pyramidal cells (PCs) during fast network oscillations. In parallel, we monitored the local field potential in the stratum pyramidale (Fig. 1 and fig. S1). During gamma-frequency activity, CA3 PCs discharged phase-locked with the oscillations, but only at a low frequency (*8*–*10*) of 3.5 ± 0.5 Hz (Fig. 1A). Unexpectedly, the frequency of action currents (ACs) in axons recorded >600 μm from the soma was higher by a factor of 4 to 5, with a mean frequency of 16.1 ± 1.4 Hz (Fig. 1, B and C). These results indicate that in the distal axon of PCs, EAPs are generated at high frequencies during gamma oscillations; however, most of these APs do not reach the somatodendritic compartment. To directly demonstrate that axonal spikes are ectopically generated and fail to invade the soma, we performed dual somatic and axonal cell-attached recordings from individual cells (Fig. 1, D to F). We again found a low discharge frequency in the soma (2.7 ± 0.5 Hz) but a considerably higher frequency in the axon (15.8 ± 0.7 Hz; n = 9 cells) (Fig. 1, E and F).

The absence of EAP invasion of the soma may reflect strong γ-aminobutyric acid type A ($GABA_A$) receptor ($GABA_AR$)–mediated inhibition in the soma or at the AIS of PCs. We therefore applied $GABA_AR$ antagonist during dual axonal and somatic recordings from PCs. Bath application of $GABA_AR$ antagonist gabazine considerably increased the probability of the back-propagation of antidromic APs (from 19.3 ± 2.9% to 91.2 ± 1.2%, before and after gabazine application, respectively; n = 3) (fig. S2, A to C). Somatic invasion of APs in the presence of gabazine was maintained during hyperpolarization to −90 mV (92.7 ± 1.8%; n = 3), further indicating that APs are initiated antidromically in the distal axon. These results provide evidence that $GABA_AR$-mediated inhibition effectively controls axosomatic coupling and prevents the back-propagation of EAPs to the soma.

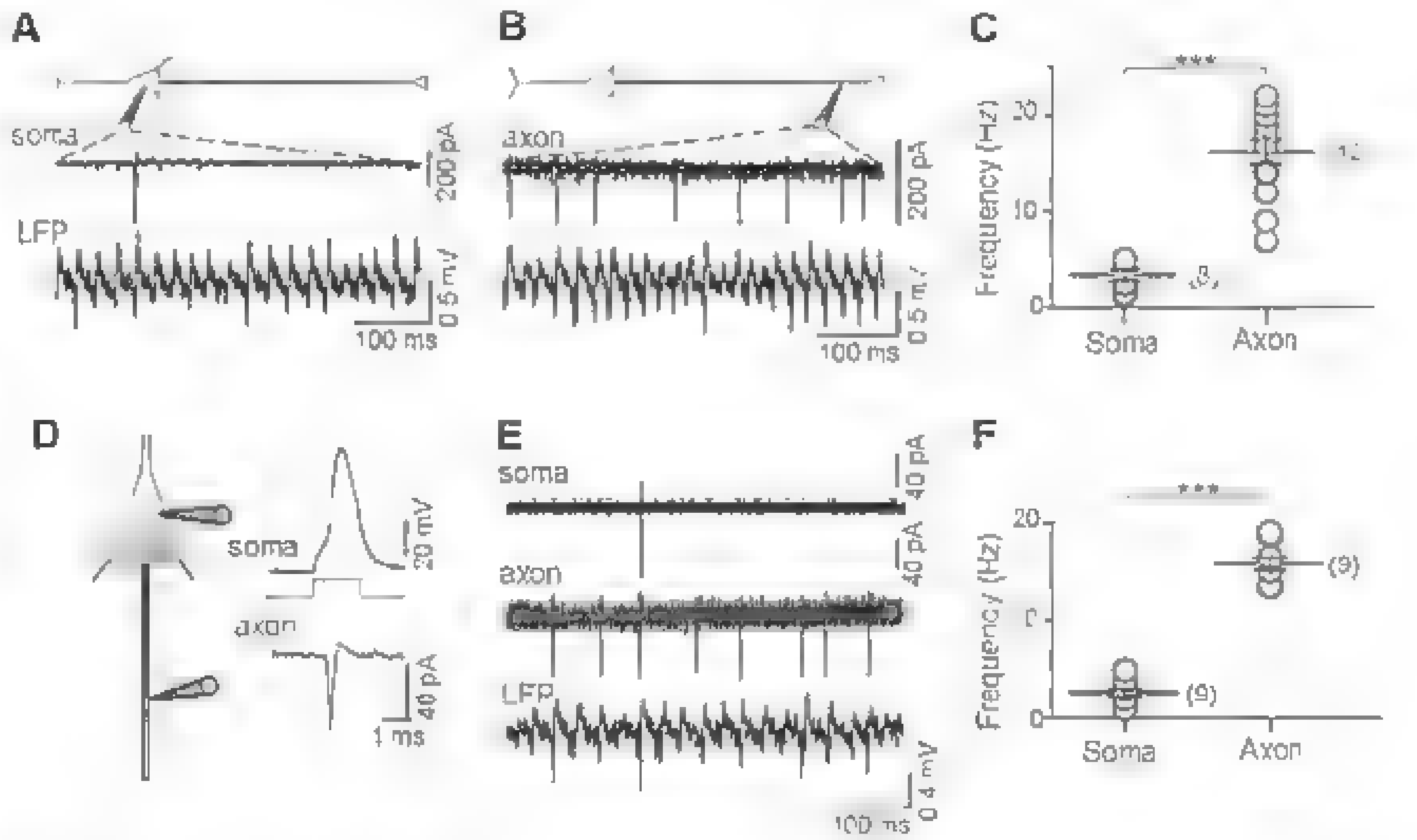

Fig. 1. High-frequency discharge of the axon, but not the soma, of hippocampal CA3 pyramidal cells during gamma-frequency oscillations in vitro. **(A and B)** Schematic representation of the recording configuration (top). Somatic (A) and axonal (B) cell-attached patch-clamp recordings were obtained from PCs during kainic acid (KA)–induced gamma oscillations in the local field potential (LFP). **(C)** Summary plot of AC frequency in the soma (8 cells) and axon (12 cells) reveals a significant difference between the two compartments (***P < 0.0001). **(D)** Scheme of dual somatic and axonal recording configuration. APs evoked in whole-cell configuration by brief depolarizing current injection into the soma (800 pA) (inset) reliably induced ACs in the axon, confirming that recordings are made from two compartments of the same cell. **(E)** Dual somatic and axonal cell-attached recordings directly demonstrate that high-frequency axonal spikes fail to invade the soma during gamma-frequency oscillations (LFP). **(F)** Summary plot shows the highly significant difference in the discharge frequency observed at the soma and proximal axon in dual recordings (n = 9 cells) during network oscillations.

[1]Institute of Neurophysiology, Charité-Universitätsmedizin Berlin, Charitéplatz 1, 10117 Berlin, Germany. [2]Neuroscience Research Center, Charité-Universitätsmedizin Berlin, Charitéplatz 1, 10117 Berlin, Germany. [3]Bernstein Center for Computational Neuroscience Berlin, Unter den Linden 6, 10099 Berlin, Germany. [4]Cluster of Excellence, NeuroCure, Charitéplatz 1, 10117 Berlin, Germany. [5]Institute of Neuroscience, Medical School, University of Newcastle, Framlington Place, Newcastle upon Tyne NE2 4HH, UK.

*To whom correspondence should be addressed. E-mail: tengis.gloveli@charite.de

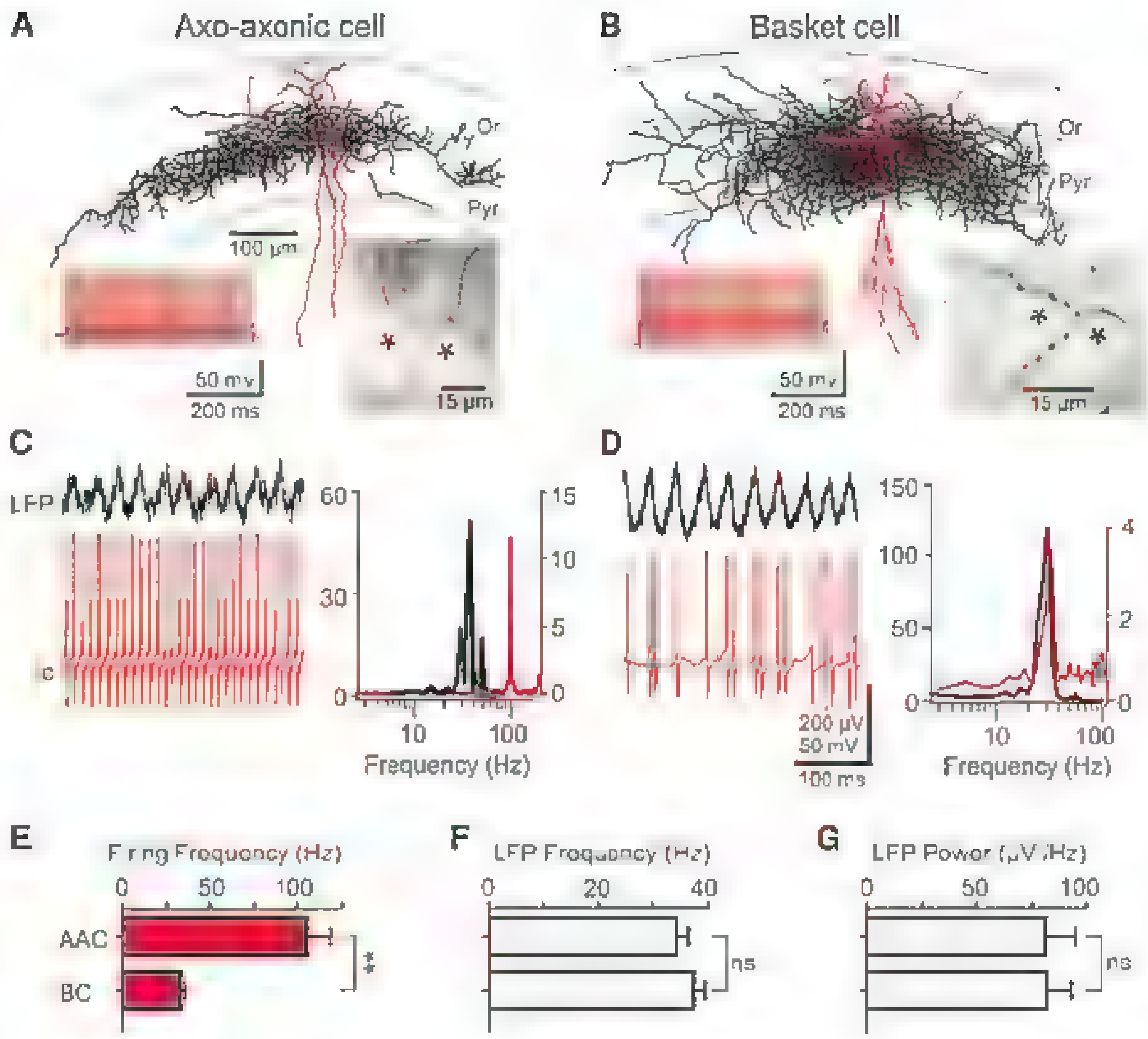

Fig. 2. AACs and BCs are differentially involved in gamma-frequency oscillations. (**A** and **B**) Reconstructions of a recorded and biocytin-filled AAC (A) and BC (B) in the CA3 area. The axon (in black) of the AAC is found at the border of the pyramidal layer (Pyr.) and stratum oriens (Or.), where AISs of pyramidal cells are localized. The light micrograph shows axo-axonic cartridges of labeled AAC along the AIS of two unstained PCs. Asterisks mark PC somata. In contrast, the BC shows a broader distribution of the axon in the pyramidal layer and adjacent region of the strata oriens and radiatum. The high-power photomicrograph shows two PC somata surrounded by biocytin-labeled axonal baskets. Inset traces illustrate the characteristic fast-spiking discharge of the interneurons in response to 0.3 nA depolarizing current pulses. (**C**) Whole-cell recording from an AAC reveals that the cell discharges at a constant high frequency (left, red trace, ic) during KA-induced network gamma oscillations (black trace, LFP). Spectral analysis of the AAC discharge shows a sharp peak at 104 Hz (right, red curve, right *y* axis; mV^2/Hz), separate from the peak in the power spectrum of the extracellular oscillations (30 Hz, black curve, left *y* axis; $\mu V^2/Hz$). (**D**) Corresponding data from a BC. In contrast to the AAC, the BC discharged at gamma frequencies (30 Hz) with clear phase-locking to the oscillations. (**E** to **G**) The firing frequencies of the two types are different during network activity (E), although there was no significant difference in the mean frequency (F) and power (G) of LFP between the two sets of recordings ($n = 4$ and 6, respectively).

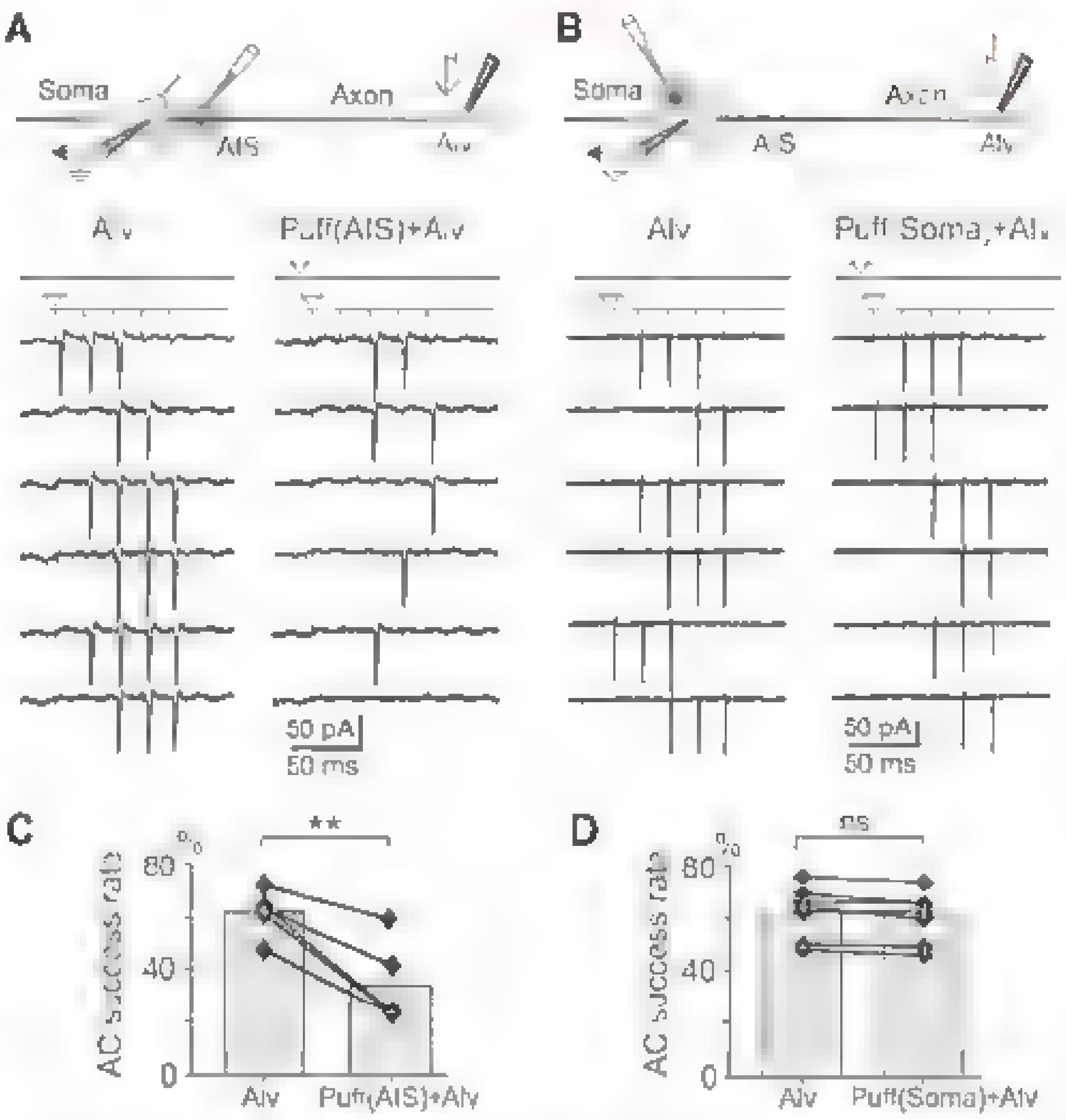

Fig. 3. GABA-mediated inhibition at the AIS reduces the back-propagation of ACs from the axon to the soma. (**A**) Schematic representation of the experimental configuration (top). Antidromic AC recorded from the PC in cell-attached configuration in response to alveus stimulation (five pulses at 50 Hz) in control conditions (bottom left, Alv, triangle) and in combination with puff-application of GABA to the AIS (100 μM; pressure 10 to 15 pounds per square inch; five pulses at 100 Hz) (bottom right, Puff(AIS)+Alv, triangle). (**B**) Corresponding data obtained in experiments with GABA application to the soma. (**C**) Bar chart shows that antidromic ACs can be recorded with high probability from the soma under control conditions (62.4 ± 4.1%), whereas the probability is reduced significantly when GABA is applied to the AIS (34.5 ± 7.3%, $P = 0.006$, data from 5 cells). (**D**) When GABA was puff-applied to the soma, the probability of antidromic AC at the soma was not significantly different between control conditions and GABA application in cell-attached configuration (62.0 ± 3.7% and 60.0 ± 3.6%, respectively; $n = 7$, $P = 0.7$). All these experiments were carried out in the presence of antagonists of fast glutamatergic transmission.

Inhibition to the soma and the AIS is mediated by basket cells (BCs) and axo-axonic cells (AACs), respectively. We next examined the relative contributions of these two sources of inhibition to the blockade of back-propagation. Consistent with previous reports (*9–11*), BCs discharged at gamma frequencies (33.6 ± 2.6 Hz; 6 BCs) phase-locked to the oscillation in the field potential (Fig. 2, B and D). In contrast, morphologically identified AACs fired at markedly higher frequencies (mean 105.3 ± 13.3 Hz; $n = 4$) and did not show correlation with the field oscillations (Fig. 2, A and C). The stark contrast between the behavior of AACs and the rhythmic activity of other inhibitory interneuron types (*9–11*) suggests that AACs play a unique role in gamma activity: They do not contribute to phasic inhibition underlying these oscillations but instead provide tonic inhibitory control to the AIS of PCs.

To better understand the function of AAC-mediated inhibition during gamma oscillations, we next explored whether $GABA_AR$ activation at the AIS has a hyperpolarizing or depolarizing effect (fig. S3). Both depolarizing (*12*) and hyperpolarizing (*13*) AAC effects have been reported. To avoid interference with the intracellular ionic environment, in particular the Cl^- concentration, cell-attached current-clamp recordings (*14*) were obtained from somata of CA3 PCs. Under these conditions, local GABA application to the AIS of the PCs resulted in transient hyperpolarizing

responses (fig. S3, A and B). Similar hyperpolarizing inhibitory effects were observed when GABA was applied to the soma (fig. S3, A and B). Bath application of the antagonist bicuculline (10 μM) reversibly blocked the hyperpolarizing responses (by 83.6 ± 4.8% and 86.0 ± 2.2% at the AIS and soma, respectively; $n = 4$ each), confirming that they were indeed mediated by fast ionotropic $GABA_A$Rs (*15*).

These results convergently indicated that AACs firing at high frequency could produce strong inhibition in the AIS of CA3 PCs during network activity. Could this inhibition underlie the failure of EAPs to back-propagate to the soma? We thus examined the effect of local GABA application on antidromic APs elicited by brief trains of electrical pulses to the distal axon in nonoscillating slices. AP invasion of the soma was detected by recording ACs in cell-attached voltage-clamp configuration. Without GABA application, ACs were recorded with high probability in response to the antidromic stimulation, indicating the reliable back-propagation of axonal APs. Application of GABA to the AIS during the stimulation significantly reduced the rate of ACs recorded at the soma (Fig. 3, A and C, and fig. S4, A and B). We repeated our experiments in whole-cell configuration, voltage clamping the PCs at −100 mV to prevent the generation of APs in the soma and the AIS. Without GABA application, antidromic ACs were recorded at the soma with similar high probability, indicating that these events were initiated by the extracellular stimuli in the distal axon rather than in the AIS or the soma. Application of GABA to the AIS of the hyperpolarized PCs resulted in a substantial reduction in the probability of back-propagating ACs (fig. S4C), which suggests that the shunting effect of inhibition, rather than membrane potential hyperpolarization, blocks the back-propagation of EAPs. In contrast, when GABA was applied to the soma, no significant reduction in the rate of ACs was observed (Fig. 3, B and D).

We then investigated whether a single AAC could provide sufficient GABAergic input in the AIS to suppress antidromically evoked APs. Simultaneous patch-clamp recordings were taken from synaptically coupled AAC and CA3 PC pairs (Fig. 4). The identity of the interneurons was confirmed by subsequent visualization and morphological analysis (Fig. 4, A to C). When the PC axon was stimulated without activating the presynaptic interneurons, ACs were observed with high probability at the soma (Fig. 4, D and E). Conversely, when a train of APs was elicited in the AACs during the stimulation of the PC axon, the probability of somatically recorded ACs was significantly lowered (Fig. 4, D and E). In stark contrast, activation of single BCs did not significantly decrease the rate of antidromic ACs in synaptically coupled CA3 PCs (Fig. 4E).

To further analyze the mechanisms underlying the control of somatic invasion by EAPs, we have used computational models of CA3 pyramidal cells (*16*), AACs, and BCs (figs. S5 to S7). In agreement with our experimental findings, brief high-frequency activation of a presynaptic AAC reliably blocked the invasion of AIS and the somatodendritic domain by antidromic APs (fig. S5C). For AACs, peak conductance amplitudes >0.01 μS reliably abolished the back-propagation of antidromic APs, whereas for BCs, a conductance larger by a factor of 3, 0.03 μS, was required (fig. S5, D and E). Qualitatively similar results were obtained when various parameters, including the reversal potential for $GABA_{AR}$-mediated inhibition, were changed (fig. S5, F and G), further indicating that the shunting effect of the inhibitory conductance at the AIS plays the major role in blocking the back-propagation of EAPs from the distal axon.

Finally, to investigate whether the AACs are also more efficient in controlling orthodromic

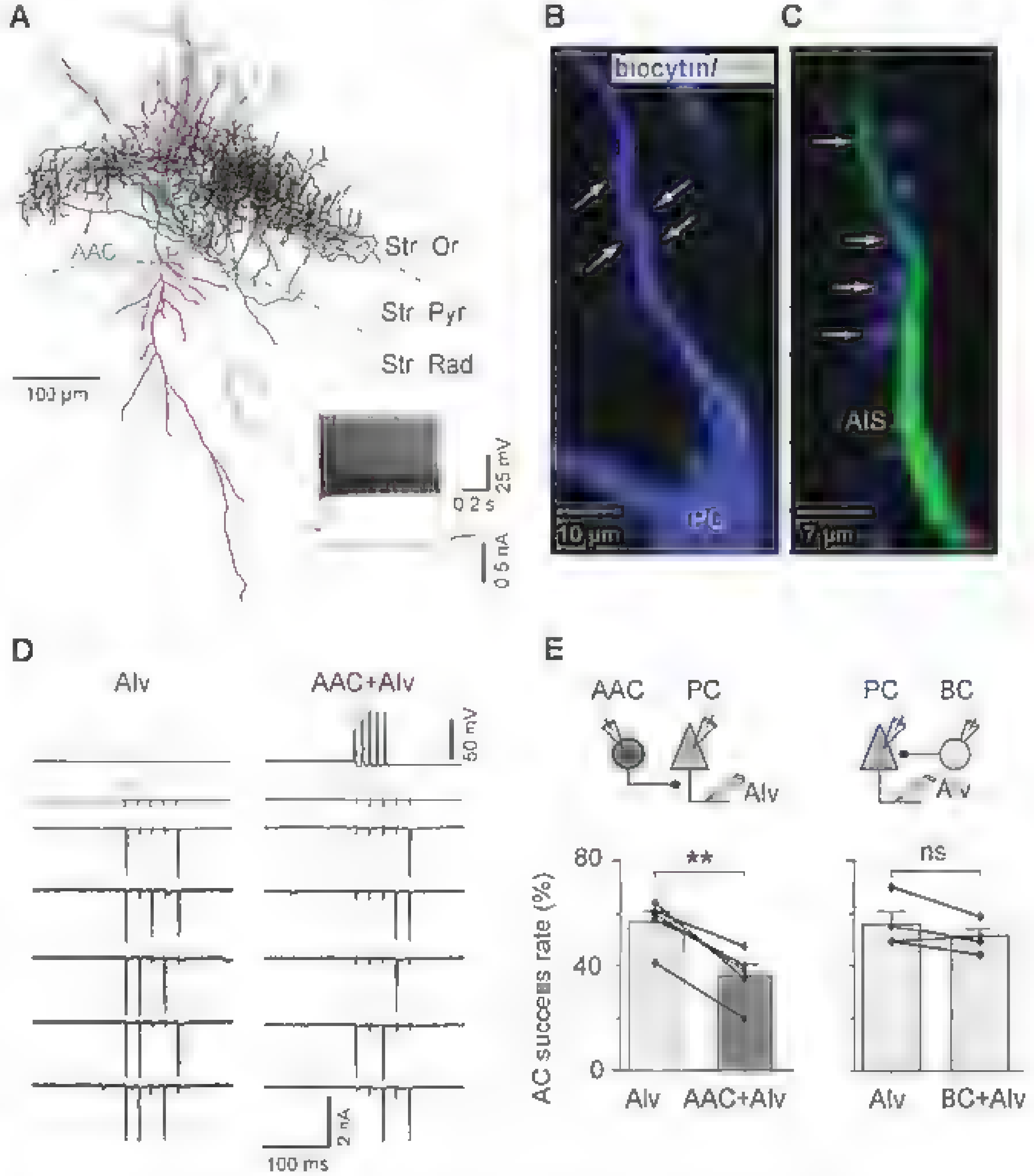

Fig. 4. Activation of a single AAC suppresses antidromic AP invasion of the soma in synaptically coupled PCs. **(A)** Neurolucida reconstruction of a synaptically coupled AAC and PC pair in the CA3 area (soma and dendrites of the AAC are in blue, axon in black; soma and dendrites of the PC are in pink, axon in green). The inset, bottom, illustrates the characteristic fast-spiking discharge of the AAC in response to a depolarizing current pulse. **(B)** Projection of a confocal image stack of the same PC AIS. Arrows indicate the location of putative synaptic contacts formed by AAC axon varicosities in close apposition with the AIS. The AIS (blue), with immunostaining for the marker phospho-IκBa superimposed (green), is shown. **(C)** The axon of the interneuron formed a series of boutons (blue, arrows) in close apposition with other PC AISs immunolabeled using antibodies against phospho-IκBa (green), confirming the identity of the AAC. **(D)** Antidromic ACs were recorded from the whole-cell voltage-clamped PCs in response to alveus stimulation (5 pulses at 50 Hz) under control conditions (left, Alv, triangle) and after the activation of the synaptically coupled AAC (right, AAC+Alv; train of 5 APs elicited at 100 Hz by brief somatic current injection during the stimulus train to the axon). **(E)** Schemes (top) illustrate the experimental configurations. Summary bar charts on the effect of AAC (bottom left) and BC (bottom right) activation on the probability of antidromic AC invasion of the soma of postsynaptic PCs. Whereas activation of AACs (five paired recordings) results in a significant reduction in the probability of AC invasion (AAC+Alv) in comparison with the control condition (Alv) (**$P = 0.002$), activation of BCs (four paired recordings) had no significant impact ($P = 0.2$).

initiation of APs, we compared the impact of AAC- and BC-mediated inhibition on the generation of APs in response to somatic current injections in a computational model. High-frequency activation of a single AAC or BC did not change the site of AP initiation but shifted the current threshold to higher values (fig. S8A). However, activation of BCs resulted in a larger increase of the threshold at high (>0.04 μS) inhibitory conductances. Thus, although AACs are more efficient in preventing the back-propagation of antidromic APs, BCs can better control the initiation of orthodromic APs in response to strong excitatory inputs. This conclusion was supported by experimental evidence: Application of GABA to the AIS transiently attenuated the initiation of orthodromic ACs induced by weak, but not strong, somatic depolarization, which suggests that activation of $GABA_AR$s at the AIS is less efficient in preventing the generation of orthodromic ACs (fig. S8, B and C).

Our results reveal that cortical PCs are divided into two electrogenic compartments during gamma activity: The soma discharges at low frequency, whereas in the axon, EAPs are generated at higher frequencies. This functional separation is maintained by strong inhibition that is mediated by highly active AACs. This powerful inhibition to the AIS prevents the back-propagation of EAPs to somatodendritic compartments but allows for the generation of orthodromic APs when the excitatory drive is high. Our results are in agreement with proposed models of persistent gamma oscillations, whereby the plexus of PC axons generates fast oscillations, which coexist with local field gamma oscillations (*17–19*). The net synaptic output produced by the PC axonal plexus provides the major excitatory drive onto inhibitory interneurons. These high-frequency axonal APs could orthodromically excite interneurons without necessarily causing PC somata to fire (*17*, *18*), thereby providing the drive for local oscillations even during sparse orthodromic activation of the network from upstream regions (*19*). EAPs have been suggested to arise under certain conditions as a result of the activation of presynaptic $GABA_AR$s, with a depolarizing effect and transient elevations in $(K^+)_o$ during synchronous GABA-mediated potentials (*20*). However, the potential mechanisms of EAP generation during the network oscillations remain unknown and will need future experimental evaluation.

The high-frequency, non-phase-locked discharge of AACs during gamma activity differs dramatically from that of BCs and other GABAergic interneurons. However, this discharge pattern is consistent with recent in vivo data indicating that cortical AACs, in contrast to other interneuron types, receive and respond to tonic rather than phasic excitation (*21*). AACs express significantly less extrasynaptic $GABA_AR$ α1 subunits in the plasma membrane than BCs do (*22*). This subunit contributes heavily to tonic inhibition and facilitates coincidence detection and temporally precise discharge in BCs (*22–24*). The low level of tonic inhibition in AACs, in contrast, favors temporal integration of synaptic inputs and the firing of tonic APs. Indeed, these interneurons fire vigorously when excitation levels are heightened in the network in vivo (*21*).

Our experimental data demonstrate that AACs have an inhibitory effect in the AIS of CA3 PCs in the hippocampus. Thus, during gamma activity, high-frequency discharge of AACs leads to buildup of a tonic level of inhibition in the AIS of postsynaptic neurons. The hyperpolarization and the shunting influence by the inhibitory conductance act together to efficiently block the passage of APs from the axon to the soma. The small diameter of the distal axon limits the depolarizing current flowing into the AIS produced by the antidromic AP (*25*, *26*). In contrast, when the neurons receive strong excitation onto their somatodendritic surface, sufficient charge can accumulate at the AIS to overcome inhibition and initiate APs, which then propagate to the axon and can also back-propagate to the dendrites.

Our study provides insight into the function of one of the most powerful cortical inhibitory interneuron types, AACs in cortical networks. In contrast to BCs, which provide strong inhibition to control orthodromic initiation of APs in response to excitatory synaptic inputs, AACs are more efficient at preventing the propagation of EAPs from the axon to somatodendritic compartments. Thus, AACs play an important role in functional dissociation of axonal/somatic compartments and orthodromic/antidromic activity, and they maintain the dynamic polarization of PCs in active cortical networks.

References and Notes

1. G. J. Stuart, B. Sakmann, *Nature* **367**, 69 (1994).
2. C. M. Colbert, D. Johnston, *J. Neurosci.* **16**, 6676 (1996).
3. M. J. Gutnick, D. A. Prince, *Science* **176**, 424 (1972).
4. S. F. Stasheff, M. Hines, W. A. Wilson, *J. Neurophysiol.* **70**, 961 (1993).
5. D. Pinault, R. Pumain, *Neuroscience* **31**, 625 (1989).
6. M. E. Sheffield, T. K. Best, B. D. Mensh, W. L. Kath, N. Spruston, *Nat. Neurosci.* **14**, 200 (2011).
7. D. Debanne, E. Campanac, A. Bialowas, E. Carlier, G. Alcaraz, *Physiol. Rev.* **91**, 555 (2011).
8. J. Csicsvari, B. Jamieson, K. D. Wise, G. Buzsaki, *Neuron* **37**, 311 (2003).
9. T. Gloveli *et al.*, *J. Physiol.* **562**, 131 (2005).
10. J. J. Tukker, P. Fuentealba, K. Hartwich, P. Somogyi, T. Klausberger, *J. Neurosci.* **27**, 8184 (2007).
11. N. Hajos *et al.*, *J. Neurosci.* **24**, 9127 (2004).
12. J. Szabadics *et al.*, *Science* **311**, 233 (2006).
13. L. L. Glickfeld, J. D. Roberts, P. Somogyi, M. Scanziani, *Nat. Neurosci.* **12**, 21 (2009).
14. K. L. Perkins, *J. Neurosci. Methods* **154**, 1 (2006).
15. E. H. Buhl, K. Halasy, P. Somogyi, *Nature* **368**, 823 (1994).
16. P. Hemond *et al.*, *Hippocampus* **18**, 411 (2008).
17. R. D. Traub *et al.*, *Eur. J. Neurosci.* **12**, 4093 (2000).
18. R. D. Traub *et al.*, *Proc. Natl. Acad. Sci. U.S.A.* **100**, 11047 (2003).
19. M. A. Whittington, R. D. Traub, *Trends Neurosci.* **26**, 676 (2003).
20. M. Avoli, M. Methot, H. Kawasaki, *Eur. J. Neurosci.* **10**, 2714 (1998).
21. Y. Zhu, R. L. Stornetta, J. J. Zhu, *J. Neurosci.* **24**, 5101 (2004).
22. A. Baude, C. Bleasdale, Y. Dalezios, P. Somogyi, T. Klausberger, *Cereb. Cortex* **17**, 2094 (2007).
23. J. R. Geiger, J. Lubke, A. Roth, M. Frotscher, P. Jonas, *Neuron* **18**, 1009 (1997).
24. T. Klausberger, P. Somogyi, *Science* **321**, 53 (2008).
25. H. R. Luscher, M. E. Larkum, *J. Neurophysiol.* **80**, 715 (1998).
26. Z. F. Mainen, J. Joerges, J. R. Huguenard, T. J. Sejnowski, *Neuron* **15**, 1427 (1995).

Acknowledgments: We thank R. Traub, M. Brecht, and J. Geiger for critically reading the manuscript; F. W. Johenning for help with two-photon imaging; A. McMurtrie for her contribution to morphological reconstruction; C. Schultz for generously sharing the IκBα antibody; and H. Monyer for providing the parvalbumin-positive enhanced green fluorescent protein mice. This work was supported by the Deutsche Forschungsgemeinschaft (SFB-TR 3/B5 and GL 254/5-1 to T.G., EXC 257 to D.S. and I.V.) and the Bundesministerium für Bildung und Forschung (BCCN 1A3 to T.G.).

Supplementary Materials

www.sciencemag.org/cgi/content/full/336/6087/1458/DC1
Materials and Methods
Figs. S1 to S8
References (*27–39*)

15 March 2012; accepted 3 May 2012
10.1126/science.1222017

New Products

SPECTROPHOTOMETER

The new Genova Plus life science ultraviolet/visible spectrophotometer from Jenway features icon-driven software with soft-key navigation and the ability to save results and methods to a USB memory stick. With dedicated modes for DNA/RNA analysis, preprogrammed methods for protein analysis plus standard spectrophotometer functions, the user-friendly Genova Plus is optimized for applications in biochemistry, forensic science, genetics, biotechnology, and other life science laboratories. The new Genova Plus incorporates a large graphical display built into the lid of the unit. Powerful icon-driven software and soft-key navigation ensure rapid analysis and ease of use. A large internal memory enables over 300 methods to be stored. In addition to dedicated modes for DNA/RNA analysis, protein assays, nucleic acid purity, and optical density, the spectrophotometer can be used as a standard spectrophotometer with measurement modes for photometrics, concentration, multiwavelength, spectrum scanning, quantitation, and kinetics.

Bibby Scientific

For info: +44-(0)-1785-812121 | www.bibby-scientific.com

WATER PURIFICATION SYSTEMS

The Elix Essential systems integrate patented Elix electrodeionization (EDI) technology along with several other complementary water purification techniques in order to produce Type 2 pure water with consistently pure and reliable water quality. The new Elix Essential system range includes models with flow rates of 3, 5, 10, or 15 L of pure water per hour, and daily production possibilities of up to 300 L. The high-quality pure water produced by the systems has resistivity values exceeding 5 MΩ·cm at 25°C (typically 10–15 MΩ·cm at 25°C) and less than 30 ppb total oxidizable carbon. Product water is recommended for a variety of uses: as feed to laboratory equipment; preparation of microbiological media, buffer and pH solutions; histology; chemical reactions run in water, and manual glassware rinsing. Elix Essential systems have a small footprint and can be installed on or under the bench as well as on a wall.

EMD Millipore

For info: 800-645-5476 | www.millipore.com

ECL IMAGER

The Thermo Scientific myECL Imager revolutionizes the capture and analysis of chemiluminescent Western blots, stained protein gels, and nucleic acid gels by simplifying the entire imaging workflow. The myECL Imager incorporates advanced CCD technology that results in greater than two times the sensitivity of X-ray film, with 10 times the dynamic range. The intuitive touchscreen controls with on-board computer simplify the image acquisition process. The improved sensitivity and small instrument footprint makes the myECL Imager an effective substitute for the laboratory darkroom. The Thermo Scientific myAnalysis Software supplied with the instrument provides a suite of programs to analyze nucleic acid or protein images, including automatic lane and band identification and molecular weight overlay analysis programs. The myAnalysis Software saves image files in a nonproprietary format for easy sharing with colleagues. Images and data reports can be exported directly to Microsoft Word, Excel, and PowerPoint programs for further analysis and presentations.

Thermo Scientific

For info: 800-874-3723 | www.thermoscientific.com/myeclimager

BRAIN-INJECTION SYRINGES

The Neuros syringe incorporates several technology firsts for significantly improved, controlled animal injections. Specifically designed for the neurosciences, Neuros syringes are available with ultrafine 30-, 32-, or 33-gauge needles that accurately dispense 50 nL to 100 µL, providing the smallest volume, thin-gauge solution on the market. Neuros syringes enable precision animal brain injections with minimal tissue damage and reduced variability. A unique, adjustable needle sleeve maintains rigidity and ensures a targeted injection path to an exact location. Two needle sleeve options are offered—one with a blind stop for cannulated applications and the other for use with stereotaxic holders—each with adjustable needle exposure of 0 to 20 mm. Neuros syringes fill a critical gap in the available microvolume choices, which required neuroscience researchers to use either larger syringes that produced dead volume, wasted sample and reduced accuracy, or small-volume syringes with larger gauge needles that damage tissue.

Hamilton Company

For info: 800-648-5950 | www.hamiltoncompany.com

TISSUE SLICERS

The EMS7000smz and EMS5000mz are high precision vibrating microtomes designed for microscopy and histology. Designed to produce the highest quality slices of the most difficult material, the EMS vibrating microtomes minimize damage to tissue surfaces and produce slices of uniform thickness. The competitively priced EMS5000mz offers a *z* axis deflection of 1–2 µm and a blade advance controllable to 10 µm/sec. The EMS7000smz delivers perfect sections with sub-micron *z* axis deflection across a broad range of vibration speeds and amplitudes and enhanced longevity of performance through an advanced vibrating mechanism. It is the finest slicer in the world for preparations for visual patch clamping. Both tissue slicers offer simple operation at the push of a button or a range of changeable and programmable parameters customizable to user preferences. Tissue cooling is accomplished by the use of either an ice-water bath or an electronically controlled thermoelectric cooler.

Electron Microscopy Sciences

For info: 215-412-8400 | www.emsdiasum.com

Electronically submit your new product description or product literature information. Go to www.sciencemag.org/products/newproducts.dtl for more information.

Newly offered instrumentation, apparatus, and laboratory materials of interest to researchers in all disciplines in academic, industrial, and governmental organizations are featured in this space. Emphasis is given to purpose, chief characteristics, and availability of products and materials. Endorsement by *Science* or AAAS of any products or materials mentioned is not implied. Additional information may be obtained from the manufacturer or supplier.

UNIVERSITÄT BASEL – PAUL SCHERRER INSTITUTE

Professor in Nano-Diffraction of Biological Specimens

The University of Basel and the Paul Scherrer Institute (PSI) in Switzerland invite applications for a Professorship in the area of *Nano-Diffraction of Biological Specimens*. We are considering applications at a tenure-track assistant or associate professor level. The position will be shared between the University of Basel and the PSI. It will be integrated into the research environment at the Biozentrum and the Swiss Nanosciences Institute (SNI) of the University of Basel and the Biology and Chemistry Department at PSI. The successful candidate will be responsible for coordinating the design and operation of the biological end station at the Swiss free electron laser (SwissFEL) at the PSI. The ideal candidate will develop a nano-diffraction setup for biomolecular samples (e.g. nanocrystals and suspensions of single particles, or viruses) for femto-second x-ray diffraction studies using free electron laser technology, and will have his/her own biological project of interest. The infrastructure of the Biomolecular Research Laboratory at PSI will support the research activities of the new professor. The successful candidate will contribute to undergraduate and postgraduate teaching at the University of Basel and will engage in collaborative projects between the University of Basel and the PSI.

The University of Basel and the PSI offer an outstanding scientific environment and an attractive research endowment, and Switzerland provides a high standard of living and a superb cultural atmosphere. Applications, including CV, list of publications and a short research summary, should be sent by e-mail (pdf or zip) to Prof. Martin Spiess, Dean, Faculty of Science, University of Basel, Klingelbergstrasse 50, 4056 Basel, Switzerland, to dekanat-philnat@unibas.ch. For informal enquiries please contact Prof. Henning Stahlberg (henning.stahlberg@unibas.ch, phone: +41-61 387 32 62) or Prof. Gebhard Schertler (gebhard.schertler@psi.ch).

The deadline for receipt of applications is August 31, 2012. Applications from female candidates are particularly welcomed.

UNI BASEL

PAUL SCHERRER INSTITUT PSI

The Ohio State University

Wexner Medical Center

Pharmacology Faculty

The Ohio State University College of Medicine seeks 5 new faculty members (one at the rank of Professor and 4 at open rank) to expand its program in genomics and pharmacogenomics.

Expertise in genomics and pharmacogenomics in the fields of cardiovascular diseases, neurosciences, cancer, immunology, and bioinformatics is preferred. Ph.D., M.D. degree required; the successful candidate will have a proven record of high impact funded research in these fields and a record of collaborative, translational and transdisciplinary research.

Faculty will be appointed to departments and centers appropriate to career orientation and may include but not limited to: The Dorothy M. Davis Heart and Lung Research Institute; The Comprehensive Cancer Center; The Department of Pharmacology; The Department of Neurosciences; The Department of Internal Medicine and the Division of Cardiovascular Medicine; The Department of Internal Medicine and the Division of Human Genetics; The Department of Molecular Virology and Immunology; The Department of Bioinformatics. The successful applicant will also participate in innovative research programs sponsored by the Clinical and Translational Science Award funded Center for Clinical and Translational Research.

Successful applicants will be expected to take advantage of the diverse resources and opportunities for collaboration available in this environment to build an expanding program of genomic and pharmacogenomic research.

Applicants should submit a copy of their CV and a description of their accomplishments and current research focus and goals to:

Wolfgang Sadee, Dr.rer.nat, Chair, Department of Pharmacology, Director, Program in Pharmacogenomics, 5078 Graves Hall, 333 W. 10th Ave, Columbus, OH 43210. Email: Ring.32@osu.edu

To build a diverse workforce The Ohio State University College of Medicine encourages applications from individuals with disabilities, veterans and women. EEO/AA employer.

徐州医学院

XUZHOU MEDICAL COLLEGE

Teaching and Research Positions At Xuzhou Medical College

Position Summary:

Xuzhou Medical College is located in Xuzhou, north of Jiangsu Province, China. It is a well-known medical institution of higher education and has developed rapidly in scientific research and personnel training in recent years. In order to accelerate the development of our College, we are sincerely searching for colleagues to join our College at the professor or associate professor or Ph.D. level. Opportunities are available in all areas including Human Anatomy, Histology and Embryology, Pathology, Immunology, Pharmacology, Physiology, Pharmaceutics, Pharmaceutical Analysis, Epidemiology and Hygienic Statistics, Anesthesiology, Nursing, Stomatology, Rehabilitation Medicine, Biochemistry and Molecular Biology, Neurobiology, Pathogenic Biology, Genetics, Biology, Pharmacokinetics, Analytical Chemistry, Imaging, Biomedical Engineering, Oral and Maxillofacial Surgery, Orthodontics, Oncology, Cell Biology, Microbiology, Internal Medicine, Pharmaceutical Chemistry, Clinical Medicine, Obstetrics and Gynaecology, Pediatrics, Urinary Surgery, Hepatobiliary Surgery, Neurology, Hematology, Basic Medicine.

Requirements/Qualifications:

- Doctoral degree holder
- Professor or associate professor

For more detailed information, please visit the following website in Chinese: **http://rsc.xzmc.edu.cn/**

Contact:

Mr. Du Gang or Mr. Li Yuandong
Personnel Department, Xuzhou Medical College
209 Tongshan Road, Xuzhou, Jiangsu Province, 221004, China
Tel/Fax:86-516-83262042, 83262238
Email: szb@xzmc.edu.cn and rsc@xzmc.edu.cn

Postdoctoral Research Fellows

The Pennsylvania State University is recruiting five exceptional postdoctoral research fellows to pursue cutting edge research in Batteries and Energy Storage, Biogeochemical Cycles, CO2 Utilization, Health and the Environment, and Water Science. Positions will be supported by the Penn State Institutes of Energy and the Environment (PSIEE) at Penn State, University Park, PA, and will include highly competitive salaries, funds for travel and supplies, and an innovative future faculty development program designed for the cohort of fellows. These positions are part of an initiative to enhance the already vigorous program of environmental and energy research and education at Penn State, and reinforces the university's internationally recognized leadership in multidisciplinary research. These positions represent an exceptional opportunity to develop new research projects in collaboration with two or more Penn State faculty.

Positions are for two years, with a start date in Fall Semester 2012. An excellent publication record and a Ph.D. in a relevant field are required. To be considered for employment, please submit a CV, a three-page research concept (proposal) that leverages the faculty and facilities at Penn State and three letters of recommendation to **Judy Cranage at jvc9@psu.edu by July 27, 2012.**

Batteries and Energy Storage - Batteries and energy storage research is a major interdisciplinary initiative at Penn State spanning from materials to cells to systems. The university has a diverse and collaborative group working in areas including novel electrode materials, electrolytes, binders, cell manufacturing, electrode structures, battery safety, advanced diagnostics and sensing, multiscale modeling, and battery control and energy storage management. Penn State also has the only fabrication facility of large-format batteries among U.S. universities. We are seeking investigators that can address length scales from materials to devices and/or devices to systems. Proposals that can bridge experiments and modeling are encouraged. Details can be found at www.best.psu.edu. For more information contact Chao-Yang Wang (cxw31@psu.edu), Michael Hickner (mah49@psu.edu), or Michael Janik (mjj13@psu.edu).

Biogeochemical Cycles - Biogeochemists at Penn State are a diverse and collaborative group working at the leading edge of their fields in areas including carbon cycle science, nutrient and acid pollution, environmental genomics, and sustainable agriculture. A partial listing of biogeochemistry faculty can be found at www.biogeochemistry.psu.edu/people.asp. Cutting-edge facilities for biological sequencing, stable isotope analysis, and geochemistry are available on campus. Applicants proposing omics-enabled research can take advantage of expertise and resources available through the Center for Environmental geoChemistry and Genomics. For more information contact Jenn Macalady (jlm80@psu.edu) or Jason Kaye (jpk12@psu.edu).

CO2 Utilization - The CO2 utilization position focuses on the capture and catalytic conversion of CO2 to either hydrocarbons or alcohols for clean energy applications. Interest is in advancing fundamental and applied research on such topics as CO2 utilization, including but not limited to: (a) development of energy efficient solvent, solid sorbent, or membrane materials and processes for CO2 separation (b) The design, characterization, and preparation of novel catalysts for CO2 activation and conversion, (c) understanding multi-center CO2 activation and multi-electron/proton (or hydrogen atom) transfer processes, and (d) the elucidation of structure/property relationships in selective CO2 reductions. We are seeking ideas and approaches that are "out of the box". Collaboration with one or more faculty members in the EMS Energy Institute, and Departments of Chemical Engineering and/or Chemistry is strongly encouraged. For more information contact Chunshan Song (csong@psu.edu), Rob Rioux (rmr189@psu.edu), or Ayusman Sen (asen@psu.edu).

Health and the Environment - A wide range of opportunities exists to work in highly collaborative groups in this field. Areas of expertise that interface with environment include nutrition, toxicology, immunology, disease dynamics or entomology. Penn State has state-of-the-art core facilities in metabolomics, flow cytometry and microscopy and genomics. Proposals that incorporate genomics, proteomics or metabolomics are encouraged. A partial list of faculty in the environment and health field can be found at www.psiee.psu.edu/psiee_people/faculty_results_az.asp. For more information contact Gary H. Perdew (ghp2@psu.edu) or Kasia Kordas (kxk48@psu.edu).

Water Science - Existing strengths at Penn State span a wide range of topics, including multi-scale modeling, integrated assessment, study of coupled hydrological and biogeochemical cycles, contaminant fate and transport, ecohydrology, polar hydrology, and resource economics. Penn State faculty and staff are involved in the Critical Zone Observatory network, the Long Term Ecological Research network, the National Atmospheric Deposition Program, and other long-term environmental observatories. We are seeking candidates who will leverage resources and expertise of several faculty via collaboration across units. A list of Penn State water scientists and engineers is available at www.psiee.psu.edu/psiee_people/faculty_results_az.asp. For more information contact Beth Boyer (ewb100@psu.edu), Mike Gooseff (mng2@psu.edu), or Li Li (lili@eme.psu.edu).

PENNSTATE

www.psiee.psu.edu/open_positions.asp

Penn State is committed to affirmative action, equal opportunity and the diversity of its workforce.

TEXAS TECH UNIVERSITY

Structural Biology: Biological NMR Spectroscopy

The Department of Chemistry and Biochemistry invites applications for a senior faculty member in the area of **Biological NMR Spectroscopy**. We are especially interested in applicants whose research programs will complement existing areas of strength at TTU, such as structure, function and dynamics of membrane proteins, biomolecules involved in cancer, and plant proteins. However, all qualified candidates are encouraged to apply. The successful candidate for this position will be part of a major new **Structural Biology** initiative at TTU that includes a commitment to the acquisition of 600 MHz and 800 MHz NMR instruments and hiring two additional biological NMR spectroscopy faculty. Evidence of a well-funded research program and a demonstrated commitment to excellence in teaching and service are essential. The successful applicant will be directly involved in the selection of the NMR equipment and in the selection of the two additional faculty to be hired at the assistant and/or associate professor level. The Department of Chemistry and Biochemistry is among the top academic units at Texas Tech University, in terms of research funding, publications and graduate education. Texas Tech University is classified as a doctoral research-extensive university by the Carnegie Foundation and has recently qualified to receive funding from the State of Texas National Research University Fund. It has an enrollment of more than 30,000 students, and is one of the major, state-supported, multidisciplinary universities of the Southwest. A School of Medicine is located on the main campus in Lubbock.

All applications must be submitted online. Online faculty application for **requisition number 85837** can be found at **http://jobs.texastech.edu**. Applications must include the names of three references. Evaluation of applications will begin on **July 1, 2012**, and continue until the position is filled. For additional information, please contact the chair of the search committee, **Dr. Joachim Weber, Department of Chemistry and Biochemistry, Texas Tech University, Box 41061, Lubbock, TX 79409-1061 (joachim.weber@ttu.edu)**.

Texas Tech University is an Affirmative Action/Equal Opportunity Employer, committed to excellence through diversity. Texas Tech welcomes applications from minorities, women, veterans, persons with disabilities, dual-career couples, and all qualified persons.

Max-Planck-Institut für molekulare Genetik

Max Planck Institute for Molecular Genetics

Announcement of a Director position

at Max Planck Institute for Molecular Genetics

The Max Planck Institute for Molecular Genetics in Berlin is in the process of identifying a new Director. The institute works at the interface of genome research and genetics. Current interests include computational genomics, the genetics of human diseases, regulatory networks in development, with a strong emphasis on genome-wide techniques and systems approaches (see http://www.molgen.mpg.de).

The Max Planck Society for the Advancement of Science is an independent, non-profit research organization that primarily promotes and supports basic research. The society currently operates 80 institutes and research facilities with more than 23,400 employees, including 4,400 scientists.

The Max Planck Society, an equal opportunity employer, is committed to diversity and inclusion in all aspects of recruiting and employment. The Max Planck Society is aiming at increasing the percentage of women among its scientific leadership, particularly at the director level and therefore strongly encourages expressions of interest from and nominations of qualified women.

Please send a letter of interest or suggestions of candidates to the Managing Director, Prof. Dr. Martin Vingron. All enquiries will be treated confidentially.

Max Planck Institute
for Molecular Genetics
Martin Vingron
Ihnestraße 63–73
14195 Berlin · Germany
or managing-director@molgen.mpg.de

The Mortimer D. Sackler, M.D. Prize for Distinguished Achievement in Developmental Psychobiology

Nominations are invited for The Mortimer D. Sackler, M.D. Prize for Distinguished Achievement in Developmental Psychobiology, a biennial prize recognizing and honoring the most creative scientists in the area of Developmental Psychobiology for research at any level, from the cultural to the molecular. The recipient of the Prize will receive $100,000, deliver Grand Rounds and participate in workshops at the Columbia and Cornell Sackler Institutes in New York City.

Nominations should include a letter of recommendation detailing the rationale for the candidate's nomination:

- How does the nominee's research embody a major advance in Developmental Psychobiology?
- Summarize his or her scientific achievements both specific to Developmental Psychobiology and across fields.

Nominations must also include curriculum vitae, a list of prior awards and recognitions, copies of 2 or 3 key papers, and no more than 2 letters of support. Nominations must be received by **October 15, 2012** and can be sent to **hlf2010@columbia.edu**.

For more information, please visit our website at **www.sacklerinstitute.org**

KGI

KECK GRADUATE INSTITUTE

of Applied Life Sciences

Junior Faculty Positions in Applied Life Sciences

Keck Graduate Institute is seeking applicants for several positions in applied life sciences to educate graduate students for careers in life sciences industries and to develop research programs that contribute new knowledge that will impact human health. We seek collaborative and entrepreneurial individuals with expertise in pharmaceutical discovery and development, biochemical engineering and bioprocessing, genomics and proteomics of personalized medicine, population genetics, and biomedical diagnostics and devices. A Ph.D. and postdoctoral experience in life science or engineering is required.

As part of recent strategic planning, KGI is focusing on rare and intractable disease as the theme for this faculty recruitment effort. We seek to build upon our successes in biomarker research, rare disease therapy, microfluidics, nucleic acid diagnostics, and systems biology to develop collaborations that will impact the ongoing discovery and development of diagnostics and therapies that address stratified medicine. We expect collaborations between biologists, chemists, and engineers to perform interdisciplinary research and development of technologies and therapies.

KGI offers unique programs to prepare its graduates for jobs in life science industry, government, and non-profits. These include a professional science masters (PSM), a postdoctoral professional masters (PPM), as well as MS and Ph.D. degrees in Applied Life Sciences. KGI is also launching a new School of BioPharmacy that may stimulate opportunities for joint appointments in both Applied Life Sciences and BioPharmacy.

Applicants should electronically submit a curriculum vitae, a synopsis of professional goals and research interests, and arrange for at least three letters of recommendation to **www.kgi.edu**.

西北农林科技大学

Northwest A&F University

Academic Talents Recruitment

Northwest A&F University, Shaanxi, China

Northwest A&F University(NWAFU) is one of the key universities in China supported by the Central Government under the "Project 985" and "Project 211". It is located in Yangling, Shaanxi Province, the birth place of Chinese agricultural civilization. Founded in 1934 as the first high education institution in modern agriculture and forestry, NWAFU has achieved significant progresses and developments in the past 78 years. Now with its 23 colleges and departments, NWAFU is the most comprehensive university in agriculture, forestry and hydro-science in China and one of the nation's premier research-oriented universities.

Recently, NWAFU has established Special Professorships in the following academic areas and invites highly talented and motivated candidates to apply

I. Academic areas with job openings

Maize genomics and molecular breeding,
Vegetable molecular breeding,
Tree genetics and breeding
Animal molecular breeding,
Apple genomics
Functional genomics of plant nutrition,
Crop functional genomics,
Soil chemistry
Soil erosion prediction model,
Animal cell engineering and embryo engineering
Pathogenic microorganisms of animals,
Plant stress biology
Material cycling in watershed ecosystem
Structural optimization and structure-function relationship of biologically active natural substances
Food safety
Theoretic and techniques of crop high-efficiency water use,
Hydrological modeling theory and methods,
Agricultural machinery and technology,
Forestry economictheory and policy,
Contemporary sociological theory and research methods

II. Applicant Eligibility

2.1 Ph.D. degree in related disciplines. Under 45 years old for applicants in natural sciences and under 50 years old for those in social sciences

2.2 Holding an assistant professor or more senior position for international applicants. A rank of full professor or equivalent for domestic applicants

III. Benefits and Salary

3.1 Entitlement of full professor and supervisor of Ph.D. students.

3.2 A minimal startup funding of ¥3 million for candidates in natural sciences and ¥1 million for those in social science

3.3 An apartment (150-180m2) and a ¥0.3 million household allowance will be provided. Ownership of the apartment will be transferred to the faculty members after serving the university for ten years

3.4 In addition to regular salary and benefits, qualified applicants will be compensated with an annual allowance of ¥0.1-0.5 million. International candidates will receive a minimal annual salary of ¥0.6 million

3.5 Spouse hiring will be accommodated

IV. Application Procedure

4.1 Applicants should provide. An English version of curriculum vitae with lists of publications, research interests and professional titles and activities, A statement of research accomplishments and future teaching and research plan, PDF copies of academic transcripts, diploma and degree certificate, five representative papers or books and documents for funded projects, awards, patents and keynote speakers at international conferences, etc; Three recommendation letters with referrers'e-mails and telephone numbers

4.2 NWAFU will conduct a preliminary screen and invite eligible candidates to Yangling for an interview and campus visit. The selected candidates need to sign a contract with the university. **See our Chinese ad at http://rcb.nwsuaf.edu.cn/show.php?articleid=539**

V. Contact

Address: No. 3Taicheng Road, Yangling, Shaanxi Province, 712100 China
Contact Persons: SUN Ma, or ZHANG Pengfei
Tel: +86-29-87082855, 87082577, Fax: +86-29-87082855
E-mail: **rencaike@nwsuaf.edu.cn; rencaiban@gmail.com.**
The university's website: **http://www.nwsuaf.edu.cn**

Fonds Fund

InBev-Baillet Latour

NOMINATIONS ARE INVITED

for the prestigious

InBev-BAILLET LATOUR HEALTH PRIZE

of

€ 250,000

(Two hundred and fifty thousand euros)

Theme for 2013: Cancer

Previous recipient in that field: Robert A. Weinberg, USA

Recipient 2012 (Neurosciences): Gero Miesenböck, UK

This annual award is intended to recognize outstanding scientific achievements in biomedical research for the benefit of human health and to encourage the laureate in the pursuit of his/her career. The Prize is open to scientists of all nationalities who have not received an equivalent Prize for their personal use. Exceptionally, the Prize may be shared between two persons who have collaborated over a long period. The laureate will be selected by an international Jury in February 2013.

The themes for the following years will be: Cardiovascular Diseases, Metabolic Disorders, Infectious Diseases and Immunology, Neurosciences.

For more information go to **www.inbevbailletlatour.com** (Medical research)

Deadline for nominations: September 14, 2012

Regulations and nomination forms can be obtained by e-mail from **prix@frs-fnrs.be**

ifr Institute of Food Research

PROFESSORIAL OPPORTUNITIES IN MICROBIOLOGY

INSTITUTE OF FOOD RESEARCH, NORWICH RESEARCH PARK, UK

IFR, strategically funded by the Biotechnology and Biological Sciences Research Council, is one of the world's premier research institutions in the area of food, diet and health. It is at the heart of the Norwich Research Park, a leading centre providing a critical mass of life and environmental science capability which, with some 35 microbiology research groups, is one of the largest clusters of microbiologists in the UK.

The IFR wishes to appoint two Professorial/Principal Scientists, one in Gastro Intestinal Tract Biology and another in Foodborne Bacterial Pathogens.

The appointees will have excellent strategic leadership skills and a strong commitment to cross and multi-disciplinary research working both within the IFR and across the Norwich Research Park – a BBSRC National Research and Innovation Campus.

Gut Microbiome

With a background in microbial genetics and physiology, s/he will develop and lead research in microbial interactions in complex commensal communities and contribute to the development of GI-tract microbiology research within the Gut Biology Programme and across the Institute.

Bacterial Foodborne Pathogens

With a background in microbial genetics or biochemistry, s/he will develop and lead a research programme on the physiology and molecular biology of a significant bacterial foodborne pathogen.

In both cases candidates with a successful general microbiology research background with the enthusiasm and dedication to align their research interests to one of the above areas, are encouraged to apply.

For further information on the Institute of Food Research and the Norwich Research Park, please see www.ifr.ac.uk and www.nrp.org.uk and for BBSRC please see www.bbsrc.ac.uk

An attractive salary and benefits package is available, reflecting the level of experience and achievement. The appointment will be tenured, full time and based at the Institute of Food Research, Norwich, UK.

Further information, including instructions on how to apply, may be obtained from the IFR's recruitment consultants, Carbon–NfP, who would be happy to have an informal and confidential discussion with the potential candidates. Please contact Sharon Taylor by email sharon.taylor@carbon-nfp.com in the first instance.

The closing date for applications is Monday, 16 July 2012.

Carbon-NfP Ltd, 17 Russell Court, Woburn Place, London WC1H 0LL.

The Institute of Food Research is a registered charity (no. 1058499) limited by guarantee and is an Equal Opportunities Employer

BBSRC bioscience for the future

POSITIVE ABOUT DISABLED PEOPLE

www.carbon-nfp.com

CARBON-NfP

POSITIONS OPEN

USDA Agricultural Research Service
www.ars.usda.gov

RESEARCH LEADER
Supervisory Research Plant Pathologist/ Geneticist (Plants)
Salary Range of $96,690 to $147,857

The Cereal Disease Research Unit in St. Paul, Minnesota, is seeking a permanent full-time Research Leader. The mission of the unit is to reduce losses in wheat, oat, and barley to major diseases including leaf rust, stem rust, crown rust, and Fusarium head blight. In addition to research responsibilities, the incumbent exercises leadership and line authority over scientists and support personnel assigned to the Unit. The incumbent is responsible for maintaining and enhancing the creativity and productivity of the Unit, hiring personnel and managing the human, fiscal, and physical resources assigned to the Unit, serving as the Unit fund holder, providing technical information and consultation both internal and external to Agricultural Research Service (ARS), and ensuring the proper interpretation and reporting of scientific research results and information. To apply, print a copy of vacancy **announcement ARS-X12E-0059** from the ARS Careers **Website: http://www.afm.ars.usda.gov/hrd/jobs/announcements/scientific.htm** and follow the application directions provided. To have a printed copy mailed, call **Pam Groth** at **telephone: 651-649-5046.** *U.S. citizenship is required.* Applications must be received by June 30, 2012.

USDA/ARS is an Equal Opportunity Employer and provider.

FACULTY POSITION in
Innate Immunology/Inflammation
Department of Immunobiology
The University of Arizona

The Department of Immunobiology at the University of Arizona College of Medicine is seeking interactive, well-qualified applicants for a Tenure-Track or Tenured position at the **ASSISTANT, ASSOCIATE,** or **FULL PROFESSOR** rank depending upon qualifications, investigating the initiation and regulation of innate and inflammatory responses. Successful applicants will be expected to bring novel expertise, develop independent research programs, and contribute to graduate (Ph.D.) and medical (M.D.) education. In addition, the candidate will be expected to invest a fraction of their effort to help build interactive and collaborative programs within and outside the Department to tackle larger biomedical problems relevant to human health.

The University of Arizona is ranked amongst the top 20 public research and education universities. It boasts excellent core facilities and a rich scientific environment that includes a number of strong, interactive departments covering a broad range of molecular and biomedical sciences. The University also offers a lively campus with nationally recognized academic, sports, and performing arts programs. It is located in sunny Tucson, which is surrounded by the majestic Sonoran Desert and bio-diverse sky islands that rise to more than 9,000 feet above the desert floor. The city boasts a vibrant multicultural population of approximately 900,000, and a strong, diverse economy.

Please complete an online application for **Job #48571** at **website: http://www.hr.arizona.edu.** Be prepared to attach your curriculum vitae.

The University of Arizona is an Equal Employment Opportunity/Affirmative Action Employer. Minorities/Women/Persons with Disabilities/Veterans.

Two **POSTDOCTORAL RESEARCH FELLOWS** are available at the Department of Pharmacology at Rush University in Chicago for studying molecular mechanism of atherosclerosis. Candidates must have a Ph.D., M.D., or comparable degree with prior experience and training in the followings: vascular biology, atherosclerosis, monocyte, platelet, endothelial cell, molecular biology, viral vectors, or diabetic vascular disease. Applicants should send curriculum vitae to: **Dr. Chunxiang "Kevin" Zhang,** Professor and Chairman, Department of Pharmacology, Rush University. **E-mail: chunxiang_zhang@rush.edu.**

POSITIONS OPEN

DIRECTOR
Bioengineering Institute,
New York University

New York University (NYU) is creating an innovative Institute for Bioengineering that will cross multiple disciplines and schools of the university. It is intended to foster close collaboration particularly among the Polytechnic Institute (NYU-Poly), Courant Institute, Faculty of Arts and Science, Center for Neural Science, Colleges of Dentistry and Nursing, as well as the School of Medicine. The combined expertise and talent available in these units is already considerable. Part of the Institute's new activities will occur on the Campus of NYU-Poly in Brooklyn while the part particularly devoted to applied biomedical research and development will be housed in a new building under construction in Manhattan near the Medical School, cohabiting with the College of Dentistry and Nursing.

We are seeking applications and nominations for the Institute Director. The primary responsibilities of the Director are to provide leadership and vision for collaborative bioengineering research among these units, recruit qualified faculty, generate resources, establish interdisciplinary Master's and Ph.D. Programs, and interface with peer departments and institutes elsewhere. The faculty of the new Institute will have tenure and teaching responsibilities in one of the units of NYU but conduct research that is not constrained by disciplinary or geographic boundaries within NYU. We are particularly interested in an individual who embraces academic entrepreneurship and whose research supports NYU-Poly's core values of invention, innovation, and entrepreneurship in an academic setting. World-class visibility in one or several of the bioengineering areas will be required. Some examples are implant and instrument design, therapeutic devices, biomedical imaging and diagnostics, biomaterials, biomedical simulation, modeling and data analysis, genomic engineering, and neuro-engineering, but this list is not exclusionary.

Applications for the position should consist of your curriculum vitae, a list of publications, a history of grant support, a summary of entrepreneurial activities, and a statement of research and teaching interests. They should be sent electronically to **e-mail: dir_bioeng_inst@poly.edu** at the Provost's Office at NYU-Poly, with "Bioengineering Institute Director" in the subject line. Applications will be accepted until the position is filled, but those received prior to June 30, 2012 will be assured of consideration.

NYU and NYU-Poly are Equal Opportunity/Affirmative Action Employers. All candidates are encouraged to apply.

DIRECTOR: Therapeutic Drug Design and Discovery at Einstein

The Albert Einstein College of Medicine is seeking a director for a new program in academic translational drug discovery and development. The program will support all pre-clinical stages including computational drug design, fragment-based discovery, chemical elaboration, animal disease model testing, PK/PD and toxicology, medicinal chemistry, drug candidate stability and local IND approval. The successful candidate will have experience in managing several of these elements and will have demonstrated achievements in the drug development pipeline in an academic and/or pharmaceutical environment. The candidate will have the ability to integrate existing pre-clinical components, and to recruit new staff to establish an integrated structure. The ability to collaborate closely with discovery and clinical researchers is of critical importance. Appointment will be at a faculty rank and position commensurate with experience. Respond to: **Director Search, Department of Biochemistry, Albert Einstein College of Medicine, 1300 Morris Park Avenue, Bronx, NY 10461.** Applications should include curriculum vitae, research experience, goals, and if appropriate, a research plan to integrate the candidate's research interests into the program. Applications must include contact information for three referees. Applications should be submitted as a single PDF to **e-mail: drugdiscovery@einstein.yu.edu.** *Equal Opportunity Employer.*

POSITIONS OPEN

UNIVERSITY OF FLORIDA
Department of Medicinal Chemistry

The Department of Medicinal Chemistry, College of Pharmacy (**website: http://www.cop.ufl.edu/**), University of Florida, invites applications for a tenure-track **ASSISTANT PROFESSOR** position. The successful candidate will establish a strong independent research program in drug discovery and development and participate in professional and graduate instructional efforts of the college. Area of specialization within medicinal chemistry is open, but should complement the interests of the department and agree with institutional strategies adopted by the University of Florida to foster interdisciplinary research in cancer, infectious diseases, and neuroscience. The department is located within the UF Health Science Center complex (**website: http://www.health.ufl.edu/**). This unique research environment offers excellent opportunities for synergistic collaborations.

Applicants should submit a cover letter, curriculum vitae, summary of research experience and proposed research, and summary of teaching experience (if any) through GatorJobs (**website: https://jobs.ufl.edu/** and search postings for **Requisition Number 0901019–Ast Prof**). Please also submit three letters of recommendation as PDF file attachments electronically to Program Assistant **David Jenkins** at **e-mail: jenkins@cop.ufl.edu.** To ensure full consideration, materials should be submitted by August 1, 2012, when the search committee will begin reviewing applications. Materials received after this date may be considered at the discretion of the committee and/or hiring authority.

The University of Florida is an Equal Opportunity Institution and encourages applications from qualified minority and female applicants.

SENIOR MANAGER, TRANSGENIC
Genotyping Services Laboratory

Opportunity for Senior Manager, Transgenic Genotyping Services Laboratory, at The Jackson Laboratory, located in Bar Harbor, Maine. Responsible for the daily operations and strategic direction of a high volume genotyping lab, overseeing laboratory personnel, assay development, production scale genotyping operations, sample chain of custody, quality control, genetic integrity of assays, laboratory supplies, equipment, technology, improved workflow processes, internal customer service, and third-party contract laboratory management. Requires minimum of Master's degree in molecular biology or genetics or foreign equivalent, and five years' experience directly managing throughput genotyping laboratory. Applicants should apply with a cover letter (required) at **website: http://www.jax.org/careers.** Please refer to **job requisition #3298.**

A **POSTDOCTORAL POSITION** is available for self-motivated, recent Ph.D. graduates to study the cell signaling mechanisms in University of Michigan at Ann Arbor, Michigan. Candidates with a strong background in molecular cell biology and excellent publications are encouraged to apply. Experiences in analyzing genetic engineering mice or protein structural analysis will be a plus. Please submit your curriculum vitae and statement of interest to **Dr. Jian-Guo Geng** at **e-mail: jgeng@umich.edu.**

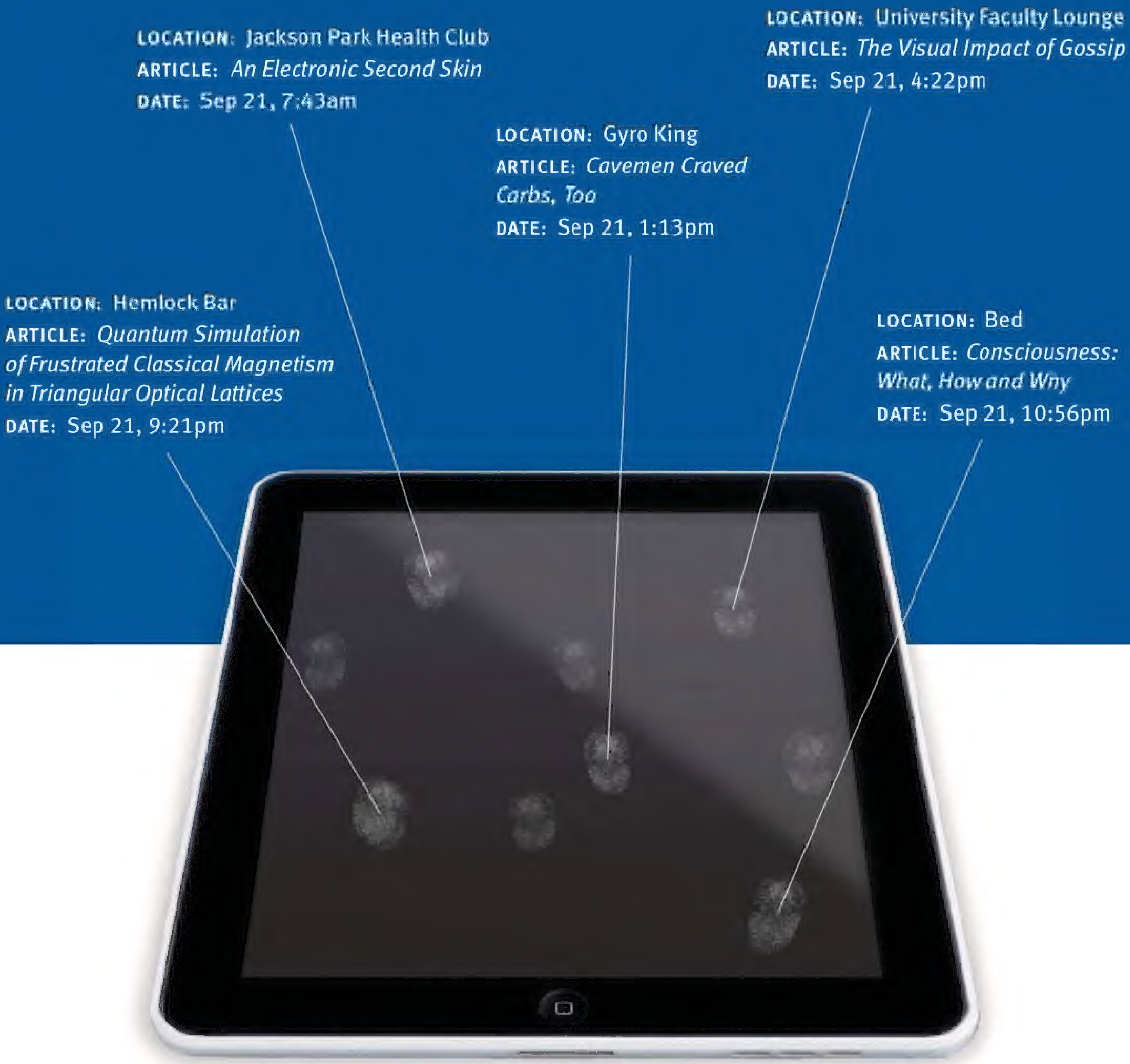
LOCATION: Jackson Park Health Club
ARTICLE: An Electronic Second Skin
DATE: Sep 21, 7:43am
LOCATION: University Faculty Lounge
ARTICLE: The Visual Impact of Gossip
DATE: Sep 21, 4:22pm
LOCATION: Gyro King
ARTICLE: Cavemen Craved Carbs, Too
DATE: Sep 21, 1:13pm
LOCATION: Hemlock Bar
ARTICLE: Quantum Simulation of Frustrated Classical Magnetism in Triangular Optical Lattices
DATE: Sep 21, 9:21pm
LOCATION: Bed
ARTICLE: Consciousness: What, How and Why
DATE: Sep 21, 10:56pm

R&D Systems

Puts Cancer Stem Cells in Your Sights

An overriding experimental limitation for cancer stem cell (CSC) researchers is the ability to identify and isolate CSCs from other tumor cells. To address this need, we offer a broad selection of tools to facilitate the identification and isolation of specific CSC populations.

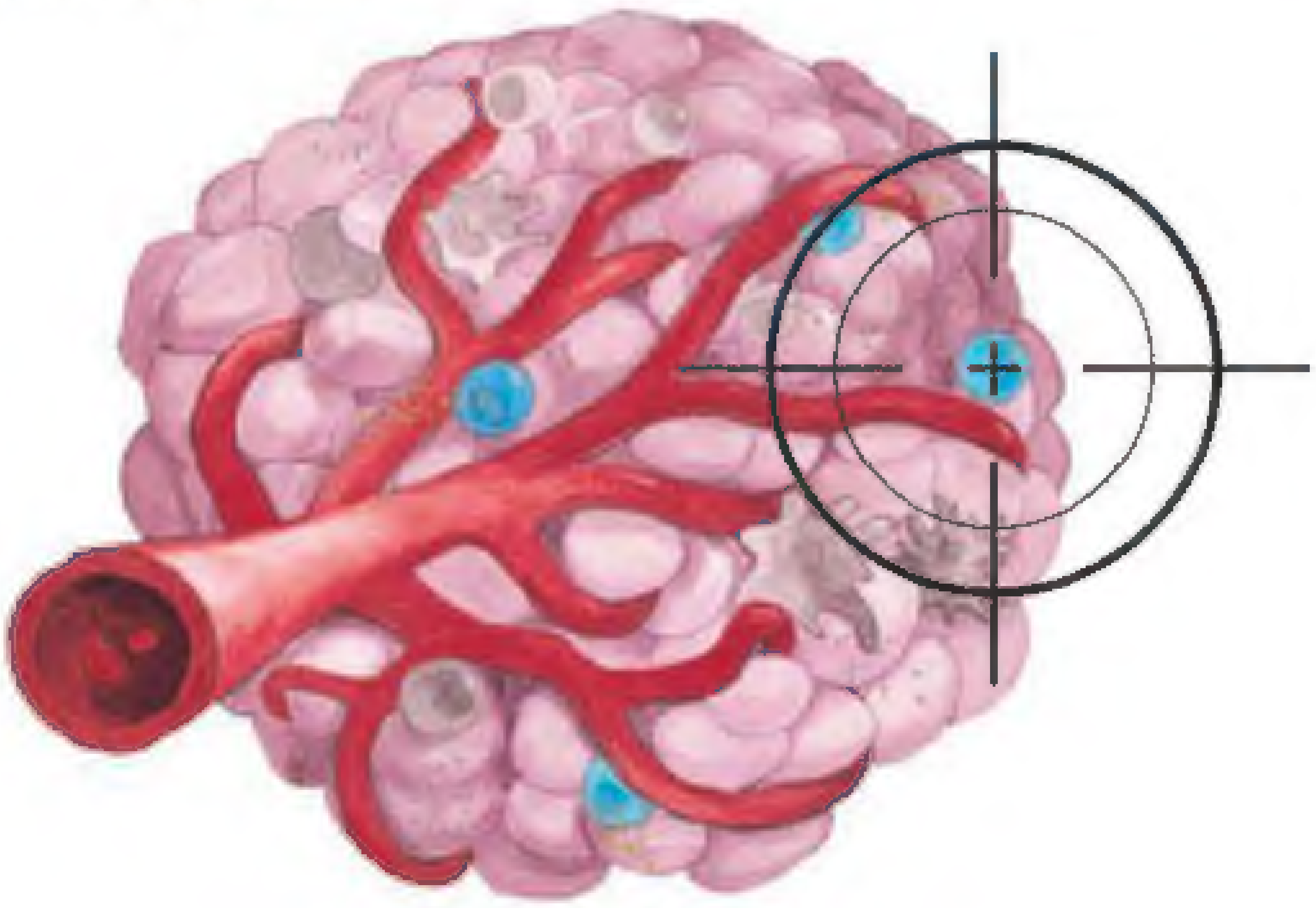

Identify

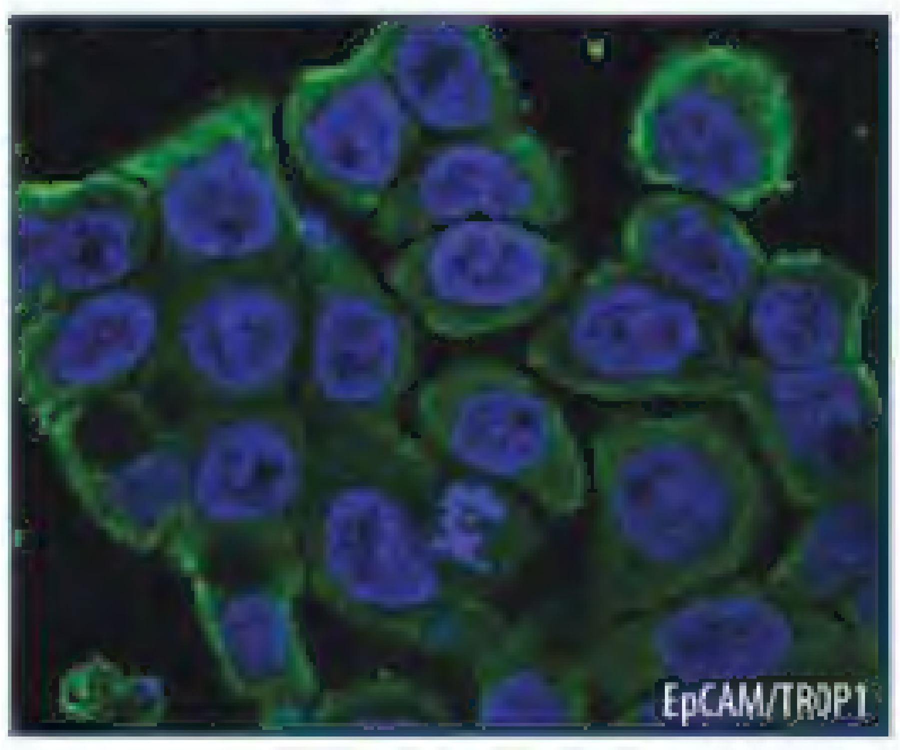

High performance antibodies for cancer stem cell identification & characterization.

Isolate

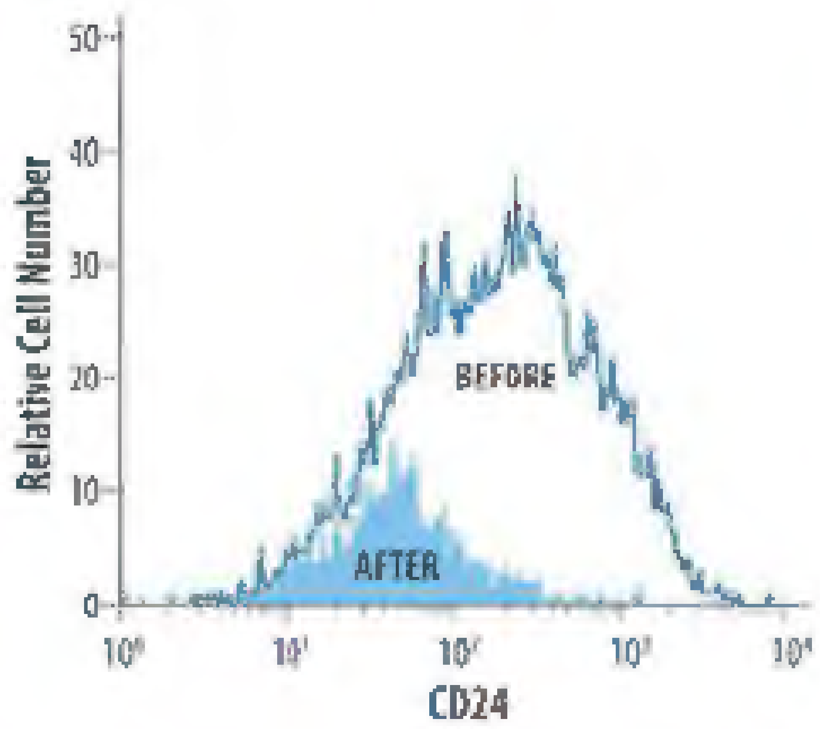

Complete kits for selection & detection, to isolate enriched cancer stem cell populations.

Investigate

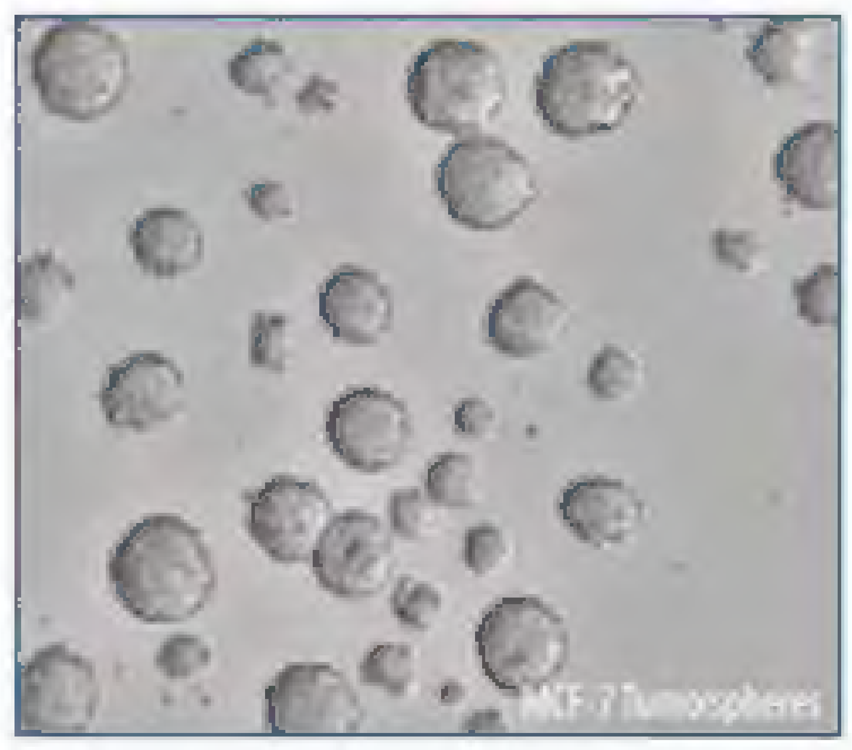

Specialized media, premium quality recombinant & natural proteins, signal transduction reagents & more!

For more information, please visit: www.RnDSystems.com/CSC

For research use only. Not for use in diagnostic procedures.

R&D Systems, Inc. www.RnDSystems.com

R&D Systems Europe, Ltd. www.RnDSystems.com

R&D Systems China Co., Ltd. www.RnDSystemsChina.com.cn